The European Physical Journal C

EPJ C

I. Antoniadis
D. Ghilencea
Editors

Recognized by European Physical Society

Supersymmetry After the Higgs Discovery

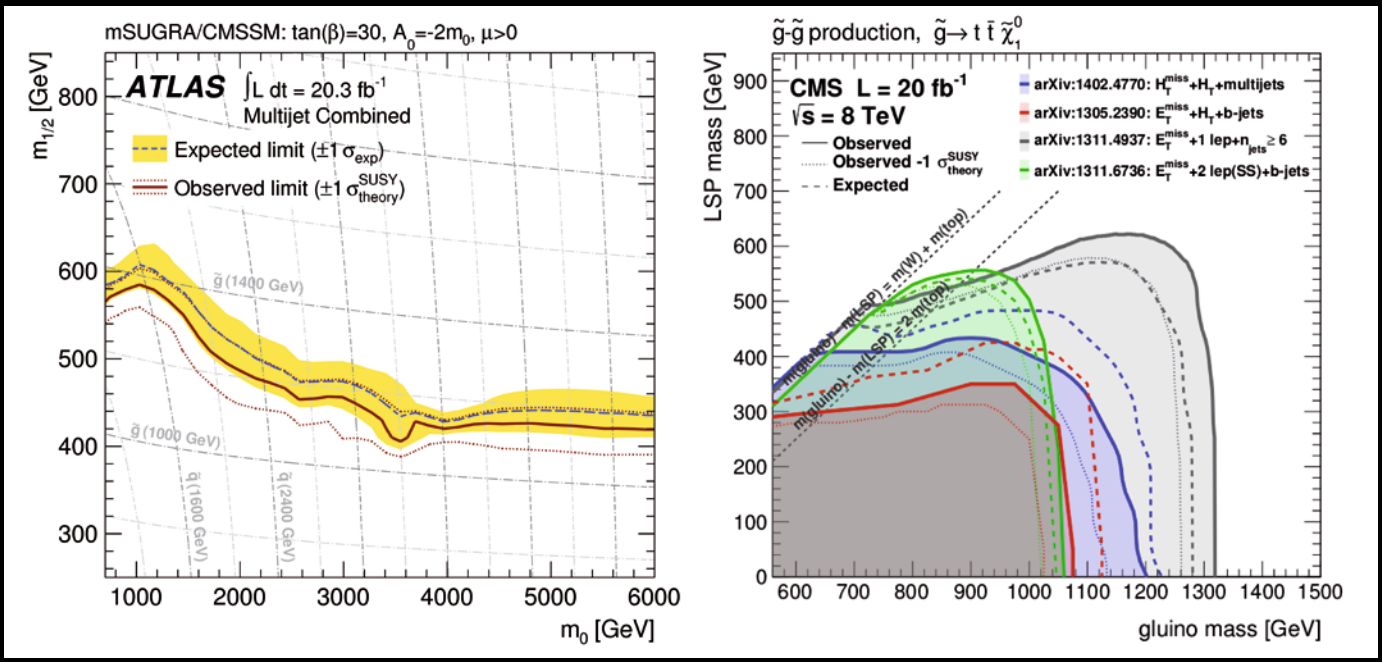

Springer

Supersymmetry After the Higgs Discovery

Ignatios Antoniadis • Dumitru Ghilencea
Editors

Supersymmetry After the Higgs Discovery

Springer

Editors
Ignatios Antoniadis
Department of Physics
CERN
Geneva, Switzerland

Dumitru Ghilencea
Theoretical Physics
National Institute of Physics NIPNE
Bucharest-Magurele, Romania

Originally published in Eur. Phys. J. C 74, 5 (2014)

ISBN 978-3-662-44171-8 ISBN 978-3-662-44172-5 (eBook)
DOI 10.1007/978-3-662-44172-5
Springer Heidelberg New York Dordrecht London

Library of Congress Control Number: 2014947341

Printed on acid-free paper

Springer is part of Springer Science+Business Media (www.springer.com)

Eur. Phys. J. C (2014) 74:2841
DOI 10.1140/epjc/s10052-014-2841-3

THE EUROPEAN PHYSICAL JOURNAL C

Editorial

Supersymmetry after the Higgs discovery

I. Antoniadis[1,a], **D. Ghilencea**[1,2,b]

[1] Department of Physics, CERN - Theory Division, 1211 Geneva 23, Switzerland
[2] Theoretical Physics Department, National Institute of Physics and Nuclear Engineering (IFIN-HH), 077125 Bucharest, Romania

Published online: 27 May 2014

These are interesting times for theoretical and experimental high energy physics. Nearly five decades after the Higgs particle theoretical prediction (1964), the ATLAS and CMS experiments of the Large Hadron Collider (LHC) at CERN confirmed (4 July 2012) the existence of the Higgs boson of the Standard Model (SM) and, implicitly, its associated (Brout–Englert–Higgs) mechanism of electroweak (EW) symmetry breaking. This confirmation is a great triumph of theoretical high energy physics and, in particular, of the principle of symmetries that modern physics is based upon, introduced early last century by E. Noether.

Supersymmetry (SUSY) is a new symmetry that relates bosons and fermions, which has strong support at both the mathematical and the physical level. At the mathematical level, SUSY avoids the restrictions of the Coleman–Mandula no-go theorem by the introduction of spinorial generators (supercharges) that makes SUSY the only possibility in which space-time beyond Poincaré and internal symmetries of the S-matrix can be combined consistently (Haag–Lopuszanski–Sohnius). The existence of a super-Poincaré (graded Lie) algebra and its representations (superfields) further supported this new symmetry on strong mathematical grounds. Moreover, if imposed as a local symmetry, general relativity is included automatically (supergravity). It is then no surprise that SUSY is also a fundamental ingredient in string theory where it plays such a crucial role, even if no trace of this symmetry is left at low energies.

At the physical level, the motivation is even stronger, when applied to the Standard Model, to obtain a (minimal) supersymmetric extension of it that could be valid at energies as low as the TeV scale. The motivation is that TeV-scale SUSY solves the mass hierarchy problem of the SM and stabilizes the EW scale in the presence of quantum corrections, by ensuring an improved ultraviolet behavior of the theory. TeV-scale SUSY is consistent with a dynamical (radiative) electroweak symmetry breaking which in the Standard Model is not explained, being an ad-hoc input. Further, in SUSY models the unification of the fundamental forces in Nature (weak, strong, and electromagnetic) is naturally achieved, to realize a long-held dream of high energy physics. This unification picture is completed by the unification with gravity, as done in various string models, like the weakly coupled heterotic string. SUSY also provides an interesting dark matter candidate, consistent with thermal relic abundance calculations, which may soon be detected by accelerator- or satellite-based experiments. All these features rely to a large extent on the existence of *low, TeV-scale* SUSY, which is thus accessible at the ongoing LHC experiments. Exact, non-perturbative results are also possible in the presence of SUSY. The consistency of all these theoretical and phenomenological advantages of SUSY made it become the most popular candidate for "new physics" beyond the Standard Model.

One initial drawback of this theory is that it more than doubles the SM spectrum, something regarded with serious skepticism by some experimentalists and even theorists. SUSY predicts a plethora of new particles (superpartners) that so far were not detected by large and small scale physics experiments. In particular the constraints from the first run of the LHC (7 and 8 TeV) restricted significantly the parameter space of various *minimal* supersymmetric models, such as the constrained minimal supersymmetric standard model. Another problem is an increased fine tuning (instability) of the EW scale in some simple models, which may question the success of SUSY in solving the hierarchy problem that motivated its introduction in the first place. These problems point to the breaking mechanism of SUSY, whose details remain somewhat mysterious.

These are, however, early days in the great effort to detect SUSY experimentally. Until Run 2 of the LHC (13 and 14 TeV) is performed and completed it is difficult to make definite statements about the existence of TeV-scale SUSY, even in minimal models. So far, the existence of a Higgs boson, in a (perturbative) region perfectly well compatible with SUSY,

[a] e-mail: ignatios.antoniadis@cern.ch
[b] e-mail: dumitru.ghilencea@cern.ch

gives us hope that this scalar particle is only one of many other scalars that we so far failed to discover. Why should there be only a *single* scalar particle, but so many fermions and gauge bosons? The optimist would even say that we already have a scalar particle and with a mass range, both *predicted* by SUSY, the Higgs boson, so we must be on the right track.

The current volume intends to be a review of these ideas, following the development of SUSY from its very early days up to present. The order of the contributions should provide the reader with the historical development as well as the latest theoretical updates and experimental constraints from particle accelerators and dark matter searches. It is a great pleasure to bring together in this volume contributions from people who initiated or contributed significantly to the development of this theory over so many years. For a balanced point of view, the volume also includes a (last) contribution that attempts to describe the physics beyond the Standard Model in the absence of SUSY.

Beloved by many theorists or shunned by as many experimentalists, the idea of SUSY remains attractive. We are fortunate that the LHC has good chances to clarify the question if SUSY really exists near the TeV scale. Its experimental confirmation would certainly dominate particle physics for many decades to come with an impact that is hard to imagine at this moment. The alternative is that this scale is pushed higher and higher, moving this beautiful idea further away from our experimental reach. This would make theorists wonder whether they pinned their hopes for too long on a single, most beautiful but elusive idea and whether the time is ripe to re-consider our view on physics near the TeV scale.

Geneva, March 2014.

Contents of this volume:

Contents

Eur. Phys. J. C (2014) 74:2698
DOI 10.1140/epjc/s10052-013-2698-x

THE EUROPEAN PHYSICAL JOURNAL C

Review

SUSY: the early years (1966–1976)

Pierre Ramond[a]

Institute for Fundamental Theory, Physics Department, University of Florida, Gainesville, USA

Received: 20 November 2013 / Accepted: 27 November 2013 / Published online: 27 May 2014

Abstract We describe the early evolution of theories with fermion–boson symmetry.

1 Introduction

By the 1940s, physicists had identified two classes of 'elementary' particles with widely different group behavior, bosons and fermions. The prototypic boson is the photon which generates electromagnetic forces; electrons, the essential constituents of matter, are fermions which satisfy Pauli's exclusion principle. This distinction was quickly extended to Yukawa's particle (boson), the generator of Strong Interactions, and to nucleons (fermions). A compelling characterization followed: matter is built out of fermions, while forces are generated by bosons.

Einstein's premature dream of unifying *all* constituents of the physical world should have provided a clue for that of fermions and bosons; yet it took physicists a long time to relate them by symmetry. This fermion–boson symmetry is called '*supersymmetry*'.

Supersymmetry, a necessary ingredient of string theory, turns out to have further remarkable formal properties when applied to local quantum field theory, by restricting its ultraviolet behavior, and providing unexpected insights into its nonperturbative behavior. It may also play a pragmatic role as the glue that explains the weakness of the elementary forces within the Standard Model of Particle Physics at short distances.

2 Early hint

In 1937, Wigner [1], with some help from his brother-in-law, publishes one of his many famous papers 'On Unitary Representations of the Inhomogeneous Lorentz Group'. He was then at the University of Wisconsin at Madison, a refugee from Princeton, which had denied him tenure. It was not an easy paper to read, but its results were very simple: there were five types of representations labeled by the values of $P^2 \equiv p^\mu p_\mu = m^2$, one of the Poincaré group's Casimir operator.

All but two representations describe familiar particles found in Nature. Massive particles come with momentum $\boldsymbol{p}$, spin j, and $2j+1$ states of polarization, e.g. electrons and nucleons with spin 1/2. There are also four types of massless representations with spin replaced by helicity (spin projection along the momentum). The first two describe massless particles with a single helicity (photons with helicity ± 1), or half-odd integer helicity, such as "massless" neutrinos with helicity $+1/2$.

The last two representations $O(\Xi)$ and $O'(\Xi)$ describe states which look like massless 'objects', particle-like in the sense that they have four-momentum, but with bizarre helicities: each representation contains an infinite tower of helicities, one with integer helicities, the other with half-odd integer helicities. These have no analogues in Nature.[1]

Physicists were slow in recognizing the importance of group representations, even though Pauli provided the first solution of the quantum-mechanical hydrogen atom using group theory. Wigner's paper does not seem to have moved any mountains, and infinite spin representations were simply ignored, except of course by Wigner.

Yet, $O(\Xi)$ and $O'(\Xi)$ contained important information: they are 'supersymmetric partners' of one another!

3 Hadrons and Mesons

Symmetries were gaining credence among physicists, not as a simplifying device but as a guide to the organiza-

[a] e-mail: ramond@phys.ufl.edu

[1] 'Infinite spin' representations do not appear in the Poincaré decomposition of the conformal group.

tion of Nature. Wigner and Stückelberg's 'supermultiplet model' unified SU(2) isospin and spin. Once Gell-Mann and Ne'eman generalized isospin to SU(3), it did not take long for Gürsey and Radicati [2], as well as Sakita [3], to propose its unification with spin into SU(6). Pseudoscalar and vector mesons (bosons) were found in the **35** representation of SU(6), while the hadrons (fermions) surprisingly lived in **56**, not in **20** [3], as expected by the statistics of the time. This non-relativistic unification proved very successful, both experimentally and conceptually, since it led to the hitherto unsuspected *color* quantum number.

In 1966, Miyazawa [4] proposed further unification. His aim was to assemble the fermionic **56** and the bosonic **35** into one mathematical structure, such as SU(9) but at the cost of disregarding spin-statistics.

To explain the bounty of strange particle discovered in the 1950s, Sakata had proposed to explain mesons as $T\overline{T}$ bound states of the spin one-half triplet

$$T = (p, n, \Lambda).$$

Miyazawa adds a *pseudoscalar* triplet

$$t = (K^+, K^0, \eta),$$

to the Sakata spinor triplet. The hadron octet would then be described by another bound state, $T\bar{t}$, but he could not describe the spin three-half baryons decimet in the **56**.

He introduces a toy model with two fundamental constituents, a spin one-half and a spin zero particle, $\mathbf{p} = (\alpha_\uparrow, \alpha_\downarrow, \gamma)$. The nine currents

$$\mathbf{p}^\dagger \lambda_i \mathbf{p} = \begin{cases} F_i, & i = 0, 1, 2, 3, 8; \\ G_i, & i = 4, 5, 6, 7, \end{cases}$$

satisfy a current algebra with both commutators and anticommutators

$$\begin{aligned} \left[F_i,\ F_j\right] &= i f_{ijk} F_k, \\ \left[F_i,\ G_j\right] &= i f_{ijk} G_k, \\ \left\{G_i,\ G_j\right\} &= d_{ijk} F_k, \end{aligned}$$

a 'generalized Jordan algebra' which he calls $V(3)$. This is the first example, albeit non-relativistic, of a superalgebra, today called SU(2/1) with even part $\mathrm{SU}(2) \times U(1)$.

In 1967, he expanded his construction [5], to general superalgebras he calls $V(n, m)$ with the idea of including the decimet. Alas, the phenomenology was not as compelling as that of SU(6); two of the quarks inside a nucleon do not seem to live together in an antitriplet color state.

In 1969, Berezin and G. I. Kac [6,7] show the mathematical consistency of graded Lie algebra which contains both commutators and anticommutators; they give its simplest example generated by the three Pauli matrices $\sigma_+, \sigma_-, \sigma_3$. Physical applications are not discussed, although Berezin's advocacy of Grassmann variables in path integrals was no doubt a motivation.

4 Dual resonance models

In the 1960s, physicists had all but given up on a Lagrangian description of the Strong Interactions, to be replaced by the S-matrix program: amplitudes were determined from general principles and symmetries, locality, causality, and Lorentz invariance. Further requirements on the amplitudes such as Regge behavior and its consequent bootstrap program were still not sufficient to determine the amplitudes.

In 1967, Dolen et al. [8] discovered a peculiar relation in $\pi - N$ scattering. At tree-level, its fermionic s-channel ($\pi N \to \pi N$) is dominated by resonances (Δ^{++}, ...), as shown by countless experiments. On the other hand, its bosonic t-channel ($\pi \bar{\pi} \to N \overline{N}$) is dominated by the ρ-meson. Using the tools of S-matrix theory in the form of 'finite energy sum rules', they found that the Regge shadow of the bosonic t-channel's ρ-meson *averaged* the fermionic resonances in the s-channel! This was totally unexpected, since these two contributions, described by different Feynman diagrams, should have been independent. Was this the additional piece of information needed to fully determine the amplitudes of Strong Interactions? This early example of fermion–boson kinship led, through an unlikely tortuous path, to modern supersymmetry.

An intense theoretical search for amplitudes where the s- and t-channel contributions are automatically related to one another followed. Under the spherical cow principle, spin was set aside and the search for DHS-type amplitudes focused on the purely bosonic process $\omega \to \pi\pi\pi$ [9]. Soon thereafter, Veneziano [10] proposed a four-point amplitude with the desired crossing symmetry,

$$A(s,t) \sim \frac{\Gamma(-\alpha(s))\Gamma(-\alpha(t))}{\Gamma(-\alpha(s) - \alpha(t))},$$

where $\alpha(x) = \alpha_0 + \alpha' x$ is the linear Regge trajectory. It displays an infinite number of poles in *both* s-channel $s > 0, t < 0$ and t-channel $s < 0, t > 0$.

Veneziano's construction was quickly generalized to n-point 'dual' amplitudes. The infinite series of poles were recognized as the vibrations of a string [11–13].

The amplitudes were linear combinations of tree chains which factorize into three-point vertices and propagators. A generalized coordinate emerged [14] from this analysis

$$Q_\mu(\tau) = x_\mu + \tau\ p_\mu + \sum_{n=1}^{\infty} \frac{1}{\sqrt{2n\alpha'}} \left(a_{n\mu} e^{in\tau} - a^\dagger_{n\mu} e^{-in\tau}\right),$$

with an infinite set of oscillators

$$\left[a_{n\mu}, a^{\dagger}_{mv}\right] = \delta_{nm} g_{\mu v}.$$

The vertex for emitting a particle of momentum k_μ from the linear chain was simple

$$V(k,\tau) =: e^{ik\cdot Q(\tau)}:.$$

Out of its corresponding generalized momentum

$$P_\mu(\tau) \;=\; \frac{\mathrm{d}Q_\mu}{\mathrm{d}\tau}, \tag{1}$$

one derived the operators

$$L_n \;=\; \frac{1}{2\pi}\int_{-\pi}^{\pi} \mathrm{d}\tau e^{in\tau} {:}P^\mu P_\mu{:} \;\equiv\; \langle {:}P^\mu P_\mu{:}\rangle_n,$$

which satisfy the Virasoro algebra[2]

$$[\,L_m\,,\,L_n\,] \;=\; (m-n)L_{n+m} + \frac{D}{12} m(m^2-1)\delta_{m,-n}.$$

Its finite subalgebra, $L_0, L_\pm$, the Gliozzi algebra, generates conformal transformations in two dimensions. The propagator was given by

$$\frac{1}{(\alpha' L_0 + 1)}.$$

5 Superstrings

The Klein–Gordon equation for a point particle

$$0 \;=\; p^2 + m^2 \;=\; \langle P^\mu\rangle_0 \langle P_\mu\rangle_0 + m^2,$$

could then be interpreted as a special case of

$$0 \;=\; \langle P^\mu P_\mu\rangle_0 + m^2$$

suggesting a correspondence [15] between point particles and dual amplitudes,

$$\langle A\rangle\langle B\rangle \;\to\; \langle A\,B\rangle.$$

Fermions should satisfy the Dirac equation

$$0 \;=\; \gamma_\mu\, p^\mu + m \;=\; \langle \Gamma_\mu\rangle_0 \langle P^\mu\rangle_0 + m.$$

This requires a generalization of the Dirac matrices as dynamical operators

$$\gamma_\mu \;\to\; \Gamma_\mu \;=\; \gamma_\mu + i\gamma_5 \sum_{n=0}^{\infty}\left(b_{n\mu}e^{in\tau} + b^{\dagger}_{n\mu}e^{-in\tau}\right)$$

where the oscillators are *Lorentz vectors*[3], which satisfy anticommuting relations

$$\{b_{n\mu}, b^{\dagger}_{n\mu}\} \;=\; \delta_{nm} g_{\mu v},$$

the sum running over the positive integers.

This led me to propose the string Dirac equation in the winter of 1970 [16], which readily followed from that correspondence:

$$0 \;=\; \langle \Gamma_\mu\, P^\mu\rangle_0 + m.$$

The basic Dirac algebra, $\{\gamma\cdot p, \gamma\cdot p\} = p^2$ is seen to be generalized to an algebra with both commutator and anticommutators

$$\{F_n,\, F_m\} \;=\; 2L_{n+m}, \quad [L_n,\, F_m] \;=\; (2m-n)F_{m+n},$$

where $F_n = \langle \Gamma_\mu P^\mu\rangle_n$, and these new L_n's also satisfy the Virasoro algebra, but with a different c-number.

Neveu and Schwarz then compute the amplitude for a dual fermion emitting three pseudoscalars with the Yukawa vertex

$$\Gamma_5 {:}e^{ik\cdot Q(\tau)}{:}, \quad \Gamma_5 \;=\; \gamma_5(-1)^{\sum b^{\dagger}_n \cdot b_n},$$

and find that the resulting amplitude contains an infinite number of poles in its fermion–antifermion channel, and even identify the residue of the first pole [17]!

A new model with bosonic poles and vertices emerges, written in terms of an infinite tower of anticommuting vector oscillators,

$$\{b_{r\mu}, b^{\dagger}_{sv}\} \;=\; \delta_{rs} g_{\mu v}, \quad r,s = \tfrac{1}{2}, \tfrac{3}{2}, \ldots.$$

The triple boson vertex is given by

$$V_{NS}(k,\tau)k^\mu \;=\; H_\mu(\tau){:}e^{ik\cdot Q(\tau)}{:},$$

where

$$H_\mu(\tau) \;=\; \sum_{r=1/2,3/2,\ldots}\left[b_{r\mu}e^{-ir\tau} + b^{\dagger}_{r\mu}e^{ir\tau}\right].$$

These are the building blocks of the 'Dual Pion model' [18, 19], published in April 1971. The algebraic structure found in the generalized Dirac equation remains the same, producing a super-Virasoro algebra which decouples unwanted modes [20], with Γ_μ replaced by H_μ, through the operators

$$G_r \;=\; \langle H\cdot P\rangle_r, \quad r = \tfrac{1}{2}, \tfrac{3}{2}, \ldots.$$

The close relation of the two sectors is soon after formalized by Gervais and Sakita [21] who write them in terms of a world-sheet σ-model, with different boundary conditions, symmetric for the fermions, antisymmetric for the bosons. They call the transformations generated by the anticommuting Virasoro operators, *supergauge transformations*, the first time the name 'super' appears in this context.

[2] A c-number is added anachronistically.

[3] Later was it realized that this made sense only in ten space-time dimensions where the little group is the spinor–vector schizophrenic SO(8).

The following years saw the formulation of the RNS (NSR to some) 'Dual Fermion Model', generating dual amplitudes with boson and fermion legs. It lived in ten space-time dimensions, with states determined in terms of transverse fermionic and bosonic harmonic oscillator operators.

In the fermionic 'R-sector', the spectrum of states is spanned by the fermionic ground state, $u|0>$ where u is a fixed 32-dimensional spinor, annihilated by both transverse bosonic and fermionic oscillators, a_{ni} and b_{ni}, $i = 1, 2 \ldots, 8$, and integer n. The fermion masses are determined by

$$\alpha' m_R^2 \;=\; \sum_{n=1}^{\infty} n \left[a_n^\dagger \cdot a_n + b_n^\dagger \cdot b_n \right].$$

The bosonic 'NS-sector' spectrum starts with a tachyon, $|0>$ annihilated by the same a_{ni}, but also by the NS fermionic oscillators b_{ri}, where r runs over half-integers. The boson masses satisfy

$$\alpha' m_{NS}^2 \;=\; \sum_{n=1}^{\infty} n a_n^\dagger \cdot a_n + \sum_{r=\frac{1}{2}} r b_r^\dagger \cdot b_r - \frac{1}{2}.$$

But there were idiosyncrasies. The correspondence between Neveu–Schwarz and the dual fermion states differed for states with an even number ($G \equiv (-1)^{\sum b_r^\dagger \cdot b_r} = -1$) of $b_r^\dagger$, and states with an odd number, and there is a tachyon in the even number spectrum, at $\alpha' m_{NS}^2 = -1/2$.

In 1976, Gliozzi et al. [22] noticed that the NS tachyon can be eliminated by requiring an odd number of anticommuting operators in the bosonic spectrum, ($G = -1$). The NS ground state

$$\alpha' m_{NS}^2 = 0: \;\; b_{1i}^\dagger |0\rangle,$$

now consists of eight bosons, transforming as the vector (=spinor) SO(8) representation. The first excited states are

$$\alpha' m_{NS}^2 = 1: \;\; b_{\frac{1}{2}i}^\dagger b_{\frac{1}{2}j}^\dagger b_{\frac{1}{2}k}^\dagger |0\rangle, \;\; b_{\frac{1}{2}i}^\dagger a_{1j}^\dagger |0\rangle, \;\; b_{\frac{3}{2}i}^\dagger |0\rangle,$$

that is, $128 = 56(8.7.6/1.2.3) + 64(8.8) + 8$ bosonic states, and so on.

In their next step, they show that the R ground state solution could also be reduced to eight fermionic degrees of freedom. In ten dimensions, while a spinor has naturally 32 degrees of freedom, they showed that one can impose *both* chiral and Majorana (reality) restrictions on it, and reduce the spinor to eight dimensions: the spinor (=vector) SO(8) representation

$$\alpha' m_R^2 = 0: \;\; \psi_\alpha |0\rangle, \;\; \alpha = 1, 2 \ldots 8.$$

The first excited state of the R-sector consists of

$$\alpha' m_R^2 = 1: \;\; b_{1i}^\dagger \psi_\alpha |0\rangle, \;\; a_{1j}^\dagger \psi_\alpha |0\rangle,$$

with $128 = 8.8 + 8.8$ fermionic states! This was no accident, and using one of Jacobi's most obtuse relations, they showed that this equality obtained at all levels. Indeed this was supersymmetry, with the same number of bosons and fermions, albeit in ten space-time dimensions.

Fermion–boson symmetry, born in its world-sheet realization, reappears as supersymmetry in ten-dimensional space-time.

Meanwhile, behind the iron curtain, …

6 Russians

In March 1971, there appears a remarkable and terse paper by Gol'fand and Likhtman [23,24] who extend the Poincaré algebra generated by P_μ and $M_{\mu\nu}$ to 'bispinor generators', W_α and $\overline{W}_\beta$, which generate spinor translations.

Cognizant that spin–statistics requires anticommutating spinors, they arrive at the parity-violating algebra

$$\{W, W\} = \left[P_\mu, P_\nu\right] = 0, \quad \{W, \overline{W}\} = \frac{(1+\gamma_5)}{2} \gamma_\mu P_\mu. \tag{2}$$

assuming no other subalgebra of the Poincaré group. With little stated motivation, they have written down the $\mathcal{N} = 1$ superPoincaré algebra in four dimensions!

They identify its simplest representation: two 'scalar hermitean' fields $\phi(x)$ and $\omega(x)$, and one left-handed spinor field $\psi_1(x)$, of equal mass, the earliest mention of the Wess–Zumino supermultiplet. They do not consider auxiliary fields nor display the transformation properties of these fields. However, they show the spinor generators as bilinears in those fields

$$W = \frac{(1+\gamma_5)}{2} \int d^3x \left[\phi^* \overset{\leftrightarrow}{\partial_0} \psi_1(x) + \omega(x) \overset{\leftrightarrow}{\partial_0} \psi_1^c(x) \right]. \tag{3}$$

They also describe that the *massive* vector multiplet follows with the vector field $A_\mu(x)$, a scalar field $\chi(x)$ and a spinor field $\psi_2(x)$. They write down its spinor current

$$W = \frac{(1+\gamma_5)}{2} \int d^3x \left[\chi \overset{\leftrightarrow}{\partial_0} \psi_2(x) + A_\mu(x) \overset{\leftrightarrow}{\partial_0} \gamma_\mu \psi_2(x) \right]. \tag{4}$$

This ground-breaking paper ends with the difficult task of writing interactions. Self-interactions of the WZ multiplet are not presented, only its interactions with a massive Abelian vector supermultiplet. This, the last formula in their paper, is a bit confusing since ϕ and ω now appear as complex fields (setting $\omega = 0$ and replacing the complex ϕ by $\phi + i\omega$ is more what they need), but it contains now-familiar features, such as the squared D-term.

Gol'fand and Likhtman had firmly planted the flag of supersymmetry in four dimensions.

Interestingly, physicists on both sides of the iron curtain seemed oblivious to this epochal paper.

Likhtman [25] seems to be the only one who followed up on this paper. He notices that the vacuum energy cancels out because of the equal number of mass bosons and fermions with the same mass. He finds scalar masses only logarithmically divergent, which he mentions in a later publication [26].

In December 1972, in an equally impressive paper, Volkov and Akulov [27,28] want to explain the masslessness of neutrinos in terms of an invariance principle. They note that the neutrino-free Dirac equation is invariant under the transformations

$$\psi \to \psi + \zeta, \quad x_\mu \to x_\mu - \frac{a}{2i}(\zeta^\dagger \sigma_\mu \psi - \psi^\dagger \sigma_\mu \zeta),$$

where ζ is a global spinor. When added to the Poincaré generators, they form a group, of the type Berezin and G. I. Kac had advocated [6,7] for algebras with commuting and anticommuting parameters. The translation of ψ makes the neutrino akin to a Nambu–Goldstone particle with only derivative couplings.

There follows a Lagrangian that describes its invariant interactions, which we can identify as a non-linear representation of supersymmetry.

The end of their paper contains this remarkable sentence 'We note that if one introduces gauge fields corresponding to the(se) transformations, then, as a consequence of the Higgs effect, a massive gauge field with spin 3/2 arises, and the Goldstone particles with spin 1/2 vanish'. This remark is followed in October 1973, when Volkov and Soroka [29, 30] generalize their transformations to local parameters and show explicitly that the fermionic Nambu–Goldstone particle indeed becomes a gauge artifact. Thus was born what became known as the 'Super Higgs Effect'.

7 Wess–Zumino

In October 1973, Wess and Zumino [31] generalize the world-sheet supergauge transformations of the RNS model to four dimensions.

Their's is the paper that launched the massive and systematic study of supersymmetric field theories in four dimensions.

The scalar (now called chiral or Wess–Zumino) multiplet is introduced. It consists of two real scalar bosons, A and B, a Weyl (Majorana) fermion ψ and two auxiliary fields F and G. Supergauge transformations generate the algebra

$$\delta A = i\overline{\alpha}\psi, \quad \delta B = i\overline{\alpha}\gamma_5\psi,$$
$$\delta\psi = \partial_\mu(A - \gamma_5 B)\gamma^\mu\alpha + n(A - \gamma_5 B)\gamma_\mu\partial_\mu\alpha + F\alpha + G\gamma_5\alpha$$
$$\delta F = i\overline{\alpha}\gamma^\mu\partial_\mu\psi + i\left(n - \frac{1}{2}\right)\partial_\mu\overline{\alpha}\gamma^\mu\psi$$
$$\delta G = i\overline{\alpha}\gamma_5\gamma^\mu\partial_\mu\psi + i\left(n - \frac{1}{2}\right)\partial_\mu\overline{\alpha}\gamma_5\gamma^\mu\psi,$$

where α is an 'infinitesimal' anticommuting spinor, and n is an integer assigned to the multiplet. With impressive algebraic strength, they are shown to close on both conformal and chiral transformations. In particular, two transformations with parameters α_1 and α_2 result in a shift of x_μ by $i\overline{\alpha}_1\gamma_\mu\alpha_2$.

The free Lagrangian for the scalar multiplet follows:

$$\mathcal{L}_{WZ} = -\frac{1}{2}\partial_\mu A\partial^\mathcal{A} - \frac{1}{2}\partial_\mu B\partial^\mu B - \frac{i}{2}\overline{\psi}\gamma_\mu\partial^\mu\psi + \frac{1}{2}(F^2 + G^2).$$

It is not invariant under supergauge transformations but since it transforms as a derivative, the action is invariant. To introduce invariant interactions, they derive the calculus necessary to produce covariant interactions, by assembling two scalar multiplets into a third, etc.

They also introduce the vector supermultiplet, consisting of four scalar fields, D, C, M, N, a vector field v_μ, and two spinor fields χ and λ, on which they derive the supergauge transformations. By identifying the vector field with the chiral current generated by a scalar multiplet

$$v_\mu = B\partial_\mu A - A\partial_\mu B - \frac{1}{2}i\overline{\psi}\gamma_5\gamma_\mu\psi,$$

and following it through the algebra, they express all the vector multiplet fields as quadratic combinations of the scalar supermultiplet. In particular $D = 2\mathcal{L}_{WZ}$.

Finally, they notice that one can drop some of these fields, C, N, M, and χ, without affecting the algebra (soon to be called the Wess–Zumino gauge), and write the vector multiplet Lagrangian in a very simple form:

$$\mathcal{L}_V = -\frac{1}{4}v_{\mu\nu}v^{\mu\nu} - \frac{1}{2}i\overline{\lambda}\gamma_\mu\partial^\mu\lambda + \frac{1}{2}D^2.$$

This paper contains many of the techniques that were soon to be used in deriving many of the magical properties of supersymmetric theories in four dimensions.

In December 1973, Wess and Zumino present the one-loop analysis [32] of an interacting Wess–Zumino multiplet, and find remarkable regularities: the SUSY tree-level relations are not altered by quantum effects, the vertex correction is finite (leaving only finally where they find that one has only wave function renormalization), and finally the quadratic divergences of the scalar and pseudoscalar fields cancel. As it was realized later, this addresses the "gauge hierarchy problem", and strongly suggests SUSY's application to the Standard Model.

8 Representations

The representations of the supersymmetry algebra were first systematically studied by Gell-Mann and Ne'eman (unpublished). They mapped the algebra in light-cone coordinates to a Fermi oscillator, and they found that in supersymmetry, the massless representations of the Poincaré group assemble into two states with helicities separated by one-half

$$\left(\lambda \pm \frac{1}{2}, \lambda\right),$$

and with the same light-like momentum, yielding an equal number of bosons and fermions. The simplest is $\lambda = 0$, with a real scalar and half a left-handed Weyl fermion. However, CPT-symmetric local field theories require the other half of the Weyl fermion, $(\frac{1}{2}, 0) + (0, -\frac{1}{2})$, which describes one Weyl fermion and a complex scalar boson, the ingredients of the Gol'fand–Likhtman–Wess–Zumino multiplet.

The massless gauge supermultiplet, $(1, \frac{1}{2}) + (-\frac{1}{2}, -1)$, describes a gauge boson, and its companion Weyl (Majorana) fermion describes the gaugino.

The supergravity supermultiplet $(2, \frac{3}{2}) + (-\frac{3}{2}, -2)$ contains the graviton and the gravitino, remarkably the ingredients of interacting supergravity [33,34]

They extend their analysis to the case of $\mathcal{N}$ supersymmetries. Disregarding particles of spin higher than two, they find two cases with manifestly self-conjugate supermultiplets.

First, we have an $\mathcal{N} = 4$ supermultiplet, with helicities

$$(1) + 4\left(\tfrac{1}{2}\right) + 6(0) + 4\left(-\tfrac{1}{2}\right) + (-1),$$

and led in 1976 to the $\mathcal{N} = 4$ superYang–Mills theory [35], which was found much later to have magical properties, such as an enhanced conformal symmetry, and ultraviolet finiteness!

Second, we have $\mathcal{N} = 8$ supergravity with helicities

$$(2) + 8\left(\tfrac{3}{2}\right) + 28(1) + 56\left(\tfrac{1}{2}\right) + 70(0) \\ +56\left(-\tfrac{1}{2}\right) + 28(-1) + 8\left(-\tfrac{3}{2}\right) + (-2),$$

which also led to a fully interacting theory, $\mathcal{N} = 8$ Supergravity [36].

Massive representations of supersymmetry can be assembled using a group theoretical Higgs mechanism. The massive vector representation contains a Dirac spinor, a massive vector, and a scalar particle

$$\left(1, \tfrac{1}{2}\right) + \left(-1, -\tfrac{1}{2}\right) + \left(0, -\tfrac{1}{2}\right) + \left(0, \tfrac{1}{2}\right),$$

all of equal mass, as considered by Gol'fand and Likhtman.

9 Towards the supersymmetric standard model

With the Wess–Zumino paper, the flood gates had been opened [37]. In short order, a supersymmetric version [38] of QED is written down, with Abelian gauge invariance, in which the Dirac electron spinor is accompanied by *two* complex spin zero fields. In January 1974, Salam and Strathdee [39,40] assemble the fields within a supermultiplet into one superfield with the help of anticommuting Grassmann variables. The same authors [41] coin the word 'super-symmetry' in a May 1974 paper which generalizes supersymmetry to Non-Abelian gauge interactions.

Before applying supersymmetry to the real world, several conceptual problems must be resolved. Firstly, the absence of fermion–boson symmetry at low energies requires it to be broken. Secondly, its application to the electroweak theory demands the extension of the Higgs mechanism. Finally, the known particles must be assigned to supermultiplets.

In 1974, Fayet and Iliopoulos [42] produce the first paper on spontaneous breaking of supersymmetry in theories with a gauged Abelian symmetry by giving its D auxiliary field a constant value. Their proposal is remarkably simple, just add to the Lagrangian for a $U(1)$ vector multiplet a D-term

$$\mathcal{L}_V^{FI} = \mathcal{L}_V + \xi D.$$

This extra term violates neither Abelian gauge invariance nor supergauge invariance, since its supergauge variation is a total derivative. The resulting field equation $\langle D \rangle_0 = \xi$ yields a theory where both gauge and supergauge invariances are broken.

A year later, O'Raifeartaigh [43] invents a different way to spontaneous breaking of supersymmetry, in theories with several interacting scalar supermultiplets. Its simplest model involves three scalar supermultiplets with equations of motion

$$F_1 = -m\phi_2^* - 2\lambda\phi_1^*\phi_3^*,\ F_2 = -m\phi_1^*,\ F_3 = \lambda(M^2 - \phi_1^{2*}),$$

where m, M, and λ are parameters. There are no solutions for which all three F_i vanish, and supersymmetry is broken. From these two early examples, the auxiliary fields are the order parameters of SUSY breaking.

Both schemes yielded an embarrassing massless Goldstone spinor, which may have impeded the application of supersymmetry[4]. None of these authors were aware of Volkov's papers.

The second hurdle is the generalization of the Higgs mechanism to supersymmetry. This is done in the context of an unusual model by Fayet [44] in December 1974. Like Volkov

[4] In 1976, Weinberg and Gildener note that supersymmetry could explain a low mass scalar boson, but bemoan that it would produce a massless fermion!

and Akulov before, Fayet builds models where the electron neutrino is the Goldstone spinor from the breakdown of supersymmetry[5] using the FI mechanism.

Although the model building in this paper did not survive the test of time, two important and more permanent concepts emerged. One is that the Higgs mechanism applies, but *two* scalar supermultiplets are needed to achieve $SU(2) \times U(1) \rightarrow U(1)$ electroweak breaking, in accord with the number of surviving scalars in the massive vector supermultiplets—also the existence of R-symmetry, a new kind of continuous symmetry acting on both the fields and the Grassmann parameters of the superfields.

It was not until July 1976 that Fayet [45] generalizes the Weinberg–Salam (soon to be called the Weinberg–Salam–Glashow, and then Standard) model to SUSY. Its distinctive features are

- There are two scalar superfields, S, T, (today's $H_{u,d}$) for EW breaking.
- Leptons and quarks are the fermions inside scalar supermultiplet.
- We have a continuous R-symmetry.

The particle content is the 'minimal supersymmetric model' (MSSM). Some kinks still need to be ironed out, having to do with SUSY breaking (*à la* Fayet–Iliopoulos in this paper), which produces a massless Goldstone spinor. The continuous R-symmetry in this paper behaves like a 'leptonic' number, but it prevents the spinor gluons from acquiring a mass.

Today, we know that SUSY breaking is an active area of theoretical research, even without the presence of a Goldstone fermion, eaten by the Super-Higgs mechanism.

10 SUSY today

By stopping this history of fermion–boson symmetry in 1976, we rob the reader of the many wonderful concepts since discovered, but they are more than adequately covered in the articles in this volume.

The seeds of today's SUSY research were planted in these early papers.

Almost 40 years later, superstring theories have blossomed into a dazzling array of connected theories; the study of $\mathcal{N} = 4$ superYang–Mills theories is an active field of research, as is the possible finiteness of $\mathcal{N} = 8$ supergravity.

The Hamiltonian is no longer fundamental, but derived from translations along SUSY's fermionic dimensions.

Few doubt the existence of a deeper connection between bosons and fermions, but opinions differ at which scale it will be revealed: the breaking of supersymmetry remains as mysterious as ever.

Yet, the recent discovery of a low mass Higgs particle suggests that the universe displays more symmetry at shorter distances.

Today, SUSY is unfulfilled, beloved by theorists, but so far shunned by experiments.

In the words of the late Sergio Fubini, *'We do not know if supersymmetry is just a beautiful painting to put on the wall, or something more'.*

[5] In 1974, the Standard Model was not yet 'standard', and many authors were still presenting alternatives.

References

1. E. Wigner, On unitary representations of theinhomogeneous Lorentz group. Annals of Mathematics **40**(1),149–204 (1939)
2. F. Gürsey, L.A. Radicati, Spin and unitary spin independence of strong interactions. Phys. Rev. Lett. **13**, 173–175 (1964)
3. B. Sakita, Supermultiplets of elementary particles. Phys. Rev. **136**, B1756–B1760 (1964)
4. H. Miyazawa, Baryon number changing currents. Progr. Theoret. Phys. (Kyoto) **36**, 1266 (1966)
5. H. Miyazawa, Spinor symmetries and symmetries of Baryons and Mesons. Phys. Rev. **170**, 1586–1590 (1968)
6. F.A. Berezin, G.I. Kac, Mat. Sbornik Tom **82** (124) (1970)
7. F.A. Berezin, G.I. Kac, Math. USSR. Sbornik **11**, 311–325 (1970)
8. R. Dolen, D. Horn, C. Schmid, Predictions of Regge parameters of ρ poles from low-energy πN data. Phys. Rev. Lett. **19**, 402–407 (1967)
9. M. Ademollo, H.R. Rubinstein, G. Veneziano, M.A. Virasoro, Bootstraplike conditions from superconvergence. Phys. Rev. Lett. **19**, 1402–1405 (1967)
10. G. Veneziano, Construction of a crossing-symmetric, Regge behaved amplitude for linearly rising trajectories. Nuovo Cim. A **57**, 190–197 (1968)
11. Y. Nambu, Quark model and the factorization of the Veneziano amplitude, EFI 69–64, in *Symmetries and Quark Model*, ed. by R. Chand (Gordon and Breach, 1970)
12. H. B. Nielsen, An almost physical interpretation of the integrand of the n-point Veneziano model. Nordita Preprint 1969, submitted to the 15th International Conference on High energy Physics, Kiev, 1970
13. L. Susskind, Harmonic-oscillator analogy for the Veneziano model. Phys. Rev. Lett. **23**, 545–547 (1969)
14. S. Fubini, D. Gordon, G. Veneziano, A general treatment of factorization in dual resonance models. Phys. Lett. B **29**, 679–682 (1969)
15. P. Ramond, An interpretation of dual theories. Nuovo Cim. A **4**, 544–548 (1971)
16. P. Ramond, Dual theory for free fermions. Phys. Rev. D **3**, 2415–2418 (1971)
17. A. Neveu, in *The Birth of String Theory*, eds by E. Cappelli, E. Castellani, F. Colombo, P. DiVecchia (Cambridge University Press, Cambridge, 2012)
18. A. Neveu, J.H. Schwarz, Tachyon-free dual model with a positive-intercept trajectory. Phys. Lett. **34B**, 517–518 (1971)

19. A. Neveu, J.H. Schwarz, Factorizable dual model of pions. Nucl. Phys. B **31**, 86–112 (1971)
20. A. Neveu, J.H. Schwarz, C. Thorn, Reformulation of the dual pion model. Phys. Lett. **35B**, 529–533 (1971)
21. J.-L. Gervais, B. Sakita, Field theory interpretation of supergauges in dual models. Nucl. Phys. B **34**, 632–639 (1971)
22. F. Gliozzi, J. Scherk, D.I. Olive, Supersymmetry, supergravity theories and the dual spinor model. Nucl. Phys. B **122**, 253–290 (1977)
23. Yu.A. Golfand, E.P. Likhtman, Extension of the algebra of poincare group generators and violation of p invariance. JETP Lett. **13**, 323–326 (1971)
24. Yu.A. Golfand, E.P. Likhtman, Pisma Zh.Eksp. Teor. Fiz. **13**, 452–455 (1971)
25. E. P. Likhtman, *Irreducible Representations of the Extension of the Algebra of the Poincaré Generators by the Bispinor Generators*. Report of the Lebedev Institute no. 41 (1971) (retroprinted http://arxiv.org/pdf/hep-ph/0101209.pdf)
26. E.P. Likhtman, JETP Lett. **21**, 109 (1975)
27. D.V. Volkov, V.P. Akulov, Possible universal neutrino interaction. JETP Lett. **16**, 438–440 (1972)
28. D.V. Volkov, V.P. Akulov, Pisma Zh.Eksp. Teor. Fiz. **16**, 621–624 (1972)
29. D.V. Volkov, V.A. Soroka, Higgs effects for goldstone particles with spin 1/2. JETP Lett. **18**, 312–314 (1973)
30. D.V. Volkov, V.A. Soroka, Pisma Zh.Eksp. Teor. Fiz. **18**, 529–532 (1973)
31. J. Wess, B. Zumino, Supergauge transformations in four dimensions. Nucl. Phys. B **70**, 39–50 (1974)
32. J. Wess, B. Zumino A Lagrangian model invariant under supergauge transformations. Phys. Lett. B **49**, 52 (1974)
33. D.Z. Freedman, P. van Nieuwenhuizen, S. Ferrara, Progress toward a theory of supergravity. Phys. Rev. D **13**, 3214–3218 (1976)
34. S. Deser, B. Zumino, Consistent supergravity. Phys. Lett. **62B**, 335 (1976)
35. L. Brink, John H. Schwarz, Joel Scherk, Supersymmetric Yang-Mills theories. Nucl. Phys. **121B**, 77 (1977)
36. E. Cremmer, B. Julia, The SO(8) supergravity. Nucl. Phys. **159B**, 141 (1979)
37. S. Ferrara, Review by Pierre Fayet. Phys. Rep. **32**, 249–334 (1977)
38. J. Wess, B. Zumino, Nucl. Phys. **78B** (1974)
39. A. Salam, J.A. Strathdee, Supergauge transformations. Nucl. Phys. B **76**, 477 (1974)
40. A. Salam, J.A. Strathdee, On superfields and fermi-bose symmetry. Phys. Rev. D **11**, 1521–1535 (1975)
41. A. Salam, J.A. Strathdee, "Super-symmetry and Nonabelian Gauges". Phys. Lett. B **51**, 353–355 (1974)
42. P. Fayet, J. Iliopoulos, "Spontaneously Broken Supergauge Symmetries and Goldstone Spinors. Phys. Lett. B **51**, 461–464 (1974)
43. L. O'Raifeartaigh, Spontaneous Symmetry Breaking for Chiral Scalar Superfields. Nucl. Phys. B **96**, 331 (1975)
44. P. Fayet, Supergauge Invariant Extension of the Higgs Mechanism and a Model for the Electron and its Neutrino. Nucl. Phys. B **90**, 104–124 (1975)
45. P. Fayet, Supersymmetry and Weak, Electromagnetic and Strong Interactions. Phys. Lett. B **64**, 159–162 (1976)

Eur. Phys. J. C (2014) 74:2837
DOI 10.1140/epjc/s10052-014-2837-z

THE EUROPEAN PHYSICAL JOURNAL C

Review

The supersymmetric standard model

with a Brout–Englert–Higgs boson as spin-0 partner of the Z

Pierre Fayet[a]

Laboratoire de Physique Théorique de l'ENS (UMR 8549 CNRS), 24 rue Lhomond, 75231 Paris Cedex 05, France

Received: 25 March 2014 / Accepted: 26 March 2014 / Published online: 27 May 2014

Abstract Supersymmetric extensions of the standard model lead us to expect superpartners for all particles, spin-0 squarks and sleptons and spin-$\frac{1}{2}$ gluinos, charginos, and neutralinos, with an odd R-parity making the lightest one stable. The electroweak breaking is induced by a pair of spin-0 doublets, leading to several charged and neutral BE-Higgs bosons. These theories also lead to gauge/Higgs unification by providing spin-0 bosons as *extra states for spin-1 gauge bosons* within massive gauge multiplets. In particular, the 125 GeV/c^2 boson recently observed at CERN, most likely a BE-Higgs boson associated with the electroweak breaking, may also be interpreted, up to a mixing angle induced by supersymmetry breaking, as *the spin-0 partner of the Z* under *two* supersymmetry transformations. We also discuss how the compactification of extra dimensions, relying on R-parity and other discrete symmetries, may determine both the grand-unification and the supersymmetry-breaking scales.

1 Introduction

Is there a "superworld" of new particles? Could half of the particles at least have escaped our observations? Do new states of matter exist? After the prediction of antimatter by Dirac, supersymmetric extensions of the standard model lead to anticipate the possible existence, next to quarks and leptons, of associated spin-0 *squarks* and *sleptons*, with the gluons, $W^{\pm}$, Z, and photon also associated with new superpartners, *gluinos, charginos* and *neutralinos* [1–5]. These new states are characterized by a quantum number called *R-parity* related to baryon and lepton numbers, obtained from a discrete remnant of a continuous $U(1)_R$ symmetry acting chirally on the supersymmetry generator, broken to R-parity by the gravitino and gluino masses [6,7].

The spontaneous breaking of the electroweak symmetry is induced, in contrast with the standard model [8,9], by *a pair of spin-0 doublets* responsible for charged-lepton and down-quark masses, and up-quark masses, respectively [1–3]. This leads to expect *charged spin-0 bosons* $H^{\pm}$, and additional neutral ones. Such theories possess many attractive features, providing in particular a natural place for fundamental spin-0 bosons next to spin-1 and spin-$\frac{1}{2}$ particles, and the possibility of associating spin-1 with spin-0 particles within massive gauge multiplets of supersymmetry. We keep waiting for signs of superpartners [10,11] and additional Brout–Englert–Higgs bosons [12,13], beyond the one recently found at the CERN LHC [14,15].

This new boson with a mass close to 125 GeV/c^2 may actually be interpreted (up to a mixing angle, possibly small, induced by supersymmetry breaking) as *a spin-0 partner of the spin-1 Z* within a massive gauge multiplet of supersymmetry, providing within a theory of electroweak and strong interactions the first example of *two known fundamental particles of different spins related by supersymmetry*—in spite of their different electroweak properties.

We shall review here the main steps followed in the construction of the supersymmetric standard model, parallel to related developments in $N = 2$ and $N = 4$ supersymmetric theories. These more speculative theories may also be expressed using extra compact dimensions, which may play an essential role in the breaking of the supersymmetry and grand-unification symmetries at the compactification scale(s) [16–18]. We also refer the reader to the standard review articles [19–22], and leave more detailed discussions on the present status of supersymmetric theories, including the role of neutralinos as possible dark matter candidates and the effect of the new particles on gauge-coupling unification, to subsequent contributions to this volume.

2 Relate bosons with fermions, yes, but how?

To begin with, according to common knowledge, supersymmetry relates, or should relate, bosons with fermions:

[a] e-mail: fayet@lpt.ens.fr

$$\underbrace{\text{Bosons}}_{\text{integer spin}} \overset{\text{SUSY}}{\longleftrightarrow} \underbrace{\text{Fermions}}_{\text{half-integer spin}} . \tag{1}$$

But can such an idea be of any help in understanding the real world of particles and interactions? Could one relate, for example, mesons with baryons,

$$\text{Mesons} \longleftrightarrow \text{Baryons?} \tag{2}$$

as attempted by Miyazawa in the 1960s [23,24] within a non-relativistic framework? Or in a more modern way dealing now with fundamental particles, can one relate the bosons, messengers of interactions, with the fermions, constituents of matter, to arrive at some sort of unification

$$\text{Forces} \longleftrightarrow \text{Matter?} \tag{3}$$

This would be very attractive, but unfortunately things do not work out that way.

Indeed it turns out that supersymmetry should associate known bosons with new fermions, and known fermions with new bosons. While this is now often presented as obvious, it was long taken, and even mocked, as a sign of the irrelevance of supersymmetry. Still, part of the utopic association (3) between forces and matter may turn out to be relevant in the case of *dark matter*, for which supersymmetric theories provide a natural candidate in connection with R-parity conservation (cf. (92,93) in Sect. 7).

The supersymmetry algebra

$$\begin{cases} \{Q,\ \bar{Q}\} = -2\,\gamma_\mu P^\mu \\ [Q,\ P^\mu] = 0 \end{cases} \tag{4}$$

relates supersymmetry transformations with spacetime translations. It was introduced in the years 1971–1973 [25–28] with various motivations, including: is it at the origin of parity non-conservation [26], or is the neutrino a Goldstone particle [27]? More interestingly, the intimate connection of supersymmetry with spacetime translations implies that a theory invariant under local supersymmetry transformations must include general relativity, leading to supergravity theories [29–31].

However, even knowing about the mathematical existence of such an algebra, with bosonic and fermionic degrees of freedom jointly described using superfields [32,33], fundamental bosons and fermions do not seem to have much in common. It is hard to imagine how they could be related by a spin-$\frac{1}{2}$ generator, in a relativistic theory. Beyond the obvious fact that bosons and fermions have different masses, to which we shall return later, the gauge bosons, mediators of interactions, and the quarks and leptons do not have the same gauge quantum numbers.

In addition supersymmetric gauge theories [34–36] systematically involve spin-$\frac{1}{2}$ Majorana fermions, unknown in Nature (with a possible exception for neutrinos in case lepton number turns out not to be exactly conserved). In contrast known fundamental fermions, quarks and leptons, correspond to Dirac spinors carrying conserved quantum numbers, baryon number B and lepton number L. These are even known, or were known in the past, as *fermionic numbers*, to emphasize that they are carried by fundamental fermions only, not by bosons. Of course this no longer appears as necessary today, now that we got familiar with supersymmetric extensions of the standard model and ready to accept the possible existence of spin-0 bosons, squarks and sleptons, carrying B and L almost by definition [2,3], but this was once viewed as quite a heretic hypothesis. Furthermore, just attributing B and L to squarks and sleptons does not necessarily guarantee that these quantum numbers are going to be conserved, at least to a sufficiently good approximation. This is also where R-symmetry and R-parity are going to play an essential role [2–5].

Altogether supersymmetry first seemed irrelevant to the description of the real world, and many physicists kept this point of view for quite some time.

3 General features

3.1 The specificities of spontaneous supersymmetry breaking

There is also the difficult question of how to obtain a spontaneous breaking of the supersymmetry. This is by far not trivial owing to the specificities of its algebra, allowing one to express the hamiltonian from the squares of the four components of the supersymmetry generator, as

$$H = \frac{1}{4} \sum_\alpha Q_\alpha^2 . \tag{5}$$

It implies that *a supersymmetric vacuum state must have a vanishing energy*, which first seemed to prevent any spontaneous breaking of supersymmetry to possibly occur [37]. In any case such a breaking should lead to a massless spin-$\frac{1}{2}$ Goldstone fermion, unobserved.

Nevertheless, in spite of this apparently general argument, spontaneous supersymmetry breaking turned out to be possible, although it is very severely constrained. Indeed in global supersymmetry, instead of simply trying to make a supersymmetric vacuum state unstable, as one would normally do for any ordinary symmetry, one has to arrange for such a symmetric state to be *totally absent*, as it would otherwise have vanishing energy and be stable owing to the relation (5) between the hamiltonian and supersymmetry generator.

Such a very special situation may be obtained using either a mechanism relying on a $U(1)$ gauge group and associated ξD term included in the Lagrangian density [38]. Or using an appropriate set of chiral superfields including at least a gauge singlet one with its corresponding σF term from a

linear term in the superpotential [39,40], interacting through a suitable superpotential carefully chosen *with the help of an R symmetry* [1]. These models also lead to the systematic existence of *classically flat directions* of the potential (valleys) associated with classically massless particles (*moduli* or *pseudomoduli*), in connection with the fact that one makes it impossible for all auxiliary components to vanish simultaneously; and this in a generic way, thanks to the use of an R symmetry.

In most situations on the other hand, spin-0 fields generally tend, in order to minimize the energy, to adjust their vacuum expectation values so that all auxiliary fields vanish simultaneously, with supersymmetry remaining conserved. At the same time the other symmetries may well be, quite easily, spontaneously broken, including charge and color gauge symmetries if some charged-slepton or squark fields were to acquire non-vanishing v.e.v.'s. This would be, also, a real disaster ! In practice one will always have to pay sufficient attention to the supersymmetry-breaking mechanism, so that *all* squarks and sleptons (and charged BE-Higgs bosons) acquire large positive mass^2 (i.e. *no tachyons*), and the vacuum state preserves electric charge and color as required, avoiding charge-or-color-breaking (CCB) minima.

3.2 Gluino masses and metastable vacua

Note that *metastable vacuum states* with a very long lifetime may have to be considered, separated by a potential barrier from a lower-energy stable minimum of the energy, for which charge or color symmetries could be spontaneously broken. This may the case, in particular, in the presence of additional spin-0 gluon fields introduced in [7] to turn gluinos into Dirac particles, with an underlying motivation from extended supersymmetry [41,42].

Gluinos would remain massless in the presence of an unbroken continuous R symmetry, also denoted $U(1)_R$, acting chirally on them. Gluino mass terms, however, may be generated radiatively from their Yukawa couplings to a new set of massive *messenger-quark superfields vectorially coupled to gauge superfields*, sensitive both to the source of supersymmetry breaking (e.g. through auxiliary-component v.e.v.'s $< F >$ or $< D >$), and to a source of R-symmetry breaking, for Majorana gluinos [7]. It is, however, difficult to generate radiatively large gluino masses, unless one accepts to consider really very large masses for messenger quarks, as frequently done now.

One can also generate in this way a Dirac gluino mass term, which preserves the continuous R-symmetry. The new spin-0 gluon fields introduced to turn gluinos into Dirac particles, now called "sgluons", tend, however, to acquire radiatively generated negative mass^2 from their couplings to messenger quarks [7, footnote 5], so that the corresponding desired vacuum state must be stabilized in order to avoid color breaking.

This may be done by adding in the Lagrangian density a direct gauge-invariant chiral-octet-superfield mass term, breaking explicitly the $U(1)_R$ symmetry down to R-parity. It includes, next to a "sgluon" mass^2 term, a direct $\Delta R = \pm 2$ gluino Majorana mass term for the second octet of "paragluinos" breaking the continuous $U(1)_R$. This Majorana mass term splits the Dirac gluino octet into two Majorana mass eigenstates through the *see-saw mechanism for Dirac gluinos*. This one is formally analogous to the see-saw mechanism for neutrinos that became popular later. While the color-preserving vacuum, with massive gluinos, gets locally stabilized in this way, it is only *metastable* [7, footnote 6], an interesting feature compatible with phenomenological requirements also occurring in other situations, which attracted some attention later [43].

Let us return to Majorana gluinos. Their mass terms are not forbidden in the supergravity framework where the gravitino acquires a mass $m_{3/2}$ so that R-symmetry gets reduced to R-parity, allowing for direct gaugino mass terms [6], which may be generated from gravity-induced supersymmetry breaking. Jointly with the direct higgsino mass term μ (or effective mass term $\mu_{\rm eff}$), these terms allow for *both charginos* to be *heavier than* m_W, as is now necessary [44–46].

3.3 The fate of the Goldstone fermion, and related interactions of a light gravitino

A massless Goldstone fermion appears in spontaneously broken globally supersymmetric theories, which is in principle viewed as an embarrassment. This Goldstone fermion, however, may be eliminated by the super-Higgs mechanism within supergravity theories [29–31,47]. Still it may actually survive under the form of the $\pm\frac{1}{2}$ polarization states of a massive but possibly very light spin-$\frac{3}{2}$ gravitino. But a very light gravitino still behaves as a (quasi-massless) spin-$\frac{1}{2}$ goldstino according to the equivalence theorm of supersymmetry [6], in which case we get back to our starting point, still having to discuss the fate of the Goldstone fermion !

Thanks to R-parity, however, this Goldstone fermion, being R-odd, has no direct couplings to ordinary particles only. It couples bosons to fermions within the multiplets of supersymmetry, i.e. ordinary particles to superpartners (as yet unseen), in a way fixed by the boson-fermion mass spectrum through the supercurrent conservation equation. Furthermore, its interactions may be much weaker than weak interactions, if the supersymmetry-breaking scale parameter ($\sqrt{d}$ or $\sqrt{F}$), related to the gravitino mass by $m_{3/2} = \kappa d/\sqrt{6} = \kappa F/\sqrt{3}$ with $\kappa^2 = 8\pi G_N$, is sufficiently large [5,6]. Supersymmetry is then said to be bro-

ken "at a high scale", the spin-$\frac{1}{2}$ polarization states of such a light gravitino behaving as an "almost-invisible" goldstino.

The gravitino is then the lightest supersymmetric particle, or LSP, with a very-weakly interacting [48] and thus early decoupling gravitino appearing as a possible candidate for the non-baryonic dark matter of the Universe [49,50]. With such a light gravitino LSP, the next-to-lightest supersymmetric particle (NLSP), usually a neutralino, is expected to decay, possibly with a long lifetime, according to

$$\text{neutralino} \to \gamma + \text{unobserved gravitino}, \tag{6}$$

leading to an experimental signature through the production of photons + missing energy-momentum, as is the case in the so-called GMSB models.

Conversely, how the spin-$\frac{1}{2}$ Goldstone fermion (goldstino) field couples to boson-fermion pairs determines how the boson and fermion masses get split within the multiplets of supersymmetry [5,6].

4 Electroweak breaking with two spin-0 doublets

4.1 Introducing R symmetry, and $U(1)_A$, in a two-doublet model

One of the initial difficulties in supersymmetric theories was to construct massive Dirac spinors carrying a conserved quantum number that could be attributed to leptons, although supersymmetric theories involve self-conjugate Majorana fermions which in principle cannot carry such a quantum number. This led to the definition of R-symmetry, first obtained within a toy model for "leptons", soon reinterpreted as the charginos and neutralinos of the supersymmetric standard model [1].

This first supersymmetric electroweak model [1] was obtained from a related pre-SUSY 2-spin-0-doublet vector-like one [51], that was actually an "inert-doublet model", close to being a supersymmetric theory. This one already included a Q symmetry precursor of the R symmetry, acting on the two doublets ($\varphi'' = h_1$ and $\varphi' = h_2^c$) according to

$$h_1 \to e^{i\alpha}\, h_1, \quad h_2 \to e^{i\alpha}\, h_2\,. \tag{7}$$

This Q symmetry, jointly with $U(1)_Y$, allowed one to rotate independently the two doublets h_1 and h_2, restricting the structure of the Yukawa and quartic couplings very much as for Higgs and higgsino doublets within supersymmetry. There it acts according to

$$\begin{aligned} H_1\,(x,\theta) &\overset{Q}{\to} e^{i\alpha}\, H_1\,(x,\theta\, e^{-i\,\alpha}),\\ H_2\,(x,\theta) &\overset{Q}{\to} e^{i\alpha}\, H_2\,(x,\theta\, e^{-i\,\alpha}), \end{aligned} \tag{8}$$

allowing in particular for a $\mu\, H_1 H_2$ mass term in the superpotential (with the Higgs mass parameter μ equal to the higgsino one m).

This original definition of the Q-symmetry acting on the supersymmetry generator was then modified into the now-familiar definition of R-symmetry, acting according to

$$\begin{aligned} H_1\,(x,\theta) &\overset{R}{\to} H_1\,(x,\theta\, e^{-i\,\alpha}),\\ H_2\,(x,\theta) &\overset{R}{\to} H_2\,(x,\theta\, e^{-i\,\alpha}), \end{aligned} \tag{9}$$

so as to leave h_1 and h_2 invariant and survive the electroweak breaking induced by $< h_1 >$ and $< h_2 >$, while forbidding a $\mu\, H_1 H_2$ mass term in the superpotential.

Going from Q to R was done through the relation

$$R \;=\; Q\, U^{-1}\,. \tag{10}$$

The additional $U(1)$ symmetry also defined in [1], later called $U(1)_A$, transforms h_1 and h_2 as in (7) but commutes with supersymmetry, in contrast with Q and R. It acts according to

$$H_1 \overset{U(1)_A}{\to} e^{i\alpha}\, H_1, \quad H_2 \overset{U(1)_A}{\to} e^{i\alpha}\, H_2, \tag{11}$$

also forbidding the $\mu H_1 H_2$ term in the superpotential (as what was called later a $U(1)_{PQ}$ symmetry), with its definition extended to act axially on quark and lepton fields and superfields [2,3]. Just as $U(1)_A$ (and in contrast with Q), R symmetry forbids a $\mu\, H_1 H_2$ mass term in the superpotential. This one was then replaced by an "R-invariant" trilinear coupling $\lambda\, H_1 H_2 S$ with an extra singlet S transforming according to

$$\begin{aligned} S(x,\theta) &\overset{R}{\to} e^{2\,i\,\alpha}\, S(x,\theta\, e^{-i\,\alpha}),\\ S &\overset{U(1)_A}{\to} e^{-2i\alpha}\, S. \end{aligned} \tag{12}$$

This continuous R-symmetry gets subsequently reduced to R-parity, in the presence of Majorana gravitino and gaugino mass terms.

4.2 Avoiding an "axion"

The μ term first considered in [1] does not allow one to have both $< h_1 >$ and $< h_2 >$ non-zero, then leading to a massless chargino. Indeed even in the presence of the weak-hypercharge $\xi D'$ term splitting the h_1 and h_2 mass^2 terms apart from μ^2 we only get a non-vanishing v.e.v. for one doublet, the other being "inert". Taking $\mu = 0$ to allow for v_1 and v_2 non-zero, with $\tan\beta = v_2/v_1$ (then denoted $\tan\delta = v'/v''$), would only fix the difference $v_2^2 - v_1^2$, leaving us with *two flat directions* associated with the chiral superfield

$$H_A = H_1^0\, \sin\beta + H_2^0\, \cos\beta, \tag{13}$$

leading to two classically massless spin-0 bosons, h_A and A.

Indeed the field

$$A = \sqrt{2}\ \mathrm{Im}\,(h_1^0 \sin\beta + h_2^0 \cos\beta), \tag{14}$$

orthogonal to the Goldstone combination $z_g = \sqrt{2}\ \mathrm{Im}(-h_1^0 \cos\beta + h_2^0 \sin\beta)$ eaten away by the Z, is associated with the breaking of the $U(1)_A$ symmetry in (11). It corresponds to an axionlike or even axion pseudoscalar once quarks get introduced, present in the mass spectrum [1–3] together with its corresponding real part,

$$h_A = \sqrt{2}\ \mathrm{Re}\,(h_1^0 \sin\beta + h_2^0 \cos\beta) \tag{15}$$

("saxion"). Both would remain classically massless in the absence of the extra singlet S, with superpotential interactions breaking explicitly the $U(1)_A$ symmetry.[1] But there was no need then to explain how we got rid of such an unwanted spin-0 "axion" A by breaking explicitly the $U(1)_A$ symmetry; indeed this notion was brought to attention three years later [52,53], in connection with a possible solution to the CP problem.

Avoiding such an "axion" and classically massless associated scalar h_A was done through an explicit breaking of the $U(1)_A$ symmetry (now often known as a PQ symmetry). It was realized through the superpotential interactions $f(S)$ of an extra singlet S coupled through a trilinear superpotential term $\lambda\, H_1 H_2 S$. This one is invariant under $U(1)_A$, defined in [1] as

$$H_1 \overset{U(1)_A}{\to} e^{i\alpha} H_1, \quad H_2 \overset{U(1)_A}{\to} e^{i\alpha} H_2,$$
$$S \overset{U(1)_A}{\to} e^{-2i\alpha} S. \tag{16}$$

The superpotential interactions $f(S)$, including terms proportional to S, S^2 or S^3, break explicitly $U(1)_A$, so that a massless or light axionlike spin-0 boson A, in particular, is avoided. (This one may of course reappear with a small mass, in the presence of a small explicit breaking of $U(1)_A$, as e.g. in the $U(1)_A$ limit of the NMSSM, with a small $\frac{\kappa}{3} S^3$ superpotential term.)

Selecting among possible $f(S)$ interactions, including S, S^2 or S^3 terms as in the general NMSSM, the sole linear term proportional to S presented the additional interest of leading to an "R-invariant" (nMSSM) superpotential [1]

$$\mathcal{W} = \lambda\, H_1 H_2\, S + \sigma\, S. \tag{17}$$

Indeed H_1, H_2, and S transform as

$$H_{1,2}(x,\theta) \overset{R}{\to} H_{1,2}(x, \theta\, e^{-i\alpha}),$$
$$S(x,\theta) \overset{R}{\to} e^{2i\alpha}\, S(x, \theta\, e^{-i\alpha}), \tag{18}$$

so that the superpotential (17) transforms with $R = 2$ according to

$$\mathcal{W}(x,\theta) \overset{R}{\to} e^{2i\alpha}\, \mathcal{W}(x, \theta\, e^{-i\alpha}), \tag{19}$$

as required for its last F component to be R-invariant.

We then get a conserved additive quantum number R carried by the supersymmetry generator and associated with this unbroken $U(1)_R$ symmetry, in fact the progenitor of R-parity, $R_p = (-1)^R$. Such a superpotential has also the interest of triggering spontaneous electroweak breaking even in the absence of any supersymmetry breaking, in contrast with the MSSM.

Another possibility to avoid the would-be "axion" A is to eliminate it by gauging the extra $U(1)_A$ (taking $f(S) = 0$ and assuming anomalies appropriately canceled), as in the USSM [2,3].

5 Gauge/BE-Higgs unification within supersymmetry

5.1 The massive gauge multiplet for the Z boson

In the first electroweak model [1] the Goldstone fermion was related to the photon by supersymmetry. I.e. the spin-$\frac{1}{2}$ Goldstone fermion, now called the goldstino, was identical to the spin-$\frac{1}{2}$ partner of the photon, known as the photino. Only charged particles are then sensitive to supersymmetry breaking, namely the $W^\pm$, the charged BE-Higgs boson $H^\pm$ (then called $w^\pm$) and their associated charginos. The neutral ones, uncoupled to the photon and thus to the goldstino, still remain mass-degenerate implying at this stage [1]

$$m_Z = m\,(\text{Dirac zino}) = m\,(\text{neutral spin-0 BEH boson}). \tag{20}$$

The Dirac zino is obtained from chiral gaugino and higgsino components transforming in opposite ways under R symmetry, according to

$$\text{gaugino} \overset{R}{\to} e^{\gamma_5 \alpha}\,\text{gaugino},$$
$$\text{higgsino} \overset{R}{\to} e^{-\gamma_5 \alpha}\,\text{higgsino}. \tag{21}$$

This R quantum number, first presented as a toy-model "lepton number", was reinterpreted as corresponding to a new class of R-odd particles, known as charginos and neutralinos.

In present notations, $< h_i^0 > = v_i/\sqrt{2}$ with $\tan\beta = v_2/v_1$ replacing the original $\tan\delta = v'/v'' = v_2/v_1$, the Goldstone field eaten away by the Z is described by $z_g = \sqrt{2}\ \mathrm{Im}\,(-h_1^0 \cos\beta + h_2^0 \sin\beta)$, orthogonal to the pseudoscalar combination A in (14). Together with the corresponding real part denoted by z in [1],[2]

[1] With $\tan\beta = v_2/v_1 \equiv \tan\delta = v'/v''$, $h_1^\circ = \varphi''^\circ$, $h_2^0 = \varphi'^{0*}$, the complex field $\varphi''^{0*} \sin\delta + \varphi'^0 \cos\delta = (h_1^0 \sin\beta + h_2^0 \cos\beta)^*$, massless in the absence of S [1], represents the would-be axionlike boson A in (14) and associated scalar h_A.

[2] There we defined $z = \varphi_1''^0 \cos\delta - \varphi_1'^0 \sin\delta = \sqrt{2}\ \mathrm{Re}\,(h_1^0 \cos\beta - h_2^0 \sin\beta)$. We include here an optional change of sign in the definition (22) of z, to avoid a $-$ sign for large $\tan\beta$.

$$z \,=\, \sqrt{2}\ \mathrm{Re}\,(-h_1^0\,\cos\beta + h_2^0\,\sin\beta), \tag{22}$$

it is described by the chiral superfield combination,

$$H_z = -H_1^0\,\cos\beta + H_2^0\,\sin\beta \,=\, \frac{z+iz_g}{\sqrt{2}} + \cdots, \tag{23}$$

orthogonal to

$$H_A = H_1^0\,\sin\beta + H_2^0\,\cos\beta \,=\, \frac{h_A + iA}{\sqrt{2}} + \cdots \tag{24}$$

describing the pseudoscalar A as in (14). This scalar z is, independently of the value of β, the spin-0 field getting related with the Z under supersymmetry, with a mass term

$$-\frac{1}{2}\,m_Z^2\,z^2 \tag{25}$$

in the Lagrangian density.

One of the first implications of supersymmetric theories is thus the possible existence, *independently of* $\tan\beta$, of a neutral spin-0 BE-Higgs boson degenerate in mass with the Z, i.e. of mass (say m_h, for the reader used to MSSM notations)

$$m_h \,\simeq\, 91\ \mathrm{GeV/c^2}\ \text{up to supersymmetry-breaking effects.} \tag{26}$$

Neutral (or charged) *spin-0 BE-Higgs bosons get associated with massive gauge bosons*, and related inos, within massive gauge multiplets of supersymmetry [1], according to

$$Z \overset{SUSY}{\longleftrightarrow} 2\,\text{Majorana zinos} \overset{SUSY}{\longleftrightarrow} \text{neutral spin-0 BEH boson}\,. \tag{27}$$

The two Majorana zinos are obtained, in the usual formalism, from mixings of neutral gaugino and higgsino components transforming under R as in (21). The continuous R symmetry gets subsequently reduced to R-parity through the effects to the μ term (directly included as in the MSSM, or possibly resurrected from a translation of S), and direct gaugino mass terms ($m_{1/2}$) generated from supergravity or radiative corrections. These have $\Delta R = \pm 2$ and mix neutralinos into four Majorana mass eigenstates, from the two Majorana zinos in (20), the photino and the neutral higgsino described by H_A, as in the MSSM. There may also be more, as in the presence of additional N/nMSSM or USSM singlinos described by the singlet S or an extra-$U(1)$ gauge superfield.

5.2 Yukawa couplings "of the wrong sign" for the z, spin-0 partner of the Z

The new boson found at CERN with a mass close to 125 GeV/c^2 [12–15], believed to a BE-Higgs boson associated with the electroweak breaking, may well also be interpreted, in general up to a mixing angle as we shall see, as a spin-0 partner of the 91 GeV/c^2 Z boson under *two* infinitesimal supersymmetry transformations.

We can compare the z field in (22) with the SM-like scalar field,

$$h_{\mathrm{SM}} = \sqrt{2}\ Re\,(h_1^0\,\cos\beta + h_2^0\,\sin\beta), \tag{28}$$

so that

$$< h_{\mathrm{SM}}\,|\,z > \,=\, -\cos 2\beta. \tag{29}$$

The two fields are at an angle $\pi - 2\beta$ in field space, getting very close for large $\tan\beta$. The spin-0 z, directly related with the Z under supersymmetry, tends for large $\tan\beta$ to behave very much as the SM-like h_{SM}.

Furthermore, while the SM-like scalar field h_{SM} has Yukawa couplings to quarks and charged leptons

$$\frac{m_{q,l}}{v} \,=\, 2^{1/4}\,G_F^{1/2}\,m_{q,l}\,, \tag{30}$$

the z field, spin-0 partner of the spin-1 Z, has almost-identical Yukawa couplings

$$\frac{m_{q,l}}{v}\,2\,T_{3\,q,l} \,=\, 2^{1/4}\,G_F^{1/2}\,m_{q,l}\,2\,T_{3\,q,l}\,, \tag{31}$$

simply differing by *a relative change of sign for d quarks and charged leptons* (with $2\,T_{3\,d,l} = -1$) which acquire their masses through $< h_1^0 >$, as compared to u quarks. This may also be understood from the expression of the axial part in the weak neutral current $J_Z^\mu = J_3^\mu - \sin^2\theta\,J_{\mathrm{em}}^\mu$, proportional to $J_{3\ \mathrm{ax}}^\mu$, the Z boson coupled to J_Z^μ getting its mass by eliminating the would-be Goldstone boson z_g that is the pseudoscalar partner of the spin-0 z, as seen from (23).

The z has, however, *reduced trilinear couplings to the* $W^\pm$ *and* Z, by a factor $-\cos 2\beta$, with

$$\begin{cases} (z\,VV)\ \text{couplings} = (h_{SM}\,VV)\ \text{couplings}\ \times\ (-\cos 2\beta), \\ (z\,ff)\ \text{couplings}\ = (h_{SM}\,VV)\ \text{couplings} \\ \qquad\qquad\qquad \times \left(2T_{3f} \,=\, \begin{cases} +1\ u,c,t \\ -1\ d,s,b;\ e,\mu,\tau \end{cases}\right). \end{cases} \tag{32}$$

The expected production of a spin-0 z in the ZZ^* or WW^* decay channels would then be *decreased by* $\cos^2 2\beta$ as compared to a SM boson, with respect to fermionic quark and lepton channels (the change of sign in d-quarks and charged-lepton couplings also affecting the $z \to \gamma\gamma$ decay).

But *the z field does not necessarily correspond to a mass eigenstate*, and further mixing effects induced by supersymmetry breaking must be taken into account, as discussed soon for the MSSM in Sect. 5.4.

Additional information on the production and decay rates of the new boson may tell whether it can originate from a single doublet as in the standard model, or if two doublets h_1 and h_2 are also allowed or possibly required. The role of the spin-0 combination z in (22) as related to the Z by two supersymmetry transformations is then guaranteed if supersymmetry is indeed relevant, even if no "supersymmetric particle" has been found yet.

The observation of a new spin-0 particle with a mass not too far from m_Z, possibly related to the Z by supersymmetry, thus appears as an important indication in favor of this symmetry.

According to this gauge-Higgs unification (already within $N = 1$ theories in four dimensions), BEH bosons naturally appear as *extra spin-0 states of massive spin-1 gauge bosons*. This, in spite of the fact that they have *different gauge-symmetry properties*—thanks to the spontaneous breaking of the electroweak symmetry. We also have, in a similar way,

$$W^{\pm} \overset{SUSY}{\longleftrightarrow} 2\,\text{Dirac winos} \overset{SUSY}{\longleftrightarrow} \text{charged spin-0 boson } H^{\pm}, \tag{33}$$

with a mass term

$$-\,m_W^2\,|H^{\pm}|^2\,, \tag{34}$$

up to supersymmetry-breaking effects. This is why the charged boson now known as $H^{\pm}$, appearing as a spin-0 partner of the massive $W^{\pm}$, was initially denoted $w^{\pm}$ in [1].

5.3 Charged and neutral spin-0 BE-Higgs bosons as described by $W^{\pm}$ and Z massive gauge superfields

Even more remarkably, these massive spin-1, spin-$\frac{1}{2}$, and spin-0 particles may all be described by (neutral or charged) *massive gauge superfields* [54,55]. This is true *in spite of their different electroweak gauge-symmetry properties*, spin-1 fields transforming as a gauge triplet and a singlet while spin-0 BEH fields transform as electroweak doublets; although gauge and BE-Higgs bosons have *very different couplings to quarks and leptons*, BEH bosons being coupled proportionally to masses as seen from (31), in contrast with gauge bosons. This may first appear very puzzling but is elucidated in [55].

To do so we must *change picture* in our representation of such spin-0 bosons. The previous z and $w^{\pm}$ ($\equiv H^{\pm}$) cease being described by spin-0 components of the chiral doublet BEH superfields H_1 and H_2, to get described, through a non-polynomial change of fields, by the lowest (C) components of the Z and $W^{\pm}$ superfields, now massive. This explicit association between massive gauge bosons and spin-0 BEH bosons can be realized in a manifestly supersymmetric way (at least for the Z superfield for which supersymmetry stays unbroken at this stage) by completely gauging away the three (Goldstone) chiral superfields H_1^-, H_2^+, and $H_z = -\,H_1^0 \cos\beta + H_2^0 \sin\beta$, taken identical to their v.e.v.'s:

$$H_1^- \equiv H_2^+ \equiv 0,$$
$$H_z = -\,H_1^0 \cos\beta + H_2^0 \sin\beta \equiv -\,\frac{v}{\sqrt{2}}\,\cos 2\beta. \tag{35}$$

The corresponding $< H_1^0 > = v_1/\sqrt{2}$ and $< H_2^0 > = v_2/\sqrt{2}$ generate mass terms $\frac{1}{2}\,m_Z^2 |Z|^2$ and $m_W^2\,|W^+|^2$ for the gauge superfields $Z(x,\theta,\bar\theta)$ and $W^{\pm}(x,\theta,\bar\theta)$. The previous z and $w^{\pm}$ ($\equiv H^{\pm}$) get described by the lowest (C) spin-0 components of these *massive* Z and $W^{\pm}$ superfields, expanded as

$$Z(x,\theta,\bar\theta) \,=\, C_Z(x) + \cdots - \theta\sigma_\mu\bar\theta\; Z^\mu(x) + \cdots\,,$$
$$W^{\pm}(x,\theta,\bar\theta) \,=\, C_W^{\pm}(x) + \cdots - \theta\sigma_\mu\bar\theta\; W^{\mu\,\pm}(x) + \cdots\,. \tag{36}$$

Their last (C) components now correspond to physical dynamical degrees of freedom describing, through *non-polynomial field transformations*, linearized as

$$z \,=\, m_Z\, C_Z + \cdots\,, \quad w^{\pm} = m_W\, C_{\pm} + \cdots\,, \tag{37}$$

the spin-0 BE-Higgs fields previously referred to as z and $w^{\pm}$, now known as $H^{\pm}$ [55]:

massive gauge superfields now describe also spin-0 BEH fields! (38)

Their subcanonical ("χ") spin-$\frac{1}{2}$ components also correspond to physical degrees of freedom, describing (again through non-polynomial field transformations) the spin-$\frac{1}{2}$ fields previously known as higgsinos.

We then keep only

$$H_A = H_1^0 \sin\beta + H_2^0 \cos\beta = \frac{h_A + i\,A}{\sqrt{2}} + \cdots\,, \tag{39}$$

as an ("uneaten") chiral superfield, describing as in (14,15) the pseudoscalar $A = \sqrt{2}\;\mathrm{Im}\,(h_1^0 \sin\beta + h_2^0 \cos\beta)$ and associated scalar $h_A = \sqrt{2}\;\mathrm{Re}\,(h_1^0 \sin\beta + h_2^0 \cos\beta)$.

5.4 The BE-Higgs boson as spin-0 partner of Z, in the MSSM and beyond

This applies in particular to the specific model known as the MSSM, here expressed as including the soft dimension-2 supersymmetry-breaking gauge-invariant mass term

$$-\,m_A^2\;|h_1 \sin\beta - h_2^c \cos\beta|^2\,. \tag{40}$$

It may be considered as an "inert-doublet" mass term, chosen to vanish for $< h_i^0 > = v_i/\sqrt{2}$ with $\tan\beta = v_2/v_1$. This term thus *does not modify the vacuum state considered*, initially taken as having a spontaneously broken supersymmetry in the gauge-and-Higgs sector, with the photino playing the role of the Goldstone fermion so that the mass equalities (20) applies for neutral particles, with $m_{H^{\pm}}^2 = m_W^2$ for charged ones [1–3].

The gauge-and-Higgs sector, first considered with a spontaneously broken supersymmetry, admits two neutral classically flat directions of the potential, associated with the scalar and pseudoscalar fields h_A and A described by the initially massless chiral superfield $H_A = H_1^0 \sin\beta + H_2^0 \cos\beta$ in

(13,39). There is indeed initially, in the absence of the inert-doublet mass term (40), a classically massless pseudoscalar

$$A = \sqrt{2}\ \mathrm{Im}\,(h_1^0\ \sin\beta + h_2^0\ \cos\beta), \tag{41}$$

associated with the breaking of the $U(1)_A$ symmetry $h_1 \to e^{i\alpha}\, h_1,\ h_2 \to e^{i\alpha}\, h_2$ in (7, 16) [1], which acquires a mass m_A from the added soft supersymmetry-breaking terms (40) that break explicitly $U(1)_A$.

Defining

$$\begin{cases} \varphi_{\rm sm} = h_1 \cos\beta + h_2^c \sin\beta, \\ \varphi_{\rm in} = h_1 \sin\beta - h_2^c \cos\beta, \end{cases} \tag{42}$$

the two previously flat directions associated with A and h_A get lifted by the mass term (40) for the inert combination $\varphi_{\rm in}$. With

$$|\varphi_{\rm in}|^2 = |\, h_1 \sin\beta - h_2^c \cos\beta\,|^2 = |H^+|^2 + \frac{1}{2}\, A^2 + \frac{1}{2}\ |\sqrt{2}\ \mathrm{Re}\,(h_1^0 \sin\beta - h_2^0 \cos\beta)\,|^2 \tag{43}$$

it also provides an additional supersymmetry-breaking contribution m_A^2 to $m_{H^\pm}^2$ in addition to the supersymmetric one m_W^2, so that

$$m_{H^\pm}^2 = m_W^2 + m_A^2. \tag{44}$$

Adding the supersymmetric contribution m_Z^2 from (22, 25) and supersymmetry-breaking one m_A^2 from (40, 43) we get *directly* the 2×2 spin-0 scalar mass^2 matrix

$$\mathcal{M}_\circ^2 = \begin{pmatrix} c_\beta^2\, m_Z^2 + s_\beta^2\, m_A^2 & -s_\beta c_\beta\,(m_Z^2 + m_A^2) \\ -s_\beta c_\beta\,(m_Z^2 + m_A^2) & s_\beta^2\, m_Z^2 + c_\beta^2\, m_A^2 \end{pmatrix}, \tag{45}$$

verifying

$$\begin{aligned} \mathrm{Tr}\,\mathcal{M}_\circ^2 &= m_H^2 + m_h^2 = m_Z^2 + m_A^2, \\ \det \mathcal{M}_\circ^2 &= m_H^2\, m_h^2 = m_Z^2\, m_A^2\, \cos^2 2\beta, \end{aligned} \tag{46}$$

so that

$$m_{H,h}^2 = \frac{m_Z^2 + m_A^2}{2} \pm \sqrt{\left(\frac{m_Z^2 + m_A^2}{2}\right)^2 - m_Z^2 m_A^2\, \cos^2 2\beta} \quad (+\,\text{radiative corrections}). \tag{47}$$

This implies the well-known relation $m_h < m_Z |\cos 2\beta|$ at the classical level, up to radiative corrections which must be significant if one is to reach $\simeq 125$ GeV/c^2 from a classical value between 0 and m_Z. This classical value of m_h can approach m_Z for large $\tan\beta$ with large m_A i.e. large supersymmetry-breaking effects. We must then also count on significant quantum corrections from large supersymmetry breaking (e.g. from very heavy stop squarks), if the resulting m_h is to reach the observed $\simeq 125$ GeV/c^2.

These scalar mass eigenstates behave for large m_A as

$$\begin{cases} H \to \sqrt{2}\ Re\,(h_1^0 \sin\beta - h_2^0 \cos\beta) \\ \quad \text{with large mass } m_H \simeq m_A, \\ h \to h_{\rm SM} = \sqrt{2}\ Re\,(h_1^0 \cos\beta + h_2^0 \sin\beta) \\ \quad \text{with standard-model couplings.} \end{cases} \tag{48}$$

Indeed $\varphi_{\rm sm} = h_1 \cos\beta + h_2^c \sin\beta$ in (42) is the "active" SM-like Higgs doublet acquiring a v.e.v., with h_{SM} coupled as in the standard model. The h field, presumably to be associated with the 125 GeV/c^2 boson observed at CERN, is very close to the z in (22) for large $\tan\beta$, thus justifying *an almost complete association of this* 125 GeV /c^2 *boson with the spin-1 Z*, as indicated by (29).

But we do not want to stick too closely to the specific case of the MSSM, as we felt from the beginning that its 2-doublet structure ought to be extended to the extra singlet S with a trilinear superpotential coupling $\lambda\, H_1 H_2 S$. It is now very strongly constrained, in many of its interesting regions in parameter space. Furthermore this extra N/nMSSM singlet S introduced by turning the μ parameter into a dynamical superfield in superspace according to

$$\mu \to \mu(x,\theta) = \lambda\, S(x,\theta), \tag{49}$$

leads to a new quartic spin-0 coupling independent of the gauge couplings, which helps making the lightest BE-Higgs boson sufficiently heavy. Indeed *the lightest neutral spin-0 mass may already be equal to* m_Z *at the classical level, even before any breaking of the supersymmetry*, and independently of $\tan\beta$ [1]. This is in sharp contrast with the MSSM for which it would at best vanish (for $\mu = 0$) or worse, in which one does not even get any electroweak breaking in the absence of supersymmetry breaking (for $\mu \neq 0$).

But let us now turn to another direction explored in a parallel way, leading us from $N = 1$ supersymmetric theories with a continuous $U(1)_R$ symmetry to $N = 2$ and $N = 4$ theories, naturally expressed in an extended spacetime with extra compact dimensions, before coming back to the $N = 1$ supersymmetric standard model in Sect. 7.

6 From *R*-symmetry to $N = 2$ and $N = 4$ supersymmetry, and extra dimensions

6.1 *F*-breaking of supersymmetry, with *R*-symmetry

Let us return to the second classical mechanism of spontaneous breaking of the global supersymmetry, relying on non-vanishing v.e.v.'s for auxiliary F-components of chiral superfields [39,40]. In order to do so *the superpotential must be very carefully chosen* to avoid the existence of one or usually several supersymmetric vacuum states with vanishing energy, which would necessarily be stable, with supersymmetry remaining conserved.

Indeed for n interacting chiral superfields, the set of n analytic equations $F_i(\varphi_j) = 0$ (of degree 2 at most for a renormalizable theory) for n complex variables φ_j has solutions in almost all situations, excepted very special ones. All auxiliary F components can then vanish simultaneously, leading to a stable vacuum state (or usually several vacuum states) for which supersymmetry is preserved, with $< H > = 0$.

This choice of suitable superpotentials, for which such *supersymmetric vacua are totally avoided* (rather than just been made unstable, which is not possible here as discussed in Sect. 3.1) is realized with the help of an additional R symmetry [1] acting chirally on the supersymmetry generator according to

$$Q \overset{R}{\to} e^{-\gamma_5 \alpha}\, Q. \tag{50}$$

It relies both on $R = 2$ and $R = 0$ chiral superfields transforming according to

$$\Phi(x,\theta) \overset{R}{\to} e^{i\, R_\Phi\, \alpha}\, \Phi(x, \theta\, e^{-i\,\alpha}), \tag{51}$$

products of superfields being allowed in the superpotential only if they verify $\sum R_\Phi = 2$.

The original example of [39] involves, in nMSSM-like notations, two chiral doublets H_1 and H_2 having $R = 0$, interacting with a triplet $\boldsymbol{T}$ and a singlet S having $R = 2$, through the superpotential

$$\mathcal{W} \,=\, H_1\, (\lambda\, \boldsymbol{\tau}.\boldsymbol{T} + \lambda' S)\, H_2 + \sigma\, S, \tag{52}$$

with a global $SU(2) \times U(1)$ electroweak-like symmetry. It is a global version of the electroweak model [1] with the gauge superfields omitted, supplemented with an additional triplet $\boldsymbol{T}$ next to the (N/nMSSM) singlet S, already having in mind for its gauged version an $N = 2$ extended supersymmetric, or "hypersymmetric" theory [41], with (H_1, H_2) describing an $N = 2$ (matter) *hypermultiplet*.

We thus have in this model of spontaneous supersymmetry breaking through auxiliary F-component v.e.v.'s *the same number of* $R = 0$ *and* $R = 2$ *chiral superfields*, four in each case. (This is also in connection with the underlying $N = 2$ structure of the model when it is gauged, and its extra global $SU(2)$ symmetry acting on the $N = 2$ supersymmetry generators, softly broken through the weak-hypercharge $\xi\, D'$ and/or $\sigma\, F_S$ terms). They transform under R as in (9,12), according to

$$\begin{cases} H_{1,2}\,(x,\theta) \overset{R}{\to} H_{1,2}\,(x, \theta\, e^{-i\,\alpha})\,, \\ S(x,\theta) \overset{R}{\to} e^{2\,i\,\alpha}\, S(x, \theta\, e^{-i\,\alpha})\,, \\ \boldsymbol{T}(x,\theta) \overset{R}{\to} e^{2\,i\,\alpha}\, \boldsymbol{T}(x, \theta\, e^{-i\,\alpha})\,. \end{cases} \tag{53}$$

R-symmetry requires that the superpotential $\mathcal{W}$ be *a linear function of the* $R = 2$ *superfields*, S, and $\boldsymbol{T}$, the triplet $\boldsymbol{T}$ being excluded by the $SU(2)$ electroweak-like symmetry. It excludes in particular a $\mu\, H_1 H_2$ superpotential term, so that $\mathcal{W}$ transforms with $R = 2$ as in (19) [1,39].

With such suitably chosen superpotentials [39,40] all auxiliary F-components cannot vanish simultaneously, the set of equations $F_i(\varphi_j) = 0$ being constructed so as to have no solution, thanks in particular to the requirement of R-symmetry. As a result supersymmetry gets spontaneously broken. A systematic consequence of this mechanism is the existence of an infinite set of inequivalent classically degenerate vacua associated with *classically flat directions* (valleys) corresponding to classically massless particles (*pseudomoduli*) other than Goldstone bosons.

This includes in particular two classically flat directions associated with the spin-0 component of one of the $R = 2$ chiral superfields, leading to the possibility of discussing, depending on radiative corrections, the spontaneous (or quasi-spontaneous) breaking of R-symmetry. It would lead to a massless R Goldstone boson, if the R symmetry is non-anomalous; or to an R-axion, as the R symmetry, which acts axially on gluinos, is usually anomalous [56].

6.2 From $N = 1$ with a $U(1)_R$ symmetry to $N = 2$

We now consider the global $SU(2) \times U(1)$ symmetry of this model of interacting chiral superfields [39] as returning to local, as in [1] extended by an extra chiral triplet $\boldsymbol{T}$ next to the nMSSM singlet S. For a special choice of the trilinear superpotential couplings λ and λ' in (52) in terms of the gauge couplings g and g' the gaugino fields (λ_L) described by the electroweak gauge superfields may be related to the spin-$\frac{1}{2}$ fermion fields (ζ_L) described by the singlet and triplet chiral superfields S and $\boldsymbol{T}$ through an extra global $SU(2)$ symmetry, also acting on the two spin-0 doublets ($\varphi'' = h_1$ and $\varphi' = h_2^c$) described by H_1 and H_2 but not on their higgsino counterparts. It thus acts on the $N = 2$ supersymmetry generators themselves, now transforming as a chiral doublet under this $SU(2)$ symmetry [41].

Then

$$\begin{pmatrix} \lambda_L \\ \zeta_L \end{pmatrix} \to SU(2) \text{ doublets of } N = 2 \text{ gauginos} \tag{54}$$

transform as (global) $SU(2)$ doublets of left-handed spinors with $R = 1$. This places the fermions ζ_L in adjoint chiral multiplets on the same footing as the adjoint chiral λ_L associated with the Majorana gauginos in the gauge multiplets, upgrading ζ_L up to a new gaugino status. λ_L and ζ_L in (54) globally behave as an isodoublet of gauginos, for an enlarged $N = 2$ extended supersymmetry ("hypersymmetry") algebra. The two chiral doublets H_1 and H_2 responsible for electroweak breaking jointly describe electroweak doublets of spin-$\frac{1}{2}$ and spin-0 fields forming an $N = 2$ *"hypermultiplet"*. Each hypermultiplet describes a Dirac spinor and two complex spin-0 fields, i.e. 4 fermionic + 4 bosonic field degrees of freedom.

This additional $SU(2)$ symmetry leading to $N=2$ supersymmetry requires H_1 and H_2 to interact with trilinear superpotential couplings as in (52) but fixed by g and g' according to $\lambda = g/\sqrt{2},\ \lambda' = g'/\sqrt{2}$, so that

$$\mathcal{W} = \frac{1}{\sqrt{2}}\, H_1\, (g\, \boldsymbol{\tau}.\boldsymbol{T} + g' S)\, H_2 + \sigma S, \tag{55}$$

the trilinear superpotential terms getting totally fixed by the gauge couplings.

D-breaking and F-breaking mechanisms for $N=1$ spontaneous supersymmetry breaking then get unified within $N=2$. It allows for an abelian $\xi D'$ term responsible for D-breaking within a non-abelian theory [1] to be rotated into a related σF_S term responsible for F-breaking [39], through a global $SU(2)$ rotation acting on the $N=2$ supersymmetry generators [41]. This theory involves triplet and singlet chiral superfields $\boldsymbol{T}$ and S, next to the H_1 and H_2 doublets, with a superpotential first restricted by R-invariance as in (52), then by the (softly broken) global $SU(2)$ as in (55). In this specific example the two Goldstone fermions (goldstinos) are the two photinos, related to the photon and two additional *spin-0 photons* by $N=2$ supersymmetry. Only charged particles are then sensitive at lowest order to the spontaneous breaking of the supersymmetry. Neutral ones remain mass degenerate within two $N=2$ gauge multiplets, a massless one with the photon and a massive one associated with the Z.

Indeed the two neutral ($N=1$) gauge superfields associated with W_3 and W' (i.e. the Z and photon superfields) join the four neutral chiral ones T_3, S, H_1^0, and H_2^0 to describe, ultimately, a massive $N=2$ gauge multiplet (with the Z, 4 Majorana zinos and five spin-0 bosons), and a massless one (with the photon, two Majorana photinos and two spin-0 photons). This leads us to discuss again gauge/BE-Higgs unification, this time within $N=2$ theories.

6.3 Gauge/BE-Higgs unification in $N=2$

As we just saw the $N=2$ associations

$$\begin{aligned} \gamma &\overset{N=2}{\longleftrightarrow} \text{2 Majorana photinos} \\ &\overset{N=2}{\longleftrightarrow} \text{two neutral spin-0 photons,} \end{aligned} \tag{56}$$

and

$$\begin{aligned} Z &\overset{N=2}{\longleftrightarrow} \text{four Majorana zinos} \\ &\overset{N=2}{\longleftrightarrow} \text{five neutral spin-0 bosons,} \end{aligned} \tag{57}$$

were initially obtained in the $N=2$ (hypersymmetric) $SU(2)\times U(1)$ electroweak model [41], with the $N=2$ supersymmetry spontaneously broken through one, or a combination, of the D-breaking [1,38] and F-breaking [39] mechanisms, becoming equivalent and unified within $N=2$. The two associated goldstinos are then the two gaugino partners of the photon, known as photinos, within a $N=2$ gauge multiplet. As for $N=1$ in [1] boson-fermion mass splittings are felt only by charged particles. Neutral ones remain mass-degenerate at the classical level within the massive Z and massless photon multiplets of $N=2$ supersymmetry, as shown above in (56, 57).

Extending (56) to QCD leads to

$$\begin{aligned} \text{gluons} &\overset{N=2}{\longleftrightarrow} \text{2 Majorana gluino octets} \\ &\overset{N=2}{\longleftrightarrow} \text{2 neutral spin-0 gluon octets.} \end{aligned} \tag{58}$$

Extending (57) to the $W^\pm$ requires *four doublet BE-Higgs superfields* H_1, H_1', and H_2, H_2' rather than the usual two, so as to describe, altogether, a massive $N=2$ gauge multiplet said to be *of type I* as for the Z multiplet in (57) (cf. Sect. 6.6 soon), with

$$W^\pm \overset{N=2}{\longleftrightarrow} \text{4 Dirac winos} \overset{N=2}{\longleftrightarrow} \text{five charged spin-0 bosons.} \tag{59}$$

This attractive property of gauge-Higgs unification applies to other gauge bosons including those associated with grand-unified theories, or with an extra-$U(1)$ gauge group. These theories may also be obtained from an extended spacetime with additional compact dimensions [16–18,42,57], with

$$\text{spin-0 photons, gluons, ...} \leftrightarrow \text{extra components of six-dimensional gauge fields} V^{\hat{\mu}} = \begin{pmatrix} V^\mu \\ V^5 = a \\ V^6 = b \end{pmatrix}, \tag{60}$$

etc. The latter associations correspond to *a different type of gauge/BE-Higgs unification* as compared to the one discussed earlier for $N=1$ supersymmetry in Sect. 5 [1,54,55]. This one was conceptually more subtle by relating spin-1 and spin-0 fields with different gauge-symmetry properties, in contrast with (60). Both types are physically relevant and get combined when dealing with supersymmetric GUTs with extra dimensions [16–18,57]. This also corresponds, in four dimensions, to different types of massive gauge multiplets of $N=2$, of types I, II, or III, as will be discussed in Sect. 6.8.

This opens the question of the breaking of the $N=2$ supersymmetry, even harder than for $N=1$ especially if we also aim at a realistic theory with quarks and leptons acquiring masses from Yukawa couplings to spin-0 doublets, and without abandoning too much of the extended symmetries that the theory is supposed to have. Before that, let us pursue for a while in the direction of further increasing the symmetry.

6.4 From $N=2$ to $N=4$

A further step in this direction of increasing the symmetry is obtained with a $N=2$ supersymmetric Yang–Mills theory

describing a $N = 2$ gauge multiplet interacting with a massless spin-$\frac{1}{2}$-spin-0 hypermultiplet in the adjoint representation of the gauge group. This leads to (P. Fayet, unpublished, 1976) [42]

$$\begin{cases} N = 2 \text{ supersymmetric Y-M theory} \\ \text{with } N = 2 \text{ adjoint "matter" hypermultiplet} \\ \rightarrow \ N = 4 \text{ supersymmetric Y-M theory,} \end{cases} \tag{61}$$

involving a set of four chiral adjoint gauginos

$$\begin{pmatrix} \lambda_L \\ \zeta_{1L} \\ \zeta_{2L} \\ \zeta_{3L} \end{pmatrix} \rightarrow SU(4)\text{-quartet of } N = 4 \text{ gauginos.} \tag{62}$$

They transform as a quartet of the global $SU(4)$ $(\sim O(6))$ symmetry group acting on the set of $N = 4$ supersymmetry generators, also transforming as a chiral quartet of $SU(4)$. These theories describe, from the three chiral adjoint $N = 1$ superfields involved, a $SU(4)$ sextet of spin-0 fields in the adjoint representation of the gauge group, so that

$$\begin{aligned} &N = 4 \text{ gauge multiplet} \\ &\quad = \big(1 \text{ spin-1} \ + \ 4 \text{ spin-}\tfrac{1}{2} + 6 \text{ spin-0}\big) \\ &\qquad \text{adjoint gauge fields.} \end{aligned} \tag{63}$$

These $N = 4$ supersymmetric Yang–Mills theories may be obtained directly from $N = 2$ theories in four dimensions (P. Fayet, 1976) [42], or equivalently from dimensional reduction of a $N = 1$ supersymmetric Yang–Mills theories in 10 dimensions [58,59]. They involve a single gauge coupling with no arbitrary Yukawa or quartic couplings, and are totally fixed in four dimensions up to the choice of the Yang–Mills group, and vacuum state for which gauge symmetry may be spontaneously broken. This implies, however, a reduced flexibility taking us farther away from a realistic theory of particles and interactions.

6.5 Spontaneous generation of central charges in $N = 2$ or 4 supersymmetry algebras

A remarkable feature of such $N = 2$ and $N = 4$ theories is that the supersymmetry algebra gets *spontaneously modified* when the Yang–Mills symmetry gets spontaneously broken [42]. Indeed an intriguing phenomenon occurs, which had to be properly elucidated before asserting that we are actually dealing with a *bona fide* $N = 4$ supersymmetry algebra, supposed to be

$$\begin{cases} \{Q_i, \ \bar{Q}_j\} = -2\,\gamma_\mu P^\mu\,\delta_{ij}, \\ [Q_i, \ P^\mu] = 0. \end{cases} \tag{64}$$

But when the Yang–Mills symmetry gets spontaneously broken, with the $N = 4$ supersymmetry generators Q_i remaining unbroken, we generate *a new sort of massive multiplet*, necessarily complex. Each one describes one spin-1, four Dirac spin-$\frac{1}{2}$, and 5 spin-0 fields, with (6+10) bosonic + 16 fermionic degrees of freedom altogether [42]. This corresponds to a massive multiplet of particles with maximum spin 1, which, however, is *not a representation of the* $N = 4$ *supersymmetry algebra* (64)! So, what is going on?

Actually the supersymmetry algebra (64) is valid up to field-dependent gauge-transformations (and terms proportional to field equations of motion). When the Yang–Mills symmetry gets spontaneously broken through the translation of some of the adjoint spin-0 gauge fields, these field-dependent gauge transformations acquire spontaneously generated constant parts. They correspond to some of the unbroken Yang–Mills generators, now *promoted to abelian* as the other Yang–Mills generators, with which they would not commute, get spontaneously broken. They thus belong to the center of the (super)symmetry algebra.

These *spontaneously generated central charges* then appear in the right-hand side of the anticommutation relations (64) [42]. This extended supersymmetry algebra gets thus spontaneously modified, to include central charges in its anticommutation relations. This leads to the same kind of algebra as in [60], even if its conclusions cannot be applied directly as its conditions of validity are not met.

As we shall see these central charges play an essential role in the framework of grand-unification [61,62], when moving from the standard model to a grand-unification gauge group like $SU(5)$ or $O(10)$, ….

6.6 Massive multiplets for $N = 2$ grand unification with gauge/BE-Higgs unification

Modifying the algebra, spontaneously or not, to include central charges on the right-hand side of the anticommutation relations (64) allows for new massive multiplets (sometimes referred to as BPS) to appear as representations of this algebra. We get in particular new massive ("short") multiplets with maximum spin $N/4$, instead of $N/2$ in the absence of such central charges. The first example is *the massive (matter) hypermultiplet of* $N = 2$, describing a Dirac spin-$\frac{1}{2}$ and two spin-0 particles, all charged, with 4 bosonic + 4 fermionic degrees of freedom [41]. Another example is *the massive gauge multiplet of* $N = 4$, describing one spin-1, four Dirac spin-$\frac{1}{2}$, and five spin-0 particles, charged, with 16 + 16 d.o.f. altogether [42].

The $N = 2$ massive gauge multiplet such as the Z one in (57), real, does not admit a central charge. It describes one spin-1, two Dirac spin-$\frac{1}{2}$ (or four Majorana) fermions and five spin-0 particles, with 8 + 8 d.o.f., and similarly for the $W^\pm$ multiplet in (59), charged, with 16 + 16 d.o.f.. These massive gauge multiplets *of type I*, relevant for the description of electroweak interactions, do not require a central charge

(Z) in the anticommutation relations, even though they may be complex as for the $W^{\pm}$ multiplet.

Other types of $N = 2$ massive gauge multiplets, however, require a central charge and are necessarily complex. They play a crucial role in $N = 2$ extended supersymmetric grand-unified theories [57]. The massive gauge multiplet *of type II* describes one spin-1, two Dirac spin-$\frac{1}{2}$, and one spin-0 particles, all charged, with 8 + 8 d.o.f., times 3 when dealing with $SU(3)$ antitriplets or triplets. This "smaller" multiplet is relevant to describe the $X^{\pm 4/3}$ in a $SU(5)$, $O(10)$ or $E(6)$ … grand-unified theory, with a central charge $Z = \pm m_X$ on the right-hand side of the anticommutation relations of the $N = 2$ supersymmetry generators.

Yet another type of multiplet, *of type III*, has the same field content as a complex *type I* multiplet, but with a non-vanishing value of the central charge Z. It describes one spin-1, four Dirac spin-$\frac{1}{2}$ fermions and five spin-0 particles, with 16 + 16 d.o.f. as for the $W^{\pm}$ multiplet, times 3 when dealing with $SU(3)$ antitriplets or triplets. It is relevant to describe the $Y^{\pm 1/3}$ in a grand-unified theory, with a central charge $Z = \pm m_X$, and a mass $m_Y = \sqrt{m_X^2 + m_W^2} > |Z| = m_X$.

One ultimately gets, in a $N = 2$ $SU(5)$-type supersymmetric GUT, the following X and Y multiplets [57]:

$$\begin{cases} X^{\pm 4/3} & \overset{N=2}{\longleftrightarrow} & 2 \text{ Dirac xinos} & \overset{N=2}{\longleftrightarrow} & 1 \text{ charged spin-0 boson} & \text{(type II)} \\ Y^{\pm 1/3} & \overset{N=2}{\longleftrightarrow} & 4 \text{ Dirac yinos} & \overset{N=2}{\longleftrightarrow} & 5 \text{ charged spin-0 bosons} & \text{(type III)} \end{cases} \tag{65}$$

both with the same value $Z = \pm m_X$ of the central charge Z. The mass relation

$$m_Y^2 = m_W^2 + m_X^2, \tag{66}$$

is interpreted by viewing m_W and m_Z as mass parameters already present in the five- or six-dimensional spacetime as a result of the electroweak breaking. m_X is associated with extra components of the momenta along the compact dimensions, m_W^2 and m_X^2 both contributing to the $Y^{\pm 1/3}$ mass^2 in four dimensions, according to (66) [16–18].

This is essential when discussing $N = 2$ extended supersymmetric electroweak or grand-unified theories, which now require *four rather than two spin-0 BEH electroweak doublets*, or grand-unification quintuplets [16–18,57].

6.7 Electroweak breaking with an unbroken $SU(4)$ *electrostrong* symmetry, in six dimensions

$N = 2$ theories [41,42], and extended $N = 2$ supersymmetric GUTs may be formulated from a higher (five- or six-) dimensional spacetime [16–18,57], with

$$V^{\hat{\mu}} = \begin{pmatrix} V^{\mu} \\ V^5 = a \\ V^6 = b \end{pmatrix}. \tag{67}$$

In this higher-dimensional space, the $SU(5)$ symmetry is broken through the BEH-quintuplet v.e.v.'s, providing in six dimensions equal masses to the $Y^{\pm 1/3}$ and $W^{\mp}$ gauge fields, according to

$$SU(5) \overset{\text{EW breaking}}{\longrightarrow} SU(4) \text{ electrostrong gauge group in six dimensional spacetime,} \tag{68}$$

with

$$SU(5)\ \underline{\mathbf{24}} \begin{cases} g, \gamma,\ X^{\pm 4/3} & & \underline{\mathbf{15}} & \text{adjoint } SU(4), \\ Y^{\pm 1/3},\ W^{\mp} & \to & (\underline{\bar{\mathbf{4}}} + \underline{\mathbf{4}}) & \text{quartets}, \\ Z & & \underline{\mathbf{1}} & \text{singlet}. \end{cases} \tag{69}$$

The $\underline{\mathbf{15}}$ adjoint $SU(4)$ gauge bosons remain massless in 6d, the quartet and antiquartet having mass $m_Y = m_W$ in 6d, and the singlet Z, $m_Z = m_W/\cos\theta$ where $\sin^2\theta = 3/8$ at this stage.

6.8 Grand unification and supersymmetry breaking from extra dimensions

The extra compact space dimensions may then play an essential role in the breaking of the supersymmetry and grand-unification symmetries, with boundary conditions involving continuous or, more interestingly, discrete symmetries, including R-parity and various parity-like or similar symmetries in compact space. The breaking of supersymmetry (i.e. of the $N = 2$ supersymmetry generators after reduction to four dimensions) may be obtained by identifying the action of performing a complete loop in compact space (e.g. a translation $x^6 \to x^6 + L_6$ on a flat torus) with a discrete R-parity transformation, $R_p = (-1)^{3(B-L)}\ (-1)^{2S}$.

In a similar way, the breaking of the $SU(4)$ electrostrong symmetry present in six dimensions may be obtained by identifying performing a complete loop (e.g. a translation $x^5 \to x^5 + L_5$ on a torus) with a discrete Z_2 GUT-parity transformation G_p. This one may be defined as

$$\text{GUT-parity } G_p = G' \times e^{\frac{3}{5}Y} = \pm 1, \tag{70}$$

where G' is a global symmetry operator commuting with $SU(5)$ and supersymmetry. It acts on matter multiplets, associated with quarks and leptons including mirror partners, and BE-Higgs multiplets, in quintuplet representations of $SU(5)$. The $X^{\pm 4/3}$ and $Y^{\pm 1/3}$ fields, and associated supersymmetry multiplets, have $G_p = -1$ and get excluded from the low-energy spectrum as a result of the compactification. The gluons, photon, $W^{\pm}$, and Z have $G_p = +1$, thus surviving as massless or light fields as compared to the compactification scales. Within quintuplet BEH representations electroweak doublets have $G_p = +1$ and color triplets $G_p = -1$. Generating m_X in this way, in connection with GUT parity, automatically solves the so-called "doublet-triplet splitting prob-

lem". The R-parity and GUT-parity operators R_p and G_p have ± 1 eigenvalues, and commute.

A breaking of chirality in four dimensions is required if we are to avoid mirror quarks and leptons in the low-energy theory. It may be obtained by considering a discrete reflection symmetry, or rotation of π, in the 2d compact space, transforming x^5, x^6 into $-x^5$, $-x^6$ in view of identifying opposite points. As the $V^5 = a$ and $V^6 = b$ components of the $V^{\hat{\mu}}$ gauge fields transform with a $-$ sign, these extra components describing four-dimensional fields associated with spin-0 gluons and photons (or more generally spin-0 electroweak gauge fields), with mirror parity $M_p = -1$, and coupling ordinary particles to their mirror partners (also with $M_p = -1$), disappear from the low-energy spectrum, as well as the mirror quarks and leptons to which they would couple. This operation truncates away half of the states, leaving only a $N = 1$ supersymmetry in the low-energy sector after reduction to four dimensions, without mirror particles nor spin-0 gluons or photons. This one is further reduced to $N = 0$, i.e. no surviving supersymmetry below the compactification scale, using boundary conditions involving R-parity.

This leads to the possibility of fixing the scales associated with these breakings in terms of the compactification scales for the extra dimensions [16–18]. With relations like, in the simplest cases of two flat extra dimensions,

$$\begin{cases} m_{3/2} = \dfrac{\pi}{L_6} = \dfrac{1}{2R_6} \\ \quad \text{(from identification R-parity} \equiv \text{translation of } L_6), \\ m_X = \dfrac{\pi}{L_5} = \dfrac{1}{2R_5} \\ \quad \text{(from identification GUT-parity} \equiv \text{translation of } L_5). \end{cases} \tag{71}$$

This use of *discrete boundary conditions*, involving for supersymmetry R-parity rather than a continuous symmetry, allows one to link rigidly these $m_{3/2}$ and m_X parameters to the compactification scales. This is in contrast with the initial approach of [77,78], intended to generate four-dimensional supersymmetry-breaking parameters of moderate size in an extended supergravity theory, ignoring all states at the compactification scale.

6.9 Proton stability, and quark and lepton masses

GUT parity also leads to *stabilize the proton* through the mechanism of replication of quark and lepton families introduced for $N = 2$ supersymmetry in four dimensions [63], a duplication getting sufficient in five or six dimensions to constitute *pairs of $SU(5)$ representations with opposite G_p parities*. For example the usual u_L and $\bar{u}_L$ fields, normally related by $SU(5)$ under which they form a $SU(4)$ sextet, and coupled through the $X^{\pm 4/3}$ gauge boson, are now forbidden to do so by the boundary conditions involving GUT parity. They can no longer be described by $SU(5)$ components of a single representation of higher-d fields, as both need to have GUT parity $G_p = +1$ to survive at low-energy. This requires a doubling of $SU(5)$ matter representations, not needed for the four quintuplet BE-Higgs representations in six dimensions, whose triplet components are unwanted at low energy. Thus

$$\begin{aligned} \text{GUT parity} &\rightarrow \text{doubling of matter representations} \\ &\rightarrow \text{stability of the proton,} \end{aligned} \tag{72}$$

at least in the simplest situations considered.

Constructing a mass term for the matter fermions in six dimensions, however, is normally impossible here, these being represented by *six-dimensional 8-component Weyl spinors of the same chirality* $-$, as for higgsinos, owing to supersymmetry [16–18]. Indeed gauginos, of chirality $+$, must have six-dimensional Yukawa couplings to both higgsinos and matter fermions. For example the electron and mirror-electron fields are described by the six-dimensional Weyl spinors of chirality $-$,

$$\begin{pmatrix} e_{M\,R} \\ -- \\ e_L \end{pmatrix} \text{(in an electroweak doublet)}, \quad \begin{pmatrix} e_R \\ -- \\ e_{M\,L} \end{pmatrix} \text{(singlet)}, \tag{73}$$

verifying in particular

$$\begin{aligned} e(x^\mu, -x^5, -x^6) &= e(x^\mu, x^5, x^6), \\ e_M(x^\mu, -x^5, -x^6) &= -e_M(x^\mu, x^5, x^6), \text{ etc.,} \end{aligned} \tag{74}$$

for their $M_p = +1$ and -1 field components, respectively. Quark and lepton fields (and wave functions) are developed proportionally to $\cos(2\pi n_5 x_5/L_5)\cos(2\pi n_6 x_6/L_6)$, with n_5 and n_6 integers ≥ 0, or $\sin(2\pi n_5 x_5/L_5)\sin(2\pi n_6 x_6/L_6)$. Mirror quark and lepton fields involve $\cos(2\pi n_5 x_5/L_5)\sin(2\pi n_6 x_6/L_6)$ or $\sin(2\pi n_5 x_5/L_5)\cos(2\pi n_6 x_6/L_6)$, as for spin-0 gluons and electroweak spin-0 bosons, etc., such states being absent in the low-energy spectrum, for which $n_5 = n_6 = 0$.

To bypass this obstruction for generating quark and lepton masses we need to connect upper to lower components, for different six-dimensional Weyl spinors of chirality $-$, with right-handed upper components and left-handed lower ones as in (73). These Weyl spinors have different electroweak properties and should connect through a doublet spin-0 six-dimensional field, in an $SU(5)$ quintuplet.

This may be done by coupling $\overline{\psi'_-}(x^{\hat{\mu}})\,\Gamma_5\,\psi_-(x^{\hat{\mu}})$ and $\overline{\psi'_-}(x^{\hat{\mu}})\,\Gamma_6\,\psi_-(x^{\hat{\mu}})$ to spin-0 quintuplets, with their real and imaginary parts coupled to $\overline{\psi'_-}\,\Gamma_5\,\psi_-$ and $\overline{\psi'_-}\,\Gamma_6\,\psi_-$ very much as for the fifth and sixth components of a $V^{\hat{\mu}}$ gauge

field. This requires, however, abandoning Lorentz symmetry between ordinary and compact dimensions in six dimensions, remembering also that it is in any case broken by the various boundary conditions used in the compactification. The six-dimensional Weyl matter fields in the $\underline{\bar{\mathbf{5}}}$ and $\underline{\mathbf{10}}$ representations of $SU(5)$ get coupled to the four spin-0 fields in quintuplet representations h_1 and h_2 (with mirror parity $M_p = +1$), and h'_1 and h'_2 (with $M_p = -1$). Only the former survive at low-energy, acquiring v.e.v.'s $v_1/\sqrt{2}$ and $v_2/\sqrt{2}$ breaking $SU(5)$ to $SU(4)$ in six dimensions. This generates six-dimensional mass terms such as

$$-m_e\,(\,\bar{e}(x^{\hat{\mu}})\,e(x^{\hat{\mu}}) + \bar{e}_M(x^{\hat{\mu}})\,e_M(x^{\hat{\mu}})\,),\ldots, \tag{75}$$

for charged leptons and quarks together with their mirror and spin-0 partners, with

$$m_e = h_e v_1/\sqrt{2}\,,\ \ m_d = h_d v_1/\sqrt{2}\,,\ \ m_u = h_u v_2/\sqrt{2}\,. \tag{76}$$

This also provides a way to escape the sometimes unwanted GUT mass relations $m_d = m_e,\ m_\mu = m_s,\ m_b = m_\tau$ valid at the grand-unification scale. Indeed owing to the replication of quark and leptons families [63] associated with GUT parity, d quarks and charged leptons, with GUT parity $+1$, now sit in different representations of $SU(5)$, together with their replicas having GUT parity -1. (d, e'^{+}), (s, μ'^{+}), (b, τ'^{+}), and (d', e^{+}), (s', μ^{+}), (b', τ^{+}) are thus associated within six quartets of the $SU(4)$ electrostrong gauge group, only e, μ, τ and d, s, b surviving at low-energy owing to the boundary conditions involving GUT parity.

$N = 2$ supersymmetry gets reduced to $N = 0$ in the four-dimensional low-energy theory by the compactification process. Heavy states carrying compact momenta remain organized in a $N = 2$ spectrum, before it gets broken in the compactification process using R-parity. This leads to the four-dimensional spectrum

$$\begin{cases} m^2(q, l, \text{and mirrors}) & = m_{lq}^2 + \left(\frac{2\pi n_5}{L_5}\right)^2 + \left(\frac{2\pi n_6}{L_6}\right)^2, \\ & \quad n_5, n_6 \text{ integer}, \\ m^2(\tilde{q},\ \tilde{l}, \text{and smirrors}) & = m_{lq}^2 + \left(\frac{2\pi n_5}{L_5}\right)^2 + \left(\frac{2\pi n_6}{L_6}\right)^2, \\ & \quad n_5 \text{ integer}, n_6 \text{ half-integer}, \end{cases} \tag{77}$$

using (74) for counting the states at each level, with e.g. two electron and two mirror electron states, etc., for each set of integers $(n_5 \neq 0,\ n_6 \neq 0)$.

For $n_5 = 0$ i.e. below the GUT scale, the spectrum starts e.g. with the electron at m_e^2, two selectrons and two mirror selectrons at $m^2 = m_e^2 + (\pi/L_6)^2$, an electron and a mirror electron at $m^2 = m_e^2 + (2\pi/L_6)^2$ and so on, etc.; and similarly for all particles from the six-dimensional spectrum already obtained for the X, Y, W, Z, γ, and gluon multiplets of supersymmetry, combined with the compactification using R-parity, GUT parity, and reflection symmetry in compact space. (But we might also consider, to better respect the underlying extended supersymmetry, generating six-dimensional masses only for quarks and leptons with $n_5 = n_6 = 0$, leaving (s)quarks, (s)leptons and (s)mirror particles carrying compact momenta massless in six dimensions.)

Two of the four six-dimensional spin-0 doublets, h_1 and h_2, with $M_p = +1$, remain in the low-energy spectrum, breaking spontaneously the electroweak symmetry and generating quark and lepton masses. h'_1 and h'_2, with $M_p = -1$, couple quarks and leptons to their mirror partners but do not survive in the low-energy spectrum. The four-dimensional theory has the same content as the standard model at low-energy, but with the two spin-0 doublets h_1 and h_2 making possible the gauge/BE-Higgs unification that is one of the most interesting features of supersymmetric theories.

6.10 Consequences for the grand unification and supersymmetry-breaking scales

Independently of specific aspects on quark and lepton mass generation, that may still be further discussed or questioned, this indicates that supersymmetry may only show up manifestly through the presence of R-odd superpartners at the compactification scale, i.e.

$$m(R\text{-odd superpartners}) \ \approx\ \text{compactification scale}. \tag{78}$$

This one is not necessarily directly tied to the electroweak scale, especially as *the electroweak breaking can be directly formulated in the higher five- or six-dimensional spacetime*, independently of the compactification scale. It may even be quite high, especially if we consider that two compactification scales of comparable order may determine both the supersymmetry and the grand-unification scales, as hinted to by (71). This would imply

$$m(\text{R-odd superpartners}) \ \approx\ \text{GUT scale}, \tag{79}$$

seriously decreasing the hope of finding directly superpartners very soon. On the positive side, however, it would alleviate or solve the difficulties associated with flavor-changing neutral current processes induced by squark or slepton exchanges. The possible stability of the proton in this framework might allow for the grand-unification scale to be lower than usually expected …

7 Back to the supersymmetric standard model

7.1 The need for superpartners

Let us now return to the more familiar story of simple $(N = 1)$ supersymmetric theories, in four spacetime dimensions. Irrespectively of all the difficulties, one first had to find which bosons and fermions could be related. One may try as a warm-up exercise the tentative associations

$$\begin{cases} \text{photon} & \overset{?}{\longleftrightarrow} & \text{neutrino}, \\ W^{\pm} & \overset{?}{\longleftrightarrow} & e^{\pm}, \\ \text{gluons} & \overset{?}{\longleftrightarrow} & \text{quarks}, \\ & \cdots & \end{cases} \tag{80}$$

But we have no chance to realize in this way systematic associations of known fundamental bosons and fermions, especially as we know more fundamental fermionic field degrees of freedom, describing quarks and leptons (90), than bosonic ones (28, including the newly found boson). In addition these fields have different gauge and internal (B and L) quantum numbers.

Still the exercise of trying to relate, within a first electroweak model, the photon with a "neutrino" and the W^- with an "electron", accompanyied by a "heavy electron" and charged BE-Higgs boson H^-, turned out to be very fruitful. While illustrating how far one could go when trying to relate known particles and the limitations of this approach, it provided through a reinterpretation of its fermions as charginos and neutralinos the electroweak sector of supersymmetric extensions of the standard model [1]. The initial need for a conserved quantum number carried by the "lepton" candidates led to a $U(1)_R$ symmetry acting chirally on the supersymmetry generator according to

$$Q \overset{R}{\rightarrow} e^{-\gamma_5 \alpha}\, Q. \tag{81}$$

Both doublets h_1 and h_2 used for the electroweak breaking having $R = 0$, this continuous R-symmetry survives this breaking, leading to an additive quantum number R differing by ± 1 unit between bosons and fermions within multiplets of supersymmetry, gauge and BE-Higgs bosons having $R = 0$, and their superpartners, known as gauginos and higgsinos, $R = \pm 1$. The would-be "neutrino", however, uncoupled to the Z, cannot be interpreted as a ν_e or ν_μ, the ν_τ being still unknown. It has to be viewed as a neutrino of a new type, a "photonic neutrino" that became the photino [2,3]. The "lepton" candidates are thus interpreted as *charginos* and *neutralinos*, providing the electroweak gauge-and-Higgs sector of the supersymmetric standard model.

We also have to deal with the systematic appearance of *self-conjugate Majorana fermions*, while Nature seems to know only Dirac fermions. How can we obtain the usual Dirac fermions, and attribute them conserved quantum numbers like B and L? This problem gets more acute as baryon number B and lepton number L are carried by fundamental fermions only, quarks and leptons, not by bosons. This gets impossible to realize in a supersymmetric theory where bosons and fermions are related. It also seemed to make supersymmetry irrelevant to the real world. The solution consists first in accepting the existence of Majorana fermions as belonging to a new class of particles. The photon gets associated with its own new "neutrino", a *photonic neutrino* called in 1977 the *photino*; and similarly for the gluons associated with *gluinos*, etc. [2,3,6]. The Majorana fermions of supersymmetry are thus identified as gluinos and neutralinos, or they combine into charginos. At the same time one introduces new bosons carrying baryon and lepton numbers, known as *squarks and sleptons*—although this does not necessarily guarantee yet that B and L will always remain conserved at least to a sufficiently good approximation.

Supersymmetry thus does not relate directly known bosons and fermions. All particles get associated with new superpartners, according to

$$\begin{cases} \text{known bosons} & \longleftrightarrow \text{new fermions}, \\ \text{known fermions} & \longleftrightarrow \text{new bosons}. \end{cases} \tag{82}$$

This was long mocked as a sign of the irrelevance of supersymmetry. But times have changed, and the same feature now gets frequently viewed, rather naively, as an "obvious" consequence of the supersymmetry algebra.

7.2 The basic ingredients

However, even after accepting the introduction of superpartners one still has to face another potential problem. With so many spin-0 particles, including squarks and sleptons carrying B and L, how can we get interactions mediated by spin-1 gauge bosons, avoiding unwanted squark and slepton exchanges that would lead to B and L violations? R-parity plays here an essential role by *automatically forbidding direct exchanges of squarks and leptons* between quarks and leptons, which might otherwise lead to proton decay at a much too high rate.

The required ingredients for a supersymmetric extension of the standard model are [2,3]

$$\begin{cases} 1)\ SU(3) \times SU(2) \times U(1) \text{ gauge superfields}, \\ 2) \text{ chiral quark and lepton superfields}, \\ 3) \text{ the two doublet BE-Higgs superfields } H_1 \text{ and } H_2, \\ 4) \text{ a trilinear superpotential } \mathcal{W}_{l,q} \text{ responsible for } q \text{ and } l \text{ masses}. \end{cases} \tag{83}$$

We must use *two* doublet Higgs superfields. With a single one, say H_1, we could only construct, from $\widetilde{W}^-_{L+R}$ and $\tilde{h}^-_{1L}$, a single massive Dirac chargino $\tilde{h}^-_{1L} + \widetilde{W}^-_R$ acquiring its mass from $< h^\circ_1 >$, getting stuck with a surplus massless chiral chargino $\widetilde{W}^-_L$. Two doublet Higgs superfields now called

$$H_1 = \begin{pmatrix} H_1^0 \\ H_1^- \end{pmatrix} \quad \text{and} \quad H_2 = \begin{pmatrix} H_2^+ \\ H_2^0 \end{pmatrix} \tag{84}$$

are required to get *two* massive Dirac charginos (or actually winos) from gaugino ($\lambda^- = \widetilde{W}^-_{L+R}$) and higgsino ($\tilde{h}^-_{1L}$ and $(\tilde{h}^+_{2L})^c$) components.

To account for B and L conservation the superpotential $\mathcal{W}$ should be taken as *an even function of quark and lepton superfields* i.e. invariant under R-parity [2,3]. It includes the

trilinear terms

$$\mathcal{W}_{l,q} \;=\; h_e\, H_1\,.\,\bar{E}\, L \;+\; h_d\, H_1\,.\,\bar{D}\, Q \;-\; h_u\, H_2\,.\,\bar{U}\, Q\,. \quad (85)$$

H_1 and H_2 are separately responsible for charged-lepton and down-quark masses, and up-quark masses, respectively, with

$$m_e = h_e\, v_1/\sqrt{2}\,,\; m_d = h_d\, v_1/\sqrt{2}\,,\; m_u = h_u\, v_2/\sqrt{2}\,, \quad (86)$$

and $\tan\beta = v_2/v_1$. This tends to favor a smaller v_1 as compared to v_2 i.e. a large $\tan\beta$, in view of the large mass of the t quark as compared to b.

The superpotential $\mathcal{W}_{l,q}$ is also "invariant" under the continuous R symmetry (53) under which [1–3]

$$\begin{cases} V(x,\theta,\bar{\theta}) & \overset{R}{\to}\; V(x,\theta\, e^{-i\,\alpha},\bar{\theta}\, e^{i\,\alpha}), \\ H_{1,2}\,(x,\theta) & \overset{R}{\to}\; H_{1,2}\,(x,\theta\, e^{-i\,\alpha}), \\ (L,\,Q,\,\bar{E},\,\bar{D},\,\bar{U})(x,\theta) & \overset{R}{\to}\; e^{i\,\alpha}\,(L,\,Q,\,\bar{E},\,\bar{D},\,\bar{U})(x,\theta\, e^{-i\,\alpha}), \end{cases} \quad (87)$$

so that it transforms according to $\mathcal{W}_{l,q}\,(x,\theta) \;\to\; e^{2\,i\,\alpha}\,\mathcal{W}_{l,q}\,(x,\theta\, e^{-i\,\alpha})$ as in (19). The $\mu H_1 H_2$ superpotential mass term, however, does not, the higgsino mass term transforming chirally under R (as a gaugino mass term but in the opposite way). The superpotential $\mathcal{W}_{l,q}$ is also invariant under the extra $U(1)_A$ symmetry under which [1–3]

$$\begin{cases} V(x,\theta,\bar{\theta}) & \overset{U(1)_A}{\to}\; V(x,\theta,\bar{\theta}), \\ H_{1,2}\,(x,\theta) & \overset{U(1)_A}{\to}\; e^{i\,\alpha}\; H_{1,2}\,(x,\theta), \\ (L,\,Q,\,\bar{E},\,\bar{D},\,\bar{U})(x,\theta) & \overset{U(1)_A}{\to}\; e^{-i\,\alpha/2}\,(L,\,Q,\,\bar{E},\,\bar{D},\,\bar{U})(x,\theta), \end{cases} \quad (88)$$

as in (16). The $\mu H_1 H_2$ mass term, however, is not, the higgsino mass term transforming chirally under $U(1)_A$.

A continuous R-invariance, however, would force Majorana gluinos to remain massless. It must get reduced to R-parity, so that gluinos, in particular, can acquire a mass. This also applies to the gravitino, and to gravity-induced supersymmetry-breaking terms including gaugino mass terms [44,45,64–67]. (We leave aside the possibility of Dirac gluinos [7] considered in Sect. 3.2 and in theories with extra dimensions [16–18] as discussed in Sect. 6.8, with Dirac gluinos at the compactification scale, making somewhat obsolete the other usual mechanisms for generating supersymmetry-breaking terms.)

Indeed massless or light gluinos would combine with quarks, antiquarks and gluons to form light *R-hadrons*, *R-mesons* $\tilde{g}q\bar{q}$ and *R-baryons* $\tilde{g}qqq$ [4,7,68]. They are expected to decay into ordinary hadrons plus unobserved neutralinos (taken at the time as photinos or very light gravitinos) carrying away missing energy-momentum. They were not observed, leading to consider massive gluinos, with the $U(1)_R$ symmetry group reduced to its discrete Z_2 R-parity subgroup, with $R_p = (-1)^R$. The existence of gluinos lighter than ~ 1 TeV/c^2 has now been explored at LHC, and often excluded in this mass range in many situations of interest.

R-parity is thus simply

$$R_p = (-1)^R = \begin{cases} +1 \text{ for gauge and BEH bosons, quarks and leptons,} \\ -1 \text{ for superpartners.} \end{cases} \quad (89)$$

As $(-1)^{2S} \equiv (-1)^{3B+L}$ for ordinary particles, it may be reexpressed as [4]

$$R_p \;=\; (-1)^R \;\equiv\; (-1)^{2S}\,(-1)^{3B+L}\,, \quad (90)$$

or equivalently $(-1)^{2S}\,(-1)^{3(B-L)}$. This symmetry, if conserved, requires that supersymmetric particles be produced in pairs, their decays producing again particles of $R_p = -1$ (or an odd number of them), the "lightest supersymmetric particle", or LSP, being stable.

The LSP is usually taken as a neutralino, although other superpartners may also play this role. The pair-production of supersymmetric particles [2,3], first considered for gluinos [4,68], sleptons [69–71], and photinos [72,73], then extended to many processes at much higher energies [10,11,46], should ultimately lead to two unobserved neutralinos, the famous "missing energy-momentum" signature often used to search for supersymmetry. These neutralinos may have interactions of roughly weak-interaction strength, although there magnitude depends significantly of the mass spectrum, including squark and slepton masses.

Once we accept that supersymmetry does not relate directly known bosons and fermions, we have to account for the fact that superpartners have not been observed, which requires them to be sufficiently heavy. If a few GeV/c^2 or $\gtrsim$ 15 GeV/c^2 could be sufficient in the late 1970s or early 1980s [68–71], at the time of PETRA and PEP experiments, we know now, from LEP, Fermilab, and LHC experiments [10,11,46], that superpartners, excepted possibly some of the neutralinos, should be rather heavy, i.e. more than $\approx$ 1 TeV or so in most cases for strongly interacting squarks and gluinos. Indirect constraints, discussed in other articles in this volume, may point in the direction of even heavier squarks and sleptons, to avoid unwanted flavor-changing neutral current effects, depending also on the structure of the supersymmetry-breaking terms considered.

The mass splittings between squarks and quarks would be generated in global supersymmetry from the auxiliary $< D >$'s of neutral gauge superfields [1,38] and $< F >$'s of chiral ones [39,40] most notably H_1^0 and H_2^0, in connection with the supercurrent conservation equation [6], resulting in the mass sum rule [5]

$$\overline{\Sigma}\, m^2(\text{squarks}) = \overline{\Sigma} m^2(\text{quarks}) \times \begin{cases} \text{in global supersymmetry,} \\ \text{up to radiative corrections,} \\ \text{with } SU(3)\times SU(2)\times U(1) \text{ or } SU(5) \text{ gauge group.} \end{cases} \quad (91)$$

Table 1 Minimal particle content of the supersymmetric standard model. The gaugino fields $\tilde{W}_3$ and $\tilde{W}'$ mix with the higginos $\tilde{h}_1^\circ$, $\tilde{h}_2^\circ$ into four Majorana neutralinos; or more, as in the presence of an extra N/nMSSM singlet S coupled through a $\lambda\, H_1 H_2\, S$ superpotential

Spin 1	Spin 1/2	Spin 0
gluons g photon γ	gluinos $\tilde{g}$ photino $\tilde{\gamma}$	
$W^\pm$ Z	winos $\widetilde{W}_{1,2}^\pm$ zinos $\widetilde{Z}_{1,2}$ higgsino $\tilde{h}^\circ$	$H^\pm$ H $h,\ A$ } BE-Higgs bosons
	leptons l quarks q	sleptons $\tilde{l}$ squarks $\tilde{q}$

For the first family, $m^2(\tilde{u}_1)+m^2(\tilde{u}_2)+m^2(\tilde{d}_1)+m^2(\tilde{d}_2) = 2\,(m_u^2 + m_d^2)$, so that one of the squarks should have a very small or in fact negative mass^2, then leading to a charge and color-breaking vacuum state as discussed in Sect. 3.1. Making all squarks heavy, initially done through the $< D >$ from an extra $U(1)$ with non-vanishing axial couplings [2,3], is now usually realized by generating soft supersymmetry-breaking terms from supergravity or radiative corrections, in "gravity-mediated" or "gauge-mediated" models [22,44,45,64–67], characterized, in the latter case, by a very light gravitino LSP.

Once they acquire a sizable-enough mass as from gravity-induced gaugino mass terms, these weakly interacting neutralinos [48] (or WIMPs, for "weakly interacting massive particles"), stable from R-parity conservation, can annihilate sufficiently to satisfy cosmological constraints. They became natural candidates for the non-baryonic dark matter of the Universe, as soon as the need for such particles became manifest [74–76]. With the neutral gaugino fields $\tilde{W}_3$ and $\tilde{W}'$ mixing with the higginos $\tilde{h}_1^\circ$, $\tilde{h}_2^\circ$ into Majorana neutralinos, according to

$$\{W_3,\ W';\ h_1^\circ,\ h_2^\circ;\ldots\} \overset{SUSY}{\longleftrightarrow} \underbrace{\{\tilde{W}_3,\ \tilde{W}';\ \tilde{h}_1^\circ,\ \tilde{h}_2^\circ;\ldots\}}_{\text{neutralinos}}, \quad (92)$$

the association

$$\text{neutral gauge } (\gamma,\ Z,\ldots) \text{ and BEH bosons } (h,\ H,\ A,\ \ldots) \longleftrightarrow \text{dark matter} \quad (93)$$

serves as a substitute for (3), now relating the mediators of electroweak forces (or mass generation) to *dark matter*, rather than normal matter. The neutralino sector, and thus the LSP which serves as a natural dark matter candidate, may also involve an extra higgsino (*singlino*) described by a chiral singlet superfield S coupled to H_1 and H_2 through a $\lambda\, H_1 H_2\, S$ superpotential as in the N/nMSSM, or *another gaugino* associated with an extra $U(1)$ as in the USSM.

The quartic interactions of the doublets h_1 and h_2 now appear as *electroweak gauge interactions*, with a well-specified potential [1]

$$V_{\text{quartic}} = \frac{g^2+g'^2}{8}\,(h_1^\dagger h_1 - h_2^\dagger h_2)^2 + \frac{g^2}{2}\,|h_1^\dagger h_2|^2\,, \quad (94)$$

present in all versions of the supersymmetric standard model, from the MSSM to the N/nMSSM, USSM, etc. *These quartic Higgs couplings, now fixed by the electroweak gauge couplings g and g′*, to $(g^2+g'^2)/8$ and $g^2/2$, are responsible for the mass terms m_W^2 and m_Z^2 for the charged and neutral spin-0 BEH fields $w^\pm$ ($\equiv H^\pm$) and z that appear as spin-0 partners of the $W^\pm$ and Z. This is at the root of the gauge/BE-Higgs unification described in Sect. 5, and resulting mass relations.

7.3 Turning μ into a dynamical superfield variable in superspace

One can introduce as in [1] (μ being then called m) the $\mu\, H_1 H_2$ superpotential term, leading to the mass terms

$$V_\mu = \mu^2\,(h_1^\dagger h_1 + h_2^\dagger h_2)\,. \quad (95)$$

But even in the presence of the weak-hypercharge $\xi D'$ term splitting the h_1 and h_2 mass^2 terms apart from μ^2 we cannot get non-vanishing v.e.v.'s for both h_1 and h_2 but only for one of them, the other being "inert", getting stuck with a massless chargino. Adding a soft term proportional to $h_1 h_2$ that would cure the problem but at the price of making the theory non-supersymmetric was not considered, at the time, as a valid option. The $\mu\, H_1 H_2$ term is also not invariant under the continuous R symmetry, which would require μ to transform according to $\mu \to e^{2i\alpha}\mu$. The μ parameter was thus made dynamical in superspace by being promoted to a superfield variable $\mu(x,\theta)$ through the introduction of the extra singlet S, with the replacement

$$\mu \to \mu(x,\theta) = \lambda\, S(x,\theta) \text{ so that } \mu\, H_1 H_2 \to \lambda\, H_1 H_2\, S. \quad (96)$$

The resulting superpotential $\mathcal{W}$ reads, when R-invariance is not required,

$$\mathcal{W} = \lambda\, H_1 H_2\, S\, [+\mu\, H_1 H_2] + f(S) + \mathcal{W}_{lq}, \quad (97)$$

with

$$f(S) = \frac{\kappa}{3}\,S^3 + \frac{\mu_S}{2}\,S^2 + \sigma\, S, \quad (98)$$

as in the general NMSSM.

The additional requirement of R-invariance (i.e. $U(1)_R$) was initially intended to get an additive quantum number R carried by Dirac fermions, leading to *Dirac* neutralinos and charginos. Demanding R-invariance (acting as in (18, 87)) reduced the singlet superpotential $f(S)$ to the sole linear term

$f(S) = \sigma\, S$ of the nMSSM, with

$$\mathcal{W} \;=\; \lambda\, H_1 H_2\, S + \;\sigma\, S \;+\; \mathcal{W}_{lq}. \tag{99}$$

The extra trilinear and bilinear terms $\frac{\kappa}{3}\, S^3$ and $\frac{\mu_S}{2}\, S^2$, excluded by the continuous R as well as the μ term, possibly regenerated from $< S >$ according to

$$\mu_{\rm eff} \;=\; \lambda \;< S >, \tag{100}$$

may be reintroduced if we do not insist on this symmetry (as required for Majorana gluino and gravitino masses). This leads to the chargino (wino) mass matrix

$$\mathcal{M} \;=\; \begin{pmatrix} m_2 & m_W\,\sqrt{2}\,\sin\beta \\ m_W\,\sqrt{2}\,\cos\beta & \mu_{\rm eff} \end{pmatrix}, \tag{101}$$

where non-diagonal terms respect the continuous R while diagonal ones violate it by $\Delta R = \pm 2$. Having both m_2 and $\mu_{\rm eff}$ different from zero is essential to have both charginos (winos) heavier than m_W, as now necessary [44–46].

The μ parameter, although "supersymmetric" (and possibly regenerated from $< S >$ as $\mu_{\rm eff}$) may be protected from being too large as it comes in violation of both the continuous R-symmetry and the chiral $U(1)_A$ acting according to [1]

$$\begin{aligned} &H_{1,2}\,(x,\theta) \;\overset{R}{\rightarrow}\; H_{1,2}\,(x, \theta\, e^{-i\,\alpha}), \\ &H_{1,2}(x,\theta) \;\overset{U_A}{\rightarrow}\; e^{i\alpha}\, H_{1,2}(x,\theta). \end{aligned} \tag{102}$$

The same continuous R symmetry may prevent gluino and other gaugino masses from being too large. It is even so efficient in doing so that it makes difficult to generate significant gluino masses from radiative corrections involving messenger quarks [7] unless these are taken really very heavy (introducing a new scale much larger than electroweak scale). μ and gaugino mass parameters ($m_{1/2}$) may then naturally be of the same order, i.e.

$$\mu \;\;(\text{or } \mu_{\rm eff}) \approx m_{\rm gauginos} \approx m_{\rm gravitino} \text{ in view of } R \text{ symmetry}. \tag{103}$$

A further advantage of the dynamical change $\mu \rightarrow \lambda\, S$ comes with the introduction of new quartic couplings in the potential, independent of gauge couplings. The doublet mass terms for h_1 and h_2 get replaced by $\lambda^2\,|s|^2\,(h_1^\dagger h_1 + h_2^\dagger h_2)$, with the quartic potential (94) replaced as in [1] (where λ^2 was called $h^2/2$, with $\tan\beta = v_2/v_1 \equiv \tan\delta = v'/v''$) by

$$\begin{aligned} V = \frac{g^2+g'^2}{8}\;\,(h_1^\dagger h_1 - h_2^\dagger h_2)^2 + \frac{g^2}{2}\;\,|h_1^\dagger h_2|^2 \\ + \left|\lambda\, h_1 h_2 + \frac{\partial f(s)}{\partial s}\right|^2 + \lambda^2\,|s|^2\,(h_1^\dagger h_1 + h_2^\dagger h_2) \;+ \cdots . \end{aligned} \tag{104}$$

The extra quartic coupling

$$V^{\lambda}_{\rm quartic} = \lambda^2\,|h_1\, h_2|^2 \;+\; \lambda^2\,|s|^2\,(h_1^\dagger h_1 + h_2^\dagger h_2) \tag{105}$$

comes in addition to the $(g^2+g'^2)/8$ and $g^2/2$ terms in (94) and is essential to make all spin-0 BE-Higgs bosons sufficiently heavy. It now leads to

$$m_h^2 \;\leq\; m_Z^2\,\cos^2 2\beta \;+\; \frac{\lambda^2\, v^2}{2}\;\sin^2 2\beta \quad (+\,\text{rad. corr.}), \tag{106}$$

i.e. to an upper bound larger than m_Z (+ radiative corrections), for $\lambda > \sqrt{(g^2+g'^2)/2}$ so that $\lambda v/\sqrt{2} > m_Z$, independently of $\tan\beta$. This makes it much easier to obtain a lightest spin-0 mass of 125 GeV/c^2 in the N/nMSSM, without having to rely on large contributions from radiative corrections involving very heavy stop quarks. If sizable enough, the coupling λ of the trilinear superpotential $\lambda\, H_1 H_2 S$ also makes it easier to consider smaller $\tan\beta$ that may be ≈ 1, in contrast with the MSSM which tends to require large $\tan\beta$.

8 Conclusions and perspectives

Our first aims were to understand how supersymmetry may allow for a description of fundamental particles and interactions, and discuss resulting implications. At the time weak interactions through neutral currents were just recently discovered, the structure of the weak neutral current unknown, the $W^\pm$ and Z hypothetical, with a lower limit on m_W as low as about 5 GeV/c^2 in 1974. No fundamental spin-0 boson was known, and many physicists did not really believe in their existence, preferring to think of spontaneous symmetry breaking as induced by v.e.v.'s for bilinear products of fermion fields. Lots of efforts were made developing theories trying to avoid such unwanted fundamental spin-0 fields and particles [79–83].

In contrast supersymmetric theories, leading to superpartners with extra charged and neutral BE-Higgs bosons from the two electroweak spin-0 doublets [1–5], provide a natural framework for fundamental spin-0 fields by relating them to chiral spin-$\frac{1}{2}$ ones (and spin-1 fields as we saw), so that

spin-0 fields acquire, within supersymmetry,
equal dignity as spin-$\frac{1}{2}$ ones. (107)

Spin-0 mass parameters are equal, up to supersymmetry-breaking effects, to spin-$\frac{1}{2}$ ones, free from quadratic divergences, all benefiting from remarkable non-renormalization properties [37].

The electroweak scale is the most natural one where to search for supersymmetric particles, with supersymmetry usually expected to show up a not-too-high scale, now typically considered to be $\lesssim$ a few TeV at most. But no supersymmetric particle has shown up yet, with lower limits on squarks and gluinos often reaching $\simeq$ TeV scale [10,11]. Still *we keep hoping that the next round of LHC experiments*

will lead to a direct discovery of the new superpartners. In between, the finding at CERN of a new particle likely to be a spin-0 BE-Higgs boson [12–15] seems to indicate that we are indeed on the right track, in contrast with other anticipations about the nature of electroweak breaking.

At which energy scale we may expect to find supersymmetric particles depends on the magnitude of the parameters describing supersymmetry breaking, in connection with the amount of breaking of the continuous R symmetry. Gaugino mass parameters ($m_{1/2}$ i.e. m_1, m_2, m_3) break both supersymmetry and R symmetry, while the higgsino mass parameter μ (or $\mu_{\rm eff}$ if regenerated from $< S >$) also comes in violation of R symmetry, making natural for them to be of the same order.

Squark and slepton supersymmetry-breaking mass^2 parameters ($m_\circ^2$) may be of this same order, as frequently considered. Or they could be significantly larger as they do not violate R symmetry, leading one to consider situations such as

$$m(\tilde{q},\tilde{l}) \;\approx\; m_\circ \left\{ \begin{matrix} \gg ? \\ \approx ? \end{matrix} \right\},$$
$$m_{\rm gauginos} \;\approx\; \mu_{\rm eff} \;\gtrsim\; \text{a few}\, m_W \,\text{to TeV}\,. \qquad (108)$$

One may also consider other situations, e.g. with moderate $m_\circ$ as compared to very large $m_{3/2}$ and $\mu_{\rm eff}$. What should be the mass scale for the new particles, if it is not $\sim$ TeV scale as was commonly expected, remains an open question.

As supersymmetry breaking and electroweak breaking are in general *two independent phenomena*, we should take seriously the possibility that their breaking scales be of different magnitudes. The supersymmetry-breaking scale could then be significantly larger, *especially if a new physical phenomenon not directly related to electroweak breaking is involved in this process*, such as the compactification of an extra dimension.

This could fix the supersymmetry-breaking scale in terms of the compactification scale ($\approx \hbar/Lc$) using R-parity and other discrete symmetries for the boundary conditions in compact space. Identifying

performing a complete loop in compact space
$$\equiv\; R\text{-parity transformation}, \qquad (109)$$

we get relations like $m_{3/2} \approx \pi/L$ (or $1/(2R)$), in the simplest case [16–18]. We may then face the eventuality that superpartner masses be considerably larger than the presently accessible $\approx$ TeV scale, especially if the compactification of extra dimensions also sets the scale for grand-unification breaking. This may tell us that supersymmetry should only show up manifestly through the presence of R-odd superpartners at the compactification scale, i.e.

$$m(R\text{-odd superpartners}) \approx \text{compactification scale?} \qquad (110)$$

This one is not necessarily directly tied to the electroweak scale, especially as *the electroweak breaking can be directly formulated in the higher five- or six-dimensional spacetime* (where it leaves an *electrostrong symmetry* unbroken), independently of the compactification scale. It may be quite high, especially if two similar compactification scales determine both the supersymmetry and the grand-unification scales, as hinted to by (71). This would imply

$$m(R\text{-odd superpartners}) \approx \text{GUT scale??} \qquad (111)$$

with the further possibility that the GUT scale be lower than usually considered, in connection with the possible stability of the proton associated with GUT parity.

Fortunately, supersymmetric theories also lead to gauge/BE-Higgs unification by providing spin-0 bosons as extra states for spin-1 gauge bosons within massive gauge multiplets, in spite of their different gauge-symmetry properties (and independently of extra dimensions) [1,54,55]. Massive gauge superfields now describe spin-0 BE-Higgs bosons, next to massive spin-1 gauge bosons. In particular, the 125 GeV/c^2 boson recently observed at CERN may also be interpreted, up to a mixing angle induced by supersymmetry breaking, as the spin-0 partner of the Z under *two* supersymmetry transformations,

$$\text{spin-1}\; Z \;\overset{SUSY}{\longleftrightarrow}\overset{SUSY}{\longleftrightarrow}\; \text{spin-0 BEH boson}, \qquad (112)$$

providing the first example of two fundamental particles of different spins related by supersymmetry. *Supersymmetry may thus be tested in the gauge-and-BE-Higgs sector* at present and future colliders, in particular through the properties of the new boson, even if R-odd supersymmetric particles were still to remain out of reach for some time.

References

1. P. Fayet, Nucl. Phys. B **90**, 104 (1975)
2. P. Fayet, Phys. Lett. B **64**, 159 (1976)
3. P. Fayet, Phys. Lett. B **69**, 489 (1977)
4. G. Farrar, P. Fayet, Phys. Lett. B **76**, 575 (1978)
5. P. Fayet, Phys. Lett. B **84**, 416 (1979)
6. P. Fayet, Phys. Lett. B **70**, 461 (1977)
7. P. Fayet, Phys. Lett. B **78**, 417 (1978)
8. S. Weinberg, Phys. Rev. Lett. **19**, 1264 (1967)
9. A. Salam, Proc. Nobel Symp. El. Part. Th., ed. Svartholm (1968), p. 367
10. https://twiki.cern.ch/twiki/bin/view/AtlasPublic/SupersymmetryPublicResults
11. https://twiki.cern.ch/twiki/bin/view/CMSPublic/PhysicsResultsSUS

12. https://twiki.cern.ch/twiki/bin/view/AtlasPublic/HiggsPublicResults
13. https://twiki.cern.ch/twiki/bin/view/CMSPublic/PhysicsResultsHIG
14. ATLAS coll., Phys. Lett. B **716**, 1 (2012)
15. CMS coll., Phys. Lett. B **716**, 30 (2012)
16. P. Fayet, Phys. Lett. B **159**, 121 (1985)
17. P. Fayet, Nucl. Phys. B **263**, 649 (1986)
18. P. Fayet, Proc. 2nd Nobel Symp. El. Part. Phys., Phys. Scripta T **15**, 46 (1987)
19. P. Fayet, S. Ferrara, Phys. Rep. **32**, 249 (1977)
20. H. Nilles, Phys. Rep. **110**, 1 (1984)
21. H. Haber, G. Kane, Phys. Rep. **117**, 75 (1985)
22. S. Martin, A Supersymmetry Primer, hep-ph/9709356 (2011)
23. H. Miyazawa, Progr. Theor. Phys. **36**, 1266 (1966)
24. H. Miyazawa, Phys. Rev. **170**, 1586 (1968)
25. P. Ramond, SUSY: the early years (1966–1976). Eur. Phys. J. C **74**, 2698 (2014). doi:10.1140/epjc/s10052-013-2698-x. arXiv:1401.5977
26. Yu. Gol'fand, E. Likhtman, ZhETF Pis. Red. **13**, 452 (1971) [JETP Lett. **13**, 323 (1971)]
27. D. Volkov, V. Akulov, Phys. Lett. B **46**, 109 (1973)
28. J. Wess, B. Zumino, Nucl. Phys. B **70**, 39 (1974)
29. D. Volkov, V. Soroka, Pisma Zh. Eksp. Teor. Fiz. **18**, 529 (1973) [JETP Lett. **18**, 312 (1973)]
30. S. Ferrara, D. Freedman, P. van Nieuwenhuizen, Phys. Rev. D **13**, 3214 (1976)
31. S. Deser, B. Zumino, Phys. Lett. B **62**, 335 (1976)
32. A. Salam, J. Strathdee, Nucl. Phys. B **76**, 477 (1974)
33. S. Ferrara, J. Wess, B. Zumino, Phys. Lett. B **51**, 239 (1974)
34. J. Wess, B. Zumino, Nucl. Phys. B **78**, 1 (1974)
35. S. Ferrara, B. Zumino, Nucl. Phys. B **79**, 413 (1974)
36. A. Salam, J. Strathdee, Phys. Lett. B **51**, 353 (1974)
37. J. Iliopoulos, B. Zumino, Nucl. Phys. B **76**, 310 (1974)
38. P. Fayet, J. Iliopoulos, Phys. Lett. B **51**, 461 (1974)
39. P. Fayet, Phys. Lett. B **58**, 67 (1975)
40. L. O'Raifeartaigh, Nucl. Phys. B **96**, 331 (1975)
41. P. Fayet, Nucl. Phys. B **113**, 135 (1976)
42. P. Fayet, Nucl. Phys. B **149**, 137 (1979)
43. K. Intriligator, N. Seiberg, D. Shih, JHEP **04**, 021 (2006)
44. E. Cremmer, P. Fayet, L. Girardello, Phys. Lett. B **122**, 41 (1983)
45. P. Fayet, Phys. Lett. B **125**, 178 (1983)
46. J. Beringer et al., Particle data group, Phys. Rev. D **86**, 010001 (2012)
47. E. Cremmer et al., Nucl. Phys. B **147**, 105 (1979)
48. P. Fayet, Phys. Lett. B **86**, 272 (1979)
49. P. Fayet, in *Proceedings of 16th Rencontres de Moriond*, Les Arcs, vol. 1 (1981), p. 347
50. H. Pagels, J. Primack, Phys. Rev. Lett. **48**, 223 (1982)
51. P. Fayet, Nucl. Phys. B **78**, 14 (1974)
52. F. Wilczek, Phys. Rev. Lett. **40**, 279 (1978)
53. S. Weinberg, Phys. Rev. Lett. **40**, 223 (1979)
54. P. Fayet, Nuovo Cim. A **31**, 626 (1976)
55. P. Fayet, Nucl. Phys. B **237**, 367 (1984)
56. P. Fayet, Nucl. Phys. B **187**, 184 (1981)
57. P. Fayet, Nucl. Phys. B **246**, 89 (1984)
58. F. Gliozzi, J. Scherk, D. Olive, Nucl. Phys. B **122**, 253 (1977)
59. L. Brink, J. Scherk, J. Schwarz, Nucl. Phys. B **121**, 77 (1977)
60. R. Haag, J. Lopuszanski, M. Sohnius, Nucl. Phys. B **88**, 257 (1975)
61. H. Georgi, S. Glashow, Phys. Rev. Lett. **32**, 438 (1974)
62. H. Georgi, H. Quinn, S. Weinberg, Phys. Rev. Lett. **33**, 451 (1974)
63. P. Fayet, Phys. Lett. B **397**, 417 (1985)
64. A. Chamseddine, R. Arnowitt, P. Nath, Phys. Rev. Lett. **49**, 970 (1982)
65. R. Barbieri, S. Ferrara, C. Savoy, Phys. Lett. B **119**, 343 (1982)
66. H. Nilles, M. Srednicki, D. Wyler, Phys. Lett. B **120**, 346 (1983)
67. L. Hall, J. Lykken, S. Weinberg, Phys. Rev. D **27**, 2359 (1983)
68. G. Farrar, P. Fayet, Phys. Lett. B **79**, 442 (1978)
69. G. Farrar, P. Fayet, Phys. Lett. B **89**, 191 (1980)
70. D. Barber et al., Phys. Rev. Lett. **45**, 1904 (1980)
71. H. Behrend et al., Phys. Lett. B **114**, 287 (1982)
72. P. Fayet, Phys. Lett. B **117**, 460 (1982)
73. J. Ellis, J. Hagelin, Phys. Lett. B **122**, 303 (1983)
74. H. Goldberg, Phys. Rev. Lett. **50**, 1419 (1983)
75. J. Ellis et al., Nucl. Phys. B **238**, 453 (1984)
76. G. Bertone, D. Hooper, J. Silk, Phys. Rep. **405**, 279 (2005)
77. J. Scherk, J. Schwarz, Phys. Lett. B **82**, 60 (1979)
78. J. Scherk, J. Schwarz, Nucl. Phys. B **153**, 61 (1979)
79. S. Weinberg, Phys. Rev. D **13**, 974 (1976)
80. S. Weinberg, Phys. Rev. D **19**, 1277 (1979)
81. L. Susskind, Phys. Rev. D **20**, 2619 (1979)
82. S. Dimopoulos, L. Susskind, Nucl. Phys. B **155**, 237 (1979)
83. E. Eichten, K. Lane, Phys. Lett. B **90**, 125 (1980)

Eur. Phys. J. C (2014) 74:2801
DOI 10.1140/epjc/s10052-014-2801-y

THE EUROPEAN PHYSICAL JOURNAL C

Review

Lessons for SUSY from the LHC after the first run

I. Melzer-Pellmann[1,a], **P. Pralavorio**[2,b]

[1] DESY, Notkestr. 85, 22607 Hamburg, Germany
[2] CPPM, Univ. Aix-Marseille and CNRS/IN2P3, 163 Avenue de Luminy, Case 902, 13288 Marseille Cedex 09, France

Received: 10 February 2014 / Accepted: 17 February 2014 / Published online: 27 May 2014

Abstract A review of direct searches for new particles predicted by Supersymmetry (SUSY) after the first run of the LHC is proposed. This review is based on the results provided by the ATLAS and CMS experiments.

1 Introduction

Ernest Rutherford once said at the beginning of the twentieth century 'Theorists play games with their symbols while we discover truths about the Universe'. This was before the birth of the Bohr atom and quantum mechanics. At the beginning of the twenty-first century this sentence can probably be reverted, as the predictions of the theory are so successful that experimental discoveries of the last 40 years perfectly fit in the Standard Model (SM) theory framework. In this respect, the systematic exploration of the electroweak (EW) scale at the Large Hadron Collider (LHC) [1] could have represented an even greater confirmation of the theory predictions since most Beyond Standard Model (BSM) theories and, in particular, low-energy Supersymmetry (SUSY) expect new particles with masses close to the EW scale. As it will be discussed extensively in this article, this is clearly not the case. The direct searches conducted at the first LHC run by the general purpose experiments ATLAS [2] and CMS [3] did not reveal the presence of any new particle beyond that of the Standard Model. In contrary, the Standard Model is now fully established by the discovery of the Higgs boson [4,5].

The article is based on currently published results obtained at a center-of-mass energy of $\sqrt{s} = 8$ TeV for an integrated luminosity of 20 fb^{-1} of LHC data. In case they are not available, previous results, obtained with $\sqrt{s} = 7$ TeV and 5 fb^{-1} of LHC data, are discussed. The most important analyses are based on 8 TeV LHC data, either from ATLAS or CMS (or both). Therefore, even if the fully final result from Run 1 has not yet been published for all individual search channels, lessons for SUSY discussed here are not expected to change.

This article is organized as follows: First, a brief recap of the SUSY framework used for the LHC searches is proposed in Sect. 2. Then the experimental challenges faced by the ATLAS and CMS experiments in terms of object reconstruction and background modeling are explained in Sect. 3. The limit setting procedure is also briefly summarized in this section. The discussion of the results is split in three different sections, representing the main avenues of the SUSY searches at LHC: gluino and squarks of first/second generation at the energy frontier in Sect. 4, third-generation squarks in Sect. 5, and electroweak SUSY in Sect. 6. All assume R-parity conservation and prompt decay of the SUSY particles. Section 7 is devoted to escape routes beyond R-parity conservation and prompt decays, as well as more exotic SUSY scenarios. Prospects with the coming runs of LHC and the conclusions are discussed in Sects. 8 and 9, respectively.

2 SUSY framework for the search at LHC

This section provides the reader with the minimum vocabulary and knowledge needed to understand the experimental results presented later in this article.

As discussed elsewhere in this review, SUSY [6,7] can be realized in many different ways. Even if the LHC cannot explore the full SUSY phase space, it can probe extensively the low-energy (or weak-scale) realization of N = 1 SUSY, called the Minimal Supersymmetric Standard Model (MSSM) [8]. This model predicts new particles, called sparticles, that are superpartners of each SM particle in the chiral multiplets, as shown in Fig. 1. A new quantum number, R-parity, is created and defined as $P_R = (-1)^{2s+3B+L}$, where s is the spin, B the baryon number and L the lepton number. It is negative/positive for SUSY/SM particles. Therefore, the sparticles have the same quantum numbers as their SM

[a] e-mail: isabell.melzer-pellmann@cern.ch
[b] e-mail: pascal.pralavorio@cern.ch

Fig. 1 SUSY particles in MSSM [8]

Names	Spin	P_R	Gauge Eigenstates	Mass Eigenstates
Higgs bosons	0	+1	$H_u^0\ H_d^0\ H_u^+\ H_d^-$	$h^0\ H^0\ A^0\ H^\pm$
squarks	0	−1	$\widetilde{u}_L\ \widetilde{u}_R\ \widetilde{d}_L\ \widetilde{d}_R$ $\widetilde{s}_L\ \widetilde{s}_R\ \widetilde{c}_L\ \widetilde{c}_R$ $\widetilde{t}_L\ \widetilde{t}_R\ \widetilde{b}_L\ \widetilde{b}_R$	(same) (same) $\widetilde{t}_1\ \widetilde{t}_2\ \widetilde{b}_1\ \widetilde{b}_2$
sleptons	0	−1	$\widetilde{e}_L\ \widetilde{e}_R\ \widetilde{\nu}_e$ $\widetilde{\mu}_L\ \widetilde{\mu}_R\ \widetilde{\nu}_\mu$ $\widetilde{\tau}_L\ \widetilde{\tau}_R\ \widetilde{\nu}_\tau$	(same) (same) $\widetilde{\tau}_1\ \widetilde{\tau}_2\ \widetilde{\nu}_\tau$
neutralinos	1/2	−1	$\widetilde{B}^0\ \widetilde{W}^0\ \widetilde{H}_u^0\ \widetilde{H}_d^0$	$\widetilde{N}_1\ \widetilde{N}_2\ \widetilde{N}_3\ \widetilde{N}_4$
charginos	1/2	−1	$\widetilde{W}^\pm\ \widetilde{H}_u^+\ \widetilde{H}_d^-$	$\widetilde{C}_1^\pm\ \widetilde{C}_2^\pm$
gluino	1/2	−1	$\widetilde{g}$	(same)
goldstino (gravitino)	1/2 (3/2)	−1	$\widetilde{G}$	(same)

partners, except for the spin which differs by half a unit, and R-parity. The spectrum is characterized by 25 elementary scalars and 10 elementary fermions without counting the SM particles.

For self-containment, we just recap the names and main characteristics of the new particles. To generate the masses of the up- and down-type fermions, the SM Higgs sector is extended by adding another $SU(2)_L$ complex doublet. Each doublet has a vacuum expectation value (vev) labeled v_u and v_d, constrained by the SM Higgs vev, v ($v = \sqrt{v_u^2 + v_d^2}$). Their ratio is traditionally written $\tan\beta = v_u/v_d$. As a result, eight mass eigenstates exist after electroweak (EW) symmetry breaking: three neutral Higgs bosons (h^0, the one with the lightest mass, H^0 and A^0), two charged Higgs bosons ($H^\pm$) and three Goldstone bosons (G^0, $G^\pm$), 'eaten' to give masses to the Z and $W^\pm$ bosons. The Higgs boson discovered by ATLAS and CMS is assumed to be the lightest neutral Higgs of the MSSM (h^0), since it possesses similar properties to the SM one when $m_{A^0}^2 \gg m_Z^2$ and $\tan\beta > 1$ (also called the decoupling limit).[1] The squarks ($\widetilde{q}$) and sleptons ($\widetilde{l}$) are the spin-0 partners of the SM fermions. Similarly, winos ($\widetilde{W}^0$, $\widetilde{W}^\pm$), binos ($\widetilde{B}^0$), and higgsinos ($\widetilde{H}_u^0$, $\widetilde{H}_d^0$, $\widetilde{H}_u^+$, $\widetilde{H}_d^-$) are the spin-1/2 superpartners of the electroweak bosons. To complete the list, colored gluinos ($\widetilde{g}$) and the gravitino ($\widetilde{G}$) are the partners of the gluon and graviton. With this setup, the number of fermions and bosons is equalized and the Lightest SUSY Particle (LSP) is stable if R-parity is conserved.

[1] It could still be H^0, implying that h^0 is lighter and still to be discovered; but this is presently disfavored by the data [9].

Note also that left- and right-handed fermions have two different SUSY partners $\widetilde{f}_{L,R}$ that can mix in $\widetilde{f}_{1,2}$, provided the SM partner is heavy, like in the third generation. Similarly, the wino, bino, and higgsino, governed by the gauge eigenstate mass terms M_1, M_2, and μ, mix to give four neutralinos ($\widetilde{\chi}_{1,2,3,4}^0$) and four charginos ($\widetilde{\chi}_{1,2}^\pm$). To simplify the discussion of results in this sector, this article often considers one of the three typical scenarios, shown in Fig. 2. Each corresponds to a different $\widetilde{\chi}_1^0$ flavor: (a) bino-like, (b) wino-like or co-NLSP [10], and (c) higgsino-like. The last one is favored by naturalness arguments, as discussed in the next paragraph.

When choosing the parameters such that the hierarchy or naturalness problem is solved within the MSSM [11], stringent constraints appear on the masses of the new predicted particles, especially the ones which are most closely related to the Higgs, as can be seen in Fig. 3. Interestingly, there was no experimental sensitivity to this spectrum before the startup of the LHC. Moreover, by design, the LHC is perfectly suited to access this particular region of phase space, already with its first run at $\sqrt{s} = 7$–8 TeV. Searches for hints in this particular spectrum generally shape the analysis strategy at the LHC.

In the MSSM framework, three main theoretical unknowns influence the search direction: the LSP nature, the compression (or not) of the SUSY spectra, and the status of R-parity. For the first one, experimental constraints restrict the LSP to be the lightest neutralino ($\widetilde{\chi}_1^0$) or the almost massless gravitino. In the latter case, the final states are increased compared to the former. The reason is that the Next-to-Lightest SUSY Particle (NLSP) which can be any of the SUSY particles (squark, gluino, slepton, chargino or neutralino) will

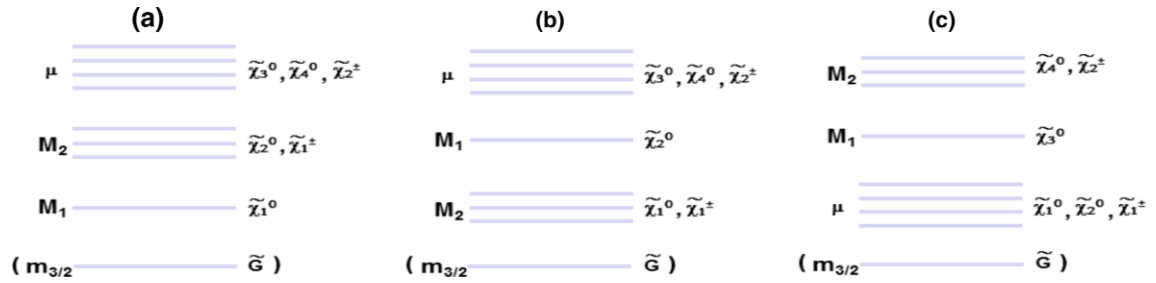

Fig. 2 Three possible EW SUSY mass spectra depending of the relative values of the M_1, M_2, and μ parameters

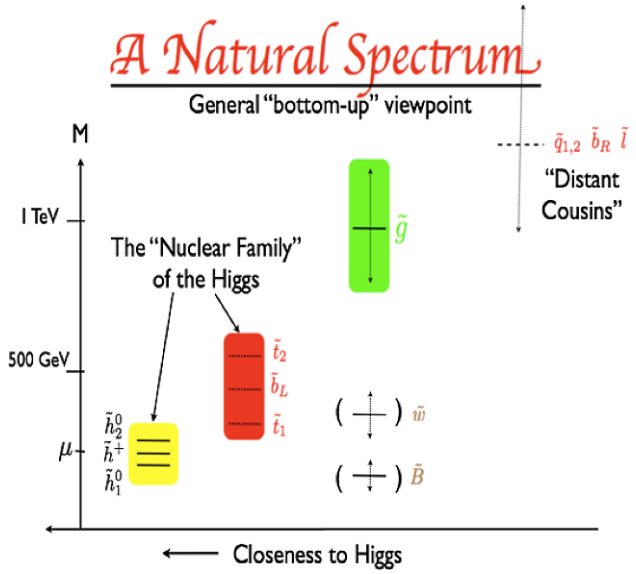

Fig. 3 Natural SUSY particle mass spectra giving less than 10 % tuning [13]

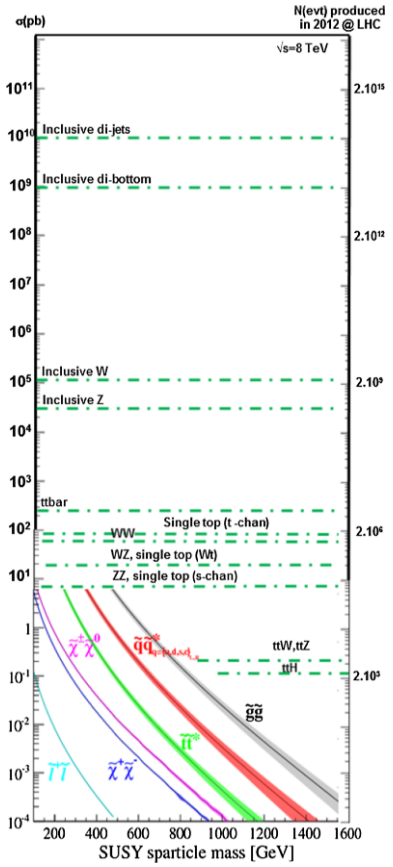

Fig. 4 Cross sections of several SUSY production channels [14], superimposed with Standard Model process at $\sqrt{s} = 8$ TeV. The *right-handed* axis indicates the number of events for 20 fb^{-1}

decay to the gravitino and the SM partner of the NLSP [12].[2] The second MSSM theory unknown is the difference (ΔM) between the mass of the highest sparticle produced at the LHC (M_{SUSY}) and the LSP (M_{LSP}), resulting in compressed or open spectra, i.e. soft or hard objects in the final state. The third MSSM theory unknown is the status of R-parity. In a plain vanilla MSSM scenario R-parity is conserved (RPC), but it could well be violated (RPV) or even a continuous symmetry. It is important to mention that in the huge MSSM phase space long-lived particles decaying within the detector or even outside often exist. This situation could arise from the low mass difference between two sparticles in the spectrum, very weak coupling to the LSP, very small R-parity Yukawa couplings, etc.

Typical SUSY cross sections of pair-produced sparticles at the LHC are given in Fig. 4—for two different sparticles mass degeneracy is assumed.[3] Since each SM particle and its superpartner belong to the same multiplet, the sparticle decay generally involves the SM partner and the LSP. However, due to the high number of new particles many dif-

[2] The most 'natural' situation is that the NLSP is the $\widetilde{\chi}_1^0$ (Fig. 3), whose decay will depend on its flavor (bino-, wino- or higgsino-like of Fig. 2) and results in $\widetilde{\chi}_1^0 \rightarrow \gamma\widetilde{\mathrm{G}}$, $\widetilde{\chi}_1^0 \rightarrow \gamma/\mathrm{Z}\widetilde{\mathrm{G}}$ or $\widetilde{\chi}_1^0 \rightarrow \mathrm{Z/h}^0\widetilde{\mathrm{G}}$ decays, respectively. The relative proportion of γ, Z and h^0 depends also on other parameters θ_{W} or $\tan\beta$.

[3] Following an ATLAS–CMS agreement [14], all SUSY cross sections are calculated in the MSSM at NLO precision in the strong coupling constant, including the resummation of soft gluon emission at next-to-leading-logarithmic (NLO + NLL) accuracy, using PROSPINO and NLL-fast [15–19].

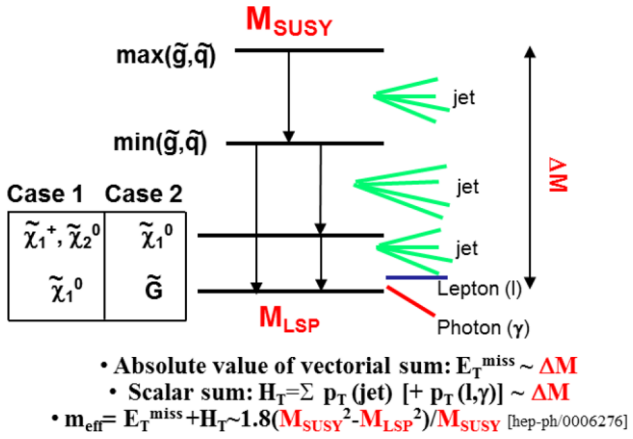

Fig. 5 Typical decay of a colored SUSY particle at LHC. The two cases shown at the bottom of the SUSY spectrum correspond to the two considered LSP types

ferent decays are possible depending on the sparticle mass spectrum, generating long decay chains. Plain vanilla MSSM searches are therefore characterized by pair-produced particles, two LSPs escaping the detection and long decay chains involving jets and/or leptons and photons as depicted in Fig. 5. Note that for the gravitino LSP scenario, the mass difference with the NLSP is always sizeable in the natural spectrum, O(100) GeV, because the gravitino is almost massless. If the masses of all colored particles are too high to be produced at LHC, the production may be dominated by chargino–neutralino pair production, resulting in less complicated final states, generally containing several leptons. Finally, non-prompt sparticle decays can generate striking signatures as displayed in Fig. 6.

3 Experimental challenges for SUSY searches at LHC

This section is mainly addressed to non-experts in LHC analyses and analysers or theorists who want to understand better the many experimental facets of a SUSY analysis at LHC.

Discovering SUSY at the LHC is an extremely challenging task, even within the restricted framework of the MSSM. First, every corner of the parameter space needs to be covered, including all possible decay channels which provide a high number of final states with different mixtures of reconstructed objects (photon, electron, muon, tau, jets, b-jets, missing transverse energy). Second, due to the presence of many scalars and weakly interacting particles, cross sections are generally extremely tiny with respect to the SM background (cf. Fig. 4). In the plain vanilla MSSM scenario, the few signal events are generally located in the tails of the kinematic distributions, requiring challenging trigger, powerful discriminating variables and accurate background modeling in a complicated region of the phase space. In other SUSY scenarios where R-parity is violated and/or non-prompt decays are possible, the experimental challenge generally shifts to taking the best performance of each subdetector to improve secondary vertex reconstruction, timing resolution, jet substructure reconstruction, lepton coverage, etc. Therefore, SUSY searches provide an excellent way to push the detector and analyser capabilities to their best.

This section is organized as follows. Experimental matters, i.e. LHC data, trigger and detector/object performance relevant for SUSY searches, are treated in Sect. 3.1. Commonly used discriminating variables for the design of the signal regions are then discussed in Sect. 3.2 and methods to estimate the remaining background in these signal regions are described in Sect. 3.3. Finally, the limit setting tools and SUSY models used for interpretations are briefly reviewed in Sects. 3.4 and 3.5, respectively.

3.1 LHC data and detector performance

After a brief reminder of the main characteristics of the LHC data (Sect. 3.1.1), ATLAS and CMS detectors (Sect. 3.1.2), the object and detector performance relevant to SUSY searches are discussed (Sects. 3.1.3 and 3.1.4).

3.1.1 LHC data

The LHC is a particle collider at CERN, 'probably the largest and the most complex machine ever constructed by humans' [20]. It is housed in a 27 km long tunnel ~100 m underground and is ultimately designed to collide proton beams at a center-of-mass energy of up to $\sqrt{s} = 14$ TeV at a rate of 40 MHz.

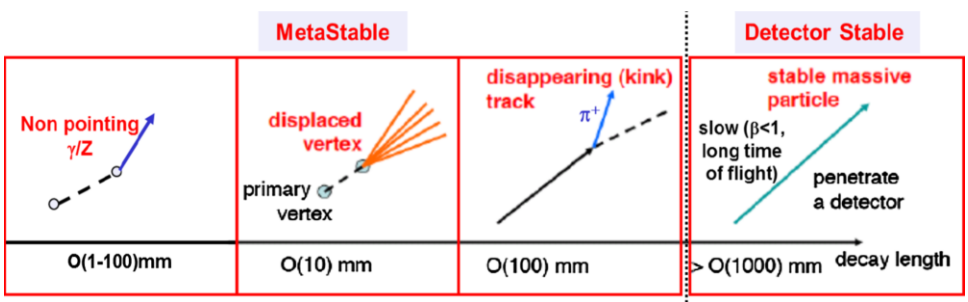

Fig. 6 Possible signatures from non-prompt sparticle decay

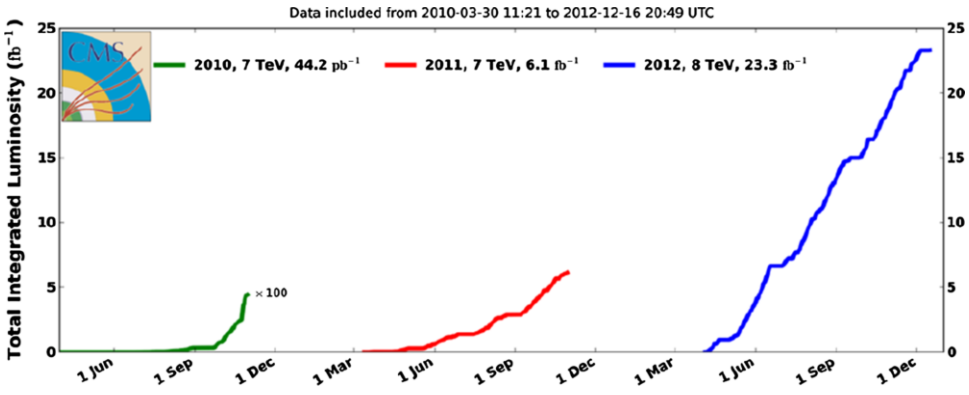

Fig. 7 LHC luminosity recorded by the CMS experiment

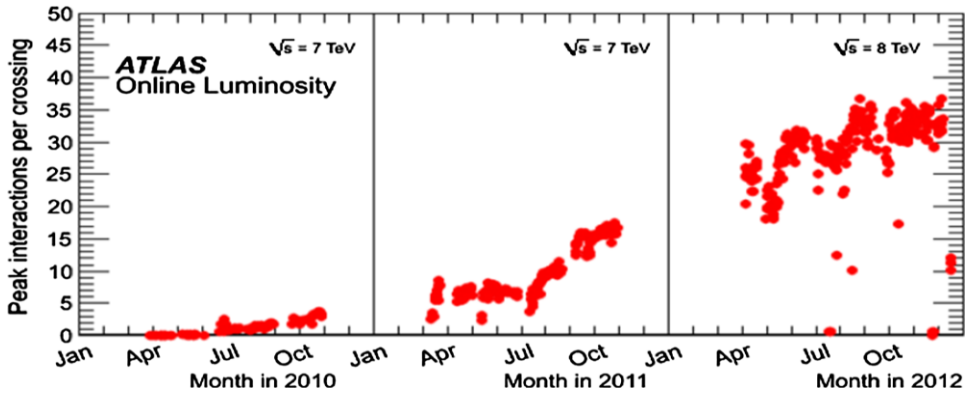

Fig. 8 Corresponding number of pile-up events as a function of time

The first proton–proton run of the LHC (Run 1) lasted from March 2010 to December 2012 with $\sqrt{s} = 7$ TeV and 8 TeV, and collisions every 50 ns. It was extremely successful and provided more than 20 fb^{-1} in 3 years, as shown in Fig. 7. Because of the increase of the proton density per bunch and the tuning of the beam optics, the number of interactions per beam crossing (pile-up) increased regularly during Run 1 to reach more than 30 at the end of 2012; see Fig. 8. This increases the complexity of the event reconstruction, as discussed later. For practical considerations, unless mentioned otherwise, searches presented in this article make use of the full $\sqrt{s} = 8$ TeV dataset.

3.1.2 ATLAS and CMS detectors

Four large detectors have been built at the collision points. Among these, ATLAS and CMS are the two general-purpose experiments. Because of the huge complexity of the detectors that can cope with very high collision rate and high pile-up conditions, world-wide collaborations of a few thousands of physicists and engineers were set up, giving these projects the flavor of a modern cathedral, dedicated to science.

The interesting particles are produced over the full solid angle down to small polar angles (θ) with respect to the incoming beams (a fraction of a degree corresponding to pseudorapidities of $|\eta|$ up to 5, where $\eta = -\ln[\tan(\theta/2)]$) and in the full azimuth $0 \leq \phi \leq 2\pi$. The transverse plane plays a special role for LHC analyses: the vectorial sum of all particle momenta produced by the collision is null and it is the bending plane in the central part. Therefore, selections generally rely on transverse momenta, labeled p_{T}.

The two detectors are based on two different technologies for the central magnets that are used to bend the charged particle trajectories: CMS uses a 4-T superconducting solenoid magnet of 3 m radius, fully containing the trackers and the calorimeters, while ATLAS chose a smaller central solenoid (2 T and 1.2 m radius), complemented by outer toroids. These choices influence the design of all detector technologies [21].

Inner tracking systems measure the momentum of charged particles, which are bent by the magnetic field. To achieve this, ATLAS and CMS have designed tracker systems providing a similar geometrical coverage (over $|\eta| < 2.4-2.5$). They are based on the same silicon detector technology near the interaction vertex, i.e. below 50 cm, with a silicon pixel and strip tracker, providing around 10 precision points per track. However, they differ considerably at larger radii: ATLAS uses straw-tube detectors (TRT), allowing 35 extra measurements per track in the bending plane for $|\eta| < 2.0$, with drift-time information for momentum measurements and pattern recognition, while CMS extends the silicon-strip technology up to a radius of ∼110 cm. Stand-alone tracker performance is generally better for CMS because of the higher magnetic field.

The electromagnetic (EM) calorimeter is the key system for measuring the kinematics of electrons and photons. CMS chose ∼75000 scintillating $PbWO_4$ crystals with an excellent energy resolution but extremely low light yield, while ATLAS built a granular lead/liquid argon sampling calorimeter with ∼200k channels. This last technology is robust and well known, with poorer energy resolution at low energy, but comparable to CMS in the 0.1–1 TeV energy range.

Key parameters for the hadronic calorimeters are the coverage up to $|\eta| < 5$ for both ATLAS and CMS, the depth in interaction length ($\lambda \sim 10$) and the sampling fraction, three times better in ATLAS than in CMS [21].

Finally, the muon spectrometers are also quite different: in ATLAS they can provide an independent and high-accuracy measurement of muons over $|\eta| < 2.7$ coverage, whereas CMS relies on a combined measurement of muon chambers and inner tracker up to $|\eta| < 2.4$.

The ability of ATLAS and CMS to use more than 90 % of the high-quality data delivered by the LHC for physics analyses demonstrates the excellent functioning of both experiments.

3.1.3 Object reconstruction performance relevant to SUSY searches

Because of different detector concepts, the final-state reconstruction differs quite a lot between ATLAS and CMS.

In ATLAS, electrons, photons, and jets are seeded by calorimeter clusters. Electrons and photons are eventually combined with the tracker information. In CMS, all final-state particles are reconstructed with the particle-flow method [22], generally seeded in the inner detector and further combined with the information from all sub-detectors.

Jets are reconstructed using the anti-kt jet clustering algorithm [23,24] with a distance parameter of 0.4 and 0.5 for ATLAS and CMS, respectively. After calibration, pile-up corrections and cleaning, jets are generally considered only above $p_{\mathrm{T}} > 20$ GeV. The jet energy scale uncertainty (and the jet energy resolution to a lesser extent) is generally the dominant systematic uncertainty for R-parity conserving strong production. It is lower than 2 % for $p_{\mathrm{T}} > 100$ GeV, degrading to 4 % for jets with $p_{\mathrm{T}} = 20$ GeV [25,26].

Identifying b-jets from light-quark and gluon jets is crucial for all third-generation searches and is possible thanks to secondary vertex information provided by the tracker. Dedicated algorithms are used by ATLAS [27] and CMS [28]. Typically with a 60–70 % b-jet identification efficiency, a light-quark jet rejection between 100 and 1000 is obtained depending on p_{T} and η. Similarly, hadronically decaying taus can be separated from light-quark jets with O(10) less rejection power than for a b-jet assuming a 60 % tau identification efficiency [29].

Leptons are key ingredients for SUSY searches targeting compressed spectra, EW production, and/or RPV final states. Due to trigger requirements, the leading lepton has to be generally above 20–25 GeV in p_{T}, but it is possible to lower the p_{T} down to 6–7 GeV in analyses considering multi-leptons. Further separation from jets is obtained by requiring the leptons to be isolated in the calorimeters and/or the tracker.

A crucial variable for SUSY searches at the LHC is the magnitude of the missing transverse momentum vector ($E_{\mathrm{T}}^{\mathrm{miss}}$). In ATLAS, it is based on the vector sum of transverse momenta of jets, leptons and all calorimeter clusters not associated to such objects (within $|\eta| < 5$). In CMS, it is based on all particles reconstructed by the particle-flow method which compensate for the lower calorimeter jet energy resolution. Because of the hadronic environment, fake $E_{\mathrm{T}}^{\mathrm{miss}}$ can arise from jet mismeasurements which can be efficiently removed by rejecting events where a high-energetic jet (or lepton) and $\mathbf{E}_{\mathrm{T}}^{\mathrm{miss}}$ are close-by (with a relative angle of $\Delta\phi(j, E_{\mathrm{T}}^{\mathrm{miss}}) < 0.4$). Detector malfunctions and poorly instrumented regions can cause high $E_{\mathrm{T}}^{\mathrm{miss}}$ as well. In some lepton-veto analyses, $H_{\mathrm{T}}^{\mathrm{miss}}$ is considered, i.e. the vectorial sum of jets above few tens of GeV in p_{T}, to decrease the sensitivity to low-energy jets coming from pile-up.

Obviously the very first experimental challenge at the LHC is the trigger. In Run 1, ATLAS and CMS concentrated their efforts on single triggers ($E_{\mathrm{T}}^{\mathrm{miss}}$, multi-jets, electrons, and muons), but they also allocated a part of the bandwidth to combined triggers (di- and multi-leptons, jets + $E_{\mathrm{T}}^{\mathrm{miss}}$, several central jets, leptons in combination with large hadronic energy, etc.) which are more analysis-specific.

3.1.4 Detector performance relevant to SUSY searches

Performance of specific sub-detectors are crucial to detect non-prompt sparticle decays or heavy stable charged particles which are slowly moving ($\beta = v/c < 0.9$).

In this respect, the tracker provides a lot of relevant information: (i) the ionization energy loss ($\mathrm{d}E/\mathrm{d}x$) measured in the silicon detectors, significantly higher for low β than for minimum ionizing particles, (ii) characteristics of displaced vertices via dedicated algorithms, and (iii) for ATLAS a continuous outer tracker, the TRT, to identify late decays. Note that RPC searches generally veto long-lived particles decaying in the tracker by imposing impact parameter requirements to reject cosmic muons.

Low-β particles or particles coming from long-lived particle decays in the tracker will arrive late in the calorimeter. The excellent timing resolution of the ATLAS and CMS EM calorimeters, around 0.3–0.4 ns per cell, is a very powerful tool to discriminate against SM particles. In the case of ATLAS, stand-alone pointing capability can also be used. Similarly, the excellent control of the calorimeter noise yields sensitivity to late-decaying particles trapped in the detector.

Finally, the time-of-flight measured in the muon spectrometer can be exploited as well. Stand-alone resolution of the order of 5 % or better can be achieved over the whole η range of the spectrometer. It can be ultimately improved by combining information with the calorimeter; see for example [30].

3.2 Discriminating variables

In RPC searches, the main background for SUSY signals is generally caused by processes involving particles with masses close to the weak scale (W, Z, H, top), or QCD multi-jet production with real or fake $E_{\mathrm{T}}^{\mathrm{miss}}$; see Fig. 4. These processes can have cross sections that are up to ten orders of magnitude higher than the SUSY signal. Therefore, finding SUSY at the LHC requires to design signal regions (SR) by exploiting at best the main characteristics of the decay cascade: the presence of two stable LSPs, whose momentum is directly proportional to $E_{\mathrm{T}}^{\mathrm{miss}}$, and/or long decay chains involving jets, i.e. large calorimeter activity in the event. The latter is efficiently measured by the scalar sum, H_{T}, of the transverse energy of reconstructed objects (for some analyses, only a part of the objects can also be considered). Rectangular cuts can then be applied on H_{T} and $E_{\mathrm{T}}^{\mathrm{miss}}$ (or $H_{\mathrm{T}}^{\mathrm{miss}}$).

Sensitivity can be improved by taking advantage of the correlation between H_{T} and $E_{\mathrm{T}}^{\mathrm{miss}}$ and by computing $m_{\mathrm{eff}} = H_{\mathrm{T}} + E_{\mathrm{T}}^{\mathrm{miss}}$, called the effective mass [31]. This is illustrated in Fig. 9. The other advantage is that m_{eff} can be linked to characteristic SUSY parameters like M_{SUSY}, the mass of the highest colored object, M_{LSP}, the LSP mass, and their mass difference ΔM; see Fig. 5. Typically m_{eff} will

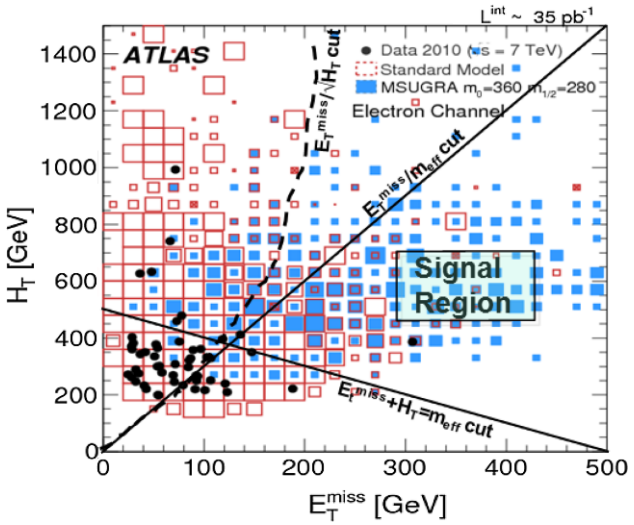

Fig. 9 Illustration of the variables used in a standard SUSY search for strong production at LHC with one-lepton, three jets and $E_{\mathrm{T}}^{\mathrm{miss}}$ final state [33]. For completeness the variable $E_{\mathrm{T}}^{\mathrm{miss}}/\sqrt{H_{\mathrm{T}}}$ is also represented in this plane

peak at $1.8(M_{\mathrm{SUSY}}^2 - M_{\mathrm{LSP}}^2)/M_{\mathrm{SUSY}}$ [32]. For open spectra ($\Delta M = M_{\mathrm{SUSY}} - M_{\mathrm{LSP}} > \mathrm{O}(500)$ GeV), this value is well above the SM background which has no correlation between $E_{\mathrm{T}}^{\mathrm{miss}}$ and H_{T}, and therefore peaks at lower values. However, for compressed spectra ($\Delta M < 500$ GeV), m_{eff} loses its separation power and selection requirements have to be relaxed, or other discriminant variables have to be used.

An alternative approach, which can also served as a cross-check, is to take advantage of the kinematic distribution of the decay of two heavy sparticles (typically gluinos or squarks around 1 TeV). By grouping the reconstructed objects in two hemispheres, two mega-jets can be formed and kinematic properties used to distinguish signal from SM background. Two common variables are α_{T} [34], the ratio of the p_{T} of the second hardest jet and the invariant mass formed from the two hardest jets, and *Razor* [35]. In the former case, SM dijet events are back-to-back and trail off at $\alpha_{\mathrm{T}} = 0.5$, whereas a SUSY signal can be asymmetric (causing $\alpha_{\mathrm{T}} > 0.5$) because of the presence of the LSP in the decay. For *Razor*, the idea is to use the transverse and longitudinal information to reconstruct the mass M_R of the two mega-jets in the rest frame of the two-jet system (R-frame). For signal with open spectra M_R will peak at M_{SUSY} and at m_{t} or m_{W} for $\mathrm{t\bar{t}}$ and WW events. Other quantities related to the R-frame (transverse mass, Lorentz boost) can be used to increase the discrimination against the background.

If the presence of lepton(s) is required, several types of invariant transverse masses could be considered as discriminant variables. The simplest case corresponds to the single lepton channel. There, the leptonic W-boson background, either coming from W (+jets) or $\mathrm{t\bar{t}}$ production, is efficiently removed by requiring that the transverse mass m_{T} is above the W mass. This variable is defined as $m_{\mathrm{T}} \equiv \sqrt{2E_{\mathrm{T}}^{\mathrm{miss}}\, p_{\mathrm{T}}^{l}(1-\cos(\Delta\phi))}$, where p_{T}^{l} is the transverse momentum of the lepton and $\Delta\phi$ the difference in the azimuthal angle between the lepton and the $E_{\mathrm{T}}^{\mathrm{miss}}$ direction. The m_{T} variable has an end-point for backgrounds containing a single leptonically decaying W boson, while signal events contain additional $E_{\mathrm{T}}^{\mathrm{miss}}$ due to the LSPs, leading to an excess at large m_{T}. When two leptons are considered the best discriminant variables are the generalized transverse masses m_{T2} [36–38] and m_{CT} [39,40]. It can be applied for example to search for direct slepton production $\tilde{l}^{+}\tilde{l}^{-} \rightarrow l_1 l_2 \tilde{\chi}_1^0(\mathrm{p}_1)\tilde{\chi}_1^0(\mathrm{p}_2)$. m_{T2} minimises the larger of the two transverse masses and is defined as

$$m_{\mathrm{T2}}^2 = \min_{\mathbf{p}_{1\mathrm{T}}+\mathbf{p}_{2\mathrm{T}}=\mathbf{E}_{\mathrm{T}}^{\mathrm{miss}}} \left\{ \max\left(m_{\mathrm{T}}^2\left(\mathrm{l}_1, \mathrm{p}_1\right), m_{\mathrm{T}}^2\left(\mathrm{l}_2, \mathrm{p}_2\right)\right)\right\} \quad (1)$$

while m_{CT} is a simple combination of the visible decay products and is defined as

$$m_{\mathrm{CT}}^2 = [E_{\mathrm{T}}(\mathrm{l}_1) + E_{\mathrm{T}}(\mathrm{l}_2)]^2 - [\mathbf{p}_{\mathrm{T}}(\mathrm{l}_1) - \mathbf{p}_{\mathrm{T}}(\mathrm{l}_2)]^2, \quad (2)$$

with $E_{\mathrm{T}} = \sqrt{p_{\mathrm{T}}^2 + m^2}$. In both cases—assuming that leptons are massless—a signal end-point is defined by $(m^2_{\tilde{l}^{\pm}} - m^2_{\tilde{\chi}^0_1})/m_{\tilde{l}^{\pm}}$ while the $\mathrm{t\bar{t}}$'s end-point is $(m_{\mathrm{t}}^2 - m_{\mathrm{W}}^2)/m_{\mathrm{t}} \sim 135$ GeV, providing a very powerful discriminating variable for open spectra, i.e. $m_{\tilde{\mathrm{t}}^{\pm}} - M_{\tilde{\chi}^0_1} > \mathrm{O}(100\ \mathrm{GeV})$. This approach can be applied to all sparticle direct production (where the sparticle decays as SM partner and the LSP). As for m_{eff}, if SUSY is discovered this will provide a way to measure sparticle masses. Other possibilities exist for mass constraining variables and are described in Ref. [41].

3.3 Background modeling

As just discussed, the signal regions are generally located in extreme regions of the phase space which are not necessarily well understood and described in simulation. As a consequence, the number of remaining background events in the signal region needs to be estimated as precisely as possible (to increase the sensitivity to the SUSY signal), preferably without relying only on simulation. Several methods using data in the background determination are possible, e.g. a semi data-driven approach using background enriched 'control' regions (CR) in data, or even a fully data-driven approach.

The fully data-driven approach is particularly suited for background processes with very large cross sections and fake $E_{\mathrm{T}}^{\mathrm{miss}}$-like dijet production, fake lepton/photon in leptonic/photonic channels and long-lived particle searches. The first type of background is estimated with the jet smearing method, where the jet response for well-measured and badly measured jets is estimated in dedicated samples (see more details in [42]). The second type of background is estimated by counting the number of leptons/photons passing a loose lepton/photon selection but failing a tight one. With the measure of the true and fake lepton/photon efficiency to pass or fail the tight criteria from dedicated orthogonal samples, it is possible to estimate the number of fake leptons/photons in the tight selection. Finally, background to long-lived particles is estimated with a template method.

The semi data-driven approach is particular suited for SM processes with large cross section, as top-quark, W-, or Z-boson production. The definition of the control region is a trade-off between kinematic requirements as similar as possible to the signal region to minimize systematics, the highest achievable purity and minimization of the contamination from potential signal. This is illustrated in Fig. 10. The simulation is normalized to the event yield in the control region (*scale* factor), and the background in the signal region is estimated by extrapolating the background level via simulation from the control region to the signal region (*transfer* factor).

Determination from Monte Carlo simulations only is generally adequate for backgrounds that are expected to be very small in the signal region (e.g. diboson production for strong

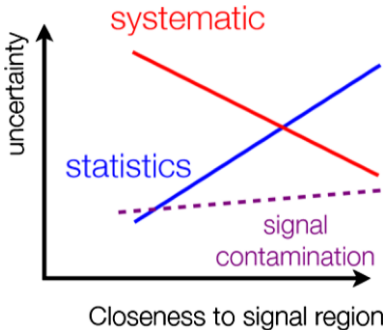

Fig. 10 Parameters entering in the design of a control region

SUSY searches), or for rare processes with very small cross sections (e.g. $\mathrm{t\bar{t}H}$ or triboson production).

Monte Carlo (MC) simulated event samples therefore play a central role in SUSY analyses. They allow not only to develop and validate the analysis procedure but also, in many cases, to evaluate the SM backgrounds, and to calculate the acceptance and efficiency of the studied signal samples. SUSY analyses rely heavily on the progress made in the last 20 years in the calculations and simulation of high Q^2 processes in hadronic collisions. Simulated samples of top (including $\mathrm{t\bar{t}W}$ and $\mathrm{t\bar{t}Z}$) and W- or Z-boson production with multiple jets are produced with multi-parton generators such as ALPGEN [43], SHERPA [44] or MADGRAPH [45], with (in some cases) up to six additional partons in the matrix element. The next-to-leading-order (NLO) generators MC@NLO [46] and POWHEG [47–49] are generally used for top or diboson production. Parton shower and fragmentation processes are simulated with either HERWIG [50] or PYTHIA [51].

All SM backgrounds are then fed into a GEANT4-based [52] model of the CMS or ATLAS detector. Due to the large amount of signal points, the signal events are usually processed with a fast detector simulation [53,54]. The effect of multiple proton–proton collisions from the same or different bunch crossings is included in all simulations by overlaying minimum bias events onto hard-scattering events. The distribution of the number of interactions per bunch crossing is reweighted in the simulation to match the data.

Systematics are often estimated by comparing two generators of the same type, by using different parton distribution functions, and by changing the factorization, renormalization, and matching scales. The choice of the generator is made case-by-case and is analysis dependent: RPC strong production searches with a large number of jets generally use multi-parton generators, whereas EW production searches preferably use next-to-leading order generators.

3.4 Limit extraction

After all cuts have been applied, the number of data events n is counted in the signal region ('cut-and-count' method). It is

compared to the expected number of SM events to enter the signal region. For that, a likelihood function for observing n_B background events in the signal region is constructed as the product of Poisson probability distributions for event counts in the signal region and each of the main control regions, and of constraints for systematic uncertainties on the expected yields, called nuisance parameters.[4] The Poisson probability density functions also include free parameters, for example to scale the expected contributions from the major backgrounds. The free parameters and nuisance parameters are adjusted to maximize the likelihood function. The result of the likelihood fit includes therefore a set of estimates and uncertainties for the background in the SR[5]. The significance of an excess is the probability that a background-only experiment is more signal-like than observed and is computed following the *CLs* prescription [55].

If no excess is observed, limits at 95 % confidence level (CL) are set. Note that to obtain more constraining limits, some analyses make use of the discriminant variable shape. For each public result, efficiency maps are provided to allow theorists to test their own models. Following an ATLAS–CMS agreement, the numbers quoted for exclusion refer to the observed limit minus one standard deviation.

3.5 SUSY models for interpretation

The sensitivity of the SUSY searches are estimated by three complementary approaches, given that it is not possible to cover the entire parameter phase space.

First, constrained SUSY models, where boundary conditions at a high energy scale reduce the number of parameters to a few making it realistic to scan systematically, are tested. Benchmark models are MSUGRA/CMSSM [56–60], minimal GMSB [61] and AMSB [62,63] models. Each model corresponds to a particular SUSY breaking messenger: gravity for the former and the latter and gauge bosons for GMSB. Similarly the LSP is generally the bino-like $\widetilde{\chi}_1^0$ for MSUGRA/CMSSM, the wino-like $\widetilde{\chi}_1^0$ for AMSB, and always the gravitino for GMSB.

Second, we have topological or simplified models [64–66] where only a few SUSY particles are involved, while the masses of all other SUSY particles are set to multi-TeV values, out of range at the LHC. The cascade decay of the remaining particles to the LSP, typically with zero or one intermediate step, is only characterized by the particle masses. These models are particularly suited for direct sparticle production.

Finally, results can also be interpreted in phenomenological MSSM (pMSSM) [67] models where the number of MSSM parameters is reduced to 19 by assuming the absence of new sources of flavor changing neutral currents and CP violation and universality of the first and second generation. By sampling a limited number of pMSSM parameters, the sensitivity of the searches to more 'realistic' configurations of SUSY particle masses and branching ratios can be assessed.

4 Gluino and first/second generation of squarks

In the MSSM, TeV-scale squarks and gluinos produced in pp collisions will decay promptly in long decay chains containing mainly quark and gluon jets and the LSP. SUSY events are therefore characterized by multiple energetic jets as well as transverse missing energy (E_T^{miss}) originating from the undetected LSP energies; see Fig. 5. Depending on the sparticle present (or not) in between the squarks/gluinos and the LSP, charged lepton(s) and/or photons could also appear in the cascade. This section summarizes the present status of searches for gluinos and first/second-generation squarks when the $\widetilde{\chi}_1^0$ is the LSP (Sect. 4.1) and when the gravitino is the LSP (Sect. 4.2).

4.1 SUSY models with $\widetilde{\chi}_1^0$ as LSP

To improve the sensitivity to these models, searches are usually divided in lepton-veto (Sect. 4.1.1) and leptonic (Sect. 4.1.2) searches. The former target more inclusive or generic scenarios, while the latter are generally more optimal for specific models. In both cases, requiring that some jets are originating from a b quark can increase the sensitivity (Sect. 4.1.3). A summary is given in Sect. 4.1.4.

4.1.1 Lepton-veto searches

The preferred gluino (squark) decay modes are $\widetilde{g} \rightarrow q\widetilde{q}$ ($\widetilde{q} \rightarrow q\widetilde{\chi}_1^0, q\widetilde{g}$), which generate signatures with two to $\geq$10 jets. Low jet multiplicities probe squark–squark (two jets or more), squark–gluino (three jets or more) or gluino–gluino (four jets or more) production. Additional jets compared to the tree level processes originate from initial- and final-state radiation jets (ISR/FSR) or from the presence of a top quark in the decay chain. In the last case, an increase of sensitivity is possible by requiring the presence of one or several b-tagged jets (see Sect. 4.1.3 for more details).

Several optimizations are possible, depending on the discriminating variables chosen, and this section only discusses the already published results based on rectangular cuts on E_T^{miss} and H_T [68], H_T^{miss} and H_T [69] on one side and

[4] Nuisance parameters are modeled by a Gaussian probability density function with a width given by the size of the uncertainty.

[5] The procedure is checked by building 'validation regions' in between the control and the signal and comparing with data.

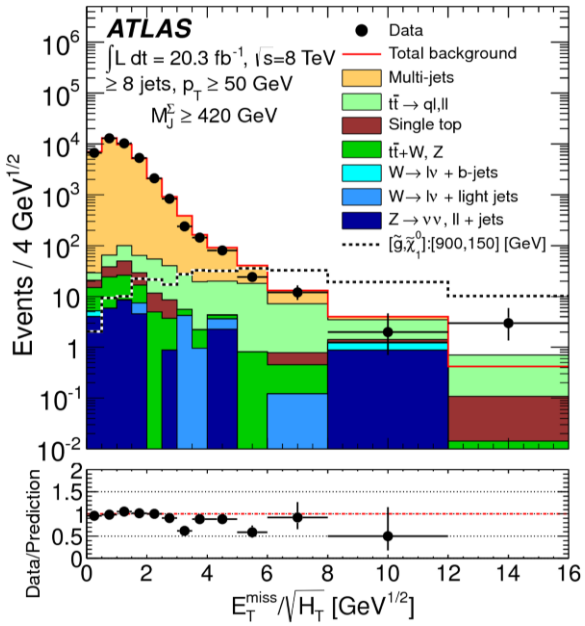

Fig. 11 Example of a discriminating variable: the $E_{\mathrm{T}}^{\mathrm{miss}}$ significance from [70]

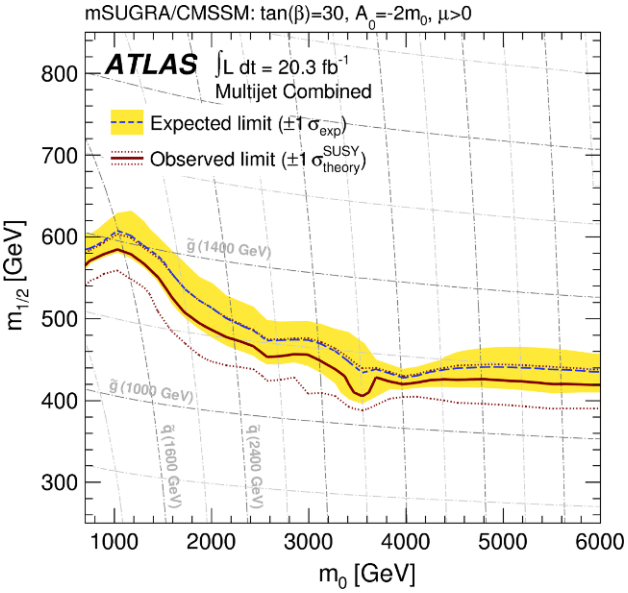

Fig. 12 Typical exclusion limit at 95 % CL from the lepton-veto inclusive search in the MSUGRA/CMSSM scenario [70]

$E_{\mathrm{T}}^{\mathrm{miss}}$ significance [70] on the other side. As an example Fig. 11 shows the $E_{\mathrm{T}}^{\mathrm{miss}}$ significance distribution. The SM background, composed of W + jets, Z($\rightarrow \nu\nu$) + jets, $\mathrm{t\bar{t}}$ and QCD multi-jets, peaks at low $E_{\mathrm{T}}^{\mathrm{miss}}$ significance value. A typical SUSY signal, where gluinos of mass 900 GeV are pair produced and decay each to a $\mathrm{t\bar{t}}$ pair and a LSP of mass of 150 GeV, leads to much higher values. The signal region is defined as $E_{\mathrm{T}}^{\mathrm{miss}}/\sqrt{H_{\mathrm{T}}} > 4\ \mathrm{GeV}^{1/2}$.

In all lepton-veto analyses, the challenge is to properly estimate backgrounds that are poorly modeled by Monte Carlo simulations: the QCD multi-jet background is obtained with a jet smearing method or a template method for the $E_{\mathrm{T}}^{\mathrm{miss}}$ significance search. Z($\rightarrow \nu\nu$) + jets estimate relies on a close-by Standard Model process like γ + jets or Z($\rightarrow \mu\mu$) + jets samples. W + jets and $\mathrm{t\bar{t}}$ are estimated by designing control regions close to the signal regions—requiring one lepton for example. Note that other searches with m_{eff} or Razor as discriminating variables will become available soon. Searches with α_{T} are only available for half the luminosity of the 2012 data [71]. All these analyses are generally more powerful than [68–70] but will not change the overall picture given in the rest of this section.

All these searches are particularly efficient for open spectra where the mass difference between the LSP and the gluino/squark is large ($\Delta M > \mathrm{O}(500)$ GeV), providing high-energetic jets. This is for example the case in the constrained SUSY model MSUGRA/CMSSM where the two most relevant parameters, the universal scalar and fermion masses at Grand Unified Theory (GUT) scale, m_0 and $m_{1/2}$, are varied to construct a grid of points.[6] Figure 12 shows the limits obtained with the $E_{\mathrm{T}}^{\mathrm{miss}}$ significance search. Squark and gluino masses at the EW scale are proportional to the m_0 and $m_{1/2}$ parameters and shown by the isolines, which indicate that gluino and degenerate squark masses below 1.2 TeV are excluded. For equal degenerate squark and gluino masses a limit of 1.3 TeV is reached.

Another way to represent the power of the lepton-veto searches is to use simplified models where $\tilde{\mathrm{g}} \rightarrow \mathrm{q\bar{q}}\tilde{\chi}_1^0$ decays are enforced. Here again a limit of 1.2 TeV on the gluino mass is obtained (for massless LSPs); see Fig. 13. However, for more compressed spectra the limits degrade and LSP masses cannot be excluded beyond 500 GeV. A similar situation occurs when considering mass-degenerate light flavor squarks forced to decay as $\tilde{\mathrm{q}} \rightarrow \mathrm{q}\tilde{\chi}_1^0$; see Fig. 14. Compared to the gluino situation, the limits are degraded to 800 GeV for squark masses (again in the case of massless LSPs), and LSP masses cannot be excluded beyond 300 GeV. These limits are reduced to 400 and 100 GeV, respectively, when only one light squark is considered.

Overall these results represent an increase of about one order of magnitude compared to the previous limits from Tevatron and LEP. From the lepton-veto analyses, the strongest limits are obtained for the gluino in open SUSY spectra, and they exclude a large part of the favored region from naturalness (cf. Fig. 3).

[6] The other fixed parameters (tan β, A_0, and the sign of μ) are chosen to accommodate a 126 GeV Higgs mass.

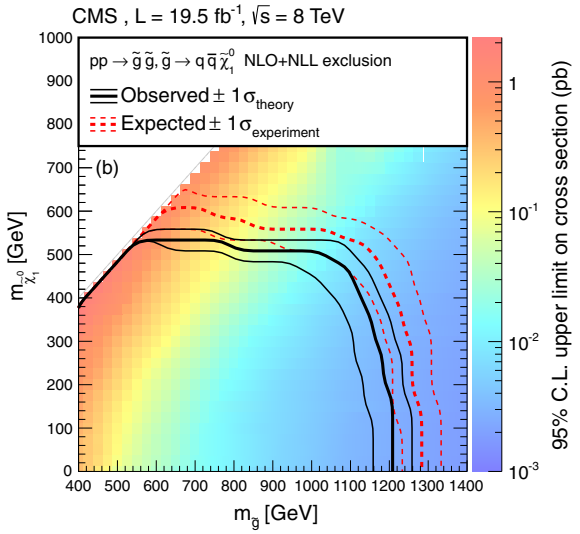

Fig. 13 Exclusion limits at 95 % CL on the gluino–gluino production in the gluino–LSP mass plane [68]. The gluino always decays as $\tilde{g} \to q\bar{q}\tilde{\chi}_1^0$ and all other SUSY particles are decoupled

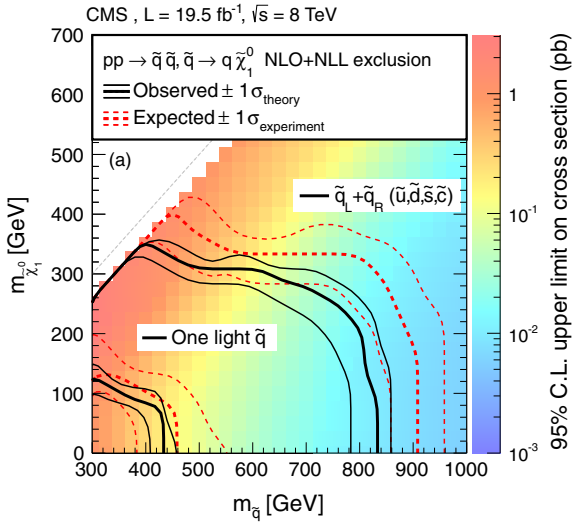

Fig. 14 Exclusion limits at 95 % CL on the squark–squark production in the squark–LSP mass plane [68]. The squark always decays as $\tilde{q} \to q\tilde{\chi}_1^0$ and all other SUSY particles are decoupled

4.1.2 Leptonic searches

Requiring one or two isolated leptons (electron or μ) on top of multi-jets and $E_{\mathrm{T}}^{\mathrm{miss}}$ allows to probe other regions of parameter space, and especially more compressed mass spectra. The lepton generally comes from W leptonic decays originating from chargino, top or from slepton decay. Experimental challenges drastically change: lepton triggers can be exploited and requirements on jet kinematics can be reduced. Lowering cuts on $E_{\mathrm{T}}^{\mathrm{miss}}$ and H_{T} is possible since the multi-jet QCD background is naturally suppressed by the presence of isolated lepton(s). Very soft leptons (in the 6–25 GeV range) are also considered to probe the compressed gluino–chargino–LSP case [72]. Finally, other variables exist like the transverse mass m_{T}, which efficiently reduces $\mathrm{t\bar{t}}$ and W + jets backgrounds by requiring $m_{\mathrm{T}} > m_{\mathrm{W}}$, as discussed in Sect. 3.2. This allows one to compensate the loss due to the leptonic branching ratio(s) when comparing with lepton-veto analyses. While this works well for single-lepton analyses to be competitive with lepton-veto analyses, this is generally not sufficient when two leptons are considered.[7] In that case, it is more advantageous to consider two leptons of same-sign since this signature is almost not produced by SM processes and appears naturally in many SUSY decays. The two reasons are: (i) gluinos are Majorana particles and produced in pairs, therefore if leptons are present in each leg they have 50 % probability to be of same-sign, (ii) multi-W final states occur frequently through top and chargino decays and leptonic W decay will ensure the presence of two same-sign leptons in most cases. For a same-sign dilepton analysis, the main background is caused by the rare $\mathrm{t\bar{t}}X$ ($X = \mathrm{h}^0, \mathrm{Z}, \mathrm{W}$) SM processes, fake leptons and mis-measured lepton charge because of the process $\mathrm{l} \to \mathrm{l}\gamma \to \mathrm{ll\bar{l}}$ where $\bar{\mathrm{l}}$ inherits most of the energy of the original lepton.

4.1.3 Multi b-tagged jet searches

As for leptons, identifying b-tagged jets in the multi-jet final states can be a precious help, especially together with leptons. This is particularly true for the decay $\tilde{g} \to \mathrm{t\bar{t}} \to \mathrm{t\bar{t}}\tilde{\chi}_1^0$, favored by the natural mass spectrum. This will provide four tops + $E_{\mathrm{T}}^{\mathrm{miss}}$ final states. Several dedicated analyses have been designed to reach this striking final state and obtain extra sensitivity compared to lepton-veto analyses described in Sect. 4.1. Reducing the dominant $\mathrm{t\bar{t}} \to \mathrm{W^+W^-b\bar{b}}$ background is possible when considering (i) a single isolated lepton and at least five jets, two or three of which are identified as b-tagged jets [73], (ii) two same-sign leptons with one, two or three b-tagged jets [74].[8] The best sensitivity is obtained by the former, which can exclude gluino masses up to 1.3 TeV for LSP masses below 600 GeV, assuming a 100 % branching ratio for the decay $\tilde{g} \to \mathrm{t\bar{t}}\tilde{\chi}_1^0\tilde{\chi}_1^0$. The same-sign dilepton analysis allows one to probe the compressed spectra part when one top is off-shell. The relative strengths of the different analyses for this model can be judged from Fig. 15. Similar results are obtained for $\tilde{g} \to \mathrm{b\bar{b}}\tilde{b}_{\mathrm{L}} \to \mathrm{b\bar{b}}\tilde{\chi}_1^0\tilde{\chi}_1^0$.

[7] This final state could be very useful to determine SUSY parameters but is generally not for discovery.

[8] The case of three b-tagged jets without a lepton is also considered but no public results exist yet at $\sqrt{s} = 8$ TeV.

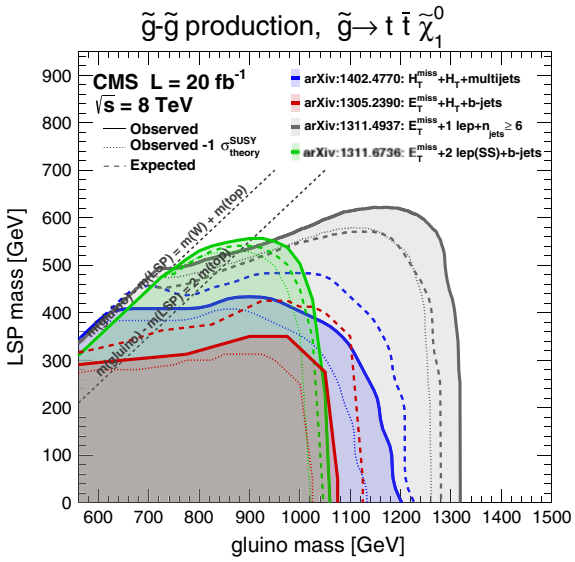

Fig. 15 Exclusion limits at 95 % CL on the gluino–gluino production in the gluino–LSP mass plane for a simplified model where gluino decays promptly via off-shell top squark and a LSP. The other sparticle masses are assumed to be decoupled. Four different analyses are shown

4.1.4 Summary

Ultimate limits from the first LHC run on gluino and squark masses when the $\widetilde{\chi}_1^0$ is the LSP will be obtained by combining all lepton-veto and leptonic analyses—many results are still to come. However, it is already fair to say that the most important constraint from the LHC experiments is the exclusion of the gluino mass below 1 TeV for open spectra. This fairly generic limit excludes a great part of the favored region from naturalness (cf. Fig. 3). Since the gluino mass is governed by only one parameter (M_3) and enters in the top squark and EWKino masses through loop corrections, this has the general effect to pull up the whole natural spectrum [75]. Compressed spectra are still poorly explored, but more work is still going on to exploit monojet-like final states provided by ISR/FSR. Extra sensitivity will also be brought by analyses based on reduced lepton and jet thresholds—this is possible when the peak luminosity decreases at the end of a LHC run. Another important information is coming from the LSP mass constraint which can reach up to 600 GeV in leptonic analyses, though it is less generic than the gluino limit. Finally, squark-mass constraints are more model-dependent and single squark-mass limits are at most of the order of 500 GeV.

4.2 SUSY models with $\widetilde{\mathrm{G}}$ as LSP

SUSY scenarios where the gravitino is the LSP generate a variety of final states driven by the NLSP-gravitino coupling. While some of these final states are common with Sect. 4.1, when the NLSP is the gluino or a squark, some need the development of new dedicated analyses, when NLSP is a slepton, chargino or neutralino. The most natural solution is $\widetilde{\chi}_1^0$ as the NLSP, leading to final states with extra γ, Z or h^0, depending on the SUSY parameters.

Among all possible final states, the ones containing photons, jets and $E_{\mathrm{T}}^{\mathrm{miss}}$ from the gluino/squark cascade could have escaped searches described in Sect. 4.1. In this case, the most dangerous background is caused by multi-jet or γ + jets events when the jet is mimicking a photon. This background type can be drastically reduced with a good photon/jet rejection—measured to be $O(10^4)$ in the $H \to \gamma\gamma$ channel—and by requiring a high value for $E_{\mathrm{T}}^{\mathrm{miss}}$. The other type of background are SM electroweak processes, especially $\mathrm{W}(\to \mathrm{e}\nu_{\mathrm{e}})\gamma$, where the electron is reconstructed as a photon and true $E_{\mathrm{T}}^{\mathrm{miss}}$ is caused by the neutrino. In both cases, data-driven methods are used for the background estimate. As an example, the distribution of $E_{\mathrm{T}}^{\mathrm{miss}}$, the main discriminating variable for the $\gamma\gamma$ searches is shown in Fig. 16. A high sensitivity is observed for the SUSY signal at high $E_{\mathrm{T}}^{\mathrm{miss}}$. Assuming a bino-like $\widetilde{\chi}_1^0$ NLSP, Fig. 17 shows that it is possible to exclude gluino masses below 1 TeV regardless of the NLSP mass [76].

When the $\widetilde{\chi}_1^0$ is higgsino-like, the preferred solution from naturalness arguments, $\widetilde{\chi}_1^0 \to \mathrm{h}^0(\to \mathrm{b\bar{b}})\widetilde{\mathrm{G}}$ final states is expected. No analysis presently attempts to search for a $4\mathrm{b}+E_{\mathrm{T}}^{\mathrm{miss}}$ final state. However, assuming that $\widetilde{\chi}_1^0$ is also partly bino-like, the signature will be $\gamma + \mathrm{b} + E_{\mathrm{T}}^{\mathrm{miss}}$ and this has been searched for. A second photon and a lepton veto are applied to remain orthogonal with other searches and remove final states with leptonic W decays [78]. In this case also the gluino mass limit reaches values around 1 TeV, as shown in Fig. 18.

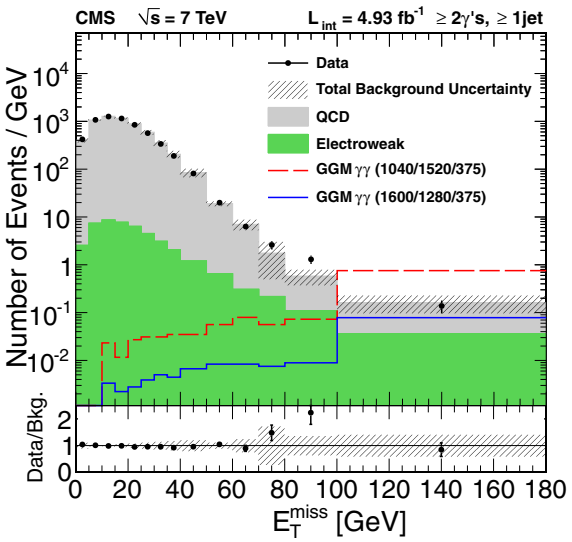

Fig. 16 $E_{\mathrm{T}}^{\mathrm{miss}}$ distribution in the diphoton analysis [77]

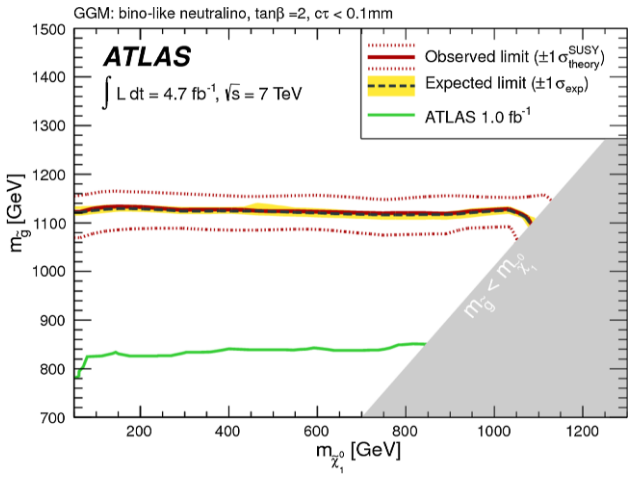

Fig. 17 Exclusion limits at 95 % CL on the gluino–gluino production in the gluino–LSP mass plane from the diphoton + $E_{\mathrm{T}}^{\mathrm{miss}}$ analysis [76]. The simplified model assumes a bino-like NLSP and a gravitino LSP. The other sparticle masses are assumed to be decoupled

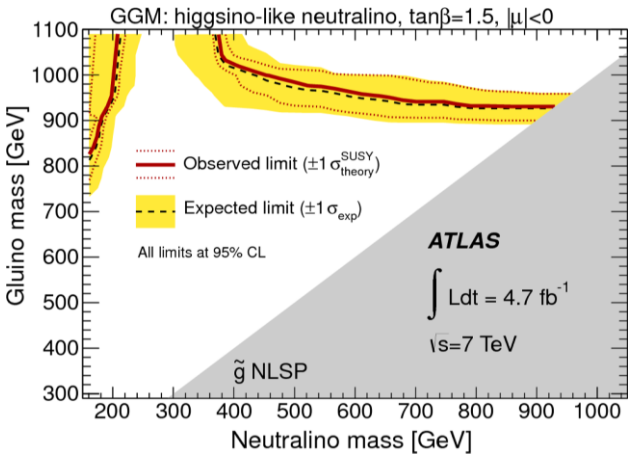

Fig. 18 Exclusion limits at 95 % CL on the gluino–gluino production in the gluino–LSP mass plane from the $\gamma + \mathrm{b} + E_{\mathrm{T}}^{\mathrm{miss}}$ analysis [78]. The simplified model assumes a higgsino-like NLSP. The other sparticle masses are assumed to be decoupled

All other NLSP cases are generally already well covered by the searches discussed in Sect. 4.1 [12]. However, it is possible to gain a bit in sensitivity by searching for one or two τ + jets + $E_{\mathrm{T}}^{\mathrm{miss}}$ final states [79,80], especially when $\widetilde{\tau}$ is the NLSP or co-NLSP with other sleptons. In this case, it is possible to combine with a 2-lepton + jets + $E_{\mathrm{T}}^{\mathrm{miss}}$ search [72] and even a 3-lepton + jets + $E_{\mathrm{T}}^{\mathrm{miss}}$ search [81]. In all cases, the gluino mass limit is always above 1 TeV.

As for models with the $\widetilde{\chi}_1^0$ as LSP, SUSY scenarios where the $\widetilde{\mathrm{G}}$ is the LSP provide strong constraints on sparticle masses and particularly on the gluino mass which is generally excluded below 1 TeV whatever the NLSP nature and mass are. Less stringent limits are obtained for squarks. It is worth to note that these conclusions are based on 7 TeV results—presently only one 8 TeV result is available.

5 Third generation of squarks

As already discussed in Sect. 2, naturalness predicts light third-generations squarks. Another motivation for the third-generation squarks to be the lightest colored sparticles is that the squark mass eigenstates $(\widetilde{\mathrm{q}}_1, \widetilde{\mathrm{q}}_2)$ depend on orthogonal combinations of the gauge eigenstates $(\widetilde{\mathrm{q}}_{\mathrm{R}}, \widetilde{\mathrm{q}}_{\mathrm{L}})$, e.g. for the lighter squark given by $\widetilde{\mathrm{q}}_1 = \widetilde{\mathrm{q}}_{\mathrm{L}} \cos(\Theta_{\widetilde{\mathrm{q}}}) + \widetilde{\mathrm{q}}_{\mathrm{R}} \sin(\Theta_{\widetilde{\mathrm{q}}})$. The off-diagonal elements of the mass matrix $\Theta_{\widetilde{\mathrm{q}}}$ are proportional to the mass of the SM partner particle, the Higgs-related parameters μ and $\tan\beta$. Therefore, the mass of the $\widetilde{\mathrm{t}}_1$, predominantly $\widetilde{\mathrm{t}}_{\mathrm{R}}$, can be small due to the large top quark mass, and the $\widetilde{\mathrm{b}}_1$ mass is expected to be light for large $\tan\beta$. For small $\tan\beta$ the $\widetilde{\mathrm{b}}_{\mathrm{L}}$ is still expected to be small due to the effects of the large top Yukawa coupling, as it is part of the doublet containing $\widetilde{\mathrm{t}}_{\mathrm{L}}$.

The following two sections review the status of the searches for models with $\widetilde{\chi}_1^0$ being the LSP (Sect. 5.1), and the $\widetilde{\mathrm{G}}$ being the LSP (Sect. 5.2).

5.1 SUSY models with $\widetilde{\chi}_1^0$ as LSP

If the third-generation squarks are lighter than gluinos, they are likely to appear in gluino decay chains. But if the gluino masses are too heavy to be produced at the LHC energy, searches for direct third-generation squark pair production might be the only way to observe them, even though these branching ratios are more than one order of magnitude lower than those for gluino–gluino production (see Fig. 4).

For top squarks, the possible decays and therewith connected search strategies depend on the masses of the accessible particles. Assuming that the $\widetilde{\mathrm{t}}_1$, the $\widetilde{\chi}_1^{\pm}$ and the $\widetilde{\chi}_1^0$ are the only accessible SUSY particles, the possible decays in the $m_{\widetilde{\mathrm{t}}_1} - m_{\widetilde{\chi}_1^0}$ parameter plane are displayed in Fig. 19.

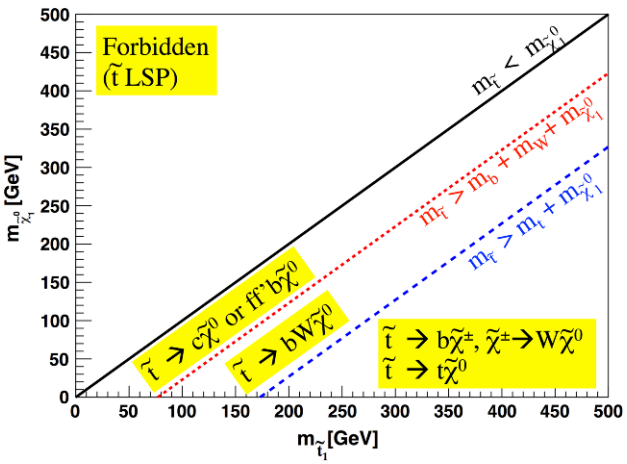

Fig. 19 Overview of the possible top squark decays depending on the mass of the $\widetilde{\mathrm{t}}_1$ and the $\widetilde{\chi}_1^0$

The most obvious decay chain is given for $m_{\tilde{t}_1} > m_t + m_{\tilde{\chi}_1^0}$: here the top squark will decay either like $\tilde{t} \to t\tilde{\chi}_1^0$ or $\tilde{t} \to b\tilde{\chi}_1^\pm$, where $\tilde{\chi}_1^\pm \to W^\pm\tilde{\chi}_1^0$, with cross sections depending on the $\tilde{\chi}_1^\pm$ mass. In both cases this gives two W bosons, resulting in a large probability to have (at least) one electron or muon in the final state. Hence, the searches requiring zero or one lepton in the final state are the strongest. Zero-lepton searches are expected to have a slightly higher reach in the $\tilde{t}_1$ mass for low $\tilde{\chi}_1^0$ masses, while one-lepton analyses tend to reach closer to the diagonal line at $m_{\tilde{t}_1} - m_{\tilde{\chi}_1^0} = m_t$. The region around this line is very difficult to cover with current searches, as the kinematics of the decay are similar to the SM top decay kinematics. An option to test this parameter space exists for cases where the $\tilde{t}_2$ is not too heavy either. A decay chain to search for would be $\tilde{t}_2 \to Z\tilde{t}_1$. Requiring same-flavor dileptons from the Z boson decay in addition to a lepton from the $\tilde{t}_1 \to t\tilde{\chi}_1^0$ decay provide a powerful background rejection [82].

When the $\tilde{t}_1$ is lighter than the top, in the region defined by $m_b + m_W + m_{\tilde{\chi}_1^0} < m_{\tilde{t}_1} < m_t + m_{\tilde{\chi}_1^0}$ the top squark will decay as $\tilde{t} \to b\tilde{\chi}_1^\pm$, with the subsequent decay $\tilde{\chi}_1^\pm \to W^\pm\tilde{\chi}_1^0$. This can best be tested with an analysis requiring two leptons and two b-tagged jets, which also has sensitivity to the three-body decay $\tilde{t} \to bW^\pm\tilde{\chi}_1^0$, which becomes important for high $\tilde{\chi}_1^\pm$ masses. Also a one-lepton search has sensitivity in this area, as shown below.

For $m_{\tilde{t}_1} < m_b + m_W + m_{\tilde{\chi}_1^0}$, the $\tilde{t}_1$ is expected to decay to $c\tilde{\chi}_1^0$. This case is best tested with a monojet analysis, which can contain a charm-tag as well, which is not yet published. The results of top squark searches are discussed in Sect. 5.1.1.

Searches for the decay of the bottom squark via $\tilde{b}_1 \to b\tilde{\chi}_1^0$, are usually performed in zero-lepton analyses requiring two b-tagged jets, as no prompt leptons are expected from b decays. If $m_{\tilde{b}_1} > m_t + m_{\tilde{\chi}_1^0}$, the decay $\tilde{b}_1 \to t\tilde{\chi}_1^-$, with $\tilde{\chi}_1^- \to W^-\tilde{\chi}_1^0$, is open as well, and searches with lepton signatures are again advisable, e.g. a same-sign dilepton search is well suited due to the low SM background in this channel. For $\tilde{b}$ decays to a bottom quark and $\tilde{\chi}_2^0$, the $\tilde{\chi}_2^0$ can decay with a certain probability to a Z or Higgs boson and $\tilde{\chi}_1^0$. The additional boson could be tagged to further reduce the background. The results of bottom squark searches are discussed in Sect. 5.1.2.

5.1.1 Search for direct top squark production

The first search [83] discussed here is focused on the direct production of two top squarks, with two possible decay modes of the top squark: $\tilde{t} \to t\tilde{\chi}_1^0$ and $\tilde{t} \to b\tilde{\chi}_1^\pm$, with $\tilde{\chi}_1^\pm \to W^\pm\tilde{\chi}_1^0$, for which a one-lepton final state is a favorable final state.

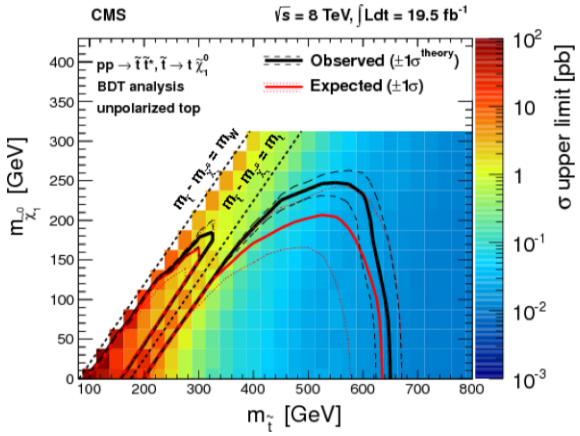

Fig. 20 Exclusion limits at 95 % CL on the top squark pair production in the top squark–LSP mass plane for a simplified model assuming $\tilde{t} \to t\tilde{\chi}_1^0$ [83]. All other sparticles are decoupled

The dominant $t\bar{t}$ background, where both W bosons decay leptonically, is reduced by the quantity m_{T2}^W, which is defined as the minimum mother particle mass compatible with all transverse momenta and mass-shell constraints [84]. This variable is similar to the m_{T2} variable (cf. Sect. 3.2). m_{T2}^W has by construction an end-point at the top-quark mass in the case of a dileptonic top-quark decay, where one lepton is not identified or lies outside the acceptance of the analysis. In the search for the decay $\tilde{t} \to t\tilde{\chi}_1^0$, the dilepton $t\bar{t}$ background is further suppressed by requiring that three of the jets in the event are consistent with the $t \to bW \to bq\bar{q}$ decay chain.

The exclusion limits are shown in Fig. 20 for the simplified model describing $\tilde{t} \to t\tilde{\chi}_1^0$. Here the top is unpolarized, and a maximum limit of 620 GeV for the top squark mass and of 225 GeV for the $\tilde{\chi}_1^0$ mass can be set. In the case of 100 % right-handed tops one would expect leptons with larger p_T leading to a larger acceptance, and hence to an extension of the limit at high masses by 25–50 GeV. Accordingly, a 100 % left-handed top would reduce the limit by the same amount. Also, one has to take into account that the simplified model assumes a probably too optimistic branching fraction of 100 %. If the branching fraction would be reduced to 60 % with no possibility to detect other decay chains, the excluded limit would drop to $m_{\tilde{t}} < 500$ GeV and $m_{\tilde{\chi}_1^0} < 125$ GeV.

Effects of similar size are also observed for the simplified model describing $\tilde{t} \to b\tilde{\chi}_1^\pm$, with $\tilde{\chi}_1^\pm \to W^\pm\tilde{\chi}_1^0$. Figure 21 shows this model for the unpolarized chargino, left–right symmetric $W\tilde{\chi}_1^0\tilde{\chi}_1^\pm$ coupling, and the mass parameter of the $\tilde{\chi}_1^\pm$ set to $m_{\tilde{\chi}_1^\pm} = xm_{\tilde{t}} + (1-x)m_{\tilde{\chi}_1^0}$ with $x = 0.5$. For a larger mass parameter (with $x = 0.75$) the excluded top squark and $\tilde{\chi}_1^0$ mass is shifted up by about 25–50 GeV, while for a lower mass parameter ($x = 0.25$) the limit becomes slightly weaker. For right-handed charginos and right-handed $W\tilde{\chi}_1^0\tilde{\chi}_1^\pm$ couplings the limit is up to 50 GeV stronger, while it is weaker for other combinations of polarizations of chargino

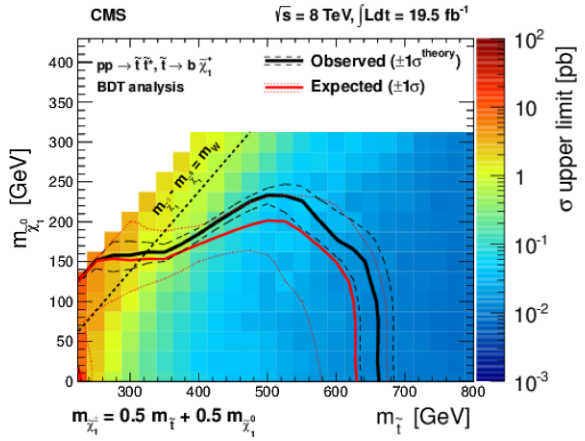

Fig. 21 Exclusion limits at 95 % CL on the top squark pair production in the top squark–LSP mass plane for a simplified model assuming $\widetilde{t} \to b\widetilde{\chi}_1^{\pm}$, with $\widetilde{\chi}_1^{\pm} \to W^{\pm}\widetilde{\chi}_1^0$. The $\widetilde{\chi}_1^{\pm}$ mass parameter is $x = 0.5$ (see text) [83]. All other sparticles are decoupled

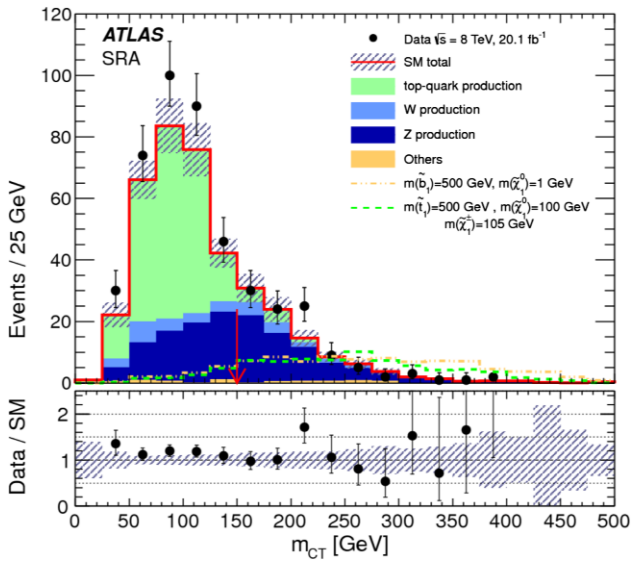

Fig. 22 The m_{CT} distribution with all selection criteria applied except for the m_{CT} thresholds [86]

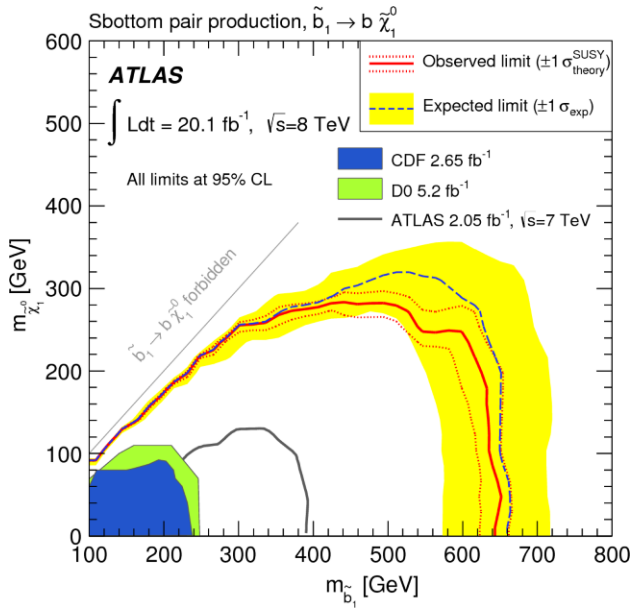

Fig. 23 Exclusion limits at 95 % CL on the bottom squark pair production in the bottom squark–LSP mass plane for a simplified model assuming $\widetilde{b} \to b\widetilde{\chi}_1^0$ [86]. All other sparticles are decoupled

and $W\widetilde{\chi}_1^0\widetilde{\chi}_1^{\pm}$ couplings. Searches for top squarks can also be performed in 2-lepton final states [85], and lead to slightly less stringent results, which are compatible with the 1-lepton search results.

In summary, top squarks around 600 GeV can be excluded for $\widetilde{\chi}_1^0$ masses lower than 200 GeV, assuming that $\widetilde{\chi}_1^{\pm}$ and $\widetilde{\chi}_1^0$ are the only lighter SUSY particles, in which case the branching fractions for the investigated decays are large. This result excludes for the first time a large part of the phase space allowed by naturalness. Here it should be mentioned that the limit is not so strong for models with rich EWKino and slepton spectra with masses below the top squark mass. In such models many more decay chains may open up, leading partly to very soft objects in the final state and therefore deteriorating the acceptance and hence the achievable limit.

5.1.2 Search for direct bottom squark production

Assuming $\widetilde{b}_1 \to b\widetilde{\chi}_1^0$, direct bottom squark production are searched for by requiring a lepton-veto, two b-tagged jets and a moderate amount of missing energy due to the LSPs ($E_{\mathrm{T}}^{\mathrm{miss}} > 150$ GeV) [86]. Further discriminating variables are the minimum angle $\Delta\phi$ between the $E_{\mathrm{T}}^{\mathrm{miss}}$ vector and either of the three highest-p_{T} jets, which is expected to be larger for signal than for background from multi-jet events, and a requirement on the contransverse mass m_{CT} (cf. Sect. 3.2), which is displayed in Fig. 22.

Figure 23 shows the exclusion limit for direct bottom squark pair production. Bottom squark masses up to 620 GeV and $\widetilde{\chi}_1^0$ masses up to 260 GeV are excluded at 95 % CL. Up to bottom squark masses of 300 GeV, mass differences of at least 50 GeV between $\widetilde{b}$ and $\widetilde{\chi}_1^0$ can be excluded. Again, these limits correspond to a branching fraction of 100 %. If a lower branching fraction of 60 % and no possibility to detect other decay chains are assumed, the limit drops to $m_{\widetilde{b}} < 520$ GeV and $m_{\widetilde{\chi}_1^0} < 150$ GeV. Note that this search is also sensitive to the direct production of top squarks with subsequent decay to $\widetilde{t} \to b\widetilde{\chi}_1^{\pm}$, with $\widetilde{\chi}_1^{\pm} \to W^{\pm}\widetilde{\chi}_1^0$. The sensitivity of this search is comparable to the one-lepton search discussed above for small chargino–neutralino mass differences of a few GeV, where the leptons are too soft to be detected.

The results of the same-sign dilepton search [74], discussed in Sect. 4.1.2, can also be interpreted in terms of

a direct bottom squark search, where the bottom squarks are pair-produced and then each decay as $\tilde{b} \to t\tilde{\chi}_1^-$, with $\tilde{\chi}_1^- \to W^-\tilde{\chi}_1^0$ (and charge conjugate, respectively). Here, same-sign dileptons can originate from leptonic top-quark and W-boson decays. Bottom squark masses below 500 GeV can be excluded for chargino masses up to 350 GeV and neutralino masses up to 150 GeV, if $m_{\tilde{\chi}_1^0}/m_{\tilde{\chi}_1^\pm} = 0.5$. Slightly higher neutralino masses, up to 180 GeV can be excluded for $m_{\tilde{\chi}_1^0}/m_{\tilde{\chi}_1^\pm} = 0.8$.

In summary, directly produced bottom squark have been searched for the first time in the region predicted by naturalness. Bottom squark masses below 600 GeV up to $\tilde{\chi}_1^0$ masses of 250 GeV can be excluded assuming large branching fractions to the examined final states.

5.2 SUSY models with $\tilde{G}$ as LSP

GMSB models where only the $\tilde{t}_R$ and the higgsinos are accessible [87] provide a perfect example of a natural scenario. The lightest chargino and the two lighter neutralinos are almost pure higgsinos and therefore nearly mass degenerate, which corresponds to scenario (c) of Fig. 2. The following decay is therefore considered: $\tilde{t}_R \to \tilde{\chi}_1^+ b \to ff'\tilde{\chi}_1^0 b \to ff' h^0(\to \gamma\gamma, b\bar{b})\tilde{G}b$ where f and f′ are low-energetic quarks or leptons. SM background events are suppressed by requiring the invariant mass of two photons to be within the Higgs mass window, exploiting the sidebands for the background estimation. In addition, two b-tagged jets are required, originating from the top squark decay. As shown in Fig. 24, top squark masses below 360 to 410 GeV are excluded, depending on the higgsino mass. Note that the direct $\tilde{\chi}_1^+\tilde{\chi}_1^-$ production channel can have a similar final state when b-tagged jets are coming from one of the h^0. Considering this decay therefore increases the sensitivity for low $\tilde{\chi}_1^0$ mass and top squark mass above 300 GeV, where the $\tilde{\chi}_1^+\tilde{\chi}_1^-$ production cross section dominates over direct top squark production.

For the top squark decay considered, other final states can occur as well. First the two Higgs bosons could decay as $h^0 \to ZZ \to llll$ instead of $\gamma\gamma/b\bar{b}$. Second the lightest neutralino could also decay as $\tilde{\chi}_1^0 \to Z(\to ll)\tilde{G}$ giving Zh^0 or even ZZ final states. In all of these cases, the multi-lepton analysis [81], described in Sect. 4.2, is particularly sensitive. Models with a branching ratio of 100 % for $\tilde{\chi}_1^0 \to Z\tilde{G}$ and a branching ratio of 50 % for each $\tilde{\chi}_1^0$ decay are considered. As shown in Fig. 25, for a branching ratio of 100 % to Z bosons and $\tilde{G}$, top squark masses below 510 GeV can be excluded for $\tilde{\chi}_1^\pm$ masses of up to 450 GeV. The limits for the other two cases are weaker.

In summary, the mass reach of GMSB top squark searches is about 200 GeV weaker than for models with $\tilde{\chi}_1^0$ as LSP. No dedicated bottom squark search in the GMSB model is published yet, but a similar limit should be obtained since the final-state $\tilde{b}_1 \to \tilde{\chi}_1^0 b$ is very similar to that of the top squark ($\tilde{t}_1 \to \tilde{\chi}_1^+ b \to ff'\tilde{\chi}_1^0$) when the low-energetic fermions f and f′ are not reconstructed.

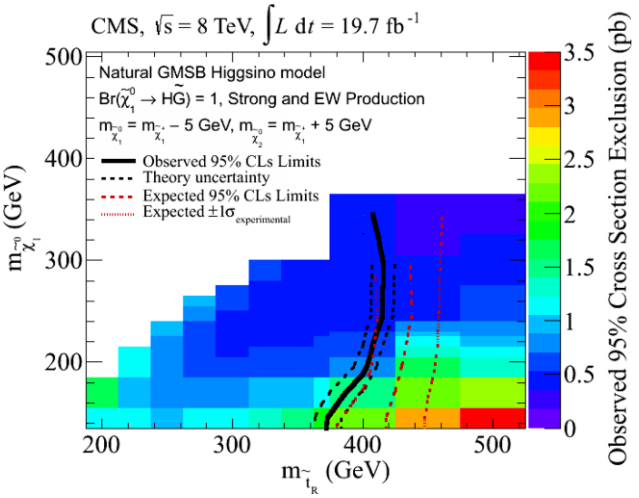

Fig. 24 Exclusion limits at 95 % CL on the top squark pair production in the top squark–LSP mass plane for a simplified model assuming $\tilde{t}_R \to \tilde{\chi}_1^+ b$. Further assumptions are that $\tilde{\chi}_1^+$ is higgsino-like, $\tilde{\chi}_1^0$ is the NLSP decaying as $\tilde{\chi}_1^0 \to h^0\tilde{G}$ and $\tilde{G}$ is the LSP [87]

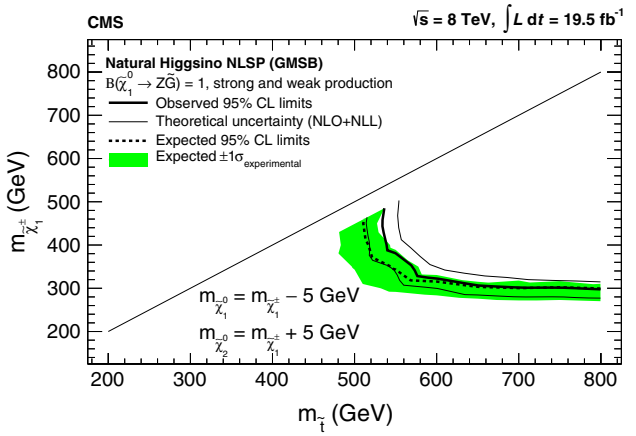

Fig. 25 Exclusion limits at 95 % CL on the top squark pair production in the top squark–LSP mass plane for a simplified model assuming $\tilde{t} \to \tilde{\chi}_1^+ b$. Further assumptions are that $\tilde{\chi}_1^+$ is higgsino-like, $\tilde{\chi}_1^0$ is the NLSP decaying as $\tilde{\chi}_1^0 \to Z\tilde{G}$ and $\tilde{G}$ is the LSP [81]

6 Electroweak SUSY sector

In natural SUSY, many weakly interacting particles are expected to be close to the EW scale. Searches for neutral and charged Higgses with positive R-parity are presented in Sect. 6.1. Searches for partners of the Higgses and electroweak gauge bosons, called electroweakinos (EWKinos), are discussed in Sect. 6.2. Finally, the limits on the sleptons are discussed in Sect. 6.3.

6.1 SUSY Higgses

As already mentioned in Sect. 2, the Higgs boson discovered is assumed to be the lightest neutral Higgs of the MSSM (h^0). It is worth to note that a value of 126 GeV is close to the upper mass bound possible for h^0 in MSSM and requires O(1 TeV) top squark mass or a fine-tuned value of top squark mixing. This creates a tension with the natural SUSY spectrum where the top squark mass should be 600 GeV maximum. Results of searches are extensively discussed in [9] of this review. This section therefore proposes only a short summary.

Extra neutral and charged Higgses, which preferentially couple to the most massive down-type fermions, are actively searched. At tree level, their masses only depend on $\tan\beta$ and m_{A^0}.[9] At LHC, neutral Higgses are produced singly or accompanied by b-jet(s) and decay via $\tau^+\tau^-$, $b\bar{b}$ and more marginally $\mu^+\mu^-$ final states. Charged Higgses with lower masses than the top quark will predominantly appear in the top decay via $t \to bH^{\pm}$. When charged Higgses have higher masses than the top quark, they will be produced in association with top and bottom quarks. In both cases, they mainly decay via $H^{\pm} \to \tau^{\pm}\nu$. Results from searches favor neutral and charged SUSY Higgses with masses higher than h^0, even if no model-independent limits exist yet.

It is worth to mention that more intricate searches are also investigated. For example, searches for a topology in which a H^0 decays via a cascade of lighter charged and neutral Higgs bosons[10] have been performed by ATLAS [88].

6.2 EWKinos

As discussed in Sect. 2, neutralino and chargino masses are obtained by mixing gauge eigenstates. The sensitivity to the three typical scenarios shown in Fig. 2 and corresponding to (a) bino-like, (b) wino-like, and (c) higgsino-like $\widetilde{\chi}_1^0$ are now reviewed both for $\widetilde{\chi}_1^0$ (Sect. 6.2.1) and the gravitino (Sect. 6.2.2) being the LSP.

6.2.1 SUSY models with $\widetilde{\chi}_1^0$ as LSP

At LHC, most efforts concentrate on processes involving the two lightest neutralinos ($\widetilde{\chi}_1^0$, $\widetilde{\chi}_2^0$) and the lightest chargino ($\widetilde{\chi}_1^{\pm}$). Assuming that the EWKinos are the lightest sparticles of the spectrum (Fig. 3), the main production occurs via the s-channel exchange of a virtual gauge boson. EWKinos then naturally decay as $\widetilde{\chi}_2^0 \to Z/h^{0(*)}\widetilde{\chi}_1^0$ and $\widetilde{\chi}_1^{\pm} \to W^{(*)}\widetilde{\chi}_1^0$. Given the low values of cross sections compared to SM backgrounds, searches are conducted most of the times for leptonic decays of Z and W, giving 1–4 leptons + $E_{\mathrm{T}}^{\mathrm{miss}}$ final states. Note that an excess in these channels could well be the only SUSY signal at LHC if colored sparticles are too heavy or decay through intricate chains.

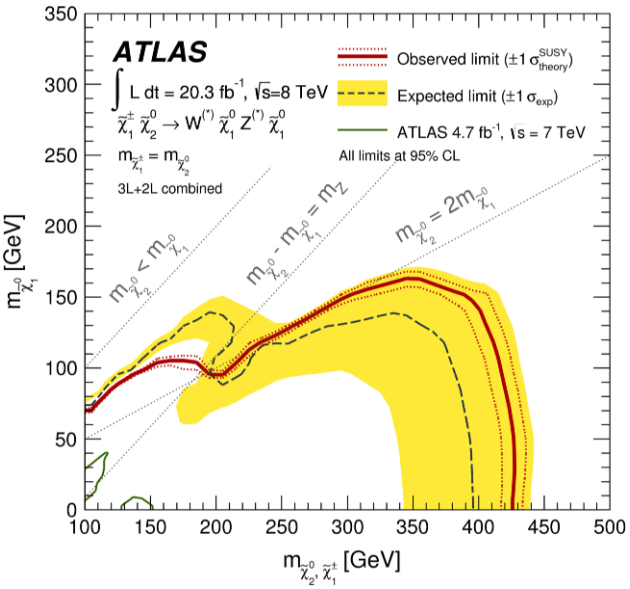

Fig. 26 Exclusion limits at 95 % CL on the $\widetilde{\chi}_1^{\pm}\,\widetilde{\chi}_2^0$ production in the $\widetilde{\chi}_1^{\pm}$-LSP mass plane [76] for a simplified model assuming $\widetilde{\chi}_1^{\pm}$ and $\widetilde{\chi}_2^0$ are mass degenerate and decay via $\widetilde{\chi}_1^{\pm} \to W^{\pm(*)}\widetilde{\chi}_1^0$ and $\widetilde{\chi}_2^0 \to Z^{0(*)}\widetilde{\chi}_1^0$. All other SUSY particles are decoupled

At LHC, scenario (a) with bino-like $\widetilde{\chi}_1^0$ and wino-dominated $\widetilde{\chi}_2^0$ and $\widetilde{\chi}_1^{\pm}$ is the most favorable scenario, especially when the mass difference between $\widetilde{\chi}_2^0$ and $\widetilde{\chi}_1^{\pm}$ and the LSP allows for on-shell Z, h^0, and W. The highest cross section is coming from $\widetilde{\chi}_1^{\pm}\widetilde{\chi}_2^0$ production, covered by a 3-lepton + $E_{\mathrm{T}}^{\mathrm{miss}}$ search. Most sensitive signal regions require the three leptons to be electrons or muons (the leading one should have $p_{\mathrm{T}} > 25$ GeV) and the invariant mass of the two same-flavor opposite-sign leptons (m_{SFOS}) to be close to the Z-boson mass. Further discrimination is obtained by selecting ranges of $E_{\mathrm{T}}^{\mathrm{miss}}$ and m_{T} (formed with $E_{\mathrm{T}}^{\mathrm{miss}}$ and the lepton not forming the SFOS lepton pair). The search sensitivity is driven by the ability to reduce and control the WZ background. Assuming mass degeneracy between $\widetilde{\chi}_1^{\pm}$ and $\widetilde{\chi}_2^0$, stringent limits are obtained on EWKinos: $m_{\widetilde{\chi}_2^0,\widetilde{\chi}_1^{\pm}} <$ 340 GeV for LSP masses lower than 70 GeV are excluded [89].[11] Recent efforts were made to cover the case where Z and/or W are not on-shell and where h^0 is present in the decay. This is done by considering bins of m_{SFOS} outside the Z-mass and requiring the presence of tau-lepton(s). In this case the reducible background coming from jets or photons faking leptons is also of importance and could dominate over WZ, altering the sensitivity to this more compressed EWKino

[9] For charged Higgses $m^2_{H^{\pm}} = m^2_A + m^2_W$ at tree level. Other SUSY parameters enter via radiative corrections and are fixed to particular benchmark values, chosen to exhibit certain MSSM features.

[10] $H^0 \to W^{\mp}H^{\pm} \to W^{\mp}W^{\pm}h^0 \to W^{\mp}W^{\pm}b\bar{b}$.

[11] Note that with no mass degeneracy these upper bounds can be significantly lower.

mass spectrum. However, together with the increase in luminosity and $\sqrt{s}$, this provides considerable improvement over 7 TeV results, even if the compressed scenario case still has poor sensitivity.

The 3-lepton + $E_{\mathrm{T}}^{\mathrm{miss}}$ final state is less favorable for scenario (a) where $M_1 \ll \mu < M_2$, since the $\widetilde{\chi}_1^{\pm}\widetilde{\chi}_2^0$ production cross section is divided by 3 due to the lower coupling of the higgsino to SM gauge bosons. Similarly scenario (b) suffers from the too large $\widetilde{\chi}_1^{\pm}$–$\widetilde{\chi}_2^0$ mass difference. Finally, no sensitivity is expected from scenario (c) because of the closeness of $\widetilde{\chi}_1^{\pm}$, $\widetilde{\chi}_2^0$, and $\widetilde{\chi}_1^0$, resulting in too soft objects in the final state. To partially recover the sensitivity, other channels with 2-lepton + $E_{\mathrm{T}}^{\mathrm{miss}}$ final state targeting the search for $\widetilde{\chi}_1^+\widetilde{\chi}_1^- \rightarrow \mathrm{W}^+(\rightarrow 1^+\nu)\mathrm{W}^-(\rightarrow 1^-\nu)\widetilde{\chi}_1^0\widetilde{\chi}_1^0$ and $\widetilde{\chi}_1^+\widetilde{\chi}_2^0 \rightarrow \mathrm{W}^+(\rightarrow \mathrm{qq}')\mathrm{Z}^0(\rightarrow 1^-1^+)\widetilde{\chi}_1^0\widetilde{\chi}_1^0$ are being developed [76]. In scenario (a) for massless $\widetilde{\chi}_1^0$, the former excludes chargino masses in the range $100 < m_{\widetilde{\chi}_1^{\pm}} < 160$ GeV while the latter extends further the $\widetilde{\chi}_1^{\pm}/\widetilde{\chi}_2^0$ mass limit to 410 GeV; see Fig. 26. Other modes like $\widetilde{\chi}_1^+\widetilde{\chi}_1^0 \rightarrow \mathrm{W}^+(\rightarrow 1^+\nu)\widetilde{\chi}_1^0\widetilde{\chi}_1^0$ and $\widetilde{\chi}_2^0\widetilde{\chi}_1^0 \rightarrow \mathrm{Z}^0(\rightarrow 1^+1^-)\widetilde{\chi}_1^0\widetilde{\chi}_1^0$ are not yet explored due to the very low cross section and overwhelming inclusive W and Z cross section. Finally, even in the most favorable scenario (a), $\widetilde{\chi}_1^0\widetilde{\chi}_1^0$ and $\widetilde{\chi}_2^0\widetilde{\chi}_2^0$ productions are heavily suppressed at production level—O(1 fb) for 100 GeV $\widetilde{\chi}$ mass—and cannot be searched for at LHC even in dedicated monojet analyses [90,91].

6.2.2 SUSY models with $\widetilde{G}$ as LSP

As for the strong production, new final states and search possibilities can emerge when the gravitino is the LSP. In scenario (a), the final state will contain two additional photons, reducing drastically the background from gauge bosons and therefore increasing the reach in mass. Reinterpreting the two 2-photons + $E_{\mathrm{T}}^{\mathrm{miss}}$ analysis described in Sect. 4.2, and considering $\widetilde{\chi}_1^{\pm}\widetilde{\chi}_1^0$ production which have the highest cross section, exclude $m_{\widetilde{\chi}_1^{\pm}} < 500$ GeV independently of the $\widetilde{\chi}_1^0$ mass [77]. Similarly scenario (b) implies $\widetilde{\chi}_1^{\pm} \rightarrow \mathrm{W}^+\widetilde{\mathrm{G}}$ and $\widetilde{\chi}_1^0 \rightarrow \gamma/\mathrm{Z}\widetilde{\mathrm{G}}$ and it could be searched for in the 1-lepton + 1-photon channel, but no publication exists yet. Finally, scenario (c) is accessible thanks to the decay $\widetilde{\chi}_1^0 \rightarrow \gamma/\mathrm{Z}/\mathrm{h}^0\widetilde{\mathrm{G}}$ where the branching ratios to γ, Z, and h^0 depend primarily on $\tan\beta$ and on the mass difference between $\widetilde{\chi}_1^0$ and $\widetilde{\mathrm{G}}$. In the case of Z-rich higgsino (low $\tan\beta$ value and positive μ), final states with 4-leptons + $E_{\mathrm{T}}^{\mathrm{miss}}$ or 2-leptons + 2-jets will provide interesting sensitivity, as shown in Fig. 27 for the 2011 LHC data [92]. Mixed Z/h^0 (higher $\tan\beta$ value) scenarios can be covered by 2-leptons + 2b + $E_{\mathrm{T}}^{\mathrm{miss}}$ final states. h^0-rich higgsino scenarios (low $\tan\beta$ value and negative μ) can be covered by 4b + $E_{\mathrm{T}}^{\mathrm{miss}}$.

More complicated situations can occur beyond the three scenarios discussed in Fig. 2. For example, if M_1 and μ are approximately equal and the NLSP is a bino/higgsino admixture, large branching ratios to photons and Higgs bosons are generated. The 1b + photon + $E_{\mathrm{T}}^{\mathrm{miss}}$ final state, described in Sect. 4.2, can exclude $\widetilde{\chi}_1^0$ masses between 200 and 400 GeV, see Fig. 18.

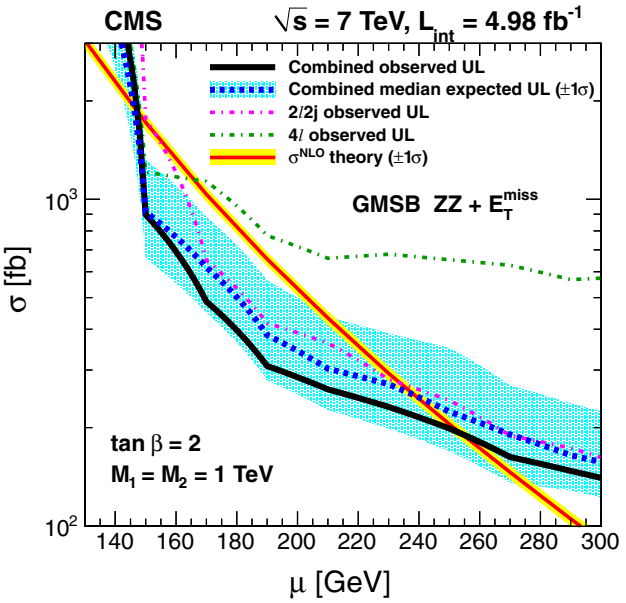

Fig. 27 Exclusion limits at 95 % CL on the production cross section of higgsino-like EWKinos $\widetilde{\chi}_1^0$, $\widetilde{\chi}_2^0$,$\widetilde{\chi}_1^{\pm}$. The decay of the NLSP $\widetilde{\chi}_1^0 \rightarrow \mathrm{Z}^{0(*)}\widetilde{\mathrm{G}}$ is forced and all other SUSY particles are decoupled [92]

In conclusion, EWKino searches provide presently much weaker constraints on the natural SUSY scenario than the strong production searches. Limits are still model-dependent and rely on many assumptions. More results are still expected in the near future, and ultimately the limits should be set in the pMSSM to understand better how complete the current searches are. Given that, it is fair to say that a complete exploration of this sector is still to come and will greatly benefit from the high luminosity program of LHC.

6.3 Sleptons

Sleptons ($\widetilde{\mathrm{e}}$, $\widetilde{\mu}$, $\widetilde{\tau}$, and $\widetilde{\nu}$) are governed by five parameters: masses of the left-handed and right-handed $\widetilde{\mathrm{e}}/\widetilde{\mu}$, which are assumed to be mass degenerate in the MSSM, masses of the left-handed and right-handed staus and the stau mixing angle. $\widetilde{\nu}$ masses can be related to the charged slepton parameters. From naturalness arguments O(1 TeV) slepton masses are expected: the very low slepton production cross section, see Fig. 4, will therefore prevent their discovery. However, searching for O(500 GeV) sleptons could be achievable with high luminosity. The reason is that these very low cross sections with respect to EWKino production, are largely recovered by the more favorable branching ratio $\mathrm{BR}(\widetilde{\mathrm{l}}^+ \rightarrow 1^+\widetilde{\chi}_1^0) = 100$ % compared to leptonic branching

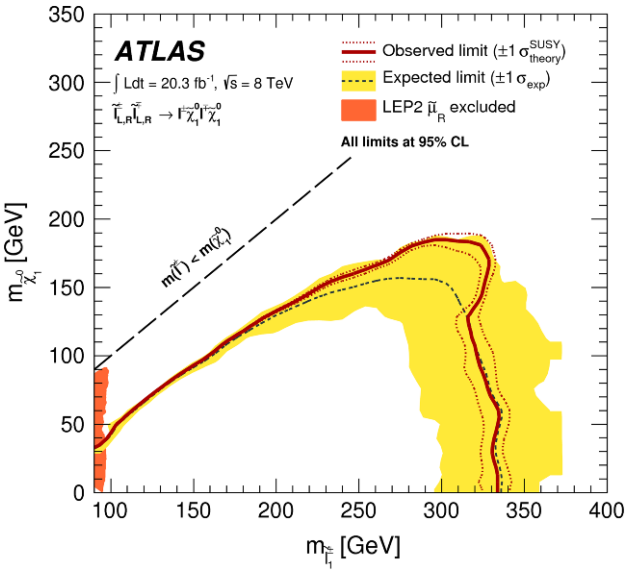

Fig. 28 Exclusion limits at 95 % CL on the slepton–slepton production in the slepton-LSP mass plane. The slepton decay $\widetilde{l} \to l\widetilde{\chi}_1^0$ is forced and all other SUSY particles are decoupled [93]

ratios of W and Z. Lepton searches rely almost entirely on the very powerful discriminant variables like m_{T2} or m_{CT} and electron(s) or muon(s) in the final states (presently no sensitivity is obtained for staus). Like in the direct bottom squark search (Fig. 22), the edge of slepton events with $m_{\widetilde{l}} - m_{\widetilde{\chi}_1^0} > O(100\,\text{GeV})$ appears far above the top and WW background ones.

The most promising final state is 2-lepton + E_T^{miss}, coming from $\widetilde{l}^+\widetilde{l}^- \to l\bar{l}\widetilde{\chi}_1^0\widetilde{\chi}_1^0$. Mass degenerate left- and right-handed selectrons and smuons are excluded below 325 GeV masses for massless neutralinos, largely exceeding the LEP limit for right-handed smuons as shown in Fig. 28 [93]. Upper limits for left- and right-handed slepton masses are also obtained and give 250 GeV and 300 GeV for massless neutralinos.

Direct slepton production can also be accessed when the gravitino is the LSP. Various final states can be considered depending on the nature of the NSLP generating final states very similar to the EWKino searches. A particular interesting one corresponds to the NSLP slepton scenario where right-handed $\widetilde{e}/\widetilde{\mu}$ decay to an electron/muon and a right-handed $\widetilde{\tau}_R$ gives a tau and a gravitino. This generates a multi-lepton final state where the lepton multiplicity depends on the tau decay [81]. $\widetilde{\tau}_R$ masses can then be excluded up to 200 GeV.

To be complete, a very favorable situation arises if the sleptons are interleaved between $\widetilde{\chi}_2^0/\widetilde{\chi}_1^\pm$ and $\widetilde{\chi}_1^0$ in scenario (a). Two cases can be envisaged: assume that all sleptons are mass degenerate (a1) and consider that only $\widetilde{\tau}$ and $\widetilde{\nu}_\tau$ are light (a2). In both cases, the EWKinos will couple to the sleptons generating 2-leptons + E_T^{miss} and 3-lepton + E_T^{miss} final states with higher $\sigma \times$ BR than in the direct slepton or direct EWKino case discussed previously in this section. If the slepton masses are exactly in between $\widetilde{\chi}_2^0/\widetilde{\chi}_1^\pm$ and $\widetilde{\chi}_1^0$, mass limits reached in Fig. 26 are increased by a factor 2 to 3 for scenario (a1) and remain similar for scenario (a2) [89].

7 Escape routes: *R*-parity violation, long-lived particle searches and beyond MSSM signatures

Given the absence of signal from plain vanilla MSSM signatures, it is of paramount importance to look at scenarios where *R*-parity is violated (Sect. 7.1) and/or sparticle decays are not prompt (Sect. 7.2). In both cases, the stringent limits discussed in Sects. 4, 5 and 6 generally do not apply. Pushing further this idea, sensitivity to signatures appearing in scenarios beyond MSSM are also discussed in Sect. 7.3.

7.1 *R*-parity violation searches

R-parity conservation implies pair production of the superpartners and requires the lightest superpartners to be stable, leading to typical missing transverse energy signatures in the detector. If *R*-parity is not conserved these constraints do not exist anymore and dedicated searches need to be performed.

In RPV scenarios, the current limits of the proton decay can be met if only either *B* or *L* (and not both) is violated and the violation is sufficiently small [94]. Such models can also accommodate non-zero neutrino masses and neutrino oscillations. The RPV superpotential W_{RPV} includes three trilinear terms parameterized by the 48 Yukawa couplings λ_{ijk}, λ'_{ijk}, λ''_{ijk}:

$$W_{RPV} = \frac{1}{2}\lambda_{ijk} L_i L_j \bar{E}_k + \lambda'_{ijk} L_i Q_j \bar{D}_k + \lambda''_{ijk} \bar{U}_i \bar{D}_j \bar{D}_k, \quad (3)$$

where i, j, k are generation indices, L and Q the $SU(2)_L$ doublet superfields of the leptons and quarks, and $\bar{E}$, $\bar{D}$ and $\bar{U}$ the $SU(2)_L$ singlet superfields of the charged leptons and the up- and down-type quarks.

The nature of the LSP—which is neutral and colorless in *R*-parity conserving models—might be different in RPV models and might be charged and/or carry color as well.

Searches for models with leptonic RPV interactions ($\lambda_{ijk} \neq 0$ or $\lambda'_{ijk} \neq 0$) are discussed in Sects. 7.1.1 and 7.1.2, respectively, while the quark RPV interactions ($\lambda''_{ijk} \neq 0$) are reviewed in Sect. 7.1.3. Because of present constraints on RPV couplings, the values considered are generally in the range $O(10^{-2}-10^{-5})$. If the phase space for the LSP decay is very small ($\lambda < 10^{-5}$), it might also be long-lived. Such cases are covered in Sect. 7.2.

7.1.1 Search for leptonic RPV interactions ($\lambda_{ijk} \neq 0$)

With leptonic RPV interactions, multi-lepton final states are expected, which is particularly favorable at LHC where the

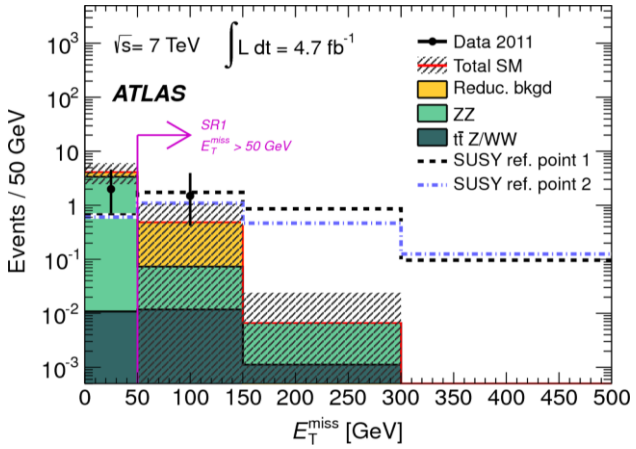

Fig. 29 $E_{\mathrm{T}}^{\mathrm{miss}}$ distribution for events with at least four leptons and no Z-boson candidates. 'SUSY ref. point 1' is a simplified model point defined by $m_{\widetilde{\chi}_1^{\pm}} = 500$ GeV and $m_{\widetilde{\chi}_1^0} = 300$ GeV, while 'SUSY ref. point 2' is a MSUGRA/CMSSM model point defined by $m_{1/2} = 860$ GeV and $\tan\beta = 37$ [95]

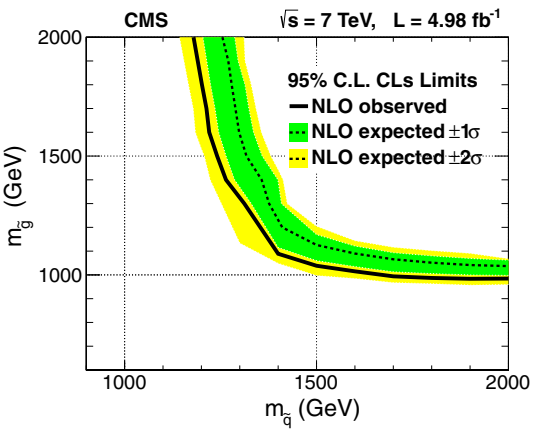

Fig. 30 Exclusion limits at 95 % CL in the squark and gluino mass plane for a GMSB RPV model with $\lambda_{123} = 0.05$ [97]

QCD background overwhelmingly dominates. The plethora of models considered is discussed in terms of the same order as for the RPC models, starting with strong production, then focusing on the third-generation, EWKino production and, finally, slepton production.

As a first example, a search with four or more leptons (electrons or muons) in the final state is discussed [95]. A non-zero coupling of λ_{121} is chosen as a representative model. To veto low-energy resonances, the invariant mass of any opposite-sign same-flavor pair must be above 20 GeV and outside a window around the Z-boson mass. Two signal regions according to different signal scenarios are defined. The first one requires $E_{\mathrm{T}}^{\mathrm{miss}} > 50$ GeV to be sensitive to models with missing energy originating from neutrinos. As an illustration, the $E_{\mathrm{T}}^{\mathrm{miss}}$ distribution is displayed in Fig. 29. The other one is tuned to scenarios with a large multiplicity of high-p_{T} objects originating from heavier sparticles, by requiring $m_{\mathrm{eff}} > 300$ GeV.

The strong production case is considered by looking at a full model, taken from Ref. [96], and tested in a MSUGRA/CMSSM parameter plane ($m_{1/2}$, $\tan\beta$), for m_0, A_0 both zero, μ positive, and $\lambda_{121} = 0.032$ at the unification scale. In this model, the $\widetilde{\tau}_1$ is the LSP and it decays through a virtual slepton or sneutrino as $\widetilde{\tau}_1 \to \tau e\mu\nu_{\mathrm{e}}$ or $\widetilde{\tau}_1 \to \tau ee\nu_{\mu}$. Values of $m_{1/2}$ below 820 GeV are excluded for $10 < \tan\beta < 40$. Note, however, that weak processes contribute to the SUSY pair production, dominating for $m_{1/2} > 600$ GeV. Therefore, a corresponding gluino mass below 1 TeV is excluded in this model.

Multi-lepton final states can also arise when gravitino is the LSP and all right-handed sleptons are flavor degenerate —known as slepton co-NLSP scenario. Pair-produced gluinos and squarks eventually decay to the $\widetilde{\chi}_1^0$, which further decays to a slepton and a lepton, with the (right-handed) slepton decaying further to another lepton and the gravitino, yielding four leptons in the final state. Gluino masses below 1.2 TeV and squark masses below 1 TeV can be excluded with a 7 TeV analysis [97], assuming an RPV coupling of $\lambda_{123} = 0.05$, as shown in Fig. 30.

Leptonic RPV interactions can also arise in a search for direct top squark production [98], where each top squark decays to a top quark and an intermediate on- or off-shell bino which decays further through leptonic RPV interactions (λ_{122} or λ_{233}), via $\widetilde{\chi}_1^{0*} \to l_i + \nu_j + l_k$ or $\widetilde{\chi}_1^{0*} \to \nu_i + l_j + l_k$, where the indices i, j, k refer to the ones in Eq. (3). The signature of direct top squark pair production with RPV decays is different from the one of RPC models, which implies a large amount of missing energy. In the RPV search, three or more isolated leptons (including hadronic τ candidates) and one or more b-tagged jets are required, but only low $E_{\mathrm{T}}^{\mathrm{miss}}$. Instead m_{eff} is used as discriminating variable.

The limits are extracted in the bino top squark mass plane, and found to be approximately independent of the bino mass. Top squark masses below 1020 GeV can be excluded for bino masses of 200 to 1300 GeV for a non-zero λ_{122}, and top squark masses below 820 GeV for a non-zero λ_{233}.

The results of the 4-lepton + $E_{\mathrm{T}}^{\mathrm{miss}}$ search [95], discussed at the beginning of this section, can also be interpreted in a simplified model where the lightest chargino and neutralino are the only sparticles with masses below the TeV scale. The pair-produced charginos decay each into a W boson and bino-like $\widetilde{\chi}_1^0$ as in scenario (a) of Fig. 2. The LSP then decays through a virtual slepton or sneutrino as $\widetilde{\chi}_1^0 \to \mathrm{e}\mu\nu_{\mathrm{e}}$ or $\widetilde{\chi}_1^0 \to \mathrm{ee}\nu_{\mu}$ with a branching fraction of 50 % each. The width of the $\widetilde{\chi}_1^0$ is fixed to 100 MeV to ensure prompt decays. Choosing the best expected limit for each of the model points, with the $\sqrt{s} = 7$ TeV data, chargino masses up to about 500 GeV are excluded for LSP masses between 100 and 540 GeV in the simplified model.

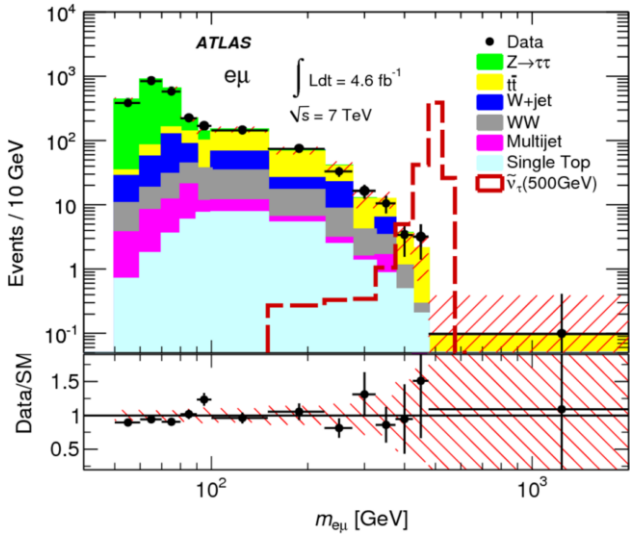

Fig. 31 Observed and predicted invariant eμ-mass distribution. Signal simulations are shown for sneutrino mass of 500 GeV, $\lambda'_{311} = 0.11$, and $\lambda_{132} = 0.07$ [99]

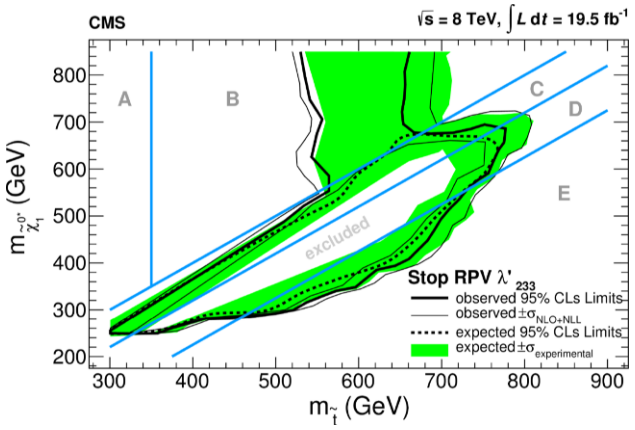

Fig. 32 Exclusion limits at 95 % CL for RPV top squark decay in the top squark-LSP mass plane with non-zero λ'_{233} coupling. The region inside the curve is excluded. The different regions, A, B, C, D, and E, mark different kinematic regions with different top squark decay products [98]

In RPV SUSY, single sneutrinos can be produced via λ'_{311} coupling and then decay through λ_{ijk} couplings to lepton pairs of different flavor. Searches for such scenarios have been performed in all possible combinations of different-flavor dilepton selections [99]. An example for a possible signal that is compatible with current exclusion limits on the strength of the RPV interactions from precision low-energy experiments [100], expectation, is given in Fig. 31 for the eμ channel. Sneutrino masses of up to 1.6 TeV are excluded in the eμ selection (for $\lambda'_{311} = 0.11$ and $\lambda_{132} = 0.07$), where the mass resolution is better than in the channels including hadronically decaying tau leptons. The latter lead to sneutrino mass exclusion limits of the order of 1.1 TeV for the same RPV interaction strength.

To summarize, as leptonic RPV interactions usually lead to signatures with many leptons, most scenarios are well covered with the current searches, and often result in sparticle mass limits that are stronger than those of RPC searches.

7.1.2 Search for semi-leptonic RPV interactions ($\lambda'_{ijk} \neq 0$)

Such signatures are specifically covered by the HERA experiments [101,102], which put stringent limits on the coupling between the first and second generation due to the nature of the unique $e^{\pm}p$ accelerator. Therefore, LHC searches focus more on the third generation, as detailed below.

Signatures of models where the top squarks are light, while the other squarks and gluinos are decoupled, resemble those of third-generation leptoquarks. Trilinear RPV operators allow the lepton-number-violating decay $\tilde{t}_1 \to \tau b$ with a coupling $\lambda'_{333} \neq 0$, resulting in the same final state as from third-generation leptoquark decay, with similar kinematics. They can be tested by dedicated searches for τ and b quarks in the final state [103]. With 7 TeV data, top squarks up to 525 GeV are excluded assuming a simplified model with a branching ratio of 100 % for $\tilde{t}_1 \to \tau b$.

The top squark search [98], discussed in Sect. 7.1.1, can also be exploited for semileptonic RPV interactions (λ'_{233}), via $\tilde{\chi}_1^{0*} \to l_i + q_j + q_k$ or $\tilde{\chi}_1^{0*} \to \nu_i + q_j + q_k$, where the indices i, j, k refer to the ones in Eq. (3). Limits are set for λ'_{233}, where different kinematic regions lead to different allowed decays, ranging from two-body decays (for $m_t + m_{\tilde{\chi}_1^0} < m_{\tilde{t}_1}$) to four-body decays (e.g. for $m_{\tilde{\chi}_1^0} > m_{\tilde{t}_1} > 2m_t$). The resulting excluded region is shown in Fig. 32.

In summary, the signatures of semi-leptonic RPV interactions are similar to those expected in leptoquark decays. The LHC experiments can complement these searches with analyses including the third generation, where the most stringent limits up to now could be achieved.

7.1.3 Search for quark RPV interactions ($\lambda''_{ijk} \neq 0$)

The quark RPV interactions described by λ''_{ijk} can be well tested with multi-jet resonance searches [104,105]. We here discuss an analysis searching for three-jet resonances [106], which tests two different RPV Yukawa couplings. While one search is inclusive, testing λ''_{122}, the other one requires at least one jet of each resonance decay to be b-tagged and is sensitive to λ''_{113} and λ''_{223}. The jet-ensemble technique [107,108] is used to combine the six highest-p_T jets into all possible unique triplets.

Limits are set on the gluino pair-production cross section times the branching fraction as a function of the gluino mass, as shown in Fig. 33. Gluinos with masses below 650 GeV decaying to light-flavor jets can be excluded. Decays includ-

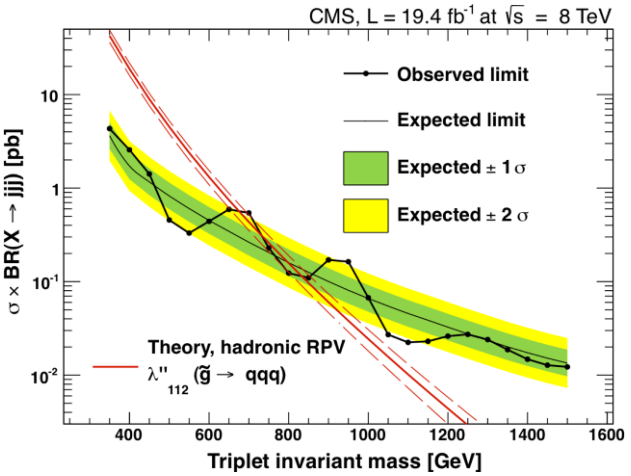

Fig. 33 Exclusion limits at 95 % CL on the production cross section of pair-produced gluinos for the inclusive RPV multi-jet search [106]

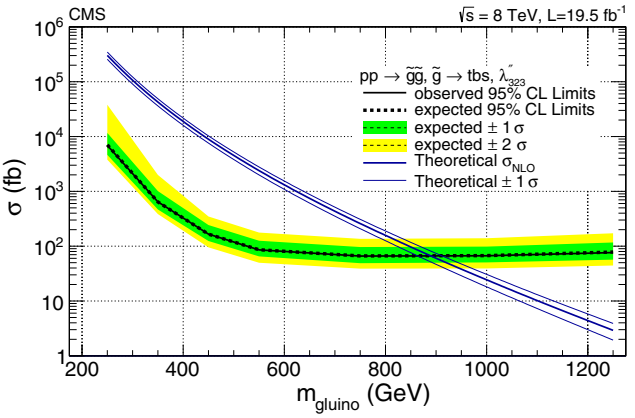

Fig. 34 Exclusion limits at 95 % CL on the production cross section of pair-produced gluinos for the same-sign dilepton analysis including heavy-flavor jets [74]

ing heavy-flavor jets can be excluded for even larger gluino masses, between 200 and 835 GeV.

Two other approaches exist. The first one counts the number of six-jets events above a given p_T threshold to search for high mass gluinos and the second one takes profit of the large boost of the low-mass gluinos [109]. With 7 TeV data, gluino masses up to 666 and 255 GeV can be excluded, respectively. The limit of the first approach is expected to reach 1 TeV with 8 TeV data.

Another scenario is given by a gluino decay to two quarks and one $\widetilde{\chi}_1^0$, which then further decays through a λ''_{ijk} interaction to three quarks, leading to final states with ten jets when gluino pair production is assumed. A search for such scenarios is currently performed, but it has not yet been published.

The results of the same-sign dilepton search [74], discussed in Sect. 4.1.2, can also be interpreted in an RPV model, where gluinos are pair-produced and decay to three quarks via $\widetilde{g} \to \text{tbs}(\bar{t}\bar{b}\bar{s})$, testing the λ''_{323} coupling. In this decay 50 % of the W bosons are expected to be same-sign, when both W bosons decay leptonically. As shown in Fig. 34, gluino masses up to 860 GeV can be excluded.

In summary, a plethora of models with different RPV interactions exists, and those with the most striking signatures have been tested up to now, excluding a large phase space, but leaving holes for more complicated signatures still to be found with more data. This still leaves a large parameter space for not-yet-detectable RPV SUSY.

7.2 Long-lived particle searches

As no metastable particles are present in the Standard Model, long-lived particle searches are generally free of SM background. In turn, they require a deep understanding of the detector performance, which represents the only background, as discussed in Sect. 3.1.4. Metastable particles appear generally in the SUSY GUT theory framework [110–114]. They arise in three main situations: very low mass difference ($\leq$O(1 GeV)) between a SUSY particle and the LSP in RPC models, very weak R-parity violation, i.e. λ, λ' or $\lambda'' \leq \text{O}(10^{-5})$, or very weak coupling to the gravitino in GMSB models. Depending on the SUSY mass spectrum, the metastable particle can be colored (squarks and gluinos) or not (sleptons, lightest chargino or neutralino). The experimental signatures probed at LHC are now reviewed by going from the left to the right of Fig. 6.

Non-pointing photons arise in GMSB models where the NLSP is the lightest neutralino with bino-like flavor, i.e. scenario (a) of Fig. 2. If the coupling strength with the gravitino is weak, the $\widetilde{\chi}_1^0$ lifetime is in the range O(0.1–100 ns) accessible by the experiments, provided the $\widetilde{\chi}_1^0$ mass is close to the EW scale. In the EM calorimeter, non-pointing photons exhibit a singular geometric shape for the energy deposit and a late arrival. Results of the search are shown in Fig. 35 in the $\widetilde{\chi}_1^0$ lifetime–mass plane.[12] The stronger limits obtained by ATLAS [116] for long lifetimes are explained by the standalone pointing capability of its calorimeter, whereas at short lifetimes CMS exploits better the correlation between E_T^{miss} and photon energy [117]. Non-pointing photons are not the only possibility in GMSB models. NLSP $\widetilde{\chi}_1^0$ will give non-pointing Z or Higgs. Slepton or squark/gluino NLSPs will give non-pointing leptons or jets. However, in all of these cases, no public results exist yet.

Reconstructing a displaced vertex with high mass and many tracks is undoubtedly a striking sign of new physics, as shown in Fig. 36. SUSY models with $\widetilde{\chi}_1^0$ LSP and very small RPV couplings can provide a plethora of possibilities: with leptons (electrons, muons or taus) attached to the

[12] Weaker limits from converted photons reconstructed by the tracker as an electron–positron pair are not shown [115].

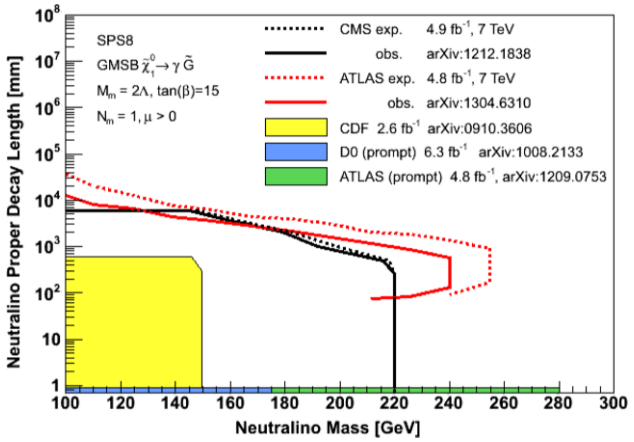

Fig. 35 Exclusion limits for non-pointing photon searches at 95 % CL in the mass–lifetime plane of the $\tilde{\chi}_1^0$, assumed to be bino-like NLSP

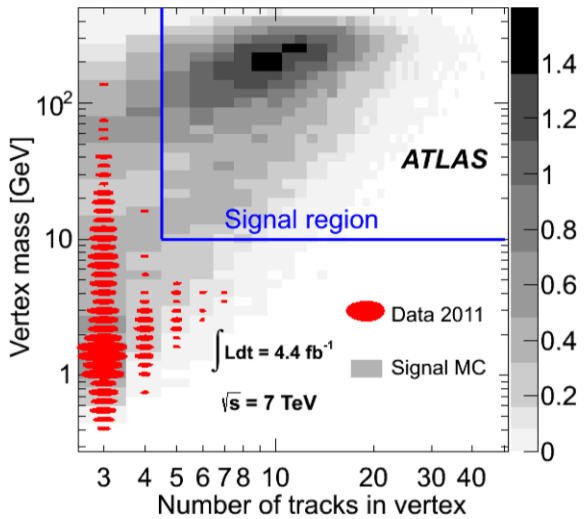

Fig. 36 Mass–track multiplicity plane of the displaced vertex selected by the ATLAS search. One muon is also asked to point to the displaced vertex. The SUSY model considered has 700 GeV squarks, 500 GeV $\tilde{\chi}_1^0$ and $\lambda'_{2ij} = 0.3 \times 10^{-5}$ [118]

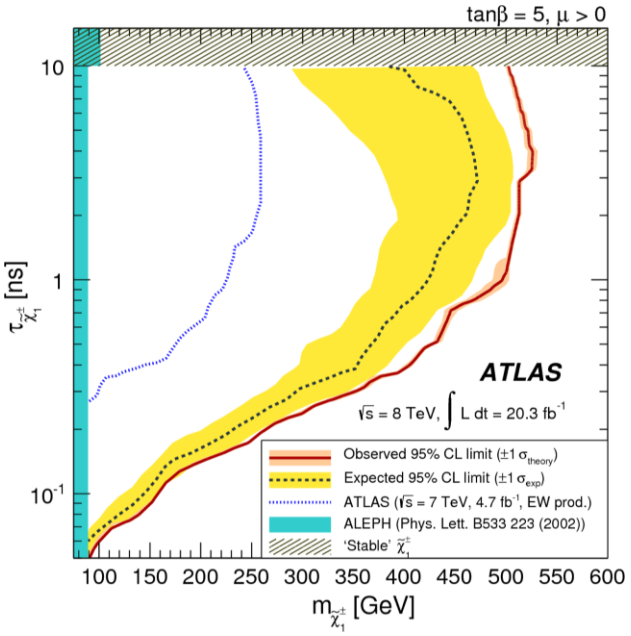

Fig. 37 Exclusion limit at 95 % CL for disappearing track searches in mass-lifetime plane of the $\tilde{\chi}_1^\pm$ [120]

displaced vertex or without leptons. While the latter case requires tracker and calorimeter information (cluster size, track multiplicity pointing to the cluster, etc.), the former relies on a dedicated tracking algorithm for non-standard displaced-vertex reconstruction. To date the only publicly available search interpreted in SUSY models is the one from ATLAS [118]. SUSY models with the simplified decay chain $\tilde{q}/\tilde{g} \to q/q\bar{q} + \tilde{\chi}_1^0 \to q/q\bar{q} + \mu q_i q_j$ are excluded for $\tilde{\chi}_1^0$ lifetimes below 1 m and squark (gluino) masses below 0.7 (0.9) TeV. Other searches looking for long-lived neutral bosons decaying in two leptons [119] could be useful to reject some SUSY models—though it is not yet done. In this case the displaced vertex is required to be at a distance of more than five standard deviations from the primary vertex in the transverse plane. Similar study is ongoing with two jets.

AMSB [62,63] provides a well motivated case for metastable charginos, since $\tilde{\chi}_1^\pm$ and $\tilde{\chi}_1^0$ are almost degenerate and $m_{\tilde{\chi}_1^\pm} - m_{\tilde{\chi}_1^0} \geq 140$ MeV. The situation is similar to scenario (b) of Fig. 2. The chargino therefore decays after O(10 cm) to undetectable particles, a soft pion and the LSP. This will cause the chargino track to 'disappear'. When produced directly ($\tilde{\chi}_1^+ \tilde{\chi}_1^-$, $\tilde{\chi}_1^\pm \tilde{\chi}_1^0$) with an additional jet from initial-state radiation to trigger the event, one (or two) tracks may have no/few associated hits in the outer region of the tracking system. The continuous TRT tracking of the outer part of the ATLAS inner detector gives sensitivity to this signature. With the additional requirement of a high-energetic isolated track, regions beyond the LEP limits can be excluded in the lifetime–mass plane of the chargino, as shown in Fig. 37 [120]. Although originally motivated by AMSB, this result is largely model independent and fits also predictions in many 'unnatural' SUSY models [121–124], where the chargino and the LSP are the only accessible sparticles at LHC.

If the gluino and the LSP are almost mass degenerate, the gluino lifetime could be long enough for it to hadronize in *R*-hadrons ($\tilde{g}q\bar{q}$, $\tilde{g}qqq'$) or *R*-gluino balls ($\tilde{g}$ g).[13] These composite particles are detector-stable, highly ionizing, slowly moving (i.e. non-relativistic) and could change sign when they interact with the detector material. The signature can thus be a detector-stable charged particle, but also a charged particle turning neutral, or even a charged particle turning neutral and turning back charged. To fully explore all possibilities one needs to combine all possible detector mea-

[13] A similar reasoning applies to squarks.

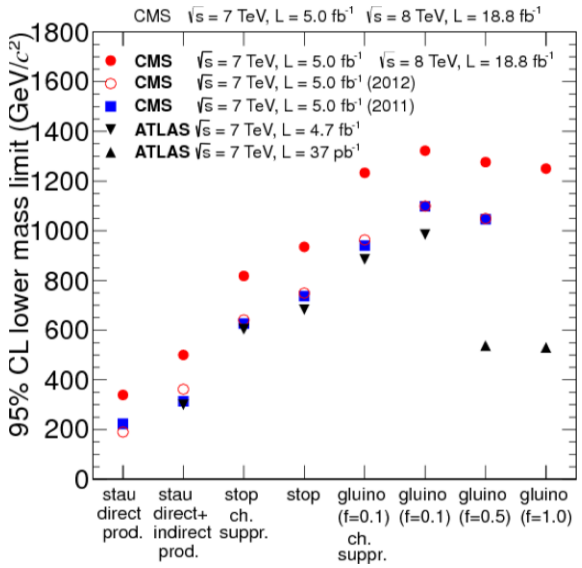

Fig. 38 Lower mass limit at 95 % CL on different scenarios for long-lived particles [125]

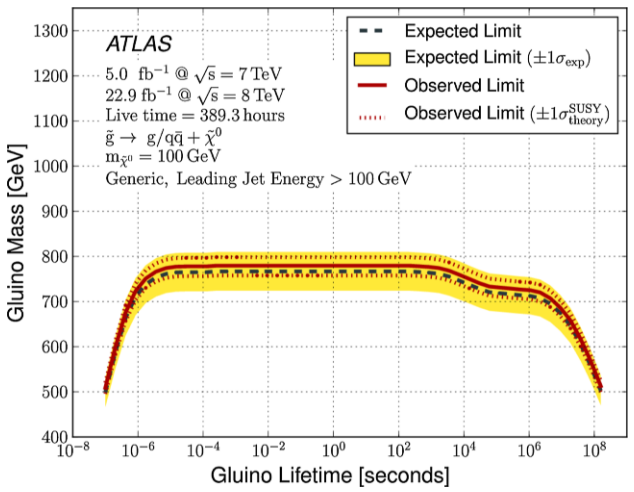

Fig. 39 Exclusion limit at 95 % CL for the stopped gluino searches in mass-lifetime plane of the gluino [126]

surements: $\beta\gamma$[14] from the pixel detector by inverting the Bethe–Bloch function, and β from the calorimeter and muon spectrometer by measuring the arrival time in these devices. Together with the measure of the particle momentum p in the tracker, or in the muon spectrometer, the composite particle mass $m = p/(\beta\gamma)$ can be inferred.

Events are selected by dedicated slow muon or $E_{\mathrm{T}}^{\mathrm{miss}}$ triggers—the latter case is justified by the modest calorimeter energy depositions of the R-hadrons combined with high-energetic jets from initial-state radiation. The background is evaluated by building templates for p, β, and $\beta\gamma$ in signal depopulated regions (like in Fig. 36, signal regions are generally background free). Non-colored particles can also be detector-stable and behave like heavy muons. Therefore, the analysis techniques are similar to the ones used for colored particles. However, in that case, the best performing signal regions are the ones requiring two detector-stable slepton candidates.

The current mass limits from detector-stable particles are presented in Fig. 38 [125]—note that the ATLAS results are still those from the 7 TeV run [30]. Because no Standard Model backgrounds exist, the limits obtained are generally higher than in the prompt-decay case. This is especially true for top and bottom squarks and staus—where no limits on the direct production exist in the RPC prompt case. The gluino masses below 1.2 TeV are excluded independent of the hypotheses made for the interaction of the R-hadrons and R-gluino balls.

A fraction of these slow-moving particles may come to rest within the detector volume and only decay later as $\tilde{g} \to q\bar{q}\tilde{\chi}_1^0, g\tilde{\chi}_1^0$. A particular case is given when this happens in the calorimeter. The signature consists of a high-energetic jet(s) in absence of collisions. The main background is then caused by calorimeter noise bursts, cosmic rays with high energy deposit or beam halo—the leading background. Gluinos below 850 GeV are excluded for a gluino lifetime between 10 μs and 15 min; see Fig. 39 [126]. This signature is generally present in unnatural SUSY models, where the gluino and the LSP are the only accessible sparticles at the LHC.

7.3 Beyond MSSM

The MSSM has firmly been established since 30 years and serves as a basis for most of the SUSY searches at the LHC. However, many possible extensions exist, as shown in Fig. 40. With mild departure from MSSM parsimony, they could explain the current absence of SUSY signals at LHC. In addition, they generally predict new signatures that could be searched for at LHC. We briefly review here the status of these beyond MSSM searches.

The first category of models adds a gauge-singlet superfield to the MSSM. More specifically in the NMSSM [128], two additional Higgs bosons and one neutralino (singlino, $\widetilde{S}$) are added to the MSSM. The extra Higgs are searched for as a peak around 10 GeV in the invariant di-muon mass [129]. The naturalness constraints from the 126 GeV Higgs mass are relaxed and singlino-like LSPs with very small couplings are possible—changing the phenomenology of the SUSY EW sector. Because of this addition, these models predict final states with multi-leptons and $E_{\mathrm{T}}^{\mathrm{miss}}$. Even if no dedicated searches exist yet at LHC, reinterpretations of present EWKino searches, presented in Sect. 6, have already started to constrain NMSSM models [130]. Apart from NMSSM,

[14] The variable β is the particle velocity and γ is the Lorentz boost.

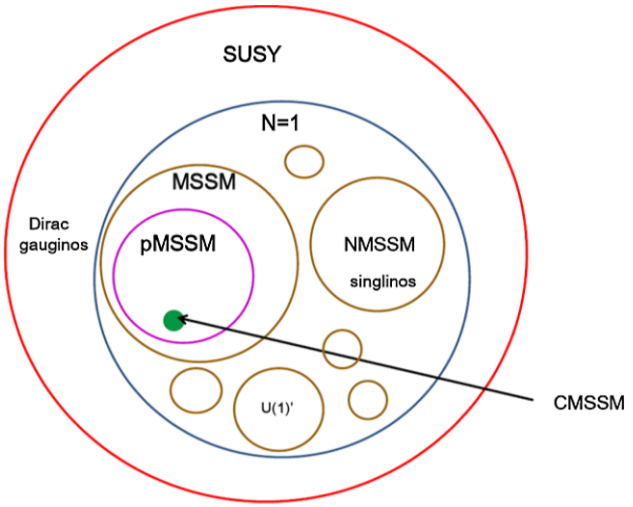

Fig. 40 SUSY phase space and associated theories [127]

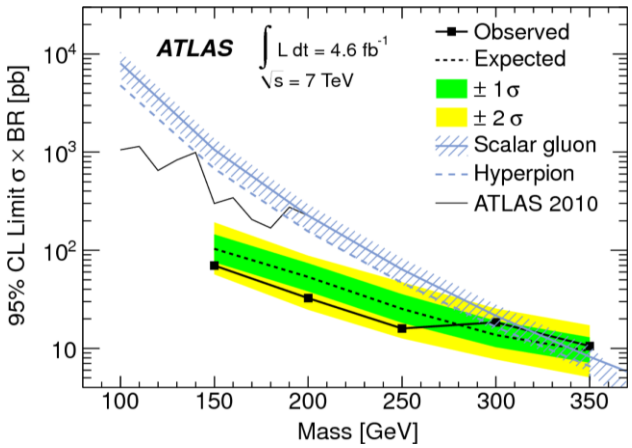

Fig. 41 Exclusion limits at 95 % CL on the sgluon pair production cross section as a function of the sgluon mass [136]

another popular model is stealth SUSY [131], where the invisible singlet and singlino are mass degenerate and light, which reduces drastically the amount of $E_{\mathrm{T}}^{\mathrm{miss}}$—all SUSY cascade decays end like $\widetilde{\mathrm{S}} \rightarrow \mathrm{S}(\rightarrow \mathrm{jj})\widetilde{\mathrm{G}}$ with a poorly boosted $\widetilde{\mathrm{G}}$. Experimental signatures comprise a low $E_{\mathrm{T}}^{\mathrm{miss}}$, displaced vertex and high-multiplicity final states including photons and a high number of b-jets. CMS already places a limit on stealth scenarios where S decays via a photon [132]. Limits of 1.5 TeV on squarks initiating cascade decays are obtained. More refined searches are currently going on.

The second category of models postulates the gluino to be of Dirac type instead of Majorana as in the MSSM.[15] This happens in theories which extend the R-parity concept to a continuous symmetry (MRSSM [133]), hybrid $\mathrm{N} = 1/\mathrm{N} = 2$ model [134] and Supersoft SUSY (SSSM [135]). For the two first models, a new particle (the sgluon) completes the MSSM multiplet composed of gluons and gluinos. In all models, the constraint on the gluino mass in the natural spectrum is relaxed since the radiative corrections are truncated. Because of that, gluino–gluino cross sections are expected to be lower than in the MSSM, weakening the current constraint. The sgluon provides also new signatures to search for. Above a mass of 350 GeV, sgluons dominantly decay in two tops. They can for example be searched for by asking two same-sign leptons (no public results are presently available). At lower mass, sgluons decay in two gluons, giving a pair of two-jet resonances with equal mass. A unique pairing of the four highest energetic jets is achieved for each event by minimizing the pairwise separation. A peak in the dijet mass distribution is then searched for, while the shape and the normalization of the multi-jet background are estimated by a data-driven method. Sgluons are excluded for masses below 300 GeV; see Fig. 41 [136]. It is interesting to note that this signature, unique in BSM models at LHC, is limited at low mass by the multi-jet energy trigger threshold and therefore strong limits are already obtained with the first run at 7 TeV in 2010.

[15] It can also be the case for other gauginos but only the gluino is considered since LHC limits are generally quite strong on the gluino mass.

8 SUSY prospects at LHC beyond the first run

The LHC program is approved until 2022. In this program, the center-of-mass energy will be 13 TeV at the restart and it should reach gradually 14 TeV. Expected luminosities are $\sim$100 fb^{-1} at the end of 2017 and $\sim$300 fb^{-1} in 2022. A possible extension, called High-Luminosity-LHC (HL-LHC), is planned from 2024 to 2030–2035 (Run 3) and could deliver ultimately $\sim$3000 fb^{-1}. The average number of pile-up events per bunch crossing is expected to rise up to 140 in 2030. Expected discovery sensitivities and exclusion limits have recently been extracted by ATLAS and CMS for benchmark processes of plain vanilla MSSM, i.e. R-parity conservation and $\widetilde{\chi}_1^0$ LSP [137,138].

With the increase in beam energy in 2015, the strong SUSY cross sections are greatly enhanced, opening a new phase space to explore with already a low integrated luminosity recorded (1–10 fb^{-1}). A few examples are given here for sparticles at the energy frontier. The cross section for gluino–gluino production (with squarks decoupled) is enhanced by more than a factor of 20 for gluino masses of around 1.3 TeV. The cross section for the pair production of squarks of the first/second generation as well as for third-generation squarks rises by about a factor of 10 for squark masses of 800 GeV. With 300 fb^{-1}, mass degenerate squarks (of the first and second generation) and gluinos of up to 2.7 TeV could be discovered with 5σ significance. For higher gluino (squarks)

masses, e.g. 3.5 TeV, squark (gluino) masses could be discovered up to 2.5 (2) TeV. With the HL-LHC, a gain of about 300 GeV in the mass range is expected. Finally, the top squark could be discovered up to masses of about 800 (1000) GeV with 300 (3000) fb^{-1}, assuming a 100 % branching ratio to a top quark and a $\widetilde{\chi}_1^0$.

Searches for electroweak particles like neutralinos and charginos benefit more from the large expected integrated luminosity than for the increase in $\sqrt{s}$ due to their low cross sections. By the end of Run 3, neutralinos ($\widetilde{\chi}_2^0$) and charginos ($\widetilde{\chi}_1^{\pm}$) decaying to $Z\widetilde{\chi}_1^0$ and $W\widetilde{\chi}_1^0$, respectively, as in scenario (a) of Fig. 2, can be discovered up to a mass of 700 GeV for $\widetilde{\chi}_1^0$ masses of up to 200 GeV with a 5σ significance. In the case of no signal, the exclusion limits are about 200 to 300 GeV higher. Some sensitivity is also expected in the compressed and more natural scenario (c) of Fig. 2 where the $\widetilde{\chi}_1^0$ is higgsino-like.

In summary, the full harvest of the LHC, including the HL-LHC, could explore the largest part of the most interesting weak-scale SUSY phase space, which will remain a hot topic to be tested for at least the next two decades.

9 Conclusions

ATLAS and CMS, the two general-purpose LHC experiments, have developed a coherent and ambitious program to search for new particles at the energy frontier, $O(0.1\text{–}1$ TeV) with 25 fb^{-1} of proton–proton collision data with center-of-mass energies of 7 and 8 TeV. These efforts were successful: a Higgs boson of 126 GeV mass was discovered after two years of running, closing the list of Standard Model particles to be found.

This discovery fits with expectations from the minimal realization of N = 1 SUSY, a.k.a. weak-scale SUSY or MSSM. However, this model also predicts new particles at the energy frontier that could solve the gauge hierarchy problem of the Standard Model, i.e. the quadratic divergence of the Higgs mass at higher energy. Assuming that R-parity is conserved, the plain vanilla SUSY solution predicts a 'natural' or low fine-tuning mass spectrum composed of gluino masses around 1 TeV, top squark and left-handed bottom squark masses around 500 GeV, and chargino/neutralino masses below 500 GeV. All other SUSY particles could be of much higher mass. In this framework, the two favored LSP candidates could be the lightest neutralino or the gravitino. ATLAS and CMS experiment have probed, by direct searches, the uncharted heart of the MSSM spectrum, attracting high attention from the community. To date, these dedicated searches, mainly based on the presence of multi-jets and $E_{\mathrm{T}}^{\mathrm{miss}}$ (but not only these), have not revealed any sign of new physics.

Not all results from Run 1 are currently available but the following general conclusions could be drawn: the gluino mass, governed by only one SUSY parameter, M_3, could be excluded below 1 TeV irrespective of the SUSY mass spectrum in between the gluino and the LSP, and the nature of the LSP. This conclusion applies well for open SUSY spectra, i.e. a mass difference between gluino and the LSP above O(500 GeV). But the excluded gluino mass region should be lowered to 600 GeV when considering more and more compressed spectra, because the jet and $E_{\mathrm{T}}^{\mathrm{miss}}$ softening decreases the acceptance—the presence of isolated lepton(s) can partially correct for that.

Constraints on squarks of the first and second generation are generally softer and less general, since mass degeneracy between families is often assumed. A strong focus was put on the third squark generation (top and bottom squark) because of their particular position in the natural spectrum. When top and bottom squarks are directly produced, final states are generally less complex than for the gluino and squarks of the first and second generation and composed of multiple b-jets and lepton(s). Dedicated searches dramatically shrink the allowed window, but they are (presently) unsuccessful. As an illustration, holes in the top squark searches are presently located near the top mass funnel, $m_{\tilde{\mathrm{t}}} = m_{\mathrm{t}} + m_{\widetilde{\chi}_1^0}$, for $m_{\widetilde{\chi}_1^0} > 100$ GeV, at low mass difference between top squark and $\widetilde{\chi}_1^0$ or in very intricate top squark decay chains.

The weak SUSY sector (charginos, neutralinos, and sleptons) is also probed extensively at LHC. Because of the lower cross section, the Standard Model background is only reducible considering multi-lepton final states. These leptons are provided by the leptonic decay of the W, Z, Higgs and/or sleptons. Compared with the other sectors no strong general conclusions are drawn (yet) because of the high number of possible final states and the complexity of the sector governed by around 10 parameters. Nonetheless, constraints are generally always going beyond the LEP ones, and biting the natural spectrum in many cases.

Therefore it is fair to say that even if not all 8 TeV results are currently available, plain vanilla MSSM is under high pressure. More definitive conclusions will come when all these results will be interpreted with a full scan of the main 19–20 MSSM parameters (some assumptions are made on the other 105-19 parameters), which will happen in 2014. Meanwhile, more focus has been put on searches for long-lived particles, R-parity violating scenarios and new theoretical ideas (Stealth SUSY, Dirac gauginos, extra gauge-singlet superfield) that provide many striking signatures, generally background free and relying more on detector performance. Such scenarios are in most cases compatible with the absence of experimental evidence for plain vanilla MSSM. A huge number of possibilities exist and the most important ones have been covered (or are worked on), with presently no sign

of SUSY. It is interesting to note that the gluino mass is constrained to be above 1 TeV in the models that have been considered.

All these direct searches for new particles have been complemented by indirect searches, which we briefly mention for completeness. At LHC, the main improvement comes from the measurement of the $B_s^0 \to \mu^+\mu^-$ branching ratio, where the leading SUSY contributions involve SUSY Higgses (A^0 and H^0) in penguin diagrams. Good agreement with the Standard Model was found [139,140], and no irreducible limit exists on SUSY models. Other indirect evidence for new physics could be found when searching for the flavor-changing decay of the top quark like $t \to cH$, which is very strongly suppressed in the Standard Model $BR = O(10^{-15})$. Contributions from SUSY Higgses in virtual loops of the decay amplitude can enhance the cross section significantly, by factors up to nine orders of magnitude. Nevertheless, up to now, no evidence for this decay has been found when considering $H \to WW, ZZ, \tau\tau$ leptonic decay [69] and $H \to \gamma\gamma$ decay [141].

A new phase of exploration will be opened in 2015 with the restart of the LHC at higher energy. But the present situation after the first run could well fit an Ernest Rutherford quote: 'An alleged scientific discovery has no merit unless it can be explained to a barmaid'. We can now happily discuss with the barmaid of the SM bar, but we could not yet find the door of the SUSY bar!

Acknowledgments We would like to thank our colleagues in CMS and ATLAS who helped us producing the combined plots.

References

1. L. Evans, P. Briant, JINST **3**, S08001 (2008)
2. ATLAS Collaboration, JINST **3**, S08003 (2008)
3. CMS Collaboration, JINST **3**, S08004 (2008)
4. ATLAS Collaboration, Phys. Lett. B **716**, 1 (2012)
5. CMS Collaboration, Phys. Lett. B **716**, 30 (2012)
6. P. Ramond, SUSY: the early years (1966–1976). Eur. Phys. J. C **74**, 2698 (2014). doi:10.1140/epjc/s10052-013-2698-x. arXiv:1401.5977
7. P. Fayet, SUSY: From 1976 to the LEP years (2014)
8. S.P. Martin, A Supersymmetry Primer (2011). arXiv:hep-ph/9709356
9. A. Djouadi, Implications of the Higgs discovery for the MSSM. Eur. Phys. J. C **74**, 2704 (2014). doi:10.1140/epjc/s10052-013-2704-3. arXiv:1311.0720
10. S.P. Martin, P. Ramond, Phys. Rev. D **48**, 5365 (1993)
11. G.G. Ross, SUSY: Quo Vadis?. Eur. Phys. J. C **74**, 2699 (2014). doi:10.1140/epjc/s10052-013-2699-9
12. Y. Kats, P. Meade, M. Reece, D. Shih, JHEP **1202**, 115 (2012)
13. L. Hall, Searches for SUSY at the LHC. LBL Workshop, 19–21 Oct 2011 (2011)
14. M. Kramer, A. Kulesza, R. Van der Leeuw, M. Mangano, S. Padhi, T. Plehn, X. Portell, Supersymmetry production cross sections in pp collisions at $\sqrt{s} = 7$ TeV (2012). arXiv:1206.2892
15. W. Beenakker, R. Hopker, M. Spira, P.M. Zerwas, Nucl. Phys. B **492**, 51 (1997)
16. A. Kulesza, L. Motyka, Phys. Rev. Lett. **102**, 111802 (2009)
17. A. Kulesza, L. Motyka, Phys. Rev. D **80**, 095004 (2009)
18. W. Beenakker, S. Brensing, M. Kramer, A. Kulesza, E. Laenen et al., JHEP **0912**, 041 (2009)
19. W. Beenakker, S. Brensing, M. Kramer, A. Kulesza, E. Laenen et al., Int. J. Mod. Phys. A **26**, 2637 (2011)
20. The Royal Swedish Academy of Sciences. Press release of the 2013 Physics Nobel Prize (2013)
21. D. Froidevaux, P. Sphicas, Ann. Rev. Nucl. Part. Sci. **56**, 375 (2006)
22. CMS Collaboration, Commissioning of the particle-flow reconstruction in minimum-bias and jet events from pp collisions at 7 TeV. CMS-PAS-PFT-10-002 (2010)
23. M. Cacciari, G.P. Salam, G. Soyez, JHEP **0804**, 063 (2008)
24. M. Cacciari, G.P. Salam, Phys. Lett. B **641**, 57 (2006)
25. CMS Collaboration, JINST **6**, P11002 (2011)
26. ATLAS Collaboration, Eur. Phys. J. C **73**, 2304 (2013)
27. ATLAS Collaboration, Commissioning of the ATLAS high-performance b-tagging algorithms in the 7 TeV collision data. ATLAS-CONF-2011-102 (2011)
28. CMS Collaboration, JINST **8**, P04013 (2013)
29. CMS Collaboration, JINST **7**, P01001 (2012)
30. ATLAS Collaboration, Phys. Lett. B **720**, 277 (2013)
31. I. Hinchliffe, F.E. Paige, M. Shapiro, J. Soderqvist, W. Yao, Phys. Rev. D **55**, 5520 (1997)
32. D. Tovey, Phys. Lett. B **498**, 1 (2001)
33. ATLAS Collaboration, Phys. Rev. Lett. **106**, 131802 (2011)
34. L. Randall, D. Tucker-Smith, Phys. Rev. Lett. **101**, 221803 (2008)
35. C. Rogan, Kinematics for new dynamics at the LHC (2010). arXiv:1006.2727
36. C. Lester, D. Summers, Phys. Lett. B **463**, 99 (1999)
37. A. Barr, C. Lester, P. Stephens, J. Phys. G **29**, 2343 (2003)
38. M. Burns, K. Kong, K.T. Matchev, M. Park, JHEP **0903**, 143 (2009)
39. D. Tovey, JHEP **0804**, 034 (2008)
40. G. Polesello, D. Tovey, JHEP **1003**, 030 (2010)
41. A.J. Barr, T.J. Khoo, P. Konar, K. Kong, C.G. Lester, K.T. Matchev, M. Park, Phys. Rev. D **84**, 095031 (2011)
42. ATLAS Collaboration, Phys. Rev. D **87**, 012008 (2013)
43. M.L. Mangano, M. Moretti, F. Piccinini, R. Pittau, A.D. Polosa, JHEP **0307**, 001 (2003)
44. T. Gleisberg, S. Hoeche, F. Krauss, M. Schonherr, S. Schumann et al., JHEP **0902**, 007 (2009)
45. J. Alwall, M. Herquet, F. Maltoni, O. Mattelaer, T. Stelzer, JHEP **1106**, 128 (2011)
46. S. Frixione, F. Stoeckli, P. Torrielli, B.R. Webber, C.D. White, The MCaNLO 4.0 Event Generator (2010). arXiv:1010.0819
47. P. Nason, JHEP **0411**, 040 (2004)
48. S. Frixione, P. Nason, C. Oleari, JHEP **0711**, 070 (2007)
49. S. Alioli, P. Nason, C. Oleari, E. Re, JHEP **1006**, 043 (2010)
50. M. Bahr, S. Gieseke, M. Gigg, D. Grellscheid, K. Hamilton et al., Eur. Phys. J. C **58**, 639 (2008)
51. T. Sjöstrand, S. Mrenna, P.Z. Skands, JHEP **05**, 026 (2006)
52. GEANT4 Collaboration, Nucl. Instrum. Methods A **506**, 250 (2003)
53. S. Abdullin, P. Azzi, F. Beaudette, P. Janot, A. Perrotta, in *CHEP 2011*. J. Phys.: Conference Series, vol. 331, p. 032049 (2010)

54. ATLAS Collaboration, The simulation principle and performance of the ATLAS fast calorimeter simulation FastCaloSim. ATL-PHYS-PUB-2010-013 (2010)
55. A. Read, J. Phys. G: Nucl. Part. Phys. **28**, 2693 (2002)
56. A.H. Chamseddine, R.L. Arnowitt, P. Nath, Phys. Rev. Lett. **49**, 970 (1982)
57. R. Barbieri, S. Ferrara, C.A. Savoy, Phys. Lett. B **119**, 343 (1982)
58. L.J. Hall, J.D. Lykken, S. Weinberg, Phys. Rev. D **27**, 2359 (1983)
59. R. Arnowitt, P. Nath, Phys. Rev. Lett. **69**, 725 (1992)
60. G.L. Kane, C.F. Kolda, L. Roszkowski, J.D. Wells, Phys. Rev. D **49**, 6173 (1994)
61. M. Dine, A.E. Nelson, Y. Nir, Y. Shirman, Phys. Rev. D **53**, 2658 (1996)
62. L. Randall, R. Sundrum, Nucl. Phys. B **557**, 79 (1999)
63. G.F. Giudice, M.A. Luty, H. Murayama, R. Rattazzi, JHEP **9812**, 027 (1998)
64. N. Arkani-Hamed, P. Schuster, N. Toro, J. Thaler, L.-T. Wang et al., MARMOSET: The path from LHC data to the new standard model via on-shell effective theories (2007). arXiv:hep-ph/0703088
65. J. Alwall, P. Schuster, N. Toro, Phys. Rev. D **79**, 075020 (2009)
66. D. Alves et al., J. Phys. G **39**, 105005 (2012)
67. A. Djouadi et al., The minimal supersymmetric standard model: group summary report (1998). arXiv:hep-ph/9901246
68. CMS Collaboration, Phys. Lett. B **725**, 243 (2013)
69. CMS Collaboration, Search for new physics in multijets and missing momentum final state in proton–proton collisions at $\sqrt{s} = 8$ TeV. JHEP (2014) (Accepted). arXiv:1402.4770
70. ATLAS Collaboration, JHEP **1310**, 130 (2013)
71. CMS Collaboration, Eur. Phys. J. C **73**, 2568 (2013)
72. ATLAS Collaboration, Phys. Rev. D **86**, 092002 (2012)
73. CMS Collaboration, Phys. Lett. B. (2013) (Submitted). arXiv:1311.4937
74. CMS Collaboration, JHEP **1401**, 163 (2014). arXiv:1311.6736
75. A. Arvanitaki, M. Baryakhtar, X. Huang, K. Van Tilburg, G. Villadoro, JHEP **1403**, 022 (2014). arXiv:1309.3568
76. ATLAS Collaboration, Phys. Lett. B 718, 411 (2012)
77. CMS Collaboration, JHEP **1303**, 111 (2013)
78. ATLAS Collaboration, Phys. Lett. B **719**, 261 (2013)
79. ATLAS Collaboration, Eur. Phys. J. C **72**, 2215 (2012)
80. CMS Collaboration, Eur. Phys. J. C **73**, 2493 (2013)
81. CMS Collaboration, Search for anomalous production of events with three or more leptons in pp collisions at $\sqrt{s} = 8$ TeV. Phys. Rev. D (2014) (Submitted). arXiv:1404.5801
82. ATLAS Collaboration, Search for direct top squark pair production in events with a Z boson, b-jets and missing transverse momentum in pp collisions at $\sqrt{s} = 8$ TeV with the ATLAS detector. Eur. Phys. J. C (2014) (Submitted). arXiv:1403.5222
83. CMS Collaboration, Eur. Phys. J. C **73**, 2677 (2013)
84. Y. Bai, H. Cheng, J. Gallicchio, J. Gu, JHEP **1207**, 110 (2012)
85. ATLAS Collaboration, Search for direct top-squark pair production in final states with two leptons in pp collisions at $\sqrt{s} = 8$ TeV with the ATLAS detector. Eur. Phys. J. C (2014) (Submitted). arXiv:1403.4853
86. ATLAS Collaboration, JHEP **1310**, 189 (2013)
87. CMS Collaboration, Phys. Rev. Lett. **112**, 161802 (2014). arXiv:1312.3310
88. ATLAS Collaboration, Phys. Rev. D **89**, 032002 (2014). arXiv:1312.1956
89. ATLAS Collaboration. JHEP **1404**, 169 (2014). arXiv:1402.7029
90. CMS Collaboration, JHEP **1209**, 094 (2012)
91. ATLAS Collaboration, JHEP **1304**, 075 (2013)
92. CMS Collaboration, JHEP **1211**, 147 (2012)
93. ATLAS Collaboration, Search for direct production of charginos, neutralinos and sleptons in final states with two leptons and missing transverse momentum in pp collisions at $\sqrt{s} = 8$ TeV with the ATLAS detector JHEP (2013). (Submitted). arXiv:1403.5294
94. R. Barbier, C. Berat, M. Besancon, M. Chemtob, A. Deandrea et al., Phys. Rep. **420**, 1 (2005)
95. ATLAS Collaboration, JHEP **1212**, 124 (2012)
96. K. Desch, S. Fleischmann, P. Wienemann, H. Dreiner, S. Grab, Phys. Rev. D **83**, 015013 (2011)
97. CMS Collaboration, JHEP **1206**, 169 (2012)
98. CMS Collaboration, Phys. Rev. Lett. **111**, 221801 (2013)
99. ATLAS Collaboration, Phys. Lett. B **723**, 15 (2013)
100. M. Chemtob, Prog. Part. Nucl. Phys. **54**, 71 (2005)
101. ZEUS Collaboration, Phys. Rev. D **86**, 012005 (2012). arXiv:1205.5179
102. H1 Collaboration, Phys. Lett. B **704**, 388 (2011). arXiv:1107.3716
103. CMS Collaboration, Phys. Rev. Lett. **110**, 081801 (2013)
104. R.S. Chivukula, M. Golden, E.H. Simmons, Phys. Lett. B **257**, 403 (1991)
105. R.S. Chivukula, M. Golden, E.H. Simmons, Nucl. Phys. B **363**, 83 (1991)
106. CMS Collaboration, Phys. Lett. B **730**, 193 (2014). arXiv:1311.1799
107. CDF Collaboration, Phys. Rev. Lett. **107**, 042001 (2011)
108. CMS Collaboration, Phys. Rev. Lett. **107**, 101801 (2011)
109. ATLAS Collaboration, JHEP **1212**, 086 (2012)
110. S. Raby, Phys. Rev. D **56**, 2852 (1997)
111. H. Baer, K. Cheung, J.F. Gunion, Phys. Rev. D **59**, 075002 (1999). arXiv:hep-ph/9806361
112. A. Mafi, S. Raby, Phys. Rev. D **63**, 055010 (2001)
113. S. Raby, Phys. Lett. B **422**, 158 (1998)
114. A. Mafi, S. Raby, Phys. Rev. D **62**, 035003 (2000)
115. CMS Collaboration, JHEP **1211**, 172 (2012)
116. ATLAS Collaboration, Phys. Rev. D **88**, 012001 (2013)
117. CMS Collaboration, Phys. Lett. B **722**, 273 (2013)
118. ATLAS Collaboration, Phys. Lett. B **719**, 280 (2013)
119. CMS Collaboration, JHEP **1302**, 085 (2013)
120. ATLAS Collaboration, Phys. Rev. D **88**, 112006 (2013)
121. L.J. Hall, Y. Nomura, S. Shirai, JHEP **1301**, 036 (2013)
122. A. Arvanitaki, N. Craig, S. Dimopoulos, G. Villadoro, JHEP **1302**, 126 (2013)
123. N. Arkani-Hamed, A. Gupta, D.E. Kaplan, N. Weiner, T. Zorawski, Simply Unnatural Supersymmetry (2012). arXiv:1212.6971
124. M. Ibe, S. Matsumoto, T.T. Yanagida, Phys. Rev. D **85**, 095011 (2012)
125. CMS Collaboration, JHEP **1307**, 122 (2013)
126. ATLAS Collaboration, Phys. Rev. D **88**, 112003 (2013)
127. T. Rizzo, The BSM Zoo. 40th SLAC Summer Institute (2012)
128. U. Ellwanger, C. Hugonie, A.M. Teixeira, Phys. Rept. **496**, 1 (2010)
129. CMS Collaboration, Phys. Rev. Lett. **109**, 121801 (2012)
130. U. Ellwanger, JHEP **1311**, 108 (2013)
131. J. Fan, M. Reece, T. Ruderman, JHEP **1111**, 012 (2012)
132. CMS Collaboration, Phys. Lett. B **719**, 42 (2013)
133. G.D. Kribs, E. Poppitz, N. Weiner, Phys. Rev. D **78**, 055010 (2008)
134. S.Y. Choi, M. Drees, A. Freitas, P.M. Zerwas, Phys. Rev. D **78**, 095007 (2008)
135. G.D. Kribs, A. Martin, Phys. Rev. D **85**, 115014 (2012)
136. ATLAS Collaboration, Eur. Phys. J. C **73**, 2263 (2013)
137. Y. Gershtein, M. Luty, M. Narain, L.T. Wang, D. Whiteson et al., New Particles Working Group Report of the Snowmass 2013 Community Summer Study (2013). arXiv:1311.0299

138. D. Abbaneo et al., ECFA High Luminosity LHC Experiments Workshop: Physics and Technology Challenges. ECFA-13-284 (2013)
139. LHCb Collaboration, Phys. Rev. Lett. **110**, 021801 (2013)
140. CMS Collaboration, Phys. Rev. Lett. **111**, 101804 (2013)
141. ATLAS Collaboration, Search for top quark decays t $\rightarrow$ q H with H $\rightarrow \gamma\gamma$ using the ATLAS detector, JHEP (2014) (Submitted). arXiv:1403.6293

Eur. Phys. J. C (2014) 74:2732
DOI 10.1140/epjc/s10052-014-2732-7

THE EUROPEAN PHYSICAL JOURNAL C

Review

Supersymmetric fits after the Higgs discovery and implications for model building

John Ellis[1,2,a]

[1] Department of Physics, King's College London, London WC2R 2LS, UK
[2] Theory Division, CERN, 1211 Geneva 23, Switzerland

Received: 20 November 2013 / Accepted: 27 November 2013 / Published online: 27 May 2014

Abstract The data from the first run of the LHC at 7 and 8 TeV, together with the information provided by other experiments such as precision electroweak measurements, flavour measurements, the cosmological density of cold dark matter and the direct search for the scattering of dark matter particles in the LUX experiment, provide important constraints on supersymmetric models. Important information is provided by the ATLAS and CMS measurements of the mass of the Higgs boson, as well as the negative results of searches at the LHC for events with $E/_T$ accompanied by jets, and the LHCb and CMS measurements of BR($B_s \to \mu^+\mu^-$). Results are presented from frequentist analyses of the parameter spaces of the CMSSM and NUHM1. The global χ^2 functions for the supersymmetric models vary slowly over most of the parameter spaces allowed by the Higgs mass and the $E/_T$ search, with best-fit values that are comparable to the χ^2 for the standard model. The 95 % CL lower limits on the masses of gluinos and squarks allow significant prospects for observing them during the LHC runs at higher energies.

1 Introduction

The discovery of a Higgs boson at the LHC [1,2] has given new heart to advocates of supersymmetry [3]. Its mass is consistent with the predictions of minimal supersymmetric models that the lightest Higgs boson should weigh $\lesssim$130 GeV [4–11]. Indeed, the measured value of m_h lies in the range where new physics seems to be required to stabilize the electroweak vacuum [12], which might well be supersymmetry [13]. Moreover, the measurements of Higgs couplings to other particles are consistent with the predictions of many supersymmetric models, which are close to those in the standard model. There are no signs so far of the deviations from the standard model couplings that are characteristic of models in which electroweak symmetry breaking is driven by some new dynamics [14].

On the other hand, neither are there any signs for other types of new physics, such as might be responsible for dark matter in the form of massive, weakly interacting particles whose production could be inferred in searches for events with jets and missing transverse energy, $E/_T$ at the LHC. Supersymmetry with conserved R parity is one such model that suggests the existence of a dark matter particle that was in thermal equilibrium in the early Universe and should weigh $\sim$ 1 TeV if it is to have the appropriate cosmological relic density [15]. It is assumed here that the lightest supersymmetric particle (LSP) that constitutes the dark matter is the lightest neutralino χ [16,17], though there are other candidates such as the gravitino. Important constraints on such dark matter models are imposed by direct and indirect searches for dark matter, as well as by LHC searches for $E/_T$ events, none of which have found convincing signals [18].

Even if R conservation is assumed, the interpretation of all these constraints is quite model dependent. For simplicity, we consider here only the minimal supersymmetric extension of the standard model (the MSSM), though there are well-motivated extensions, e.g., to include any extra singlet superfield (the NMSSM [19]). The MSSM already has over 100 parameters, and it is natural to consider simplifying hypotheses such as minimal flavour violation (MFV), in which all flavour violation is related to Cabibbo–Kobayashi–Maskawa mixing [20,21]. In principle, this model has six additional CP-violating phases [22], but upper limits on electric dipole moments offer no suggestion that they are large. Many studies of experimental constraints focus on versions of the MSSM with MFV in which the soft supersymmetry-breaking contributions to sfermion, Higgs and gaugino masses, m_0 and $m_{1/2}$, respectively, as well as trilinear couplings A_0, are constrained to be universal at some high input scale (the CMSSM) [23–32], or in generalizations in which the soft

[a] e-mail: john.ellis@cern.ch

supersymmetry-breaking contributions to Higgs masses are allowed to be non-universal but equal (the NUHM1) [33–35]. One example of a more restrictive model is minimal supergravity (mSUGRA), in which the gravitino mass is forced to be equal to the input scalar mass: $m_{3/2} = m_0$, and the trilinear and bilinear soft supersymmetry-breaking parameters are related: $A_0 = B_0 + m_0$.

As we shall see, the LHC $E/_T$ searches impose strong constraints on models with universal soft supersymmetry-breaking parameters such as the CMSSM, NUHM1 and mSUGRA, stimulating interest in 'natural' models in which the third-generation squarks are much lighter than those of the first and second generations, for which experiments give weaker constraints. Also, searches for specific $E/_T+$ jets signatures have been interpreted within simplified models in which these topologies are assumed to be the dominant supersymmetric signatures. There has also been interest in using searches for $E/_T+$ monojet, monophoton and mono-W/Z topologies to look for the direct pair-production of dark matter particles without passing via the cascade decays of heavier sparticles.

In view of its importance for constraining supersymmetric models, in Sect. 2 of this review there is a discussion of Higgs mass calculations and their uncertainties, as well as indications of their implications for the parameter spaces of supersymmetric models. Section 3 presents some results of global fits [36] to the CMSSM and NUHM1 using the full $E/_T$ data from Run 1 of the LHC at 7 and 8 TeV [37], the measurement by CMS and LHCb of BR($B_s \to \mu^+\mu^-$) [38–42], and the latest constraints on dark matter scattering from the LUX experiment [43]. These results include 95 % CL lower limits on sparticle masses and the prospects for discovering them in Run 2 of the LHC at 13/14 TeV. Section 4 summarizes some pertinent results within other frameworks such as mSUGRA, 'natural' and simplified models. Finally, Sect. 5 draws some conclusions for supersymmetric model-building.

2 The Higgs mass and supersymmetry

As is well known, the two complex Higgs doublets of the MSSM have eight degrees of freedom, of which three give masses to the $W^\pm$ bosons and to the Z^0 via the electroweak symmetry breaking, leaving five physical Higgs bosons in the physical spectrum: two neutral Higgs bosons h, H that are CP-even (scalar), one neutral boson A that is CP-odd (pseudoscalar), and two charged bosons $H^\pm$. The tree-level masses of the scalar supersymmetric Higgs bosons are

$$m^2_{h,H} = \frac{1}{2}\left(m^2_A + m^2_Z \mp \sqrt{(m^2_A + m^2_Z)^2 - 4m^2_A m^2_Z \cos^2 2\beta}\right) \quad (1)$$

where $\tan\beta$ is the ratio of Higgs v.e.v.s, from which we see that m_h is bounded from above by m_Z. [1] However, there are important radiative corrections to m_h (1) [4–11], of which the most important is the one-loop correction due to the top quark and stop squark:

$$\Delta m^2_h = \frac{3m^4_t}{4\pi^2 v^2} \ln\left(\frac{m_{\tilde{t}_1} m_{\tilde{t}_2}}{m^2_t}\right) + \cdots, \quad (2)$$

where $m_{\tilde{t}_{1,2}}$ are the physical masses of the stops. We see in (2) that the correction Δm^2_h depends quartically on the mass of the top, and it implies that the mass of the lightest Higgs boson may be as large as

$$m_h \lesssim 130\ \text{GeV}. \quad (3)$$

for stop masses of about a TeV, consistent with the ATLAS and CMS measurements [1,2].

If one wishes to use (2) to estimate the stop mass scale, it is clear that the answer is exponentially sensitive to the Higgs mass, and it is therefore important to refine the one-loop calculation. Several codes are available that provide complete two-loop calculations and include the leading dependences of three- and higher-loop contributions on the strong coupling α_s and the top Yukawa coupling α_t. It is also important to estimate the theoretical uncertainty in the calculation of m_h for given values of the supersymmetric model parameters, which is typically $\sim$ 1.5 to 3 GeV. In the following, results from the `FeynHiggs 2.10.0` code for calculating m_h are used, which is a significant improvement over previous versions. As an example of the importance for inferences about the supersymmetric mass scale from the measured value of m_h, Fig. 1 displays the $(m_{1/2}, m_0)$ plane in the CMSSM for $\tan\beta = 30$, $\mu > 0$ and $A_0 = 2.5 m_0$ [44].

The brown shaded wedge at large $m_{1/2}$ and small m_0 is excluded because there the LSP would be the charged $\tilde{\tau}_1$, whereas the lighter stop, $\tilde{t}_1$, would be the LSP. Adjacent to these wedges are narrow blue strips where the relic LSP density falls within the range favoured by astrophysics and cosmology. Measurements of $b \to s\gamma$ exclude the region shaded green, whereas in the pink region the discrepancy between the standard model and experimental values of the anomalous magnetic moment of the muon, $g_\mu - 2$, could be explained by supersymmetry [51]. The 95 % CL limit on $E/_T$ + jets events at the LHC [37] is represented by the purple line, and the green lines represent 68 and 95 % CL limits from the value of BR($B_s \to \mu^+\mu^-$) measured by the CMS and LHCb experiments [38–42]. Finally, the black lines are contours of m_h calculated with the current version `2.10.0` of the `FeynHiggs` code [45–50], which includes the leading and next-to-leading

[1] This upper limit appears because the quartic Higgs coupling λ is fixed in the MSSM to be equal to the square of the electroweak gauge coupling, up to numerical factors.

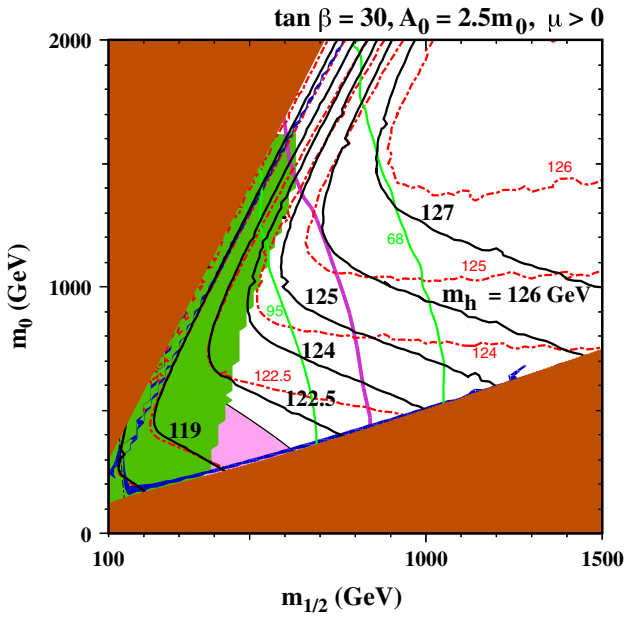

Fig. 1 The allowed regions in the $(m_{1/2}, m_0)$ plane for $\tan\beta = 30$ and $A_0 = 2.5m_0$ [44]. The *line styles* and *shadings* are described in the text. The section of the dark blue coannihilation strip in the range $m_{1/2} \in (840, 1{,}050)$ GeV is compatible with the constraints from BR$(B_s \to \mu^+\mu^-)$ (*green lines* marking the 68 and 95 % CL) [38–42] and the ATLAS 20/fb MET search (*purple line*) [37], as well as with the LHC m_H measurement. Good consistency with all the constraints is found if the improved `FeynHiggs 2.10.0` code [45–50] is used (*black lines*): results from a previous version of `FeynHiggs` are indicated by *red dotted lines*

$\log(m_{\tilde{t}}/m_t)$ terms in all orders of perturbation theory, as calculated using the two-loop renormalization-group equations (RGEs). The red dashed lines are calculated with an earlier version of `FeynHiggs`, which did not include these refinements, and we see that the m_h contours diverge significantly at large $m_{1/2}$, in particular. We also see that there is a region with $(m_{1/2}, m_0) \sim (1{,}200, 600)$ GeV that is compatible with dark matter and laboratory constraints (except for $g_\mu - 2$) and corresponds to $m_h \sim 125$ GeV according to the latest version of `FeynHiggs`, whereas the earlier version would have yielded $m_h < 124$ GeV [44].

Smaller values of $\tan\beta$ would yield smaller values of m_h, and larger values of $\tan\beta$ would be more tightly constrained by BR$(B_s \to \mu^+\mu^-)$, though values of $\tan\beta \lesssim 50$ may be compatible with all the constraints. Smaller values of A_0 would also yield smaller values of m_h along the strip near the boundary of the $\tilde{\tau}_1$ LSP wedge where the appropriate dark matter density is obtained, and this dark matter strip would only extend to lower $m_{1/2}$ in this case. There is a second dark matter strip close to the boundary with the $\tilde{t}_1$ LSP region, but m_h is too small except possibly at very large values of m_0 [44]. In general, CMSSM models with an LHC-compatible value of m_h do not make a significant contribution to resolving the $g_\mu - 2$ discrepancy [51].

3 Global fits in the CMSSM and NUHM1

After this first taste of the interplay between the LHC $E\!\!\!/_T$, m_h, BR$(B_s \to \mu^+\mu^-)$, dark matter and other constraints, and their potential implications for models, I now present some results from a global fit to the relevant data within the CMSSM [36]. These are compared with the results of a fit within the NUHM1, which offers, in principle, new ways to reconcile some of the constraints discussed in the previous section.

These fits are based on a frequentist approach developed by the MasterCode collaboration [52–69], and the `MultiNest` tool is used to sample the CMSSM and NUHM1 parameter spaces [70–72]. The global χ^2 function is calculated including precision electroweak observables such as M_W and measurements at the Z^0 peak, as well as $g_\mu - 2$. Also included is a full suite of flavour observables such as $b \to s\gamma$ and $B \to \tau\nu$ as well as BR$(B_s \to \mu^+\mu^-)$ [36]. In addition to the dark matter density, a contribution from the LUX direct search [43] for the scattering of astrophysical dark matter is also included.

Figure 2 displays $(m_0, m_{1/2})$ planes in the CMSSM (left panel) and the NUHM1 (right panel), both with $\mu > 0$.[2] The best-fit points are indicated by green stars, the $\Delta\chi^2 = 2.30$ contours, which correspond approximately to the 68 % CL are shown as red lines, and the $\Delta\chi^2 = 5.99$ contours, which correspond approximately to the 95 % CL are shown as blue lines. The results of the current fit [36] are indicated by solid lines and solid stars, whilst the dashed lines and open stars represent the results of fits to the data used in [61], reanalyzed using the current version of `MasterCode`.

In both the CMSSM and the NUHM1, we see two distinct regions: a smaller region around $(m_0, m_{1/2}) \sim (500, 1{,}000)$ GeV and a larger region extending to larger values of $(m_0, m_{1/2}$. The low-mass regions correspond to the $\tilde{\tau}_1$ coannihilation strip mentioned in the previous section, and in the high-mass regions other mechanisms bring the relic LSP density into the range allowed by astrophysics and cosmology, notably rapid LSP annihilation via direct-channel H/A resonances when $m_\chi \sim m_{H/A}/2$, and neutralino–chargino coannihilation, which becomes more important when the LSP has a significant Higgsino component. The extra parameter in the NUHM1 Higgs sectors offers more possibilities for these effects, enabling the relic density constraint to satisfied at larger values of $m_{1/2}$ and smaller values of $\tan\beta$ than in the CMSSM [44].

As we see in Table 1, the minimum values of χ^2 in the low- and high-mass regions differ by less than unity in both the CMSSM and the NUHM1. In the case of the CMSSM, the contribution from $g_\mu - 2$ is smaller in the low-mass region, but the contribution from the ATLAS jets + $E\!\!\!/_T$ search is

[2] Results for the CMSSM with $\mu < 0$ can be found in [36].

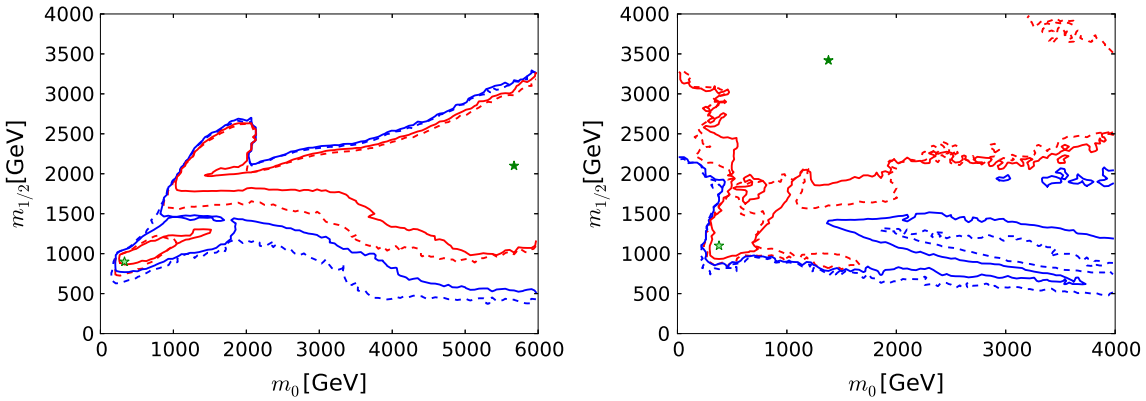

Fig. 2 The $(m_0, m_{1/2})$ planes in the CMSSM (*left*), and the NUHM1 (*right*), after implementing the ATLAS $E/_T$, BR$(B_s \to \mu^+\mu^-)$, m_h, dark matter density, LUX and other relevant constraints [36]. The results of the current fits are indicated by *solid lines* and *filled stars*, and fits to previous data [61] using the same implementations of the constraints are indicated by *dashed lines* and *open stars*. The *red lines* denote $\Delta\chi^2 = 2.30$ contours (corresponding approximately to the 68 % CL), and the *red lines* denote $\Delta\chi^2 = 5.99$ (95 % CL) contours

Table 1 The best-fit points found in global CMSSM and NUHM1 fits with $\mu > 0$, using the ATLAS $E/_T$ constraint [37], and the combination of the CMS and LHCb constraints on BR$(B_s \to \mu^+\mu^-)$[38–42]. We list the parameters of the best-fit points in both the low- and the high-mass regions in Fig. 2. The overall likelihood function is quite flat in both the CMSSM and the NUHM1, so that the precise locations of the best-fit points are not very significant, and we do not quote uncertainties. This table is adapted from [36]

Model	Region	Minimum χ^2	m_0 (GeV)	$m_{1/2}$ (GeV)	tan β
CMSSM	Low-mass	35.8	670	1,040	21
	High-mass	35.1	5,650	2,100	51
NUHM1	Low-mass	33.3	470	1,270	11
	High-mass	32.7	1,380	3,420	39

larger. This is also the case in the NUHM1, but other observables such as $A_{fb}(b)$ and A_ℓ(SLD) also contribute differences in χ^2 between the low- and high-mass regions that are $\mathcal{O}(1)$ [36]. In general, the global χ^2 function varies little over much of the $(m_0, m_{1/2})$ planes explored. Also, the value of χ^2 at the global minimum in the CMSSM is not significantly different from that in the standard model, whereas that in the NUHM1 is ~ 2 lower [36]. The CMSSM and NUHM1 confer no convincing advantages over the standard model in the global fits reported here.

Comparing the current fits (solid lines and filled stars) with the results of fits to the data available in mid-2012 (dashed lines and open stars) reanalyzed with the current versions of `FeynHiggs` and other codes, we see that the overall extensions and shapes of the regions allowed at the 95 % CL and favoured at the 68 % CL are quite similar [36]. There is some erosion of the preferred regions at low $m_{1/2}$, due to the stronger ATLAS jets + $E/_T$ limit, but the most noticeable features are the shifts to larger masses of the best-fit points. However, as noted above, the differences between the values of the global χ^2 function in the low- and high-mass regions are not significant. The lower-mass regions would require less fine-tuning and hence seem more natural [73–75]. However, the interpretation of the degree of naturalness is uncertain in the absence of a more complete theoretical framework.

Figure 3 displays the one-dimensional χ^2 functions for some sparticle masses in the CMSSM (left) and the NUHM1 (right) [36]. The upper panels are for the gluino mass $m_{\tilde{g}}$, and the lower panels are for a generic right-handed squark mass $m_{\tilde{q}_R}$. The χ^2 function for $m_{\tilde{g}}$ in the CMSSM falls almost monotonically, whereas the other χ^2 functions exhibit more structure, corresponding to the structures visible in the $(m_0, m_{1/2})$ planes in Fig. 2. In each case, the χ^2 functions have been pushed up at low mass by the ATLAS jets + $E/_T$ limit, as seen by comparing the solid and dotted lines.

The χ^2 function for the mass of the lighter stop squark $m_{\tilde{t}_1}$ in the CMSSM, shown in the upper left panel of Fig. 4, exhibits a local minimum at $m_{\tilde{t}_1} \sim 1{,}000$ GeV and a local maximum at $m_{\tilde{t}_1} \sim 2{,}000$ GeV [36]. On the other hand, the χ^2 function for $m_{\tilde{t}_1}$ in the NUHM1, shown in the upper right panel of Fig. 4, exhibits a local maximum at $m_{\tilde{t}_1} \sim 1{,}000$ GeV and a local minimum at $m_{\tilde{t}_1} \sim 2{,}000$ GeV, followed by another local maximum at $m_{\tilde{t}_1} \sim 2{,}600$ GeV.

The lower panels of Fig. 4 show the χ^2 functions for the lighter stau in the CMSSM (left) and the NUHM1 (right). In both cases, we see that low masses are strongly disfavoured, and that the χ^2 functions are almost flat above 1,000 GeV, with local maxima at $m_{\tilde{\tau}_1} \sim 700$ GeV.

There is no indication of a preferred supersymmetric mass scale, but one may set the following 95 % CL lower limits in GeV units [36]:

$$\begin{aligned} &m_{\tilde{g}} > 1{,}810 \text{ (CMSSM)}, 1{,}920 \text{ (NUHM1)}, \\ &m_{\tilde{q}_R} > 1{,}620 \text{ (CMSSM)}, 1{,}710 \text{ (NUHM1)}, \\ &m_{\tilde{t}_1} > 750 \text{ (CMSSM)}, 1120 \text{ (NUHM1)}, \\ &m_{\tilde{\tau}_1} > 340 \text{ (CMSSM)}, 450 \text{ (NUHM1)}. \end{aligned} \tag{4}$$

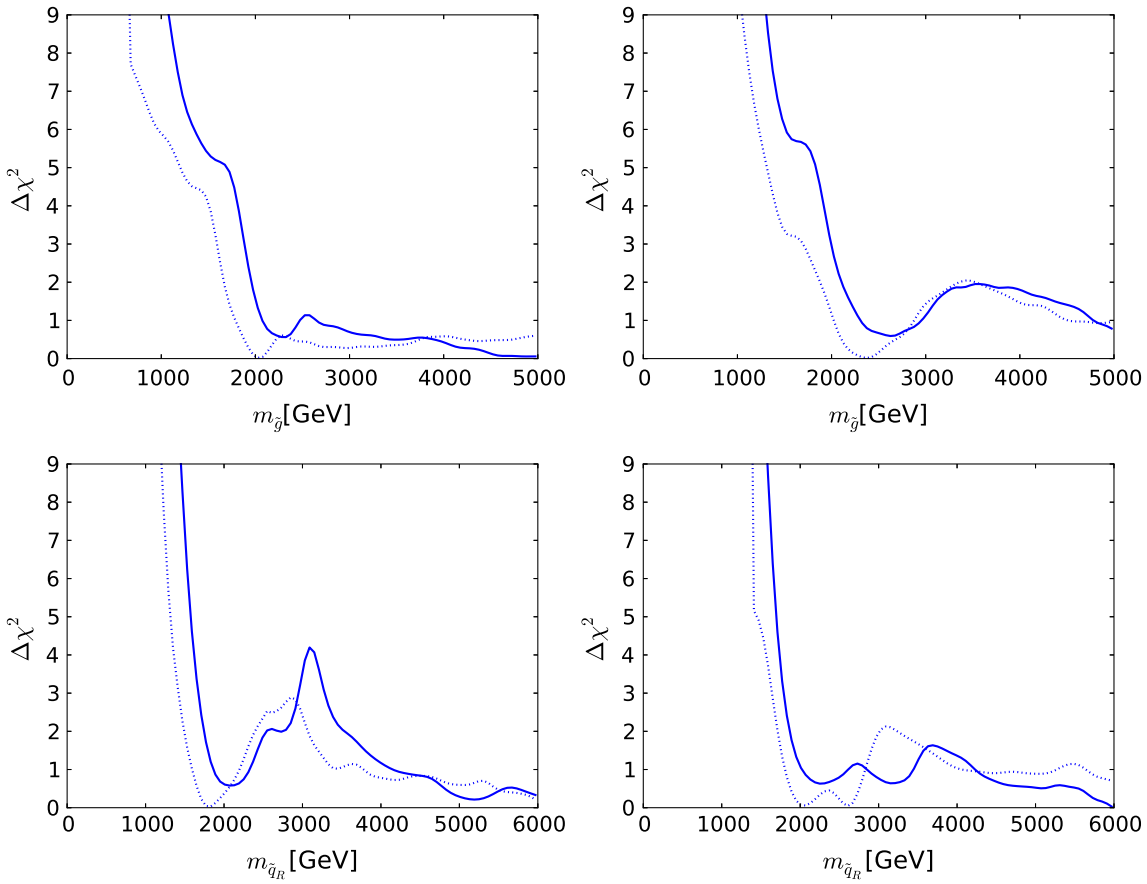

Fig. 3 The one-dimensional χ^2 likelihood functions in the CMSSM (*left*) and the NUHM1 (*right*) for the gluino mass $m_{\tilde{g}}$ (*upper*) and a generic right-handed squark mass $m_{\tilde{q}_R}$ (*lower*) [36]. In each *panel*, the *solid line* is derived from a global analysis of the present data, and the *dotted line* is derived from an analysis if the data set used in [61], using the same implementations of the m_h and dark matter scattering constraints

For comparison, estimates of the supersymmetry discovery reach of the LHC with 14 TeV can be found in [76], e.g., the $(m_0, m_{1/2})$ plane displayed in Fig. 5. It was estimated in [76] that the 5σ discovery reach for squarks and gluinos with 300/fb of high-energy luminosity should be to $m_{\tilde{g}} \sim 3,500$ GeV and $m_{\tilde{q}_R} \sim 2{,}000$ GeV if $m_\chi \ll m_{\tilde{g}}, m_{\tilde{q}_R}$, and similar sensitivities are expected in the CMSSM and the NUHM1. The discovery range with 3,000/fb of luminosity would extend a few hundred GeV further, so large parts of the CMSSM and NUHM1 parameter spaces will be accessible in future runs of the LHC.

On the other hand, the lower panels in Fig. 4 and the 95 % CL lower limits on $m_{\tilde{\tau}_1}$ given in (4) suggest, within the CMSSM and NUHM1, that the lighter stau and other sleptons may lie beyond the reach of a low-energy e^+e^- collider. However, it should be emphasized that this observation is necessarily model dependent, as there is no direct information on $m_{\tilde{\tau}_1}$. If the universality assumptions of the CMSSM and the NUHM1 were to be modified appropriately, one might be able to explain the $g_\mu - 2$ discrepancy as well as offering more hope for $\tilde{\tau}_1$ detection in e^+e^- collisions.

Figure 6 displays the $(m_\chi, \sigma_p^{\rm SI})$ planes in the CMSSM (left) and the NUHM1 (right), again with solid (dashed) lines representing the current analysis [36] and the constraints of [61], respectively, the red (blue) lines representing 68 (95) % CL contours, respectively, with the filled (open) green stars denoting the corresponding best-fit points. We see that values of $\sigma_p^{\rm SI}$ in range $10^{-47} \lesssim \sigma_p^{\rm SI} \lesssim 10^{-43}$ cm^2 are allowed in the CMSSM at the 95 % CL, though the best-fit point yields $\sigma_p^{\rm SI} \lesssim 10^{-46}$ cm^2. In the NUHM1, the range of $\sigma_p^{\rm SI}$ preferred at the 68 and 95 % CL extends to lower values $\lesssim 10^{-48}$ cm^2, whilst the best-fit point yields $\sigma_p^{\rm SI} \sim 10^{-45}$ cm^2, higher than the CMSSM best-fit value. These global fits indicate that $\sigma_p^{\rm SI}$ may lie considerably below the current upper limit from the LUX experiment [43], though significantly above the level of the background from neutrino scattering, and hence potentially accessible to future experiments searching for the scattering of astrophysical dark matter.

There have been several claims to have observed signatures of the scattering of relatively low-mass dark matter particles, which could not be accommodated within the class of universal models discussed here. Moreover, these claims

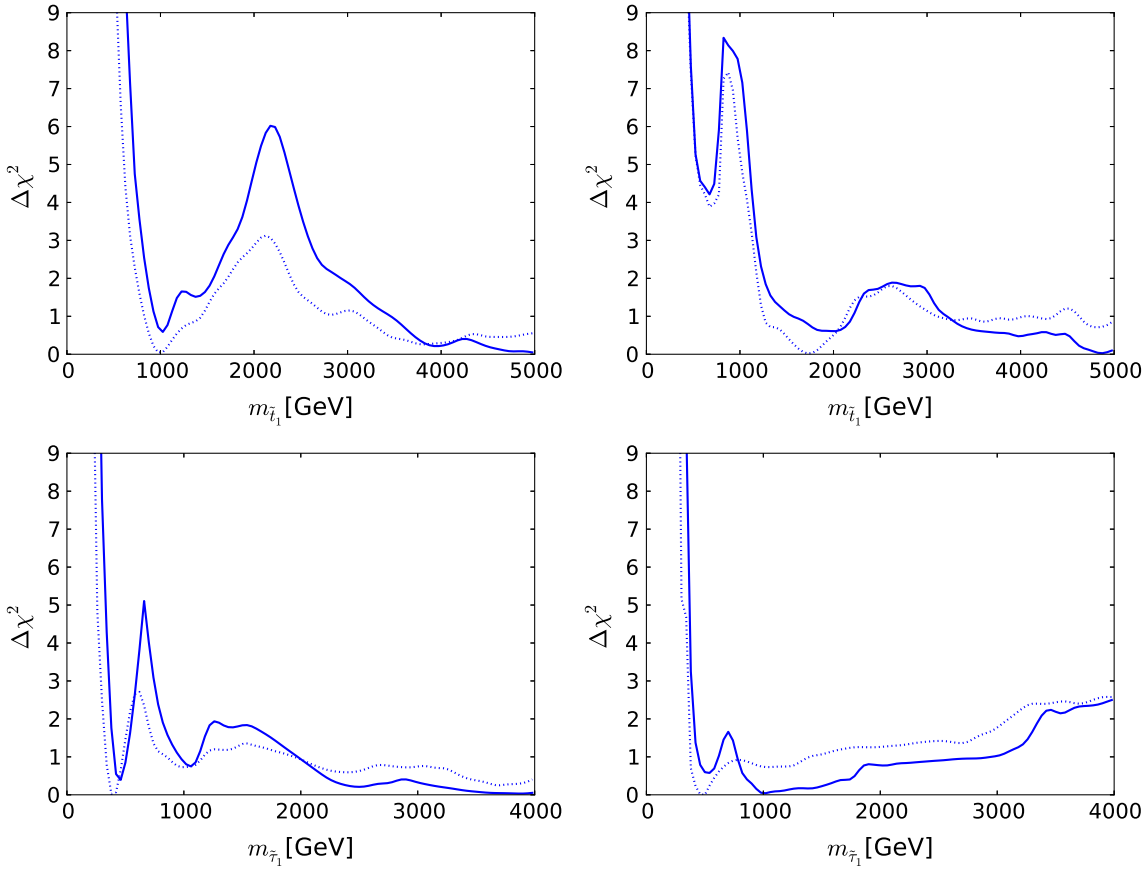

Fig. 4 The one-dimensional χ^2 likelihood functions for $m_{\tilde{t}_1}$ (*upper*) and $m_{\tilde{\tau}_1}$ (*lower*) in the CMSSM (*left*) and the NUHM1 (*right*) [36]. In each *panel*, the *solid line* is derived from a global analysis of the present data, and the *dotted line* is derived from an analysis if the data set used in [61], using the same implementations of the m_h and dark matter scattering constraints

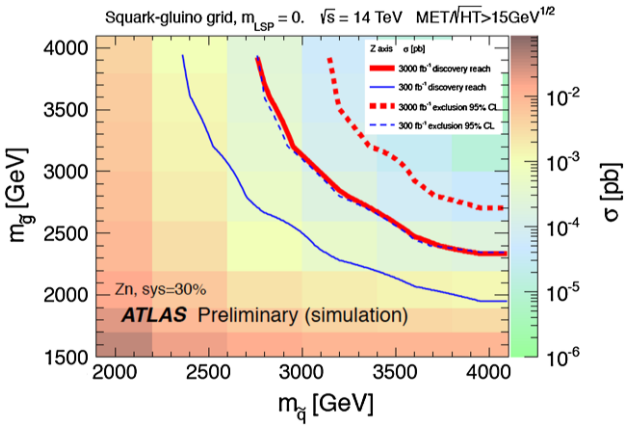

Fig. 5 The physics reach of the LHC in the $(m_0, m_{1/2})$ plane provided by searches for squarks and gluinos assuming that the LSP mass is negligible [76]. The *different colours* represent the production cross section at 14 TeV. The *solid* (*dashed*) *lines* display the 5σ discovery reach (95 % CL exclusion limit) with 300/fb and 3,000/fb, respectively

were not easy to reconcile with other negative results, e.g., from XENON100, and seem now to have been ruled out by the first results of the LUX experiment [43]. Likewise, there are various claims to have observed what might be indirect signatures of annihilations of astrophysical dark matter particles that are also difficult to accommodate within the class of models discussed here, and that will not be discussed further.

4 Alternative approaches

The above results were in the CMSSM and NUHM1 frameworks, and they are quite specific to those models. This section contains some discussions of other models and proposals for model-independent analyses of LHC data.

4.1 mSUGRA

As already mentioned, mSUGRA is a more restrictive framework than the CMSSM, since the gravitino mass is equal to the scalar mass: $m_{3/2} = m_0$, and the trilinear and bilinear soft supersymmetry-breaking parameters are related: $A_0 = B_0 + m_0$. The former relation restricts the part of the $(m_{1/2}, m_0)$ plane in which the lightest neutralino is the LSP, and the second relation allows the value of $\tan\beta$ to be

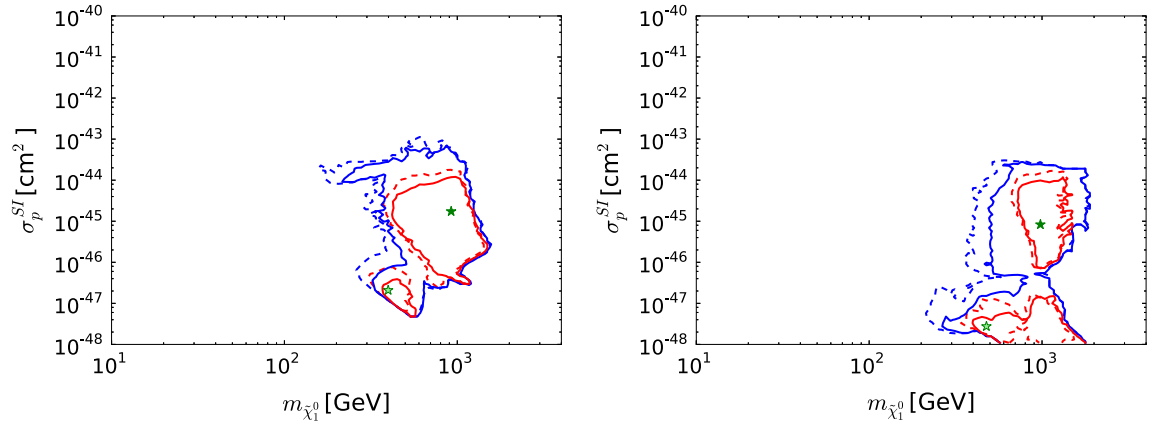

Fig. 6 The $(m_\chi, \sigma_p^{\rm SI})$ planes in the CMSSM (*left*) and the NUHM1 (*right*) [36]. In both *panels*, the *solid lines* are derived from a global analysis of the present data, and the *dotted lines* are derived from an analysis of the data used in [61], with the current implementations of the m_h and $\sigma_p^{\rm SI}$ constraints. The *red lines* denote the $\Delta\chi^2 = 2.30$ contours, the *blue lines* denote the $\Delta\chi^2 = 5.99$ contours in each case, and the *filled* (*open*) *green stars* denote the corresponding best-fit points

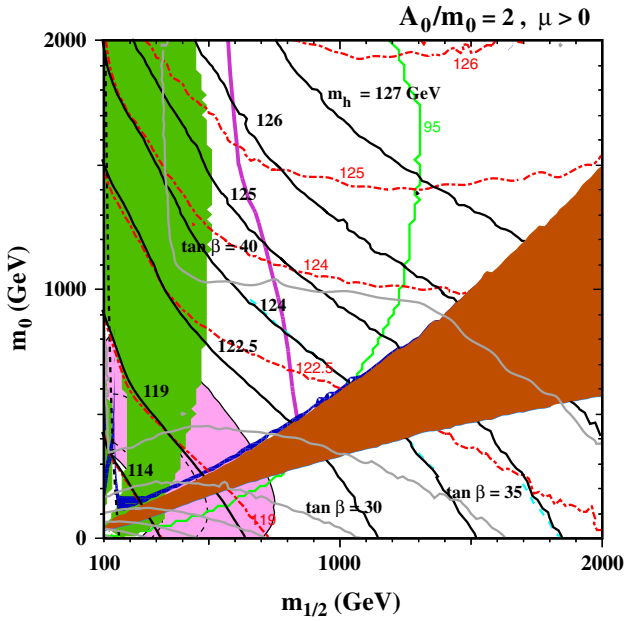

Fig. 7 The $(m_{1/2}, m_0)$ plane in a mSUGRA model with $A_0/m_0 = 2$ [44]. In addition to the *line* and *shade* conventions used in Fig. 1, the values of $\tan\beta$ derived from the electroweak vacuum conditions are shown as *solid grey contours*

fixed at each point in the $(m_{1/2}, m_0)$ plane by the electroweak vacuum conditions. Figure 7 displays a typical mSUGRA $(m_{1/2}, m_0)$ plane for the particular choice $A_0/m_0 = 2$ [44]. The same conventions as in Fig. 1 are used to represent the experimental and cosmological density constraints, and the grey lines are contours of $\tan\beta$. There is a (brown) wedge of the plane where the LSP is the lighter stau, flanked by a neutralino LSP region at larger $m_0 = m_{3/2}$ and a gravitino LSP region at smaller $m_0 = m_{3/2}$. The ATLAS $E/_T$ search is directly applicable only in the neutralino LSP region, and would require reconsideration in the gravitino LSP region.

In addition, in this region there are important astrophysical and cosmological limits on long-lived charged particles (in this case staus). The (purple) ATLAS $E/_T$ constraint intersects the (dark blue) dark matter coannihilation strip just above this wedge where $m_{1/2} \sim 850$ GeV, and the (green) BR$(B_s \to \mu^+\mu^-)$ constraint intersects the coannihilation strip at $m_{1/2} \sim 1{,}050$ GeV. The portion of the coannihilation strip between this value and its tip at $m_{1/2} \sim 1{,}250$ GeV is consistent with all the constraints. In particular, in this section of the coannihilation strip the nominal value of m_h provided by `FeynHiggs 2.10.0` is $\in$ (124, 125) GeV, compatible with the experimental measurement within the theoretical uncertainties due to the 1–2 GeV shift in m_h found in the new version of `FeynHiggs`, whereas the previous version would have given $m_h < 124$ GeV.

4.2 'Natural' models

In view of the absence of supersymmetry in conventional jets + $E/_T$ searches, the fact that the lighter stop squark $\tilde{t}_1$ is lighter than first- and second-generation squarks in many models (as we saw earlier in the cases of the CMSSM and the NUHM1), and the fact that the naturalness (or fine-tuning) argument applies most strongly to the stop, there have been many studies of so-called 'natural' models in which it is assumed that $m_{\tilde{t}_1} \ll m_{\tilde{q}_R}, m_{\tilde{g}}$. Figure 8 summarizes the results of dedicated stop searches by the CMS Collaboration [77]. We see explicitly that the sensitivity of search depends on the stop decay mode assumed as well as the LSP mass assumed, and we should recall that in a realistic model stop decays may not be dominated by a single mode. So far, the dedicated stop searches do not impinge significantly on the parameter spaces of the CMSSM and the NUHM1, but this may change in the future.

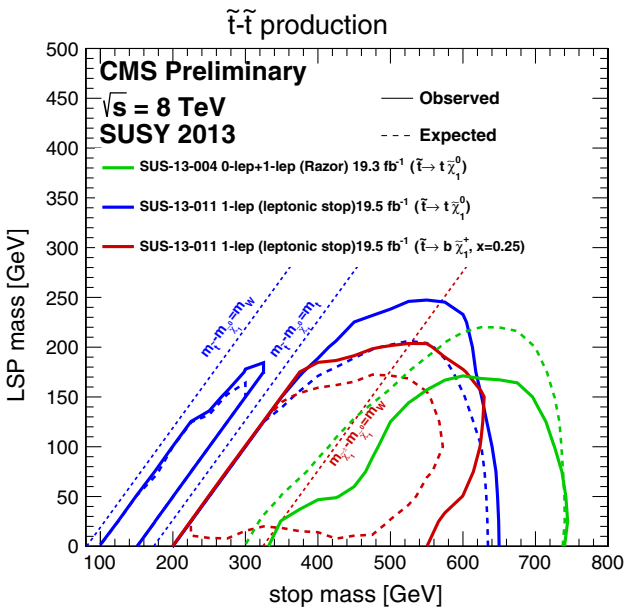

Fig. 8 Exclusion limits from stop searches by the CMS Collaboration [77]

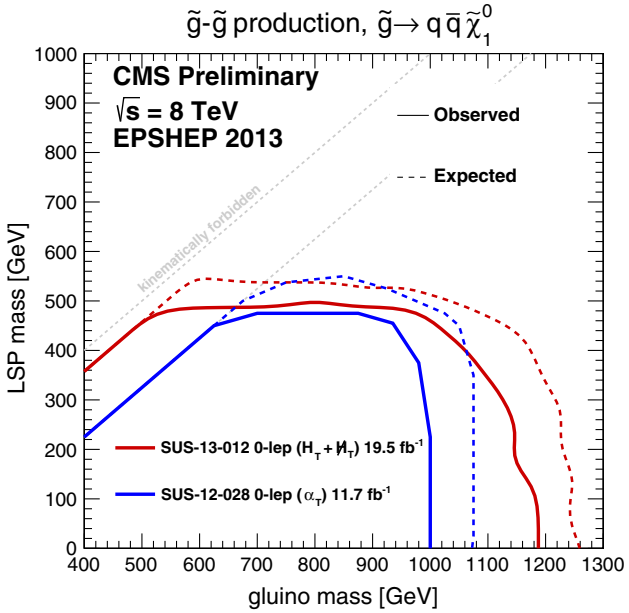

Fig. 9 Exclusion limits from searches by the CMS Collaboration in the simplified model topology $\tilde{g}\tilde{g} \rightarrow \bar{q}q\bar{q}q\chi\chi$ [77]

4.3 Simplified models

Another approach has been to benchmark supersymmetric searches by assuming simplified models in which some specific cascade signature is assumed to dominate sparticle production and decay at the LHC. For example, it might be assumed that the gluinos are much lighter than all the squarks and decay dominantly into $\bar{q}q\chi$ final states. Figure 9 shows the exclusion limits obtained by the CMS Collaboration from a search for pair-production of gluinos in this heavy-squark limit followed by decays into $\bar{q}q\chi$ final states with 100 % branching ratios [77]. We see that this search also does not reach the 95 % CL lower limits in the CMSSM and the NUHM1 that were discussed earlier. We also note that such simplified models are in general over-simplified, in that typical branching ratios are <100 %, on the one hand, and realistic models may be tackled simultaneously using several signatures in parallel. A possible way forward building on the simplified model approach may be to parameterize a realistic model in terms of the probabilities with which specific model signatures occur and combine different signatures with a 'mix and match' approach to obtain the overall sensitivity to that model [78].

4.4 Combining searches

An interesting step in this direction was taken in [79], where it was shown that certain combinations of searches yield a sensitivity to a class of models that is almost independent of the specific parameters of the model within that class. The idea here was to combine searches for $E/_T$ + jets without leptons, with a single lepton and with same- and opposite-sign dileptons, and apply them to a class of 'natural-like' supersymmetric spectra. As can be seen in Fig. 10 where this approach was applied to 7 TeV data, the confidence level with which a particular set of gluino, third-generation squark and LSP masses ($m_{\tilde{g}} = 1$ TeV, $m_{\tilde{q}_3} = 700$ GeV, $m_{\chi} = 100$ GeV)

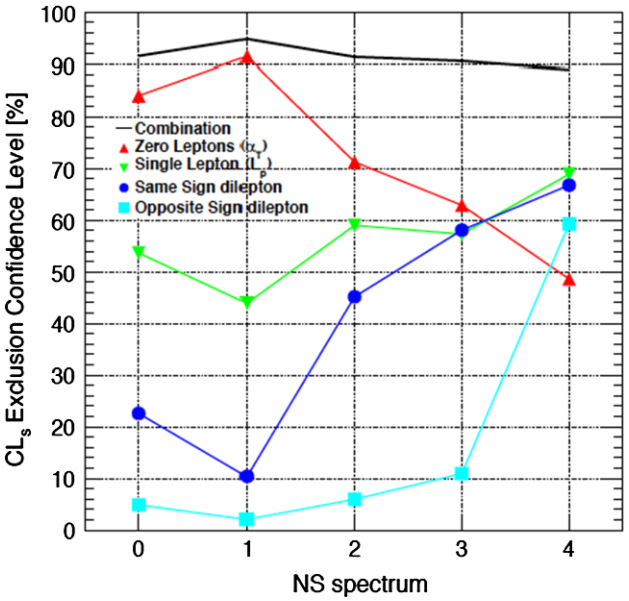

Fig. 10 The confidence levels for excluding a class of 'natural-like' supersymmetric models by combining searches at 7 TeV for several different topologies: $E/_T$ + jets without leptons, with a single lepton and with same- and opposite-sign dileptons [79]

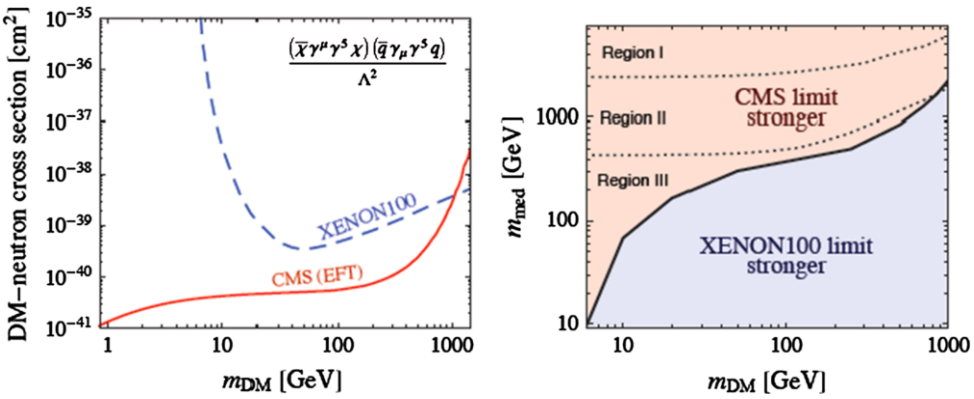

Fig. 11 It is shown in the *left panel* that, in the effective field theory (EFT) approximation, monojet searches are more sensitive than the XENON100 search for a spin-dependent dimension-6 interaction of the form $(\bar{\chi}\gamma_\mu\gamma_5\chi)(\bar{q}\gamma_\mu\gamma_5 q)/\Lambda^2$. However, the *right panel* shows that this conclusion depends on the mass controlling the form factor of the dimension-6 interaction [80]

could be excluded was found to be essentially independent of other details of the spectrum and associated branching ratios.

4.5 Monojet searches

In all the above searches, the production and cascade decays of heavier supersymmetric particles were considered. A different approach, which aims to be more model independent, is to look directly for pair-production of LSPs χ with the signature of an accompanying monojet (due predominantly to initial-state gluon radiation) or electroweak boson (γ, $W^\pm$ or Z^0). The idea was to use such searches to constrain higher-dimensional operators that could also mediate the scattering of astrophysical dark matter. In particular, it was hoped that this approach would clarify the confusion that existed for a long time about possible experimental hints for low-mass cold dark matter particles.

This approach looks promising for the case of spin-dependent dark matter scattering via an effective dimension-6 operator of the form $(\bar{\chi}\gamma_\mu\gamma_5\chi)(\bar{q}\gamma_\mu\gamma_5 q)/\Lambda^2$, as seen in the left panel of Fig. 11 [80]. However, one should remember that the kinematics of dark matter scattering (which has a very small space-like momentum transfer) and pair-production (where the momentum transfer is time-like and $> 4m_\chi^2$). This raises the possibility that there may be a non-trivial form factor for the effective operator, which could suppress the sensitivity in the LHC searches for monojets, etc.. The right panel of Fig. 11 illustrates the potential importance of this effect. Whereas the LHC limit appears stronger than the XENON100 limit in the effective field theory (EFT) limit (left panel), we see that the XENON100 limit may actually be stronger, depending on the details of the theory underlying the EFT model [80]. That said, this approach is an interesting supplement to more conventional $E/_T$ + jets searches, and may play an increasingly important rôle in searches for supersymmetry and other new physics when the LHC restarts at high energy.

5 Summary and prospects

The first run of the LHC leaves a bittersweet taste in the mouths of high-energy physicists. On the one hand, the ATLAS and CMS Collaborations have discovered a Higgs boson, an experimental Holy Grail since it was first postulated in 1964. On the other hand, they have found no trace of any other new physics, in particular no sign of supersymmetry. However, the appearance of an apparently elementary Higgs boson poses severe problems of naturalness and fine-tuning, so theorists should rejoice that they have new challenges to meet. Supersymmetry still seems to the present author to be the most promising framework for responding to these challenges, and I argue that the LHC measurements of the low mass and standard model-like couplings of the Higgs boson provide additional circumstantial arguments for supersymmetry.

The LHC searches for supersymmetry, the Higgs mass, the measurement of $\mathrm{BR}(B_s \to \mu^+\mu^-)$ and other experiments, notably those on dark matter, can be combined in global fits to the parameters of specific supersymmetric models [36,62–69]. The two examples discussed here are the CMSSM and the NUHM1: analyzing models with more parameters in an equally thorough way would be far more computationally intensive. Results of global fits to the CMSSM and the NUHM1, including best-fit points, regions preferred at the 68 % CL and allowed at the 95 % CL have been presented in this paper, as well as 95 % CL lower limits on some sparticle masses. Within these models, there are reasonable prospects for discovering supersymmetry at the LHC at higher energy, as well as for observing the scattering of astrophysical dark matter.

Various alternative approaches to supersymmetry phenomenology have also been discussed, including 'natural' models, simplified models, combined analyses of benchmark signatures, and searches for monoboson events. Although none of these impinges significantly on the CMSSM and NUHM1 parameter spaces, all of them are likely to play

greater rôles in future studies of supersymmetry at the LHC at higher energies, particularly as interest broadens to a wider range of models.

We await with impatience the advent of high-energy LHC running with increasing luminosity.

Acknowledgments I thank fellow members of the MasterCode Collaboration, particularly Oliver Buchmueller, Sven Heinemeyer, Jad Marrouche, Keith Olive and Kees de Vries for many discussions on this subject. This work was supported in part by the London Centre for Terauniverse Studies (LCTS), using funding from the European Research Council via the Advanced Investigator Grant 267352.

References

1. G. Aad et al. [ATLAS Collaboration], Phys. Lett. B **716**, 1 (2012). [arXiv:1207.7214 [hep-ex]]
2. S. Chatrchyan et al. [CMS Collaboration], Phys. Lett. B **716**, 30 (2012). [arXiv:1207.7235 [hep-ex]]
3. P. Ramond, SUSY: the early years (1966-1976). Eur. Phys. J. C **74**, 2698 (2014). doi:10.1140/epjc/s10052-013-2698-x. arXiv:1401.5977
4. J.R. Ellis, G. Ridolfi, F. Zwirner, Phys. Lett. B **257**, 83 (1991)
5. J.R. Ellis, G. Ridolfi, F. Zwirner, Phys. Lett. B **262**, 477 (1991)
6. Y. Okada, M. Yamaguchi, T. Yanagida, Prog. Theor. Phys. **85**, 1 (1991)
7. A. Yamada, Phys. Lett. B **263**, 233 (1991)
8. Howard E. Haber, Ralf Hempfling, Phys. Rev. Lett. **66**, 1815 (1991)
9. M. Drees, M.M. Nojiri, Phys. Rev. D **45**, 2482 (1992)
10. P.H. Chankowski, S. Pokorski, J. Rosiek, Phys. Lett. B **274**, 191 (1992)
11. P.H. Chankowski, S. Pokorski, J. Rosiek, Phys. Lett. B **286**, 307 (1992)
12. G. Degrassi, S. Di Vita, J. Elias-Miro, J.R. Espinosa, G.F. Giudice, G. Isidori, A. Strumia, JHEP **1208**, 098 (2012). [arXiv:1205.6497 [hep-ph]]
13. J.R. Ellis, D. Ross, Phys. Lett. B **506**, 331 (2001). [arXiv:hep-ph/0012067]
14. See, for example, J. Ellis, T. You, JHEP 1306 (2013) 103 [arXiv:1303.3879 [hep-ph]]
15. R. Catena, L. Covi, SUSY dark matter(s). Eur. Phys. J. C **74**, 2703 (2014). doi:10.1140/epjc/s10052-013-2703-4. arXiv:1310.4776
16. H. Goldberg, Phys. Rev. Lett. **50**, 1419 (1983). [Erratum-ibid. 103 (2009) 099905]
17. J.R. Ellis, J.S. Hagelin, D.V. Nanopoulos, K.A. Olive, M. Srednicki, Nucl. Phys. B **238**, 453 (1984)
18. ATLAS and CMS contributions to this volume
19. A. Djouadi, Implications of the Higgs discovery for the MSSM. Eur. Phys. J. C **74**, 2704 (2014). doi:10.1140/epjc/s10052-013-2704-3. arXiv:1311.0720
20. R.S. Chivukula, H. Georgi, Phys. Lett. B **188**, 99 (1987)
21. G. D'Ambrosio et al., Nucl. Phys. B **645**, 155 (2002). [arXiv:hep-ph/0207036]
22. J.R. Ellis, J.S. Lee, A. Pilaftsis, Phys. Rev. D **76**, 115011 (2007). [arXiv:0708.2079 [hep-ph]]
23. M. Drees, M.M. Nojiri, Phys. Rev. D **47**, 376 (1993). [arXiv:hep-ph/9207234]
24. G.L. Kane, C.F. Kolda, L. Roszkowski, J.D. Wells, Phys. Rev. D **49**, 6173 (1994). [arXiv:hep-ph/9312272]
25. H. Baer, M. Brhlik, Phys. Rev. D **53**, 597 (1996). [arXiv:hep-ph/9508321]
26. H. Baer, M. Brhlik, Phys. Rev. D **57**, 567 (1998). [arXiv:hep-ph/9706509]
27. J.R. Ellis, T. Falk, K.A. Olive, M. Schmitt, Phys. Lett. B **388**, 97 (1996). [arXiv:hep-ph/9607292]
28. V.D. Barger, C. Kao, Phys. Rev. D **57**, 3131 (1998). [arXiv:hep-ph/9704403]
29. L. Roszkowski, R. Ruiz de Austri, T. Nihei, JHEP **0108**, 024 (2001). [arXiv:hep-ph/0106334]
30. A. Djouadi, M. Drees, J.L. Kneur, JHEP **0108**, 055 (2001). [arXiv:hep-ph/0107316]
31. U. Chattopadhyay, A. Corsetti, P. Nath, Phys. Rev. D **66**, 035003 (2002). [arXiv:hep-ph/0201001]
32. J.R. Ellis, K.A. Olive, Y. Santoso, New Jour. Phys. **4**, 32 (2002). [arXiv:hep-ph/0202110]
33. H. Baer, A. Mustafayev, S. Profumo, A. Belyaev, X. Tata, Phys. Rev. D **71**, 095008 (2005). [arXiv:hep-ph/0412059]
34. H. Baer, A. Mustafayev, S. Profumo, A. Belyaev, X. Tata, JHEP **0507**, 065 (2005). [arXiv:hep-ph/0504001]
35. J.R. Ellis, K.A. Olive, P. Sandick, Phys. Rev. D **78**, 075012 (2008). [arXiv:0805.2343 [hep-ph]]
36. O. Buchmueller, R. Cavanaugh, A. De Roeck, M. J. Dolan, J. R. Ellis, H. Flacher, S. Heinemeyer, G. Isidori et al., [arXiv:1312.5250 [hep-ph]]
37. ATLAS Collaboration, http://cds.cern.ch/record/1547563/files/ATLAS-CONF-2013-047.pdf
38. S. Chatrchyan et al., CMS Collaboration. Phys. Rev. Lett. **111**, 101804 (2013). [arXiv:1307.5025 [hep-ex]]
39. R. Aaij et al., LHCb Collaboration. Phys. Rev. Lett. **111**, 101805 (2013). [arXiv:1307.5024 [hep-ex]]
40. R.Aaij et al. [LHCb and CMS Collaborations], LHCb-CONF-2013-012, CMS PAS BPH-13-007
41. F. Palla, CERN, seminar, Aug. 6th, 2013
42. J. Serrano, CERN, seminar, Aug. 6th, 2013
43. D.S. Akerib et al. [LUX Collaboration], [arXiv:1310.8214 [astro-ph.CO]]
44. O. Buchmueller, M. Dolan, J. Ellis, T. Hahn, S. Heinemeyer, W. Hollik, J. Marrouche, K. A. Olive et al. [arXiv:1312.5233 [hep-ph]]
45. For previous versions of FeynHiggs, see: G. Degrassi, S. Heinemeyer, W. Hollik, P. Slavich, G. Weiglein, Eur. Phys. J. C **28**, 133 (2003). [arXiv:hep-ph/0212020]
46. S. Heinemeyer, W. Hollik, G. Weiglein, Eur. Phys. J. C **9**, 343 (1999). [arXiv:hep-ph/9812472]
47. S. Heinemeyer, W. Hollik, G. Weiglein, Comput. Phys. Commun. **124**, 76 (2000). [arXiv:hep-ph/9812320]
48. M. Frank et al., JHEP **0702**, 047 (2007). [arXiv:hep-ph/0611326]
49. T. Hahn, S. Heinemeyer, W. Hollik, H. Rzehak, G. Weiglein, Comput. Phys. Commun. **180**, 1426 (2009)
50. T. Hahn, S. Heinemeyer, W. Hollik, H. Rzehak, G. Weiglein, [arXiv:1312.4937 [hep-ph]]
51. For a review and references, see: T. Blum, A. Denig, I. Logashenko, E. de Rafael, B.L. Roberts, T. Teubner, G. Venanzoni, [arXiv:1311.2198 [hep-ph]]
52. O. Buchmueller et al., Phys. Lett. B **657**, 87 (2007). [arXiv:0707.3447 [hep-ph]]
53. O. Buchmueller et al., JHEP **0809**, 117 (2008). [arXiv:0808.4128 [hep-ph]]
54. O. Buchmueller et al., Eur. Phys. J. C **64**, 391 (2009). [arXiv:0907.5568 [hep-ph]]
55. O. Buchmueller et al., Phys. Rev. D **81**, 035009 (2010). [arXiv:0912.1036 [hep-ph]]

56. O. Buchmueller et al., Eur. Phys. J. C **71**, 1583 (2011). [arXiv:1011.6118 [hep-ph]]
57. O. Buchmueller et al., Eur. Phys. J. C **71**, 1634 (2011). [arXiv:1102.4585 [hep-ph]]
58. O. Buchmueller et al., Eur. Phys. J. C **71**, 1722 (2011). [arXiv:1106.2529 [hep-ph]]
59. O. Buchmueller et al., Eur. Phys. J. C **72**, 1878 (2012). [arXiv:1110.3568 [hep-ph]]
60. O. Buchmueller et al., Eur. Phys. J. C **72**, 2020 (2012). [arXiv:1112.3564 [hep-ph]]. For more information and updates, please see http://cern.ch/mastercode/
61. O. Buchmueller et al., Eur. Phys. J. C **72**, 2243 (2012). [arXiv:1207.7315 [hep-ph]]
62. For a sampling of other post-LHC analyses, see: P. Bechtle et al., arXiv:1102.4693 [hep-ph]
63. M. Farina, M. Kadastik, D. Pappadopulo, J. Pata, M. Raidal, A. Strumia, Nucl. Phys. B **853**, 607 (2011). [arXiv:1104.3572 [hep-ph]]
64. M. Baak, M. Goebel, J. Haller, A. Hoecker, D. Ludwig, K. Moenig, M. Schott, J. Stelzer, Eur. Phys. J. C **72**, 2003 (2012). [arXiv:1107.0975 [hep-ph]]
65. N. Bhattacharyya, A. Choudhury, A. Datta, Phys. Rev. D **84**, 095006 (2011). [arXiv:1107.1997 [hep-ph]]
66. A. Fowlie, A. Kalinowski, M. Kazana, L. Roszkowski, Y.L.S. Tsai, Phys. Rev. D **85**, 075012 (2012). [arXiv:1111.6098 [hep-ph]]
67. T.J. LeCompte, S.P. Martin, Phys. Rev. D **85**, 035023 (2012). [arXiv:1111.6897 [hep-ph]]
68. L. Roszkowski, E. M. Sessolo, Y.-L.S. Tsai, [arXiv:1202.1503 [hep-ph]]
69. P. Bechtle, K. Desch, H.K. Dreiner, M. Hamer, M. Krmer, B. O'Leary, W. Porod, X. Prudent et al., [arXiv:1310.3045 [hep-ph]]
70. F. Feroz, M.P. Hobson, M. Bridges, Mon. Not. Roy. Astron. Soc. **398**, 1601 (2009). [arXiv:0809.3437 [astro-ph]]
71. F. Feroz, M.P. Hobson, Mon. Not. Roy. Astron. Soc. **384**, 449 (2008). [arXiv:0704.3704 [astro-ph]]
72. F. Feroz, K. Cranmer, M. Hobson, R. Ruiz de Austri, R. Trotta, JHEP **1106**, 042 (2011). [arXiv:1101.3296 [hep-ph]]
73. J.R. Ellis, K. Enqvist, D.V. Nanopoulos, F. Zwirner, Mod. Phys. Lett. A **1**, 57 (1986)
74. R. Barbieri, G.F. Giudice, Nucl. Phys. B **306**, 63 (1988)
75. G.G. Ross, SUSY: Quo Vadis?. Eur. Phys. J. C **74**, 2699 (2014). doi:10.1140/epjc/s10052-013-2699-9
76. ATLAS Collaboration, [arXiv:1307.7292 [hep-ex]]
77. For a compilation of these and other CMS results, see: https://twiki.cern.ch/twiki/bin/view/CMSPublic/PhysicsResultsSUS
78. K. Sakurai, private communication
79. O. Buchmueller, J. Marrouche, [arXiv:1304.2185 [hep-ph]]
80. O. Buchmueller, M.J. Dolan, C. McCabe, [arXiv:1308.6799 [hep-ph]]

Eur. Phys. J. C (2014) 74:2704
DOI 10.1140/epjc/s10052-013-2704-3

THE EUROPEAN PHYSICAL JOURNAL C

Review

Implications of the Higgs discovery for the MSSM

Abdelhak Djouadi[1,2,a]

[1] Laboratoire de Physique Théorique, U. Paris–Sud and CNRS, 91405 Orsay, France
[2] *Present address:* TH Unit, CERN, Geneva, Switzerland

Received: 20 November 2013 / Accepted: 27 November 2013 / Published online: 27 May 2014

Abstract The implications of the discovery of the Higgs boson at the LHC with a mass of approximately 125 GeV are summarised in the context of the minimal supersymmetric extension of the Standard Model, the MSSM. Discussed are the implications from the measured mass and production/decay rates of the observed particle and from the constraints in the search for the heavier Higgs states at the LHC.

1 Introduction

The historical discovery by ATLAS and CMS of a particle with a mass of approximately 125 GeV [1,2] and properties that are compatible with those of a scalar Higgs boson [3–8] has far reaching consequences not only for the Standard Model (SM) of the electroweak and strong interactions, but also for new physics models beyond it. This is particularly true for supersymmetric theories (SUSY) [9–11] that are widely considered to be the most attractive extensions of the SM as they naturally protect the Higgs mass against large radiative corrections and stabilise the hierarchy between the electroweak and Planck scales, besides of allowing for the unification of the three gauge coupling constants and providing a good candidate for the dark matter in the universe, the lightest SUSY particle.

In the minimal supersymmetric extension of the SM (MSSM), two Higgs doublet fields H_u and H_d are required to break the electroweak symmetry, leading to a physical spectrum with five Higgs particles: two CP-even, h and H, a CP-odd, A, and two charged, $H^\pm$, states [6,8]. Two parameters are needed to describe the MSSM Higgs sector at the tree level: one Higgs mass, which is generally taken to be that of the pseudoscalar boson M_A, and the ratio of vacuum expectation values of the two Higgs fields, $\tan\beta = v_d/v_u$, expected to lie in the range $1 \lesssim \tan\beta \lesssim 60$. The masses of the CP-even h, H and the charged $H^\pm$ states, as well as the mixing angle α in the CP-even sector are uniquely defined in terms of these two inputs at tree level, but this nice property is spoiled at higher orders [12–28].

At high M_A values, $M_A \gg M_Z$, one is in the so-called decoupling regime [29] in which the neutral CP-even state h is light and has almost exactly the properties of the SM Higgs boson, i.e. its couplings to fermions and gauge bosons are the same as the standard Higgs, while the other CP-even H and the charged $H^\pm$ bosons become heavy and mass degenerate with the A state, $M_H \approx M_{H^\pm} \approx M_A$, and they decouple from the massive gauge bosons. In this regime, the MSSM Higgs sector thus looks almost exactly like the one of the SM with its unique Higgs boson.

There is, however, one major difference between the two cases: while in the SM the Higgs mass is essentially a free parameter (and should simply be smaller than about 1 TeV in order to ensure unitarity in the high-energy scattering of massive gauge bosons), the lightest MSSM CP-even Higgs particle mass is bounded from above and, depending on the SUSY parameters that enter the important quantum corrections, is restricted to $M_h^{\max} \approx 90$–130 GeV. The lower value comes from experimental constraints, in particular Higgs searches at LEP [30,31], while the upper bound assumes a SUSY-breaking scale that is not too high, $M_S \lesssim \mathcal{O}$ (1 TeV), in order to avoid too much fine-tuning in the model. Hence, the requirement that the MSSM h boson coincides with the one observed at the LHC, i.e. with $M_h \approx 125$ GeV and almost SM-like couplings as the LHC data seem to indicate, would place very strong constraints on the MSSM parameters, in particular the SUSY scale M_S, through their contributions to the radiative corrections to the Higgs sector. This comes in addition to the limits that have been obtained from the search of the heavier Higgs states at the LHC, as well as from the negative search for supersymmetric particles.

In this review, we summarise the implications of the available LHC Higgs results for the MSSM Higgs sector. We first discuss the consequences of the M_h measured value for the various unconstrained (with the many free parameters

[a] e-mail: djouadi@th.u-psud.fr

defined at the weak scale) and constrained (with parameters obeying some universal boundary conditions at the high scale) versions of the MSSM. We then discuss the impact of the measured production and decay rates of the observed particle on the various Higgs couplings and, hence, the MSSM parameters. The impact of the negative search of the heavy H, A and $H^\pm$ states is summarised. An outlook is given in a concluding section.

2 Implications of the Higgs mass value

2.1 The Higgs masses in the MSSM

In the MSSM, the tree-level masses of the CP-even h and H bosons depend only on M_A and $\tan\beta$. However, many parameters of the MSSM such as the masses of the third generation stop and sbottom squarks $m_{\tilde{t}_i}, m_{\tilde{b}_i}$ and their trilinear couplings A_t, A_b enter M_h and M_H through quantum corrections. In the basis (H_d, H_u), the CP-even Higgs mass matrix can be written in full generality as

$$\mathcal{M}^2 = M_Z^2 \begin{pmatrix} c_\beta^2 & -s_\beta c_\beta \\ -s_\beta c_\beta & s_\beta^2 \end{pmatrix} + M_A^2 \begin{pmatrix} s_\beta^2 & -s_\beta c_\beta \\ -s_\beta c_\beta & c_\beta^2 \end{pmatrix} + \begin{pmatrix} \Delta\mathcal{M}_{11}^2 & \Delta\mathcal{M}_{12}^2 \\ \Delta\mathcal{M}_{12}^2 & \Delta\mathcal{M}_{22}^2 \end{pmatrix} \tag{1}$$

where we use the short-hand notation $s_\beta \equiv \sin\beta$ etc. and introduce the radiative corrections by a general 2×2 matrix $\Delta\mathcal{M}_{ij}^2$. One can then easily derive the neutral CP even Higgs boson masses and the mixing angle α that diagonalises the h and H states, $H = \cos\alpha H_d^0 + \sin\alpha H_u^0$ and $h = -\sin\alpha H_d^0 + \cos\alpha H_u^0$:

$$M_{h/H}^2 = \frac{1}{2}\big(M_A^2 + M_Z^2 + \Delta\mathcal{M}_{11}^2 + \Delta\mathcal{M}_{22}^2 \mp N\big) \tag{2}$$

$$\tan\alpha = \frac{2\Delta\mathcal{M}_{12}^2 - (M_A^2 + M_Z^2)s_\beta}{\Delta\mathcal{M}_{11}^2 - \Delta\mathcal{M}_{22}^2 + (M_Z^2 - M_A^2)c_{2\beta} + N} \tag{3}$$

$$N = \sqrt{M_A^4 + M_Z^4 - 2M_A^2 M_Z^2 c_{4\beta} + C}$$
$$C = 4\Delta\mathcal{M}_{12}^4 + (\Delta\mathcal{M}_{11}^2 - \Delta\mathcal{M}_{22}^2)^2 - 2(M_A^2 - M_Z^2) \times (\Delta\mathcal{M}_{11}^2 - \Delta M_{22}^2)c_{2\beta} - 4(M_A^2 + M_Z^2)\Delta\mathcal{M}_{12}^2 s_{2\beta} \tag{4}$$

The by far leading one-loop radiative corrections to the mass matrix of Eq. (1) are controlled by the top Yukawa coupling, $\lambda_t = m_t/v\sin\beta$ with $v = 246\,\text{GeV}$, which appears with the fourth power. One obtains a very simple analytical expression for the radiative correction matrix $\Delta\mathcal{M}_{ij}^2$ if only this contribution is taken into account [12–14]

$$\Delta\mathcal{M}_{11}^2 \sim \Delta\mathcal{M}_{12}^2 \sim 0\,, \tag{5}$$
$$\Delta\mathcal{M}_{22}^2 \sim \epsilon = \frac{3\bar{m}_t^4}{2\pi^2 v^2 \sin^2\beta}\left[\log\frac{M_S^2}{\bar{m}_t^2} + \frac{X_t^2}{M_S^2}\left(1 - \frac{X_t^2}{12M_S^2}\right)\right]$$

where M_S is the geometric average of the two stop masses $M_S = \sqrt{m_{\tilde{t}_1} m_{\tilde{t}_2}}$ defined to be the SUSY-breaking scale and X_t is the stop mixing parameter given by $X_t = A_t - \mu/\tan\beta$ with μ the higgsino mass parameter; $\bar{m}_t$ is the running $\overline{\text{MS}}$ top quark mass to account for the leading two-loop QCD corrections in a renormalisation-group improved approach (some refinements can be include as well).

Other soft SUSY-breaking parameters, in particular μ and A_b (and in general the corrections controlled by the bottom Yukawa coupling $\lambda_b = m_b/v\cos\beta$, which at large value of $\mu\tan\beta$ become relevant) as well as the gaugino mass parameters $M_{1,2,3}$, provide a small but non-negligible correction to $\Delta\mathcal{M}_{ij}^2$ and can thus also have an impact on the loop corrections [15,16,25–28].

The maximal value of the h mass, $M_h^{\max}$ is given in the leading one–loop approximation above by

$$M_h^2 \overset{M_A \gg M_Z}{\to} M_Z^2 \cos^2 2\beta + \Delta\mathcal{M}_{22}^2 \tag{6}$$

and is obtained for the choice of parameters [25–28]:

- a decoupling regime with heavy A states, $M_A \sim \mathcal{O}(\text{TeV})$;
- large values of the parameter $\tan\beta$, $\tan\beta \gtrsim 10$;
- heavy stops, i.e. large M_S values and we choose in general $M_S \leq 3\,\text{TeV}$ to avoid a too large fine-tuning [32,33];
- a stop trilinear coupling $X_t = \sqrt{6}M_S$, the so-called maximal mixing scenario that maximises the stop loops [34].

If the parameters are optimised as above, the maximal h mass value can reach the level of $M_h^{\max} \approx 130\,\text{GeV}$.

An important aspect is that in the decoupling regime $M_A \gg M_Z$, the heavier CP-even and the charged Higgs states become almost degenerate in mass with the CP-odd state, $M_H \approx M_{H^\pm} \approx M_A$, while the mixing angle α becomes close to $\alpha \approx \frac{\pi}{2} - \beta$ making the couplings of the light h state to fermions and massive gauge bosons SM-like, and decoupling the H, $H^\pm$ from the weak bosons as is the case for the state A by virtue of CP invariance.

In this section, we discuss the implications of the measured mass value of the observed Higgs boson at the LHC [35–62] that we identify with the lightest state h of the MSSM. We consider the phenomenological MSSM [63] in which the relevant soft SUSY parameters are allowed to vary freely (but with some restrictions) and constrained MSSM scenarios such as the minimal supergravity (mSUGRA) [64–67], gauge mediated (GMSB) [68–72] and anomaly mediated (AMSB) [73–75] supersymmetry-breaking models (for a review, see again Ref. [8]). We also discuss the implications of such an M_h value for scenarios in which the supersymmetric spec-

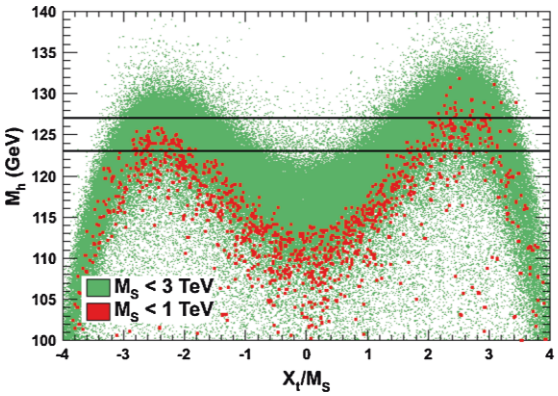

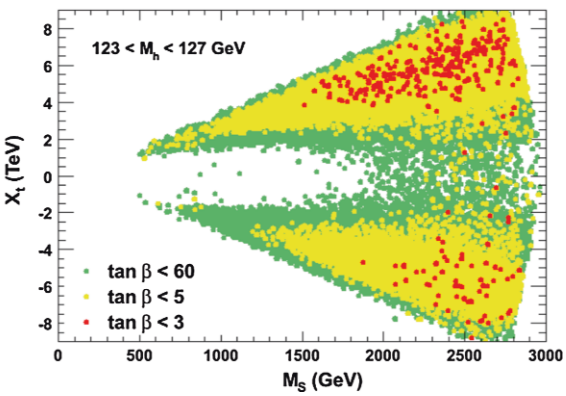

Fig. 1 The maximal value of the h boson mass as a function of X_t/M_S in the pMSSM when all other soft SUSY-breaking parameters and $\tan\beta$ are scanned (*left*) and the contours for the Higgs mass range $123 < M_h < 127\,\text{GeV}$ in the $[M_S, X_t]$ plane for some selected range of $\tan\beta$ values (*right*); from Ref. [35]

trum is extremely heavy, the so-called split SUSY [76–78] or high-scale SUSY models [79,80]. Finally, a new parametrisation of the Higgs sector, which uses the crucial information $M_h = 125$ GeV, is discussed [81].

2.2 Implications for the phenomenological MSSM

In an unconstrained MSSM, there is a large number of soft SUSY-breaking parameters, $\mathcal{O}(100)$, but analyses can be performed in the so-called "phenomenological MSSM" (pMSSM) [63], in which CP conservation, flavour diagonal sfermion mass and coupling matrices and universality of the first and second sfermion generations are imposed. The pMSSM involves then 22 free parameters in addition to those of the SM: besides $\tan\beta$ and M_A, these are the higgsino mass μ, the three gaugino masses $M_{1,2,3}$, the diagonal left- and right-handed sfermion mass parameters $m_{\tilde{f}_{L,R}}$ and the trilinear sfermion couplings A_f.

As discussed above, an estimate of the upper bound on M_h can be obtained by including the corrections that involve only the parameters M_S and X_t. However, to be more precise, one could scan the full pMSSM 22 parameter space in order to include the subleading corrections. To do so, one can use RGE programs such as `Suspect` [82] which calculate the Higgs and superparticle spectrum in the MSSM including the most up-to-date information [25].

To obtain the value $M_h^{\max}$ with the full radiative corrections, a large scan of the pMSSM parameters in an uncorrelated way was performed [35,36] in the domains:

$$\begin{aligned} 1 \le \tan\beta \le 60,\ 50\,\text{GeV} \le M_A \le 3\,\text{TeV},\\ -9\,\text{TeV} \le A_t, A_b, A_\tau \le 9\,\text{TeV},\\ 50\,\text{GeV} \le m_{\tilde{f}_L}, m_{\tilde{f}_R}, M_3 \le 3\,\text{TeV},\\ 50\,\text{GeV} \le M_1, M_2, |\mu| \le 1.5\,\text{TeV}. \end{aligned} \tag{7}$$

The results are shown in Fig. 1, where, in the left-hand side, the obtained maximal value $M_h^{\max}$ is displayed as a function of the ratio of parameters X_t/M_S. The resulting values are confronted to the mass range $123\,\text{GeV} \le M_h \le 127\,\text{GeV}$ when the parametric uncertainties from the SM inputs such as the top quark mass and the theoretical uncertainties in the determination of M_h are included[1].

For $M_S \lesssim 1$ TeV, only the scenarios with X_t/M_S values close to maximal mixing $X_t/M_S \approx \sqrt{6}$ survive. The no-mixing scenario $X_t \approx 0$ is ruled out for $M_S \lesssim 3$ TeV, while the typical mixing scenario, $X_t \approx M_S$, needs large M_S and moderate to large $\tan\beta$ values. From the scan, one obtains a maximum $M_h^{\max} = 136$, 126 and 123 GeV with maximal, typical and zero mixing, respectively.

What are the implications for the mass of the lightest stop state $\tilde{t}_1$? This is illustrated in the right-hand side of Fig. 1, where the contours are shown in the $[M_S, X_t]$ plane in which one obtains $123 < M_h < 127\,\text{GeV}$ from the pMSSM scan; the regions in which $\tan\beta \lesssim 3, 5$ and 60 are highlighted. One sees again that a large part of the parameter space is excluded if the Higgs mass constraint is imposed. In particular, large M_S values, in general corresponding to large $m_{\tilde{t}_1}$ are favoured. However, as $M_S = \sqrt{m_{\tilde{t}_1} m_{\tilde{t}_2}}$, the possibility that $m_{\tilde{t}_1}$ is of the order of a few 100 GeV is still allowed, provided that stop mixing (leading to a significant $m_{\tilde{t}_1}, m_{\tilde{t}_2}$ splitting) is large [36,57–59].

[1] This uncertainty is obtained by comparing the outputs of `SuSpect` and `FeynHiggs` [83] which use different schemes for the radiative corrections: while the former uses the $\overline{\text{DR}}$ scheme, the latter uses the on-shell scheme; the difference in the obtained M_h amounts to $\approx \pm 2$–3 GeV in general. To this, one has to add an uncertainty of ± 1 GeV from the top quark mass measurement at the Tevatron, $m_t = 173 \pm 1$ GeV [85]. Note that it is not entirely clear whether this mass is indeed the pole quark mass. A more rigorous determination of the pole mass from the measured top-pair cross section at the Tevatron gives a lower value with a larger uncertainty, $m_t^{\text{pole}} = 171 \pm 3$ GeV [84].

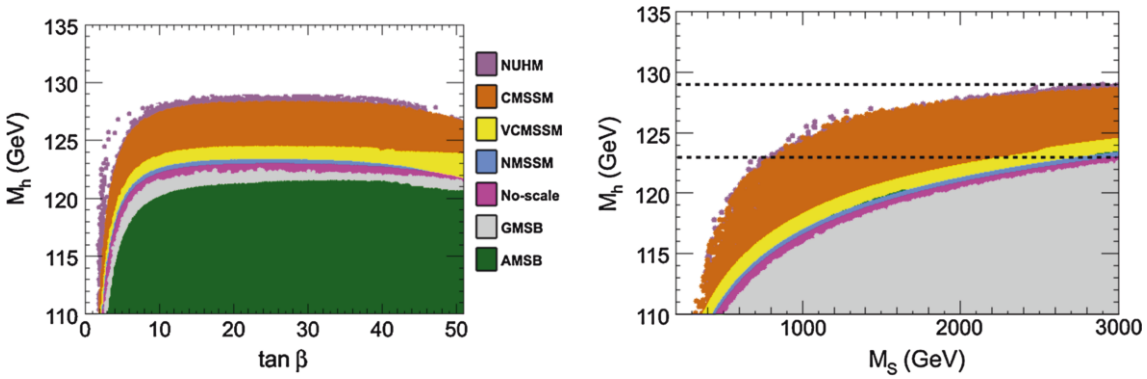

Fig. 2 The maximal value of the h boson mass as a function of $\tan\beta$ (*left*) and M_S (*right*) with a scan of all other parameters in various constrained MSSM scenarios. The range $123 < M_h < 129$ GeV for the light h boson mass is highlighted. From Ref. [35]

Masses above 1 TeV for the scalar partners of light quarks and for the gluinos are also required by the direct searches of SUSY particles at the LHC [86,87], confirming the need of high M_S values. Nevertheless, relatively light stops as well as electroweak sparticles such as sleptons, charginos and neutralinos are still possible allowing for a "natural SUSY" [33] in spite of the value $M_h \approx 125$ GeV. Nevertheless, the present LHC SUSY searches [86,87] are constraining more and more this natural scenario.

2.3 Implications for constrained MSSM scenarios

In constrained MSSM scenarios (cMSSM), the various soft SUSY-breaking parameters obey a number of universal boundary conditions at a high energy scale, thus reducing the number of basic input parameters to a handful. The various soft SUSY-breaking parameters are evolved via the MSSM renormalisation group equations down to the low energy scale M_S where the conditions of proper electroweak symmetry breaking (EWSB) are imposed.

Three classes of such models have been widely discussed in the literature. There is first the minimal supergravity (mSUGRA) model [64–67] in which SUSY-breaking is assumed to occur in a hidden sector which communicates with the visible sector only via flavour-blind gravitational interactions, leading to universal soft breaking terms, namely a common $m_{1/2}, m_0, A_0$ values for the gaugino masses, sfermion masses and sfermion trilinear couplings. Then come the gauge mediated [68–72] and anomaly mediated [73–75] SUSY-breaking (GMSB and AMSB) scenarios in which SUSY-breaking is communicated to the visible sector via, respectively, gauge interactions and a super-Weyl anomaly.

These models are described by $\tan\beta$, the sign of μ and a few continuous parameters. Besides of allowing for both signs of μ, requiring $1 \leq \tan\beta \leq 60$ and, to avoid excessive fine-tuning in the EWSB conditions, imposing the bound $M_S = M_{\rm EWSB} < 3$TeV, we adopt the following ranges for the input parameters of these scenarios:

mSUGRA	$50\ \text{GeV} \leq m_0 \leq 3\ \text{TeV}$	$50\ \text{GeV} \leq m_{1/2} \leq 3\ \text{TeV}$	$\lvert A_0\rvert \leq 9$ TeV
GMSB	$10\ \text{TeV} \leq \Lambda \leq 1000\ \text{TeV}$	$1 \leq M_{\rm mess}/\Lambda \leq 10^{11}$	$N_{\rm mess} = 1$
AMSB	$1\ \text{TeV} \leq m_{3/2} \leq 100\ \text{TeV}$	$50\ \text{GeV} \leq m_0 \leq 3\ \text{TeV}$	

Hence, in contrast to the pMSSM, the various parameters which enter the radiative corrections to M_h are not all independent in these constrained scenarios, as a consequence of the relations between SUSY-breaking parameters that are set at the high-energy scale and the requirement that electroweak symmetry breaking is triggered radiatively for each set of input parameters. The additional constraints make that it is not possible to freely tune the parameters that enter the Higgs sector to obtain the pMSSM maximal value of M_h. In order to obtain even a rough determination of $M_h^{\rm max}$ in a given constrained SUSY scenario, it is necessary to scan through the allowed range of values for the basic input parameters.

Using again the program `Suspect`, a full scan of these scenarios has been performed in Ref. [35] and the results for $M_h^{\rm max}$ are shown in the left-hand side of Fig. 2 as a function of $\tan\beta$, the input parameter that is common to all models, and in the right-hand side of the figure as a function of M_S. In the adopted parameter space of the models and with the central values of the SM inputs, the obtained upper h mass value is $M_h^{\rm max} \approx 121$ GeV in the AMSB scenario, i.e. much less that 125 GeV, while in the GMSB scenario one has $M_h^{\rm max} \approx 122$ GeV (these values are obtained for $\tan\beta \approx 20$). Thus, clearly, these two scenarios are disfavoured if the lightest h particle has indeed a mass in the range 123–127 GeV and $M_S \lesssim 3$ TeV. In mSUGRA, one obtains $M_h^{\rm max} = 128$ GeV and, thus, some parameter space would still survive the M_h constraint.

The upper bound on M_h in these scenarios can be qualitatively understood by considering in each model the allowed values of the trilinear coupling A_t, which essentially determines the stop mixing parameter X_t and thus the value of M_h for a given scale M_S. In GMSB, one has $A_t \approx 0$ at relatively high scales and its magnitude does not significantly increase in the evolution down to the scale M_S; this implies that we are almost in the no-mixing scenario which gives a low value of $M_h^{\max}$ as can be seen from Fig. 1. In AMSB, one has a non-zero A_t that is fully predicted at any renormalisation scale in terms of the Yukawa and gauge couplings; however, the ratio A_t/M_S with M_S determined from the overall SUSY breaking scale $m_{3/2}$ turns out to be rather small, implying again that we are close to the no-mixing scenario. Finally, in the mSUGRA model, since we have allowed A_t to vary in a wide range as $|A_0| \leq 9\,\text{TeV}$, one can get a large A_t/M_S ratio, which leads to a heavier Higgs particle. However, one cannot easily reach A_t values such that $X_t/M_S \approx \sqrt{6}$ so that we are not in the maximal-mixing scenario and the higher upper bound on M_h in the pMSSM cannot be reached.

In the case of mSUGRA, one can study several interesting special cases: the no-scale scenario with $m_0 \approx A_0 \approx 0$ [88,89], the scenario $m_0 \approx 0$ and $A_0 \approx -\frac{1}{4}m_{1/2}$, which approximately corresponds to the constrained next-to-MSSM (cNMSSM) [90,91], $A_0 \approx -m_0$, which corresponds to a very constrained MSSM (VCMSSM) [92], and a non-universal Higgs mass model (NUHM) [93] in which the soft SUSY-breaking scalar mass terms are different for the sfermions and for the two Higgs doublet fields.

In two particular cases, namely the "no-scale" and the "approximate cNMSSM" scenarios, the upper bound on M_h is much lower than in the more general mSUGRA case and, in fact, barely reaches $M_h \approx 123\,\text{GeV}$. The main reason is that these scenarios involve small values of A_0 at the GUT scale, $A_0 \approx 0$ for no-scale and $A_0 \approx -\frac{1}{4}m_{1/2}$ for the cNMSSM, which lead to A_t values at the weak scale that are too low to generate a significant stop mixing and, hence, one is again close to the no-mixing scenario. Thus, only a very small fraction of the parameter space of these two sub-classes of the mSUGRA model survive if we impose $123 < M_h < 127\,\text{GeV}$. These models should thus have a very heavy sfermion spectrum as a value $M_S \gtrsim 3\,\text{TeV}$ is required to increase $M_h^{\max}$. In the VCMSSM case, the value $M_h \simeq 125\,\text{GeV}$ can be reached as $|A_0|$ can be large for large m_0, $A_0 \approx -m_0$, allowing for typical mixing.

Finally, since the NUHM is more general than mSUGRA as we have two more free parameters, the $[\tan\beta, M_h]$ area shown in Fig. 2 is larger than in mSUGRA. However, since we are in the decoupling regime and the value of M_A does not matter much (as long as it a larger than a few hundred GeV) and the key weak-scale parameters entering the determination of M_h, i.e. $\tan\beta$, M_S and A_t are approximately the same in both models, one obtains a bound $M_h^{\max}$ that is only slightly higher in NUHM compared to the mSUGRA case.

In these constrained scenarios and, in particular in the general mSUGRA model, most of the scanned points giving the appropriate Higgs mass correspond to the decoupling regime of the MSSM Higgs sector and, hence, to an h boson with a SM–Higgs cross section and branching ratios. Furthermore, as the resulting SUSY spectrum for $M_h = 125 \pm 2\,\text{GeV}$ is rather heavy in these scenarios (easily evading the LHC limits from direct sparticle searches [86]), one obtains very small contributions to observables like the anomalous muon magnetic moment $(g-2)_\mu$ and to B-physics observables such as the rates $\text{BR}(B_s \to \mu^+\mu^-)$ or $\text{BR}(b \to s\gamma)$ [94]. Hence, the resulting spectrum complies with all currently available constraints. In addition, as will be discussed later, the correct cosmological density for the LSP neutralino required by recent measurements [95] can easily be satisfied. The M_h value provides thus a unique constraint in this decoupling regime.

2.4 Split and high-scale SUSY models

In the preceding discussion, we have always assumed that the SUSY-breaking scale is relatively low, $M_S \lesssim 3\,\text{TeV}$, which implies a natural SUSY scenario [33] with supersymmetric and heavier Higgs particles that could be observed at the LHC. However, as already mentioned, this choice is mainly dictated by fine-tuning considerations which are a rather subjective matter as there is no compelling criterion to quantify the acceptable amount of tuning. One could well abandon the SUSY solution to the hierarchy problem and have a very high M_S, which implies that, except for the lightest h boson, no other scalar particle is accessible at the LHC or at any foreseen collider.

This argument has been advocated to construct the so-called split SUSY scenario [76–78] in which the soft SUSY-breaking mass terms for all the scalars of the theory, except for one Higgs doublet, are extremely large, i.e. their common value M_S is such that $M_S \gg 1$ TeV (such a situation occurs e.g. in some string motivated models [96]). Instead, the mass parameters for the spin-$\frac{1}{2}$ particles, the gauginos and the higgsinos, are left in the vicinity of the EWSB scale, allowing for a solution to the dark matter problem and a successful gauge coupling unification, the two other SUSY virtues. The split SUSY models are much more predictive than the usual pMSSM as only a handful parameters are needed to describe the low-energy theory. Besides the common value M_S of the soft SUSY-breaking sfermion and one Higgs mass parameters, the basic inputs are essentially the three gaugino masses $M_{1,2,3}$ (which can be unified to a common value at M_{GUT} as in mSUGRA), the higgsino parameter μ and $\tan\beta$. The trilinear couplings A_f, which are expected to have values

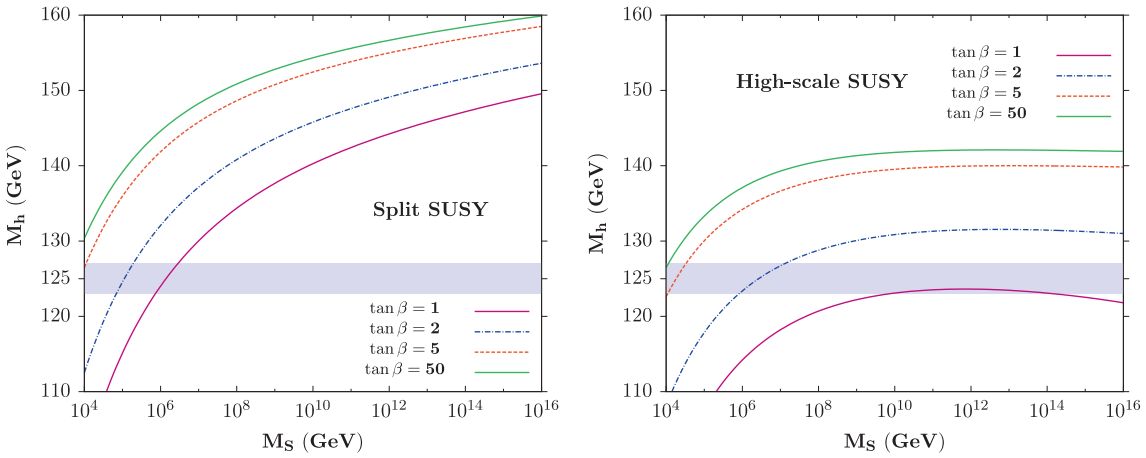

Fig. 3 The value of h boson mass as a function of the SUSY scale M_S for several values of $\tan\beta = 1, 2, 5, 50$ in the split-SUSY (*left*) and high-scale SUSY (*right*) scenarios. From Ref. [35]

close to the EWSB scale set by the gaugino/higgsino masses that are much smaller than M_S, will play a negligible role.

Concerning the Higgs sector, the main feature of split SUSY is that at the high scale M_S, the boundary condition on the quartic Higgs coupling is determined by SUSY:

$$\lambda(M_S) = \frac{1}{4}\left[g^2(M_S) + g'^2(M_S)\right]\cos^2 2\beta. \tag{8}$$

where g and g' are the SU(2) and U(1) gauge couplings. Here, $\tan\beta$ is not a parameter of the low-energy effective theory as it enters only the boundary condition above and cannot be interpreted as the ratio of the two Higgs vevs.

If the scalars are very heavy, they will lead to radiative corrections in the Higgs sector that are significantly enhanced by large logarithms, $\log(M_S/M_{\rm EWSB})$ where $M_{\rm EWSB} \approx |\mu|, M_2$. In order to have reliable predictions, one has to properly decouple the heavy states from the low-energy theory and resum the large logarithmic corrections; in addition, the radiative corrections due to the gauginos and the higgsinos have to be implemented. Following the early work of Ref. [76–78], a comprehensive study of the split SUSY spectrum has been performed in Ref. [97]. All the features of the model have been implemented in the code `SuSpect` [82] upon which the analysis presented in Ref. [35] and summarised here is based.

One can adopt an even more radical attitude than in split SUSY and assume that the gauginos and higgsinos are also very heavy, with a mass close to the scale M_S; this is the case in the so-called high-scale SUSY model [79,80]. Here, one abandons not only the SUSY solution to the fine-tuning problem but also the solution to the dark matter problem by means of the LSP and the successful unification of the gauge couplings. However, there will still be a trace of SUSY at low energy: the matching of the SUSY and low-energy theories is indeed encoded in the Higgs quartic coupling λ of Eq. (8). Hence, even if broken at very high scales, SUSY would still lead to a "light" Higgs whose mass will give information on M_S and $\tan\beta$.

The treatment of the Higgs sector of the high-scale SUSY scenario is similar to that of split SUSY: one simply needs to decouple the gauginos and higgsinos from the low-energy spectrum (in particular remove their contributions to the renormalisation group evolution of the gauge and Yukawa couplings and to the radiative corrections to M_h) and set their masses to M_S. The version of the program `Suspect` which handles the split SUSY case can be adapted to also cover the $M_1 \approx M_2 \approx M_3 \approx |\mu| \approx M_S$ case.

Using this tool, a scan in the $[\tan\beta, M_S]$ plane has been performed to determine the value of M_h in the split SUSY and high-scale SUSY scenarios; in the former case, $M_{\rm EWSB} \approx \sqrt{|M_2\mu|} \approx 246$ GeV was chosen for the low scale. The results are shown in Fig. 3, where M_h is displayed as a function of M_S for selected values of $\tan\beta$ in both split (left plot) and high-scale (right plot) SUSY.

As expected, the maximal M_h values are obtained at high $\tan\beta$ and M_S values and, at the scale $M_S \approx 10^{16}$ GeV at which the couplings g and g' approximately unify in the split SUSY scenario, one obtains $M_h \approx 160$ GeV for the higher $\tan\beta = 50$ value. Not included is the error bands in the SM inputs that would lead to an uncertainty of about 2 GeV on M_h, which is now mainly due to the 1 GeV uncertainty on m_t. In addition, the zero-mixing scenario was assumed as the parameter A_t is expected to be much smaller than M_S; this approximation might not be valid for M_S values below 10 TeV and a maximal mixing $A_t/M_S = \sqrt{6}$ would increase the Higgs mass value by up to 10 GeV at $M_S = \mathcal{O}(1$ TeV) as was discussed earlier for the pMSSM. In the high-scale SUSY scenario, one obtains a value $M_h \approx 142$ GeV (with again an uncertainty of approximately 2 GeV from the top mass) for high $\tan\beta$ values and at the unification scale $M_S \approx$

10^{14} GeV [79,80]. Much smaller M_h values, in the 120 GeV range, can be obtained for lower scales and $\tan\beta$.

Hence, the requirement that the Higgs mass is in the range $123 \lesssim M_h \lesssim 127$ GeV imposes strong constraints on the parameters of these two models. For this mass range, very large scales are needed for $\tan\beta \approx 1$ in the high-scale SUSY scenario, while scales not too far from $M_S \approx 10^4$ GeV are required at $\tan\beta \gg 1$ in both the split and the high-scale scenarios. In this case, SUSY should manifest itself at scales much below $M_{\rm GUT}$ if $M_h \approx 125$ GeV.

2.5 Splitting the Higgs and sfermion sectors

In the previous high-scale scenarios, the Higgs mass parameters were assumed to be related to the mass scale of the scalar fermions in such a way that the masses of the heavier Higgs particles are also of the order of the SUSY scale, $M_A \approx M_S$. However, this needs not to be true in general and one can, for instance, have a NUHM-like scenario where the Higgs masses are decoupled from those of the sfermions. If one is primarily concerned with the MSSM Higgs sector, one may be rather conservative and allow any value for M_A irrespective of the SUSY-breaking scale M_S. This is the quite "model-independent" approach that has been advocated in Refs. [98–101]: take M_A as a free parameter of the pMSSM, with values ranging from $\mathcal{O}(100\,\text{GeV})$ up to $\mathcal{O}(M_S)$, but make no restriction on M_S, which can be set to any value, even very high.

An important consequence of this possibility is that it reopens the low $\tan\beta$ region, $\tan\beta \lesssim 3$, which was long thought to be forbidden if one requires a SUSY scale $M_S \lesssim 1$ TeV, as a result of the limit $M_h \gtrsim 114$ GeV from the negative search of a SM-like Higgs boson at LEP [31]. If the SUSY scale is large enough, these small $\tan\beta$ values would become viable again. To estimate the required magnitude of M_S, one can still use `Suspect` in which the possibility $M_S \gg 1$ TeV is implemented [97] with the full set of radiative corrections up to two loops included. In Fig. 4, displayed are the contours in the plane $[\tan\beta, M_S]$ for fixed mass values $M_h = 120$–132 GeV of the observed Higgs state (these include a 3 GeV theoretical uncertainty and also a 3 GeV uncertainty on the top quark mass [84] that is conservatively added linearly in the extreme cases). The maximal mixing $X_t = \sqrt{6}M_S$ scenario is assumed with 1 TeV gaugino/higgsino mass parameters.

One observes that values of $\tan\beta \approx 1$ are possible and allow for an acceptable M_h value provided the scale M_S is large enough. For instance, while one can accommodate a scale $M_S \approx 1$ TeV with $\tan\beta \approx 5$, a large scale $M_S \approx 20$ TeV is required to obtain $\tan\beta \approx 2$; to reach the limit $\tan\beta = 1$, an order of magnitude increase of M_S will be required. Outside the decoupling regime, the obtained M_S for a given M_h value will be of course larger. For completeness,

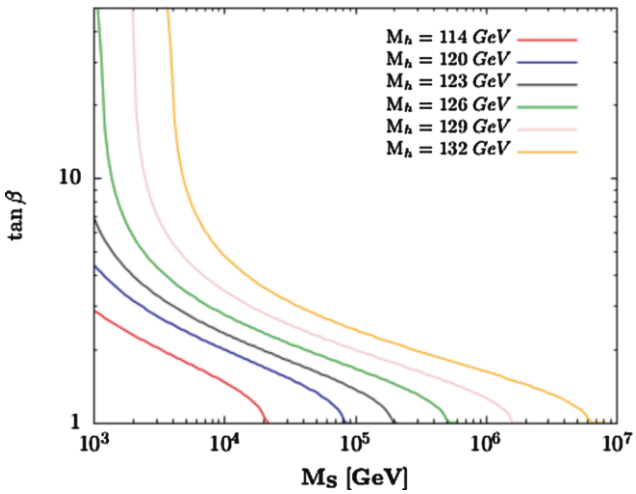

Fig. 4 Contours for fixed values $M_h = 120, 123, 126, 129$ and 132 GeV in the $[\tan\beta, M_S]$ plane in the decoupling limit $M_A \gg M_Z$; the "LEP2 contour" for $M_h = 114$ GeV is also shown

also shown is the contour for the LEP2 limit $M_h = 114$ GeV which illustrates the fact that $\tan\beta \approx 1$ is still allowed provided that $M_S \gtrsim 20$ TeV.

2.6 A new parametrisation of the Higgs sector

It was pointed out in Refs. [98,102–104] that when the measured value of the h boson mass $M_h = 125$ GeV is taken into account, the MSSM Higgs sector with solely the dominant radiative corrections included can be again described with only two free parameters such as $\tan\beta$ and M_A as was the case at tree level. In other words, the dominant radiative corrections that involve the SUSY parameters are fixed by the value of M_h. This observation leads to a rather simple parametrisation of the MSSM Higgs sector.

More specifically, let us assume that in the 2×2 matrix for the radiative corrections to the CP-even Higgs mass matrix Eq. (1), only the leading $\Delta\mathcal{M}^2_{22}$ entry of Eq. (5) that involves the by far dominant stop–top sector contribution is taken into account; this is the so-called ϵ approximation and its refinements [15,16,28]. In this $\Delta\mathcal{M}^2_{22} \gg \Delta\mathcal{M}^2_{11}, \Delta\mathcal{M}^2_{12}$ limit, one can simply trade $\Delta\mathcal{M}^2_{22}$ for the by now known h mass value $M_h = 125$ GeV and obtain

$$
\begin{aligned}
M_H^2 &= \frac{\left(M_A^2 + M_Z^2 - M_h^2\right)\left(M_Z^2 c_\beta^2 + M_A^2 s_\beta^2\right) - M_A^2 M_Z^2 c_{2\beta}^2}{M_Z^2 c_\beta^2 + M_A^2 s_\beta^2 - M_h^2} \\
\alpha &= -\arctan\left(\frac{(M_Z^2 + M_A^2) c_\beta s_\beta}{M_Z^2 c_\beta^2 + M_A^2 s_\beta^2 - M_h^2}\right)
\end{aligned}
\tag{9}
$$

This was called the habemus MSSM or hMSSM in Ref. [81].

However, this interesting and simplifying feature has to been demonstrated for all MSSM parameters and, in particular, one needs to prove that the impact of the subleading

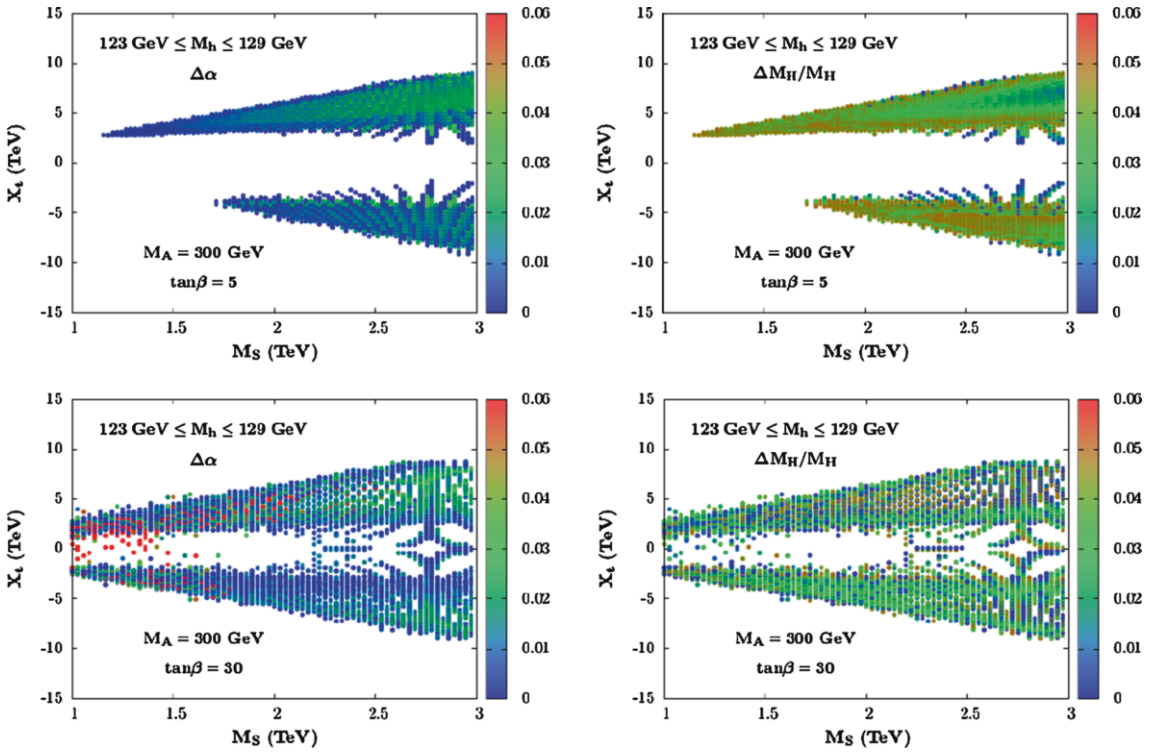

Fig. 5 The variation of the mass M_H and the mixing angle α are shown as separate *vertical colored* scales, in the plane $[M_S, X_t]$ when the full two loop corrections are included with and without the subleading matrix elements $\Delta\mathcal{M}^2_{11}$ and $\Delta\mathcal{M}^2_{12}$. $M_A = 300\,\text{GeV}$, $\tan\beta = 5$ or and 30 are taken and the other parameters are varied as described in the text [81]

corrections $\Delta\mathcal{M}^2_{11}$ and $\Delta\mathcal{M}^2_{12}$ is small. To do so, a scan of the pMSSM parameter space using the program `SuSpect`, in which the full two-loop radiative corrections to the Higgs sector are implemented, has been performed [81]. For a chosen ($\tan\beta$,M_A) input set, the soft-SUSY parameters that play an important role in the Higgs sector are varied in the following ranges: $|\mu| \leq 3\,\text{TeV}$, $|A_t, A_b| \leq 3M_S$, $1\,\text{TeV} \leq M_3 \leq 3\,\text{TeV}$ and $0.5\,\text{TeV} \leq M_S \leq 3\,\text{TeV}$ ($\approx$3 TeV is the scale up to which programs such as `SuSpect` are expected to be reliable). The usual GUT relation between the weak scale gaugino masses $6M_1 = 3M_2 = M_3$ has been assumed and $A_u, A_d, A_\tau = 0$ has been set (these last parameters have little impact on the radiative corrections). The MSSM Higgs sector parameters have been computed all across the parameter space, selecting the points which satisfy the constraint $123 \leq M_h \leq 129\,\text{GeV}$ when uncertainties are included. For each of theses points, the Higgs parameters have been compared to those obtained in the simplified MSSM approximation, $\Delta\mathcal{M}^2_{11} = \Delta\mathcal{M}^2_{12} = 0$, with the lightest Higgs boson mass as input. While the requirement that M_h should lie in the range 123–129 GeV has been made, M_h was allowed to be different from the one obtained in the "exact" case $\Delta\mathcal{M}^2_{11}, \Delta\mathcal{M}^2_{12} \neq 0$.

Displayed in Fig. 5 are the differences between the values of the mass M_H and the mixing angle α that are obtained when the two possibilities $\Delta\mathcal{M}^2_{11} = \Delta\mathcal{M}^2_{12} = 0$ and $\Delta\mathcal{M}^2_{11}, \Delta\mathcal{M}^2_{12} \neq 0$ are considered. This is shown in the plane $[M_S, X_t]$ with $X_t = A_t - \mu\cot\beta$ when all other parameters are scanned as above. The A boson mass was fixed to $M_A = 300\,\text{GeV}$ (a similar result was obtained for $M_A \approx 1\,\text{TeV}$) and two representative values $\tan\beta = 5$ and 30 are used. The conservative approach of plotting only points which maximise these differences has been adopted.

In all cases, the difference between the two M_H values is very small (in fact, much smaller than the H boson total decay width Γ_H), less than a few percent, while for α the difference does not exceed $\approx$0.025 for low values of $\tan\beta$, but at high $\tan\beta$ values, one can reach the level of $\approx$0.05 in some rare situations (large values of μ, which enhance the $\mu\tan\beta$ contributions). Nevertheless, at high enough $\tan\beta$, we are far in the decoupling regime already for $M_A \gtrsim 200\,\text{GeV}$ and such a difference does not significantly affect the couplings of the h and H bosons which, phenomenologically, are the main ingredients.

Hence, even when including the full set of radiative corrections, it remains a good approximation to use Eq. (9) to derive the parameters M_H and α in terms of the inputs $\tan\beta$, M_A and the measured M_h value.

In the case of the charged Higgs boson (whose physics is described by $\tan\beta$, $M_{H^\pm}$ and eventually α), the radiative

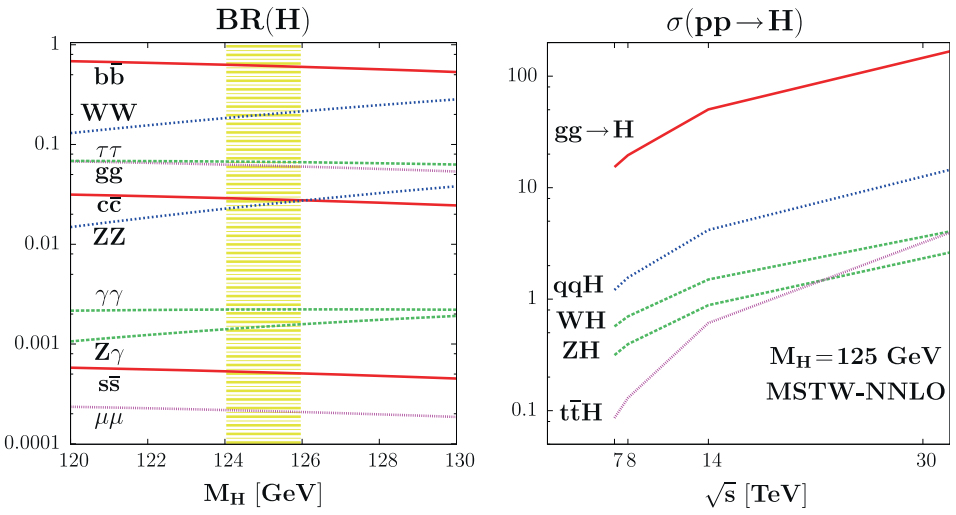

Fig. 6 The SM-like Higgs boson branching ratios in the mass range 120–130 GeV (*left*) and its production cross sections at proton colliders as a function of the c.m. energy (*right*) [107]

corrections to $M_{H^\pm}$ are much smaller for large enough M_A and one has, at the few percent level in most cases (which is again smaller than the total $H^\pm$ decay width),

$$M_{H^\pm} \simeq \sqrt{M_A^2 + M_W^2}. \tag{10}$$

In conclusion, this approximation allows to ignore the radiative corrections to the Higgs masses and their complicated dependence on the MSSM parameters and to use a simple formula to derive the other parameters of the Higgs sector, α, M_H as well as $M_{H^\pm}$. This considerably simplifies phenomenological analyses in the MSSM Higgs sector which up to now rely either on large scans of the parameter space (as in the previous subsections) or resort to benchmark scenarios in which most of the MSSM parameters are fixed (as is the case of Ref. [105] for instance).

3 Implications of the Higgs production rates

3.1 Light Higgs decay and production at the LHC

In many respects, the Higgs particle was born under a very lucky star as the mass value of ≈125 GeV (although too high for a natural SUSY) allows to produce it at the LHC in many redundant channels and to detect it in a variety of decay modes. This allows detailed studies of the Higgs properties as will be discussed in this section.

We start by summarizing the production and decay at the LHC of a light SM-like Higgs particle, which should correspond to the lightest MSSM h boson in the decoupling regime. First, for $M_h \approx 125$ GeV, the Higgs mainly decays into $b\bar{b}$ pairs but the decays into WW^* and ZZ^* final states, before allowing the gauge bosons to decay leptonically $W \to \ell\nu$ and $Z \to \ell\ell$ ($\ell = e, \mu$), are also significant. The $h \to \tau^+\tau^-$ channel (as well as the gg and $c\bar{c}$ decays that are not detectable at the LHC) is also of significance, while the clean loop induced $h \to \gamma\gamma$ mode can be easily detected albeit its small rates. The very rare $h \to Z\gamma$ and even $h \to \mu^+\mu^-$ channels should be accessible at the LHC but only with a much larger data sample. This is illustrated in the left-hand side of Fig. 6, where the decay branching fractions of a SM-like Higgs are displayed for the narrow mass range $M_h = 120$–130 GeV

On the other hand, many Higgs production processes have significant cross sections as is shown in the right-hand side of Fig. 6, where they are displayed at a proton collider at various past, present and foreseen center of mass energies for a 125 GeV SM-like Higgs boson; the MSTW parton densities [106] have been used.

While the by far dominant gluon fusion mechanism $gg \to h$ (ggF) has extremely large rates (≈20 pb at $\sqrt{s} = 7$–8 TeV), the subleading channels, i.e. the vector boson fusion (VBF) $qq \to hqq$ and the nHiggs-strahlung (HV) $q\bar{q} \to hV$ with $V = W, Z$ mechanisms, have cross sections which should allow for a study of the Higgs particle already at $\sqrt{s} \gtrsim 8$ TeV with the amount of integrated luminosity, ≈25 fb^{-1}, which has been collected by each experiment. The Higgs–top associated process $pp \to t\bar{t}h$ (ttH) would require higher energy and luminosity.

This pattern already allows the ATLAS and CMS experiments to observe the Higgs boson in several channels and to measure some its couplings in a reasonably accurate way. The channels that have been searched are $h \to ZZ^* \to 4\ell^\pm$, $h \to WW^* \to 2\ell 2\nu$, $h \to \gamma\gamma$ where the Higgs is mainly produced in ggF with subleading contributions from hjj in the VBF process, $h \to \tau\tau$ where the Higgs is produced in association with one (in ggF) and two (in VBF) jets, and finally $h \to b\bar{b}$ with the Higgs produced in the HV process. One can ignore for the moment the additional search channels $h \to \mu\mu$ and $h \to Z\gamma$ for which the sensitivity is still too low with the data collected so far.

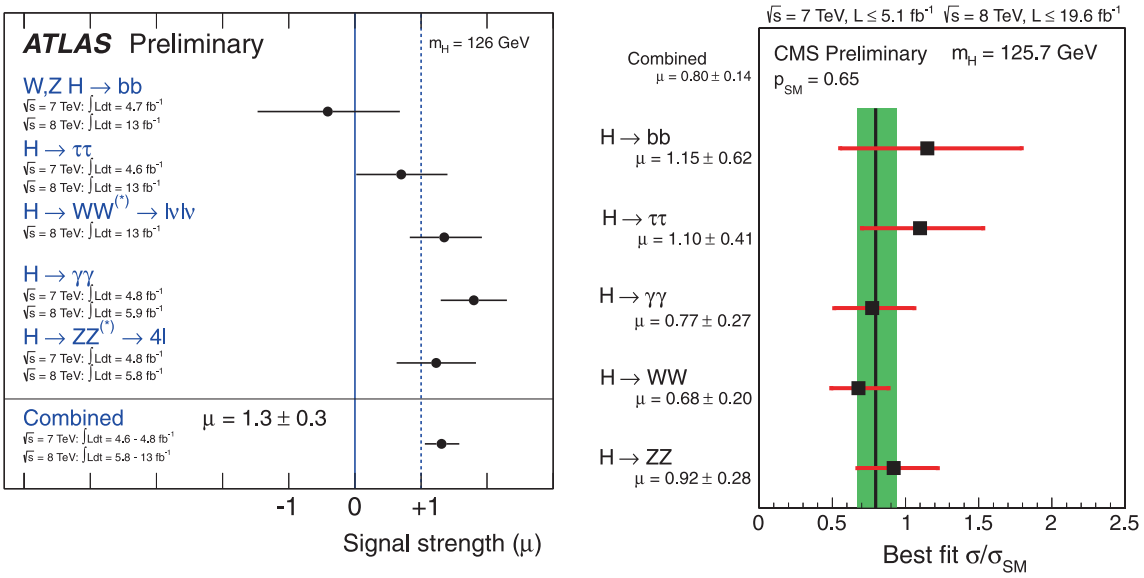

Fig. 7 The signal strengths on the SM Higgs boson in the various search channels provided by ATLAS [108] and CMS [109] with the data collected so far at $\sqrt{s} = 7$+8 TeV

A convenient way to scrutinise the couplings of the produced h boson is to consider their deviation from the SM expectation. One then considers for a given search channel the signal strength modifier μ, which, with some approximation, can be identified with the Higgs production cross section times decay branching fractions normalised to the SM value. For the $h \to XX$ decay channel, one would have in the narrow width approximation,

$$\mu_{XX}|_{\rm th} = \frac{\sigma(pp \to h \to XX)}{\sigma(pp \to h \to XX)|_{\rm SM}} = \frac{\sigma(pp \to h) \times {\rm BR}(h \to XX)}{\sigma(pp \to h)|_{\rm SM} \times {\rm BR}(h \to XX)|_{\rm SM}}. \quad (11)$$

which, from the experimental side would correspond to

$$\mu_{XX}|_{\rm exp} \simeq \frac{N^{\rm ev}_{XX}}{\epsilon \times \sigma(pp \to h)|_{\rm SM} \times {\rm BR}(h \to XX)|_{\rm SM} \times \mathcal{L}} \quad (12)$$

where $N^{\rm ev}_{XX}$ is the measured number of events in the XX channel, ϵ the selection efficiency and $\mathcal{L}$ the luminosity.

ATLAS and CMS have provided the signal strengths for the various final states with a luminosity of, respectively, $\approx$5 fb^{-1} for the 2011 run at $\sqrt{s} = 7$ TeV and $\approx$20 fb^{-1} for the 2012 run at $\sqrt{s} = 8$ TeV. The constraints given by the two collaborations are shown in Fig. 7.

When the various analysed Higgs search channels are combined, this leads to a global signal strength [108,109]

$$\begin{aligned} &\text{ATLAS}: \mu_{\rm tot} = 1.30 \pm 0.30 \\ &\text{CMS}: \mu_{\rm tot} = 0.87 \pm 0.23 \end{aligned} \quad (13)$$

which shows a good agreement with the SM expectation. In fact, when the ATLAS and CMS values are combined, one finds a global signal strength that is very close to unity, implying that the observed Higgs is rather SM-like.

Hence, already with the rather limited statistics at hand, the accuracy of the measurements in Eq. (13) is reaching the 20 % level for the ATLAS and CMS collaborations. This is at the same time impressive and worrisome. Indeed, as mentioned earlier the main Higgs production channel is the top and bottom quark loop mediated gluon fusion mechanism and, at $\sqrt{s} = 7$ or 8 TeV, the three other mechanisms contribute at a level below 15 % when their rates are added and before kinematical cuts are applied. The majority of the signal events presently observed at the LHC, in particular in the main search channels $h \to \gamma\gamma$, $h \to ZZ^* \to 4\ell$, $h \to WW^* \to 2\ell 2\nu$ and, to a lesser extent, $h \to \tau\tau$, thus come from the ggF mechanism which is known to be affected by large theoretical uncertainties.

As a matter of fact, although the cross section $\sigma(gg \to h)$ is known up next-to-next-to-leading order (NNLO) in perturbative QCD (and at least at NLO for the electroweak interaction) [110], there is a significant residual scale dependence which points to the possibility that still higher order contributions beyond NNLO cannot be totally excluded. In addition, as the process is of $\mathcal{O}(\alpha_s^2)$ at LO and is initiated by gluons, there are sizable uncertainties due to the gluon parton distribution function (PDF) and the value of the coupling α_s. A third source of theoretical uncertainties, the use of an effective field theory (EFT) approach to calculate the radiative corrections beyond the NLO approximation, should in principle also be considered [111,112]. In addition, large uncertainties arise when the $gg \to h$ cross section is broken into the jet categories $h+0j$, $h+1j$ and $h+2j$ [113]. In total, the combined theoretical uncertainty has been estimated to be of

order $\Delta^{\rm th} \approx \pm 15\,\%$ by the LHC Higgs cross section working group [110] and it would increase up to $\Delta^{\rm th} \approx \pm 20\,\%$ if the EFT uncertainty is also included[2] [112].

Hence, the theoretical uncertainty is already at the level of the accuracy of the cross section measured by the ATLAS and CMS collaborations, Eq. (13). Another drawback of the analyses is that they involve strong theoretical assumptions on the total Higgs width since some contributing decay channels not accessible at the LHC are assumed to be SM-like and possible invisible Higgs decays in scenarios beyond the SM are supposed not to occur.

In Ref. [107], following earlier work [114–117], it has been suggested to consider the decay ratios D_{XX} defined as

$$D^{\rm p}_{XX} = \frac{\sigma^{\rm p}(pp \to h \to XX)}{\sigma^{\rm p}(pp \to h \to VV)} \tag{14}$$

$$= \frac{\sigma^{\rm p}(pp \to h) \times {\rm BR}(h \to XX)}{\sigma^{\rm p}(pp \to h) \times {\rm BR}(h \to VV)} \tag{15}$$

$$= \frac{\Gamma(h \to XX)}{\Gamma(h \to VV)} \propto \frac{c_X^2}{c_V^2} \tag{16}$$

for a specific production process p = ggF, VBF, VH or all (for inclusive production) and for a given decay channel $h \to XX$ when the reference channel $h \to VV$ is used. In these ratios, the cross sections $\sigma^p(pp \to h)$ and hence, their significant theoretical uncertainties will cancel out, leaving out only the ratio of decay branching fractions and hence of partial decay widths. These can be obtained with the program HDECAY [118] which includes all higher order effects and are affected by much smaller uncertainties. Thus, the total decay width which includes contributions from channels not under control such as possible invisible Higgs decays, do not appear in the ratios $D^{\rm p}_{XX}$. Some common experimental systematical uncertainties such as the one from the luminosity measurement and the small uncertainties in the Higgs decay branching ratios also cancel out. We are thus, in principle, left with only with the statistical uncertainty and some (non common) systematical errors. The ratios D_{XX} involve, up to kinematical factors and known radiative corrections, only the ratios $|c_X|^2/\,|c_V|^2$ of the Higgs reduced couplings to the particles X and V compared to the SM expectation, $c_X \equiv g_{hXX}/g^{\rm SM}_{hXX}$.

For the time being, three independent ratios can be considered: $D_{\gamma\gamma}$, $D_{\tau\tau}$ and D_{bb}. $D_{\gamma\gamma}$ is the ratio of the inclusive ATLAS and CMS di-photon and ZZ channels that are largely dominated by the ggF mechanism; $D_{\tau\tau}$ is the signal strength ratio in the $\tau\tau$ and WW searches where one selects Higgs production in ggF with an associated jet or in the VBF production mechanism; D_{bb} is the ratio of the $h \to b\bar{b}$ and $h \to WW$ decays in hV production for which the sensitivities are currently too low.

In order to test the compatibility of the couplings of the $M_h = 125$ GeV Higgs state with the SM expectation, one can perform a fit based on the χ^2_R function

$$\chi^2_R = \frac{\left[D^{ggF}_{\gamma\gamma} - \frac{\mu_{\gamma\gamma}}{\mu_{ZZ}}|^{ggF}_{\rm exp}\right]^2}{\left[\delta\left(\frac{\mu_{\gamma\gamma}}{\mu_{ZZ}}\right)_{ggF}\right]^2} + \frac{\left[D^{VH}_{bb} - \frac{\mu_{bb}}{\mu_{WW}}|^{Vh}_{\rm exp}\right]^2}{\left[\delta\left(\frac{\mu_{bb}}{\mu_{WW}}\right)_{Vh}\right]^2}$$
$$+ \frac{\left[D^{ggF}_{\tau\tau} - \frac{\mu_{\tau\tau}}{\mu_{WW}}|^{ggF}_{\rm exp}\right]^2}{\left[\delta\left(\frac{\mu_{\tau\tau}}{\mu_{WW}}\right)_{ggF}\right]^2} + \frac{\left[D^{\rm VBF}_{\tau\tau} - \frac{\mu_{\tau\tau}}{\mu_{WW}}|^{\rm VBF}_{\rm exp}\right]^2}{\left[\delta\left(\frac{\mu_{\tau\tau}}{\mu_{WW}}\right)_{\rm VBF}\right]^2} \tag{17}$$

The errors $\delta(\mu_{XX}/\mu_{VV})$ are computed assuming no correlations between the different final state searches. The uncertainties on the ratios are derived from the individual errors that are dominated by the experimental uncertainties as one expects that the theoretical uncertainties largely cancel out in the ratios $D_{\gamma\gamma}$, D_{bb} and $D_{\tau\tau}$.

For the signal strengths above, the theoretical uncertainties have to be treated as a bias (and not as if they were associated with a statistical distribution) and the fit has to be performed for the two extremal values of the signal strengths: $\mu_i|_{\rm exp} \pm \delta\mu_i/\mu_i|_{\rm th}$ with the theoretical uncertainty $\delta\mu_i/\mu_i|_{\rm th}$ conservatively assumed to be $\pm 20\,\%$ for both the gluon and the vector boson fusion mechanisms (because of the contamination due to $gg \to h + 2j$ in the latter case) and $\approx 5\,\%$ for hV associated production.

3.2 Fit of the Higgs couplings and their ratios

A large number of analyses of the Higgs couplings from the LHC data have been performed in the SM and its extensions and a partial list is given in Refs. [119–150].

In the MSSM, the couplings of the CP-even Higgs particles h and H to gauge bosons and fermions, compared to the SM Higgs couplings, are changed by factors that involve the sine and the cosine of the mixing angles β and α. Outside the decoupling regime where they reach unity, the reduced couplings (i.e. normalised to their SM values) of the lighter h state to third generation t, b, τ fermions and gauge bosons $V = W/Z$ are for instance given by

$$c^0_V = \sin(\beta - \alpha),\ c^0_t = \cos\alpha/\sin\beta,\ c^0_b = -\sin\alpha/\cos\beta \tag{18}$$

[2] Note that also in the VBF process, despite the fact that the inclusive cross section has only a few percent combined scale and PDF uncertainty [110], the contamination by the $gg \to h + 2j$ channel makes the total uncertainty in the $h + jj$ final "VBF" sample rather large. Indeed $\mathcal{O}(30\,\%)$ $gg \to h + 2j$ events will remain even after the specific cuts that select the VBF configuration have been applied, and the rate is affected by a much larger uncertainty than the inclusive $gg \to h$ process, up to 50 % when one adds the scale and PDF uncertainties [113].

They thus depend not only on the two inputs $[\tan\beta, M_A]$, as occurs at tree level, but, a priori, on the entire MSSM spectrum as a result of the radiative corrections, in the same way as the Higgs masses. In principle, as discussed earlier, knowing $\tan\beta$ and M_A and fixing M_h to its measured value, the couplings can be determined in general. However, this is true when only the radiative corrections to the Higgs masses are included. Outside the regime in which the pseudoscalar A boson and the supersymmetric particles are very heavy, there are also direct radiative corrections to the Higgs couplings not contained in the mass matrix of Eq. (1) and which can alter this simple picture.

First, in the case of b-quarks, additional one-loop vertex corrections modify the tree–level $hb\bar{b}$ coupling: they grow as $m_b\mu\tan\beta$ and can be very large at high $\tan\beta$. The dominant component comes from the SUSY–QCD corrections with sbottom–gluino loops that can be approximated by $\Delta_b \simeq 2\alpha_s/(3\pi) \times \mu m_{\tilde{g}} \tan\beta/\max(m^2_{\tilde{g}}, m^2_{\tilde{b}_1}, m^2_{\tilde{b}_2})$ [151]. Outside the decoupling regime the c_b coupling reads

$$c_b \approx c_b^0 \times [1 - \Delta_b/(1+\Delta_b) \times (1 + \cot\alpha \cot\beta)] \tag{19}$$

with $\tan\alpha \to -1/\tan\beta$ for $M_A \gg M_Z$. A large Δ_b would significantly alter the dominant $h \to b\bar{b}$ partial width and affect the branching fractions of all other decay modes.

In addition, the $ht\bar{t}$ coupling is derived indirectly from the $gg \to h$ production cross section and the $h \to \gamma\gamma$ decay branching ratio, two processes that are generated by triangular loops. In the MSSM, these loops involve not only the top quark (and the W boson in the decay $h \to \gamma\gamma$) but also contributions from supersymmetric particles, if not too heavy. In the case of $gg \to h$ production, only the contributions of stops is generally important. Including the later and working in the limit $M_h \ll m_t, m_{\tilde{t}_{1,2}}$, the coupling c_t from the ggF process[3] is approximated by [152]

$$c_t \approx c_t^0 \left[1 + \frac{m_t^2}{4m^2_{\tilde{t}_1} m^2_{\tilde{t}_2}} \left(m^2_{\tilde{t}_1} + m^2_{\tilde{t}_2} - X_t^2 \right) \right] \tag{20}$$

which shows that indeed, $\tilde{t}$ contributions can be very large for light stops and for large stop mixing. In the $h \to \gamma\gamma$ decay rate, because the $t, \tilde{t}$ electric charges are the same, the $ht\bar{t}$ coupling is shifted by the same amount. If one ignores the usually small contributions of the other sparticles (to be discussed in the next subsection), the $ht\bar{t}$ vertex can be simply parametrised by the effective coupling of Eq. (20).

We note that the h couplings to τ leptons and c quarks do not receive the direct corrections of Eqs. (19) and (20) and one should still have $c_c = c_t^0$ and $c_\tau = c_b^0$. However, using $c_{t,b}$ or $c^0_{t,b}$ in this case has almost no impact in practice as these couplings appear only in the branching ratios for the decays $h \to c\bar{c}$ and $\tau^+\tau^-$, which are small and the direct corrections should not be too large. One can thus, in a first approximation, assume that $c_c = c_t$ and $c_\tau = c_b$. Another caveat is due to the invisible Higgs decays which are assumed to be absent and which will be discussed later.

Hence, because of the direct corrections, the Higgs couplings cannot be described only by β and α as in Eq. (18). To characterise the Higgs particle at the LHC, it was advocated that at least three independent h couplings should be considered, namely c_t, c_b and $c_V = c_V^0$ [81]. One can thus define the following effective Lagrangian:

$$\begin{aligned}\mathcal{L}_h = {} & c_V g_{hWW} h W^+_\mu W^{-\mu} + c_V g_{hZZ} h Z^0_\mu Z^{0\mu} - c_t y_t h \bar{t}_L t_R \\ & - c_t y_c h \bar{c}_L c_R - c_b y_b h \bar{b}_L b_R - c_b y_\tau h \bar{\tau}_L \tau_R + \text{h.c.}\end{aligned} \tag{21}$$

where $y_{t,c,b,\tau} = m_{t,c,b,\tau}/v$ are the Yukawa couplings of the heavy SM fermions, $g_{hWW} = 2M_W^2/v$ and $g_{hZZ} = M_Z^2/v$ the hWW and HZZ couplings and v the SM Higgs vev.

In Ref. [81], a three-dimensional fit of the h couplings was performed in the space $[c_t, c_b, c_V]$, assuming $c_c = c_t$ and $c_\tau = c_b$ as discussed above and of course the custodial symmetry relation $c_V = c_W = c_Z$, which holds in supersymmetric models. The results of this fit are presented in Fig. 8 for $c_t, c_b, c_V \geq 0$. The best-fit value for the couplings, with the $\sqrt{s} = 7{+}8\,\text{TeV}$ ATLAS and CMS data turns out to be $c_t = 0.89$, $c_b = 1.01$ and $c_V = 1.02$.

In scenarios where the direct corrections in Eqs. (19) and (20) are not quantitatively significant (i.e. considering either not too large values of $\mu\tan\beta$ or high sfermion masses), one can use the MSSM relations of Eq. (18) to reduce the number of effective parameters down to two. This allows to perform two-parameter fits in the planes $[c_V, c_t]$, $[c_V, c_b]$

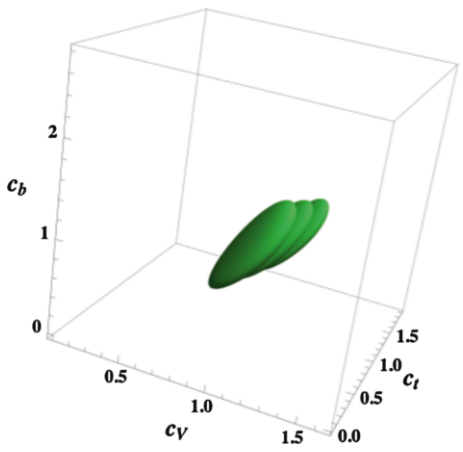

Fig. 8 The best-fit region at 68 % CL for the Higgs signal strengths in the $[c_t, c_b, c_V]$ space [81]. The three overlapping regions are for the central and extreme choices of the theoretical prediction for the Higgs rates including uncertainties

[3] In the case of the production process $gg/q\bar{q} \to ht\bar{t}$, it is still c_t^0, which should describe the $ht\bar{t}$ coupling, but the constraints on the h properties from this process are presently very weak.

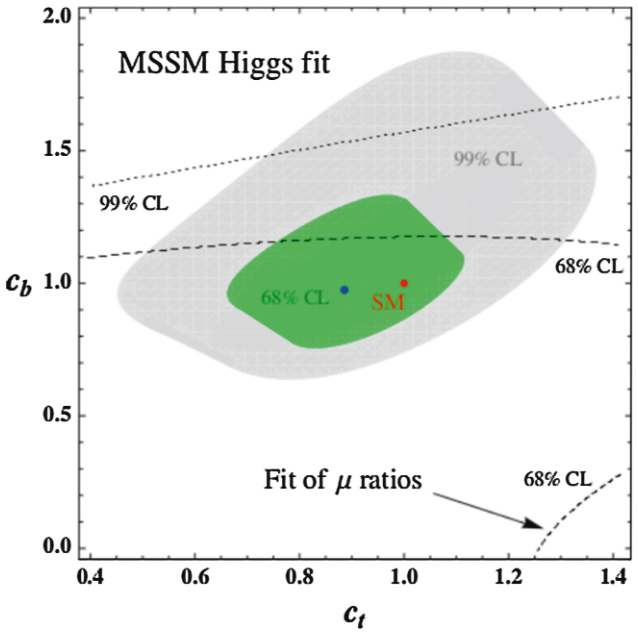

Fig. 9 Best-fit regions at 68 % and 99 % CL for the Higgs signal strengths and their ratios in the plane $[c_t, c_b]$. The best-fit point is indicated in *blue*. From Ref. [81]

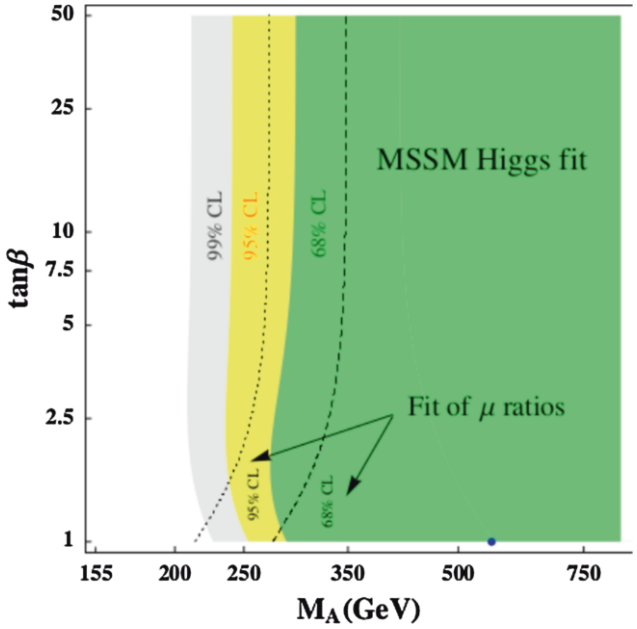

Fig. 10 Best-fit regions for the signal strengths and their ratios in the plane [tan β, M_A]; the best point is in *blue* [81]

and $[c_t, c_b]$. As an example, the fit of the signal strengths and their ratios in the $[c_t, c_b]$ plane is displayed in Fig. 9. In this two-dimensional case, the best-fit point is located at $c_t = 0.88$ and $c_b = 0.97$, while $c_V \simeq 1$. Note that although for the best-fit point one has $c_b \lesssim 1$, actually $c_b \gtrsim 1$ in most of the 1σ region.

Using the formulae Eq. (9) for the angle α and using the input $M_h \approx 125\,\text{GeV}$, one can make a fit in the plane [tan β, M_A]. This is shown in Fig. 10, where the 68, 95 and 99 % CL contours from the signal strengths and their ratios are displayed when the theory uncertainty is taken as a bias. The best-fit point when the latter uncertainty is set to zero is obtained for the values $\tan\beta = 1$ and $M_A = 557$ GeV, which implies for the other parameters using $M_h = 125\,\text{GeV}$: $M_H = 580\,\text{GeV}$, $M_{H^\pm} = 563\,\text{GeV}$ and $\alpha = -0.837$ rad, which leads to $\cos(\beta - \alpha) \simeq -0.05$. Such a point with $\tan\beta \approx 1$ implies an extremely large value of the SUSY scale, $M_S = \mathcal{O}(100)\,\text{TeV}$, for $M_h \approx 125\,\text{GeV}$. One should note, however, that the χ^2 value is relatively stable all over the 1σ region. Hence, larger values of $\tan\beta$ (and lower values of M_A) could also be accommodated reasonably well by the fit, allowing thus for not too large M_S values. In all, cases one has $M_A \gtrsim 200\,\text{GeV}$ though.

3.3 An excess in the $\gamma\gamma$ channel?

In the early LHC data, a significant excess in the $h \to \gamma\gamma$ detection channel was observed, raising the hope that it could be the first signal for physics beyond the SM. This excess has unfortunately faded away with more statistics and with the full $25\,\text{fb}^{-1}$ data collected at $\sqrt{s} = 7{+}8\,\text{TeV}$, there is now only a $\approx 2\sigma$ excess in ATLAS which measures $\mu_{\gamma\gamma} = 1.6 \pm 0.3$, while the signal strength measured by the CMS collaboration is $\mu_{\gamma\gamma} = 0.9 \pm 0.3$, which is SM-like. Nevertheless, it would be interesting to briefly discuss this excess as, besides the fact that it has triggered a vast literature, the $h \to \gamma\gamma$ channel is the one where new physics, and SUSY in particular, is most likely to manifest itself.

First, it has been realised early that this excess, if not due to a statistical fluctuation, can be easily explained or reduced in the context of the SM by invoking the large theoretical uncertainties that affect the production times decay rate in the dominant channel, $gg \to h \to \gamma\gamma$. This is shown in Fig. 11, where the ATLAS and CMS ratios $R_{\gamma\gamma} \equiv \mu_{\gamma\gamma}$ and their combination, obtained with the $\approx 10\,\text{fb}^{-1}$ data collected at $\sqrt{s} = 7{+}8\,\text{TeV}$, is compared to the theory uncertainty bands obtained by the LHC Higgs group [110] and in Ref. [112]. It is clear that including the theory uncertainty as a bias helps to reduce the discrepancy between measurement and expectation and e.g. the excess reduces to 1.3σ from the original $\gtrsim 2\sigma$ value.

Ignoring this option, let us summarise the various possibilities that could explain this excess in the context of the MSSM. Deviations of $\mu_{\gamma\gamma}$ from the SM value may be due to modifications of either the production cross section or the decay branching fraction or to both. The h decay branching fractions may be modified by a change of the h total decay width. Since the dominant decay mode is $h \to b\bar{b}$, a change of the effective $hb\bar{b}$ coupling by the direct vertex correc-

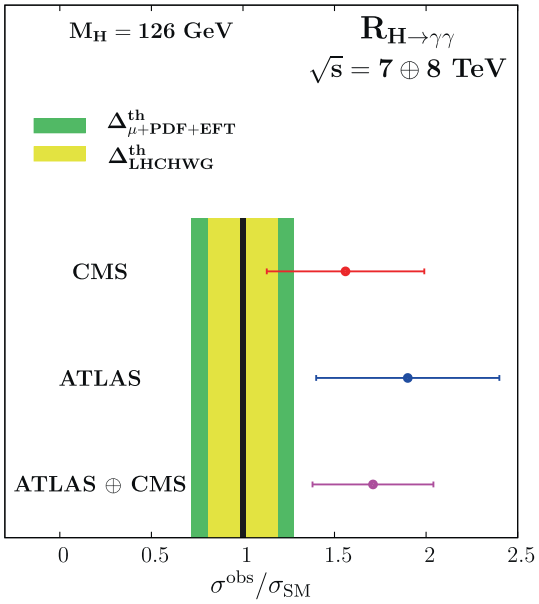

Fig. 11 The value of $\mu_{\gamma\gamma}$ given by the ATLAS and CMS collaborations with the ≈10 fb^{-1} data collected at $\sqrt{s} = 7$ and 8 TeV, as well as their combination, compared to two estimates of the theoretical uncertainty bands; from Ref. [153]

tions of Eq. (19) outside the decoupling regime can change all other Higgs rates including $h \to \gamma\gamma$. The total width can also be modified by additional decay channels to SUSY particles and the only ones that are allowed by experimental constraints are invisible decays into the LSP that will be discussed later.

Nevertheless, these two possibilities would not only affect the $h \to \gamma\gamma$ rate but also those of other channels such as $h \to ZZ$ where no excess has been observed. It is thus more appropriate to look at deviation in the $h \to \gamma\gamma$ loop induced decay only. In the MSSM, the $h \to \gamma\gamma$ process receives contributions from scalar top and bottom quarks, staus and charginos as briefly is summarised below.

- Light stops: as already discussed, the $M_h = 125$ GeV constraint requires large $M_S = \sqrt{m_{\tilde{t}_1} m_{\tilde{t}_2}}$ and/or X_t values. If $m_{\tilde{t}_1} \lesssim 500$ GeV, one should have maximal mixing $X_t \approx \sqrt{6} M_S$ and, in this case, the $h\tilde{t}_1\tilde{t}_1$ coupling of Eq. (20) is large and leads to a sizeable change of the $gg \to h \to \gamma\gamma$ rate; cf. Fig. 12 (left). However, an enhancement of the $h \to \gamma\gamma$ rate is over-compensated by a suppression of $\sigma(gg \to h)$ that seems not to occur. $\mu_{\gamma\gamma}$ is enhanced only in the no-mixing case, $X_t \approx 0$, which requires very heavy stops which decouple from the amplitude [57–59,152].
- Light sbottoms: a light $\tilde{b}_R$ state does not conflict with the M_h value as its corrections to the mass are small. For $m_{\tilde{b}_1} \lesssim 500$ GeV, it contributes to the hgg loop but it reduces the $gg \to h$ production rate; Fig. 12 (right). In turn, it has little impact on the $h \to \gamma\gamma$ rate because of the largely dominating W loop and the small $\tilde{b}_1$ electric charge. For $m_{\tilde{b}_1} \gtrsim 1$ TeV, as indicated by direct LHC searches, $\mu_{\gamma\gamma}$ is unaffected by sbottoms loops [152].
- Light staus: they lead to the largest contributions and have received most of the attention in the literature; see e.g. Ref. [154–156]. For low $m_{\tilde{\tau}_{L/R}}$ values, a few 100 GeV, and large mixing $X_\tau = A_\tau - \mu \tan\beta$, with $\tan\beta \approx 60$ and $|\mu|$=0.5–1 TeV, the lighter stau state has a mass close to the LEP2 bound, $m_{\tilde{\tau}_1} \approx 100$ GeV and its coupling to the h boson, $g_{h\tilde{\tau}\tilde{\tau}} \propto m_\tau X_\tau$, is huge. The $\tilde{\tau}_1$ contribution can hence significantly increase BR($h \to \gamma\gamma$), up to 50 % [154–156], but this occurs only for extreme choices of the parameters.
- Light charginos: the $h\chi_i^+\chi_i^-$ couplings are in general small and are maximal when the $\chi_i^\pm$ states are almost equal higgsino–wino mixtures. For a mass above 100 GeV and maximal couplings to the h boson, the $\chi_1^\pm$ contributions to the $h \to \gamma\gamma$ rate do not exceed the 10–15 % level (with a sign being the same as the sign of μ) [157,158].

Fig. 12 The deviation of $\mu_{\gamma\gamma}$ from its SM expectation from stop (*left*) and sbottom (*right*) contributions in various scenarios to the $\sigma(gg \to h) \times$ BR($h \to \gamma\gamma$) rate; from Ref. [152]

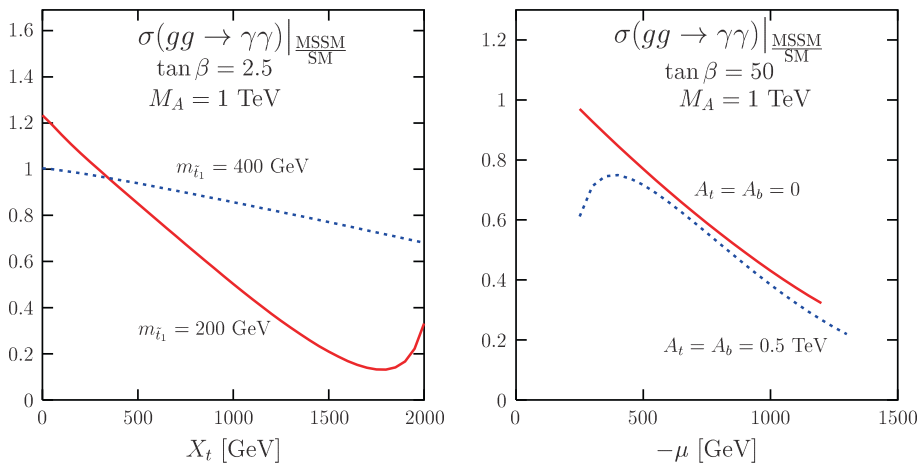

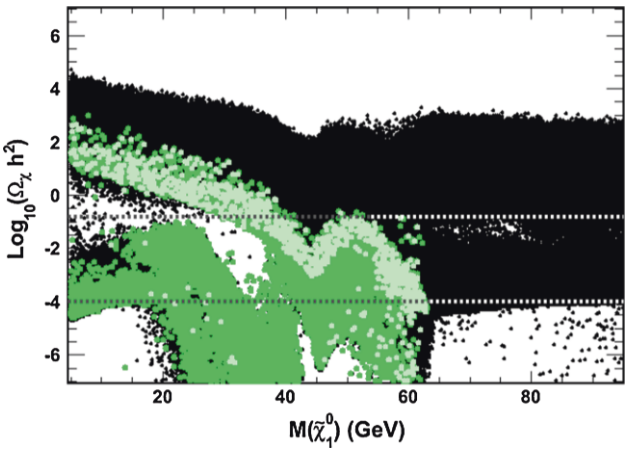

Fig. 13 The neutralino relic density $\log_{10}(\Omega_\chi h^2)$ as a function of $m_{\chi_1^0}$ compatible with $\mathrm{BR}(h \to \chi_1^0\chi_1^0) \geq 15\,\%$ (*green*) and the LHC Higgs data at 90 % CL (*light green*). The *horizontal lines* show the WMAP constraint on $\Omega_\chi h^2$. From Ref. [149]

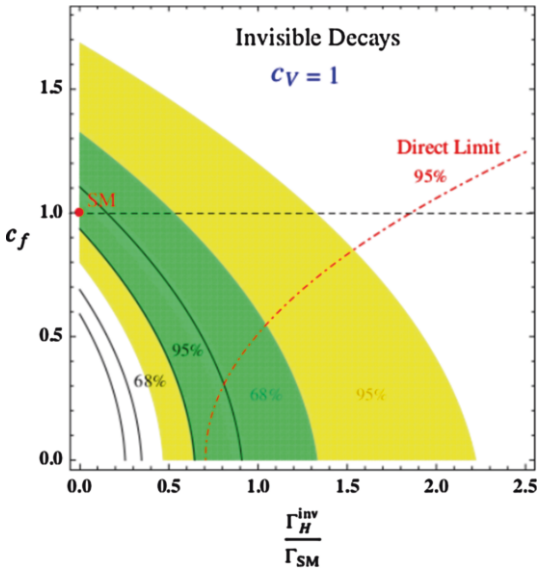

Fig. 14 1σ and 2σ domains from μ_{ZZ} for $c_V = 1$ in the plane $[c_f, \Gamma_H^{\mathrm{inv}}/\Gamma_H^{\mathrm{tot}}]$ [150]. The dependence on the theory uncertainties are shown by the *black curves* that indicate the other possible extreme domains. The direct upper limit on Γ_H^{inv} from direct searches at LHC for $c_V = c_f = 1$ [159] is also shown

Of course, different contributions can sum up resulting in more sizeable shifts. However, a 50 % deviation of the rate is unlikely and occurs only in extreme situations.

3.4 Invisible Higgs decays?

Invisible decays can also affect the properties of the observed h particle. In the MSSM, because of the LEP2 constraints, the only possible invisible channel for the h boson is into pairs of the LSP neutralinos, $h \to \chi_1^0\chi_1^0$. $\mathrm{BR}_{\mathrm{inv}}$ can be important for $m_{\tilde{\chi}_1^0} < 60$GeV and for not too large M_1 and $|\mu|$ values which make the LSP a higgsino–gaugino mixture with significant couplings to the h state. Such an LSP would have the relic density Ωh^2 required by the WMAP results [95] since it will annihilate efficiently through the s-channel exchange of the h boson. However, $\mathrm{BR}_{\mathrm{inv}}$ should be small in this case. This is exemplified in Fig. 13, where $\log_{10}(\Omega_\chi h^2)$ is shown as a function of $m_{\chi_1^0}$ for the pMSSM points that satisfy the LHC Higgs constraints and $\mathrm{BR}(h \to \chi_1^0\chi_1^0) \geq 15\,\%$. Only a small area in the region $30 \lesssim m_{\chi_1^0} \lesssim 60$ GeV fulfils these conditions.

The invisible Higgs decay width can be constrained indirectly by a fit of the Higgs couplings and in particular with the signal strength μ_{ZZ}, which is the most accurate one and has the least theoretical ambiguities. Γ_H^{inv} enters in the signal strength through the total width Γ_H^{tot}, $\mu_{ZZ} \propto \Gamma(H \to ZZ)/\Gamma_H^{\mathrm{tot}}$ with $\Gamma_H^{\mathrm{tot}} = \Gamma_H^{\mathrm{inv}} + \Gamma_H^{\mathrm{SM}}$ and Γ_H^{SM} calculated with free coefficients c_f and c_V. The resulting 1σ or 2σ ranges are shown in Fig. 14, where c_f is freely varied while $c_V = 1$ [150]. This gives $\Gamma_H^{\mathrm{inv}}/\Gamma_H^{\mathrm{SM}} \lesssim 50\,\%$ at the 95 % CL if the assumption $c_f = c_V = 1$ is made.

A more model independent approach would be to perform direct searches for missing transverse energy. These have been conducted by ATLAS [159] and CMS [163] in the $pp \to hV$ process with $V \to jj, \ell\ell$ and in the VBF channel, $qq \to qqE\!\!\!/_T$. As an example, we show in Fig. 15 (left) the CMS results for the Higgs cross section times $\mathrm{BR}_{\mathrm{inv}}$ versus M_h when the two channels are combined. For $M_h \approx 125$ GeV a bound $\mathrm{BR}_{\mathrm{inv}} \lesssim 50\,\%$ is obtained at the 95 % CL.

A more promising search for invisible decays is the monojet channel. In the ggF mode, an additional jet can be emitted at NLO leading to $gg \to hj$ final states and, because the QCD corrections are large, $\sigma(H + 1j)$ is not much smaller than $\sigma(h + 0j)$. The NNLO corrections besides significantly increasing the $h + 0j$ and $h + 1j$ rates, lead to $h + 2j$ events that also occur in VBF and VH. Hence, if the Higgs is coupled to invisible particles, it may recoil against hard QCD radiation, leading to monojet events.

In Refs. [160–162], it has been shown that the monojet signature carries a good potential to constrain the invisible decay width of a ≈ 125 GeV Higgs boson. In a model independent fashion, constraints can be placed on the rates

$$R_{\mathrm{inv}}^{\mathrm{ggF}} = \frac{\sigma(gg \to h) \times \mathrm{BR}(h \to \mathrm{inv.})}{\sigma(gg \to h)_{\mathrm{SM}}} \tag{22}$$

Recent monojet searches made by CMS and ATLAS [164, 165] are sensitive to R_{inv} close to unity. This is shown in Fig 15 (right) where the best-fit region to the LHC Higgs data is displayed in the $\mathrm{Br}_{\mathrm{inv}}$–$c_{gg}$ plane, where c_{gg} is the deviation of $\sigma(gg \to h)$ from the SM expectation [160]. For the SM value $c_{gg} = 0$, $\mathrm{Br}_{\mathrm{inv}} \gtrsim 20\,\%$ is disfavoured at 95 % CL while for $c_{gg} > 0$, a larger rate is allowed, up to $\mathrm{Br}_{\mathrm{inv}} \sim 50\,\%$.

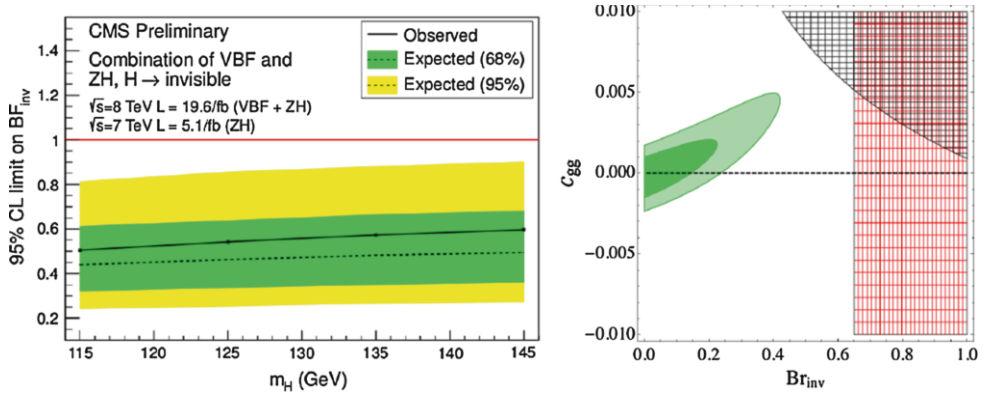

Fig. 15 *Left:* the Higgs cross section times invisible Higgs decay branching ratio normalised to the total SM cross section in the combined hV and VBF channels from CMS with the $\approx$ 20 fb^{-1} data at 8 TeV [163]. *Right*: 68 % CL (*light green*) and 95 % CL (*dark green*) best-fit regions to the combined LHC Higgs data. The *black region* is excluded by the monojet constraints while the *red region* is excluded by the ATLAS $Z + E_T$ search [159]; from Ref. [160]

The Higgs invisible rate and the dark matter detection rate in direct astrophysical searches are correlated in Higgs-portal models. Considering the generic cases of scalar, fermionic and vectorial dark matter particles χ that couple only to the Higgs, one can translate in each case the LHC constraint BR($h \to$ inv.) into a constraint on the Higgs couplings to the χ particles. It turns out that these constraints are competitive with those derived from the bounds on the dark matter scattering cross section on nucleons from the best experiment so far, XENON [95].

This is shown in Fig. 16, where the maximum allowed values of the scattering cross sections are given in the three cases assuming $\mathrm{BR}_\chi^{\mathrm{inv}} \lesssim 20\,\%$. The obtained spin-independent rates $\sigma_{\chi p}^{\mathrm{SI}}$ are stronger than the direct limit from the XENON100 experiment in the entire $M_\chi \ll \frac{1}{2} M_h$ range. In other words, the LHC is currently the most sensitive dark matter detection apparatus, at least in the context of simple Higgs-portal models.

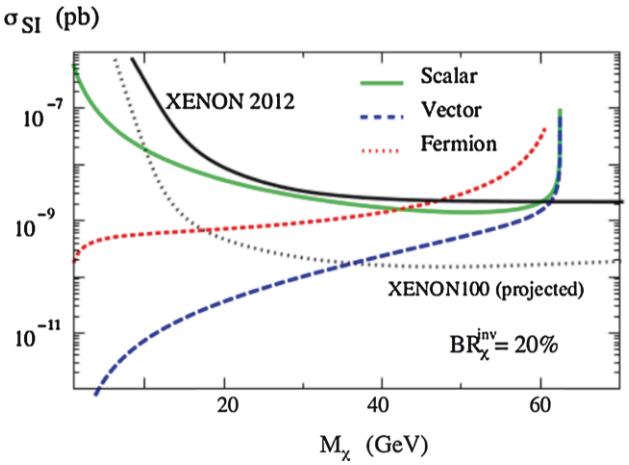

Fig. 16 Bounds on the spin-independent direct detection cross section $\sigma_{\chi p}^{\mathrm{SI}}$ in Higgs-portal models derived for an invisible branching fraction of 20 % (*colored lines*) for a 125 GeV Higgs. These are compared to the current and future direct bounds from the XENON experiment (*black lines*). From Ref. [166]

3.5 Determination of the Higgs parity

Apart from the measurement of the couplings, one also needs in principle to establish that the observed Higgs state is indeed a CP even scalar particle and hence with $\mathrm{J}^{\mathrm{PC}} = 0^{++}$ quantum numbers[4]. It is known that the Higgs to vector boson (hVV) coupling is a possible tool to probe these quantum numbers at the LHC [170,171]. This can be done by studying various kinematical distributions in the Higgs decay and production processes. One example is the threshold behaviour of the M_{Z^*} spectrum in the $h \to ZZ^* \to 4\ell$ decay channel and another is the azimuthal distribution between the decay planes of the two lepton pairs arising from the Z, Z^* bosons from the Higgs decay. These are sensitive to both the spin and the parity of the Higgs.

With the 25 fb^{-1} data collected so far, the ATLAS and CMS collaborations performed a matrix-element likelihood analysis which exploits the kinematics and Lorenz structure of the $h \to ZZ^* \to 4\ell$ channel to see whether the angular distributions are more compatible with the 0^+ or 0^- hypothesis (as well as the spin-2 possibility) [172,173]. Assuming that it has the same couplings as the SM Higgs boson and

[4] To be more general, the spin of the particle needs also to be determined. The observation of the $h \to \gamma\gamma$ decay channel rules out the spin-1 case by virtue of the Landau–Yang theorem [167,168] and leaves only the spin 0 and $\geq$2 possibilities. The graviton-like spin-2 option is extremely unlikely and, already from the particle signal strengths in the various channels, it is ruled out in large classes of beyond the SM models; see e.g. Ref. [169].

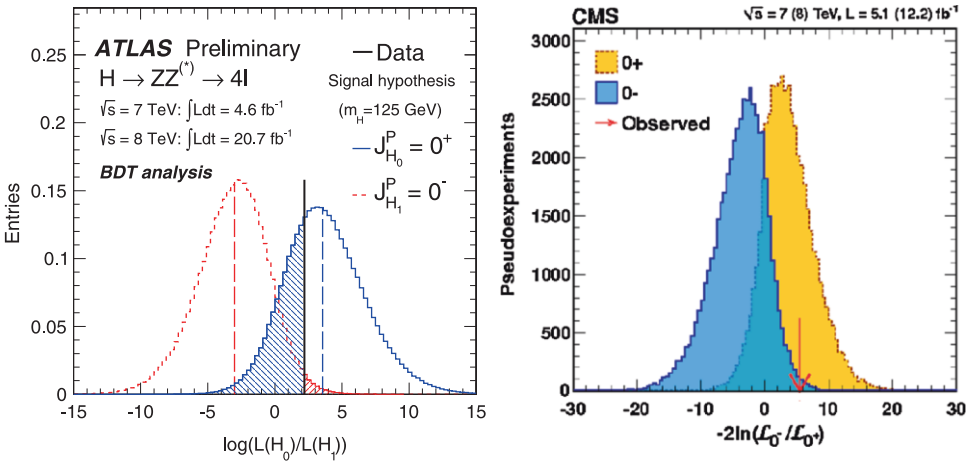

Fig. 17 Discrimination between the 0^+ and 0^- parity hypotheses for the observed Higgs boson using the kinematics of the $h \to ZZ^* \to 4\ell$ channel by the ATLAS (*left*) and CMS (*right*) collaborations with the data collected at 7+8 TeV [172,173]

that it is produced mainly from the dominant ggF process, the observed particle is found to be compatible with a 0^+ state and the 0^- possibility is excluded at the 97.8% confidence level or higher; see Fig. 17.

Other useful diagnostics of the CP nature of the Higgs boson that also rely on the different tensorial structure of the hVV coupling can be made in the VBF process. It was known since a long time that in this channel, the distribution in the azimuthal angle between the two jets produced in association with the Higgs discriminates a CP-even from a CP-odd state [174]. This has been extended recently to other observables in this process, like the rapidity separation between the two jets [175–178].

Recently, the VBF channel $pp \to Hjj$ has been reanalysed in the presence of an anomalous hVV vertex that parametrises different spin and CP assignments of the produced Higgs boson [178]. The anomalous hVV coupling is introduced by allowing for an effective Lagrangian with higher dimensional operators, which include four momentum terms which are absent in the SM. It was shown that the kinematics of the forward tagging jets in this process is highly sensitive to the structure of the anomalous coupling and that it can effectively discriminate between different assignments for the spin (spin-0 versus spin-2) and the parity (CP-even versus CP-odd) of the produced particle. In particular, it was found that the correlation between the separation in rapidity and the transverse momenta of the scattered quarks, in addition to the already discussed distribution of the azimuthal jet separation, can be significantly altered compared to the SM expectation.

This is exemplified in Fig. 18, where the difference in rapidity between tagging jets (Δy_{jj}) for each of the higher dimensional operators in the hVV couplings is displayed.

These kinematical variables define new corners of the phase space that have not been explored by the experiments at the LHC to probe anomalous hVV couplings and to check the Higgs parity. In addition, some of these observables sig-

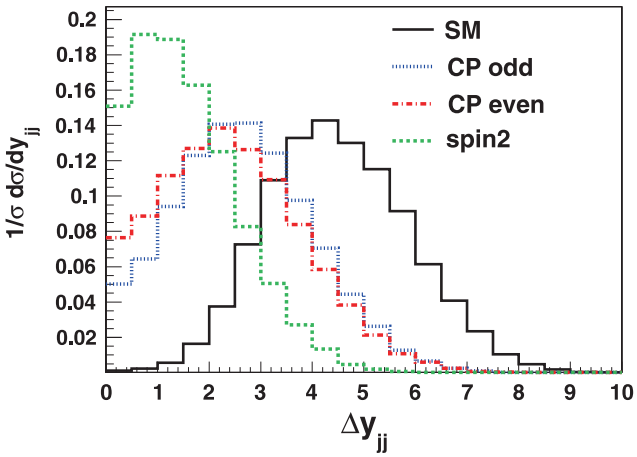

Fig. 18 Normalised distribution of the difference in rapidity between the scattered jets in VBF for each of the SM and BSM operators (spin-2, CP-even and CP-odd) individually [178]

nificantly depend on the c.m. energy and strong constraints on anomalous couplings can be obtained by performing measurements at the LHC with energies of $\sqrt{s} = 8$ and 14 TeV. Finally, the associated hV production channel can be used as the invariant mass of the Vh system as well as the p_T and rapidities of the h and V bosons are also sensitive to anomalous hVV couplings.

Nevertheless, there is a caveat in the analyses relying on the hVV couplings. Since a CP-odd state has no tree-level VV couplings, all the previous processes project out only the CP-even component of the hVV coupling [179–182] even if the state is a CP-even and -odd mixture. Thus, in the CP studies above, one is simply verifying a posteriori that indeed the CP-even component is projected out.

A better way to measure the parity of the Higgs boson is to study the signal strength in the $h \to VV$ channels [150,183]. Indeed, the hVV coupling takes the general form $g^{\mu\nu}_{hVV} =$

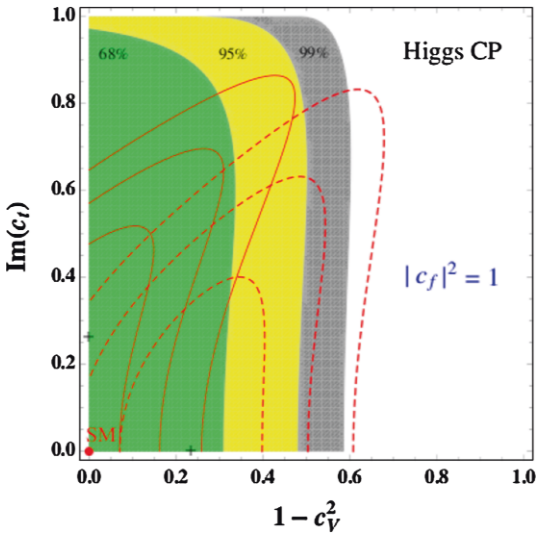

Fig. 19 Best-fit regions at 68, 95 and 99 % CL in the plane $[1 - c_V^2, \mathrm{Im}(c_t)$ for $|c_t|^2 = |c_f|^2 = 1$. Superimposed are the best-fit regions when including a theory uncertainty of ±20 % [150]

$-ic_V(M_V^2/v)\ g^{\mu\nu}$ where c_V measures the departure from the SM: $c_V = 1$ for a pure 0^+ state with SM-like couplings and $c_V \approx 0$ for a pure 0^- state. The measurement of c_V should allow to determine the CP composition of the Higgs if it is indeed a mixture of 0^+ and 0^- states.

However, having $c_V \neq 1$ does not automatically imply a CP-odd component: the Higgs sector can be enlarged to contain other states h_i with squared $h_i VV$ couplings $\Sigma_i c_{V_i}^2\, g_{h_i VV}^2$ that reduce to the SM coupling g_{hVV}^2. This is what occurs in the MSSM with complex soft parameters [170, 171]: one has three neutral states h_1, h_2 and h_3 with indefinite parity and their CP-even components share the SM hVV coupling, $c_{V_1}^2 + c_{V_2}^2 + c_{V_3}^2 = 1$. But in all cases, the quantity $1 - c_V^2$ gives an *upper bound* on the CP-odd contribution to the hVV coupling.

Using μ_{VV} and the ratios $\mu_{\gamma\gamma}/\mu_{VV}$ and $\mu_{\tau\tau}/\mu_{VV}$ as in Eq. (17), it was demonstrated that the particle has indeed a large CP component, $\gtrsim$50 % at the 95 % CL, if the Higgs couplings to fermions are SM like. This is shown in Fig. 19, where one sees that the pure CP-odd possibility is excluded at the 3σ level, irrespective of the (mixed CP) Higgs couplings to fermions provided that $|c_f|^2 = 1$.

4 Implications from heavy Higgs searches

We turn now to the constraints on the MSSM Higgs sector that can be obtained from the search of the heavier H/A and $H^\pm$ states at the LHC and start with a brief summary of their production and decay properties.

4.1 H, A, $H^\pm$ decays and production at the LHC

The production and decay pattern of the MSSM Higgs bosons crucially depend on $\tan\beta$. In the decoupling regime that is indicated by the h properties, the heavier CP-even H boson has approximately the same mass as the A state and its interactions are similar. Hence, the MSSM Higgs spectrum will consist of a SM-like Higgs $h \equiv H_{\rm SM}$ and two pseudoscalar-like particles, $\Phi = H/A$. The $H^\pm$ boson will also be mass degenerate with the Φ states and the intensity of its couplings to fermions will be similar. In the high $\tan\beta$ regime, the couplings of the non-SM like Higgs bosons to b quarks and to τ leptons are so strongly enhanced, and the couplings to top quarks and massive gauge bosons suppressed, that the pattern is rather simple.

This is first the case for the decays: the $\Phi \to t\bar{t}$ channel and all other decay modes are suppressed to a level where their branching ratios are negligible and the Φ states decay almost exclusively into $\tau^+\tau^-$ and $b\bar{b}$ pairs, with branching ratios of $\mathrm{BR}(\Phi \to \tau\tau) \approx 10\,\%$ and $\mathrm{BR}(\Phi \to b\bar{b}) \approx 90\,\%$. The $H^\pm$ boson decay into $\tau\nu_\tau$ final states with a branching fraction of almost 100 % for $H^\pm$ masses below the tb threshold, $M_{H^\pm} \lesssim m_t + m_b$, and a branching ratio of only ≈10 % for masses above this threshold while the rate for $H^\pm \to tb$ will be at the ≈90 % level in most cases.

Concerning the production, the strong enhancement of the b-quark couplings at high $\tan\beta$ makes that only two processes are relevant in this case: $gg \to \Phi$ fusion with the b-loop included and associated production with b-quarks, $gg/q\bar{q} \to b\bar{b} + \Phi$, which is equivalent to the fusion process $b\bar{b} \to \Phi$ when no additional final b-quark is present. All other processes, in particular $V\Phi, t\bar{t}\Phi$ and VBF have suppressed rates. In both the $b\bar{b}$ and the gg fusion cases, as $M_\Phi \gg m_b$, chiral symmetry holds and the rates are approximately the same for the CP-even H and CP-odd A bosons. While $\sigma(gg \to \Phi)$ is known up to NLO in QCD [184], $\sigma(bb \to \Phi)$ is instead known up to NNLO [185,186].

The most powerful search channel for the heavier MSSM Higgs particles at the LHC is by far the process $pp \to gg + b\bar{b} \to \Phi \to \tau^+\tau^-$. The precise values of the cross section times branching fraction for this process at the LHC have been updated in Refs. [110,112] and an assessment of the associated theoretical uncertainties has been made. It turns out that, in the production cross section, the total uncertainty from scale variation, the PDFs and α_s as well as from the b-quark mass are not that small: $\Delta^{\rm TH}\sigma(pp \to \Phi) \times \mathrm{BR}(\Phi \to \tau\tau) \approx \pm 25\,\%$ in the entire M_Φ range probed at the LHC at $\sqrt{s} = 8$ TeV; Fig. 20.

Besides the QCD uncertainty, three other features could alter the rate $\sigma(pp \to \Phi \to \tau\tau)$ in the MSSM and they are related to the impact of the SUSY particle contributions:

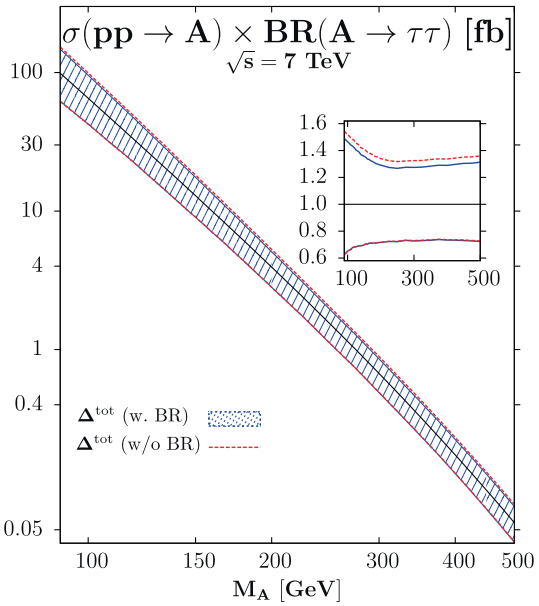

Fig. 20 The combined $\sigma(pp \to A) \times \mathrm{BR}(A \to \tau\tau)$ rate with theoretical uncertainties with and without the branching ratio; in the *inserts*, shown are the uncertainties when the rates are normalised to the central values. From Ref. [112]

(i) In the case of H (A does not couple to identical sfermions), there are squark (mainly stop) loops that contribute in addition in the $gg \to H$ process. But as they are damped by powers of $\tilde{m}_Q^2$ for $M_H \lesssim 2m_Q^2$, these contributions should be small for $\tilde{m}_Q \gtrsim 1$ TeV, in particular at high $\tan\beta$ where the b-contribution is strongly enhanced.

(ii) The vertex correction to the $\Phi b\bar{b}$ couplings, Δ_b of Eq. (19), grows as $\mu \tan\beta$ and can be very large in the high $\tan\beta$ regime. However, in the full process $pp \to \Phi \to \tau^+\tau^-$, this correction appears in both the cross section and the branching fraction and largely cancels outs as one obtains, $\sigma \times \mathrm{BR} \times (1 - \Delta_b/5)$. A very large contribution $\Delta_b \approx 1$ changes the rate only by 20 %, i.e. less than the QCD uncertainty.

(iii) The possibility of light sparticles would lead to the opening of H/A decays into SUSY channels that would reduce $\mathrm{BR}(\Phi \to \tau\tau)$. For $M_\Phi \lesssim 1$ TeV, the only possibilities are decays into light neutralinos or charginos and sleptons. These are in general disfavoured at high $\tan\beta$ as the $\Phi \to b\bar{b} + \tau\tau$ modes are strongly enhanced and dominant.

Thus, only in the unlikely cases where the decay $H \to \tilde{\tau}_1\tilde{\tau}_1$ has a branching rate of the order of 50 %, the squark loop contribution to the $gg \to H$ process is of the order 50 %, or the Δ_b SUSY correction is larger than 100 %, and one can change the $pp \to \Phi \to \tau\tau$ rate by ≈25 %, which is the level of the QCD uncertainty. One thus expects $\sigma(pp \to \Phi) \times \mathrm{BR}(\Phi \to \tau\tau)$ to be extremely robust and to depend almost exclusively on M_A and $\tan\beta$.

Finally, for the charged Higgs boson, the dominant search channel is in $H^\pm \to \tau\nu$ final states with the $H^\pm$ bosons produced in top quark decays for $M_{H^\pm} \lesssim m_t - m_b \approx 170$ GeV, $pp \to t\bar{t}$ with $t \to H^+b \to \tau\nu b$. This is particularly true at high $\tan\beta$ values when $\mathrm{BR}(t \to H^+b) \propto \bar{m}_b^2 \tan^2\beta$ is significant. For higher $H^\pm$ masses, one should rely on the three-body production process $pp \to tbH^\pm \to tb\tau\nu$, but the rates are presently rather small.

In the low $\tan\beta$ regime, $\tan\beta \lesssim 5$, the phenomenology of the heavier $A, H, H^\pm$ bosons is richer [98,187–190]. Starting with the cross sections, we display in Fig. 21 the rates for the relevant production processes at the LHC with $\sqrt{s} = 8$ TeV assuming $\tan\beta = 2.5$. For smaller $\tan\beta$ values, the rates except for $pp \to H/A + b\bar{b}$ are even larger as the $H/A + tt$ and HVV couplings are less suppressed.

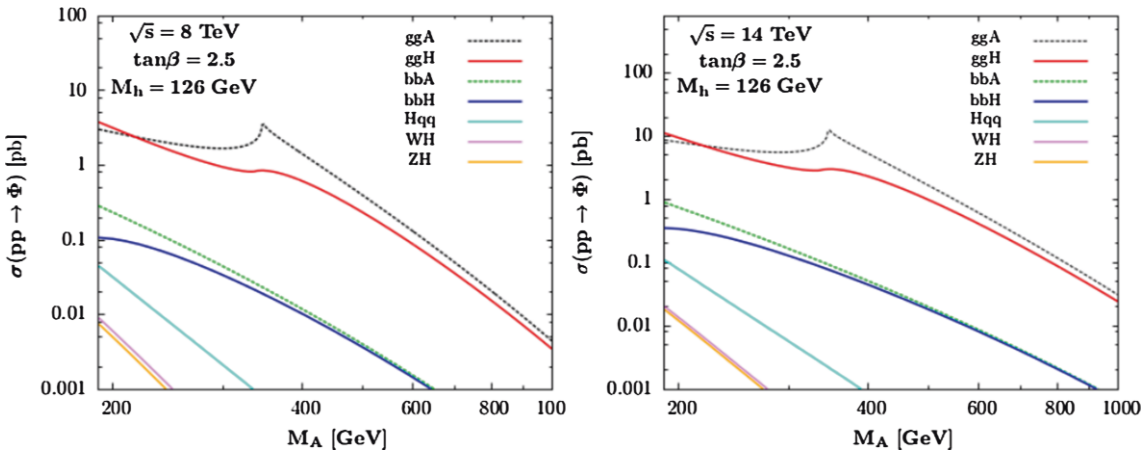

Fig. 21 The production cross sections of the MSSM heavier neutral Higgs bosons at the LHC at $\sqrt{s} = 8$ for $\tan\beta = 2.5$; only the main production channels are considered [98]

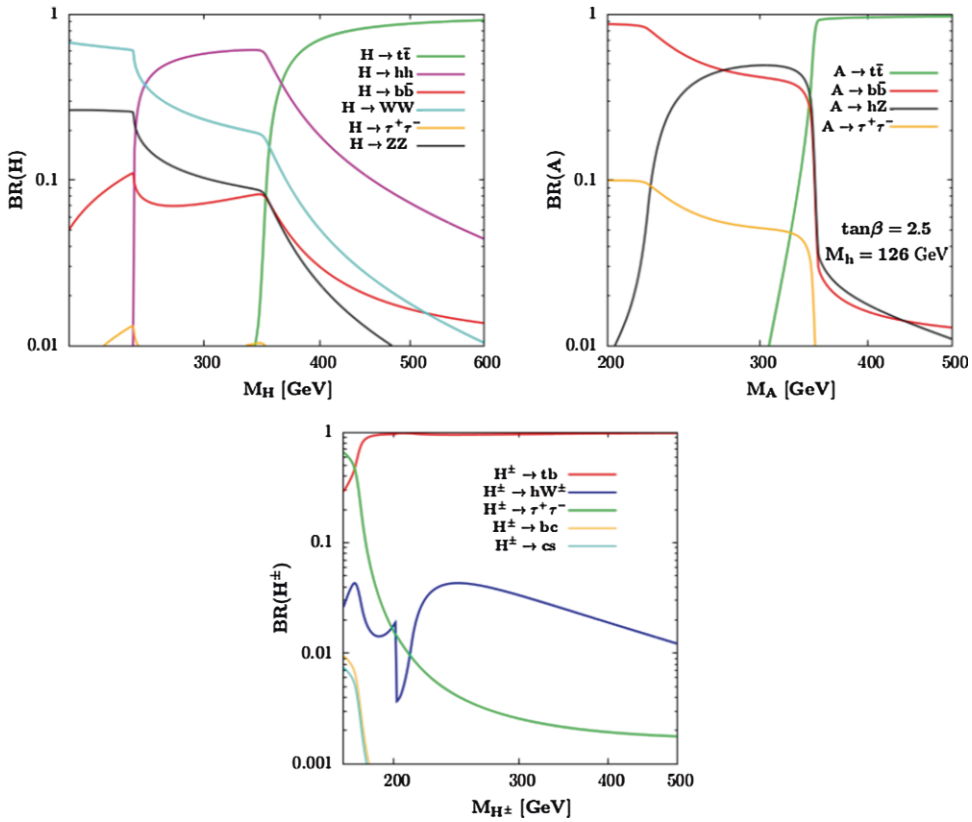

Fig. 22 The $H/A/H^\pm$ decay branching ratios as functions of the Higgs masses for $\tan\beta = 2.5$ [98]

Because of CP invariance which forbids AVV couplings, there is no AV and Aqq processes while the rates for associated $t\bar{t}A$ and $b\bar{b}A$ are small because the Att (Abb) couplings are suppressed (not sufficiently enhanced) compared to the SM Higgs. Only the $gg \to A$ process with the dominant t and sub-dominant b contributions included provides large rates. The situation is almost the same for H: only $gg \to H$ is significant at $M_H \gtrsim 300\,\text{GeV}$ and $\tan\beta \lesssim 5$; the VBF and HV modes give additional small contributions for $\tan\beta \approx 1$. For $H^\pm$, the dominant production channel is again top quark decays, $t \to H^+ b$ for $M_{H^\pm} \lesssim 170\,\text{GeV}$ as for $\tan\beta \lesssim 5$, the $m_t/\tan\beta$ piece of the $H^\pm tb$ coupling becomes large; for higher $H^\pm$ masses, the main process to be considered is $gg/q\bar{q} \to H^\pm tb$.

Turning to the $H/A/H^\pm$ decay pattern, it can be rather involved at low $\tan\beta$. A summary is as follows for $\tan\beta \lesssim 3$; see also Fig. 22, where the rates are shown for $\tan\beta = 2.5$.

- Above the $t\bar{t}$ (tb) threshold for $H/A(H^\pm)$, the decay channels $H/A \to t\bar{t}$ and $H^+ \to t\bar{b}$ are by far dominant for $\tan\beta \lesssim 3$ and do not leave space for any other mode.
- Below the $t\bar{t}$ threshold, the $H \to WW, ZZ$ decay rates are still significant as g_{HVV} is not completely suppressed.
- For $2M_h \lesssim M_H \lesssim 2m_t$, $H \to hh$ is the dominant H decay mode as the Hhh self-coupling is large at low $\tan\beta$.
- For $M_A \gtrsim M_h + M_Z$, $A \to hZ$ decays would occur but the $A \to \tau\tau$ channel is still important with rates $\gtrsim 5\,\%$.
- In the case of $H^\pm$, the channel $H^+ \to Wh$ is important for $M_{H^\pm} \lesssim 250\,\text{GeV}$, similarly to the $A \to hZ$ case.

Hence, many decay and production channels need to be considered in this low $\tan\beta$ regime.

4.2 Constraints from the LHC Higgs searches

The most efficient channel to probe the heavier MSSM Higgs bosons is by far $pp \to gg + bb \to H/A \to \tau^+\tau^-$. Searches for this process have been performed by ATLAS with $\approx 5\ \text{fb}^{-1}$ data at the 7 TeV run [191] and by CMS with $\approx 5{+}12\ \text{fb}^{-1}$ data at the 7 and 8 TeV runs [192]. Upper limits on the production cross section times decay branching ratio have been set and they can be turned into constraints on the MSSM parameter space.

In Fig. 23, the sensitivity is displayed of the CMS $pp \to \Phi \to \tau\tau$ analysis with $17\ \text{fb}^{-1}$ of data in the $[\tan\beta, M_A]$ plane. The excluded region, obtained from the observed limit at the 95 % CL, is drawn in blue. The dotted line represents the median expected limit which turns out to be weaker than the observed limit. As can be seen, this constraint is extremely restrictive and, for values $M_A \lesssim 250\,\text{GeV}$, it excludes almost the entire intermediate and high $\tan\beta$ regimes, $\tan\beta \gtrsim 5$.

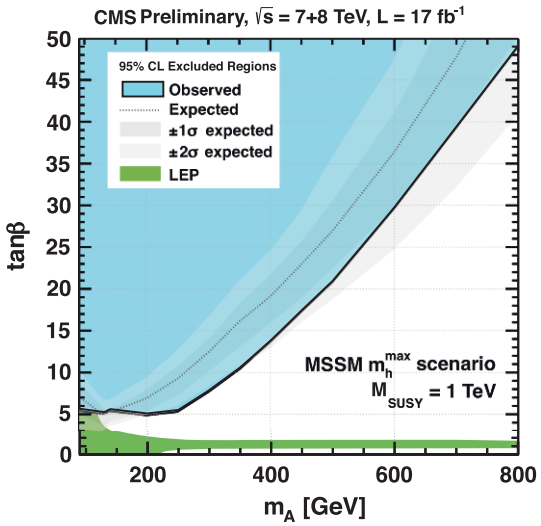

Fig. 23 The expected and observed exclusion limits in the [tan β, M_A] plane in the CMS search of the MSSM neutral Higgs bosons in the channels $pp \to h/H/A \to \tau^+\tau^-$ with ≈ 17 fb^{-1} data collected at $\sqrt{s} = 7$+8 TeV [192]

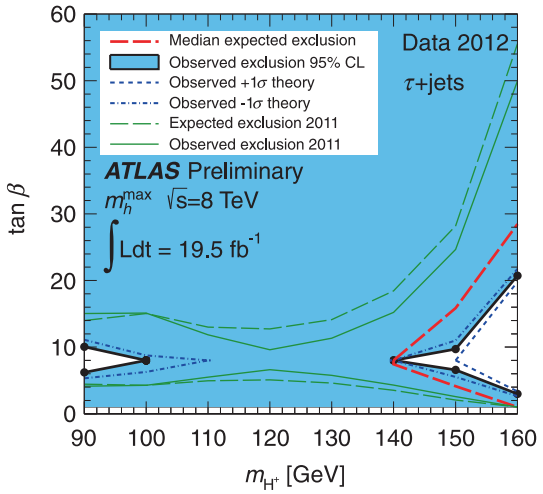

Fig. 24 The $H^\pm$ limits from ATLAS with $\sqrt{s} = 8$ TeV and $\approx$20 fb^{-1} data in the channel $t \to bH^+ \to b\tau\nu$ [194]

The constraint is less effective for a heavier A boson, but even for $M_A \approx 400$ GeV the high tan $\beta \gtrsim 10$ region is excluded and there is even sensitivity to large values $M_A \approx 800$ GeV for tan $\beta \gtrsim 50$.

There are, however, some caveats to this exclusion limit as discussed previously. The first one is that there is a theoretical uncertainty of order of $\pm 25\,\%$ that affects the $gg \to \Phi$ and $b\bar{b} \to \Phi$ production cross sections which, when included, will make the constraint slightly weaker as one then needs to consider the lower value predicted for the production rate. A second caveat is that SUSY effects, direct corrections to the production and H/A decays into sparticles, could alter the rate. However, as previously argued, $\sigma(pp \to \Phi) \times \mathrm{BR}(\Phi \to \tau\tau)$ is robust against these SUSY effects and the latter will unlikely make a substantial change of the cross section times branching fraction. Finally, the constraint is specifically given in the maximal mixing scenario $X_t/M_S = \sqrt{6}$ with $M_S = 1$ TeV. The robustness of $\sigma \times$ BR makes that the exclusion limit is actually almost model independent and is valid in far more situations than the "MSSM $M_h^{\max}$ scenario" quoted there, an assumption that can be removed without any loss.

In fact, the exclusion limit can also be extended to the low tan β region which, in the chosen scenario with $M_S = 1$ TeV, is excluded by the LEP2 limit on the lighter h mass (the green area in the figure) but should resurrect if the SUSY scale is kept as a free parameter. Note also that H/A bosons have also been searched for in the channel $gg \to b\bar{b}\Phi$ with $\Phi \to b\bar{b}$ (requiring more than three tagged b jets in the final state) but the constraints are much less severe than the ones derived from the $\tau\tau$ channel [193].

Turning to the H^+ boson [194,195], the most recent result has been provided by the ATLAS collaboration using the full $\approx$20 fb^{-1} data collected at $\sqrt{s} = 8$ TeV. The $H^\pm$ search as been performed using the τ plus jets channel with a hadronically decaying τ lepton in the final state. For $M_{H^\pm} \lesssim 160$ GeV, the results are shown in Fig. 24. Here, the relevant process is top quark decays, $t \to H^+b$ with the decay $H^+ \to \tau\nu$ having a branching ratio of almost 100 % at moderate to high tan β. For these high values, the H^+tb coupling has a component $\propto m_b \tan\beta$, which makes $\mathrm{BR}(t \to_! H^+b)$ rather large. Almost the entire tan $\beta \gtrsim 10$ region is excluded by the ATLAS analysis.

In addition, the branching fraction for the decay $t \to bH^+$ is also significant at low tan β values, when the component of the coupling $g_{tbH^+} \propto \bar{m}_t/\tan\beta$ becomes dominant. On the other hand, the branching fraction for the decay $H^\pm \to \tau\nu$ does not become very small as it has competition only from $H^+ \to c\bar{s}$, which, even for tan $\beta \approx 1$, does not dominate. Hence, the rates for $pp \to t\bar{t}$ with $t \to bH^+ \to b\tau\nu$ are comparable for tan $\beta \approx 3$ and tan $\beta \approx 30$ and the processes can also probe the low tan β region. This is exemplified in Fig. 24 where one can see that the entire area below tan $\beta \approx 5$ is also excluded. There remains then, for $H^\pm$ masses close to 90 GeV (where the detection efficiency is lower) and 160 GeV (where one is limited by the phase space), the intermediate area with tan $\beta \approx 5$–10 where the $H^\pm tb$ coupling is not strongly enhanced.

This ATLAS search has been extended to larger values of $M_{H^\pm}$ where the charged Higgs is produced in association with top quarks, $gb \to tH^+$, but the constraints are poor (only the region tan $\beta \gtrsim 50$ is excluded for $M_{H^\pm} = 200$–300 GeV) as the cross section for this process is low.

The reopening of the low tan β region allows to consider a plethora of very interesting channels for the heavier Higgs

bosons to be also investigated at the LHC: heavier CP-even H decays into massive gauge bosons $H \to WW, ZZ$ and Higgs bosons $H \to hh$, CP-odd Higgs decays into a vector and a Higgs boson, $A \to hZ$, CP-even and CP-odd Higgs decays into top quarks, $H/A \to t\bar{t}$, and even the charged Higgs decay $H^{\pm} \to Wh$. These final states have been searched for in the context of a heavy SM Higgs boson or for new resonances in some non-SUSY beyond the SM scenarios and the analyses can be adapted to the case of the heavier MSSM Higgs bosons. They would then allow to cover a larger part of the parameter space of the MSSM Higgs sector in a model-independent way, i.e. without using the information on the scale M_S and more generally on the SUSY particle spectrum that appear in the radiative corrections.

In Ref. [98] a preliminary analysis of these channels has been performed using current information given by the ATLAS and CMS collaborations in the context of searches for the SM Higgs boson or other heavy resonances (in particular new Z' or Kaluza–Klein gauge bosons that decay into $t\bar{t}$ pairs). The results are shown in Fig. 25 with an extrapolation to the full 25 fb^{-1} data of the 7+8 TeV LHC run (it has been assumed that the sensitivity scales simply as the square root of the number of events). The sensitivities from the usual $H/A \to \tau^+\tau^-$ and $t \to bH^+ \to b\tau\nu$ channels are also shown. The green and red areas correspond to the domains where the $H \to VV$ and $H/A \to t\bar{t}$ channels become constraining. The sensitivities in the $H \to hh$ and $A \to hZ$ modes are given by, respectively, the yellow and brown areas which peak in the mass range $M_A = 250$–350 GeV that is visible at low $\tan\beta$ values.

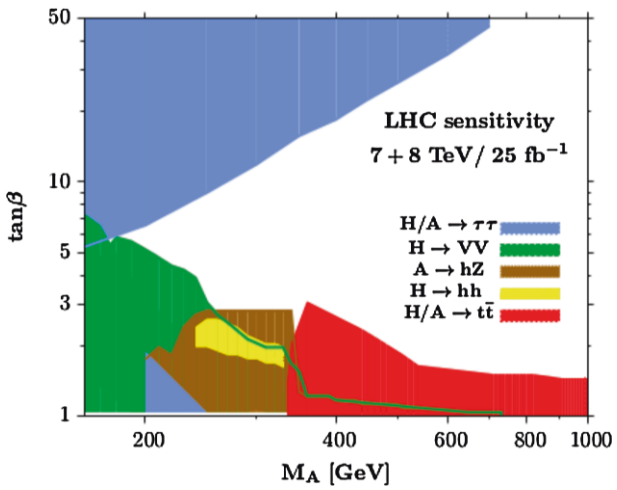

Fig. 25 The estimated sensitivities in the various search channels for the heavier MSSM Higgs bosons in the [$\tan\beta$, M_A] plane: $H/A \to \tau\tau$, $H \to WW + ZZ$, $H/A \to t\bar{t}$, $A \to hZ$ and $H \to hh$ [98]. The projection is made for the LHC with 7+8 TeV and the full 25 fb^{-1} of data collected so far. The radiative corrections are such that the h mass is $M_h = 126$ GeV

The outcome is impressive. These channels, in particular the $H \to VV$ and $H/A \to t\bar{t}$ processes, are very constraining as they cover the entire low $\tan\beta$ area that was previously excluded by the LEP2 bound up to $M_A \approx 500$ GeV. Even $A \to hZ$ and $H \to hh$ would be visible at the current LHC in small portions of the parameter space.

4.3 Could the observed state be the heavier H boson?

Let us briefly discuss the possibility, raised with the early LHC data, that the observed particle is the heavier MSSM H boson, as advocated for instance in Refs. [60–62,105]. The possibility $M_H \approx 125$ GeV, with H couplings close to those of the SM Higgs, occurs for low values of M_A, $\approx$100–120 GeV, and moderate values of $\tan\beta$, ≈ 10. In this case, H has approximately SM-like properties, while h has a mass of order 100 GeV or below and suppressed couplings to vector bosons. A dedicated scan for this region of parameter space has been performed [36] and the results were confronted with the measured Higgs mass $M_h = 123$–129 GeV and couplings that comply with the LHC ≈ 10 fb^{-1} data collected at $\sqrt{s} = 7$+8 TeV. Both the signal strengths in the various search channels of the observed Higgs boson and the limits from the $pp \to \tau^+\tau^-$ channel obtained by the CMS collaboration have been considered.

It was found that among the large flat scan with 10^8 points, only $\approx 2 \times 10^{-5}$ of the generated points would remain after imposing these LHC constraints. These points were then excluded by applying the constraints from flavour physics [94] (see also Ref. [196]), mainly the radiative decay $b \to s\gamma$ and dark matter constraints [95] (as they do not satisfy the constraint of $10^{-4} < \Omega h^2 < 0.155$ when accounting for all uncertainties). The updated $pp \to \tau^+\tau^-$ search performed by CMS with 17 fb^{-1} data, which excludes all values $\tan\beta \gtrsim 5$ for $M_A \lesssim 250$ GeV as shown in Fig. 23, now definitely rules out this scenario.

This is exemplified in Fig. 26, where we zoom in the [M_A, $\tan\beta$] plane for low values of the inputs and apply the constraints listed above. The small region in which the H boson was allowed to be the observed state (black points) by the previous $H/A \to \tau^+\tau^-$ CMS search (dashed blue line) is excluded by the new data (in red). In fact, the latest ATLAS limits from $H^{\pm}$ searches given in Fig. 24 also exclude now the possibility $M_A \approx 100$–120 GeV and, hence, the scenario where H is the observed Higgs state[5].

[5] Note that the recent $pp \to \tau\tau$ and $H^+ \to \tau\nu$ limits also exclude the so-called "intense coupling regime" [197,198], in which the three neutral Higgs bosons could be light and close in mass.

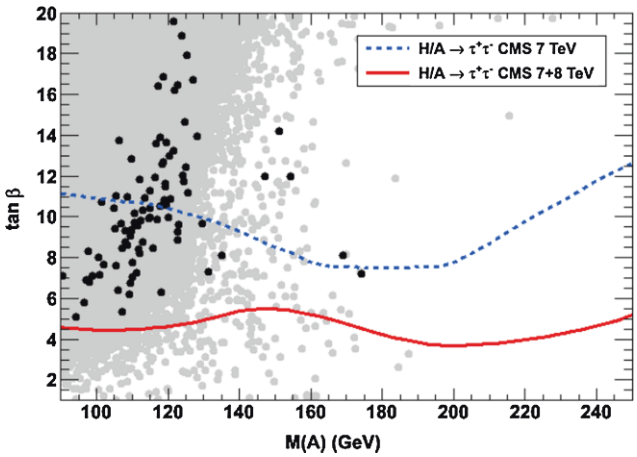

Fig. 26 The parameter space $[M_A, \tan\beta]$ with points for the heavier H boson to be observed with a mass in the range 123–129 GeV (*light grey points*) and after flavour and dark matter relic density constraints (*black points*) [36]. The CMS excluded regions from the 2011 and 2012 $\Phi \to \tau^+\tau^-$ searches are shown by the *dashed blue* and continuous *red lines*, respectively

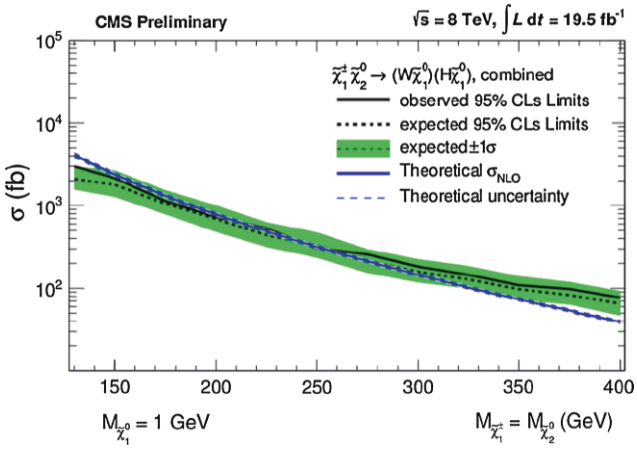

Fig. 27 The interpretations of the CMS results from the combination of all lepton and E_T searches with ≈20 fb^{-1} data collected at $\sqrt{s} = 8$ TeV. The expected and observed limits on the $pp \to \chi_2^0\chi_1^\pm$ cross section times the $\chi_2^0\chi_1^\pm \to Wh\chi_1^0\chi_1^0$ branching fraction (with the *green* band is for experimental uncertainties) is compared to the theoretical prediction [209]

4.4 Higgs production with SUSY particles

Finally, let us comment on the possibility of the Higgs bosons being produced in processes involving sparticles. First of all, there is the option of Higgs decays into SUSY particles. In the case of the lighter h boson, the only possibility when the LEP2 constraints are taken into account is the decay $h \to \chi_1^0\chi_1^0$, which has been discussed in the context of invisible Higgs decays in Sect. 3.4. In view of the strong LHC limits on squark masses, the only SUSY channels of the heavier $H/A/H^\pm$ states that might be kinematically open would be the decays into chargino, neutralinos and sleptons. For H/A, these decays have been discussed in the context of the τ searches as they might reduce the $H/A \to \tau\tau$ branching fractions but no specific search for these SUSY final states has been performed so far.

Turning to associated Higgs production with sparticles, the most important process was expected to be $pp \to \tilde{t}_1\tilde{t}_1+$ Higgs which could benefit from the possibly large Higgs–stop coupling [199–202]. The large value of M_S and hence the lightest stop mass from the current constraint makes this process unlikely. Another possibility would be associated production with staus where the phase space could be more favourable but the rates are in general much smaller.

The only channel which could lead to a detectable signal with the data collected so far would be Higgs particles from decays of charginos and neutralinos. In particular the decays $\chi_2^0 \to \chi_1^0 h$, with χ_2^0 directly produced in association with $\chi_1^\pm$ in the process $pp \to \chi_2^0\chi_1^\pm$ leading a lepton, a Higgs (decaying either into $b\bar{b}$ or into multi-leptons via $h \to ZZ^*, WW^*$) and missing energy [203–208].

The CMS collaboration has reported the results for searches of leptons and missing energy with a luminosity of ≈20 fb^{-1} data collected at $\sqrt{s} = 8$ TeV [209]. They set a limit on the cross section times branching ratio for the possible SUSY process $pp \to \chi_2^0\chi_1^\pm$ with $\chi_2^0 \to \chi_1^0 h$ and $\chi_1^\pm \to W\chi_1^0$. As can be observed from Fig. 27, where the cross section times branching ratio is displayed as a function of the masses $m_{\chi_1^\pm} = m_{\chi_2^0}$ (with the assumption that the LSP neutralino is very light, $m_{\chi_1^0} = 1$ GeV), the data show no excess over the SM backgrounds.

5 What next?

The last 2 years were extremely rich and exciting for particle physics. With the historical discovery at the LHC of a Higgs boson by the ATLAS and CMS collaboration crowned by a Nobel price this fall, and the first probe of its basic properties, they witnessed a giant step in the unravelling of the mechanism that breaks the electroweak symmetry and generates the fundamental particle masses. They promoted the SM as the appropriate theory, up to at least the Fermi energy scale, to describe three of Nature's interactions, the electromagnetic, weak and strong forces,

However, it is clear that these 2 years have also led to some frustration, as no signal of physics beyond the SM has emerged from the LHC data. The hope of observing some signs of the new physics models that were put forward to address the hierarchy problem, which is deeply rooted in the Higgs mechanisms, with supersymmetric theories being the most attractive ones, did not materialise.

The discovery of the Higgs boson and the non-observation of new particles has nevertheless far reaching consequences

for supersymmetric theories and, in particular, for their simplest low-energy formulation, the MSSM. The mass of approximately 125 GeV of the observed Higgs boson implies that the scale of SUSY-breaking is rather high, at least $\mathcal{O}$(TeV). This is backed up by the limits on the masses of strongly interacting SUSY particles set by the ATLAS and CMS searches, which in most cases exceed the TeV range [86,87]. This implies that if SUSY is indeed behind the stabilisation of the Higgs mass against very high scales that enter via quantum corrections, it is either fine-tuned at the permille level at least or its low-energy manifestation is more complicated than expected.

The production and decay rates of the observed Higgs particles, as well as its spin and parity quantum numbers, as measured by the ATLAS and CMS collaborations with the $\approx 25\,\text{fb}^{-1}$ data collected at $\sqrt{s} = 7$ and 8 TeV, indicate that its couplings to fermions and gauge bosons are approximately SM-like. In the context of the MSSM, this implies that we seem to be in the decoupling regime and this 125 GeV particle can be only identified with the lightest h boson, while the other $H/A/H^{\pm}$ states must be heavier than approximately the Fermi scale. This last feature is also backed up by the constraints from direct searches of these heavier Higgs states at the LHC.

This drives up to the question that is now very often asked in particle physics (and elsewhere): what to do next? The answer is, for me, obvious: we are only in the beginning of a new era.[6] Indeed, it was expected since a long time that the probing of the EWSB mechanism will be at least a two chapters story. The first one is the search and the observation of a Higgs-like particle that will confirm the scenario of the SM and most of its extensions, that is, a spontaneous symmetry breaking by a scalar field that develops a non-zero vacuum expectation value. This long chapter has just been closed by the ATLAS and CMS collaborations with the spectacular observation of a Higgs boson. This observation opens a second and equally important chapter: the precise determination of the Higgs profile and the unravelling of the EWSB mechanism itself.

A more accurate measurement of the Higgs couplings to fermions and gauge bosons will be mandatory to establish the exact nature of the mechanism and, eventually, to pin down effects of new physics if additional ingredients beyond those of the SM are involved. This is particularly true in weakly interacting theories such as SUSY in which the quantum effects are expected to be small. These measurements could be performed at the upgraded LHC with an energy close to $\sqrt{s} = 14$ TeV, in particular if a very high luminosity, a few ab^{-1}, is achieved [210–212].

At this upgrade, besides improving the measurements performed so far, rare but important channels such as associated Higgs production with top quarks, $pp \to t\bar{t}h$, and Higgs decays into $\mu^+\mu^-$ and $Z\gamma$ states could be probed. Above all, a determination of the self-Higgs coupling could be made by searching for double Higgs production e.g. in the gluon fusion channel $gg \to hh$ [213–215]; this would be a first step towards the reconstruction of the scalar potential that is responsible of EWSB. A proton collider with an energy $\sqrt{s} = 30$ to 100 TeV could do a similar job [212].

In a less near future, a high-energy lepton collider, which is nowadays discussed in various options (ILC, TLEP, CLIC, μ collider) would lead to a more accurate probing of the Higgs properties [216–224], promoting the scalar sector of the theory to the high-precision level of the gauge and fermionic sectors achieved by LEP and SLC [30].

Besides the high precision study of the already observed Higgs, one should also continue to search for the heavy states that are predicted by SUSY, not only the superparticles but also the heavier Higgs bosons. The energy upgrade to $\approx$14 TeV (and eventually beyond) and the planed order of magnitude (or more) increase in luminosity will allow to probe much higher mass scales than presently.

In conclusion, it is not yet time to give up on supersymmetry and on new physics in general but, rather, to work harder to be fully prepared for the more precise and larger data that will be delivered by the upgraded LHC. It will be soon enough to "philosophise" in 2 years from now, when the physics landscape will become clearer.

Acknowledgments This review relies heavily on work performed in the last two years in collaboration with S. Alekhin, A. Arbey, J. Baglio, M. Battaglia, A. Falkowski, R. Godbole, R. Grober, O. Lebedev, A. Lenz, N. Mahmoudi, L. Maiani, Y. Mambrini, B. Mellado, K. Mohan, G. Moreau, M. Muhlleitner, J. Quevillon, A. Polosa, V. Riquer and M. Spira. I thank them all for their input and for having made these two last years very fruitful and extremely exciting. Discussions with members of ATLAS and CMS (whom I congratulate in passing) are also acknowledged. I thank the CERN Theory Unit for its hospitality during this period. This work is supported by the ERC Advanced Grant Higgs@LHC.

References

1. The ATLAS collaboration, Phys. Lett. B **716**, 1 (2012)
2. The CMS collaboration, Phys. Lett. B **716**, 30 (2012)
3. P. Higgs, Phys. Lett. **12**, 132 (1964)
4. F. Englert, R. Brout, Phys. Rev. Lett. **13**, 321 (1964)

[6] One can rightfully use here the words of Winston Churchill in November 1942 after the battle of El Alamein (which in Arabic literally means "the two flags" but could also mean "the two worlds" or even "the two scientists"!): "Now, this is not the end; it is not even the beginning to the end; but it is, perhaps, the end of the beginning".

5. G. Guralnik, C. Hagen, T. Kibble, Phys. Rev. Lett. **13**, 585 (1964)
6. J. Gunion, H. Haber, G. Kane, S. Dawson, *The Higgs Hunter's Guide* (Reading, 1990)
7. A. Djouadi, Phys. Rep. **457**, 1 (2008)
8. A. Djouadi, Phys. Rep. **459**, 1 (2008)
9. M. Drees, R. Godbole, P. Roy, *Theory and Phenomenology of Sparticles* (World Sci., 2005)
10. H. Baer, X. Tata, *Weak Scale Supersymmetry: From Superfields to Scattering Events* (Cambridge U Press, Cambridge, 2006)
11. S. Martin, arXiv:hep-ph/9709356
12. Y. Okada, M. Yamaguchi, T. Yanagida, Prog. Theor. Phys. **85**, 1 (1991)
13. J. Ellis, G. Ridolfi, F. Zwirner, Phys. Lett. B **257**, 83 (1991)
14. H.E. Haber, R. Hempfling, Phys. Rev. Lett. **66**, 1815 (1991)
15. M. Carena, J.R. Espinosa, M. Quiros, C.E. Wagner, Phys. Lett. B **355**, 209 (1995)
16. H. Haber, R. Hempfling, A. Hoang, Z. Phys, C **75**, 539 (1997)
17. S. Heinemeyer, W. Hollik, G. Weiglein, Phys. Rev. D **58**, 091701 (1998)
18. S. Heinemeyer, W. Hollik, G. Weiglein, Eur. Phys. J. C **9**, 343 (1999)
19. G. Degrassi, P. Slavich, F. Zwirner, Nucl. Phys. B **611**, 403 (2001)
20. A. Brignole, G. Degrassi, P. Slavich, F. Zwirner, Nucl. Phys. B **631**, 195 (2002)
21. A. Brignole, G. Degrassi, P. Slavich, F. Zwirner, Nucl. Phys. B **643**, 79 (2002)
22. S. Martin, Phys. Rev. D **75**, 055005 (2007)
23. P. Kant, R. Harlander, L. Mihaila, M. Steinhauser, JHEP **1008**, 104 (2010)
24. J. Feng et al., Phys. Rev. Lett. **111**, 131802 (2013)
25. B. Allanach et al., JHEP **0409**, 044 (2004)
26. S. Heinemeyer, W. Hollik, G. Weiglein, Phys. Rep. **425**, 265 (2006)
27. S. Heinemeyer, IJMPA **21**, 2659 (2006)
28. M. Carena, H. Haber, Prog. Part. Nucl. Phys. **50**, 63 (2003)
29. See for instance H.E. Haber, arXiv:hep-ph/9505240
30. J. Beringer,(PDG), et al., Phys. Rev. D **86**, 010001 (2012)
31. LEP collaborations, Phys. Lett. B **565**, 61 (2003)
32. R. Barbieri, G. Giudice, Nucl. Phys. B **306**, 63 (1988)
33. M. Papucci, J. Ruderman, A. Weiler, JHEP **1209**, 035 (2012)
34. M. Carena, S. Heinemeyer, C. Wagner, G. Weiglein, Eur. J. Phys. C **26**, 601 (2003)
35. A. Arbey et al., Phys. Lett. B **708**, 162 (2012)
36. A. Arbey et al., JHEP **1209**, 107 (2012)
37. Among the vast literature on the subject, for the (mainly) early papers in the SUSY context, see e.g.: H. Baer, V. Barger, A. Mustafayev, Phys. Rev. D **85**, 075010 (2012)
38. P. Draper, P. Meade, M. Reece, D. Shih, Phys. Rev. D **85**, 095007 (2012)
39. O. Buchmueller et al., Eur. Phys. J. C **72**, 2020 (2012)
40. S. Akula et al., Phys. Rev. D **85**, 075001 (2012)
41. C. Strege et al., JCAP **1203**, 030 (2012)
42. C. Beskidt et al., JHEP **1205**, 094 (2012)
43. M. Carena et al., JHEP **1207**, 175 (2012)
44. M. Carena, I. Low, C. Wagner, JHEP **1208**, 060 (2012)
45. M. Cahill-Rowley et al., Phys. Rev. D **86**, 075015 (2012)
46. P. Lodone, Int. J. Mod. Phys. A **27**, 1230010 (2012)
47. M. Kadastik et al., JHEP **1205**, 061 (2012)
48. U. Ellwanger, JHEP **1203**, 044 (2012)
49. S. King, M. Muhlleitner, R. Nevzorov, Nucl. Phys. B **860**, 207 (2012)
50. D. Ghilencea, Nucl. Phys. B **876**, 16 (2013)
51. J. Cao et al., Phys. Lett. B **710**, 665 (2012)
52. L. Aparicio, D. Cerdeno, L. Ibanez, JHEP **1204**, 126 (2012)
53. J. Ellis, K. Olive, Eur. Phys. J. C **72**, 2005 (2012)
54. J. Cao et al., JHEP **1203**, 086 (2012)
55. F. Boudjema, G.D. La Rochelle, Phys. Rev. D **86**, 015018 (2012)
56. F. Brummer, S. Kraml, S. Kulkarni, JHEP **1208**, 089 (2012)
57. L. Hall, D. Pinner, J. Ruderman, JHEP **1204**, 131 (2012)
58. A. Arvanitaki, G. Villadoro, JHEP **1202**, 144 (2012)
59. A. Delgado et al., Eur. Phys. J. C **73**, 2370 (2013)
60. S. Heinemeyer, O. Stal, G. Weiglein, Phys. Lett. B **710**, 201 (2012)
61. P. Bechtle et al., Eur. Phys. J. C **73**, 2354 (2013)
62. M. Drees, Phys. Rev. D **86**, 115018 (2012)
63. A. Djouadi et al. (MSSM WG), arXiv:hep-ph/9901246
64. A.H. Chamseddine, R. Arnowitt, P. Nath, Phys. Rev. Lett. **49**, 970 (1982)
65. R. Barbieri, S. Ferrara, C. Savoy, Phys. Lett. B **119**, 343 (1982)
66. L. Hall, J. Lykken, S. Weinberg, Phys. Rev. D **27**, 2359 (1983)
67. N. Ohta, Prog. Theor. Phys. **70**, 542 (1983)
68. M. Dine, W. Fishler, Phys. Lett. B **110**, 227 (1982)
69. C. Nappi, B. Ovrut, Phys. Lett. B **113**, 1785 (1982)
70. L. Alvarez-Gaumé, M. Claudson, M. Wise, Nucl. Phys. B **207**, 96 (1982)
71. M. Dine, A. Nelson, Y. Shirman, Phys. Rev. D **51**, 1362 (1995)
72. G.F. Giudice, R. Rattazzi, Phys. Rep. **322**, 419 (1999)
73. L. Randall, R. Sundrum, Nucl. Phys. B **557**, 79 (1999)
74. G. Giudice, M. Luty, H. Murayama, R. Rattazzi, JHEP **9812**, 027 (1998)
75. J. Bagger, T. Moroi, E. Poppitz, JHEP **0004**, 009 (2000)
76. N. Arkani-Hamed, S. Dimopoulos, JHEP **0506**, 073 (2005)
77. G.F. Giudice, A. Romanino, Nucl. Phys. B **699**, 65 (2004)
78. J.D. Wells, Phys. Rev. D **71**, 015013 (2005)
79. See, L. Hall, Y. Nomura, JHEP **1003**, 076 (2010)
80. G. Giudice, A. Strumia, Nucl. Phys. B **858**, 63 (2012)
81. A. Djouadi, L. Maiani, G. Moreau, A. Polosa, J. Quevillon, V. Riquer, arXiv:1307.5205 [hep-ph]
82. A. Djouadi, J.L. Kneur, G. Moultaka, Comput. Phys. Commun. **176**, 426 (2007)
83. S. Heinemeyer, W. Hollik, G. Weiglein, Comput. Phys. Commun. **124**, 76 (2000)
84. S. Alekhin et al., Phys. Lett. B **716**, 214 (2012)
85. Tevatron, CDF+D0 EWWG, arXiv:1305.3929 [hep-ex]
86. See the talk given by O. Buchmuller for ATLAS and CMS at the EPS conference, Stockholm, July 2013
87. For a review, see N. Craig, arXiv:1309.0528 [hep-ph]
88. For recent studies, see: A. Benhenni et al., Phys. Rev. D **84**, 075015 (2011)
89. T. Li et al., Phys. Lett. B **710**, 207 (2012)
90. A. Djouadi, U. Ellwanger, A.M. Teixeira, Phys. Rev. Lett. **101**, 101802 (2008)
91. A. Djouadi, U. Ellwanger, A.M. Teixeira, JHEP **0904**, 031 (2009)
92. J. Ellis et al., Phys. Rev. D **70**, 055005 (2004)
93. e.g. S.S. AbdusSalam et al., Eur. Phys. J. C **71**, 1835 (2011)
94. For a recent review, see e.g. T. Hurth, F. Mahmoudi, Rev. Mod. Phys. **85**, 795 (2013)
95. For a recent review, see e.g. R. Catena, L. Covi, SUSY dark matter(s). Eur. Phys. J. C **74**, 2703 (2014). doi:10.1140/epjc/s10052-013-2703-4. arXiv:1310.4776
96. For a review, see e.g. G. Kane, R. Lu, B. Zheng, Int. J. Mod. Phys. A **28**, 1330002 (2013)
97. N. Bernal, A. Djouadi, P. Slavich, JHEP **0707**, 016 (2007)
98. A. Djouadi, J. Quevillon, arXiv:1304.1787 [hep-ph]
99. A. Delgado, G.F. Giudice, Phys. Lett. B **627**, 155 (2005)
100. E. Arganda, J.L. Diaz-Cruz, A. Szynkman, Eur. Phys. J. C **73**, 2384 (2013)
101. E. Arganda, J.L. Diaz-Cruz, A. Szynkman, Phys. Lett. B **722**, 100 (2013)
102. L. Maiani, A.D. Polosa, V. Riquer, New J. Phys. **14**, 073029 (2012)
103. L. Maiani, A.D. Polosa, V. Riquer, Phys. Lett. B **718**, 465 (2012)
104. L. Maiani, A.D. Polosa, V. Riquer, Phys. Lett. B **724**, 274 (2013)

105. M. Carena et al., Eur. Phys. J. C **73**, 2552 (2013)
106. A. Martin et al., Eur. Phys. J. C **63**, 189 (2009)
107. A. Djouadi, Eur. Phys. J. C **73**, 2498 (2013)
108. The ATLAS collaboration, ATLAS-CONF-2013-034
109. The CMS collaboration, CMS-HIG-13-005
110. S. Dittmaier et al. (LHC Higgs WG), arXiv:1101.0593
111. J. Baglio, A. Djouadi, JHEP **1010**, 064 (2010)
112. J. Baglio, A. Djouadi, JHEP **1103**, 055 (2011)
113. S. Dittmaier et al. (LHC Higgs WG), arXiv:1201.3084
114. D. Zeppenfeld, R. Kinnunen, A. Nikitenko, E. Richter-Was, Phys. Rev. D **62**, 013009 (2000)
115. A. Djouadi et al., arXiv:hep-ph/0002258
116. M. Dührssen et al., Phys. Rev. D **70**, 113009 (2004)
117. K. Assamagan et al., arXiv:hep-ph/0406152
118. A. Djouadi, J. Kalinowski, M. Spira, Comput. Phys. Commun. **108**, 56 (1998)
119. D. Carmi, A. Falkowski, E. Kuflik, T. Volansky, JHEP **1207**, 136 (2012)
120. A. Azatov, R. Contino, J. Galloway, JHEP **1204**, 127 (2012)
121. J. Espinosa, C. Grojean, M. Muhlleitner, M. Trott, JHEP **1205**, 097 (2012)
122. J. Espinosa, C. Grojean, M. Muhlleitner, M. Trott, JHEP **1212**, 045 (2012)
123. J. Espinosa, C. Grojean, M. Muhlleitner, M. Trott, JHEP **1209**, 126 (2012)
124. P. Giardino, K. Kannike, M. Raidal, A. Strumia, JHEP **1206**, 117 (2012)
125. P. Giardino, K. Kannike, M. Raidal, A. Strumia, Phys. Lett. B **718**, 469 (2012)
126. T. Li, X. Wan, Y.-K. Wang, S.-H. Zhu, JHEP **1209**, 086 (2012)
127. J. Ellis, T. You, JHEP **1206**, 140 (2012)
128. A. Azatov et al., JHEP **1206**, 134 (2012)
129. M. Klute, R. Lafaye, T. Plehn, M. Rauch, D. Zerwas, Phys. Rev. Lett. **109**, 101801 (2012)
130. A. Djouadi, A. Lenz, Phys. Lett. B **715**, 310 (2012)
131. J. Chang, K. Cheung, P.-Y. Tseng, T.-C. Yuan, JHEP **1212**, 058 (2012)
132. S. Chang, C.A. Newby, N. Raj, C. Wanotayaroj, Phys. Rev. D **86**, 095015 (2012)
133. I. Low, J. Lykken, G. Shaughnessy, Phys. Rev. D **86**, 093012 (2012)
134. M. Montull, F. Riva, JHEP **1211**, 018 (2012)
135. D. Carmi et al., JHEP **1210**, 196 (2012)
136. S. Banerjee, S. Mukhopadhyay, B. Mukhopadhyaya, JHEP **1210**, 062 (2012)
137. F. Bonnet, T. Ota, M. Rauch, W. Winter, Phys. Rev. D **86**, 093014 (2012)
138. T. Plehn, M. Rauch, Europhys. Lett. **100**, 11002 (2012)
139. G. Belanger, B. Dumont, U. Ellwanger, J. Gunion, S. Kraml, JHEP **1302**, 053 (2013)
140. G. Belanger, B. Dumont, U. Ellwanger, J. Gunion, S. Kraml, arXiv:1306.2941
141. G. Altarelli, arXiv:1308.0545
142. T. Corbett et al., Phys. Rev. D **86**, 075013 (2012)
143. A. Alves et al., Eur. Phys. J. C **73**, 2288 (2013)
144. M. Peskin, arXiv:1207.2516v1 [hep-ph]
145. G. Cacciapaglia, A. Deandrea, G.D. La Rochelle, J.B. Flament, JHEP **1303**, 029 (2013)
146. A. Falkowski, F. Riva, A. Urbano, arXiv:1303.1812 [hep-ph]
147. C. Cheung, S. McDermott, K. Zurek, JHEP **1304**, 074 (2013)
148. K. Cheung, J.S. Lee, P. Tseng, JHEP **1305**, 134 (2013)
149. A. Arbey et al., Phys. Lett. B **720**, 153 (2013)
150. A. Djouadi, G. Moreau, arXiv:1303.6591
151. See e.g., M. Carena et al., Nucl. Phys. B **577**, 88 (2000)
152. A. Djouadi, Phys. Lett. B **435**, 101 (1998)
153. J. Baglio et al., Phys. Lett. B **716**, 203 (2012)
154. See e.g. M. Carena, S. Gori, N. R. Shah, C.E.M. Wagner, JHEP **1207**, 175 (2012) (and references therein)
155. G.F. Giudice, P. Paradisi, A. Strumia, JHEP **1210**, 186 (2012)
156. U. Haisch, F. Mahmoudi, arXiv:1210.7806
157. A. Djouadi, V. Driesen, W. Hollik, J.I. Illana, Eur. Phys. J. C **1**, 149 (1998)
158. J.A. Casas, J.M. Moreno, K. Rolbiecki, B. Zaldivar, JHEP **1309**, 099 (2013)
159. The ATLAS collaboration, ATLAS-CONF-2013-011
160. A. Djouadi, A. Falkowski, Y. Mambrini, J. Quevillon, Eur. Phys. J. C **73**, 2455 (2013)
161. Y. Bai, P. Draper, J. Shelton, JHEP **1207**, 192 (2012)
162. C. Englert, J. Jaeckel, E. Re, M. Spannowsky, Phys. Rev. D **85**, 035008 (2012)
163. The CMS collaboration, CMS-PAS-HIG-13-013
164. The CMS collaboration, arXiv:1206.5663 [hep-ex]
165. The ATLAS collaboration, ATLAS-CONF-2012-147
166. A. Djouadi, O. Lebedev, Y. Mambrini, J. Quevillon, Phys. Lett. B **709**, 65 (2012)
167. L. Landau, Dokl. Akad. Nauk Ser. Fiz. **60**, 207 (1948)
168. C. Yang, Phys. Rev. **77**, 242 (1950)
169. J. Ellis, V. Sanz, T. You, Phys. Lett. B **726**, 244 (2013)
170. For a review of the CP Higgs issue, see e.g. S. Kraml (ed.) et al., arXiv:hep-ph/0608079
171. a more recent study with references, see A. Alloul, B. Fuks, V. Sanz, arXiv:1310.5150
172. The ATLAS collaboration, Phys. Lett. B **726**, 120 (2013)
173. The CMS collaboration, Phys. Rev. Lett. **110**, 081803 (2013)
174. T. Plehn, D. Rainwater, D. Zeppenfeld, Phys. Rev. Lett. **88**, 051801 (2002)
175. K. Hagiwara, Q. Li, K. Mawatari, JHEP 0907 (2009)
176. J. Frank, M. Rauch, D. Zeppenfeld, Phys. Rev. D **87**, 055020 (2013)
177. C. Englert, D. Gonsalves-Netto, K. Mawatari, T. Plehn, JHEP **1301**, 148 (2013)
178. A. Djouadi, R.M. Godbole, B. Mellado, K. Mohan, Phys. Lett. B **723**, 307 (2013)
179. V. Barger et al., Phys. Rev. D **49**, 79 (1994)
180. B. Grzadkowski, J. Gunion, X. He, Phys. Rev. Lett. **77**, 5172 (1996)
181. J. Gunion, J. Pliszka, Phys. Lett. B **444**, 136 (1998)
182. P. Bhupal Dev et al., Phys. Rev. Lett. **100**, 051801 (2008)
183. A. Freitas, P. Schwaller, Phys. Rev. D **87**, 055014 (2013)
184. M. Spira et al., Nucl. Phys. B **453**, 17 (1995)
185. R. Harlander, W. Kilgore, Phys. Rev. D **68**, 013001 (2003)
186. R. Harlander, S. Liebler, H. Mantler, Comp. Phys. Comm. **184**, 1605 (2013)
187. A. Arbey, M. Battaglia, F. Mahmoudi, Phys. Rev. D **88**, 015007 (2013)
188. P. Bechtle et al., arXiv:1305.1933
189. N. Craig, J. Galloway, S. Thomas, arXiv:1305.2424
190. N. Christensen, T. Han, S. Su, Phys. Rev. D **85**, 115018 (2012)
191. The ATLAS collaboration, arXiv:1211.6956
192. The CMS collaboration, CMS-PAS-HIG-12-050
193. The CMS collaboration, CMS-PAS-HIG-12-033
194. The ATLAS collaboration, ATLAS-CONF-2013-090
195. The CMS collaboration, arXiv:1205.5736
196. G. Barenboim et al., arXiv:1307.5973 [hep-ph]
197. E. Boos et al., Phys. Rev. D **66**, 055004 (2002)
198. E. Boos, A. Djouadi, A. Nikitenko, Phys. Lett. B **578**, 384 (2004)
199. A. Djouadi, J.L. Kneur, G. Moultaka, Phys. Rev. Lett. **80**, 1830 (1998)
200. A. Djouadi, J.L. Kneur, G. Moultaka, Nucl. Phys. B **569**, 53 (2000)
201. G. Bélanger et al., Eur. Phys. J. C **9**, 511 (1999)
202. A. Dedes, S. Moretti, Eur. Phys. J. C **10**, 515 (1999)

203. A. Datta et al., Phys. Rev. D **65**, 015007 (2002)
204. A. Datta et al., Nucl. Phys. B **681**, 31 (2004)
205. D. Ghosh, M. Guchait, D. Sengupta, Eur. Phys. J. C **72**, 2141 (2012)
206. K. Howe, P. Saraswat, JHEP **1210**, 065 (2012)
207. A. Arbey, M. Battaglia, F. Mahmoudi, arXiv:1212.6865 [hep-ph]
208. T. Han, S. Padhi, S. Su, arXiv:1309.5966 [hep-ph]
209. The CMS collaboration, CMS-PAS-SUS-13-017
210. The ATLAS collaboration, arXiv:1307.7292 [hep-ex]
211. The CMS collaboration arXiv:1307.7135 [hep-ex]
212. S. Dawson et al., arXiv:1310.8361 [hep-ex]
213. See e.g., J. Baglio et al., JHEP **1304**, 151 (2013)
214. M. Dolan, C. Englert, M. Spannowsky, JHEP **1210**, 112 (2012)
215. W. Yao, arXiv:1308.6302 [hep-ph]
216. H. Abramowicz, arXiv:1307.5288 [hep-ex]
217. M. Bicer et al., arXiv:1308.6176 [hep-ex]
218. H. Baer et al., arXiv:1306.6352 [hep-ph]
219. J. Brau et al., arXiv:1210.0202 [hep-ph]
220. For earlier work, see e.g.: G. Arons et al., arXiv:0709.1893
221. J. Aguilar-Saavedra, arXiv:hep-ph/0106315
222. E. Accomando et al., Phys. Rep. **299**, 1 (1998)
223. M. Peskin, H. Murayama, Ann. Rev. Nucl. Part. Sci. **46**, 533 (1996)
224. A. Djouadi, Int. J. Mod. Phys. A **10**, 1 (1995)

Eur. Phys. J. C (2014) 74:2699
DOI 10.1140/epjc/s10052-013-2699-9

THE EUROPEAN PHYSICAL JOURNAL C

Review

SUSY: Quo Vadis?

G. G. Ross[a]

Rudolf Peierls Centre for Theoretical Physics, University of Oxford, 1 Keble Road, Oxford OX1 3NP, UK

Received: 27 November 2013 / Accepted: 27 November 2013 / Published online: 27 May 2014

Abstract Given that there is currently no direct evidence for supersymmetric particles at the LHC it is timely to re-evaluate the need for low scale supersymmetry and to ask whether it is likely to be discoverable by the LHC running at its full energy. We review the status of simple SUSY extensions of the Standard Model in the light of the Higgs discovery and the non-observation of evidence for SUSY at the LHC. The need for large radiative corrections to drive the Higgs mass up to 126 GeV and for the coloured SUSY states to be heavy to explain their non-observation introduces a little hierarchy problem and we discuss how to quantify the associated fine tuning. The requirement of low fine tuning requires non-minimal SUSY extensions and we discuss the nature and phenomenology of models which still have perfectly acceptable low fine tuning. A brief discussion of SUSY flavour-changing and CP-violation problems and their resolution is presented.

1 Introduction

To date, the data from the LHC running at 8 TeV has shown no indication of supersymmetric partners of the Standard Model states nor, indeed, any indication of other physics 'Beyond the Standard Model' (BSM). Moreover the discovery of a new state whose properties look just like those of the Higgs boson predicted by the Standard Model has led to a re-evaluation of the need for such BSM physics. In this paper we will briefly review the reasons why supersymmetry was and still is the most promising extension of the Standard Model (SM) and why the new supersymmetric states are expected to be relatively low in mass and accessible to discovery when the LHC runs at its full energy.

The SM provides an amazingly precise description of the strong, weak and electromagnetic interactions of the fundamental states of matter, the quarks and leptons. However, there are several reasons to think that it is incomplete. The SM does not have a viable candidate for dark matter. The measurement of neutrino masses and the observation of non-trivial mixing in the lepton sector certainly require an extension of the original formulation of the SM—the most elegant possibility is to add right-handed (RH) neutrinos, which restores the symmetry between quarks and leptons and allows for neutrino masses and mixing. It has a large number of unrelated parameters needed to describe the strengths and properties of the fundamental interactions and the masses and mixing angles of the quarks and leptons suggesting there is a more fundamental theory capable of fixing these parameters. Although the Standard Model does provide a measure of unification between the weak and electromagnetic interactions it falls short of a complete unification of the fundamental forces. There is also no mechanism in the original SM for baryogenesis or an explanation of the strong CP problem. Lastly, and most pressing, the Standard Model suffers from the hierarchy problem, namely the difficulty in field theory of separating mass scales so that the electroweak scale is expected to be driven close to any high scale associated with BSM physics, such as the Planck scale or the Grand Unified (GUT) scale. Given the importance of looking for evidence of BSM physics, particularly timely in view of the LHC programme, let us address these reasons in turn.

The need for dark matter is certainly important but does not, by itself, set the scale for the new physics. It could, for example, be due to axions associated with a very high scale of new physics, perhaps even as high as the Planck scale, and evidence for it may not be accessible at laboratory energy scales. Similarly the new physics associated with neutrino masses could be very large. Indeed if the RH neutrinos have mass close to the GUT scale the smallness of the observed (LH) neutrino's mass is naturally explained via the see-saw mechanism.

The possibility of further unification is certainly appealing and there is significant circumstantial evidence in favour

[a] e-mail: g.ross1@physics.ox.ac.uk

of it. In particular it is notable that the SM representations of the quarks and leptons of a single family fit neatly in the relatively simple $\bar{5} + 10$ representation of a SU(5) GUT. This immediately explains the fact that the charges of the quarks are third integrally quantised relative to the charged leptons, the 1/3 factor coming from the fact that quarks come in three colours. Moreover the underlying SU(5) symmetry explains why both the quark and the lepton electroweak SU(2) doublets are left-handed. The resulting simplicity is further enhanced if the GUT group is enlarged to SO(10) for all the states of a single family fit into a single 16 dimensional representation of SO(10). Moreover the remaining state needed to complete the 16 dimensional representation requires the existence of a right-handed neutrino and thus naturally allows for neutrino masses and mixing. Of course it is important that the Higgs should also fit into a GUT multiplet and, in the original simple formulations, this led to a problem because the coloured Higgs partners required by the GUT have not been observed. Indeed they are required to be super-heavy or absent if nucleon decay is to be sufficiently suppressed and this led to the need for very large GUT representations that somewhat reduced the elegance of the GUT paradigm. However, the more recent approaches based on an underlying string unification have provided an elegant explanation for the absence of light coloured partners as they can be projected out at the stage of compactification and the associated breaking of the gauge group by Wilson lines, without the need for large GUT representations.

The existence of an underlying GUT also leads to relations amongst the parameters of the SM, most importantly the $SU(3) \times SU(2) \times U(1)$ gauge couplings. In SU(5) or SO(10) there is a single gauge coupling and, using the renormalisation group (RG) equations, it is straightforward to determine the strong, electromagnetic and weak couplings at low scales, as measured in the laboratory, in terms of the unified gauge coupling and the unification scale. Eliminating these unknowns leads to a relation between the gauge couplings at low energies. In the non-supersymmetric case this relation fails by more than 11 standard deviations but, in a supersymmetric GUT, the relation is accurate to better than 5 % for the case of light (TeV scale) supersymmetric (SUSY) partners. However, as the dependence of this relation on the SUSY masses is only logarithmic, it is not possible to say that gauge coupling unification requires that the SUSY states should be within the reach of the LHC.

This leaves the need to solve the hierarchy problem as the only unambiguous reason to expect new states at a mass scale accessible to direct discovery at the LHC. The problem arises if the SM is an effective field theory descending from new physics at a high scale, such as the GUT scale or the string or Planck scale. In this case the radiative corrections that arise in field theory connect the low and high scale sectors and prevent a separation of the electroweak breaking scale from the high scale associated with BSM physics. Support for the idea that the SM is an effective field theory (EFT) comes from the fact that it predicts that the only elementary spin-one states in the theory should be associated with a local gauge principle and that the only fermions in the theory should be chiral. This immediately follows because the only symmetry capable of forbidding a vector boson mass is a local gauge symmetry and the only symmetry capable of forbidding a fermion mass is a chiral symmetry; in the absence of such symmetries one would expect the states to have the high scale mass associated with the new scale of physics. It is significant that this is just what is found in the SM. The gluons, the photon and the W and Z bosons are the gauge bosons coming from the $SU(3) \times SU(2) \times U(1)$ local gauge symmetry. The fermions are chiral with respect to the SU(2) gauge group, the LH fermions transform as SU(2) doublets and the RH fermions transform as SU(2) singlets. Moreover the EFT description requires that the unbroken gauge interactions should be vectorlike, as observed, otherwise there can be no fermion masses.

This pleasing agreement of the SM structure with that required by an EFT is broken by the scalar sector because there is no symmetry that forbids a scalar mass. As a result the EFT expectation is that the Higgs mass and the associated electroweak breaking scale should be at the high scale. Even if for some reason the Higgs mass does not arise at tree level radiative corrections are expected to generate it close to the high scale. This is the hierarchy problem. The solutions that have been suggested require new physics at a low scale, potentially accessible to discovery at the LHC. In this review I will concentrate on the supersymmetric possibility in which the Higgs mass is forbidden by a combination of supersymmetry (SUSY) and a chiral symmetry. In this case the SUSY extension of the SM fits in perfectly with the EFT picture. It also allows for a consistent underlying unified theory, GUT or string based, that gives the precision prediction relating the gauge couplings and string-based models can even predict the correct unification scale in therms of the string or Planck scale. Indeed, due to the inevitable coupling between the Higgs and the scalars responsible for GUT breaking at a high scale, the SUSY extension of the GUT is an essential feature of unification.

The discovery of a Higgs candidate at 126 GeV [1,2] has lent some support to the SUSY paradigm but at the same time made it more difficult to realise. The support comes because the Higgs mass lies in the relatively small range favoured by SUSY. Moreover the observed properties of the candidate Higgs are just what are expected of an elementary state whose interactions are in the perturbative domain, as is expected in SUSY with gauge coupling unification. Thus at least the simplest composite Higgs explanation of the hierarchy problem looks less likely than the SUSY explanation. The fact that the Higgs looks very much like the SM Higgs

is not an argument against SUSY for, in the limit the SUSY breaking is large, the properties of the SUSY Higgs very closely approximate those of the SM Higgs. The difficulty comes from the relatively high mass of the Higgs that typically requires significant fine tuning in SUSY models due to the need of large radiative corrections to the Higgs mass and the corresponding need for heavy SUSY states. This fact largely maps out the possible nature of SUSY extensions of the SM after the Higgs discovery for it limits the available parameter space and structure of SUSY models and may indicate the need for a non-minimal SUSY extension of the SM. In this paper we consider these possibilities in more detail and the prospects for SUSY discovery at LHC14.

The structure of the paper is as follows. In Sect. 2 the status of simple SUSY models after the Higgs discovery is reviewed and their implications for the masses of the coloured SUSY states, particularly relevant to the LHC. In Sect. 3 we discuss the hierarchy problem and the quantitative 'fine tuning' measure of the hierarchy problem that is needed to obtain a prediction for the SUSY partner mass scale and the prospects for finding SUSY at the LHC. In Sect. 4 we review the applications of the measure to SUSY extensions of the SM and discuss whether there remain viable SUSY theories capable of solving the 'little' hierarchy problem, the particular SUSY signals implied by them and the prospects for testing them at the LHC. In Sect. 5 we discuss SUSY implications for flavour physics in the light of the constraints the LHC results have imposed on SUSY, concentrating on the most sensitive flavour-changing and CP-violating processes. Finally in Sect. 6 we present a summary and our conclusions.

2 Status of simple SUSY models after the Higgs

In this section we briefly review the status of fits to data of the simplest and most studied of the SUSY extensions of the SM, taking account of the Higgs discovery, the limits on SUSY states coming from the LHC and other experiments and the constraints imposed by the observed dark matter abundance.

In such models the Higgs mass is strongly constrained. At tree level it is bounded by the Z mass but there can be sizeable radiative contributions increasing it. However, these contributions cannot be made arbitrarily large unless the SUSY breaking scale is taken so high that unacceptable fine tuning is needed to generate the EW breaking scale. The 125 GeV Higgs lies at the upper end of this range. On the one hand it may be considered a success for the SUSY prediction of a light Higgs with couplings in the perturbative domain. On the other hand it is sufficiently heavy for considerable fine tuning of the fundamental parameters of the model to be needed, at least in the minimal implementations of SUSY.

In the next section we will quantify this fine tuning but in this section we choose to ignore it, assuming that the underlying theory fixes the necessary correlations between the parameters needed to get the correct EW breaking scale or that higher dimension operator contributions due to new states at a higher scale are present (cf. the discussion in Sect. 4.4). The spectrum of the simplest models is that of the MSSM with the minimal set of chiral super fields, ϕ^i, needed to accommodate the matter fields of the SM plus the two Higgs doublets needed to give mass to the up and down quarks. The scalar potential then has the form

$$V(\phi^i) = \left|\frac{\partial W}{\partial \phi^i}\right|^2 + \left(A_0 W^{(3)} + B_0 W^{(2)} + \text{h.c.}\right) + m_0^2 \phi^i \phi_i^*, \tag{1}$$

where W is the superpotential for the matter fields given by

$$\begin{aligned} W_{\text{MSSM}} &= W_{\text{Yukawa}} + W_\mu \\ W_{\text{Yukawa}} &= y_e H_d L e^c + y_d H_d Q d^c + y_u H_u Q u^c \\ W_\mu &= \mu H_u H_d, \end{aligned} \tag{2}$$

The form of the SUSY breaking terms assumed here is that of the constrained MSSM (CMSSM) with scalar mass universality, applicable at some initial scale, M_X, which is usually associated with the Grand Unification scale. In these equations the family and SU(2) indices have been suppressed, $W^{(3)}$ is the trilinear part of the superpotential and $W^{(2)}$ is the bilinear part. Gaugino mass universality characterised by $m_{1/2}$ is also assumed at the same input scale M_X.

Minimisation of the Higgs potential leads to two vacuum conditions at the weak scale, which can be expressed as

$$\mu^2 = \frac{m_1^2 - m_2^2 \tan^2\beta + \frac{1}{2} m_Z^2 (1 - \tan^2\beta) + \Delta_\mu^{(1)}}{\tan^2\beta - 1 + \Delta_\mu^{(2)}} \tag{3}$$

and

$$B\mu = -\frac{1}{2}\left(m_1^2 + m_2^2 + 2\mu^2\right) \sin 2\beta + \Delta_B, \tag{4}$$

where $m_{1,2}$ are the soft supersymmetry-breaking Higgs masses (evaluated at the weak scale), $\tan\beta$ is the ratio of the two Higgs vacuum expectation values, and Δ_B and $\Delta_\mu^{(1,2)}$ are loop corrections [3–5]. Using these relations we see that the CMSSM can be defined by $m_{1/2}$, m_0, A_0, $\tan\beta$ and the sign of μ.

The Higgs mass is given by [6–8]

$$m_h^2 \simeq m_Z^2 \cos^2 2\beta + \frac{3}{(4\pi)^2}\left[\ln\frac{M_S^2}{m_t^2} + \frac{X_t^2}{m_{\tilde{t}}^2}\left(1 - \frac{X_t^2}{12 m_{\tilde{t}}^2}\right)\right] \tag{5}$$

where $M_S^2 = m_{\tilde{t_L}} m_{\tilde{t_R}}$, $X_t = A_0 - \mu \cot\beta$ and the parameters are evaluated at the EW scale. From this one may see that to get large radiative corrections requires a large stop mass

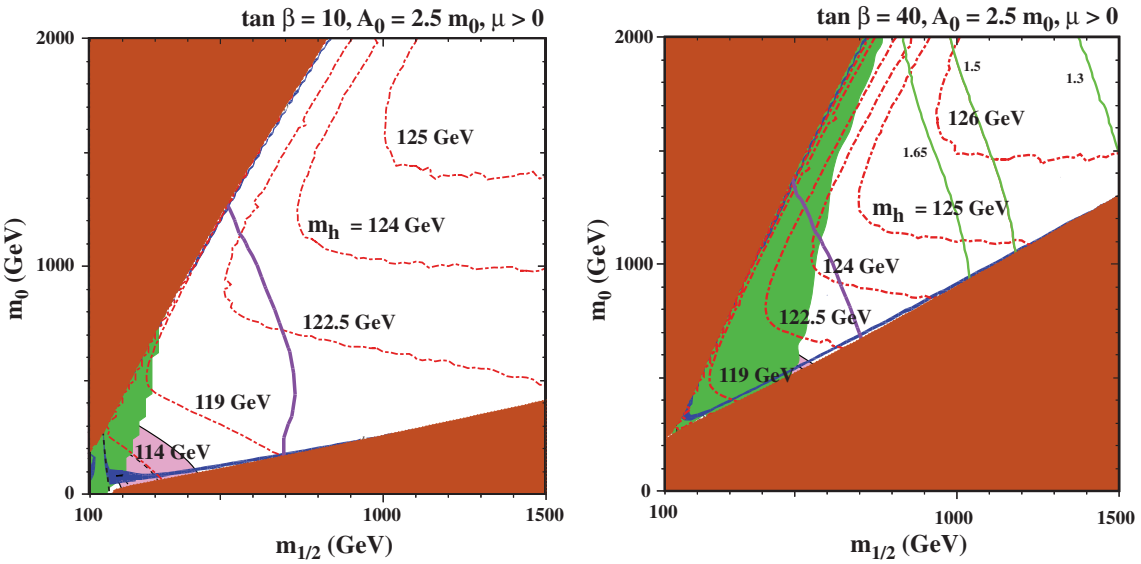

Fig. 1 The CMSSM $(m_{1/2}, m_0)$ planes for $\mu > 0$, with $\tan\beta = 10$ (*left*) and 40 (*right*), $A_0 = 2.5\,m_0$, as calculated for $m_t = 173.2$ GeV using the latest version of the SSARD code [79]. The interpretations of the *shadings* and *contour colours* are described in the text

and/or X_t, leading to very heavy coloured SUSY states in the TeV range.

2.1 CMSSM fits

Several groups [9–59] have performed detailed CMSSM fits to the LHC data from Atlas and CMS [60,61]. In these models the lightest SUSY particle (LSP), usually a combination of a neutralino and a Higgsino, is stable and a dark matter (DM) candidate. The fits that we discuss require that the DM should saturate at or be below the preferred cosmological range $\Omega_{\rm CDM}h^2 = 0.112 \pm 0.006$ [62], where h is the present Hubble expansion rate in units of 100 km/s/Mpc. In addition the dark matter should be consistent with the direct detection bounds, the strongest in the mass range of interest being that of XENON100 [63]. Constraints are also provided by flavour physics, especially $b \to s\gamma$ [64–67] and $B_s \to \mu^+\mu^-$ [68–73]. The LHCb measurement of the latter with a value close to the SM prediction provides particularly strong constraints on the large $\tan\beta$ region. In addition the measured value [74,75] of the anomalous magnetic moment of the muon, $g_\mu - 2$, plays a significant role in the fits. We will discuss further aspects of flavour-changing and CP-violation constraints in Sect. 5.

In Fig. 1 we show the results of a recent fit [54] to all the available data, including the latest LHCb measurement of $B_s \to \mu^+\mu^-$, for the parameters m_0 and $m_{1/2}$ as a function of the Higgs mass contours (red dashed lines). In each panel, the region at high $m_{1/2}$ and low m_0 where the $\tilde{\tau}_1$ is the LSP is shaded brown, as is the region at low $m_{1/2}$ and high m_0 where the stop becomes the LSP (or tachyonic). The regions excluded by $b \to s\gamma$ are shaded green, those favoured by $g_\mu - 2$ are shaded pink, and those favoured by $\Omega_\chi h^2$ are shaded dark blue[1]. The LEP chargino exclusion is shown as a near-vertical dashed black line at small $m_{1/2}$ [76]. The ATLAS exclusion from the absence of missing transverse energy events (MET) is shown by the purple lines. Also shown as solid green lines are three contours of $\mathrm{BR}(B_s \to \mu^+\mu^-)/\mathrm{BR}(B_s \to \mu^+\mu^-)_{\rm SM} = 1.65, 1.5$ (the present 95 % CL upper limit from LHCb and combined experiments), and 1.3 (the 68 % upper limit from LHCb).

Over the range shown in the $(m_0, m_{1/2})$ plane a large value for A_0 is needed to get to the observed Higgs mass[2]. For larger values of $\tan\beta$ the Higgs mass increases but the $B_s \to \mu^+\mu^-$ rate still requires that m_0 and $m_{1/2}$ are above 1 TeV. However, taking account of the dark matter constraint, for $\tan\beta = 10$, M_h does not grow above ∼121 GeV, whereas for $\tan\beta = 40$ there is compatibility for $m_{1/2} \geq 1$ TeV along the stau co-annihilation strip (SC) close to the stau LSP boundary[3]. This region is also compatible with the LHC MET constraint, but not with the supersymmetric interpretation of $g_\mu - 2$. Interestingly the sensitivity of upcoming direct DM searches will be sufficient to test the most likely regions of the CMSSM DM space providing complementary tests to the LHC SUSY searches. LUX will be sensitive to a substantial proportion of the favoured regions and XENON1T will cover almost

[1] For reasons of visibility the wider strips $0.06 < \Omega_\chi h^2 < 0.2$ are shown here.

[2] $M_h = 125.7 \pm 1.0$ GeV [1,2] although, including theoretical errors, values greater than 122 GeV are probably acceptable.

[3] The focus point (FP) region, in which the DM unpolarised annihilation cross section is enhanced by a significant Higgsino component of the LSP, is excluded by the XENON100 bound.

all of the rest. This complementarity is important because the majority of points have a very heavy Higgsino LSP, of $O(1\,\text{TeV})$, possibly beyond the reach of LHC14.

In the absence of the fine tuning constraint the upper bound on the SUSY mass spectrum comes from the requirement that the SUSY LSP should provide the observed dark matter abundance. For example, a recent Baysian fit [77] finds $m_{\tilde{g}} = 3.4\,\text{TeV}$, $m_{\tilde{t}} = 2.8\,\text{TeV}$, $m_{\tilde{u}_L} = 3.5\,\text{TeV}$ and $m_\chi = 700\,\text{GeV}$[4] as the most probable values suggesting that even LHC14 may not discover evidence for SUSY.

2.2 Beyond the CMSSM

As we have seen, the LHC and dark matter constraints have forced the CMSSM parameter space into a tight corner that requires large values of $\tan\beta$, A_0 and $m_{1/2}$ and a correspondingly heavy SUSY spectrum. However, by extending the parameters of the model the fit constraints can be more readily satisfied, particularly that of obtaining acceptable dark matter abundance. One possibility is to allow the Higgs masses to differ from the squark and slepton masses at the initial scale [16,18,80–93] and in this case it is not difficult to find regions of the parameter space where the cosmological cold dark matter density falls within the preferred range, even if the sparticle masses are relatively large, as required by the LHC MET and M_h constraints. For example [54], this may happen in a transition region where the χ LSP has a relatively large Higgsino component, a region disfavoured in the CMSSM by the XENON100 upper limit on cold dark matter scattering. Another possibility is to lower the initial scale, M_X, which compresses the spectrum making more co-annihilation processes important, thus suppressing the relic density below the range expected in the CMSSM. While these generalisations of the CNMSSM open up the phase space of acceptable solutions they still require large values of the SUSY breaking parameters corresponding to heavy SUSY spectra similar to those found in the CMSSM.

2.2.1 The CNMSSM

Another possibility that has been widely studied is to increase the particle content, for example by adding a gauge singlet chiral super field, S. The simplest version of this, the NMSSM (for reviews see [94,95]), has the superpotential

$$W_{\text{NMSSM}} = \lambda S H_u H_d + \frac{\kappa}{3} S^3 + W_{\text{Yukawa}}, \tag{6}$$

where additional terms are forbidden by the Z_3 symmetry of W_{NMSSM}. This lacks the bare μ term of the CMSSM, Eq. (2), but an effective term, μ_{eff}, is generated at the stage of EW breaking when the scalar component of S acquires a vacuum expectation value (VEV). The advantage of this is that μ_{eff} is automatically of the order of the EW breaking scale in comparison to the MSSM case in which the symmetries allow an arbitrarily large μ term. In the constrained version of the model (CNMSSM) the soft SUSY breaking terms associated with the Higgs sector at the initial scale have the form

$$V_{\text{soft}} = m_0^2|H_u|^2 + m_0^2|H_d|^2 + m_S^2|S|^2 + \left(\lambda A_0 S H_u H_d + \frac{1}{3}\kappa A_0 S^3 + \text{h.c.}\right), \tag{7}$$

with scalar mass universality assumed for all scalars apart from the new singlet. In this case the parameters of the CNMSSM may be chosen as m_0, $m_{1/2}$, A_0, $\tan\beta$, λ, m_S and the sign of μ_{eff}.

Several groups have analysed the NMSSM after the Higgs discovery [96–118]. Here we present results from a very recent study [118] that takes account of the measurement of $B_s \to \mu^+\mu^-$. In the upper figures of Fig. 2 we present the results of a CNMSSM Baysian fit showing $(m_o, m_{1/2})$ planes for $\mu_{\text{eff}} > 0$. Because of the additional singlet scalar state there are two CP even Higgs states involving mixtures of the EW doublet and singlet states. Two cases are shown, case 1 in which the lightest CP even Higgs has mass $m_{h_1} = 125.8\,\text{GeV}$ and case 2 in which the second lightest CP even Higgs has mass $m_{h_2} = 125.8\,\text{GeV}$. Note that in the second of the top figures the right-hand favoured region is already excluded by XENON100 so in both cases both the squarks and the gluinos are in the TeV range with the gluinos typically heavier than the squarks.

In the lower figure of Fig. 2 we show the (m_{h_1}, m_{h_2}) planes for these two cases. One may see from the first figure that the second state, which is mainly singlet, is expected to be very heavy, in the TeV range, while in the second figure the mainly singlet state can be relatively light but, because of its small doublet component, would not have been detected at LEP. Not shown here is an interesting third case in which both Higgs states have mass in the 126 GeV region.

The fit to the model shows that in case 1 there are two viable DM regions, one, the A-funnel region in which neutralinos annihilate through the resonance with the lightest pseudoscalar and a second (SC) in which the dominant annihilation process is through stau-coannilation. In the upper left figure the SC region is that including the best fit point, while the AF region corresponds to the top part of the plot. Both regions lie below the XENON100 limits but will be partly probed by XENON1T. In case 2 the best fit region is again SC and its interaction cross section lies below even the sensitivity of XENON1T. However, the other region corresponds to the focus point region and is already inconsistent with the XENON100 bound.

[4] These values are close to the favoured upper values in [78].

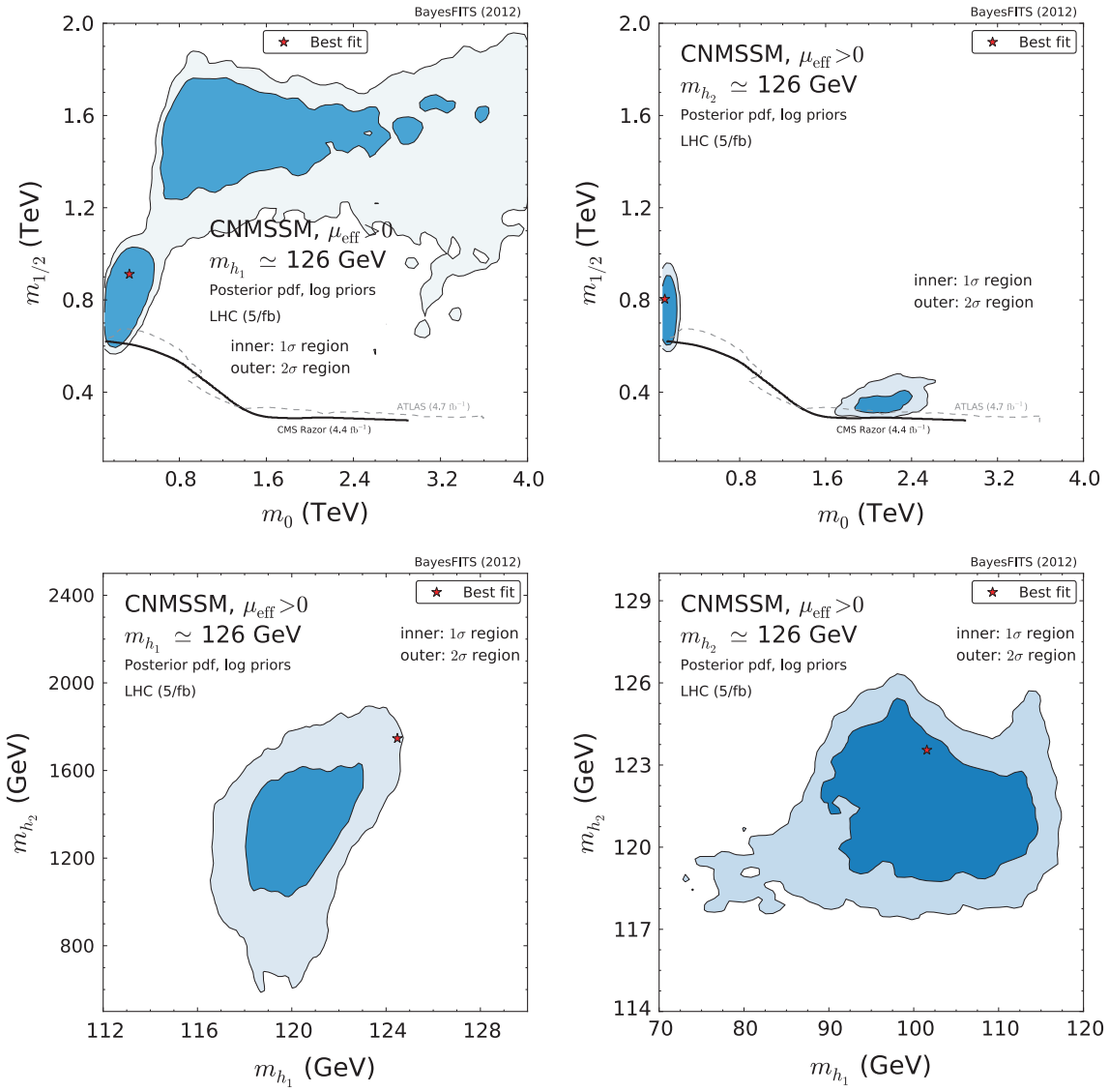

Fig. 2 CNMSSM marginalised 2D posterior pdf in the $(m_0, m_{1/2})$ plane for case 1 (*top left*), and case 2 (*top right*) and in the (m_{h_1}, m_{h_2}) plane for case 1 (*bottom left*), and case 2 (*bottom right*). The 68 % credible regions are shown in *dark blue*, and the 95 % credible regions in *light blue*. The *stars* denote the best fit points. In the *top figures* the *solid black* (*dashed grey*) line shows the CMS and ATLAS hadronic 95 % C.L. exclusion bound

The favoured values for the SUSY mass spectrum following from the requirement that the SUSY LSP should provide the observed dark matter abundance gives $m_{\tilde{g}} = 2.8\,\text{TeV}$, $m_{\tilde{t}} = 2.2\,\text{TeV}$, $m_{\tilde{u}_L} = 3.0\,\text{TeV}$ and $m_{\chi} = 600$ GeV as the most probable values, slightly lower than that found for the CMSSM, but still in the range that may be beyond LHC14 discovery.

3 The hierarchy problem

As these simple models demonstrate the non-observation of SUSY states, or indeed any significant deviations from the SM, drives the SUSY partner mass scale into the TeV region. Indeed, if one ignores the hierarchy problem, it can be made arbitrarily high if there is a non-SUSY explanation for dark matter. This emphasises the importance of the hierarchy problem for it is really only the SUSY solution to the hierarchy problem that has led us to expect low-scale SUSY, accessible to LHC discovery.

A very simple illustration of the hierarchy problem was given in [119] and follows from expanding the formula for the Z mass in Eq. (3) in terms of the input parameters. Allowing for different gaugino and scalar masses at the input scale, M_X, and simplifying by working at tree level one finds, for example for $\tan\beta = 2.5$,

$$\begin{aligned}\frac{M_Z^2}{2} = &-0.87\,\mu^2(M_X) + 3.6\,M_3^2(M_X)\\ &-0.12\,M_2^2(M_X) + 0.007\,M_1^2(M_X)\\ &-0.71\,m_{H_U}^2(M_X) + 0.19\,m_{H_D}^2(M_X)\\ &+0.48\,(m_Q^2(M_X) + m_U^2(M_X))\\ &-0.34\,A_t(M_X)\,M_3(M_X) - 0.07\,A_t(M_X)\,M_2(M_X)\\ &-0.01\,A_t(M_X)\,M_1(M_X) + 0.09\,A_t^2(0)\\ &+0.25\,M_2(M_X)\,M_3(M_X) + 0.03\,M_1(M_X)\,M_3(M_X)\\ &+0.007\,M_1(M_X)\,M_2(M_X). \end{aligned} \tag{8}$$

One may see that for the input parameters much greater than M_Z it is necessary to fine tune the parameters to arrange for significant cancellation between the terms. For the case these parameters are at the TeV scale this fine tuning is more than 1 part in 100. This is the hierarchy problem and it clearly gets worse as the input parameters increase.

Of course if the underlying theory relevant at M_X requires correlations between the input parameters the fine tuning may be reduced. As an example of this we consider the CMSSM case with universal scalar masses m_0 and universal gaugino masses $m_{1/2}$. In this case Eq. (8) becomes

$$\begin{aligned}\frac{M_Z^2}{2} = &-0.87\,\mu^2(M_X) + 3.78\,m_{1/2}^2 + 0.44\,m_0^2\\ &-0.42\,A_0\,m_{1/2} + 0.09\,A_0^2. \end{aligned} \tag{9}$$

It is instructive to consider why the coefficient of m_0 is relatively small in the CMSSM. The dominant terms in the RG equation for $m_{H_u}^2$, which sets the EW scale, involving m_0 are those proportional to the square of the top Yukawa coupling, y_t and can be integrated to give

$$\begin{aligned} m_{H_u}^2\left(Q^2\right) &= m_{H_u}^2\left(M_X^2\right) + \frac{1}{2}\left(m_{H_u}^2\left(M_X^2\right)\right.\\ &\left. + m_{Q_3}^2\left(M_X^2\right) + m_{\bar{u}_3}^2\left(M_X^2\right)\right)\left[\left(\frac{Q^2}{M_X^2}\right)^{\frac{3y_t^2}{4\pi^2}} - 1\right] \end{aligned} \tag{10}$$

$$= m_0^2\left(1 + \frac{3}{2}\left[\left(\frac{Q^2}{M_X^2}\right)^{\frac{3y_t^2}{4\pi^2}} - 1\right]\right), \tag{11}$$

where we have used the fact that in the CMSSM all the scalar masses are equal unification scale. When the factor in square brackets is -2/3 the coefficient of m_0^2 vanishes—this is known as the focus point (FP) [120–124]. Remarkable the focus point is close to the electroweak scale explaining the smallness of the coefficient of m_0^2 in Eq. (9). Clearly the appearance of such focus points affect the bounds on the SUSY spectrum coming from the hierarchy problem because the dependence of the other scalars, the squarks and sleptons, on m_0^2 is not suppressed and consequently, for models with the focus point, they can be much heavier than the Higgs. This nicely illustrates how correlations amongst the initial parameters can significantly reduce the fine tuning needed.

3.1 Fine tuning measures

In order to quantify the fine tuning needed to keep the electroweak scale much lower than the SUSY masses several fine tuning measures have been suggested [125,126]. Two frequently used are Δ_m and Δ_q where

$$\Delta_m = \max\left|\Delta_{\gamma_i}\right|, \quad \Delta_q = \left(\sum \Delta_{\gamma_i}^2\right)^{1/2},$$
$$\Delta_{\gamma_i} = \frac{\partial \ln v^2}{\partial \ln \gamma_i^2}, \quad \gamma_i = m_0, m_{1/2}, \mu_0, A_0, \ldots. \tag{12}$$

Here the basic measure Δ_{γ_i} roughly determines the relative magnitude of the term proportional to the parameter γ_i on the RHS of Eq. (8) to the LHS. A value of 100 means that the cancellation between terms on the RHS should be accurate to 1 part in 100. Typically one term dominates in which case Δ_m and Δ_q are nearly equal but in the case that there are several comparable terms Δ_q would seem the more reasonable measure.

3.2 The likelihood origin of the fine tuning measure

Of course the difficult question to answer when using such measures to limit the SUSY spectrum is how large the fine tuning measure can reasonably be? However, it has recently been shown how the measure arises when performing a likelihood fit to the data [127–130] and this allows us to give a quantitative estimate for acceptable fine tuning.

When testing a SUSY model with a given set of parameters (such as γ_i), one should in principle marginalise (i.e. integrate) the likelihood L over unrelated, 'nuisance' parameters that can be determined well from the data and are not of interest in the final result. Examples of such parameters are those already present in the Standard Model such as the Yukawa couplings. In the case of SUSY one may also integrate over the dependent parameters, the VEVs $v_{u,d}$ of the SUSY Higgs $H_{u,d}$ which are fixed by the vacuum minimisation constraints and which determine the EW breaking scale characterised by M_Z. If one chooses to do this, then the constrained likelihood is given by

$$\begin{aligned} L(\text{data}|\gamma_i) \propto &\int \mathrm{d}v\,\mathrm{d}(\tan\beta)\delta(m_Z - m_Z^0)\\ &\times \delta\,(f_1(\gamma_i; v, \beta, y_t, y_b))\;\delta\,(f_2(\gamma_i; v, \beta, y_t, y_b))\\ &L(\text{data}|\gamma_i; v, \beta, y_t, y_b). \end{aligned} \tag{13}$$

where $v^2 = v_u^2 + v_d^2$ and $\tan\beta = v_u/v_d$. $L(\text{data}|\gamma_i; \beta, v, y_t, y_b)$ is the likelihood to fit the data with a particular set of values for γ_i, $y_{t,b}$, etc. (the associated χ^2 is given by $\chi^2 = -2\ln(L)$), while $L(\text{data}|\gamma_i)$ is the ('constrained') likelihood

in the presence of the EW constraints and is a function of γ_i only. The functions f_i are the solutions to the minimisation equations given by

$$\begin{aligned} f_1(\gamma_i; v, \beta, y_t, y_b, \ldots) &\equiv v - \left(-\frac{m^2}{\lambda}\right)^{1/2}, \\ f_2(\gamma_i; v, \beta, y_t, y_b, \ldots) &\equiv \tan\beta - \tan\beta_0(\gamma_i, v, y_t, y_b), \\ \gamma_i &= \{m_0, m_{1/2}, \mu_0, A_0, B_0\}, \end{aligned} \tag{14}$$

where m^2 and λ are the effective Higgs mass and quartic coupling, functions of the underlying parameters of the theory as in [127].

Of particular relevance here is the delta function involving f_1 which constrains some combination of the parameters of the theory. We may choose the residual independent variables to lie in the surface, S, in γ_κ space defined by the EW constraint $f_1(\gamma_i^S;\ v_0,\ \beta,\ \tilde{y}_t(\beta),\ \tilde{y}_b(\beta)) = 0$. In this case we have $\delta(f_1(z_i)) = (1/|\nabla f_1|)\,\delta[\vec{n}.(\vec{z} - \vec{z}^S)]$, where $\vec{n} = \nabla f_1/|\nabla f_1|$ is the unit vector normal to the surface S, $\vec{z}$ has components $z_1, \ldots, z_n$ and $\vec{z}^S$ lies on S, $f(z_i^S) = 0$. With this, and taking $z_i = \ln\gamma_i$, Eq. (13) can be written as

$$\begin{aligned} L(\text{data}|\gamma_i) = \frac{1}{\Delta_q}\delta\left(\sum_{i=1}^{n} n_q(\ln\gamma_i - \ln\gamma_i^S)\right) \\ \times L\left(\text{data}|\gamma_i;\ v_0,\ \beta,\ \tilde{y}_t(\beta),\ \tilde{y}_b(\beta)\right)|_{\beta=\beta_0(\gamma_i)} \end{aligned} \tag{15}$$

where n_q are the components of the normal unit vector and Δ_q is the fine tuning in quadrature defined in Eq. (12) with $v \to \tilde{v}$. For independent variables, γ_i, this relation is only satisfied if all $\gamma_i = \gamma_i^0$, for all i, i.e. if the $f_1 = 0$ constraint is satisfied.

This shows that it is the constrained likelihood that should be maximised when fitting data, i.e. one should maximise the ratio of the unconstrained likelihood to the fine tuning Δ_q. If the fine tuning is large it reduces the overall likelihood. The terms of the associated χ^2 (χ^2_{new}) and unconstrained (χ^2_{old}) likelihoods are related by

$$\chi^2_{\text{new}} = \chi^2_{\text{old}} + 2\ln\Delta. \tag{16}$$

This relation can be used to infer what can be regarded as the 'acceptable' upper bound of the fine tuning requiring that $\Delta_q \ll \exp(n_d/2)$ where n_{df} is the number of degrees of freedom. If this is satisfied then χ^2 per degree of freedom will not be significantly worsened. For simple SUSY extensions of the SM such as the CMSSM $n_{df} = O(10)$, which requires $\Delta \ll 100$[5].

[5] See [128,129] for a detailed analysis of various SUSY models.

3.3 The real hierarchy problem

We have introduced the hierarchy problem in the context of supersymmetry but, given the lack of evidence for BSM physics at the LHC or in precision tests of the SM, it may be appropriate to make a few comments about claims that, even in the context of the SM, there is no hierarchy problem. It has become customary to introduce the hierarchy problem by noting that in the SM at leading order there is a quadratically divergent contribution to the Higgs mass coming from a top quark loop giving

$$\delta m^2_{H_u} \sim -\frac{3|y_t^2|}{4\pi^2}\Lambda^2. \tag{17}$$

In a renormalisable theory this divergent term is cancelled by a counter term but, taking the cutoff to be at a very high scale, this cancellation must be hierarchically precise. However, the quadratic divergence is not the real hierarchy problem in the sense that the divergent term is independent of the scale at which the mass is measured. Thus if, at a very high scale, there is a reason, such as underlying scale invariance or SUSY, for there to be no mass term it will not reappear at lower scales. The real hierarchy problem [131] arises when there are heavy states of mass M_X to which the Higgs couples which give corrections of the form

$$\delta m^2_{H_u}(Q^2) \propto y^2 M_X^2 ln\left(\frac{\Lambda^2}{M_X^2 + Q^2}\right). \tag{18}$$

Even if the mass vanishes at a high scale it reappears at a lower scale and, for it to be small at the electroweak scale, requires a precise cancellation with other terms. In a supersymmetric model this cancellation is between contributions involving different components of a supermultiplet and is automatic due to the symmetry. Thus in a SUSY GUT the term in Eq. (18) is cancelled up to terms suppressed by $\Delta^2_{\text{SUSY}}/M_X^2$ where Δ_{SUSY} is the SUSY breaking scale in the GUT sector. For the case of scale invariance the idea is that it is softly broken so that at high energy scales the breaking terms are small and the underlying scale invariance ensures that the quadratic terms is cancelled by the counter term. However, as the SM is not scale invariant its beta functions do not vanish and thus must change at some scale, M, to the scale invariant result. Even if the origin of the mass scale, M, is non-perturbative it has been shown recently [132] that the Higgs mass has corrections of $O(M)$. Thus to protect the Higgs mass, the scale M, corresponding to the onset of BSM physics, is limited to the TeV scale, otherwise the hierarchy problem reappears.

3.4 Fine tuning and the initial scale

For pedagogic reasons we introduced the fine tuning measure in the context of the CMSSM in which the low energy

structure of the MSSM spectrum is determined by parameters defined at a high (unification) scale. Such high scale models usually introduce large logarithmic enhancements in the fine tuning measure coming from the RG continuation to the electroweak breaking scale. As is exemplified by the scalar focus point structure discussed above the logarithmic enhancement may be significantly reduced if there are relations between the SUSY breaking parameters that an underlying theory might provide. It is perhaps interesting to ask what is a reasonable estimate for the minimum fine tuning that could come from a (presently unknown) underlying theory providing such relations. To quantify this, note that in the MSSM the electroweak scale, characterised by the Z mass, is given by

$$\frac{M_Z^2}{2} = \frac{m_{H_d}^2 + \Sigma_d^d - (m_{H_u}^2 + \Sigma_u^u)\tan^2\beta}{\tan^2\beta - 1} - \mu^2 \tag{19}$$

where Σ_u^u and Σ_d^d are one-loop contributions coming from the states that couple to the Higgs. Requiring that the theory be parameterised by just these terms, with no information about the underlying UV completion, leads to the 'EW' fine tuning measure [133–136] given by the maximum value of the individual terms[6]. We have

$$\Delta_{\rm EW} = \text{Max} \times \left(\left| \frac{|m_{H_u}^2 \tan^2\beta}{\tan^2\beta - 1} \right|, \left| \frac{\Sigma_u^u \tan^2\beta}{\tan^2\beta - 1} \right|, \ldots, |\mu^2| \right) \Big/ (M_Z^2/2). \tag{20}$$

In this case one can take squark and gluino masses to be very heavy because only Σ_u^u and Σ_d^d are sensitive to the radiative corrections. The dominant correction comes from the top squark loop

$$\Sigma_u^u \approx \frac{3y_t^2}{16\pi^2} m_{\tilde{t}}^2 \left(\ln\left(m_{\tilde{t}}^2/Q^2 \right) - 1 \right). \tag{21}$$

The EW fine tuning is determined by the SUSY spectrum and, for acceptable fine tuning, $\Delta_{\rm EW} < 30$, one can have stop (and other) squarks with mass as high as 5 TeV. Further it requires $|\mu| < 300$ GeV corresponding to the existence of light Higgsino states that may be visible at an e^+e^- collider with $E_{\rm CM} > 600$ GeV producing $\tilde{W}_1^+\tilde{W}_1^-$, $\tilde{Z}_1\tilde{Z}_1$ and $\tilde{Z}_2\tilde{Z}_2$ production. Gluinos can also be very heavy in which case the small mass gap of $O(10\,\text{GeV})$ between $\tilde{W}_1 - \tilde{Z}_2$ and $\tilde{Z}_2 - \tilde{Z}_1$ makes detection of Higgsino pair production difficult because the visible decay products are soft.

A low scale of EW fine tuning does not mean there is no fine tuning but leaves open the possibility that there is an underlying theory with this SUSY spectrum that is not fine tuned. Below we discuss UV complete models that do predict correlations among the MSSM SUSY breaking parameters which can achieve such low levels of fine tuning while preserving the successful prediction following from gauge coupling unification. In these models the mass of the coloured states are much more constrained than the upper bound coming from EW fine tuning. They do, however, have the tendency to produce compressed spectra.

[6] Of course, this assumes that the underlying theory does not correlate the terms in this equation. To date no theory capable of doing this has been proposed.

4 Fine tuning constraints on SUSY in the light of the Higgs discovery

As we have stressed the hierarchy problem provides the main motivation for low-scale SUSY, accessible to the LHC. In this section we will discuss the extent to which the postulate that SUSY solves the little hierarchy problem has been tested[7] and the prospects for a definitive test at LHC14. This will involve a discussion of non-minimal implementations of SUSY that can reduce the fine tuning and, in turn, suggest new signatures relevant to future LHC SUSY searches. In the main we will concentrate on the case that the initial scale at which the fundamental parameters are defined is close to the Grand Unified scale as is natural in GUTs and is consistent with the precision prediction of gauge coupling unification that follows in SUSY GUTs.

4.1 Fine tuning of the CMSSM

In the CMSSM the Higgs mass is given by Eq. (5). The heavier the Higgs mass is the larger the radiative correction that is needed. Before the LHC start-up the bound on the Higgs mass was 114 GeV corresponding, for small X_t, to $M_S \approx 500$ GeV. The measurement of the Higgs mass close to 126 GeV increases this to $M_S \approx 1$ TeV. Thus the Higgs discovery has pushed the SUSY threshold for the stops up and this leads to the need for significantly greater fine tuning. Of course one must also allow for the X_t contribution and perform a fit to all the available data. The result of such a fit [138] that was performed before the LHC start-up is shown in Fig. 3 where the fine tuning, $\Delta \equiv \Delta_m$, is shown as a function of the Higgs mass; note that the LEP bound on the Higgs mass was not included in the fit. The origin of the structure is due to two factors: the fall as the Higgs mass increases is due to the fact that the effective quartic interaction, $\lambda_{\rm eff}$, increases, reducing the sensitivity of the EW breaking VEV, $v^2 = m_{\rm eff}^2/\lambda\text{eff}$ to changes in $\lambda_{\rm eff}$. The sharp rise as the Higgs mass further increases is due to the fact that the sensitivity of m_{H_u} to m_0 in Eq. (11) increases rapidly as $Q^2 \sim m_{H_u}^2$ grows above $(115\,\text{GeV})^2$. Also shown in the figure is the

[7] For an earlier comparative study see [137].

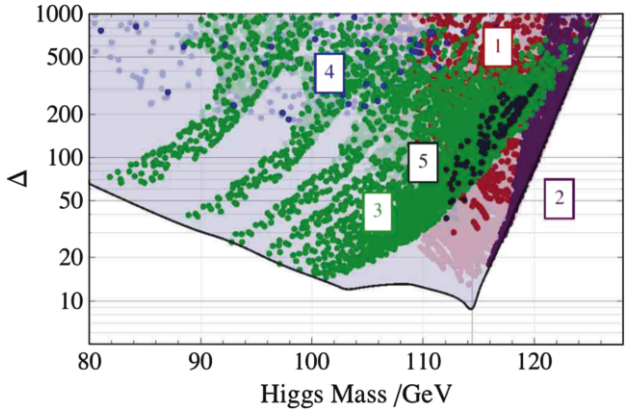

Fig. 3 Two-loop fine-tuning versus Higgs mass for the scan over CMSSM parameters with no constraint on the Higgs mass. The *solid line* is the minimum fine-tuning with $(\alpha_s, M_t) = (0.1176, 173.1\,\text{GeV})$. The *dark green*, *purple*, *crimson* and *black* coloured regions have a dark matter density within $\Omega h^2 = 0.1099 \pm 3 \times 0.0062$ (i.e. 3σ saturation) while the *lighter coloured* versions of these regions lie below this bound. The *colours* and their associated *numbers* refer to different LSP structures as described in [138]. Regions 1, 3, 4 and 5 have an LSP which is mostly bino-like. In region 2, the LSP has a significant Higgsino component

dark matter abundance colour coded [138] according to the dominant annihilation mechanism. The purple points with low fine tuning lie close to the focus point discussed above and one may see that before the LHC there are points in the parameter space scan with fine tuning less than 10, close to the LEP bound on the Higgs mass. As noted above, the points in the FP region have significant Higgsino component and the lowest fine tuned points are in conflict with the XENON100 bounds. However, the most significant effect ruling out the low fine tuned points is the measurement of the Higgs mass. For a Higgs mass in the range $m_h = 126 \pm 3$ GeV the fine tuning, Δ_m, is greater than 300, unacceptably large given the constraint of Eq. (16).

4.2 Beyond the CMSSM

Of course the CMSSM is only one particular version of the MSSM expressing the more than 100 SUSY parameters in terms of just 5 fundamental ones. One may ask if there are other MSSM parameter choices with lower fine tuning that remain to be tested. However, this is not so easy as the CMSSM has the scalar focus point that, cf. Eq. (11), desensitises the EW breaking scale to the common scalar mass m_0 and in this sense represents the class of models capable of minimising, at least part, of the fine tuning measure. In contrast, gauge mediated supersymmetry-breaking models do not have a common scalar mass and as a result the fine tuning in them may be larger [139,140] even though they may have a lower initial scale, M_X.

To do better than the CMSSM requires identifying a systematic way to reduce fine tuning. In this subsection we discuss whether the fine tuning can be reduced by theoretically well-motivated modifications of the CMSSM boundary conditions for the SUSY breaking parameters. In the next subsection we consider the possibility that the fine tuning is reduced through an extension of the particle content of the MSSM.

4.2.1 Natural SUSY

In natural SUSY the universality of squark masses is relaxed with much lighter stop squarks than those associated with the first two generations [141,142]. As we discuss in Sect. 5 the suppression of flavour-changing neutral currents and CP-violating effects place strong constraints on the first and second generation squarks favouring their mass to be in the TeV region. However, the constraint on the stop squarks is very mild and this has led to the suggestion that they may be quite light, much less than a TeV. This is consistent with present LHC bounds due to the reduction in the E_T missing signals compared to that for the first two generation squarks. Since a large contribution to fine tuning comes from the sensitivity of the EW scale to the stop quark mass one may hope that fine tuning will be substantially reduced. However, this turns out not to be the case because it is still necessary to have significant radiative corrections to the Higgs mass to drive it to 126 GeV and, for light stops, this must come from another sector of the theory, reintroducing large fine tuning. Recent studies [143,144] finds the fine tuning is at least 400 for the case the initial scale, M_X, at which the parameters are defined is close to the GUT scale, unacceptably large by the criterion in Eq. (16). Even in the case that the initial scale is low, such as in gauge mediation, there is no significant fine tuning advantage of a light stop if the gluino is in the TeV range and the fine tuning is still in the 1 % range. Interestingly [143] notes that this conclusion can be evaded in the case that the gluinos have a Dirac rather than a Majorana mass although a very recent study [144] has found the fine tuning is still severe, $\Delta \sim 100$.

4.2.2 Gaugino focus point

The second possibility that has been suggested is that there is a further focus point associated with the gauginos that reduces the sensitivity of the EW breaking scale to $m_{1/2}$[8]. This can occur if the initial values of the gaugino masses have special, non-universal, ratios [145–155]. The origin of the gaugino focus point may be seen from the RG equation

[8] As we shall discuss this can reduce the fine-tuning to an acceptable level. This conflicts with the conclusion of [144] which does not allow for such correlations between soft SUSY breaking terms.

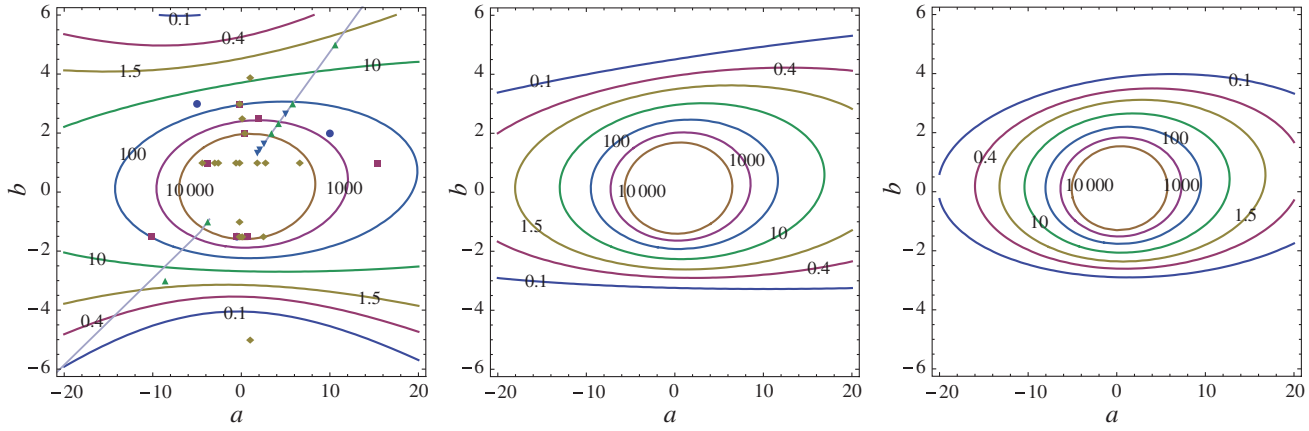

Fig. 4 Analytic results for the gaugino focus point scale contours (in units of Tev) in the MSSM for $\tan\beta = 2, 3, 10$ from *left* to *right*. The *points* and the *grey line* correspond to specific models with non-universal gaugino masses; see text for details. The contours do not change much for larger $\tan\beta$

$$16\pi^2 \frac{\mathrm{d}}{\mathrm{d}t} m_{H_u}^2 = 3\left(2|y_t|^2\left(m_{H_u}^2 + m_{Q_3}^2 + m_{\bar{u}_3}^2\right) + 2|a_t|^2\right) - 6g_2^2|M_2|^2 - \frac{6}{5}g_1^2|M_1|^2. \tag{22}$$

The first term on the RHS implicitly includes the effect of the gluino contribution to the squark masses. Although this is of higher order, since the QCD coupling is quite large, it gives a significant contribution that is comparable to that coming from the last two terms. Indeed if the gluino mass at the EW scale is similar to that of the Wino there is a cancellation between these terms that reduces the sensitivity of $m_{H_u}^2$ to the gaugino masse[9]. In Fig. 4 we show an approximate analytic estimate of the focus point scale (the scale at which the cancellation is exact) as a function of the initial gaugino mass ratios, $a, b = M_{1,2}(M_X)/M_3(M_X)$. The smallest fine tuning corresponds to values of a and b for which the gaugino focus point scale is close to the electroweak scale. For moderate a, the value $|b| \sim 2.5 - 3$ corresponds to such a low-scale gaugino focus point.

Of course, if arbitrary values of the parameters a and b are chosen, the contribution to the overall fine tuning from $\Delta_{a,b}$ should also be included in the analysis above, which typically spoils the improvement in fine tuning. However, if a and b are fixed by the underlying theory such contributions are absent. As discussed in [145–155] values of a and b in the low-focus-point region occur naturally in a variety of models. To illustrate this we show in the first plot of Fig. 4 the predicted points for the SU(5), SO(10) and E_6 GUT models (denoted by circles, squares and diamonds, respectively) considered in [157]. GUT models with F terms in **75** or **200** of SU(5), in **210** or **770** of SO(10) and in the corresponding representations of 'flipped SO(10)' embedded in E_6 predict gaugino mass ratios in the intermediate and low fine tuning region. Green triangles represent the OII orbifold model for various choices of the discrete Green Schwarz parameter, δ_{GS} [158]. The values $\delta_{\mathrm{GS}} = -5, -6, -7$ are optimal from the point of view of fine tuning. For comparison we also show points relevant for mirage mediation [147,159,160], where soft terms receive comparable contributions from gravity (modulus) and anomaly mediated SUSY breaking. In this case gaugino masses at the GUT scale have the following form:

$$M_a = m_{3/2}\left(\varrho + b_a g_a^2\right) \tag{23}$$

where g_a is the relevant gauge coupling, b_a is its β-function coefficient, while ϱ describes the relation between modulus and anomaly mediated contributions. This prescription for gaugino masses as a function of ϱ generates the grey line in Fig. 4 in the (a, b) parameter space. If ϱ is a continuous parameter there should be an additional contribution Δ_ϱ to the overall fine tuning. However, specific string models fix the value of ϱ. Four examples are shown in Fig. 4 by the blue inverted triangles:

(i) the minimal setup of KKLT-type moduli stabilisation in type II B string theory [161–163],

(ii) a model with vacuum uplifting via hidden sector matter superpotentials [161],

(iii) and (iv) the Mini Landscape of orbifold compactifications in heterotic string theory [164] with SU(4) and SU(5) hidden sector gauge groups; the type II B string theory model with vacuum stabilisation by F terms of hidden sector matter superpotentials predicts values of a and b in the low fine tuning region.

Given that there are models that naturally have the gaugino focus point at the EW scale it is interesting to ask how the

[9] Another advantage is that the accuracy of the prediction for gauge coupling unification is also improved [156].

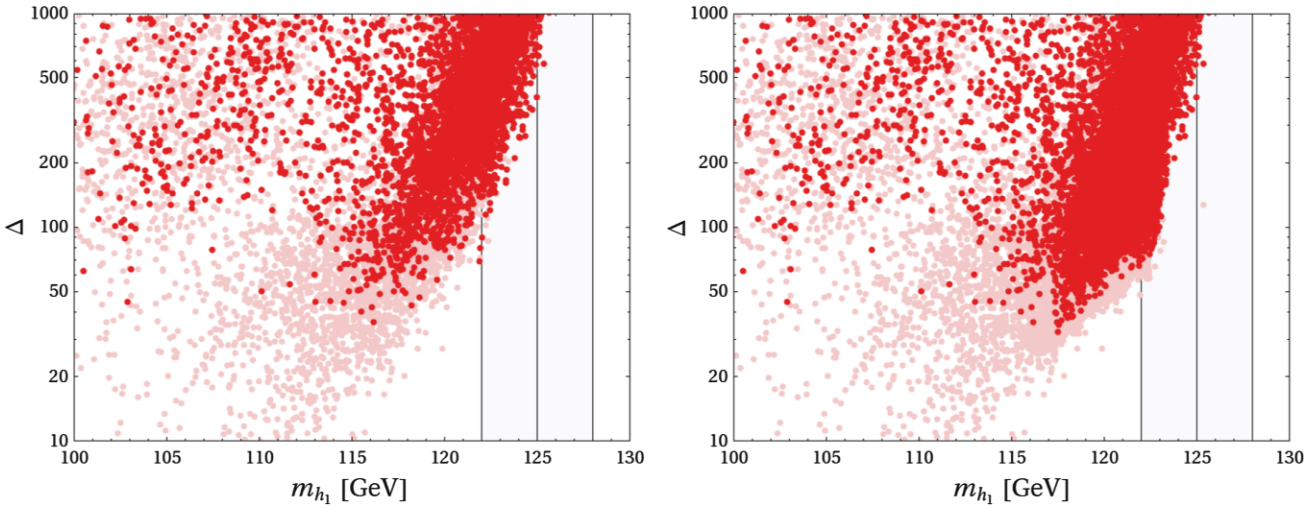

Fig. 5 Dependence of the fine tuning on the Higgs mass. The *light red points* are before any cuts while the *dark red points* take into account cuts on the SUSY masses and the relic neutralino abundance. The *left plot* is uniform in the density of the input parameters, their density reflects the likelihood for finding a viable point. The *right plot* shows additional points where we zoomed into regions of small fine tuning

overall fine tuning is affected. We consider the case of the MSSM with the CMSSM spectrum modified to allow for non-universal gaugino masses at the unification scale (the (C)MSSM) and requiring gauge coupling unification. The results of a fit to all the available data including the DM abundance is shown in Fig. 5 where it can be seen that there are some points, with a and b in the low fine tuned regions of Fig. 4, with fine tuning less than 100, marginally acceptable by the criterion of Eq. (16).

Due to the additional flexibility in the gaugino sector, a large variety of LSP compositions is possible. For points satisfying the relic abundance upper bound the LSP is mainly composed of wino and Higgsino, with typically only a very small bino component. Unlike the case for the CMSSM the direct detection cross section lies below the Xenon100 limit with the bulk of the points more than two orders of magnitude below. The correct relic abundance seems to be more easily achieved with a Higgsino-like LSP. A recent discussion of the phenomenology of the low fine tuned points can be found in [165].

4.3 Beyond the MSSM

The MSSM is the minimal extension of the SM, minimal in the sense that the fewest new states have been included when building a SUSY model. Could it be that non-minimal extensions reduce the fine-tuning constraints on SUSY and have not yet been experimentally tested?

4.4 Operator analysis

A useful way to look such extensions is to allow for a general modification of the MSSM by adding higher dimension operators [166–173] that correspond to the effective field theory that results from integrating out additional heavy degrees of freedom, of mass M_*, and ask if such operators can reduce fine tuning. There is a unique leading dimension 5 operator with the form

$$L = \frac{1}{M_*}\int \mathrm{d}^2\theta f(X)(H_u H_d) \tag{24}$$

where $X = \theta\theta m_0$ and m_0 is the SUSY breaking scale.

This gives contributions to the scalar potential of the form

$$V = (|h_u|^2 + |h_d|^2)(\chi_1 h_u h_d + \text{h.c.}) + \frac{1}{2}(\chi_2 (h_u h_d)^2 + h.c.) \tag{25}$$

where $\chi_1 = 2f(0)\mu_{\text{eff}}/M_*$, $\chi_2 = -2f'(0)m_0/M_*$ and μ_{eff} is the effective μ term. Note that the χ_1 term is supersymmetric so there are associated corrections involving Higgsinos that will generate Higgsino mass terms of the same order of magnitude as the correction to the Higgs mass terms (once the Higgs acquire their VEVs). However, in practice these corrections are going to be of $O(10\ \text{GeV})$, important to get a Higgs mass of 125 GeV but small compared to the Higgsino mass coming from the μ_{eff} term. For this reason we concentrate on the effect in the scalar sector.

The fine tuning of this model has been analysed in [174] where it was shown that the fine tuning is significantly reduced by the first term of Eq. (25) while the second term only gives a modest reduction. The dominant effect comes from the contribution of Eq. (25) to the Higgs mass after electroweak breaking and, due to the fact that the first term involves an extra power of h_u, it gives the larger contribution.

The obvious question is what new physics can give rise to the first operator corresponding to this term. The answer is

through the integration out of a new heavy gauge singlet or SU(2) triplet superfield coupling to the Higgs sector. Interestingly the operator is *not* generated in the NMSSM, the simplest singlet extension of the MSSM, as it requires an explicit mass term for the singlet super field[10] We refer to this model as the generalised NMSSM (the GNMSSM).

4.5 The GNMSSM superpotential

The most general extension of the MSSM by a gauge singlet chiral superfield consistent with the SM gauge symmetry has a superpotential of the form

$$\mathcal{W} = \mathcal{W}_{\text{Yukawa}} + \frac{1}{3}\kappa S^3 + (\mu + \lambda S) H_u H_d + \xi S + \frac{1}{2}\mu_s S^2 \tag{26}$$

$$\equiv \mathcal{W}_{\text{NMSSM}} + \mu H_u H_d + \xi S + \frac{1}{2}\mu_s S^2 \tag{27}$$

where $\mathcal{W}_{\text{Yukawa}}$ is the MSSM superpotential generating the SM Yukawa couplings and $\mathcal{W}_{\text{NMSSM}}$ is the 'normal' NMSSM with a Z_3 symmetry. One of the dimensionful parameters can be eliminated by a shift in the VEV v_s. We use this freedom to set the linear term in S in the superpotential to zero, $\xi = 0$.

The form of Eq. (12) seems to make the hierarchy problem much worse as the SM symmetries do not prevent arbitrarily high scales for the dimensionful mass terms. However, these terms can be naturally of the order of the SUSY breaking scale if there is an underlying Z_4^R or Z_8^R symmetry [176,177]. Before SUSY breaking the superpotential is of the NMSSM form. However, after supersymmetry breaking in a hidden sector with gravity mediation soft superpotential terms are generated but with a scale of order the supersymmetry-breaking scale in the visible sector characterised by the gravitino mass, $m_{3/2}$. With these the renormalisable terms of the superpotential take the form

$$\mathcal{W}_{Z_4^R} \sim \mathcal{W}_{\text{NMSSM}} + m_{3/2}^2\, S + m_{3/2}\, S^2 + m_{3/2}\, H_u\, H_d\ , \tag{28}$$

$$\mathcal{W}_{Z_8^R} \sim \mathcal{W}_{\text{NMSSM}} + m_{3/2}^2\, S \tag{29}$$

where the $\sim$ denotes that the dimensional terms are specified up to $\mathcal{O}(1)$ coefficients. Clearly the Z_4^R case is equivalent to the GNMSSM. After eliminating the linear term in S the Z_8^R case gives a constrained version of the GNMSSM with $\mu_s/\mu = 2\kappa/\lambda$.

Note that the SUSY breaking also breaks the discrete R symmetry but leaves the subgroup Z_2^R, corresponding to the usual matter parity, unbroken. As a result the lightest supersymmetric particle, the LSP, is stable and a candidate for dark matter.

4.6 Fine tuning in the GNMSSM

Several groups have recently analysed the fine-tuning implications of the GNMSSM [178–184]. Requiring that the couplings remain in the perturbative domain up to the Planck scale, the resulting fine tuning has been explored in detail for the simplified case of universal boundary conditions for the SUSY breaking parameters (CGNMSSM) [178,179]. Note that this goes beyond the operator analysis as we do not require that the singlet mass need not be large compared to the other parameters of the theory and thus cannot be integrated out. However, even allowing for the additional contribution to the Higgs mass coming from the singlet couplings, the regions of this model corresponding to low fine tuning have essentially been ruled out by a combination of LHC non-observation of SUSY and dark matter (DM) abundance. In particular the DM abundance has to be reduced below the 'over-closure' limit and this is dominantly through stau co-annihilation that is only effective for relatively low m_0 and $m_{1/2}$ and hence sparticle masses in the reach of LHC8.

For the case of non-universal gaugino masses (the (C) GNMSSM) the situation changes because the LSP can now have significant Wino/Higgsino components that ensures its efficient annihilation. In Fig. 6 we show the results of a scan [184] over the region of parameter space which allow for a rather large Higgs mass corresponding to large λ, (which implies smallish κ and small $\tan\beta$). The minimal fine tuning after the cuts were imposed is below 20, perfectly acceptable by the criterion of Eq. (16), and there are significant areas of low fine tuning remaining to be explored by LHC14.

To infer something about the typical phenomenology of the low fine tuned regions we consider viable points with fine tuning below 100. Similar to the case of the CGNMSSM the viable points have a large supersymmetric singlet mass parameter, leading to heavy singlet states. In detail this constraint comes from the need to achieve acceptable electroweak breaking consistent with the universality of scalar masses at the high scale and is why such boundary conditions are inconsistent with the NMSSM. Allowing for non-universal Higgs masses solves this problem for the MSSM and in the case of the GNMSSM it will allow for lighter singlet states.

In the universal scalar mass case considered here, the singlet states are always heavy and the dominant effect is the change to the Higgs mass that reduces the fine tuning as was found in the CGNMSSM with universal gaugino masses. However, as mentioned above, the region of parameter space of the CGNMSSM that solves the little hierarchy problem has essentially been ruled out by a combination of LHC non-

[10] Very recently it has been pointed out [175] that it is possible to enhance the effect of the second term in Eq. (25) for the case that the singlet field acquires a Dirac rather than a Majorana mass. This also leads to a significant reduction in fine tuning even for a singlet with mass in the multi TeV range.

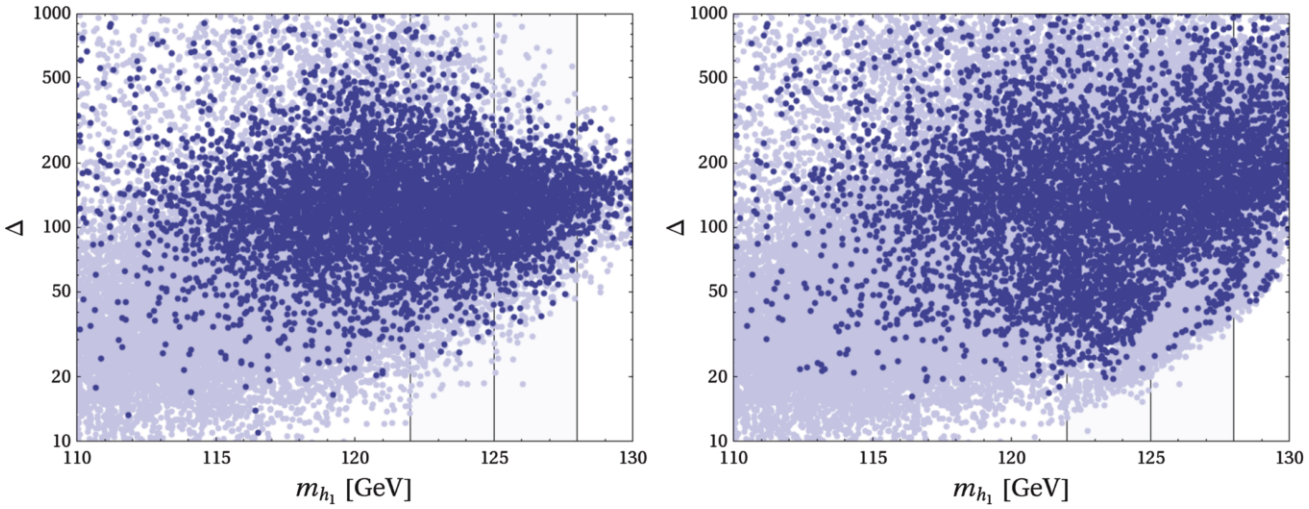

Fig. 6 Dependence of the fine tuning on the lightest Higgs mass in the (C)GNMSSM. The *light blue points* are before any cuts while the *dark blue points* take into account cuts on the SUSY masses and the relic neutralino abundance. The *left* plot is uniform in the density of the input parameters, their density reflects the likelihood for finding a viable point. The *right* plot shows additional points where we zoomed into regions of small fine tuning. The minimal fine tuning after the cuts were imposed is below 20; requiring $a = b = 1$ it is about 80

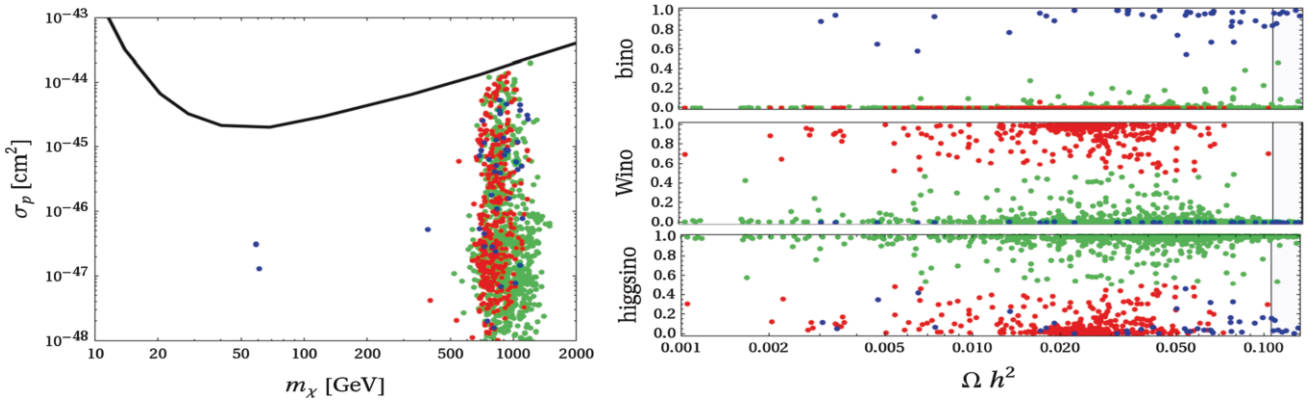

Fig. 7 (i) The dark matter direct detection cross section as a function of the neutralino mass. It has been scaled (i.e. multiplied with (Ωh^2)th$/0.1199$) to account for cases with underabundant neutralinos. Also shown is the latest bound from XENON100. (ii) The dark matter composition, that is, the bino, Wino and Higgsino fraction of the LSP, as a function of the relic density. Mostly bino-like LSPs are shown in *blue*, mostly Wino-like LSPs are shown in *red* and mostly Higgsino-like LSPs are shown in *green*, where *mostly* means a fraction >0.5. (iii) The distribution of bino-, Wino-, and Higgsino-like LSPs in the $a - b$ plane. For all points, in addition to the SUSY and Higgs cuts, a fine tuning $\Delta < 100$ was imposed. The *grey* points are before the fine tuning cut

observation of SUSY and dark matter abundance. For the case of non-universal gaugino masses the situation changes because the LSP can now have significant non-bino component to allow for its efficient annihilation. In Fig. 7 we show the direct detection cross section versus the mass of the lightest neutralino together with the latest bound from XENON100 as well as the dark matter composition as a function of the relic density. As has been observed in previous studies [185,186] of other models, it may be seen that the mass is in the TeV range, most often Higgsino-like. It can be seen that almost all of the points are below the XENON100 direct detection limit. Regarding the composition we see that for the correct relic density or an underabundance the LSP is mainly composed of wino and Higgsino, with typically only a very small bino component. As in the MSSM the correct relic abundance seems to be more easily achieved with a Higgsino-like LSP. Note that, as is the case for all cases involving universal squark and slepton masses [137], it is not possible to significantly reduce the discrepancy of SM to $g - 2$.

In Fig. 8 we show typical masses of the superpartners in the low fine tuned region. It can be seen that points with fine tuning below 100 can have gluino masses beyond 2 TeV and squark masses around 3 TeV. The squarks can be much heavier due to a contribution from m_0. This is limited by the fine tuning implications of a heavy stop unless one is near the scalar focus point. In the CMSSM these points were ruled out by direct dark matter searches as the LSP had signifi-

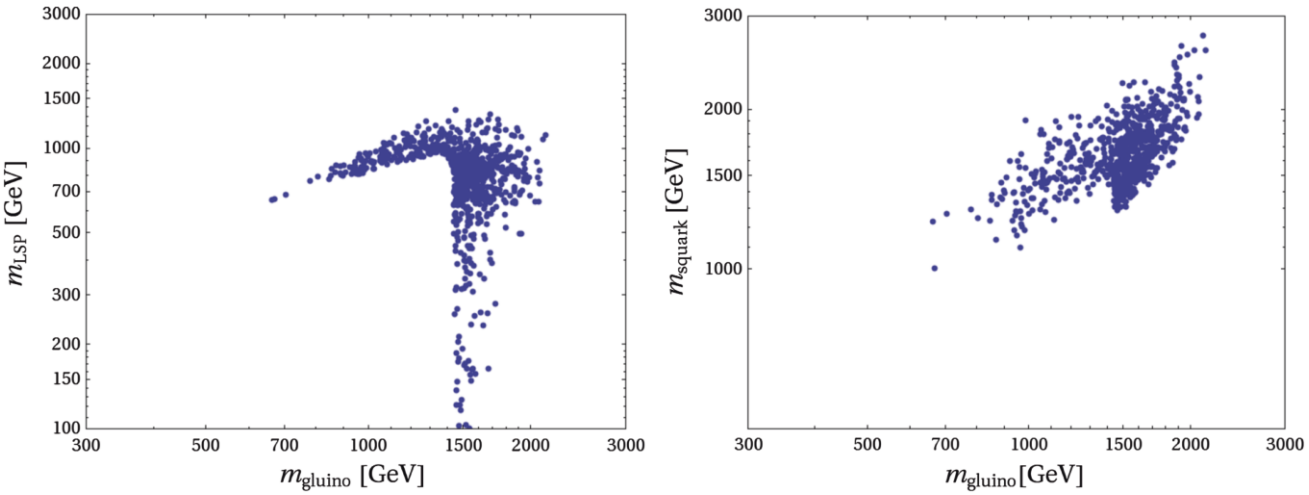

Fig. 8 Mass spectrum of points with fine tuning $\Delta < 100$ and all other cuts imposed

cant Higgsino component but in the case of non-universal gauginos this is no longer true. It is also possible that m_0 is small and the scalar masses are driven by the Gluino and Wino masses. In this case the squark masses will not be much heavier than the gluino although one must worry about sleptons being too light—in particular the neutrino should not be the LSP as this possibility has been ruled out by direct dark matter searches. For the case of heavy squarks the LHC signal is dominantly gluino pair production and decay, but this may be significantly reduced because of the compressed spectrum. Covering the whole of the low fine tuned region will be challenging and will require looking for signals sensitive to compressed spectra [187,188].

4.7 Other approaches

Several other ideas have been suggested to reduce fine tuning. One possibility is that R-parity violation reduces the LHC bounds on SUSY states. This come about because such R-parity violation allows the SUSY state to decay and, if this is dominantly into visible energy, the missing energy signals will be diluted. Of particular interest are the baryon number violating operators $\lambda_{i,j,k} U_i^c D_j^c D_k^c$ that lead to SUSY decay into quarks[11]. Such effects have been widely explored [191–203]; however, a recent analysis [144] concludes that the fine tuning is still very large in these models unless, of course, as discussed above one allows for correlations between MSSM parameters and/or an extension of the MSSM spectrum.

Another way of reducing the fine tuning that has been mentioned in Sect. 3.4 is to lower the scale at which the fundamental parameters are defined. This is the case for gauge mediation where the relevant scale is given by the gauge mediator mass. Detailed analyses of realistic models of general gauge mediation [139,140,204] find that the fine tuning may be reduced by a factor of 2 when the mediation scale is reduced from the GUT scale of $O(10^{16}$ GeV) to a scale of $O(10^6$ GeV). This reduction is quite modest and will still require extensions beyond the MSSM of the form discussed above to achieve acceptable fine tuning.

Finally it has been suggested that one should ignore the fine tuning problem altogether [205–207], perhaps appealing to anthropic arguments to justify the existence of a light Higgs capable of generating the EW breaking scale. Even so a case can be made for an underlying SUSY theory with phenomena accessible to the LHC. The reason is that the SUSY gauginos may be lighter than the underlying SUSY breaking scale due to chiral symmetry (an R-symmetry) broken at a lower scale. In this 'split SUSY' case the SUSY scalars, the squarks and the sleptons, are heavy, beyond the LHC reach, while the gauginos are quite light. The gauginos provide the dominant contribution to the difference in the beta functions between the SUSY case and the SM case and thus the success of SUSY gauge coupling unification is maintained[12]. Further, as for conventional SUSY, if the gauginos are light they can provide a viable dark matter candidate. Split SUSY has been widely studied but, due to lack of space and inclination, we do not discuss it further here.

5 SUSY and flavour physics

As we have seen the LHC results have significantly increased the lower bound on the masses of SUSY states. This in

[11] Through simple discrete symmetries [189,190] such terms can arise without the appearance of lepton number violating operators and unacceptable rates of nucleon decay.

[12] Indeed by adjusting the mass of the heavy SUSY scalars the agreement with the observed gauge couplings can be improved.

turn has implications for flavour physics and it is perhaps timely to re-examine the constraints on SUSY coming from the absence of flavour-changing neutral currents (FCNC) and CP-violating effects [208]. In supersymmetric models flavour-changing and CP-violating effects can be significantly enhanced relative to the SM, driven by processes involving squarks and leptons. In particular such models introduce new sources of CP violation such as the phase of the μ term or of the diagonal A_0 parameters which, if unsuppressed, lead to unacceptable electric dipole moments (EDM)—the SUSY CP problem. They also generate significant contributions to processes such as K^0, $\bar{K}^0$ mixing and $\mu \to e\gamma$.

In the latter case the branching ratio for this process is given by (see, e.g., [209])

$$\mathrm{BR}(\mu \to e\,\gamma) \approx 10^{-6} C \left(\frac{|m^2_{\tilde{\mu}_R \tilde{e}_R}|}{m^2_{\tilde{l}_R}}\right)^2 \left(\frac{100\,\mathrm{GeV}}{m_{\tilde{l}_R}}\right)^4 < 2.4 \times 10^{-12}, \tag{30}$$

and it is very tightly constrained by the recent measurement [210] as can be seen on the right-hand side. Indeed, for $m_{\tilde{l}_R} \sim 100\,\mathrm{GeV}$ the flavour-changing off-diagonal mass term must be very small, $m^2_{\tilde{\mu}_R \tilde{e}_R}/m^2_{\tilde{l}_R} \lesssim 10^{-3}$. Clearly if the lepton mass is above 1 TeV this constraint is weakened considerably.

Similarly, the bounds on EDMs impose strong constraints on the SUSY CP-violating phases. In a simplified approach where all relevant phases are taken to be of the same order ϕ and all soft masses are set to be of the order m_0 the different dipole moments are given by [211,212],

$$\begin{aligned} d_e &\sim 10^{-25} e\,\mathrm{cm} \times \sin\phi \left(\frac{300\,\mathrm{GeV}}{m_0}\right)^2 \left(\frac{\tan\beta}{3}\right) \\ &< 1.05 \times 10^{-27} e\,\mathrm{cm} \\ d_n &\sim 10^{-24} e\,\mathrm{cm} \times \sin\phi \left(\frac{300\,\mathrm{GeV}}{m_0}\right)^2 \left(\frac{\tan\beta}{3}\right) \\ &< 2.9 \times 10^{-26} e\,\mathrm{cm} \\ d_{Hg} &\sim 10^{-26} e\,\mathrm{cm} \times \sin\phi \left(\frac{300\,\mathrm{GeV}}{m_0}\right)^2 \left(\frac{\tan\beta}{3}\right) \\ &< 2.1 \times 10^{-28} e\,\mathrm{cm}, \end{aligned} \tag{31}$$

with the current limits [213–217] given on the right-hand side of the equations, requiring

$$\frac{1}{\sin\phi} \sim 100 \left(\frac{\tan\beta}{3}\right) \left(\frac{300\,\mathrm{GeV}}{m_0}\right)^2 \sim 100 \left(\frac{300\,\mathrm{GeV}}{m_0}\right)^2. \tag{32}$$

Again we see that TeV scale SUSY significantly eases the bound on the CP-violating phase although there is still need for small CP-violating phases, ϕ.

These estimates apply models that have no intrinsic mechanism to solve the flavour problem but the rates are considerably reduced in models in which there is family symmetry to generate viable Yukawa couplings and their related masses and mixing angles. In this case one starts with a CP-invariant theory (compactified 4D theories in string theory often are CP invariant—CP being a discrete relic of the higher dimensional Lorentz group). CP is then spontaneously broken by the familon VEVs that spontaneously break the family symmetry. Via the Froggatt Nielsen mechanism the familions generate the CP-violating Yukawa couplings in the flavour-changing sector where it is observed to be large. CP violation in the flavour conserving sector, where it is small, is driven by the flavour changing couplings and consequently is suppressed by powers of small mixing angles. The resulting models do not realise exact minimal flavour violation (MFV) as the soft A-terms do not have exactly the same structure as the Yukawa couplings and lead to additional FCNC and CP-violating effects. However, these corrections are also suppressed by powers of small mixing angles.

Detailed estimates for various SUSY models of this type have been made [218–220]. As an example of the expected rates we consider a supergravity model with an SU(3) family symmetry that, while unbroken, guarantees the degeneracy of squarks and sleptons in a given representation of the gauge group[13]. CP-violating and flavour-changing couplings are generated when the symmetry is spontaneously broken. Then the rate for $\mu \to e\gamma$ characterised by the mass insertion parameter, $|(\delta^{\ell}_{\mathrm{LR}})_{12}|$ [222–224], is given by

$$|(\delta^{\ell}_{\mathrm{LR}})_{12}| \approx 1 \times 10^{-4} \frac{A_0}{100\,\mathrm{GeV}} \frac{(200\ \mathrm{GeV})^2}{\langle \tilde{m}_l \rangle^2_{\mathrm{LR}}} \frac{10}{\tan\beta} \left(\frac{\bar{\varepsilon}}{0.13}\right)^3 |y_1|\,|x_{123} - x_{23} - x_\Sigma|\,. \tag{33}$$

where $\bar{\epsilon}$ is the expansion parameter determining the mixing in the down quark charged lepton sector [225] (of the order of the Cabibbo angle) and y_1 and $x_{123,23,\Sigma}$ are parameters that are typically of order 1. The parameter y_1 is the coefficient of the leading super potential term generating the lepton mixing and $x_{123,23,\Sigma}$ are the coefficients multiplying the natural magnitudes of the F terms of the familon fields. For the EDM one finds for the relevant mass insertion parameters [218–220]

$$\begin{aligned} |\mathrm{Im}(\delta^u_{\mathrm{LR}})_{11}| &\approx 2 \times 10^{-7} \frac{A_0}{100\,\mathrm{GeV}} \left(\frac{500\,\mathrm{GeV}}{\langle \tilde{m}_u \rangle_{\mathrm{LR}}}\right)^2 \left(\frac{\bar{\varepsilon}}{0.13}\right)^3 \left(\frac{\varepsilon}{0.05}\right)^2 |y^f_1 + y^f_2|\,|x_{123} - x_{23} - x_\Sigma| \sin\phi_1, \\ |\mathrm{Im}(\delta^d_{\mathrm{LR}})_{11}| &\approx 5 \times 10^{-7} \frac{A_0}{100\,\mathrm{GeV}} \left(\frac{500\,\mathrm{GeV}}{\langle \tilde{m}_d \rangle_{\mathrm{LR}}}\right)^2 \left(\frac{\bar{\varepsilon}}{0.13}\right)^5 \frac{10}{\tan\beta} |y^f_1 + y^f_2|\,|x_{123} - x_{23} - x_\Sigma| \sin\phi_1, \end{aligned}$$

[13] For a more general analysis and comparison with MFV expectations, see [221].

$$|\mathrm{Im}(\delta^{\ell}_{\mathrm{LR}})_{11}| \approx 2\times 10^{-7}\frac{A_0}{100\,\mathrm{GeV}}\left(\frac{200\,\mathrm{GeV}}{\langle\tilde{m}_e\rangle_{\mathrm{LR}}}\right)^2\left(\frac{\bar{\varepsilon}}{0.13}\right)^5\frac{10}{\tan\beta}$$
$$|y^f_1+y^f_2|\,|x_{123}-x_{23}-x_{\Sigma}|\sin\phi_1, \quad (34)$$

where ϵ is the expansion parameter determining the mixing in the up quark sector, y^f_i are the analogues of y_1 in the quark sector and ϕ_1 is a CP phase associated with the VEV of the relevant familon field.

The present experimental bound from the non-observation of $\mu\to e\gamma$ is $|(\delta^{\ell}_{\mathrm{LR}})_{12}|\le 10^{-5}$, which is in some tension with this bound, requiring, for example, $\tilde{m}_l = 600\,\mathrm{GeV}$ if the remaining factors in Eq. (33) are of $O(1)$. For the EDMs the most stringent bound comes from mercury and corresponds to $|\mathrm{Im}(\delta^{d}_{\mathrm{LR}})_{11}|<6.7\times 10^{-8}$ and requires $\tilde{m}_d = 1,500\,\mathrm{GeV}$ if the other factors are of $O(1)$.

It is interesting that the SUSY mass scales needed for consistency with the FCNC and CP-violating bounds are close to the increased mass scales needed to accommodate the 125 GeV Higgs mass, suggesting that the experimental limits on CP and FCNC may be quite close to the actual rates[14].

6 Summary and conclusions

The discovery of a Higgs candidate at 126 GeV may be seen as a success for the idea that there is a low-scale SUSY extension of the SM because the Higgs mass lies in the relatively small range favoured by SUSY. Moreover the observed properties of the candidate Higgs are just what are expected of an elementary state whose interactions are in the perturbative domain, as is expected in SUSY with gauge coupling unification. However, there is no doubt that evidence for SUSY is overdue in the sense that the naive expectation is that there should be SUSY partners of SM states with EW scale masses, accessible at LEP. The non-observation, to date, of coloured SUSY states at the LHC has made this discrepancy considerably worse as such states are pushed up to the TeV scale. This discrepancy is exacerbated by the Higgs discovery, as its mass lies at the upper end of the anticipated range and, at least in simple models, requires large radiative corrections to the Higgs mass and the corresponding need for large SUSY breaking parameters. Fits to the simple models, the CMSSM and the CNMSSM, show that they are under considerable pressure with only a very small region of parameter space consistent will all available data including the dark matter abundance and direct dark matter searches.

To sharpen the test of SUSY as a solution to the (little) hierarchy problem it is necessary to quantify the level of fine tuning needed to generate the observed EW scale in the presence of TeV-scale SUSY. Recent work has shown that, for the case that the EW breaking scale is treated as a nuisance variable, the fine tuning measures of fine tuning commonly used can be derived from a likelihood fit of the SUSY model to the present data. The advantage of this is that one can put an upper bound on the fine tuning consistent with an acceptable fit to the data. Applying this to simple SUSY extensions of the SM, namely the CMSSM and the CNMSSM, gives unacceptably large values of fine tuning, confirming the naive expectation. However, this does not mean that the possibility that SUSY solves the little hierarchy problem has already been excluded because it may be that non-minimal implementations of SUSY are not heavily fine-tuned. Fine tuning is strongly dependent both on the nature of the soft SUSY breaking terms and on the spectrum of the particular SUSY extension of the SM and both possibilities have been explored.

As is illustrated by the scalar focus point in the CMSSM and CNMSSM that results from the assumption of degenerate scalars at the initial (unification) scale, correlations between the soft parameters can reduce the fine-tuning substantially. The only other theoretically well-motivated focus point that has been found corresponds to gaugino masses that are non-degenerate at the initial scae so that the gluino and winos are close in mass at the EW scale. Modifying the initial conditions for gaugino masses in the CMSSM and CNMSSM to achieve this does result in a considerable reduction in fine tuning but it is still uncomfortably large.

The effect of a new states beyond those of the MSSM has, for the case these states are very heavy, been explored in a model independent way via the introduction of higher dimension operators. This shows that, even for the mass of the additional states in the multi TeV region, the fine tuning can be substantially reduced, largely by generating an additional contribution to the Higgs mass, reducing the need for very large SUSY breaking terms. The simplest way to generate the operator most significant for the reduction in fine tuning requires the addition of a singlet super field to the MSSM, as in the NMSSM. However, it requires a generalisation of the usual NMSSM through the addition of explicit EW scale mass terms for the Higgsinos and the singlet, something that can be ensured by a discrete R-symmetry. Analysis of this model shows that with the normal constrained initial spectrum the fine tuning is still uncomfortably large but allowing for non-universal gaugino masses there is a substantial region of the parameter space for which the fine-tuning drops to perfectly acceptable level even for squarks and the gluino with masses in the (1–3) TeV region. Indeed the fine tuning is close to the minimum found for the variation of the parameters at a low (EW) scale only, showing that it is possible to achieve such low fine tuning in a UV complete theory that preserves the success of gauge coupling unification. The large mass of

[14] This depends on the $O(1)$ assumption for the values of the x, y parameters. While this is the most natural value there is a mechanism capable of suppressing the rates a bit more, by an extra power of ε in $|\mathrm{Im}(\delta^{u}_{\mathrm{LR}})_{11}|$ and of $\bar{\varepsilon}$ in $|\mathrm{Im}(\delta^{d}_{\mathrm{LR}})_{11}|$ and $|\mathrm{Im}(\delta^{l}_{\mathrm{LR}})_{11}|$, respectively (for further details see [220]).

the coloured SUSY states, together with the fact that often the low fine tuned spectra are considerable compressed, corresponding to low E_T missing signals, means that it may be difficult to test the model fully even at LHC14. Dark matter can be consistent with the WMAP bounds and direct detection limits, the expectation of all the models analysed being that the LSP should be heavy, of $O(1\ \text{TeV})$, and most often with a substantial Higgsino component. However, the scattering cross section can be very low so that the low fine tuned region will not be fully tested even by XENON1T.

An associated effect of the increased bound on the SUSY masses is that the constraints from flavour-changing neutral currents and CP violation are significantly reduced. It is still necessary that the new CP-violating phases associated with the flavour singlet sector be small but this can be readily done in models with an underlying family symmetry. However, this provides only a relatively modest suppression and the expectation is that processes such as $\mu \to e\gamma$ and electric dipole moments will be close to their present limits.

References

1. G. Aad et al., ATLAS Collaboration, Phys. Lett. B **716**, 1 (2012). [arXiv:1207.7214 [hep-ex]]
2. S. Chatrchyan et al., CMS Collaboration, Phys. Lett. B **716**, 30 (2012). [arXiv:1207.7235 [hep-ex]]
3. V.D. Barger, M.S. Berger, P. Ohmann, Phys. Rev. D **49**, 4908 (1994). [arXiv:hep-ph/9311269]
4. W. de Boer, R. Ehret, D.I. Kazakov, Z. Phys, C **67**, 647 (1995). [arXiv:hep-ph/9405342]
5. M. Carena, J.R. Ellis, A. Pilaftsis, C.E. Wagner, Nucl. Phys. B **625**, 345 (2002). [arXiv:hep-ph/0111245]
6. H.E. Haber, R. Hempfling, Phys. Rev. Lett. **66**, 1815 (1991)
7. J.R. Ellis, G. Ridolfi, F. Zwirner, Phys. Lett. B **257**, 83 (1991)
8. Y. Okada, M. Yamaguchi, T. Yanagida, Prog. Theor. Phys. **85**, 1 (1991)
9. M. Drees, M.M. Nojiri, Phys. Rev. D **47**, 376 (1993). [arXiv:hep-ph/9207234]
10. H. Baer, M. Brhlik, Phys. Rev. D **53**, 597 (1996). [arXiv:hep-ph/9508321]
11. H. Baer, M. Brhlik, Phys. Rev. D **57**, 567 (1998). [arXiv:hep-ph/9706509]
12. H. Baer, M. Brhlik, M.A. Diaz, J. Ferrandis, P. Mercadante, P. Quintana, X. Tata, Phys. Rev. D **63**, 015007 (2001). [arXiv:hep-ph/0005027]
13. G.L. Kane, C.F. Kolda, L. Roszkowski, J.D. Wells, Phys. Rev. D **49**, 6173 (1994). [arXiv:hep-ph/9312272]
14. J.R. Ellis, T. Falk, K.A. Olive, M. Schmitt, Phys. Lett. B **388**, 97 (1996). [arXiv:hep-ph/9607292]
15. J.R. Ellis, T. Falk, K.A. Olive, M. Schmitt, Phys. Lett. B **413**, 355 (1997). [arXiv:hep-ph/9705444]
16. J.R. Ellis, T. Falk, G. Ganis, K.A. Olive, M. Schmitt, Phys. Rev. D **58**, 095002 (1998). [arXiv:hep-ph/9801445]
17. V.D. Barger, C. Kao, Phys. Rev. D **57**, 3131 (1998). [arXiv:hep-ph/9704403]
18. J.R. Ellis, T. Falk, G. Ganis, K.A. Olive, Phys. Rev. D **62**, 075010 (2000). [arXiv:hep-ph/0004169]
19. J.R. Ellis, T. Falk, G. Ganis, K.A. Olive, M. Srednicki, Phys. Lett. B **510**, 236 (2001). [arXiv:hep-ph/0102098]
20. V.D. Barger, C. Kao, Phys. Lett. B **518**, 117 (2001). [arXiv:hep-ph/0106189]
21. L. Roszkowski, R. Ruiz de Austri, T. Nihei, JHEP **0108**, 024 (2001). [arXiv:hep-ph/0106334]
22. A. Djouadi, M. Drees, J.L. Kneur, JHEP **0108**, 055 (2001). [arXiv:hep-ph/0107316]
23. U. Chattopadhyay, A. Corsetti, P. Nath, Phys. Rev. D **66**, 035003 (2002). [arXiv:hep-ph/0201001]
24. J.R. Ellis, K.A. Olive, Y. Santoso, New J. Phys. **4**, 32 (2002). [arXiv:hep-ph/0202110]
25. H. Baer, C. Balazs, A. Belyaev, J.K. Mizukoshi, X. Tata, Y. Wang, JHEP **0207**, 050 (2002). [arXiv:hep-ph/0205325]
26. R. Arnowitt, B. Dutta [arXiv:hep-ph/0211417]
27. J.R. Ellis, K.A. Olive, Y. Santoso, V.C. Spanos, Phys. Lett. B **565**, 176 (2003). [arXiv:hep-ph/0303043]
28. H. Baer, C. Balazs, JCAP **0305**, 006 (2003). [arXiv:hep-ph/0303114]
29. A.B. Lahanas, D.V. Nanopoulos, Phys. Lett. B **568**, 55 (2003). [arXiv:hep-ph/0303130]
30. U. Chattopadhyay, A. Corsetti, P. Nath, Phys. Rev. D **68**, 035005 (2003). [arXiv:hep-ph/0303201]
31. C. Munoz, Int. J. Mod. Phys. A **19**, 3093 (2004). [arXiv:hep-ph/0309346]
32. R. Arnowitt, B. Dutta, B. Hu [arXiv:hep-ph/0310103]
33. J. Ellis, K. A. Olive, in *Particle dark matter*, ed. by G. Bertone, pp. 142–163 [arXiv:1001.3651 [astro-ph.CO]]
34. O. Buchmueller et al. [arXiv:1207.7315 [hep-ph]]
35. C. Strege, G. Bertone, D.G. Cerdeno, M. Fornasa, R.R. de Austri, R. Trotta, JCAP **1203**, 030 (2012). [arXiv:1112.4192 [hep-ph]]
36. P. Bechtle, T. Bringmann, K. Desch, H. Dreiner, M. Hamer, C. Hensel, M. Kramer, N. Nguyen et al., JHEP **1206**, 098 (2012). [arXiv:1204.4199 [hep-ph]]
37. A. Fowlie, M. Kazana, K. Kowalska, S. Munir, L. Roszkowski, E. M. Sessolo, S. Trojanowski, Y. -L. S. Tsai [arXiv:1206.0264 [hep-ph]]
38. T. Li, J. A. Maxin, D. V. Nanopoulos, J. W. Walker [arXiv:1206.2633 [hep-ph]]
39. O. Buchmueller et al., Eur. Phys. J. C **72**, 2020 (2012). [arXiv:1112.3564 [hep-ph]]
40. H. Baer, V. Barger, A. Mustafayev, Phys. Rev. D **85**, 075010 (2012). [arXiv:1112.3017 [hep-ph]]
41. J.L. Feng, K.T. Matchev, D. Sanford, Phys. Rev. D **85**, 075007 (2012). [arXiv:1112.3021 [hep-ph]]
42. T. Li, J.A. Maxin, D.V. Nanopoulos, J.W. Walker, Phys. Lett. B **710**, 207 (2012). [arXiv:1112.3024 [hep-ph]]
43. S. Heinemeyer, O. Stal, G. Weiglein, Phys. Lett. B **710**, 201 (2012). [arXiv:1112.3026 [hep-ph]]
44. A. Arbey, M. Battaglia, A. Djouadi, F. Mahmoudi, J. Quevillon, Phys. Lett. B **708**, 162 (2012). [arXiv:1112.3028 [hep-ph]]
45. P. Draper, P. Meade, M. Reece, D. Shih, Phys. Rev. D **85**, 095007 (2012). [arXiv:1112.3068 [hep-ph]]
46. S. Akula, B. Altunkaynak, D. Feldman, P. Nath, G. Peim, Phys. Rev. D **85**, 075001 (2012). [arXiv:1112.3645 [hep-ph]]
47. M. Kadastik, K. Kannike, A. Racioppi, M. Raidal, JHEP **1205**, 061 (2012). [arXiv:1112.3647 [hep-ph]]
48. J. Cao, Z. Heng, D. Li, J.M. Yang, Phys. Lett. B **710**, 665 (2012). [arXiv:1112.4391 [hep-ph]]

49. L. Aparicio, D.G. Cerdeno, L.E. Ibanez, JHEP **1204**, 126 (2012). [arXiv:1202.0822 [hep-ph]]
50. H. Baer, V. Barger, A. Mustafayev, JHEP **1205**, 091 (2012). [arXiv:1202.4038 [hep-ph]]
51. C. Balazs, A. Buckley, D. Carter, B. Farmer, M. White [arXiv: 1205.1568 [hep-ph]]
52. D. Ghosh, M. Guchait, S. Raychaudhuri, D. Sengupta, Phys. Rev. D **86**, 055007 (2012). [arXiv:1205.2283 [hep-ph]]
53. J. Ellis, K.A. Olive, Eur. Phys. J. C **72**, 2005 (2012). [arXiv:1202. 3262 [hep-ph]]
54. J. Ellis, F. Luo, K.A. Olive, P. Sandick, Eur. Phys. J. C **73**, 2403 (2013). [arXiv:1212.4476 [hep-ph]]
55. A. Djouadi, L. Maiani, G. Moreau, A. Polosa, J. Quevillon, V. Riquer [arXiv:1307.5205 [hep-ph]]
56. C. Beskidt, W. de Boer, D. I. Kazakov [arXiv:1308.1333 [hep-ph]]
57. S. Zheng, Y. Yu, JHEP **1308**, 031 (2013). [arXiv:1303.1900 [hep-ph]]
58. P. Bechtle, S. Heinemeyer, O. Stal, T. Stefaniak, G. Weiglein, L. Zeune, Eur. Phys. J. C **73**, 2354 (2013). [arXiv:1211.1955 [hep-ph]]
59. M. Kramer, P. Bechtle, K. Desch, H.K. Dreiner, B. O'Leary, C. Robens, B. Sarrazin, P. Wienemann, Frascati Phys. Ser. **54**, 258 (2012)
60. ATLAS Collaboration. https://cdsweb.cern.ch/record/1432199/files/ATLAS-CONF-2012-033.pdf; https://cdsweb.cern.ch/record/1472710/files/ATLAS-CONF-2012-109.pdf
61. CMS Collaboration, S. Chatrchyan et al., JHEP **1210**, 018 (2012). [arXiv:1207.1798 [hep-ex]]; [arXiv:1207.1898 [hep-ex]]
62. E. Komatsu et al., WMAP Collaboration, Astrophys. J. Suppl. **192**, 18 (2011). [arXiv:1001.4538 [astro-ph.CO]]
63. E. Aprile et al., XENON100 Collaboration, Phys. Rev. Lett. **107**, 131302 (2011). [arXiv:1104.2549 [astro-ph.CO]]
64. S. Chen et al., CLEO Collaboration, Phys. Rev. Lett. **87**, 251807 (2001). [arXiv:hep-ex/0108032]
65. P. Koppenburg et al., Belle Collaboration, Phys. Rev. Lett. **93**, 061803 (2004). [arXiv:hep-ex/0403004]
66. B. Aubert et al., BaBar Collaboration [arXiv:hep-ex/0207076]
67. E. Barberio et al., Heavy Flavor Averaging, Group (HFAG) [arXiv: hep-ex/0603003]
68. G. Aad et al., ATLAS Collaboration, Phys. Lett. B **713**, 387 (2012). [arXiv:1204.0735 [hep-ex]]
69. T. Aaltonen et al., CDF Collaboration, Phys. Rev. Lett. **107**, 239903 (2011). [Phys. Rev. Lett. 107, 191801 (2011)] [arXiv: 1107.2304 [hep-ex]]
70. S. Chatrchyan et al., CMS Collaboration, Phys. Rev. Lett. **107**, 191802 (2011). [arXiv:1107.5834 [hep-ex]]
71. R. Aaij et al., LHCb Collaboration, Phys. Lett. B **699**, 330 (2011). [arXiv:1103.2465 [hep-ex]]; [arXiv:1203.4493 [hep-ex]]
72. For an official combination of the ATLAS, CMS and LHCb results, see: ATLAS, CMS, and LHCb Collaborations. http://cdsweb.cern.ch/record/1452186/files/LHCb-CONF-2012-017.pdf
73. LHCb Collaboration, R. Aaij et al., Phys. Rev. Lett. **110**, 021801 (2013). [arXiv:1211.2674 [Unknown]]
74. The Muon g-2 Collaboration, Phys. Rev. Lett. **92**, 161802 (2004). [hep-ex/0401008]
75. G. Bennett et al., The Muon g-2 Collaboration. Phys. Rev. D **73**, 072003 (2006). [arXiv:hep-ex/0602035]
76. G. Abbiendi et al., OPAL Collaboration. Eur. Phys. J. **C35**, 1–20 (2004). [hep-ex/0401026]
77. A. Fowlie, M. Kazana, K. Kowalska, S. Munir, L. Roszkowski, E.M. Sessolo, S. Trojanowski, Y.-L.S. Tsai, Phys. Rev. D **86**, 075010 (2012). [arXiv:1206.0264 [hep-ph]]
78. C. Strege, G. Bertone, F. Feroz, M. Fornasa, R. Ruiz de Austri, R. Trotta, JCAP **1304**, 013 (2013). [arXiv:1212.2636 [hep-ph]]
79. Information about this code is available from K. A. Olive: it contains important contributions from T. Falk, A. Ferstl, F. Luo, G. Ganis, A. Mustafayev, J. McDonald, K. A. Olive, P. Sandick, Y. Santoso, V. Spanos, and M. Srednicki
80. H. Baer, A. Mustafayev, S. Profumo, A. Belyaev, X. Tata, Phys. Rev. D **71**, 095008 (2005). [arXiv:hep-ph/0412059]
81. H. Baer, A. Mustafayev, S. Profumo, A. Belyaev, X. Tata, JHEP **0507**, 065 (2005). [hep-ph/0504001]
82. J.R. Ellis, K.A. Olive, P. Sandick, Phys. Rev. D **78**, 075012 (2008). [arXiv:0805.2343 [hep-ph]]
83. J. Ellis, K. Olive, Y. Santoso, Phys. Lett. B **539**, 107 (2002). [arXiv: hep-ph/0204192]
84. J.R. Ellis, T. Falk, K.A. Olive, Y. Santoso, Nucl. Phys. B **652**, 259 (2003). [arXiv:hep-ph/0210205]
85. D. Matalliotakis, H.P. Nilles, Nucl. Phys. B **435**, 115 (1995). [arXiv:hep-ph/9407251]
86. M. Olechowski, S. Pokorski, Phys. Lett. B **344**, 201 (1995). [arXiv:hep-ph/9407404]
87. V. Berezinsky, A. Bottino, J. Ellis, N. Fornengo, G. Mignola, S. Scopel, Astropart. Phys. **5**, 1 (1996). [hep-ph/9508249]
88. M. Drees, M. Nojiri, D. Roy, Y. Yamada, Phys. Rev. D **56**, 276 (1997) [Erratum-ibid. D 64 (1997) 039901] [hep-ph/9701219]
89. M. Drees, Y. Kim, M. Nojiri, D. Toya, K. Hasuko, T. Kobayashi, Phys. Rev. D **63**, 035008 (2001). [hep-ph/0007202]
90. P. Nath, R. Arnowitt, Phys. Rev. D **56**, 2820 (1997). [hep-ph/9701301]
91. A. Bottino, F. Donato, N. Fornengo, S. Scopel, Phys. Rev. D **63**, 125003 (2001). [hep-ph/0010203]
92. S. Profumo, Phys. Rev. D **68**, 015006 (2003). [hep-ph/0304071]
93. D. Cerdeno, C. Munoz, JHEP **0410**, 015 (2004). [hep-ph/0405057]
94. U. Ellwanger, C. Hugonie, A. M. Teixeira, Phys. Rep. **496**, 1–77 (2010). [arXiv:0910.1785 [hep-ph]]
95. M. Maniatis, Int. J. Mod. Phys. **A25**, 3505–3602 (2010). [arXiv: 0906.0777 [hep-ph]]
96. U. Ellwanger, JHEP **1203**, 044 (2012). [arXiv:1112.3548 [hep-ph]]
97. U. Ellwanger, C. Hugonie, Adv. High Energy Phys. **2012**, 625389 (2012). [arXiv:1203.5048 [hep-ph]]
98. S. King, M. Muhlleitner, R. Nevzorov, Nucl. Phys. B **860**, 207–244 (2012). [arXiv:1201.2671 [hep-ph]]
99. J. Cao et al., JHEP **1203**, 086 (2012). [arXiv:1202.5821 [hep-ph]]
100. D.A. Vasquez, G. Belanger, C. Boehm, J. Da Silva, P. Richardson et al., Phys. Rev. D **86**, 035023 (2012). [arXiv:1203.3446 [hep-ph]]
101. J. Rathsman, T. Rossler, Adv. High Energy Phys. **2012**, 853706 (2012). [arXiv:1206.1470 [hep-ph]]
102. D. Das, U. Ellwanger, P. Mitropoulos, JCAP **1208**, 003 (2012). [arXiv:1206.2639 [hep-ph]]
103. J.F. Gunion, Y. Jiang, S. Kraml, Phys. Rev. D **86**, 071702 (2012). [arXiv:1207.1545 [hep-ph]]
104. J.F. Gunion, Y. Jiang, S. Kraml, Phys. Rev. Lett. **110**, 051801 (2013). [arXiv:1208.1817 [hep-ph]]
105. R. Benbrik, M. Gomez, Bock, S. Heinemeyer, O. Stal, G. Weiglein, et al., Eur. Phys. J. **C72**, 2171 (2012). [arXiv:1207.1096 [hep-ph]]
106. K. J. Bae, K. Choi, E. J. Chun, S. H. Im, C. B. Park, et al., JHEP **1211**, 118 (2012). [arXiv:1208.2555 [hep-ph]]
107. Z. Kang, T. Li, J. Li, Y. Liu [arXiv:1208.2673 [hep-ph]]
108. T. Cheng, J. Li, T. Li, X. Wan, Y. K. Wang et al. [arXiv:1207.6392 [hep-ph]]
109. M. Perelstein, B. Shakya [arXiv:1208.0833 [hep-ph]]
110. G. Belanger, U. Ellwanger, J. Gunion, Y. Jiang, S. Kraml [arXiv: 1208.4952 [hep-ph]]
111. J. Cao, Z. Heng, J. M. Yang, J. Zhu, JHEP **1210**, 079 (2012). [arXiv:1207.3698 [hep-ph]]

112. G. Chalons, F. Domingo, Phys. Rev. D **86**, 115024 (2012). [arXiv: 1209.6235 [hep-ph]]
113. G. Belanger, U. Ellwanger, J. F. Gunion, Y. Jiang, S. Kraml, et al., JHEP **1301**, 069 (2013). [arXiv:1210.1976 [hep-ph]]
114. I. Gogoladze, B. He, Q. Shafi, Phys. Lett. B **718**, 1008–1013 (2013). [arXiv:1209.5984 [hep-ph]]
115. D.E. Lopez-Fogliani, J. Phys. Conf. Ser. **384**, 012014 (2012)
116. J. F. Gunion, Y. Jiang, S. Kraml, Phys. Lett. B **710**, 454–459 (2012). [arXiv:1201.0982 [hep-ph]]
117. J. Cao, F. Ding, C. Han, J. M. Yang, J. Zhu [arXiv:1309.4939 [hep-ph]]
118. K. Kowalska, S. Munir, L. Roszkowski, E.M. Sessolo, S. Trojanowski, Y.-L.S. Tsai, Phys. Rev. D **87**, 115010 (2013). [arXiv: 1211.1693 [hep-ph]]
119. G.L. Kane, S.F. King, Phys. Lett. B **451**, 113 (1999). [hep-ph/ 9810374]
120. K.L. Chan, U. Chattopadhyay, P. Nath, Phys. Rev. D **58**, 096004 (1998). [arXiv:hep-ph/9710473]
121. J.L. Feng, K.T. Matchev, T. Moroi, Phys. Rev. Lett. **84**, 2322 (2000). [hep-ph/9908309]
122. J.L. Feng, K.T. Matchev, T. Moroi, Phys. Rev. D **61**, 075005 (2000). [hep-ph/9909334]
123. J.L. Feng, K.T. Matchev, F. Wilczek, Phys. Rev. D **63**, 045024 (2001). [astro-ph/0008115]
124. J.L. Feng, K.T. Matchev, D. Sanford, Phys. Rev. D **85**, 075007 (2012). [arXiv:1112.3021 [hep-ph]]
125. J.R. Ellis, K. Enqvist, D.V. Nanopoulos, F. Zwirner, Mod. Phys. Lett. **A1**, 57 (1986)
126. R. Barbieri, G.F. Giudice, Nucl. Phys. B **306**, 63 (1988)
127. D.M. Ghilencea, G.G. Ross, Nucl. Phys. B **868**, 65 (2013). [arXiv: 1208.0837 [hep-ph]]
128. D. M. Ghilencea [arXiv:1302.5262 [hep-ph]]
129. PoS Corfu 2012, 034 (2013). [arXiv:1304.1193 [hep-ph]]
130. M.E. Cabrera, J.A. Casas, R. Ruiz de Austri, JHEP **0903**, 075 (2009). [arXiv:0812.0536 [hep-ph]]
131. C.H. Llewellyn Smith, G. G. Ross. Phys. Lett. B **105**, 38 (1981)
132. G. Marques Tavares, M. Schmaltz, W. Skiba [arXiv:1308.0025 [hep-ph]]
133. H. Baer, V. Barger, P. Huang, D. Mickelson, A. Mustafayev, W. Sreethawong, X. Tata [arXiv:1306.3148 [hep-ph]]
134. H. Baer, V. Barger, P. Huang, A. Mustafayev, X. Tata, Phys. Rev. Lett. **109**, 161802 (2012). [arXiv:1207.3343 [hep-ph]]
135. H. Baer, V. Barger, P. Huang, D. Mickelson, A. Mustafayev, X. Tata, Phys. Rev. D **87**, 115028 (2013). [arXiv:1212.2655 [hep-ph]]
136. H. Baer, V. Barger, P. Huang, D. Mickelson, A. Mustafayev, X. Tata [arXiv:1306.2926 [hep-ph]]
137. D.M. Ghilencea, H.M. Lee, M. Park, JHEP **1207**, 046 (2012). [arXiv:1203.0569 [hep-ph]]
138. S. Cassel, D.M. Ghilencea, S. Kraml, A. Lessa, G.G. Ross, JHEP **1105**, 120 (2011). [arXiv:1101.4664 [hep-ph]]
139. S. Abel, M.J. Dolan, J. Jaeckel, V.V. Khoze, JHEP **1012**, 049 (2010). [arXiv:1009.1164 [hep-ph]]
140. S. Abel, M.J. Dolan, J. Jaeckel, V.V. Khoze, JHEP **0912**, 001 (2009). [arXiv:0910.2674 [hep-ph]]
141. S. Dimopoulos, G. Giudice, Phys. Lett. B **357**, 573–578 (1995). [hep-ph/9507282]
142. A.G. Cohen, D. Kaplan, A. Nelson, Phys. Lett. B **388**, 588–598 (1996). [hep-ph/9607394]
143. E. Hardy [arXiv:1306.1534 [hep-ph]]
144. A. Arvanitaki, M. Baryakhtar, X. Huang, K. Van Tilburg, G. Villadoro [arXiv:1309.3568 [hep-ph]]
145. D. Horton, G. Ross, Nucl. Phys. B830 (2010), 221–247, [0908.0857] K. Choi, K. S. Jeong, T. Kobayashi, and K.-I. Okumura. Phys. Lett. B **633**, 355–361 (2006). [hep-ph/0508029]
146. K. Choi, K.S. Jeong, T. Kobayashi, K.-I. Okumura. Phys. Lett. B **633**, 355–361 (2006). [hep-ph/0508029]
147. K. Choi, K.S. Jeong, T. Kobayashi, K.-I. Okumura, Phys. Rev. D **75**, 095012 (2007). [hep-ph/0612258]
148. H. Abe, T. Kobayashi, Y. Omura, Phys. Rev. D **76**, 015002 (2007). [hep-ph/0703044]
149. O. Lebedev, H.P. Nilles, M. Ratz, *(2005), 211–221, hep-ph/0511320* (M. Asano and T, Higaki, 2012). 1204.0508
150. M. Asano, T. Higaki (2012). [1204.0508]
151. S. Antusch, L. Calibbi, V. Maurer, M. Monaco, M. Spinrath, JHEP **01**, 187 (2013). [1207.7236]
152. H. Abe, J. Kawamura, H. Otsuka, PTEP **2013**, 013B02 (2013). [1208.5328]
153. M. Badziak, S. Krippendorf, H.P. Nilles, M.W. Winkler, JHEP **1303**, 094 (2013). [1212.0854]
154. I. Gogoladze, F. Nasir, Q. Shafi, Int. J. Mod. Phys. **A 28**, 1350046 (2013). [1212.2593]
155. T.T. Yanagida, N. Yokozaki, Phys. Lett. **B 722**, 355–359 (2013). [1301.1137]
156. L. Roszkowski, M.A. Shifman, Phys. Rev. D **53**, 404 (1996). [hep-ph/9503358]
157. S.P. Martin, Phys. Rev. D **79**, 095019 (2009). [0903.3568]
158. A. Brignole, L.E. Ibanez, C. Munoz, Nucl. Phys. B **422**, 125–171 (1994). [hep-ph/9308271]
159. K. Choi, K.S. Jeong, T. Kobayashi, K.-I. Okumura, Phys. Lett. B **633**, 355–361 (2006). [hep-ph/0508029]
160. O. Lebedev, H. P. Nilles, M. Ratz, 211–221 (2005). [hep-ph/ 0511320]
161. K. Choi, H.P. Nilles, JHEP **0704**, 006 (2007). [hep-ph/0702146]
162. W. Cho, Y. Kim, K. Lee, C. Park, Y. Shimizu, JHEP **0704**, 054 (2007). [hep-ph/0703163]
163. K. Choi, K.S. Jeong, K.-I. Okumura, JHEP **0509**, 039 (2005). [hep-ph/0504037]
164. M. Badziak, S. Krippendorf, H.P. Nilles, M.W. Winkler, JHEP **1303**, 094 (2013). [1212.0854]
165. S. Antusch, L. Calibbi, V. Maurer, M. Monaco, M. Spinrath, JHEP **01**, 187 (2013). [1207.7236]
166. I. Antoniadis, E. Dudas, D.M. Ghilencea, P. Tziveloglou, Nucl. Phys. B **848**, 1 (2011). [arXiv:1012.5310 [hep-ph]]
167. I. Antoniadis, E. Dudas, D.M. Ghilencea, P. Tziveloglou, Nucl. Phys. B **831**, 133 (2010). [arXiv:0910.1100 [hep-ph]]
168. I. Antoniadis, E. Dudas, D.M. Ghilencea, P. Tziveloglou, Nucl. Phys. B **808**, 155 (2009). [arXiv:0806.3778 [hep-ph]]
169. D. Piriz, J. Wudka, Phys. Rev. D **56**, 4170 (1997). [hep-ph/ 9707314]
170. S.P. Martin, Phys. Rev. D **61**, 035004 (2000). [hep-ph/9907550]
171. R. Barbieri, A. Strumia, Phys. Lett. B **462**, 144 (1999). [hep-ph/ 9905281]
172. M. Dine, N. Seiberg, S. Thomas, Phys. Rev. D **76**, 095004 (2007). [arXiv:0707.0005 [hep-ph]]
173. J. A. Casas, J. R. Espinosa. I. Hidalgo [hep-ph/0402017]
174. S. Cassel, D.M. Ghilencea, G.G. Ross, Nucl. Phys. B **825**, 203–221 (2010). [0903.1115]
175. X. Lu, H. Murayama, J. T. Ruderman, K. Tobioka [arXiv:1308. 0792 [hep-ph]]
176. H.M. Lee, S. Raby, M. Ratz, G.G. Ross, R. Schieren, K. Schmidt-Hoberg, P.K.S. Vaudrevange, Phys. Lett. B **694**, 491 (2011). [arXiv:1009.0905 [hep-ph]]
177. H.M. Lee, S. Raby, M. Ratz, G.G. Ross, R. Schieren, K. Schmidt-Hoberg, P.K.S. Vaudrevange, Nucl. Phys. B **850**, 1 (2011). [arXiv: 1102.3595 [hep-ph]]
178. G.G. Ross, K. Schmidt-Hoberg, Nucl. Phys. B **862**, 710 (2012). [arXiv:1108.1284 [hep-ph]]
179. G. G. Ross, K. Schmidt-Hoberg, F. Staub, JHEP **1208**, 074 (2012). [arXiv:1205.1509 [hep-ph]]

180. A. Delgado, C. Kolda, A. de la Puente, Phys. Lett. B **710**, 460 (2012). [arXiv:1111.4008 [hep-ph]]
181. A. Delgado, C. Kolda, J.P. Olson, A. de la Puente, Phys. Rev. Lett. **105**, 091802 (2010). [arXiv:1005.1282 [hep-ph]]
182. A. Delgado, C. Kolda, J.P. Olson, A. de la Puente, Phys. Rev. D **82**, 035006 (2010). [arXiv:1005.4901 [hep-ph]]
183. L.J. Hall, D. Pinner, J.T. Ruderman, JHEP **1204**, 131 (2012). [arXiv:1112.2703 [hep-ph]]
184. A. Kaminska, G. G. Ross, K. Schmidt-Hoberg [arXiv:1308.4168 [hep-ph]]
185. L. Roszkowski, R. Ruiz de Austri, R. Trotta, Y.-L.S. Tsai, T.A. Varley, Phys. Rev. D **83**, 015014 (2011). [arXiv:0903.1279 [hep-ph]]
186. S. Akula, P. Nath, G. Peim, Phys. Lett. B **717**, 188 (2012). [arXiv:1207.1839 [hep-ph]]
187. T.J. LeCompte, S.P. Martin, Phys. Rev. D **84**, 015004 (2011). [arXiv:1105.4304 [hep-ph]]
188. H.K. Dreiner, M. Kramer, J. Tattersall, Europhys. Lett. **99**, 61001 (2012). [arXiv:1207.1613 [hep-ph]]
189. L.E. Ibanez, G.G. Ross, Nucl. Phys. B **368**, 3 (1992)
190. H.K. Dreiner, C. Luhn, M. Thormeier, Phys. Rev. D **73**, 075007 (2006). [hep-ph/0512163]
191. J. A. Evans, Y. Kats [arXiv:1209.0764]
192. Z. Han, A. Katz, M. Son, B. Tweedie [arXiv:1211.4025]
193. B. Allanach, B. Gripaios, JHEP **1205**, 062 (2012). [arXiv:1202.6616]
194. C. Brust, A. Katz, R. Sundrum, JHEP **1208**, 059 (2012). [arXiv:1206.2353]
195. CMS Collaboration Collaboration, S. Chatrchyan et al., Phys. Lett. B **718**, 329–347 (2012). [arXiv:1208.2931]
196. ATLAS Collaboration Collaboration, G. Aad et al., JHEP **1212**, 086 (2012). [arXiv:1210.4813]
197. B. Bhattacherjee, J. L. Evans, M. Ibe, S. Matsumoto, T. T. Yanagida [arXiv:1301.2336]
198. R. Franceschini, R. Mohapatra, JHEP **1304**, 098 (2013). [arXiv:1301.3637]
199. ALEPH Collaboration Collaboration, A. Heister et al., Eur. Phys. J. **C31**, 1–16 (2003). [hep-ex/0210014]
200. H.K. Dreiner, S. Grab, AIP Conf. Proc. **1200**, 358 (2010). [arXiv:0909.5407 [hep-ph]]
201. K. Desch, S. Fleischmann, P. Wienemann, H.K. Dreiner, S. Grab, Phys. Rev. D **83**, 015013 (2011). [arXiv:1008.1580 [hep-ph]]
202. H.K. Dreiner, T. Stefaniak, Phys. Rev. D **86**, 055010 (2012). [arXiv:1201.5014 [hep-ph]]
203. H.K. Dreiner, F. Staub, A. Vicente, W. Porod, Phys. Rev. D **86**, 035021 (2012). [arXiv:1205.0557 [hep-ph]]
204. T. Kobayashi, Y. Nakai, R. Takahashi, JHEP **1001**, 003 (2010). [arXiv:0910.3477 [hep-ph]]
205. N. Arkani-Hamed, S. Dimopoulos, JHEP **0506**, 073 (2005). [hep-th/0405159]
206. N. Arkani-Hamed, S. Dimopoulos, G.F. Giudice, A. Romanino, Nucl. Phys. B **709**, 3 (2005). [hep-ph/0409232]
207. G. F. Giudice and A. Romanino, Nucl. Phys. B **699**, 65 (2004) [Erratum-ibid. B 706 (2005) 65] [hep-ph/0406088]
208. J. Jaeckel, V.V. Khoze, JHEP **1211**, 115 (2012). [arXiv:1205.7091 [hep-ph]]
209. S. P. Martin, A supersymmetry primer, in *Perspectives on supersymmetry II*, ed. by G.L. Kane, pp. 1–153 [hep-ph/9709356]
210. J. Adam et al., MEG Collaboration. Phys. Rev. Lett. **107**, 171801 (2011). [arXiv:1107.5547 [hep-ex]]
211. S. Abel, S. Khalil, O. Lebedev, Nucl. Phys. B **606**, 151 (2001). [hep-ph/0103320]
212. S. Abel, O. Lebedev, JHEP **0601**, 133 (2006). [hep-ph/0508135]
213. M. Raidal, A. van der Schaaf, I. Bigi, M.L. Mangano, Y.K. Semertzidis, S. Abel, S. Albino, S. Antusch et al., Eur. Phys. J. C **57**, 13 (2008). [arXiv:0801.1826 [hep-ph]]
214. I. de Medeiros Varzielas, G. G. Ross [hep-ph/0612220]
215. J. J. Hudson, D. M. Kara, I. J. Smallman, B. E. Sauer, M. R. Tarbutt, E. A. Nature, **473**, 493 (2011)
216. C. A. Baker, D. D. Doyle, P. Geltenbort, K. Green, M. G. D. van der Grinten, P. G. Harris, P. Iaydjiev, S. N. Ivanov et al., Phys. Rev. Lett. **97**, 131801 (2006) [hep-ex/0602020]
217. W.C. Griffith, M.D. Swallows, T.H. Loftus, M.V. Romalis, B.R. Heckel, E.N. Fortson, Phys. Rev. Lett. **102**, 101601 (2009)
218. G.G. Ross, L. Velasco-Sevilla, O. Vives, Nucl. Phys. B **692**, 50 (2004). [hep-ph/0401064]
219. S. Antusch, S.F. King, M. Malinsky, JHEP **0806**, 068 (2008). [arXiv:0708.1282 [hep-ph]]
220. S. Antusch, S.F. King, M. Malinsky, G.G. Ross, Phys. Lett. B **670**, 383 (2009). [arXiv:0807.5047 [hep-ph]]
221. Z. Lalak, S. Pokorski, G.G. Ross, JHEP **1008**, 129 (2010). [arXiv:1006.2375 [hep-ph]]
222. F. Gabbiani, A. Masiero, Nucl. Phys. B **322**, 235 (1989)
223. F. Gabbiani, E. Gabrielli, A. Masiero, L. Silvestrini, Nucl. Phys. B **477**, 321 (1996). [hep-ph/9604387]
224. G. Isidori, Y. Nir, G. Perez, Annu. Rev. Nucl. Part. Sci. **60**, 355 (2010). [arXiv:1002.0900 [hep-ph]]
225. G. Ross, M. Serna, Phys. Lett. B **664**, 97 (2008). [arXiv:0704.1248 [hep-ph]]

Eur. Phys. J. C (2014) 74:2703
DOI 10.1140/epjc/s10052-013-2703-4

THE EUROPEAN PHYSICAL JOURNAL C

Review

SUSY dark matter(s)

Riccardo Catena, Laura Covi[a]

Institut für Theoretische Physik, Friedrich-Hund-Platz 1, 37077 Göttingen, Germany

Received: 20 November 2013 / Accepted: 27 November 2013 / Published online: 27 May 2014

Abstract We review the status of different dark-matter candidates in the context of supersymmetric models, in particular the neutralino as a realization of the WIMP mechanism and the gravitino. We give a summary of the recent bounds in direct and indirect detection and also of the LHC searches relevant for the dark-matter question. We also discuss the implications of the Higgs discovery for the supersymmetric dark-matter models and give the prospects for the future years.

1 Introduction

One among the most compelling pieces of evidence for physics beyond the Standard Model (SM) of particle physics is the presence of an unidentified dark-matter (DM) component in the observed Universe. This 'dark-matter problem' consists in the lack of a microscopic theory for the invisible form of matter which determines the motion of stars and galaxies in many astronomical systems, supports the large scale cosmological structure formation and constitutes about 80 % of the total matter in the Universe [1,2]. Postulated to explain the high-velocity dispersion of galaxies in a nearby galaxy cluster in 1933 by Zwicky, the DM hypothesis is nowadays corroborated by a plethora of complementary cosmological and astrophysical observations. Surveys performed from the largest structures we see in the Universe, namely galaxy clusters, down to dwarf and low surface brightness galaxies provide incontrovertible evidence in favor of the existence of a DM component in the Universe. Within the picture one obtains combining this variety of information, DM behaves like a dissipation-less and collision-less fluid manifesting itself only gravitationally. The microscopic nature of the DM component of the Universe remains, however, unknown.

One of the most popular attempts to solve the DM problem is the celebrated paradigm where the DM candidate is a weakly interacting massive particle (WIMP). In this scenario DM is made of a beyond-the-Standard-Model (BSM) particle, which is stable, initially in thermal equilibrium in the early Universe and decoupling as a non-relativistic species. The present cosmological density for such a state scales approximately with the inverse of its pair annihilation rate into lighter SM particles, and it can be accurately calculated by solving the Boltzmann equation for the WIMP number density n_χ [3,4]:

$$\frac{\mathrm{d}n_\chi}{\mathrm{d}t} = -3Hn_\chi - \langle\sigma_{\mathrm{eff}}\, v\rangle \left(n_\chi^2 - n_{\chi,\mathrm{eq}}^2\right) \tag{1}$$

where the effective thermally averaged annihilation cross section, $\langle\sigma_{\mathrm{eff}}\, v\rangle$, accounts for DM annihilations and coannihilations. Its expression in terms of particle couplings and the details of the thermal average can be found in Refs. [3,4]. Qualitatively, Eq. (1) tells us that the present WIMP number density is determined by the competition of two phenomena leading to a departure from the WIMP equilibrium number density $n_{\chi,\mathrm{eq}}$: the expansion of the Universe, which occurs with the rate H, and the DM annihilations, characterized by the rate $\Gamma_{\mathrm{ann}} = n_\chi \langle\sigma_{\mathrm{eff}}\, v\rangle$. The present value of n_χ is independent from the initial conditions, whose memory is erased in the thermal equilibrium phase. In practice, Eq. (1) has to be solved numerically and the very precise determination of the relic density achieved by current CMB experiments turns out to be a very tight constraint for many of the WIMP models proposed in the literature. The popularity of this framework relies on its very rich phenomenology and its straightforward implementation in many BSM models.

Another equally possible way to produce DM is instead to relax the assumption of equilibrium and consider the thermal evolution of the particle's abundance in the primordial plasma from a particular initial density, often taken to be zero after the inflationary dilution. In such a case, depending on

[a] e-mail: covi@theorie.physik.uni-goettingen.de

the couplings and mass of the DM candidate, different annihilation or decay rates into such particles allow one to match the present DM energy density. For this mechanism, usually candidates interacting very weakly are favored since it is vital that the particles do not reach thermal equilibrium. Here we will discuss in fact particles with non-renormalizable couplings suppressed by a large mass scale, like the Planck mass M_P for the gravitino or the Peccei–Quinn scale for the axino. The thermal-plasma contribution to their present abundance is often proportional to the maximal thermal bath temperature, since the non-renormalizable couplings are more effective at high temperature [5–10]. Otherwise also thermal bath particle decays in equilibrium can give a sufficiently large contribution to the DM density in what is called the 'FIMP' mechanism [11–15], which is instead independent of the initial conditions and temperature. Within this framework there is also the possibility to generate a DM population still exploiting the WIMP mechanism, via the decay of the decoupled WIMP into the lighter and more weakly interacting state. Such a scenario has been called the 'SuperWIMP' mechanism [16–18].

Supersymmetry (SUSY) is one of the most popular extensions of the SM and is flexible enough to offer DM candidates of both types, as we will discuss in detail in the following. After a brief introduction to the basics of SUSY, presented in Sect. 2, we review first the most popular SUSY dark-matter candidates, in Sect. 3, and then the strategies designed to detect them, in Sect. 4. Section 5 is devoted to the impact of the Higgs discovery on the field of particle dark matter, while our summary and outlook are presented in Sect. 6.

2 SUSY in a nutshell

We give here the basic concepts regarding SUSY and fix the notation, which will be needed in the next sections. A more complete treatment of the subject can be found in [19,20] or in the other reviews of this Journal.

SUSY is a unique extension of the Poincaré symmetry, which is enlarged to include also fermionic generators Q_α, $Q^{\dagger\dot{\alpha}}$. Here we will discuss only the case of a single additional fermionic generator and its conjugate corresponding to $N = 1$ SUSY. The new generators satisfy the algebra

$$\{Q_\alpha, Q^\dagger_{\dot\beta}\} = -2(\sigma^\mu)_{\alpha\dot\beta} P_\mu \tag{2}$$

and SUSY is therefore intrinsically connected to translations and space-time diffeomorphisms leading directly to gravity in the case of the promotion of SUSY from a global to a local symmetry.

The principal characteristic of supersymmetric models is that every particle has to be part of a supersymmetric multiplet consisting of different states of the same representation under the SM gauge group, but a different representation under the Lorentz group (i.e. different spin). The basic building blocks are the chiral multiplets, here denoted by Φ^i, containing the matter fermions or scalars and their superpartners, and the vector multiplets, $V = gV_aT^a$, containing the gauge bosons and their superpartners, the gauginos, one for each SM group generator T^a and gauge coupling g. SUSY not only offers a plethora of new particles, including DM candidates, but it also provides a perturbative framework for extending the SM and solving some of its shortcomings, like the hierarchy problem, and it allows for gauge coupling unification at a high scale and therefore points to a possible Grand Unification of the SM gauge group [20].

Let us turn now briefly to the case of a local supersymmetric model. The spectrum of the theory includes not only chiral and vector multiplets, but also a gravity multiplet, consisting of a spin-2 graviton and a spin-3/2 superpartner, the gravitino. The Lagrangian of such a model can be written as a function of the holomorphic superpotential $W(\Phi^i)$ and of the Kähler potential, $K(\Phi^i, \Phi^{*i})$, a hermitian function of the chiral multiplets satisfying the gauge symmetries of the SM model, and the gauge symmetry Killing vectors [19]. The kinetic terms and the gauge couplings of the chiral multiplets (at lowest order in gravity and in a Minkowski background) are generated by the Kähler potential as

$$\mathcal{L}_{kin} = \int d^2\theta d^2\theta^\dagger K_{i^*j}\Phi^{*i}e^{2V}\Phi^j \tag{3}$$

where the subscript i^*, j indicate derivative with respect to the fields Φ^{*i}, Φ^j, respectively. K_{i^*j} is the Kähler metric and gives the non-trivial structure of the scalar manifold as a non-linear σ model. The scalar potential is instead given by

$$\mathcal{V}_{\rm pot} = e^{K/M_P^2}\left[F_jK^{ji^*}F_{i^*} - 3\frac{|W|^2}{M_P^2}\right] + \text{D-terms} \tag{4}$$

where K^{ji^*} is the inverse metric to K_{i^*j} and $F_i = W_i + K_i\frac{W}{M_P^2}$ is the F-term corresponding to the chiral field Φ^i. In the limit of global SUSY, i.e. $M_P \to \infty$, the potential reduces to the simple well-known expression

$$\mathcal{V}_{\rm pot} = \sum_i |W_i|^2 + \text{D-terms} \tag{5}$$

assuming (as we will always do from now on) that the Kähler metric is canonical, i.e. $K_{i^*j} \sim \delta_{ij} + \mathcal{O}(M_P^{-2})$.

The superpotential of the MSSM contains in general quadratic and cubic interaction terms and has the form (we adopt here the same notation of [20])

$$W_{\rm MSSM} = \overline{u}\mathbf{y_u}QH_u - \overline{d}\mathbf{y_d}QH_d - \overline{e}\mathbf{y_e}LH_d + \mu H_uH_d \tag{6}$$

where we have suppressed generation indices, but where the Yukawa couplings $\mathbf{y}_i$ are matrices in family space. Here the chiral superfields Q, L denote the SM SU(2) doublets, while $\overline{u}, \overline{d}, \overline{e}$ are the SU(2) singlets. H_u and H_d are the Higgs SU(2) doublets chiral multiplets required to correctly achieve the SM particles mass generation and gauge anomaly cancellation. Note that the only dimensional term is the μ-term, which has to be at the electroweak scale to allow a 'natural' electroweak symmetry breaking. In a simple extension of the MSSM by a SM singlet multiplet S, the Next to Minimal Supersymmetric SM (NMSSM) [21–23], such scale can be obtained dynamically from another cubic term and a vacuum expectation value of the singlet. The superpotential then reads

$$W_{\mathrm{NMSSM}} = W_{\mathrm{MSSM}} + \lambda S H_u H_d + \frac{1}{3}\kappa S^3 \tag{7}$$

where λ and κ are constants. The gauge symmetries of the SM actually allow also additional renormalizable terms, which give rise to fast proton decay and are therefore usually forbidden by invoking an additional discrete Z_2 symmetry, R-parity, which distinguishes between particles and superparticles. Such terms are given by

$$\begin{aligned} W_{\mathrm{RPB}} &= \mu'^i L_i H_u \\ &\quad + \lambda'^{ijk} L_i L_j \overline{e}_k + \lambda'^{ijk} L_i Q_j \overline{d}_k + \lambda''^{ijk} \overline{u}_i \overline{d}_j \overline{d}_k. \end{aligned} \tag{8}$$

where the couplings λ^{ijk}, λ'^{ijk}, λ''^{ijk} and μ'^i carry family indices. If R-parity is unbroken, the lightest supersymmetric particle (LSP) is stable since R-parity forbids its decay into SM particles. These superpotential terms must therefore vanish or be strongly suppressed to retain a supersymmetric DM candidate in the form of the LSP. In the presence of SUSY breaking, the Lagrangian includes also soft terms, i.e. mass terms for the gauginos and the scalar fields and bilinear and trilinear scalar terms:

$$\begin{aligned} \mathcal{L}_{\mathrm{soft}} = &-\frac{1}{2}\sum_i (M_i \lambda_i \lambda_i + h.c.) - \widetilde{L}^\dagger \mathbf{m_L^2}\, \widetilde{L} - \widetilde{\overline{e}}\, \mathbf{m_{\overline{e}}^2}\, \widetilde{\overline{e}}^\dagger \\ &- \widetilde{Q}^\dagger \mathbf{m_Q^2}\, \widetilde{Q} - \widetilde{\overline{u}}\, \mathbf{m_{\overline{u}}^2}\, \widetilde{\overline{u}}^\dagger - \widetilde{\overline{d}}\, \mathbf{m_{\overline{d}}^2}\, \widetilde{\overline{d}}^\dagger \\ &- m_{H_u}^2 H_u^* H_u - m_{H_d}^2 H_d^* H_d + \mathcal{A}[W] \end{aligned} \tag{9}$$

where the three sets of gauginos (one for each factor of the SM gauge group) are denoted by λ_i, with $i = 1, 2, 3$. $\widetilde{Q}, \widetilde{L}, \widetilde{\overline{u}}, \widetilde{\overline{d}}, \widetilde{\overline{e}}$ are the scalar superpartners in the multiplets $Q, L, \overline{u}, \overline{d}, \overline{e}$ and the corresponding mass matrices are labeled with the same letters (family indices are suppressed). With this notation $\widetilde{Q}_1 = (\widetilde{u}_L, \widetilde{d}_L)$, $\widetilde{\overline{u}}_1 = \widetilde{u}_R^*$ and similarly for the other particles [20]. $\mathcal{A}[W]$ contains all the scalar bilinear and trilinear terms corresponding to the bilinear and trilinear terms in the superpotential W, e.g.

$$\begin{aligned} \mathcal{A}[W_{\mathrm{MSSM}}] = &-(\widetilde{\overline{u}}\, \mathbf{a_u}\, \widetilde{Q} H_u + \widetilde{\overline{d}}\, \mathbf{a_d}\, \widetilde{Q} H_d + \widetilde{\overline{e}}\, \mathbf{a_e}\, \widetilde{L} H_d \\ &+ b H_u H_d + h.c.). \end{aligned} \tag{10}$$

The simplest realization of the MSSM, the constrained MSSM (cMSSM), corresponds to taking at the GUT scale a single universal mass scale $m_{1/2}$ for the gauginos, a single mass m_0 for the scalar particles and a single trilinear parameter A for the three matrices $\mathbf{a_u}$, $\mathbf{a_d}$ and $\mathbf{a_e}$. The b parameter is traded for $\tan\beta = v_u/v_d$, where v_u and v_d are the VEVs of the two neutral Higgs fields, while $|\mu|$ is set by the requirement of radiative electroweak breaking. All quantities are then extrapolated to lower energies via the relevant RGEs. In other realizations, like the phenomenological MSSM (pMSSM), the different mass scales are disentangled and more parameters introduced directly at the electroweak scale.

3 SUSY dark-matter candidates

3.1 Neutralino

The most studied supersymmetric DM candidate is in many respects the lightest neutralino [24]. In the R-parity conserving MSSM there are four neutralinos in the mass spectrum of the theory and they are commonly denoted by $\tilde{\chi}_i^0$, with $i = 1, \ldots, 4$. These mass eigenstates consist of four independent linear combinations involving the neutral electroweak gauginos ($\tilde{B}$ and $\tilde{W}^0$) and the neutral Higgsinos ($\tilde{H}_d^0$ and $\tilde{H}_u^0$). The mixing between these states is a direct consequence of the electroweak symmetry breaking. In the gauge-eigenstate basis, represented here by the array $\psi = (\tilde{B}, \tilde{W}^0, \tilde{H}_d^0, \tilde{H}_u^0)$, the neutralino mass term in the MSSM Lagrangian can be writen as $-\frac{1}{2}\psi^T \mathbf{M}_{\tilde{\chi}^0}\psi$ + h.c., where the neutralino mass matrix $\mathbf{M}_{\tilde{\chi}^0}$ reads as follows [1,2,20,25]:

$$\mathbf{M}_{\tilde{\chi}^0} = \begin{pmatrix} M_1 & 0 & -g' v_d/\sqrt{2} & g' v_u/\sqrt{2} \\ 0 & M_2 & g v_d/\sqrt{2} & -g v_u/\sqrt{2} \\ -g' v_d/\sqrt{2} & g v_d/\sqrt{2} & 0 & -\mu \\ g' v_u/\sqrt{2} & -g v_u/\sqrt{2} & -\mu & 0 \end{pmatrix}.$$

The diagonal entries of this matrix, namely M_1 and M_2, stem from the gaugino mass terms present in the soft SUSY breaking Lagrangian (9). Because of the freedom to perform a phase redefinition of the fields $\tilde{B}$ and $\tilde{W}^0$, M_1 and M_2 can be chosen real and positive without loss of generality. Analogously, by a phase redefinition of the Higgs fields, v_d and v_u can be taken real and positive. The off-diagonal terms proportional to μ arise from the μ-term in the superpotential (6). The phase of μ, which cannot be reabsorbed by further phase redefinitions, is assumed to be zero in the vast majority of the analyses, to avoid potentially dangerous CP-violations. The neutralino mass matrix can be diagonalized by a unitary matrix $\mathbf{N}$ such that $\mathbf{N}^* \mathbf{M}_{\tilde{\chi}^0} \mathbf{N}^{-1} = \mathrm{diag}(m_{\tilde{\chi}_1^0}, \ldots, m_{\tilde{\chi}_4^0})$, where $m_{\tilde{\chi}_1^0}, \ldots, m_{\tilde{\chi}_4^0}$ are the masses of the four neutralinos.

The matrix **N** relates mass and gauge eigenstates as follows: $\tilde{\chi}_i^0 = \mathbf{N}_{ij}\psi_j$, where in this expression the indices i and j label, respectively, mass and gauge eigenstates. Depending on the values of the soft SUSY breaking parameters, the lightest neutralino can also be the LSP and thus a stable DM candidate for unbroken R-parity.

The neutralino interactions are determined by its composition (*i.e.* the matrix $\mathbf{N}_{ij}$), the MSSM superpotential, and the quantum numbers of its constituents: the SU(2) singlet $\tilde{B}$, the neutral components of the SU(2) doublets $(\tilde{H}_d^0, \tilde{H}_d^-)$ and $(\tilde{H}_u^+, \tilde{H}_u^0)$, and the neutral component of the SU(2) triplet $(\tilde{W}^\pm, \tilde{W}^0)$, characterized by the hypercharges 0, −1/2, 1/2 and 0, respectively. The gauge and Yukawa interactions allowed in the R-parity conserving MSSM for the neutralino constituents are shown if Fig. 1 in the form of Feynman diagrams. From these one can construct the full list of neutralino Feynman rules in the mass eigenstate basis, given for instance in [26].

The definition of the neutralino given here in the context of the MSSM can be straightforwardly generalized to the case of the NMSSM. In this model, the fermionic component of S, the 'singlino' $\tilde{S}$, mixes with the gauge eigenstates $\tilde{H}_d^0$ and $\tilde{H}_u^0$. As a result, in the mass spectrum of the theory there are five neutralino-like particles and the lightest of them has been studied by many authors as a DM candidate (see for instance [27] and references therein). A phenomenologically interesting feature of this scenario is the existence of new interaction vertices (compared to the MSSM) due to the enlarged Higgs sector of the theory, which now includes three CP-even neutral Higgs bosons and two CP-odd neutral Higgs bosons [23].

3.2 Gravitino

In local supersymmetric models we have also an electromagnetically and gauge-neutral DM candidate, i.e. the gravitino, the superpartner of the graviton. In fact, as soon as SUSY is promoted to a local symmetry, gravity is automatically included in the model and to complement the spin-2 graviton field, a spin-3/2 fermion must be added to the particle spectrum. The gravitino plays the role of 'gauge fermion' for SUSY and becomes massive via the SuperHiggs mechanism as soon as such symmetry is broken by any F or D-term having a non-vanishing expectation value.The Goldstino field, providing the spin 1/2 component of the massive gravitino is given by a combination of the chiral fermions and gauginos along the SUSY breaking direction singled out by the vector $(\langle F_i \rangle, \langle D^a \rangle)$ in field space. The gravitino mass is in general given by

$$m_{3/2} = \frac{\left\langle |W| e^{K/(2M_P^2)} \right\rangle}{M_P^2} \tag{11}$$

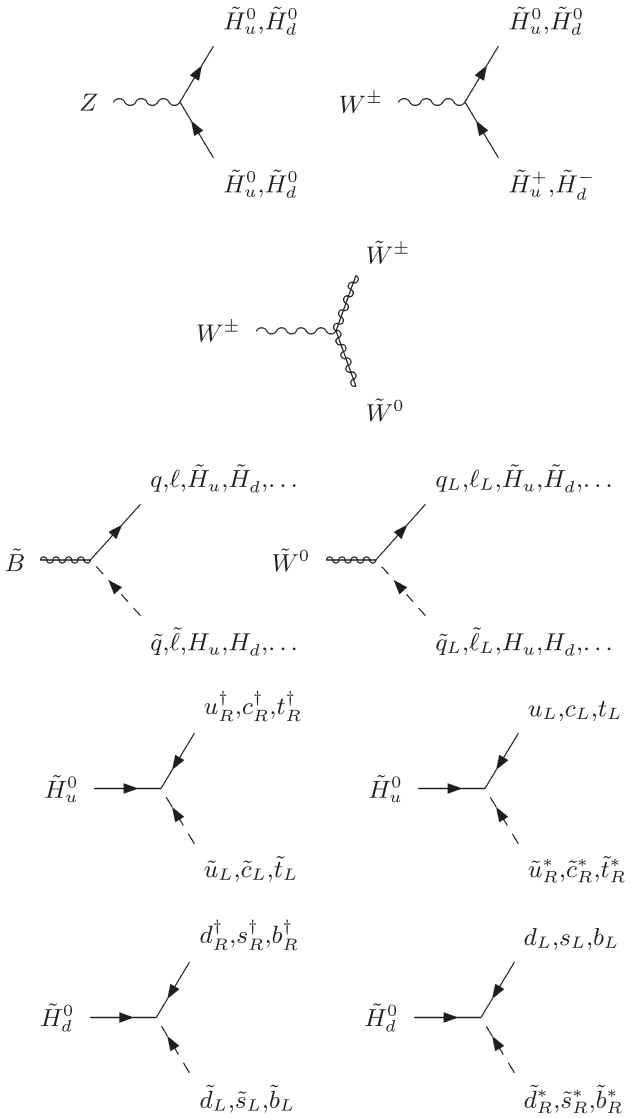

Fig. 1 Feynman diagrams for the neutralino constituents. We adopt here the same notation of Ref. [20]

where the brackets denote here the vacuum expectation value. Imposing that the cosmological constant/vacuum energy in Eq. (4) vanishes, gives, if all the D-terms vanish, also the relation

$$m_{3/2} = \frac{1}{\sqrt{3}M_P}\sqrt{\left\langle F_i F_j^* K^{ij^*} e^{K/M_P^2} \right\rangle} \sim \frac{|F|}{\sqrt{3}M_P} \tag{12}$$

where F_i is the F-term of the ith chiral superfield and F denotes the VEV of the largest non-vanishing F-term. In comparison, the SUSY breaking masses of the other superpartners are proportional to F, but they can contain a different mass scale suppression. In particular within the gauge-mediated SUSY breaking scenario [28], the gaugino masses M_i are given by the dominant F-term suppressed by the messenger masses, naturally smaller than M_P. In those type of

models it is therefore natural to have a gravitino as the lightest supersymmetric particle.

The gravitino couplings are dictated by gravity and SUSY and suppressed by the Planck mass as all gravity couplings. On the other hand, the Goldstino couples directly to the supercurrent in a derivative way and has therefore enhanced coupling in the limit of large hierarchy between the gravitino and the other sparticle masses. The general gravitino couplings can be found in [19,29,30].

3.3 Axino

Another neutral superparticle that can play the role of DM is the axino, the superpartner of the axion field. It arises naturally in extensions of the SM including also the Peccei–Quinn [31] solution to the strong CP problem in a supersymmetric setting [32,33]. The axino is a spin-1/2 fermion and it is univocally defined (and nearly massless) only in the limit of unbroken SUSY [34]. In that case in fact the whole axion supermultiplet, including the axino and the saxion as scalar partner of the pseudoscalar axion, is protected by the Goldstone nature of the axion and it is massless as long as one neglects the explicit symmetry breaking coming from QCD instantons effects. On the other hand, as soon as SUSY is broken, the axino acquires a mass and also mixes with the other neutral fermions rendering its mass and phenomenology strongly model dependent. Note that some axion models of the DFSZ-type [35,36] introduce an axion coupling to the Higgs fields in a similar way to the singlino couplings in the NMSSM, mixing in general the axino with the neutralinos, but the two models differ in the presence of cubic or quadratic couplings for the singlet field.

If the main axion/axino couplings are only with the QCD sector, as happens instead in the KSVZ-type models [37,38], the neutralino mass matrix retains an eigenstate strongly aligned with the axion direction and decoupled from the rest of the spectrum. In that case the phenomenology simplifies as one can approximate the axino couplings with the supersymmetrized axion ones [8]. Note that this requires to extrapolate the axion couplings to high scale, which may not always be possible [39,40]. Then the axino couplings are suppressed by the axion decay coupling f_a, which is constrained by axion physics considerations [41] to lie between 10^9–10^{12} GeV. The axino is therefore naturally very weakly interacting and can be a realization of the Super-WIMP mechanism if the reheat temperature is very low [8,16] or be produced by thermal decays or scatterings [8–10,12,39,40,42].

3.4 Other candidates

A variety of DM models have been developed in the literature where the DM properties are to some extent influenced by the ones of the SM neutrinos. The MSSM left-handed sneutrino $\tilde{\nu}$ has been excluded long ago as DM candidate because of its sizable coupling with the Z boson, which leads to a too large annihilation cross section (implying a too small relic density) and a too large DM–nucleon scattering cross section, which is experimentally excluded [43]. One possibility to reconcile $\tilde{\nu}$ DM with observations is to add to the MSSM spectrum a new superfield (for each neutrino flavor) whose bosonic component, the right-handed sneutrino, mixes with the left-handed sneutrino [44]. This mixing reduces the strength of the dangerous $\tilde{\nu}$–$\tilde{\nu}$–Z coupling, eventually leading to an acceptable phenomenology for the lightest sneutrino mass eigenstate, which in this context qualifies as a viable scalar DM candidate. A Higgs boson mass of 125–126 GeV restricts the allowed supersymmetric configurations to regions in parameter space where the mixed sneutrino has a mass of the order of 100 GeV [45]. At the same time in this class of theories different implementations of the seesaw mechanism provide a procedure to generate the correct masses for the light SM neutrinos (see for instance [46]). On the other hand the coupling to the Z boson of a pure right-handed sneutrino is exactly zero, a property which makes the right-handed sneutrino phenomenologically safe as non-thermal 'FIMP'-like DM candidate [13], but at the same time essentially impossible to detect if the underlying theory is the MSSM. A phenomenologically more interesting DM candidate is the right-handed sneutrino in the context of the NMSSM [47]. In this case the coupling of the right-handed sneutrino to the Higgs bosons is enhanced by new interactions which are controlled by the extra parameters of the superpotential (7) and therefore make this DM candidate potentially detectable by the next generation of ton-scale direct detection experiments. Other classes of models where the right-handed sneutrino appears as an interesting DM candidate are those which incorporate a low scale seesaw mechanism, such as the one described in Ref. [48].

We conclude this section with an alternative to the WIMP paradigm: the WIMPless scenario [49]. In this class of SUSY theories the field content is divided in three sectors: a visible (or MSSM) sector, the SUSY breaking sector and, finally, the hidden sector which contains the DM candidate. In these models the SUSY breaking is mediated to the hidden sector by gauge interactions of arbitrary strength g_χ. As for the familiar gauge-mediated SUSY breaking mechanism, this setup implies that the DM candidate acquires after SUSY breaking a mass of the order of $m_\chi \sim g_\chi^2 F/M$, where the parameters F and M parameterize the F-term and VEV of the SUSY breaking field. Assuming a standard thermal history in the hidden sector, the present DM density for this model scales as $\Omega_\chi \sim (H^*/n_\chi^*)(m_\chi^2/g_\chi^4)$, where H and n_χ are evaluated at the time t^* of the DM chemical decoupling. Hence in this framework Ω_χ depends on F and M only, for what concerns particle physics. This implies that in this

class of theories the relic density matches the observations for a broad range of DM couplings and masses, making this scenario phenomenologically very interesting.

4 SUSY dark-matter detection

In the following we will review the current status of SUSY DM searches focusing separately on two different classes of DM candidates. First we will concentrate on the neutralino which is the archetypal WIMP and has couplings of electroweak strength and a mass typically varying between a few GeV up to tens of TeV. Then we will move to a second class of particles, like the gravitino, whose interactions are much weaker than the electroweak force (*e.g.* in principle down to gravitational strength) and that are characterized by a larger range of possible masses. These candidates are commonly dubbed SuperWIMPs.

4.1 SUSY WIMPs

4.1.1 Direct detection

The aim of the direct detection technique [53] is to measure the energy released by Milky Way DM particles when scattering off nuclei in underground detectors. In the case of DM–nucleus spin-independent interactions, the differential rate of scattering events expected in a direct detection experiment, $\mathrm{d}R/\mathrm{d}Q$, is given by [1,2,25]:

$$\frac{\mathrm{d}R}{\mathrm{d}Q}(Q) = \gamma(Q)\frac{\sigma_p}{m_\chi}\int_{|\boldsymbol{v}|<v_{\min}} d^3v\,\frac{f_\odot(\boldsymbol{v},t)}{|\boldsymbol{v}|} \tag{13}$$

where $f_\odot$ is the time-dependent local DM distribution function in the detector rest frame normalized at the value of the local DM density, $v_{\min}(Q, m_\chi)$ is the minimum DM velocity required to transfer an energy Q to the detector nuclei, m_χ is the DM mass and σ_p the DM-nucleon scattering cross section. The energy-dependent function $\gamma(Q)$ incorporates the details of the detector.

The calculation of the DM–nucleus scattering cross section has been performed in various supersymmetric extensions of the SM (and we refer the reader to Ref. [54,55] for details regarding these computations). In the vast majority of the proposed scenarios—for instance in the case of a neutralino within the MSSM—this calculation reduces to the determination of the couplings, often denoted by α_{2q} and α_{3q}, appearing in the contact interactions

$$\alpha_{3q}\,\bar{\chi}\chi\bar{q}q \qquad \text{and} \qquad \alpha_{2q}\,\bar{\chi}\gamma^5\gamma^\mu\chi\bar{q}\gamma^5\gamma_\mu q \tag{14}$$

which in the non-relativistic limit lead to a spin-independent and to a spin-dependent DM–nucleus interaction, respectively. In the MSSM, these operators are the only velocity-independent operators relevant for the neutralino–nucleus scattering. For Dirac DM candidates, instead, a vector coupling of the form $\bar{\chi}\gamma^\mu\chi\bar{q}\gamma_\mu q$ is also allowed. A complete classification of the non-relativistic operators allowed by Galilean invariance as well as by energy and momentum conservation and relevant for the DM–nucleus scattering can be found in [56].

Several experiments have currently reached the sensitivity to start probing the WIMP paradigm using different target materials and detection principles, including the detection of an annual modulation signal associated with the time variation of the expected DM scattering rate in the detector due to the motion of the Earth relative to the Sun. Three collaborations, namely CRESST, CoGeNT and CDMS have also published results compatible with the detection of a small number of candidate signal events, which were not possible to ascribe to any of the considered background sources [57–59]. There is not a general consensus regarding the interpretation of these results and the picture is further complicated by the 8.9 σ C.L. detection of a modulation signal made by the DAMA/LIBRA experiment [60]. This finding has been not confirmed by other experiments and its interpretation in terms of dark mass and scattering cross section is in very strong tension with the results of other experiments, in particular of XENON100 [61], which is currently excluding the regions of the plane DM mass versus spin-independent scattering cross section favored by DAMA as well as the low WIMP mass regions favored by CRESST, CoGeNT, and CDMS. A neutralino with a mass close to 10 GeV, as required by these experiments, might be generated by relaxing the assumption of gaugino mass unification [62] (see also [63,64] for alternative approaches) while DM isospin violating interactions seem the only possibility to reconcile DAMA with XENON100 [65]. In addition, several experiments are also probing the spin-dependent DM interactions using nuclei with unpaired protons as target materials (*e.g.* see Ref. [66]).

The impact of these results on the search for SUSY WIMPs is remarkable. In Fig. 2 we report the regions in the plane DM mass m_χ versus spin-independent DM-nucleon scattering cross section σ_p favored by three independent analyses of the MSSM [50–52] (see also [67,68] for other studies exploring larger mass ranges and finding a big region at the TeV scale where DM is a Higgsino-like neutralino). Several supersymmetric configurations appear already excluded by current direct detection searches. Moreover, the next generation of ton-scale experiments will be able to probe the vast majority of the presently allowed configurations. However, DM candidates with a mass in the 10 GeV (100 GeV) range and spin-independent cross sections smaller than roughly $10^{-45}\,\mathrm{cm}^2$ ($10^{-49}\,\mathrm{cm}^2$) will be very difficult (if not impossible) to discover even with the next generation of direct

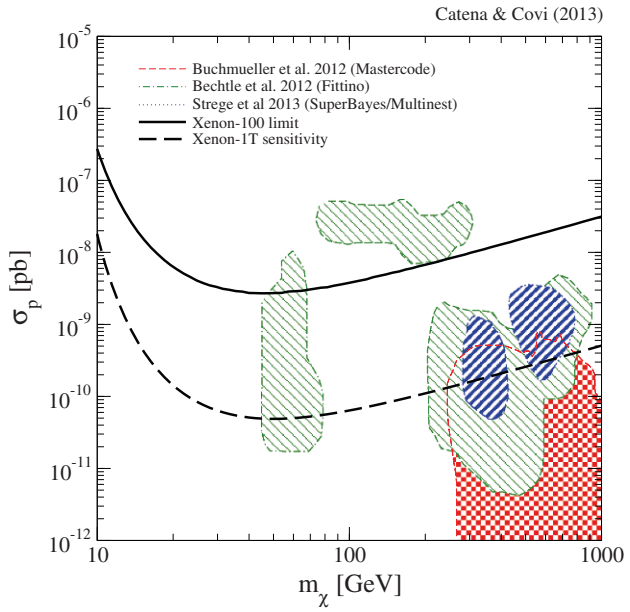

Fig. 2 Regions in the plane DM mass m_χ versus spin-independent DM-nucleon scattering cross section σ_p favored by three independent global fits of the MSSM to a variegated sample of observations including the latest LHC data, low energy observables, cosmological limits as well as DM searches. The *blue contours* include the 95% credible regions found in Ref. [50] employing log-priors, while the *red* and *green countours* represent the 95% C.L. favored regions determined in Refs. [51,52]. The *solid black line* corresponds to the present XENON100 exclusion limit. The *black dashed curve* represents instead the sensitivity of XENON-1T after 1 year of data

detection experiments, since an experiment sensitive to such a low scattering cross sections would also measure the large flux of solar and atmospheric neutrinos which would therefore constitute a copious and irreducible background source [69].

The interpretation of a DM direct detection signal in terms of DM properties is significantly affected by the uncertainties in local DM density [70], in the local DM velocity distribution function [71,72] and by the current limited knowledge of the nuclear form factors as well as of the matrix elements determining the DM-nucleon couplings [73]. For these reasons DM halo independent approaches to the WIMP direct detection have been proposed [74–78] as well as multiple targets analyses [79].

4.1.2 Indirect detection

Alternatively, DM could be revealed through the observation of SM particles produced in space by DM annihilations or decays [1,2] (the latter possibility applies to long-lived DM candidates and will be reviewed in Sect. 4.2). This detection strategy is known as the DM indirect detection technique. WIMPs are expected to copiously annihilate in galactic and extragalactic regions where the DM density is large compared to the present mean cosmic density. Annihilation products of particular interest are γ-rays [80]—which propagate along geodesics and provide therefore direct information on the region where the associated annihilations have occurred—and antimatter [81] (*e.g.* positrons, antiprotons or exotic nuclei like antideuterons [82], etc…), which is also produced by standard astrophysical sources (*e.g.* pulsars) but nevertheless sub-leading in space. In both cases the expected energy spectra exhibit a kinematical cutoff associated with the mass of the DM candidate, a feature which can be used to separate the DM signal from possible astrophysical backgrounds which (with a few exceptions) are characterized by power laws decreasing with energy.

The flux of charged annihilation products observable on top of the atmosphere is calculated solving a transport equation for the propagation and diffusion of these particles in the galactic magnetic field. This can be done either numerically [83] or semi-analitically, expanding in Bessel functions the space and energy distribution function of the DM annihilation products (see for instance Ref. [84]). For neutral annihilation products of type i, such as photons and neutrinos, the observable differential flux in a direction at an angle θ from the direction of the galactic center, at an energy E is given by [1,2]:

$$\frac{\mathrm{d}\Phi_i}{\mathrm{d}E\,\mathrm{d}\Omega}(\theta, E) = \frac{1}{4\pi m_\chi^2}\langle\sigma v\rangle\frac{\mathrm{d}N_i}{\mathrm{d}E}(E)\int_{l.o.s.}\mathrm{d}s\rho_\chi^2(r(s,\theta)) \tag{15}$$

where $\langle\sigma v\rangle$ is the average velocity-weighted annihilation cross section, $\frac{\mathrm{d}N_i}{\mathrm{d}E}$ is the differential energy spectrum of the i particles produced per annihilation and the integral of the squared DM mass density, ρ_χ^2(r), is computed along the line of sight s, where $r(s,\theta)$ is the distance from the galactic center. Therefore, we clearly see that regions in space with a high concentration of DM are good targets to look for such annihilations. For Majorana DM candidates Eq. (15) has to be divided by a factor of 2.

γ-rays from DM annihilations can be produced either through a prompt emission or as a byproduct of various processes, including the hadronization of charged annihilation products forming a π^0 subsequently decaying in a pair of photons and the inverse Compton of relativistic charged particles upscattering low energy photons from CMB, starlight and interstellar radiation [85].

A study of the signal-to-noise ratio shows that optimal targets are [86]: the galactic center (with a large expected DM signal but also a large astrophysical background), dwarf spheroidal galaxies (which are among the most DM dominated environments), the galactic halo (including the associated substructures) and, finally, massive nearby galaxy clusters. DM can be also gravitationally trapped in astrophysical

Table 1 s-channel and t-channel tree level two-body neutralino annihilations allowed in the MSSM [2]

Final state	s-channel	t-channel
$\tilde{\chi}_1^0\tilde{\chi}_1^0 \to \bar{f}f$	A, Z	$\tilde{f}$
$\tilde{\chi}_1^0\tilde{\chi}_1^0 \to W^{\pm}W^{\mp}$	h, H, Z	$\tilde{\chi}_i^{\pm}$
$\tilde{\chi}_1^0\tilde{\chi}_1^0 \to ZZ$	h, H	$\tilde{\chi}_i^0$
$\tilde{\chi}_1^0\tilde{\chi}_1^0 \to ZA$	h, H, Z	$\tilde{\chi}_i^0$
$\tilde{\chi}_1^0\tilde{\chi}_1^0 \to Zh(ZH)$	A, Z	$\tilde{\chi}_i^0$
$\tilde{\chi}_1^0\tilde{\chi}_1^0 \to W^{\pm}H^{\mp}$	A, h, H	$\tilde{\chi}_i^{\pm}$
$\tilde{\chi}_1^0\tilde{\chi}_1^0 \to hh(HH)$	h, H	$\tilde{\chi}_i^0$
$\tilde{\chi}_1^0\tilde{\chi}_1^0 \to AA$	h, H	$\tilde{\chi}_i^0$
$\tilde{\chi}_1^0\tilde{\chi}_1^0 \to Ah(AH)$	A, Z	$\tilde{\chi}_i^0$

objects like the Sun and annihilate at their center producing a potentially observable flux of energetic neutrinos [87].

The DM annihilation cross section has been calculated in various supersymmetric models. In the MSSM there are different classes of two-body final states allowed at tree level [1,2,88] (we neglect here coannihilations, which are instead crucial to calculate the DM relic density). A complete list is shown in Table 1, where we assumed that the neutralino is the DM candidate. In addition, there are also three-body final states which can play an important role in the context of the DM indirect detection, in particular those involving a single photon or electroweak gauge boson emitted as final state radiation or by the particle mediating the annihilation (the so-called virtual internal bremsstrahlung) which can lead to interesting spectral features in the γ-ray band [89]. Detailed calculations of the associated annihilation cross sections have been presented by various groups [90,91] and also implemented in publicly available numerical codes [92]. At one loop a pair of photons [93] or one photon accompanied by one Z-boson [94] can be also produced. These monochromatic lines are clearly distinguishable by standard astrophysical backgrounds but unfortunately loop-suppressed.

The last 4 years of observations in the field of indirect DM searches have been particularly rich of interesting results. Regarding DM searches in the antimatter channel, the observation of an 'anomalous' rise in the positron fraction measured by the PAMELA satellite [95] and possibly related to a nearby primary source of positrons has triggered a vigorous debate in the literature concerning the DM interpretation of this signal. Though pulsars might explain this observation as well [96,97], a clear and universally accepted interpretation of this phenomenon is still missing. Recently, a rise in the positron fraction in the 10–300 GeV range has been also observed by the AMS-02 space observatory [98], providing therefore a remarkable confirmation of the PAMELA results. Likely, future data from the AMS-02 experiment will finally clarify this intriguing puzzle. The PAMELA satellite has also provided accurate measurements of the antiproton flux on top of the atmosphere [99] which are, however, in excellent agreement with expectations from standard astrophysical sources. In addition, during the past few years γ-ray observations have also played a major role in the context of DM searches. The identification of a 130 GeV γ-ray line in the direction of the galactic center in the Fermi-LAT data [89,100] has stimulated an intense discussion regarding its nature. Though a monochromatic γ-ray line at these energies has been often referred to as the 'smoking gun' for DM searches, the global significance of this signal is constantly decreasing (currently quoted at 1.5 σ [101]), while the amount of data taken is increasing. Significant results have been also achieved observing the galactic center with HESS, a system of imaging atmospheric Cherenkov telescopes designed to investigate cosmic γ-rays in the energy range from tens of GeV to tens of TeV. Finally, observations in the radio band have also provided valuable results for DM searches through the synchrotron emission generated by relativistic charged particles produced by DM matter annihilations in the galactic magnetic field [102].

These data significantly limit the allowed regions in the plane DM mass versus annihilation cross section and consequently drastically impact the space of allowed supersymmetric configurations. For instance, the latest Fermi-LAT data from the observation of 25 dwarf spheroidal satellite galaxies constrain the DM annihilation cross section to be less than 3×10^{-26} cm^3 s^{-1} ('the thermal cross section') for DM particles with a mass less than 10 GeV (15 GeV), assuming that the dominant annihilation channel is $\bar{b}b$ ($\tau^+\tau^-$) [103]. The thermal cross section is commonly taken as an important reference when extracting bounds from indirect detection measurements, since it represents the cross section required for thermal WIMPs to match the observed relic density. This value can, however, drastically be different if the expansion rate of the Universe before DM decoupling is not the one expected from General Relativity, as typically occurs for instance in Scalar-Tensor theories of gravity and in certain models with extra spatial dimensions [104]. Indeed, a larger expansion rate, for example, implies an earlier DM chemical decoupling and therefore a larger DM density at decoupling which has thus to be compensated by a larger annihilation cross Section [105,106]. This phenomenon induces a distortion in the allowed regions of the $(m_{1/2}, m_0)$ plane of the cMSSM [107].

4.1.3 LHC searches

WIMPs could be also produced in high-energy proton–proton collisions at the LHC. Different final states are in principle relevant for DM searches. One of the most popular channel to look for DM is a final state involving a single jet or a single photon produced in association with missing transverse momentum. This class of processes is generically

expected in all models where there is an effective contact interaction involving two DM particles and two quarks (not only in SUSY theories). The single jet (or the single photon) is radiated by one of the initial state quarks. In the case of DM searches in mono-jet (and analogously for the mono-photon) events, the most relevant source of SM background consists in the production of a Z boson in association with a jet, with the Z boson decaying into a neutrino pair, or in the W plus jet production, with the W boson decaying into a neutrino and a misidentified lepton. Current measurements performed by the ATLAS and CMS collaborations focused on these channels are consistent with SM expectations [108,109]. A similar strategy currently pursued at LHC consists in searching for DM in events with a hadronically decaying W or Z boson. Also the study of this channel has, however, reported results which are consistent with SM expectations [110]. More recently, it has been proposed to search for a DM signal in mono-lepton events resulting from the production of a pair of DM particles in association with a W boson subsequently decaying into a lepton and a neutrino. The latest analysis of this channel performed using data corresponding to 20 fb^{-1} of integrated luminosity at $\sqrt{s} = 8$ TeV center-of-mass energy has found no indications of a DM signal [111].

In addition to these search strategies, which as already mentioned would also apply to non-SUSY WIMPs, there are different studies which instead aim at identifying DM explicitly assuming that the underlying theory is SUSY. An interesting example of this type of analyses is the search for neutralino DM in events involving direct slepton or gaugino production in final states with two or three leptons and missing transverse momentum [112,113]. In the case of the direct production of sleptons, which occurs via a supersymmetric version of the Drell–Yan process, the following chain of decays leads to neutralino DM production: $\bar{q}q \rightarrow \tilde{\ell}^{\pm}\tilde{\ell}^{\mp} \rightarrow (\tilde{\chi}_1^0\ell^{\pm}) + (\tilde{\chi}_1^0\ell^{\mp})$. In the case of direct gaugino production, instead, DM can be produced in various way. As an example, we mention here the decay chain: $\bar{q}q \rightarrow \tilde{\chi}_2^0\tilde{\chi}_1^{\pm} \rightarrow (\tilde{\chi}_1^0\ell^{\pm}\ell^{\mp}) + (\tilde{\chi}_1^0\ell^{\pm}\nu)$, where DM is produced in association with three leptons in the final state. Again, current searches are consistent with SM expectations [112,113]. The same conclusion also applies to another channel relevant for SUSY DM, namely the search for strongly produced supersymmetric particles in decays with two leptons and missing transverse momentum [114].

There are two main approaches to extract from these LHC searches limits on the DM mass and couplings. A first possibility consists in modeling the DM interactions within an effective field theory framework and then assuming that only certain operators are relevant when studying DM at collider [115]. This approach has the advantage of establishing explicit correlations between LHC observables, *e.g.* missing transverse momentum distributions, and other DM properties, such as for instance the DM-nucleon scattering cross section. The drawback of this approach is that it might provide an oversimplified picture of the real DM properties [116,117]. Alternatively the LHC searches for DM can be interpreted within specific particle physics framework, like for instance the pMSSM, where the SUSY spectrum is described by approximately $\mathcal{O}(10)$ parameters. In this case the large number of parameters tends to weaken the possibility of directly relating the LHC results to other DM detection strategies. Nevertheless, focusing on certain classes of supersymmetric configurations, interesting correlation patterns have been identified even in the pMSSM framework [118].

4.1.4 Complementarity of the different detection strategies

The detection strategies presented in this section probe distinct WIMP properties and are therefore complementary. This allows on the one hand to independently verify a hypothetical DM discovery made by one of the mentioned experimental techniques, on the other hand to experimentally probe a large set of different DM models.

Direct detection experiments and LHC searches can be combined in different ways. One can combine the associated measurements in a global fit to infer the properties of the underlying DM model [50] or, alternatively, use the results from one of these detection strategies to predict, within a certain particle physics framework, DM signals in the other class of experiments. For instance, LHC (real and simulated) data have been often used in the literature to try to reconstruct the DM-nucleon scattering cross section within the MSSM [119]. There have been recently also attempts to use simulated results from the next generation of ton-scale direct detection experiments to forecast certain classes of missing energy distributions observable at the LHC [118]. In this case, the basic idea is that although the direct detection technique is directly sensitive only to the DM mass and scattering cross section, indirectly this class of experiments has also the potential to constrain the parameters, or certain combinations of parameters, which most crucially enter the calculation of specific DM production cross sections at the LHC. An illustrative example of this approach can be found in Ref. [118], where this idea is applied to a light neutralino thermally produced in the early universe via resonant annihilations mediated by the CP-even Higgs boson. In this scenario a hypothetically discovered direct detection signal can be translated into a prediction for the missing energy distribution associated with a LHC final state involving three leptons and missing energy. Similar approaches to the ones presented here have been also investigated to perform combined analyses of DM searches at LHC and in space via γ-ray observations [120,121].

Direct and indirect detection searches are also highly complementary [122,123]. In the MSSM this has been clearly

shown in Ref. [122], where through a scan of the cMSSM parameter space the authors prove that in the plane $\langle\sigma v\rangle/m_\chi^2$ versus spin-independent scattering cross section σ_p, direct and indirect detection experiments probe orthogonal regions. Focusing for instance on the expected sensitivity of the next generation of imaging Cherenkov telescope arrays and assuming a set of dwarf spheroidal galaxies as target regions, in Ref. [122] it is shown that portions of the cMSSM parameter space corresponding to values of $\langle\sigma v\rangle/m_\chi^2$ smaller than 10^{-31} cm^3 s^{-1} GeV^{-2} (and to $\sigma_p > 10^{-11}$ pb) will be explored by ton-scale direct detection experiments but not by indirect searches, on the contrary, regions with $\sigma_p < 10^{-11}$ pb will be probed by indirect searches (if $\langle\sigma v\rangle/m_\chi^2 > 10^{-31}$ cm^3 s^{-1} GeV^{-2}) remaining inaccessible to direct detection experiments.

4.2 SUSY SuperWIMPs

In the case of particles with interactions much weaker than the electroweak one, the chances of DM detections are much more limited than for WIMPs. Nevertheless in particular models where the DM candidate is unstable or couples with more strongly interacting particles, like in the case of gravitino or the axino, the situation is still promising.

4.2.1 Direct detection

The direct detection of particles like the gravitino is unfortunately very difficult, since the scattering cross section is strongly suppressed and practically always below the unavoidable neutrino background. In fact the elastic scattering of a gravitino against the nucleus must proceed through the supergravity dimension-six four-fermion contact interaction or through two single-gravitino vertices, giving a rate suppressed by four powers of the Planck mass. In models where R-parity is violated, also the inelastic scattering of the gravitino into a neutrino is possible, which is instead suppressed only by two powers of the Planck scale and the smallness of the R-parity coupling. Unfortunately for values of such coupling compatible with indirect detection bounds, the rate is also in this case unobservable [30]. Also the axino interaction with quarks is unfortunately too strongly suppressed to give rise to a measurable signal. We can conclude therefore that a confirmed DM signal in a direct detection experiment would be very difficult to reconcile with the hypothesis that DM is a gravitino or axino.

4.2.2 Indirect detection

It has been realized few years ago that gravitino LSP and other SuperWIMPs can be retained as good DM candidates even if R-parity is slightly broken and the LSP is no more stable [124,125]. In fact in most cases the lifetime of the DM particle can still be long enough to exceed the lifetime of the Universe by many orders of magnitude. In the case of the gravitino such small R-parity breaking would be actually quite welcome, since it allows one to avoid any Big Bang Nucleosynthesis (BBN) constraint coming from the (too) late decay of the Next to Lightest Supersymmetric Particle (NLSP) [126]. Indeed in the presence even of a tiny violation coupling above $10^{-12} - 10^{-10}$, most of the NLSPs decay quickly in SM particles before BBN [125]. For other DM candidates like the axino the BBN constraints are less severe [127–129] and therefore the introduction of R-parity breaking perhaps less compelling, but still even in that case the possibility of a decaying DM candidate remains open [34]. Note that, on the other side, the R-parity breaking couplings cannot be too large if one wants to retain the baryonic asymmetry [130,131].

If the DM is not stable, we may be able to detect its decay in our galactic neighborhood or from any of the astrophysical targets discussed already in Sect. 4.1.2. The differential flux of SM particles produced by decaying DM is given by

$$\frac{\mathrm{d}\Phi_i}{\mathrm{d}E\mathrm{d}\Omega}(\theta, E) = \frac{1}{4\pi\tau_\chi m_\chi}\frac{\mathrm{d}N_i}{\mathrm{d}E}(E)\int_{l.o.s.}\mathrm{d}s\rho_\chi(r(s,\theta)) \quad (16)$$

where τ_χ is the DM decay time, $\frac{\mathrm{d}N_i}{\mathrm{d}E}$ is the differential energy spectrum of the SM particles of type i and energy E produced per decay and the last integral is computed along the line of sight. From this expression, we expect from decaying DM a very different spatial distribution of the signal compared to the annihilation case. Moreover the strength of the signal is not very strongly dependent on the particular DM profile density and therefore the bounds are much less affected by astrophysical uncertainties [132]. Note also that, contrary to the case of WIMPs, there is here no direct connection between the DM decay and the DM production mechanism and therefore there is no natural expectation for the DM lifetime.

The decay channels of gravitino DM depend on the particular realization of R-parity breaking. In the case of bilinear R-parity breaking, the main decay channels are into a neutrino and a gauge boson, i.e. photon, Z or Higgs, or a charged lepton and a W. The exact branching ratios depend on the gravitino mass and the supersymmetric spectrum. For a light gravitino below the W threshold, the decay goes into a neutrino and photon, giving rise to the possibility of the smoking-gun signal of a photon line. For particular configurations of the gaugino masses or low $m_{3/2}$, the gravitino decay can be sufficiently suppressed to allow for R-parity breaking couplings able to generate also the neutrino masses [133]. In general though, the Fermi-LAT data set a strong bound on the DM

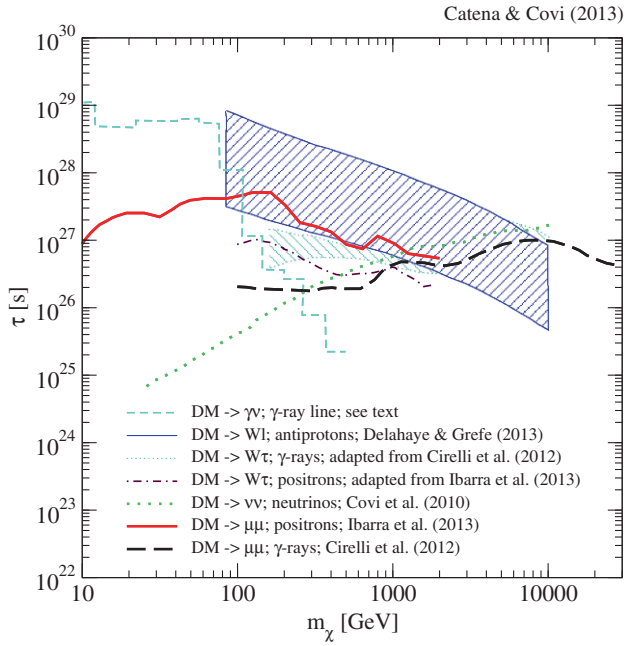

Fig. 3 A compilation of 2-σ exclusion limits in the plane DM mass versus mean DM lifetime for different decay channels. For the gravitino decay in models with bilinear R-parity violation, we give the limits from Fermi-LAT γ-ray *line* searches from [135] rescaled according to the gravitino branching ratio in [137,146] as the *light blue* (*short-dashed*) *line*. Moreover for the same gravitino decaying DM model the blue band corresponds to the limits from antiprotons recently computed in [143]. The size of this band incorporates the uncertainties in the assumed galactic diffusion model. As an indication of the reach of other channels for the same gravitino models, we also give a conservative estimate on the bounds on the dominant gravitino decay channel $W\tau$ combining the WW and $\tau\tau$ constraints from γ-rays [145] in the *green* band and positrons [144] in the *brown* (*dashed-dotted*) *line*. Finally to compare to more general decaying DM candidates, we also give in the *black dashed line* the exclusion limit obtained using the continuum γ-ray data from the Fermi-LAT and in the *red solid line* the exclusion limit derived using the AMS-02 positron flux observations in [145] and [144], respectively. These two analyses apply to generic decaying DM models where the DM candidate dominantly decays into a pair $\mu^+\mu^-$. Also we show with the *green* (*dotted*) *line* projected limits from ICEcube on the decay into two neutrinos [147]

lifetime in a photon line of the order of 5×10^{28} s [134,135], excluding the R-parity breaking parameter space giving origin to neutrino masses, if the gravitino is heavier than few GeV. The spectra from gravitino decay in bilinear R-parity models have been computed in [132,136–139]. In the case of trilinear R-parity breaking, also three-body decays can be important, because the two-body decay only arises at one-loop level [140–142]. As for the case of DM annihilation, until now no clear signal for a DM decay has been found so far. Interpreting the present data as a constraint in the case of gravitino DM, we obtain limits on its lifetime as shown in Fig. 3 collecting results on the bilinear R-parity breaking model from [30,135,143] and adapting results from [144,145].

These gravitino lifetime limits can be reinterpreted in bilinear R-parity breaking models in a limit of the order 3×10^{-8} on the bilinear R-parity breaking strength $\epsilon \sim \frac{\mu'^i}{\mu}$ below the $W\ell$ channel [135] and in even more stringent limits at larger gravitino masses [143]. For the axino case, since the couplings are less suppressed, the R-parity breaking interaction has instead to be of the order of $\sim 10^{-11}$ for axino masses around the GeV [34]. Regarding the claim of a tentative line at 130 GeV in the Fermi-LAT data [89,100], such a line signal may occur naturally with the correct intensity in bilinear R-parity breaking models, both from gravitino [148,149] or axino [150] DM decay, but unfortunately the morphology of the signal region, which appears strongly concentrated in the galactic center [100,151], is not well-fitted by the more broadly distributed decaying DM signal [148]. On the other hand, decaying gravitino DM can accommodate the positron excess observed by PAMELA [138] and AMS-02 [152].

4.2.3 LHC searches

For SuperWIMP DM the direct production at the LHC is in many cases too suppressed to allow to measure the DM candidate directly. The single-gravitino production rate at LHC has been computed in [153] and it results in a visible monojet signal only for very light gravitino with mass well below 1 eV. Such a gravitino could only be considered as a subdominant hot DM component, since the case of dominant hot DM is excluded by large scale structure observations [154,155].

So if we require the gravitino to be heavier than ∼100 keV,[1] the first evidence for gravitino (or axino) would be given by the observation of the strongly interacting superpartners like the gluino or the squark, as already discussed in the neutralino case. The only difference is the modification of the decay chains, and the possibility to have the final decay of the NLSP into gravitino, axino or SM particles in the detector.

We can therefore distinguish two broad classes of signatures depending on the NLSP lifetime: either the NLSP decays in the detector or it is stable on collider timescales. In general the NLSP decay can proceed either via the R-parity conserving (RPC) or the R-parity violating (RPV) couplings and the corresponding lifetimes, assuming e.g. a pure Bino NLSP, are

$$\tau_{\chi,\mathrm{RPC},\tilde{G}} = 1.8 \times 10^{-3}\ \mathrm{s} \left(\frac{M_1}{200\ \mathrm{GeV}}\right)^{-5} \left(\frac{m_{3/2}}{1\ \mathrm{MeV}}\right)^{2}$$

$$\tau_{\chi,\mathrm{RPC},\tilde{a}} = 3.1 \times 10^{-2}\ \mathrm{s} \left(\frac{M_1}{200\ \mathrm{GeV}}\right)^{-3} \left(\frac{f_a}{10^{11}\ \mathrm{GeV}}\right)^{2}$$

[1] This lower value for a Cold DM candidate is usually quoted for a classical thermal relic. In reality the boundary between Warm and Cold DM is fuzzy and depends strongly on the production mechanism, ensuing velocity distribution and possibly presence of other DM components, see e.g. [155].

$$\tau_{\chi,\text{bilRPV}} \sim 1.4 \times 10^{-6}\,\text{s}\left(\frac{M_1}{200\,\text{GeV}}\right)^{-1}\left(\frac{\epsilon}{10^{-9}}\right)^{-2} \quad (17)$$

where we consider the RPC decays into photon and gravitino/axino, and the bilinear R-parity breaking decay into an electroweak gauge boson and a lepton, with ϵ denoting again the overall bilinear R-parity breaking coupling (for more details see e.g. [156]). We see from the time-scales involved that the neutralino decay is prompt (without resolvable second vertex, i.e. $\tau \leq 10^{-12}$ s) only for very small gravitino mass, very large Bino mass or large R-parity breaking couplings, which are already excluded by indirect detection observations. Therefore the classical collider analysis for gauge-mediated SUSY breaking models [28] or RPV models [157] with prompt vertices does not apply to the scenario of SuperWIMP DM.

Much more probable are displaced vertices, as studied in [156,158–161], and in that case, if the decay can be observed, the type of daughter particles will give information on the model and the presence of R-parity violation. The phenomenology expected depends strongly on the type of NLSP and its decay channels. The signal from a long-lived neutralino (N)LSP, produced by squark and providing a muon in the final state, has been recently analyzed by the ATLAS collaboration [162,163] up to decay length of 1 m with no evidence of excess above the SM background. Still many other possible NLSPs and decay channels are yet unexplored.

If instead the NLSP appears stable in the detector, then the most favorable case for detection is if the NLSP is charged. In the case of a slepton NLSP, an electromagnetically charged track could be observed in the tracker and an escaping 'heavy muon' in the muon chambers [164–169], giving an unmistakable signal that a long decay and therefore a very weakly interacting sector is present in the model. Recent LHC analyses are given in [170–172] and they reach limits on the $\tilde{\tau}$ mass above 300 GeV for direct production. Also colored metastable NLSP can give a rich signal, hadronizing into R-hadrons, that can also change sign of the electric charge while they are moving in the detector [164]. The LHC collaborations are looking for such exotic metastable particles, and CMS sets already very strong constraints on the collider-stable stop and gluino (N)LSP, reaching a lower limits of the order of about 800 and 1,200 GeV, respectively [172,173]. ATLAS is performing similar searches [170,174].

Note that a charged NLSP could also be captured in the detector or the surrounding material and open up the possibility to detect the decay in the periods of no collider operation [175], as long as the detectors are kept switched on. Moreover if one could store a stau NLSP and measure not only the dominant decay, but also the radiative decay with an additional γ, it would be possible to distinguish e.g. between gravitino or axino LSP [129,176].

For a detector-stable neutral NLSP, like the neutralino or the sneutrino, instead, the phenomenology is very similar to the classical supersymmetric WIMP scenario discussed in Sect. 4.1.3.

4.2.4 Complementarity of the different detection strategies

If a DM signal will be seen in any of the above channels, it will be important to compare and check the signatures also in an independent channel. In the case of gravitino DM with RPV, this may be possible since the gravitino and NLSP decay derive from the same coupling and, especially for neutralino NLSP, they are strongly correlated [156]. Therefore from the observation of a particular DM mass and lifetime in indirect detection, one could infer at least a range of expected NLSP lifetimes and masses. On the other hand, measuring RPV at the LHC would surely strongly restrict the possible DM candidates, and it would give a prediction of the possible SuperWIMP indirect detection rate, depending on the DM mass. In this scenario the direct detection measurement could instead be vital to disentangle the case of neutral NLSP from the WIMP scenario, e.g. excluding the possibility that a neutralino seen at LHC could be the DM.

Of course if the LHC will be able to measure the complete supersymmetric spectrum and estimate some of the neutralino mixings, also detailed studies and checks on the possible DM production mechanisms could be realized extending our knowledge of the cosmological history to the electroweak scale or beyond [177–179].

5 Dark matter and the Higgs boson

The discovery of a new bosonic state at the LHC whose mass is close to 126 GeV—plausibly (one of) the celebrated Higgs boson(s)—has influenced in various ways the last year of theoretical research in particle and astroparticle physics. Though the DM properties could be in principle unrelated to those of the Higgs boson, in the vast majority of the theoretical frameworks considered to quantitatively address the DM problem, the Higgs boson discovery indirectly impacts the allowed configurations in the parameter space of the underlying DM theory. The indirect influence of the Higgs boson mass on the nature of the DM candidate has been quantified by various groups through global fits of the most popular beyond the SM theories to large data sets including the latest LHC discovery and bounds obtained from the null result of searches for new physics [50–52].

In the context of the cMSSM the latest LHC Higgs boson mass measurement has significantly pushed towards larger values of $m_{1/2}$ the favored regions in the plane $(m_{1/2}, m_0)$ [50]. This is mainly a consequence of the fact that global fits without the Higgs boson mass measure-

ment tend to prefer Higgs boson masses below 120 GeV. The requirement of reproducing the observed value for the Higgs mass therefore entails specific supersymmetric configurations characterized either by large stop masses, enhancing the Higgs mass thorough sizable stop-loop corrections, or by maximal mixing in the stop sector, which occurs when the stop mixing parameter X_t approaches the value $0.5(m^2_{\tilde{t}_1} + m^2_{\tilde{t}_2})$, where $m_{\tilde{t}_1}$ and $m_{\tilde{t}_2}$ are the masses of the stop mass eigenstates. In both scenarios low values of $m_{1/2}$ are not allowed.

The impact of a Higgs boson mass close to 126 GeV has also been discussed in the NMSSM [180] and in the context of the pMSSM [181], where the large dimensionality of the underlying parameter space allows one to accommodate more smoothly the latest LHC results. We refer the reader to the review of this series by John Ellis for further details of the role of the Higgs discovery in the context of SUSY global fits. We note only that in general a heavy spectrum is less easily reconciled with the present DM density, since the annihilation cross section determining the WIMP relic density becomes weaker with increasing masses and therefore the abundance larger. Nevertheless even in the simple cMSSM there are surviving islands of acceptable neutralino number densities compatible with heavy spectra, for example in the Higgsino/Wino scenarios, which could give a stronger direct detection signal, or also along the stau-neutralino coannihilation strip. In the latter case though, the degeneracy between the NLSP and LSP needed to give the observed DM density is so strong that such a region may be excluded soon by LHC searches for metastable massive charged particles [182].

In connection to the case of SuperWIMP DM, instead, a heavy spectrum is not in general a problem, since it actually relaxes in part the BBN bounds, thanks to the shorter NLSP lifetime. Moreover for large NLSP masses it is easier to exploit the SuperWIMP production mechanism also for charged NLSPs. On the other hand, one has to admit that a heavy supersymmetric particle spectrum increases as well the thermal production contribution to the present DM density tightening the upper bound on the reheat temperature [183]. Recent analyses of gravitino DM in different MSSM realizations after the Higgs discovery are given in Refs. [184,185].

Though all LHC measurements are consistent with SM expectations, the observation of a Higgs diphoton rate somewhat larger than expected (the ATLAS collaboration reports a deviation close to 1.5 σ [186]) has motivated studies where this result was put in relation with the Fermi-LAT 130 GeV γ-ray line in models where DM is coupled to the Higgs boson. A simple unified description of the two phenomena has been proposed in Ref. [187], which provides a concrete realization within the NMSSM of a scenario where sizable DM annihilations into photons are associated with an enhanced Higgs diphoton rate.

6 Summary and outlook

We have reviewed here different supersymmetric DM candidates, discussing in particular the two extreme cases of the neutralino WIMP and the much more weakly interacting gravitino/axino. In both cases we are still missing a convincing signal, though the LHC as well as direct and indirect detection experiments are already putting interesting constraints on the parameter space of the basic supersymmetric models. On the other hand, the supersymmetric framework for DM is still very flexible and viable regions for (nearly) any type of supersymmetric DM are open in more general settings and not only in those.

We would like to stress again that galactic and extragalactic DM searches provide information on a different sector of the DM theory than that more directly probed at the LHC and that data from all available sources will be absolutely needed to identify univocally the DM particle. In this respect we can look forward to a very productive time in the next decade since, while LHC will push the high-energy exploration further, hopefully finding soon some type of beyond the SM physics, direct and indirect detection experiments will continue to search for DM. XENON 1-ton, for instance, is expected to start the scientific phase in 2015, essentially in parallel with the high-energy run of the LHC. The Cherenkov Telescope Array, an observatory for ground-based γ-ray astronomy, is currently completing the preparatory phase while AMS-02 will continue taking high-quality data for many more years. Also the astrophysical aspects of the DM problem will be probed in depth in the next years through the Gaia space observatory, launched in November 2013 to measure the kinematical properties of about 10^9 stars in our galaxy.

In the best case scenario, there is still a reasonable hope of a contemporary detection of DM in all three detection strategies and in many different experiments, allowing to test thoroughly both the WIMP hypothesis and the supersymmetric nature of DM. In absence of a signal at the LHC, direct and indirect detection experiments may nevertheless be able to pinpoint a WIMP in the near future. On the other hand, for the case of SuperWIMPs the LHC searches are not yet optimized, but they will surely come to maturity in the next run, allowing to cover most of the supersymmetric parameter space, as long as the mass scales are within reach. In the worst case scenario, instead, where no DM signals will be identified in the next decade with the different techniques presented here, we would have nevertheless learned that many of our current paradigms, like for instance the WIMP mechanism, need to be revised in favor of different and more flexible approaches, showing once again that Nature is often more rich and sophisticated than what one might expect at first.

Acknowledgments We would like to thank Michael Grefe and Leszek Roszkowski for valuable comments on the first version of this manuscript. The authors acknowledge partial financial support by the German-Israeli Foundation for scientific research and development (GIF) and by the EU FP7 ITN Invisibles (Marie Curie Actions, PITN-GA-2011-289442).

References

1. L. Bergstrom, Rep. Prog. Phys. **63**, 793 (2000) (Preprint hep-ph/0002126)
2. G. Bertone, D. Hooper, J. Silk, Phys. Rep. **405**, 279–390 (2005) (Preprint hep-ph/0404175)
3. P. Gondolo, G. Gelmini, Nucl. Phys. B **360**, 145–179 (1991)
4. J. Edsjo, P. Gondolo, Phys. Rev. D **56**, 1879–1894 (1997) (Preprint hep-ph/9704361)
5. M. Bolz, A. Brandenburg, W. Buchmuller, Nucl. Phys. B **606**, 518–544 (2001) (Preprint hep-ph/0012052)
6. J. Pradler, F.D. Steffen, Phys. Rev. D **75**, 023509 (2007) (Preprint hep-ph/0608344)
7. V.S. Rychkov, A. Strumia, Phys. Rev. D **75**, 075011 (2007) (Preprint hep-ph/0701104)
8. V.S. Rychkov, A. Strumia, Phys. Rev. D **75**, 075011 (2007) (Preprint hep-ph/0701104)
9. A. Brandenburg, F.D. Steffen, JCAP **0408**, 008 (2004) (Preprint hep-ph/0405158)
10. A. Strumia, JHEP **1006**, 036 (2010) (Preprint 1003.5847)
11. J. McDonald, Phys. Rev. Lett. **88**, 091304 (2002) (Preprint hep-ph/0106249)
12. L. Covi, L. Roszkowski, M. Small, JHEP **0207**, 023 (2002) (Preprint hep-ph/0206119)
13. T. Asaka, K. Ishiwata, T. Moroi, Phys. Rev. D **73**, 051301 (2006) (Preprint hep-ph/0512118)
14. L.J. Hall, K. Jedamzik, J. March-Russell, S.M. West, JHEP **1003**, 080 (2010) (Preprint 0911.1120)
15. C. Cheung, G. Elor, L. Hall, Phys. Rev. D **84**, 115021 (2011) (Preprint 1103.4394)
16. L. Covi, J.E. Kim, L. Roszkowski, Phys. Rev. Lett. **82**, 4180–4183 (1999) (Preprint hep-ph/9905212)
17. J.L. Feng, A. Rajaraman, F. Takayama, Phys. Rev. Lett. **91**, 011302 (2003) (Preprint hep-ph/0302215)
18. J.L. Feng, A. Rajaraman, F. Takayama, Phys. Rev. D **68**, 063504 (2003) (Preprint hep-ph/0306024)
19. J. Wess, J. Bagger, *Supersymmetry and Supergravity* (Princeton University Press, Princeton, 1992)
20. S.P. Martin (1997) (Preprint hep-ph/9709356)
21. R. Flores, K.A. Olive, D. Thomas, Phys. Lett. B **245**, 509–515 (1990)
22. C. Hugonie, G. Belanger, A. Pukhov, JCAP **0711**, 009 (2007) (Preprint 0707.0628)
23. M. Maniatis, Int. J. Mod. Phys. A **25**, 3505–3602 (2010) (Preprint 0906.0777)
24. J. Ellis, J.S. Hagelin, D.V. Nanopoulos, K. Olive, M. Srednicki, Nucl. Phys. B **238**, 453 (1984)
25. G. Jungman, M. Kamionkowski, K. Griest, Phys. Rep. **267**, 195–373 (1996) (Preprint hep-ph/9506380)
26. H.K. Dreiner, H.E. Haber, S.P. Martin, Phys. Rep. **494**, 1–196 (2010) (Preprint 0812.1594)
27. D. Cerdeno, E. Gabrielli, D. Lopez-Fogliani, C. Munoz, A. Teixeira, JCAP **0706**, 008 (2007) (Preprint hep-ph/0701271)
28. G. Giudice, R. Rattazzi, Phys. Rep. **322**, 419–499 (1999) (Preprint hep-ph/9801271)
29. J. Pradler (2007) (Preprint 0708.2786)
30. M. Grefe (2011) (Preprint 1111.6779)
31. R. Peccei, H.R. Quinn, Phys. Rev. Lett. **38**, 1440–1443 (1977)
32. H.P. Nilles, S. Raby, Nucl. Phys. B **198**, 102–112 (1982)
33. J. Frere, J. Gerard, Lett. Nuovo Cim. **37**, 135 (1983)
34. L. Covi, J.E. Kim, New J. Phys. **11**, 105003 (2009) (Preprint 0902.0769)
35. M. Dine, W. Fischler, M. Srednicki, Phys. Lett. B **104**, 199 (1981)
36. A. Zhitnitsky, Sov. J. Nucl. Phys. **31**, 260 (1980)
37. J.E. Kim, Phys. Rev. Lett. **43**, 103 (1979)
38. M.A. Shifman, A. Vainshtein, V.I. Zakharov, Nucl. Phys. B **166**, 493 (1980)
39. K.J. Bae, K. Choi, S.H. Im, JHEP **1108**, 065 (2011) (Preprint 1106.2452)
40. K.Y. Choi, L. Covi, J.E. Kim, L. Roszkowski, JHEP **1204**, 106 (2012) (Preprint 1108.2282)
41. G.G. Raffelt, Lect. Notes Phys. **741**, 51–71 (2008) (Preprint hep-ph/0611350)
42. E.J. Chun, Phys. Rev. D **84**, 043509 (2011) (Preprint 1104.2219)
43. T. Falk, K.A. Olive, M. Srednicki, Phys. Lett. B **339**, 248–251 (1994) (Preprint hep-ph/9409270)
44. L.J. Hall, T. Moroi, H. Murayama, Phys. Lett. B **424**, 305–312 (1998) (Preprint hep-ph/9712515)
45. B. Dumont, G. Belanger, S. Fichet, S. Kraml, T. Schwetz, JCAP **1209**, 013 (2012) (Preprint 1206.1521)
46. C. Arina, F. Bazzocchi, N. Fornengo, J. Romao, J. Valle, Phys. Rev. Lett. **101**, 161802 (2008) (Preprint 0806.3225)
47. D.G. Cerdeno, C. Munoz, O. Seto, Phys. Rev. D **79**, 023510 (2009) (Preprint 0807.3029)
48. L. Basso, B. O'Leary, W. Porod, F. Staub, JHEP **1209**, 054 (2012) (Preprint 1207.0507)
49. J.L. Feng, J. Kumar, Phys. Rev. Lett. **101**, 231301 (2008) (Preprint 0803.4196)
50. C. Strege, G. Bertone, F. Feroz, M. Fornasa, R. Ruiz de Austri et al., JCAP **1304**, 013 (2013) (Preprint 1212.2636)
51. P. Bechtle, T. Bringmann, K. Desch, H. Dreiner, M. Hamer et al., JHEP **1206**, 098 (2012) (Preprint 1204.4199)
52. O. Buchmueller, R. Cavanaugh, M. Citron, A. De Roeck, M. Dolan et al., Eur. Phys. J. C **72**, 2243 (2012) (Preprint 1207.7315)
53. M.W. Goodman, E. Witten, Phys. Rev. D **31**, 3059 (1985)
54. M. Drees, M. Nojiri, Phys. Rev. D **48**, 3483–3501 (1993) (Preprint hep-ph/9307208)
55. J.R. Ellis, A. Ferstl, K.A. Olive, Phys. Lett. B **481**, 304–314 (2000) (Preprint hep-ph/0001005)
56. A.L. Fitzpatrick, W. Haxton, E. Katz, N. Lubbers, Y. Xu (2012) (Preprint 1211.2818)
57. G. Angloher, M. Bauer, I. Bavykina, A. Bento, C. Bucci et al., Eur. Phys. J. C **72**, 1971 (2012) (Preprint 1109.0702)
58. C. Aalseth, P. Barbeau, J. Colaresi, J. Collar, J. Diaz Leon et al., Phys. Rev. Lett. **107**, 141301 (2011) (Preprint 1106.0650)
59. R. Agnese et al. (CDMS Collaboration), Phys. Rev. Lett. (2013) (Preprint 1304.4279)
60. R. Bernabei et al. (DAMA Collaboration, LIBRA Collaboration), Eur. Phys. J. C **67**, 39–49 (2010) (Preprint 1002.1028)
61. E. Aprile et al. (XENON100 Collaboration), Phys. Rev. Lett. **109**, 181301 (2012) (Preprint 1207.5988)
62. N. Fornengo, S. Scopel, A. Bottino Phys. Rev. D **83**, 015001 (2011) (Preprint 1011.4743)
63. P. Bhupal Dev, S. Mondal, B. Mukhopadhyaya, S. Roy, JHEP **1209**, 110 (2012) (Preprint 1207.6542)
64. C. Boehm, P.S.B. Dev, A. Mazumdar, E. Pukartas, JHEP **1306**, 113 (2013) (Preprint 1303.5386)

65. J.L. Feng, J. Kumar, D. Marfatia, D. Sanford, Phys. Lett. B **703**, 124–127 (2011) (Preprint 1102.4331)
66. S. Kim, H. Bhang, J. Choi, W. Kang, B. Kim et al., Phys. Rev. Lett. **108**, 181301 (2012) (Preprint 1204.2646)
67. K. Kowalska, L. Roszkowski, E.M. Sessolo, JHEP **1306**, 078 (2013) (Preprint 1302.5956)
68. A. Fowlie, K. Kowalska, L. Roszkowski, E.M. Sessolo, Y.L.S. Tsai, Phys. Rev. D **88**, 055012 (2013) (Preprint 1306.1567)
69. J. Billard, L. Strigari, E. Figueroa-Feliciano (2013) (Preprint 1307.5458)
70. R. Catena, P. Ullio, JCAP **1008**, 004 (2010) (Preprint 0907.0018)
71. R. Catena, P. Ullio, JCAP **1205**, 005 (2012) (Preprint 1111.3556)
72. N. Bozorgnia, R. Catena, T. Schwetz (2013) (Preprint 1310.0468)
73. D. Cerdeno, M. Fornasa, J. Huh, M. Peiro, Phys. Rev. D **87**, 023512 (2013) (Preprint 1208.6426)
74. P.J. Fox, G.D. Kribs, T.M. Tait, Phys. Rev. D **83**, 034007 (2011) (Preprint 1011.1910)
75. P.J. Fox, J. Liu, N. Weiner, Phys. Rev. D **83**, 103514 (2011) (Preprint 1011.1915)
76. E. Del Nobile, G. Gelmini, P. Gondolo, J.H. Huh (2013) (Preprint 1306.5273)
77. J. Herrero-Garcia, T. Schwetz, J. Zupan, Phys. Rev. Lett. **109**, 141301 (2012) (Preprint 1205.0134)
78. B.J. Kavanagh, A.M. Green, Phys. Rev. Lett. **111**, 031302 (2013) (Preprint 1303.6868)
79. M. Pato, L. Baudis, G. Bertone, R. Ruiz de Austri, L.E. Strigari et al., Phys. Rev. D **83**, 083505 (2011) (Preprint 1012.3458)
80. T. Bringmann, C. Weniger, Phys. Dark Univ. **1**, 194–217 (2012) (Preprint 1208.5481)
81. P. Salati, F. Donato, N. Fornengo (2010) (Preprint 1003.4124)
82. F. Donato, N. Fornengo, P. Salati, Phys. Rev. D **62**, 043003 (2000) (Preprint hep-ph/9904481)
83. A. Strong, I. Moskalenko, Astrophys. J. **509**, 212–228 (1998) (Preprint astro-ph/9807150)
84. T. Delahaye, R. Lineros, F. Donato, N. Fornengo, P. Salati, Phys. Rev. D **77**, 063527 (2008) (Preprint 0712.2312)
85. M. Cirelli, P. Panci, Nucl. Phys. B **821**, 399–416 (2009) (Preprint 0904.3830)
86. M. Kuhlen, M. Vogelsberger, R. Angulo, Phys. Dark Univ. **1**, 50–93 (2012) (Preprint 1209.5745)
87. L. Bergstrom, J. Edsjo, P. Gondolo, Phys. Rev. D **58**, 103519 (1998) (Preprint hep-ph/9806293)
88. M. Drees, M.M. Nojiri, Phys. Rev. D **47**, 376–408 (1993) (Preprint hep-ph/9207234)
89. T. Bringmann, X. Huang, A. Ibarra, S. Vogl, C. Weniger, JCAP **1207**, 054 (2012) (Preprint 1203.1312)
90. T. Bringmann, L. Bergstrom, J. Edsjo, JHEP **0801**, 049 (2008) (Preprint 0710.3169)
91. P. Ciafaloni, M. Cirelli, D. Comelli, A. De Simone, A. Riotto et al., JCAP **1106**, 018 (2011) (Preprint 1104.2996)
92. P. Gondolo, J. Edsjo, P. Ullio, L. Bergstrom, M. Schelke et al., JCAP **0407**, 008 (2004) (Preprint astro-ph/0406204)
93. L. Bergstrom, P. Ullio, Nucl. Phys. B **504**, 27–44 (1997) (Preprint hep-ph/9706232)
94. P. Ullio, L. Bergstrom, Phys. Rev. D **57**, 1962–1971 (1998) (Preprint hep-ph/9707333)
95. O. Adriani (PAMELA Collaboration) et al., Nature **458**, 607–609 (2009) (Preprint 0810.4995)
96. D. Hooper, P. Blasi, P.D. Serpico, JCAP **0901**, 025 (2009) (Preprint 0810.1527)
97. T. Linden, S. Profumo, Astrophys. J. **772**, 18 (2013) (Preprint 1304.1791)
98. M. Aguilar (AMS Collaboration) et al., Phys. Rev. Lett. **110**, 141102 (2013)
99. O. Adriani (PAMELA Collaboration) et al., Phys. Rev. Lett. **105**, 121101 (2010) (Preprint 1007.0821)
100. C. Weniger, JCAP **1208**, 007 (2012) (Preprint 1204.2797)
101. M. Ackermann (Fermi-LAT Collaboration) et al. (2013) (Preprint 1305.5597)
102. N. Fornengo, R. Lineros, M. Regis, M. Taoso, Phys. Rev. Lett. **107**, 271302 (2011) (Preprint 1108.0569)
103. M. Ackermann (Fermi-LAT Collaboration) et al. (2013) (Preprint 1310.0828)
104. R. Catena, N. Fornengo, A. Masiero, M. Pietroni, F. Rosati, Phys. Rev. D **70**, 063519 (2004) (Preprint astro-ph/0403614)
105. R. Catena, N. Fornengo, M. Pato, L. Pieri, A. Masiero, Phys. Rev. D **81**, 123522 (2010) (Preprint 0912.4421)
106. M. Schelke, R. Catena, N. Fornengo, A. Masiero, M. Pietroni, Phys. Rev. D **74**, 083505 (2006) (Preprint hep-ph/0605287)
107. R. Catena, N. Fornengo, A. Masiero, M. Pietroni, M. Schelke, JHEP **0810**, 003 (2008) (Preprint 0712.3173)
108. 2013 Search for new physics in monojet events in pp collisions at sqrt(s) = 8 tev Tech. Rep. CMS-PAS-EXO-12-048 CERN Geneva
109. G. Aad (ATLAS Collaboration) et al., Phys. Rev. Lett. **110**, 011802 (2013) (Preprint 1209.4625)
110. G. Aad (ATLAS Collaboration) et al. (2013) (Preprint 1309.4017)
111. 2013 Search for dark matter in the mono-lepton channel with pp collision events at center-of-mass energy of 8 tev Tech. Rep. CMS-PAS-EXO-13-004 CERN Geneva
112. 2013 Search for direct-slepton and direct-chargino production in final states with two opposite-sign leptons, missing transverse momentum and no jets in 20/fb of pp collisions at sqrt(s) = 8 tev with the atlas detector Tech. Rep. ATLAS-CONF-2013-049 CERN Geneva
113. 2013 Search for direct production of charginos and neutralinos in events with three leptons and missing transverse momentum in 21 fb^{-1} of pp collisions at $\sqrt{s} = 8$ tev with the atlas detector Tech. Rep. ATLAS-CONF-2013-035 CERN Geneva
114. 2013 Search for strongly produced supersymmetric particles in decays with two leptons at $\sqrt{s} = 8$ tev Tech. Rep. ATLAS-CONF-2013-089 CERN Geneva
115. J. Goodman, M. Ibe, A. Rajaraman, W. Shepherd, T.M. Tait et al., Phys. Rev. D **82**, 116010 (2010) (Preprint 1008.1783)
116. I.M. Shoemaker, L. Vecchi, Phys. Rev. D **86**, 015023 (2012) (Preprint 1112.5457)
117. O. Buchmueller, M.J. Dolan, C. McCabe (2013) (Preprint 1308.6799)
118. G. Arcadi, R. Catena, P. Ullio (2012) (Preprint 1211.5129)
119. E.A. Baltz, M. Battaglia, M.E. Peskin, T. Wizansky, Phys. Rev. D **74**, 103521 (2006) (Preprint hep-ph/0602187)
120. G. Bertone, D. Cerdeno, M. Fornasa, L. Pieri, R. Ruiz de Austri et al., Phys. Rev. D **85**, 055014 (2012) (Preprint 1111.2607)
121. J. Kopp, E.T. Neil, R. Primulando, J. Zupan, Phys. Dark Univ. **2**, 22–34 (2013) (Preprint 1301.1683)
122. L. Bergstrom, T. Bringmann, J. Edsjo, Phys. Rev. D **83**, 045024 (2011) (Preprint 1011.4514)
123. C. Arina, G. Bertone, H. Silverwood, Phys. Rev. D **88**, 013002 (2013) (Preprint 1304.5119)
124. F. Takayama, M. Yamaguchi, Phys. Lett. B **485**, 388–392 (2000) (Preprint hep-ph/0005214)
125. W. Buchmuller, L. Covi, K. Hamaguchi, A. Ibarra, T. Yanagida, JHEP **0703**, 037 (2007) (Preprint hep-ph/0702184)
126. K. Jedamzik, M. Pospelov, New J. Phys. **11**, 105028 (2009) (Preprint 0906.2087)
127. H. Baer, S. Kraml, A. Lessa, S. Sekmen, JCAP **1011**, 040 (2010) (Preprint 1009.2959)
128. H. Baer, S. Kraml, A. Lessa, S. Sekmen, JCAP **1104**, 039 (2011) (Preprint 1012.3769)
129. A. Freitas, F.D. Steffen, N. Tajuddin, D. Wyler, JHEP **1106**, 036 (2011) (Preprint 1105.1113)
130. H.K. Dreiner, G.G. Ross, Nucl. Phys. B **410**, 188–216 (1993) (Preprint hep-ph/9207221)

131. M. Endo, K. Hamaguchi, S. Iwamoto, JCAP **1002**, 032 (2010) (Preprint 0912.0585)
132. G. Bertone, W. Buchmuller, L. Covi, A. Ibarra, JCAP **0711**, 003 (2007) (Preprint 0709.2299)
133. D. Restrepo, M. Taoso, J. Valle, O. Zapata, Phys. Rev. D **85**, 023523 (2012) (Preprint 1109.0512)
134. A. Abdo, M. Ackermann, M. Ajello, W. Atwood, L. Baldini et al., Phys. Rev. Lett. **104**, 091302 (2010) (Preprint 1001.4836)
135. G. Vertongen, C. Weniger, JCAP **1105**, 027 (2011) (Preprint 1101.2610)
136. K. Ishiwata, S. Matsumoto, T. Moroi, Phys. Rev. D **78**, 063505 (2008) (Preprint 0805.1133)
137. L. Covi, M. Grefe, A. Ibarra, D. Tran, JCAP **0901**, 029 (2009) (Preprint 0809.5030)
138. W. Buchmuller, A. Ibarra, T. Shindou, F. Takayama, D. Tran, JCAP **0909**, 021 (2009) (Preprint 0906.1187)
139. K.Y. Choi, D.E. Lopez-Fogliani, C. Munoz, R.R. de Austri, JCAP **1003**, 028 (2010) (Preprint 0906.3681)
140. S. Lola, P. Osland, A. Raklev, Phys. Lett. B **656**, 83–90 (2007) (Preprint 0707.2510)
141. N.E. Bomark, S. Lola, P. Osland, A. Raklev, Phys. Lett. B **686**, 152–161 (2010) (Preprint 0911.3376)
142. B. Bajc, T. Enkhbat, D.K. Ghosh, G. Senjanovic, Y. Zhang, JHEP **1005**, 048 (2010) (Preprint 1002.3631)
143. T. Delahaye, M. Grefe (2013) (Preprint 1305.7183)
144. A. Ibarra, A.S. Lamperstorfer, J. Silk (2013) (Preprint 1309.2570)
145. M. Cirelli, E. Moulin, P. Panci, P.D. Serpico, A. Viana, Phys. Rev. D **86**, 083506 (2012) (Preprint 1205.5283)
146. M. Grefe, J. Phys. Conf. Ser. **375**, 012035 (2012) (Preprint 1111.7117)
147. L. Covi, M. Grefe, A. Ibarra, D. Tran, JCAP **1004**, 017 (2010) (Preprint 0912.3521)
148. W. Buchmuller, M. Garny, JCAP **1208**, 035 (2012) (Preprint 1206.7056)
149. S.P. Liew, Phys. Lett. B **724**, 88–91 (2013) (Preprint 1304.1992)
150. M. Endo, K. Hamaguchi, S.P. Liew, K. Mukaida, K. Nakayama, Phys. Lett. B **721**, 111–117 (2013) (Preprint 1301.7536)
151. M. Su, D.P. Finkbeiner (2012) (Preprint 1206.1616)
152. M. Ibe, S. Iwamoto, S. Matsumoto, T. Moroi, N. Yokozaki, JHEP **1308**, 029 (2013) (Preprint 1304.1483)
153. M. Klasen, G. Pignol, Phys. Rev. D **75**, 115003 (2007) (Preprint hep-ph/0610160)
154. M. Viel, G.D. Becker, J.S. Bolton, M.G. Haehnelt, M. Rauch et al., Phys. Rev. Lett. **100**, 041304 (2008) (Preprint 0709.0131)
155. A. Boyarsky, J. Lesgourgues, O. Ruchayskiy, M. Viel, JCAP **0905**, 012 (2009) (Preprint 0812.0010)
156. S. Bobrovskyi, W. Buchmuller, J. Hajer, J. Schmidt, JHEP **1109**, 119 (2011) (Preprint 1107.0926)
157. R. Barbier, C. Berat, M. Besancon, M. Chemtob, A. Deandrea et al., Phys. Rep. **420**, 1–202 (2005) (Preprint hep-ph/0406039)
158. K. Ishiwata, T. Ito, T. Moroi, Phys. Lett. B **669**, 28–33 (2008) (Preprint 0807.0975)
159. S. Chang, M.A. Luty (2009) (Preprint 0906.5013)
160. P. Meade, M. Reece, D. Shih, JHEP **1010**, 067 (2010) (Preprint 1006.4575)
161. S. Asai, Y. Azuma, M. Endo, K. Hamaguchi, S. Iwamoto, JHEP **1112**, 041 (2011) (Preprint 1103.1881)
162. G. Aad (ATLAS Collaboration) et al., Phys. Lett. B **719**, 280–298 (2013) (Preprint 1210.7451)
163. 2013 Search for long-lived, heavy particles in final states with a muon and a multi-track displaced vertex in proton-proton collisions at sqrt(s) = 8tev with the atlas detector. Tech. Rep. ATLAS-CONF-2013-092 CERN Geneva
164. M. Fairbairn, A. Kraan, D. Milstead, T. Sjostrand, P.Z. Skands et al., Phys. Rep. **438**, 1–63 (2007) (Preprint hep-ph/0611040)
165. J.R. Ellis, A.R. Raklev, O.K. Oye, JHEP **0610**, 061 (2006) (Preprint hep-ph/0607261)
166. M. Endo, K. Hamaguchi, K. Nakaji (2011) (Preprint 1105.3823)
167. T. Ito, K. Nakaji, S. Shirai, Phys. Lett. B **706**, 314–319 (2012) (Preprint 1104.2101)
168. J. Heisig, J. Kersten, Phys. Rev. D **86**, 055020 (2012) (Preprint 1203.1581)
169. J. Heisig, J. Kersten, B. Panes, T. Robens (2013) (Preprint 1310.2825)
170. G. Aad (ATLAS Collaboration) et al., Phys. Lett. B **720**, 277–308 (2013) (Preprint 1211.1597)
171. 2013 A search for heavy long-lived sleptons using 16 fb^{-1} of pp collisions at $\sqrt{s} = 8$ tev with the atlas detector Tech. Rep. ATLAS-CONF-2013-058 CERN Geneva
172. S. Chatrchyan (CMS Collaboration) et al. **1307**, 122 (2013) (Preprint 1305.0491)
173. S. Chatrchyan (CMS Collaboration) et al. Phys. Lett. B **713**, 408–433 (2012) (Preprint 1205.0272)
174. 2013 Search for long-lived stopped gluino r-hadrons decaying out-of-time with lhc collisions in 2011 and 2012 using the atlas detector Tech. Rep. ATLAS-CONF-2013-057 CERN Geneva
175. S. Asai, K. Hamaguchi, S. Shirai, Phys. Rev. Lett. **103**, 141803 (2009) (Preprint 0902.3754)
176. A. Brandenburg, L. Covi, K. Hamaguchi, L. Roszkowski, F. Steffen, Phys. Lett. B **617**, 99–111 (2005) (Preprint hep-ph/0501287)
177. K.Y. Choi, L. Roszkowski, R. Ruiz de Austri, JHEP **0804**, 016 (2008) (Preprint 0710.3349)
178. F.D. Steffen, Phys. Lett. B **669**, 74–80 (2008) (Preprint 0806.3266)
179. A. Freitas, F.D. Steffen, N. Tajuddin, D. Wyler, Phys. Lett. B **679**, 270–277 (2009) (Preprint 0904.3218)
180. K. Kowalska, S. Munir, L. Roszkowski, E.M. Sessolo, S. Trojanowski et al., Phys. Rev. D **87**, 115010 (2013) (Preprint 1211.1693)
181. A. Arbey, M. Battaglia, A. Djouadi, F. Mahmoudi, Phys. Lett. B **720**, 153–160 (2013) (Preprint 1211.4004)
182. M. Citron, J. Ellis, F. Luo, J. Marrouche, K. Olive et al., Phys. Rev. D **87**, 036012 (2013) (Preprint 1212.2886)
183. K. Hamaguchi, F. Takahashi, T. Yanagida, Phys. Lett. B **677**, 59–61 (2009) (Preprint 0901.2168)
184. L. Roszkowski, S. Trojanowski, K. Turzynski, K. Jedamzik, JHEP **1303**, 013 (2013) (Preprint 1212.5587)
185. J. Hasenkamp, M.W. Winkler (2013) (Preprint 1308.2678)
186. G. Aad (ATLAS Collaboration) et al., Phys. Lett. B (2013) (Preprint 1307.1427)
187. K. Schmidt-Hoberg, F. Staub, M.W. Winkler, JHEP **1301**, 124 (2013) (Preprint 1211.2835)

Eur. Phys. J. C (2014) 74:2712
DOI 10.1140/epjc/s10052-013-2712-3

THE EUROPEAN PHYSICAL JOURNAL C

Review

The strings connection: MSSM-like models from strings

Hans Peter Nilles[a]

Bethe Center for Theoretical Physics (BCTP) and Physikalisches Institut der Universität Bonn, Nussallee 12, 53115 Bonn, Germany

Received: 20 November 2013 / Accepted: 27 November 2013 / Published online: 27 May 2014

Abstract String theory constructions towards the MSSM allow us to identify some general properties that could be relevant for tests at the LHC. They originate from the geometric structure of compactification and the location of fields in extra-dimensional space. Within the framework of the heterotic MiniLandscape we extract some generic lessons for supersymmetric model building. Among them is a specific pattern of SUSY breakdown based on mirage mediation and remnants of extended supersymmetry. This leads to a split spectrum with heavy scalars of the first two families of quarks and leptons and suppressed masses for gauginos, top partners and Higgs bosons. The models exhibit some specific form of hidden supersymmetry consistent with the high mass of the Higgs boson and all presently available experimental constraints. The most compelling picture is based on precision gauge coupling unification that might be in the kinematic reach of the LHC.

1 Introduction

The standard model (SM) of particle physics and its minimal supersymmetric extension (MSSM) are under experimental investigation at the Large Hadron Collider (LHC) and other high energy physics experiments. The recent discovery of the Higgs boson [1,2] has strong impact on the SM and the MSSM. While these models were constructed to understand particle physics at the TeV scale from a bottom-up perspective, it would be of interest to extend them to higher energies and find a consistent ultraviolet (UV) completion. The UV extrapolation of the MSSM seems to be consistent with a grand unified (GUT) picture where all the gauge interactions are derived from a unified group structure. The inclusion of gravitational interactions would point to a UV-completion within superstring theory. In such a unified scheme we would then hope for a better understanding of the many free parameters of the SM and the MSSM.

The construction of particle physics models from string theory started with great enthusiasm in the mid-1980s triggered by the seminal paper of Green and Schwarz [3], suggesting unified gauge groups like SO(32) and $E_8 \times E_8$. Meanwhile we can look back at model constructions within the framework of heterotic theories, type I, type IIA and B as well as M- and F-theory.[1]

Unfortunately string theories do not lead exclusively to the SM or MSSM at low energies. These models are not a generic part of the so-called "Landscape" of string theories. To find them (if at all) we have to look at specific spots and corners of this landscape. The task of string phenomenology is thus an effort to see whether the MSSM can be embedded in string theory (rather than derive it directly from string theory). Once such embeddings are found we can then try to extract common properties shared by the successful models as possible "predictions" of string theory. Relevant issues concern gauge-Yukawa unification, gauge-Higgs unification, a solution to the μ-problem, the flavor structure and the absence of exotics.

String theory is defined in $d = 10$-dimensional space-time while SM and MSSM reside in $d = 4$. Properties of the $d = 4$ models depend crucially on the compactification of the extra spatial dimensions. Here it is not only the geometry of the compact manifold, but also the geographic localization of the fields on that manifold. Essentially all low-energy physics is given by these geometrical and geographical properties. This includes the possible appearance of scale hierarchies within the framework of string theories. They could come from locations of enhanced symmetry at corners of the moduli space of the extra-dimensional manifold. String model building is thus a map of the "Landscape" of extra dimensions to the "Landscape" of string vacua with SM or MSSM structure. Such an analysis requires the construction of a vast amount

[a] e-mail: nilles@th.physik.uni-bonn.de

[1] For recent reviews and a comprehensive list of references see [4–8].

of possible string vacua followed by a selection of acceptable MSSM candidates.

Given the apparently enormous amount of string vacua we have to establish some useful rules where to look first. In Sect. 2 we shall discuss these rules followed by a discussion of the compactification in Sect. 3. This will lead to the construction of the so-called Minilandscape [9–11] in Sect. 4. In Sect. 5 we shall extract lessons from the Minilandscape, most notably for the Higgs system, the top-quark Yukawa coupling, the flavor symmetries and a specific pattern of supersymmetric breakdown. Explicit model building towards tests at the LHC will be treated in Sect. 6. In Sect. 7 we shall give a conclusion and outlook.

2 Some useful rules

The MSSM has special properties that point towards a specific UV-completion. We have the gauge group $SU(3) \times SU(2) \times U(1)$, three families of quarks and leptons and one pair of Higgs doublets. Evolution of gauge coupling constants shows unification at a scale of few times 10^{16} GeV. Neutrino mass spectra are consistent with a see-saw mechanism that requires a right handed neutrino with Majorana mass at a similar scale. One family of quarks and leptons fits exactly into one 16-dimensional spinor representation of SO(10). The families come in three identical repetitions. SO(10) (and its subgroups SU(5) or $SU(4) \times SU(2) \times SU(2)$) represents the most economical GUT-extension of $SU(3) \times SU(2) \times U(1)$. While quarks and leptons come in complete representations of the GUT group, the Higss multiplet is incomplete (known as the doublet-triplet splitting problem in the SU(5) framework). Apart from the gauge symmetries the MSSM contains many more (approximate) discrete symmetries to explain the flavor structure and the stability of the proton.

This leads us to postulate the following rules for the embedding of the SM in string theory [12,13]:

- include spinor representations of SO(10) for chiral matter multiplets and the description of quarks and leptons,
- allow simultaneously for split GUT-multiplets in case of Higgs fields (to solve the "doublet-triplet splitting" problem),
- repetition of families does not come from an enlarged gauge group but is understood as a result of the topological properties of compactified space,
- consider $N = 1$ supersymmetry in $d = 4$ to allow for gauge coupling unification
- select specific corners of moduli space (of the compact manifold) to allow for enhanced discrete symmetries.

From the string theory point of view we can also deduce some tendency towards a grand unified picture, where in particular E_8 plays a crucial role. E_8 is the largest exceptional group.

In $d = 4$ it does not allow for chiral fermion representations. This is different in $d = 10$ and E_8 is a valid GUT group provided the symmetry is broken during the process of compactification. But how does this connect to the successful grand unified gauge groups SU(5) and/or SO(10). There is a well-defined chain to descent from E_8 to smaller groups by chopping off a node of the Dynkin diagram. This leads to E_7, then to E_6 and E_5. E_5 is not an exceptionalgroup: it

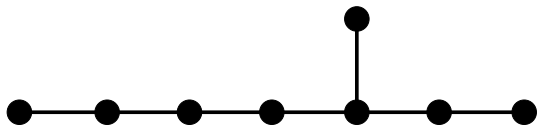

Fig. 1 E_8 is the maximal exceptional group

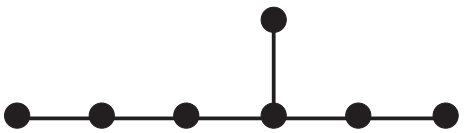

Fig. 2 The next smaller is E_7

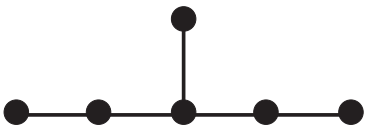

Fig. 3 E_6 allows for chiral representation in $d = 4$

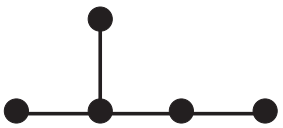

Fig. 4 E_5 coincides with $D_5 = \mathrm{SO}(10)$

Fig. 5 E_4 is equivalent to $A_4 = \mathrm{SU}(5)$

Fig. 6 E_3 connects to the standard model gauge group

coincides with $D_5 = \mathrm{SO}(10)$. Further steps in the chain are $E_4 = A_4 = \mathrm{SU}(5)$ and $E_3 = \mathrm{SU}(3) \times \mathrm{SU}(2)$ makes contact to the real world (the breakdown of the symmetries in terms of Dynkin diagrams is illustrated in Figs. 1, 2, 3, 4, 5, 6).

While E_8 looks esoteric from the point of view of the low-energy effective field theory it appears naturally in the framework of string theory. This is obvious for the $E_8 \times E_8$ heterotic string, but we can also find E_8 as a nonperturbative enhancement in M- and F-theory. Since the latter two only have a qualitative description at strong coupling, we shall concentrate here on a discussion in the framework of heterotic $E_8 \times E_8$ string [14,15], where a fully consistent global string construction is possible. Even here the MSSM is not generic but will require the selection of special corners in moduli space with enhanced discrete symmetries. Some remnants of grand unification and spinors of SO(10) will be present as well.

3 The process of compactification

Celebrated examples for compactification to $d = 4$ with $N = 1$ supersymmetry [16] are Calabi–Yau manifolds. They are beautiful objects (see Fig. 7) but quite difficult to construct. While we can make some reliable statements on topological properties, a more detailed description of the metric is barely possible. In addition Calabi–Yau compactification gives a "generic" description of moduli space and we might miss some of the "corners" of moduli space that are relevant for the appearance of small parameters in the low-energy effective action.

We thus need an approximation that is simple enough to allow for specific calculations in the framework of string theory. In addition it should encode all the topological properties

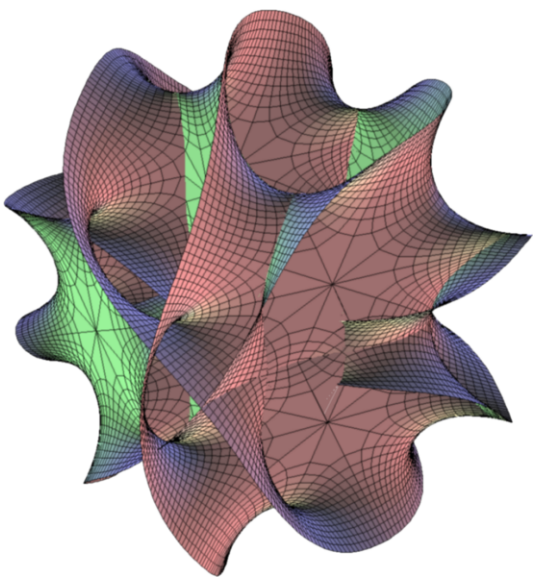

Fig. 7 An impression of a Calabi–Yau manifold

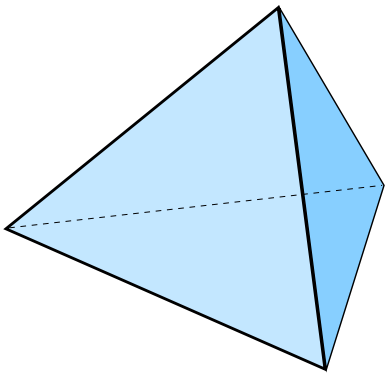

Fig. 8 A two-dimensional Z_2 orbifold

of the Calabi–Yau manifold and provide an intuitive geometrical picture of the location of fields in extra dimensions. In our approach we shall use the notion of (flat) orbifold compactifications [17–20] of the $E_8 \times E_8$ heterotic string.[2]

Orbifolds are spatially flat objects with the exception of fixed points (fixed tori) where curvature contributions are localized (see Fig. 8 for an illustration). The flatness allows an exact treatment in the framework of conformal field theory and the geometric picture is simple and intuitive. We encounter several sectors that characterize the location of fields in extra dimensions:

- $d = 10$ untwisted sector with fields traveling throughout the six compactified dimensions (bulk)
- $d = 6$ twisted sector (fixed tori in compactified extra dimensions)
- $d = 4$ twisted sector (fixed points in extra dimensions)

In addition there is also a "localization" of gauge fields in extra dimensions in the sense that we find different effective gauge groups at different loci of fields. To illustrate this we shall consider an explicit example discussed in [13] (see Fig. 9). We find different manifestations of gauge symmetry at different fixed points. The fields located at the fixed points will come with the representations of that group. So if the electron lives at the SO(10) fixed point it will come in a full spinor representation of SO(10). At other points we might have split representations with respect to SO(10). So the Higgs fields should not be localized at an SO(10) fixed point. Otherwise they would come in a full 10-dimensional representation of SO(10) and there would be SU(3) triplets in addition to the desired SU(2) doublets of the MSSM. The $d = 4$ gauge group is the common subgroup of the gauge groups at the various fixed points, here the SM gauge group $\mathrm{SU}(3) \times \mathrm{SU}(2) \times U(1)$ (see Fig. 10).

This leads to a picture called "Local Grand Unification". In $d = 4$ the gauge group is $\mathrm{SU}(3) \times \mathrm{SU}(2) \times U(1)$ while

[2] For other approaches see [21–31].

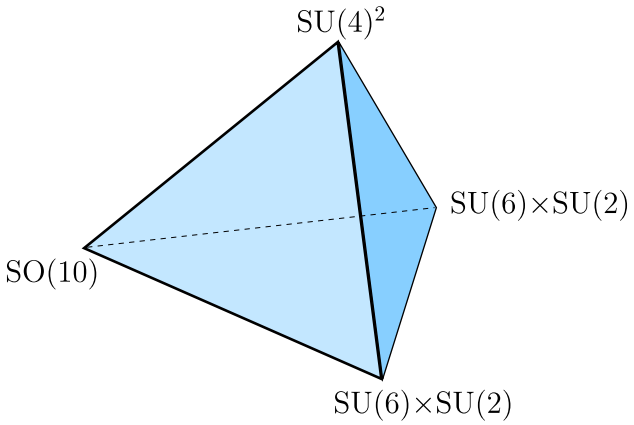

Fig. 9 The gauge symmetries at the various fixed points for a specific model constructed in Ref. [13]

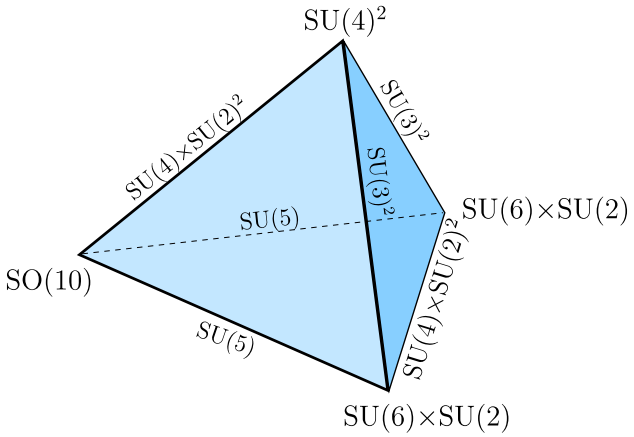

Fig. 10 The gauge symmetries at the various fixed points and their common subgroups. In the present model this leads to the standard model gauge group in the four-dimensional effective theory [13]

the gauge symmetry is enhanced at certain fixed points (fixed tori) in extra dimensions. The scheme keeps the good properties of grand unification like the complete GUT family structure for quarks and leptons. It avoids the problems like complicated $d = 4$ GUT breaking and the doublet-triplet splitting problem via the appearance of split multiplets. It is obvious that in such a picture the key properties of the $d = 4$ effective theory will depend crucially on the geography of fields in extra dimensions.

4 A MiniLandscape

To complete this program we have to construct explicit models of MSSM structure. With a sufficiently large sample of such models we should then be able to identify "fertile" patches of the string landscape and analyse the successful models to check for regularities. A first attempt to do so was an analysis of heterotic $E_8 \times E_8$ models within the orbifold compactification Z_6II. We will not repeat the details here, as they are explained in [9–11,32–35]. Meanwhile these investigations have been extended to the $Z_2 \times Z_2$ case [13,36], Z_{12} [37,38], $Z_2 \times Z_4$ [39] and Z_8 [40]. All these constructions are based on a grand unified picture at some intermediate stage. This is one of the reasons for their success. If you start with a grand unified picture it is much more likely to find successful models. Partially this comes from the fact that one family of quarks and lepton fits into the 16-dimensional spinor representation of SO(10) as we have discussed in Sect. 2.

As we have stressed before, we expect the geometry and the localization of fields in compactified dimensions to be important for properties of the low-energy MSSM effective action. Therefore we need models that are not only consistent vacua of string theory, but we also need explicit information as regards the "geography" of fields in extra dimensions. By now these two properties are only available in the orbifold constructions mentioned above. Let us illustrate this in the case of the Z_6II orbifold. These consist of a Z_2 twist θ and a Z_3 twist ω. We consider the six-dimensional compactified space as a product of three tori as shown in Fig. 11.

The fields on the orbifold can now be associated to specific sectors. First there are the fields in the untwisted sector. These are the fields that exist already on the torus and can therefore freely move through six-dimensional compactified space (so they are bulk fields that actually live in full ten-dimensional space-time). In addition we have twisted fields attached to various sectors. They do not live in the full bulk, but they are confined to fixed points and fixed tori in compactified space. For Z_6II we have three twisted sectors as shown in Figs. 12, 13 and 14, one of them with fixed points and two of them with fixed tori. For a given MSSM-candidate model we shall then be able to identify exactly the location of all the fields. These properties will be important for the interactions between fields in the given model. Fields that live close to each other (or have sufficient overlap) will couple more strongly than those at remote corners of extra-dimensional space.

Fig. 11 The bulk of six-dimensional compactified space. Fields in the untwisted sector can freely move in the bulk

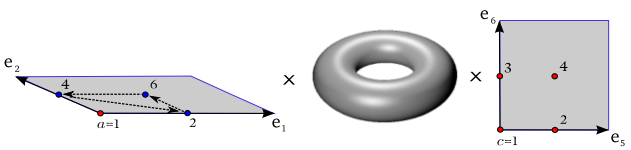

Fig. 12 The sector of Z_2 twist (θ sector) with fixed torus

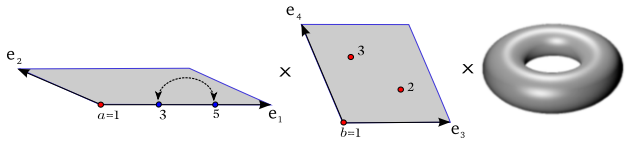

Fig. 13 The sector of Z_3 twist (ω sector) with fixed torus

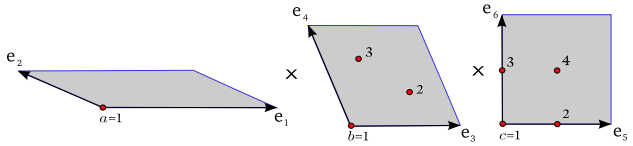

Fig. 14 The sector of Z_6 twist ($\theta\omega$ sector) with fixed points

The construction principle for the models has been given in refs. [9–11]. One identifies models at the orbifold fixed points with enhanced gauge and discrete symmetries (in this construction we typically find several additional $U(1)$- symmetries). One of the $U(1)$-symmetries is anomalous and thus induces a nontrivial Fayet–Iliopoulos (FI) term. As a result some singlet fields will develop nontrivial vacuum expectation values that break the additional $U(1)$-symmetries and allow a decoupling of exotics. As there is a small parameter ϵ involved,[3] this analysis can be done using effective field theory methods. It requires a scan of F- and D-flat directions in the effective potential. The resulting models will then inherit the symmetries at the orbifold point in a slightly broken form and various hierarchies in the model can be obtained in the spirit of the Frogatt–Nielsen mechanism [41]. This will be instrumental for the discussion of Yukawa couplings of the MSSM. Small parameters appear as powers of ϵ and are the source for the appearance of mass hierarchies (e.g. the μ-term) in the low-energy effective theory. With a sufficiently large sample of candidate models we can now "experimentally" study the properties of these models and try to extract some lessons for further model building.

5 Lessons from the MiniLandscape

All the models have gauge group $\mathrm{SU}(3) \times \mathrm{SU}(2) \times U(1)$ in the observable sector and possibly some hidden sector gauge group which might be relevant for supersymmetry breakdown (which we will not discuss here in detail). They have three families of quarks and leptons and exactly one pair of Higgs doublets H_u and H_d. All potential Higgs triplet pairs are removed and the doublet-triplet splitting problem is solved. Still there remains the question of a possible $\mu H_u H_d$ term and we shall therefore start our discussion with the Higgs system.

5.1 Lesson 1: the Higgs doublets

The Higgs system is vector-like and a μ-term $\mu H_u H_d$ is potentially allowed. As this is a supersymmetric term we would like to understand why it is small compared to the GUT scale: This is the so-called μ-problem. To avoid the problem one could invoke a symmetry that forbids the term. However, we know that μ has to be nonzero and the symmetry has to be broken and this might reintroduce the μ-term again. In string theory the problem is even amplified since typically we find several (say N) Higgs doublet pairs at the orbifold point. In the procedure to remove exotics (as described above) we have to make $N-1$ pairs heavy while keeping one light. So this last doublet has to resist the mechanism that allows to remove the others. In fact in many constructions to "solve" the μ-problem in this way the small μ-parameter is the result of a specific fine tuning of parameters arranged in such a way to remove all doublet pairs except for one, and we do not consider this as a satisfactory solution. Part of the models of the MiniLandscape are in this class, but fortunately only very few.

Most of the models provide one Higgs-doublet pair that resisted all attempts to remove them. At first we were surprised by this result and expected a "hidden" symmetry to be at work. In fact we could identify an underlying discrete R-symmetry [10] that protected the μ-parameter. In some cases this R-symmetry [42–44] was only approximate and could therefore allow a μ-parameter at a higher order in the superpotential sufficiently suppressed by a high power of the Fayet–Iliopoulos parameter (ϵ).

Where does this come from? Is there a common property in the models that is the source of this astonishing result? Indeed there is! In all of these models the Higgs fields H_u and H_d live in the untwisted sector! This is quite a special situation: Higgs pairs in $d = 4$ come from gauge fields in extra dimensions and this is called "gauge-Higgs unification". Technically the Higgs fields correspond to continuous Wilson lines in the sense described in [45,46]. But why does it lead to a solution of the μ-problem? The Higgs pair is nontrivially extended in the bulk. Therefore it might be in a nontrivial representation of the extra-dimensional Lorentz group SO(6) of SO(9, 1). The group SO(6) treats bosons and fermions differently and can thus provide the required (discrete) R-symmetry to control the μ-term. This is the first lesson from the MiniLandscape: The Higgs doublets live in the untwisted sector and are thus bulk fields (by now this has been confirmed in other constructions, like $Z_2 \times Z_2$ [13,36] and $Z_2 \times Z_4$ [39]). We believe that this result derived from the MiniLandscape might be of much more general validity.

[3] In the models of the MiniLandscape the parameter ϵ is typically of the order 1/10 to 1/100.

The R-symmetry forbids a constant term in the superpotential as well. This has two important consequences

- SUSY vacua are Minkowski vacua with vanishing vacuum energy
- SUSY breakdown requires a nontrivial constant in the superpotential, thus breaks the R-symmetry and relates μ to the value of the gravitino mass.

The MiniLandscape gives a solution to the μ-problem via an approximate (discrete) R-symmetry. Looking in detail at the models we find that the term $H_u H_d$ in the superpotential is neutral under all selection rules. Thus if a term $f(\Phi_i) H_u H_d$ (where $f(\Phi_i)$ is a polynomical of singlet fields) is allowed in the superpotential, a term $f(\Phi_i)$ is allowed as well. This is reminiscent of an earlier discussion of Casas and Munoz [47] in field theoretical models. To repeat the first lesson of the MiniLandscape: Higgs fields live in the untwisted sector, they are bulk fields.

5.2 Lesson 2: the top quark

The large mass of the top quark requires a large top-quark Yukawa coupling (in contrast to the Yukawa couplings for the first two families which should be small compared to the gauge couplings). String theory has only one coupling for gauge and Yukawa couplings. A trilinear top-quark Yukawa coupling $H_u t \bar{t}$ would be of order of the gauge couplings and thus lead to gauge-Yukawa unification.

In the construction of models of the MiniLandscape we required a Yukawa coupling at the trilinear level to accommodate a heavy top quark. Other Yukawa couplings could be suppressed within the framework of a Frogatt–Nielsen mechanism.

Inspection of the location of the top quark yields a second lesson of the MiniLandscape: both (t, b) and $\bar{t}$ reside in the untwisted sector as well. This guarantees maximal overlap with the bulk field H_u and leads to gauge-Yukawa unification in a natural way.[4] Typically the top quark is the only matter field with trilinear Yukawa coupling. The location of the other fields of the third family is strongly model-dependent, but in general they are distributed over various sectors: the third family could be called a "patchwork family".

5.3 Lesson 3: first two families of quarks and leptons

They are found to be located at fixed points in extra dimensions (Fig. 14). As such they live at points of enhanced symmetries (both gauge and discrete). The presence of these discrete symmetries is the reason for the suppressed Yukawa couplings. In the $Z_6 II$ example shown in the figure the two families live at adjacent fixed points in the third extra-dimensional torus. In fact one family is located at $a = b = c = 1$ the other at $a = b = 1$ and $c = 3$ (see Fig. 14). This leads to a D_4 family symmetry [48,49] that forbids sizeable flavor changing neutral currents and thus relieves the so-called "flavor problem". The geometric reason for small Yukawa couplings is their minimal overlap with the bulk Higgs fields. This leads to Yukawa couplings of higher order and a hierarchical generation of masses within the Frogatt–Nielsen mechanism. The FI-term provides the small parameter ϵ that controls the pattern of the masses. The first two families also live at points of enhanced gauge symmetries and enjoy the successful properties of "local grand unification".

5.4 Lesson 4: the pattern of SUSY breakdown

The question of supersymmetry breakdown is a complicated process and we shall try to extract some general lessons that are rather model-independent. Specifically we would consider gaugino condensation in the hidden sector [50–53] (realized explicitly in the MiniLandscape [54]).

A reasonable value for the gravitino mass can be obtained if the dilaton is fixed at a realistic value for the grand unified gauge coupling $\alpha_{\mathrm{GUT}} \sim 1/24$. The discussion needs the study of moduli stabilization, which, fortunately, we do not have to analyse here in detail. In fact we can rely on some specific pattern of supersymmetry breaking which seems to be common in various string theories, first observed in the framework of Type IIB theory [55–61] and later confirmed in the heterotic case [62,63]: so-called "mirage mediation". Its source is a suppression of the tree-level contribution in modulus mediation (in particular for gaugino masses and A-parameters). The suppression factor is given by the logarithm of the "hierarchy"

$$\log(M_{\mathrm{Planck}}/m_{3/2})$$

which numerically is of the order $4\pi^2$. Non-leading terms suppressed by loop factors can now compete with the tree-level contribution. In its simplest form the loop corrections are given by the corresponding β-functions, leading to "anomaly mediation" if the tree-level contribution is absent. The mirage scheme is therefore a combination of modulus and mirage mediation. At the GUT scale soft terms (say gaugino masses) receive a universal contribution from modulus mediation while the contribution of loops splits the spectrum proportional to the β-function. As the β-function for SU(3) is negative this leads to a suppressed value of the gluino mass at the GUT scale while the contributions to the wino and bino are increased. As the evolution of couplings to lower ener-

[4] An exception is the $Z_2 \times Z_2$-orbifold, which does not allow for quarks and leptons in the untwisted sector. For a detailed discussion see refs. [13,36].

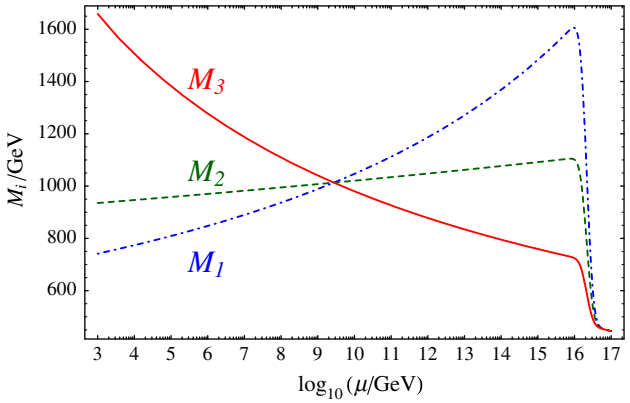

Fig. 15 The evolution of gaugino masses in mirage mediation. The scale of equality of the gaugino masses depends on the ratio of modulus versus anomaly mediation. For details see Ref. [59]

gies is determined by the same β-functions one is lead to a situation that gaugino masses coincide at some intermediate scale: the mirage point (see Fig.15).

The location of this point depends on the relative strength of modulus and anomaly mediation. It could be as low as the TeV scale. We can thus summarize the main properties of mirage mediation:

- gaugino masses and A-parameters are suppressed compared to the gravitino mass by the factor $\log(M_{\text{Planck}}/m_{3/2})$
- we obtain a compressed pattern of gaugino masses (as the SU(3) β-function is negative while those of SU(2) and $U(1)$ are positive)
- soft scalar masses m_0 are more model-dependent. In general we would expect them to be as large as $m_{3/2}$ [57].

This picture of mirage mediation is a quite generic property of string theory and has been explicitly discussed within type IIB and the heterotic string theory. It is a consequence of the mechanism to fine tune the vacuum energy to the observed value.

The models of the MiniLandscape inherit this generic picture of suppressed and compressed gaugino masses and suppressed A-parameters. But they also teach us something new on the soft scalar masses: and this leads to lesson 4 of the MiniLandscape. The scalars (Higgses as well as squarks and sleptons) reside in various sectors that feel SUSY in different ways: some of them enjoy extended SUSY (at the tree level). If we consider the untwisted sector we know that it is obtained from simple torus compactification of the $D = 10$ theory and this leads to extended $N = 4$ supersymmetry in $D = 4$. Soft terms are protected (at least at tree level) by this symmetry (and broken by loop corrections when they communicate to sectors with a smaller amount of supersymmetry). Sectors with fixed tori feel a remnant $N = 2$ supersymmetry and might be protected as well. The fields in sectors with fixed points feel only $N = 1$ SUSY and are not further protected [64,65]. Within the framework described here we would then expect soft terms $m_0 \sim m_{3/2}$ for the first two families. Other scalar fields, in particular the Higgs bosons and the scalar partners of the top quark, feel a protection from extended SUSY and are therefore suppressed compared to $m_{3/2}$ (by a loop factor of order $1/4\pi^2$).

The pattern of soft terms in the models of the MiniLandscape can thus be characterized by two scales: the gravitino mass $m_{3/2}$ and a second scale suppressed by a factor of order of $1/4\pi^2$. As a result of mirage mediation and the consequences of extended SUSY we see a characteristic hierarchical pattern. Higgs bosons, stops, gaugino masses and A-parameters are suppressed compared to the gravitino mass while squark and sleptons of the first two families are heavy. In addition we expect a compressed spectrum of gaugino masses at the TeV scale. This constitutes lesson 4 of the MiniLandscape.

6 Connections to LHC results

At the moment this is written (summer 2013) we have two important results from the first run of the LHC at center of mass energy 7–8 TeV. These are

- the discovery of the Higgs boson at a mass of 125–126 GeV providing the last missing piece of the standard model
- apparent absence of any sign of physics beyond the standard model

Given the high expectations for new physics signals at LHC both results put severe constraints on the parameter space of the MSSM. One might even ask the question whether this is still compatible with the MSSM. Does the string-inspired scheme we are discussing here survive the experimental results of the LHC?

6.1 Qualitative string "predictions"

There is no convincing way known to predict the Higgs mass directly within the models of the MiniLandscape. We have to accommodate it as an experimental fact. Pre-LHC we had the lower limit of 114 GeV for the Higgs mass from the LEP experiments. Within the MSSM we had thus a possible range of 114–130 GeV. The string-inspired scheme discussed here can, however, say something about the SUSY spectrum. The two most important results are:

- the spectrum of SUSY particles exhibits a hierarchy of scales separated by the value of $\log(M_{\text{Planck}}/m_{3/2})$. This implies that the gravitino mass $m_{3/2}$ has to be very large, presumably even bigger than 10 TeV or more. Otherwise

gaugino masses would be too small and already ruled out experimentally. This leads to heavy masses $m_0 \sim m_{3/2}$ for the scalars of the first two generations. This, in addition to the presence of the D_4 family symmetry, relieves potential tension in the absence of flavor changing neutral currents. Unfortunately we do not have a theoretical upper limit of $m_0 \sim m_{3/2}$ from the MSSM and the string-inspired system. A limitation on $m_0 \sim m_{3/2}$ would need some prejudice concerning the fine tuning one is willing to tolerate.

– a compressed spectrum of gaugino mass as given by the mirage mediation scheme. Recall that in the case of universal gaugino masses at the GUT scale we would have the ration $M_1 : M_2 : M_3 \approx 1 : 2 : 6$ at the electroweak scale. In the mirage scheme this ratio depends on the relative size of the contributions of modulus mediation and anomaly mediation. The spectrum is typically more compressed even to a point where $M_1 \approx M_2 \approx M_3$ at the TeV scale [67].

The compression of the gaugino mass scale has several characteristic consequences:

– missing energy signals at LHC will be less efficient to detect SUSY particles.
– there will be a reduced fine-tuning problem because the gluino mass is suppressed.
– we could achieve precision gauge unification.
– in the presence of an ultra-compressed spectrum we might solve potential problems of the thermal relic abundance of dark matter candidates.

We shall discuss these issues in detail later when we consider explicit models.

6.2 Lessons from LHC

The value of the Higgs mass is compatible with the MSSM but hints to a rather high value of masses of SUSY particles (see Fig.16).

We are thus driven to a corner of parameter space with large SUSY scale $M_{\rm SUSY}$. For this reason there are already many attempts in the literature to build models beyond the MSSM. Here we shall stick to the discussion of the MSSM since we do not think that the absence of experimental signals for physics beyond the SM, at this moment, is a sufficient motivation to go beyond the MSSM.

In fact we note that the high value of the Higgs mass leads to high $M_{\rm SUSY}$ in the MSSM. It should therefore be not too surprising that LHC has not found signs of SUSY in the first run. $M_{\rm SUSY}$ might be too large for supersymmetry to be just around the corner and one might even fear that the energy reach of LHC14 might not be sufficient.

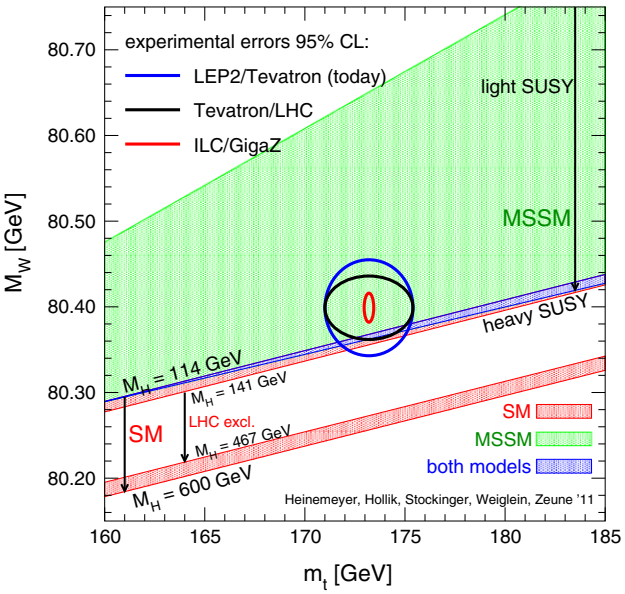

Fig. 16 Constraints on the SUSY spectrum [66] from LEP. In the MSSM a Higgs mass of 126 GeV leads to the region of "heavy SUSY"

6.3 Towards explicit models

We have the parameters $m_{3/2}$ and m_0 in the multi-TeV range, while other parameters like m_3 (stops), A and gaugino masses ($m_{1/2}$) are suppressed by a factor of $O(1/4\pi^2)$ and could be accessible at the LHC. An important role is played by the mirage parameter ϱ, which gives the ratio of modulus to anomaly mediation for gaugino masses. It defines the compression of the spectrum of gaugino masses. Model building along these lines has been discussed explicitly in refs. [64,65]. We shall here only explain the outcome and skip the details. Not surprisingly, the high value of the Higgs mass limits the parameter space drastically. We illustrate this with the plot in Fig. 17. The green regions are excluded for a Higgs mass outside the range of 124–128 GeV. The gravitino mass is pushed to values far beyond 10 TeV, and for the benchmark point shown here, the gluino mass is 3 TeV, beyond current LHC reach.[5] The scheme leads to some version of "hidden SUSY" that will be difficult to test at LHC. One reason is the high value of $m_{3/2}$ (forced upon us by the high value of the Higgs mass) another one the compressed gaugino spectrum that hides SUSY even in the cases where the gluino is accessible to production at the LHC. With a compressed spectrum the mass difference between the gluino and the lightest neutralino (LSP) is smaller than in the standard case.

[5] Lower values for gluino masses are possible, as will shall discuss later.

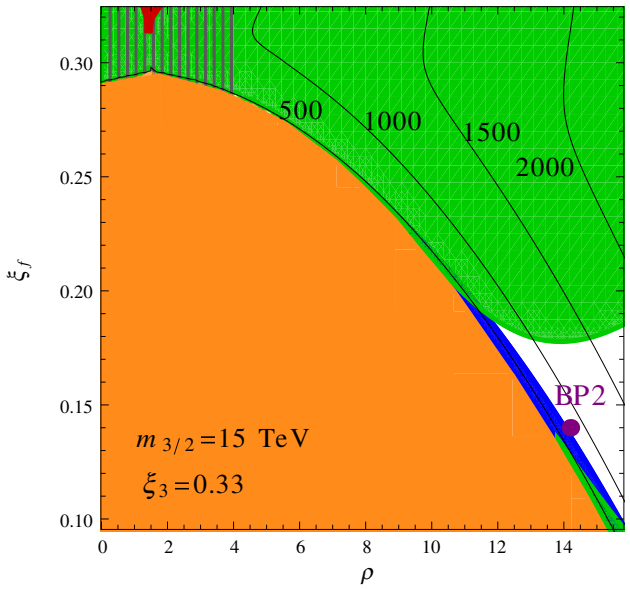

Fig. 17 Parameter scan for a benchmark model with a gluino mass of 3 TeV. The *green* regions are inconsistent with a Higgs mass in the range of 124–128 GeV (for details see [64]). The *hatched region* indicates the reach of direct searches for SUSY (as of summer 2012). It illustrates that limits of direct searches are still weak

In the decay of the gluino the LSP thus will have less kinetic energy and this reduces the "missing energy" signal of the escaping LSP. This poses a severe challenge for the LHC as we shall see in more detail in the next subsection. The LSP is the prime candidate for cold dark matter in the universe. Within the general scenario the quest for a correct thermal relic density rules out a large part of the parameter space [65]. Still the parameter space of the scheme is sufficiently large to be consistent with all presently known experimental and cosmological constraints. We need more experimental results to clarify the situation.

6.4 Precision supersymmetry

Let us therefore consider a special corner of the parameter space that is theoretically well motivated. There are two strong arguments for supersymmetry:

- solution to the electroweak hierarchy problem
- gauge coupling unification.

The latter one is motivated by the evolution of gauge couplings in the MSSM as well as theoretical arguments from string theory that only provides one fundamental coupling. It might thus be interesting to take these arguments as serious as possible and demand precision gauge coupling unification (PGU) within a scheme of minimal fine tuning [68]. The evolution of gauge coupling is given by

$$\frac{1}{g_i^2(M_{\rm GUT})} = \frac{1}{g_i^2(M_Z)} - \frac{b_i^{\rm MSSM}}{8\pi^2}\ln\left(\frac{M_{\rm GUT}}{M_Z}\right) + \frac{1}{g_{i,\rm Thr}^2}$$

We assume that the threshold corrections vanish at the high scale. Thus they come exclusively from the MSSM spectrum

$$\frac{1}{g_{i,\rm Thr}^2} = \frac{b_i^{\rm MSSM} - b_i^{\rm SM}}{8\pi^2}\ln\left(\frac{M_{\rm SUSY}}{M_Z}\right)$$

with the SUSY breakdown scale $M_{\rm SUSY}$. To quantify precision gauge unification (PGU) we define

$$\epsilon_3 = \frac{g_3^2(M_{\rm GUT}) - g_{1,2}^2(M_{\rm GUT})}{g_{1,2}^2(M_{\rm GUT})}$$

and demand $\epsilon_3 = 0$. The relation between ϵ_3 and $M_{\rm SUSY}$ is given in Fig. 18, and $\epsilon_3 = 0$ leads to $M_{\rm SUSY} \sim 2$ TeV. We now have to determine $M_{\rm SUSY}$ in a given model. In the case that all the supersymmetric partners have the same mass M, then $M_{\rm SUSY} = M$. For non- universal masses we have an effective scale

$$M_{\rm SUSY} \sim \frac{m_{\widetilde{W}}^{32/19}\, m_{\widetilde{h}}^{12/19}\, m_H^{3/19}}{m_{\widetilde{g}}^{28/19}}\, X_{\rm sfermion}$$

where $m_{\widetilde{W}}$, $m_{\widetilde{h}}$, m_H and $m_{\widetilde{g}}$ denote the mass of the wino, the higgsino, the heavy Higgs and the gluino, respectively. Within this class of models considered here the effect of sfermions is small [68]: $X_{\rm sfermion} \approx 1$. Let us first examine the value of $M_{\rm SUSY}$ in the so-called CMSSM (i.e. the MSSM with universal gaugino masses $m_{1/2}$ at the GUT scale). At the weak scale we would have the gaugino mass ratio [67]

$$M_1 : M_2 : M_3 = 1 : 2 : 6$$

and the effective SUSY scale reads

$$M_{\rm SUSY} \simeq 0.3\left(m_{\widetilde{h}}^{12}\, m_{1/2}^4\, m_H^3\right)^{1/19} X_{\rm sfermion}$$

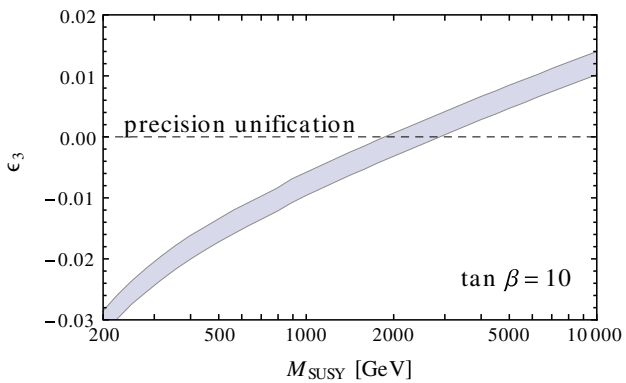

Fig. 18 Precision gauge unification ($\epsilon_3 = 0$) requires a SUSY scale around 2–3 TeV [68]

To reach a scale $M_{\rm SUSY} \approx 2$ TeV as required by precision gauge unification this leads to a large higgsino mass

$$m_{\widetilde{h}} \simeq 20\text{TeV} \times \left(\frac{\text{TeV}}{m_{1/2}}\right)^{1/3} \left(\frac{\text{TeV}}{m_H}\right)^{1/4}$$

As $m_{\widetilde{h}} \sim \mu \sim 20$ TeV we will have a severe fine-tuning problem. Since we require a minimal amount of fine tuning we shall discard the CSSM as a natural framework to obtain precision gauge unification. Are there alternatives?

The string-inspired pattern of the SUSY breaking scheme discussed earlier exhibits mirage mediation and a compressed gaugino mass spectrum. The gaugino masses can be written as

$$M_i = \frac{m_{3/2}}{16\pi^2}\left(\varrho + b_i^{\rm MSSM}\, g^2\right)$$

where $m_{3/2}$ denotes the gravitino mass and ϱ parametrizes the modulus mediated contribution to gaugino masses. This leads to

$$M_1 : M_2 : M_3 = (\varrho + 3.3) : 2(\varrho + 0.5) : 6(\varrho - 1.5)$$

and exhibits a strong compression of gaugino masses for small ϱ (and even an unphysical region where the gluino is the lightest gaugino). Now let us have another look at $M_{\rm SUSY}$:

$$M_{\rm SUSY} \sim \frac{m_{\widetilde{W}}^{32/19}\, m_{\widetilde{h}}^{12/19}\, m_H^{3/19}}{m_{\widetilde{g}}^{28/19}}$$

Key observation is the fact that an increase of the gluino mass reduces $M_{\rm SUSY}$. In the case of a compressed spectrum with wino and gluino masses of similar size we obtain PGU (i.e. $M_{\rm SUSY} \sim 2$ TeV) for a smaller value of μ and therefore less fine tuning. This is illustrated in Fig. 19.

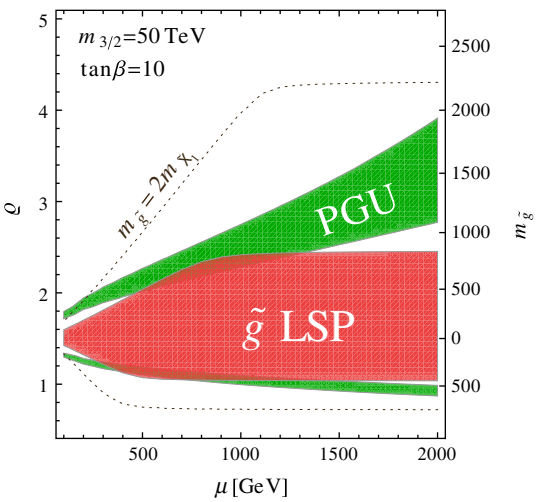

Fig. 19 Gluino mass versus μ for various values of ϱ. *Green regions* are consistent with small ϱ and an ultra-compressed spectrum of gaugino masses satisfying PGU [68]

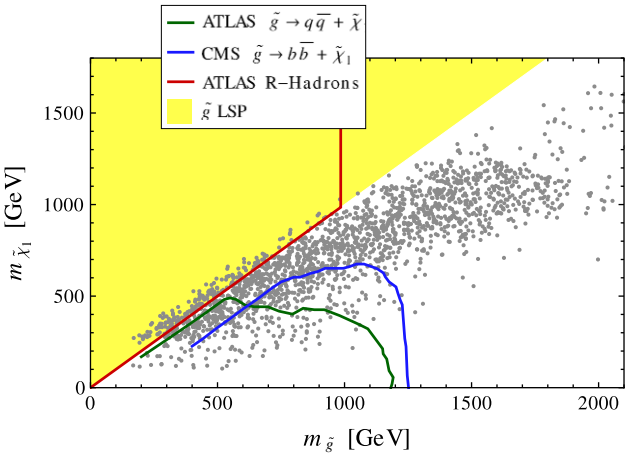

Fig. 20 Neutralino versus gluino mass for a sample of benchmark models that satisfy PGU with a compressed gaugino mass spectrum [68]. Current limits from LHC are still weak

The green regions are consistent with PGU. We see that rather small values of $m_{\widetilde{g}}$ and $\mu \sim m_{\widetilde{h}}$ allow for PGU, both in the kinematic reach of the LHC. Known results from LHC might thus constrain the models and even rule them out. To check the validity of the model, we have generated a large data sample [68] with random input parameters that lead to successful PGU. In Fig. 20 we provide a scatter plot of those parameters and include present limits from LHC (ATLAS search [69] and CMS results for b-jets and missing energy [70]; for a detailed discussion see [68]). Present LHC limits are weak. Only a small part of the parameter space is ruled out. The strongly compressed gaugino mass spectrum makes it difficult to detect even rather light gluinos. It will be interesting to see the discovery potential for the LHC in the next run, as large parts of the parameter space are kinematically accessible.

More restrictions on the model could come from the requirement of the correct thermal relic abundance of the lightest supersymmetric particle (LSP) as a candidate for cold dark matter. Prime candidates are the bino and the higgsino. Due to its small annihilation cross section, the bino density from thermal production typically exceeds the observed dark matter density by far. Higgsinos, on the other hand, undergo efficient annihilation into third generation quarks or gauge bosons, and co-annihilations with the charged higgsino further enhance their cross section. Hence, the relic density of a higgsino LSP might typically be below the dark matter density. In mirage mediation, the gaugino masses are non-universal at the high scale and lead to highly compressed gaugino spectrum at the weak scale as a consequence of PGU. This enhances the possibility for co-annihilations which is favorable for the dark matter density. In Fig. 21 we compare the neutralino relic density for the sample points with or without imposing PGU.

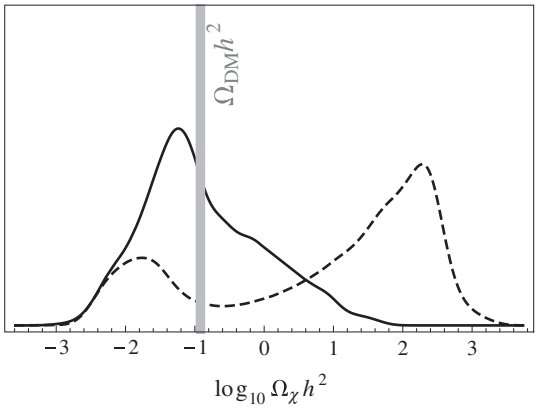

Fig. 21 Distribution of the thermal neutralino relic density for the benchmark sample with (*solid*) or without (*dashed*) the assumption of precision gauge coupling unification [68]

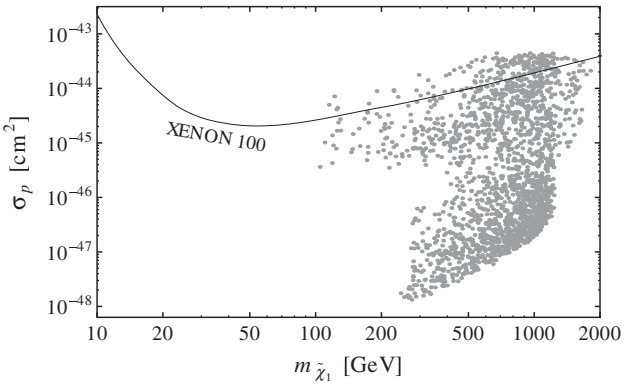

Fig. 22 Neutralino proton cross section for the benchmark points with successful PGU [68]. The current limit from XENON100 direct dark matter search is shown. The latter is only applicable if the lightest neutralino accounts for all dark matter of the universe

Models with PGU seem to be able to accomodate the correct relic density rather easily. Reach and limits from direct detection of these dark matter candidates are shown in Fig. 22.

Future experiments might probe a significant part of the parameter space of the models.

7 Conclusion

As we have seen it is a long way from string theory via the MSSM to LHC physics. To test these ideas we need consistent string theory constructions that allow explicit determination of spectrum and interactions to be confronted with the data. At this point only the models of the heterotic Mini-Landscape satisfy both criteria. Given these models we can try to extract some generic properties from the successful MSSM candidates. Essentially these are lessons originated from the geographic localization of fields in compactified extra-dimensional space. A coherent picture emerges, Higgs and top multiplets live in the bulk. This provides a solution to the μ-problem with an R-symmetry as well as a large value for the Yukawa coupling of the top quark (to be consistent with so-called gauge-Yukawa unification). The multiplets of the first two families are located at fixed points in extra-dimensional space. They enjoy enhanced gauge- and discrete symmetries that alleviate the flavor problem. A slight breakdown of these symmetries provides a small parameter (originated from a Fayet–Iliopoulos term) that could explain the hierarchies of quark and lepton masses as well as the μ-parameter. We expect these properties (derived from the heterotic string theory) to be of more general validity and should also manifest themselves in constructions based on type I, type II, M- and F-theory.

In the discussion of SUSY breakdown we can identify a rather generic scheme: mirage mediation. It has been found both in Type IIB and heterotic theory and is a consequence of the mechanism to obtain a small value of the vacuum energy (compared to the scale of the gravitino mass). The scheme is characterized by two scales for the soft terms separated by a factor $\log(M_{\rm Planck}/m_{3/2})$. Gaugino masses and A- parameters tend to be at the TeV scale, while gravitino mass and scalar masses are generically at a higher scale. A second characteristic property of the mirage scheme is the possibility of a compressed spectrum of the gaugino masses as shown in Fig. 23. It leads to hidden SUSY at the LHC and allows for the correct thermal relic density of the LSP dark matter candidate.

Within the heterotic scheme we could identify another important result concerning scalar masses, determined by the localization properties of the corresponding fields with a potential protection through extended supersymmetry. Localized fields as e.g. the scalar partners of quarks and

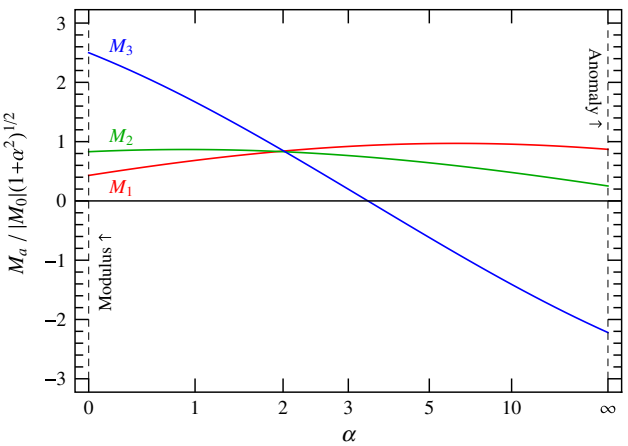

Fig. 23 Gaugino masses as a function of α, the ratio of anomaly to modulus mediated contributions (α is inversely proportional to ϱ defined earlier) [62]. We clearly see the possibility of an ultra-compressed spectrum around $\alpha = 2$

leptons of the first two families only feel $N = 1$ SUSY and would be as heavy as the gravitino. Fields at fixed tori or the bulk feel a hidden $N = 2$ or $N = 4$ SUSY and have suppressed masses comparable to those of the gaugino masses. It is this interplay of symmetries that leads to very specific properties of the spectrum of superpartners. The scheme is still consistent with all known experimental data. A large part of the parameter space is within the kinematical reach of the LHC at 14 TeV. The next run of the LHC might hopefully test these ideas.

References

1. G. Aad et al., ATLAS Collaboration. Phys. Lett. B **716**, 1 (2012). [arXiv:1207.7214 [hep-ex]]
2. S. Chatrchyan et al., CMS Collaboration. Phys. Lett. B **716**, 30 (2012). [arXiv:1207.7235 [hep-ex]]
3. M.B. Green, J.H. Schwarz, Phys. Lett. B **149**, 117 (1984)
4. H.P. Nilles, S. Ramos-Sanchez, M. Ratz, P.K.S. Vaudrevange, Eur. Phys. J. C **59**, 249 (2009). [arXiv:0806.3905 [hep-th]]
5. A.N. Schellekens, *Life at the Interface of Particle Physics and String Theory*. [arXiv:1306.5083 [hep-ph]].
6. K.-S. Choi, J.E. Kim, Quarks and leptons from orbifolded superstring. Lect. Notes Phys. **696**, 1 (2006)
7. L.E. Ibanez, A.M. Uranga, *String Theory and Particle Physics: An Introduction to String Phenomenology* (University Press, Cambridge, UK, 2012), p. 673
8. R. Blumenhagen, B. Kors, D. Lust, S. Stieberger, Phys. Rept. **445**, 1 (2007). [arXiv:hep-th/0610327]
9. O. Lebedev, H.P. Nilles, S. Raby, S. Ramos-Sánchez, M. Ratz, P.K.S. Vaudrevange, A. Wingerter, Phys. Lett. **B645**, 88 (2007). [arXiv:hep-th/0611095]
10. O. Lebedev, H.P. Nilles, S. Raby, S. Ramos-Sánchez, M. Ratz, P.K.S. Vaudrevange, A. Wingerter, Phys. Rev. **D77**, 046013 (2007). [arXiv:0708.2691 [hep-th]]
11. O. Lebedev, H.P. Nilles, S. Ramos-Sanchez, M. Ratz, P.K.S. Vaudrevange, Phys. Lett. B **668**, 331 (2008). [arXiv:0807.4384 [hep-th]]
12. H.P. Nilles, Five golden rules for superstring phenomenology, [arXiv:hep-th/0410160]
13. S. Förste, H.P. Nilles, P.K.S. Vaudrevange, A. Wingerter, Phys. Rev. **D70**, 106008 (2004). [arXiv:hep-th/0406208]
14. D.J. Gross, J.A. Harvey, E.J. Martinec, R. Rohm, Nucl. Phys. B **256**, 253 (1985)
15. D.J. Gross, J.A. Harvey, E.J. Martinec, R. Rohm, Nucl. Phys. **B267**, 75 (1986)
16. P. Candelas, G.T. Horowitz, A. Strominger, E. Witten, Nucl. Phys. B **258**, 46 (1985)
17. L.J. Dixon, J.A. Harvey, C. Vafa, E. Witten, Nucl. Phys. B **261**, 678 (1985)
18. L.J. Dixon, J.A. Harvey, C. Vafa, E. Witten, Nucl. Phys. B **274**, 285 (1986)
19. L.E. Ibáñez, H.P. Nilles, F. Quevedo, Phys. Lett. B **187**, 25 (1987)
20. L.E. Ibáñez, J.E. Kim, H.P. Nilles, F. Quevedo, Phys. Lett. B **191**, 282 (1987)
21. A.E. Faraggi, Nucl. Phys. B **387**, 239 (1992). [arXiv:hep-th/9208024]
22. F. Gmeiner, G. Honecker, JHEP **0807**, 052 (2008). [arXiv:0806.3039 [hep-th]]
23. G. Honecker, J. Vanhoof, Fortsch. Phys. **60**, 1050 (2012). [arXiv:1201.5872 [hep-th]]
24. V. Braun, Y.H. He, B.A. Ovrut, T. Pantev, Phys. Lett. B **618**, 252 (2005). [arXiv:hep-th/0501070]
25. V. Bouchard, R. Donagi, Phys. Lett. B **633**, 783 (2006). [arXiv:hep-th/0512149]
26. L.B. Anderson, J. Gray, A. Lukas, E. Palti, JHEP **1206**, 113 (2012). [arXiv:1202.1757 [hep-th]]
27. L.B. Anderson, J. Gray, A. Lukas, E. Palti, PoS CORFU **2011**, 096 (2011)
28. R. Donagi, M. Wijnholt, Adv. Theor. Math. Phys. **15**, 1237 (2011). [arXiv:0802.2969 [hep-th]]
29. C. Beasley, J.J. Heckman, C. Vafa, JHEP **0901**, 058 (2009). [arXiv:0802.3391 [hep-th]]
30. T.P.T. Dijkstra, L.R. Huiszoon, A.N. Schellekens, Nucl. Phys. B **710**, 3 (2005). [arXiv:hep-th/0411129]
31. P. Anastasopoulos, T.P.T. Dijkstra, E. Kiritsis, A.N. Schellekens, Nucl. Phys. B **759**, 83 (2006). [arXiv:hep-th/0605226]
32. T. Kobayashi, S. Raby, R.J. Zhang, Phys. Lett. B **593**, 262 (2004). [arXiv:hep-ph/0403065]
33. T. Kobayashi, S. Raby, R.J. Zhang, Nucl. Phys. B **704**, 3 (2005)
34. W. Buchmüller, K. Hamaguchi, O. Lebedev, M. Ratz, Phys. Rev. Lett. **96**, 121602 (2006). [arXiv:hep-ph/0511035]
35. W. Buchmüller, K. Hamaguchi, O. Lebedev, M. Ratz, Nucl. Phys. B **785**, 149 (2007). [arXiv:hep-th/0606187]
36. M. Blaszczyk, S. Nibbelink, Groot, M. Ratz, F. Ruehle, M. Trapletti, P.K.S. Vaudrevange. Phys. Lett. B **683**, 340 (2010). [arXiv:0911.4905 [hep-th]]
37. J.E. Kim, B. Kyae, Flipped SU(5) from Z(12-I) orbifold with Wilson line (2006). [arXiv:hep-th/0608085]
38. J.E. Kim, J.H. Kim, B. Kyae, JHEP **06**, 034 (2007). [arXiv:hep-ph/0702278]
39. D.K.M. Pena, H.P. Nilles, P.-K. Oehlmann, JHEP **1212**, 024 (2012). [arXiv:1209.6041 [hep-th]]
40. S.G. Nibbelink, O. Loukas, [arXiv:1308.5145 [hep-th]]
41. C.D. Froggatt, H.B. Nielsen, Nucl. Phys. B **147**, 277 (1979)
42. R. Kappl, H.P. Nilles, S. Ramos-Sanchez, M. Ratz, K. Schmidt-Hoberg, P.K.S. Vaudrevange, Phys. Rev. Lett. **102**, 121602 (2009). [arXiv:0812.2120 [hep-th]]
43. F. Brummer, R. Kappl, M. Ratz, K. Schmidt-Hoberg, JHEP **1004**, 006 (2010). [arXiv:1003.0084 [hep-th]]
44. H.M. Lee, S. Raby, M. Ratz, G.G. Ross, R. Schieren, K. Schmidt-Hoberg, P.K.S. Vaudrevange, Phys. Lett. B **694**, 491 (2011). [arXiv:1009.0905 [hep-ph]]
45. L.E. Ibanez, H.P. Nilles, F. Quevedo, Phys. Lett. B **192**, 332 (1987)
46. A. Font, L.E. Ibanez, H.P. Nilles, F. Quevedo, Nucl. Phys. B **307** 109 (1988). [Erratum-ibid. B 310 (1988) 764]
47. J.A. Casas, C. Muñoz, Phys. Lett. B **306**, 288 (1993). [arXiv:hep-ph/9302227]
48. T. Kobayashi, H.P. Nilles, F. Plöger, S. Raby, M. Ratz, Nucl. Phys. B **768**, 135 (2007). [arXiv:hep-ph/0611020]
49. H.P. Nilles, M. Ratz, P.K.S. Vaudrevange, Fortsch. Phys. **61**, 493 (2013). [arXiv:1204.2206 [hep-ph]]
50. H.P. Nilles, Phys. Lett. B **115**, 193 (1982)
51. S. Ferrara, L. Girardello, H.P. Nilles, Phys. Lett. B **125**, 457 (1983)
52. J.P. Derendinger, L.E. Ibáñez, H.P. Nilles, Phys. Lett. B **155**, 65 (1985)
53. M. Dine, R. Rohm, N. Seiberg, E. Witten, Phys. Lett. B **156**, 55 (1985)
54. O. Lebedev, H.P. Nilles, S. Raby, S. Ramos-Sánchez, M. Ratz, P.K.S. Vaudrevange, A. Wingerter, Phys. Rev. Lett. **98**, 181602 (2007). [arXiv:hep-th/0611203]

55. K. Choi, A. Falkowski, H.P. Nilles, M. Olechowski, S. Pokorski, JHEP **0411**, 076 (2004). [arXiv:hep-th/0411066]
56. K. Choi, A. Falkowski, H.P. Nilles, M. Olechowski, Nucl. Phys. B **718**, 113 (2005). [arXiv:hep-th/0503216]
57. O. Lebedev, H.P. Nilles, M. Ratz, Phys. Lett. B **636**, 126 (2006). [arXiv:hep-th/0603047]
58. V. Nilles, J. Plank, CCR, **42**, 736 (2012)
59. O. Lebedev, H.P. Nilles, M. Ratz, A Note on fine-tuning in mirage mediation. [arXiv:hep-ph/0511320]
60. O. Loaiza-Brito, J. Martin, H.P. Nilles, M. Ratz, Log(M(Pl) / m(3/2)). AIP Conf. Proc. **805**, 198 (2006). [arXiv:hep-th/0509158]
61. O. Lebedev, V. Lowen, Y. Mambrini, H.P. Nilles, M. Ratz, JHEP **0702**, 063 (2007). [arXiv:hep-ph/0612035]
62. V. Löwen, H.P. Nilles, Phys. Rev. **D77**, 106007 (2008). 0802.1137
63. V. Lowen, H.P. Nilles, Nucl. Phys. B **827**, 337 (2010). [arXiv:0907.4983 [hep-ph]]
64. S. Krippendorf, H.P. Nilles, M. Ratz, M.W. Winkler, Phys. Lett. B **712**, 87 (2012). [arXiv:1201.4857 [hep-ph]]
65. M. Badziak, S. Krippendorf, H.P. Nilles, M.W. Winkler, JHEP **1303**, 094 (2013). [arXiv:1212.0854 [hep-ph]]
66. S. Heinemeyer, W. Hollik, D. Stockinger, A.M. Weber, G. Weiglein, Pramana **69**, 783 (2007). [arXiv:hep-ph/0611371]
67. K. Choi, H.P. Nilles, JHEP **0704**, 006 (2007). [arXiv:hep-ph/0702146 [HEP-PH]]
68. S. Krippendorf, H.P. Nilles, M. Ratz, M.W. Winkler, Phys. Rev. D **88**, 035022 (2013). [arXiv:1306.0574 [hep-ph]]
69. ATLAS Collaboration, Search for squarks and gluinos with the ATLAS detector using final states with jets and missing transverse momentum and 5.8 fb^{-1} of $\sqrt{s}$=8 TeV, ATLAS-CONF-2012-109, ATLAS-COM-CONF-2012-140
70. CMS Collaboration, Search for Supersymmetry in pp collisions at 8 TeV in events with a single lepton, multiple jets and b-tags, CMS-PAS-SUS-13-007

Eur. Phys. J. C (2014) 74:2766
DOI 10.1140/epjc/s10052-014-2766-x

THE EUROPEAN PHYSICAL JOURNAL C

Review

Composite Higgses

Brando Bellazzini[1,2], **Csaba Csáki**[3,a], **Javi Serra**[3]

[1] Institut de Physique Théorique, CEA-Saclay and CNRS URA-2306, 91191 Gif-sur-Yvette Cedex, France
[2] Dipartimento di Fisica e Astronomia, Università di Padova and INFN Sezione di Padova, Via Marzolo 8, 35131 Padua, Italy
[3] Department of Physics, LEPP, Cornell University, Ithaca, NY 14853, USA

Received: 5 January 2014 / Accepted: 8 January 2014 / Published online: 27 May 2014

Abstract For the closing article in this volume on supersymmetry, we consider the alternative options to SUSY theories: we present an overview of composite Higgs models in light of the discovery of the Higgs boson. The small value of the physical Higgs mass suggests that the Higgs quartic is likely loop generated; thus models with tree-level quartics will generically be more tuned. We classify the various models (including bona fide composite Higgs, little Higgs, holographic composite Higgs, twin Higgs and dilatonic Higgs) based on their predictions for the Higgs potential, review the basic ingredients of each of them, and quantify the amount of tuning needed, which is not negligible in any model. We explain the main ideas for generating flavor structure and the main mechanisms for protecting against large flavor violating effects, and we present a summary of the various coset models that can result in realistic pseudo-Goldstone Higgses. We review the current experimental status of such models by discussing the electroweak precision, flavor, and direct search bounds, and we comment on the UV completions of such models and on ways to incorporate dark matter.

1 Introduction

The discovery of the Higgs boson [1,2] with mass $m_h \approx 125\,\text{GeV}$ has been an important milestone in particle physics. It allows us for the first time to finally completely fix the parameters of the SM Higgs potential

$$V(h) = -\mu^2|H|^2 + \lambda|H|^4, \tag{1.1}$$

where $\langle H\rangle = v/\sqrt{2}$, $v = 246$ GeV. The resulting experimental values are

$$\mu^2_{\text{exp}} \approx (89\,\text{GeV})^2, \quad \lambda_{\text{exp}} \approx 0.13. \tag{1.2}$$

It has also started to seriously weed out and constrain the once-crowded arena of models of electroweak symmetry breaking and the TeV scale: plain technicolor/Higgsless [3–6] models are excluded, while the simplest supersymmetric models have a difficult time reproducing the observed value of the Higgs mass. The absence of observation of missing energy events puts strong lower limits on masses of superpartners. The other articles in this volume [7–14] focus on reviewing both the history of and the implications of the Higgs discovery for SUSY. This review focuses on the other viable option: natural electroweak symmetry breaking from strong dynamics, where the strong dynamics produces a light composite Higgs doublet.

The idea of a composite Higgs boson goes back to Georgi and Kaplan in the 1980s [15–21], where it was also recognized that making it a Goldstone boson could also render the Higgs lighter than the generic scale of composites. The idea of composite Higgses has re-emerged in the guise of warped extra dimensional models in the late 1990s [22–25], and then in the form of little Higgs models [26,27] in the early 2000s, when the crucial ingredient of collective breaking was added. Collective breaking was originally [52] inspired by the deconstruction [28,29] of extra dimensional models where the Higgs is identified with a component of the gauge field. This idea was later fully utilized in a warped background in the holographic composite Higgs models [30,31], building on important earlier work [32–40]. The generic features of these constructions have been condensed into a simple 4D effective description [41,42].

This review aims at explaining the main ideas behind the various types of composite Higgs constructions, to contrast their main features, critically compare them and present the main experimental constraints on them. We will not follow the historical order of developments: instead we will present everything from the point of view of a 4D low-energy effective theory.

We start by explaining the consequences of the recent measurement of the value of the Higgs mass on the parameters of the Higgs potential: both the mass and the quartic self coupling are independently fixed. A light Higgs mass

[a] e-mail: csaki@cornell.edu

of 125 GeV implies a small quartic, which is more likely to point toward a loop-induced quartic rather than a tree-level one. We present a simple parametrization of the potential suitable for pseudo-Goldstone composite Higgs models and the tuning necessary to obtain this potential. In Sect. 3 we classify the various types of composite Higgs models based on their predictions for the Higgs potential and quantify the expected amount of tuning in these models. Section 4 contains the discussion of the various possible mechanisms for generating the Yukawa couplings, and for protecting from large flavor changing effects. We review the various coset models that can give rise to realistic patterns of symmetry breaking with SM-like Higgs bosons in Sect. 5. The signals and constraints on the composite Higgs models are summarized in Sect. 6, and we finally comment on UV completions in Sect. 7.

2 The Higgs potential of composite Higgs models and tuning

One can nicely classify the various types of composite Higgs models by the size of the Higgs potential and also by the mechanism that generates the Yukawa couplings, in particular for the top quark. We will first focus on the generic features of the potential, in order to categorize in Sect. 3 composite Higgs models based on the particulars of such a potential, and finally in Sect. 4 we will discuss the various mechanisms for the generation of the Yukawa couplings.

While the numerical values of the parameters in the Higgs potential (1.1) are now fixed, there are several different dynamical ways in which one can arrive at this potential. We will make the following assumptions regarding the dynamics responsible for generating the potential:

- The Higgs is a composite with a scale of compositeness given by f.
- There is a hierarchy between the Higgs VEV v and the scale f: $v/f < 1$ such that the Higgs potential can be expanded in powers of h/f.[1]
- The Higgs potential is (fully or partially) radiatively generated. This is generically the case when the Higgs is also a pseudo-Goldstone boson (pGB). We will also assume that the potential vanishes in the limit when the SM couplings vanish.

Using these assumptions the leading terms in the Higgs potential can be parameterized by (using $h = \sqrt{2}H$):

$$\Delta V(h) = \frac{g_{\rm SM}^2 \Lambda^2}{16\pi^2}\left(-a|h|^2 + b\frac{|h|^4}{2f^2}\right), \tag{2.1}$$

where $g_{\rm SM}$ is a typical SM coupling, the largest of which corresponds to the top Yukawa $g_{\rm SM}^2 \sim N_c y_t^2$. We have also introduced the scale Λ, which sets the overall size of the potential. Typically, this will be given by the mass of the state that is responsible for cutting off the quadratic divergence of the Higgs, so generically $\Lambda \sim m_*$. To fit the observed Higgs VEV and mass, the parameters a, b, f and Λ have to satisfy

$$\begin{aligned}(246\,\text{GeV})^2 &= v^2 = \frac{a}{b}f^2,\\ (125\,\text{GeV})^2 &= m_h^2 = 4\,b\,v^2\,\frac{g_{\rm SM}^2}{16\pi^2}\frac{\Lambda^2}{f^2}.\end{aligned} \tag{2.2}$$

We can then classify a composite Higgs model by the magnitudes of the parameters Λ, a, and b. Before we do so, we would like to make some important general remarks regarding the perturbative nature of the physics responsible for the Higgs potential and the consequences of this for fine-tuning.

One of the main physical consequence of the magnitude of the recently measured Higgs mass is that the physics generating the Higgs potential should be weakly coupled. The experimental value of the quartic is $\lambda_{\rm exp} \approx 0.13$, which is of the order expected for a weakly coupled one-loop diagram. The loop factor L is given by

$$L = 2\frac{g_{\rm SM}^2(\Lambda^2/f^2)}{16\pi^2} \sim 0.15\left(\frac{g_{\rm SM}}{\sqrt{N_c}y_t}\right)^2\left(\frac{\Lambda/f}{2}\right)^2, \tag{2.3}$$

where the separation between $\Lambda \sim m_*$ and f determines the magnitude of the coupling of the states at m_*, $g_* = \Lambda/f$. We can see that for $g_* \sim 2$ the loop is about the right size for the value of the observed quartic. This leads us to conclude that the new physics responsible for cutting off the potential is weakly coupled,

$$g_* \equiv \Lambda/f \ll 4\pi, \tag{2.4}$$

implying that the mass scale for new particles appears much before the true strong coupling scale $\Lambda_{\rm C} \sim 4\pi f$ is reached. While this perturbativity sounds like a welcome news for the calculability of the Higgs potential, it is also the origin of the tuning for these composite Higgs models. If the idea of a true loop-induced potential with a loop factor $L \sim 0.15$ is taken seriously, one would also expect the same factor to set the magnitude of the Higgs mass parameter, yielding the relation $f^2 = \mu^2/L \approx v^2$. However, as we will see in Sects. 6.1 and 6.3, electroweak precision tests (EWPTs) and the Higgs coupling measurements imply that $f > v$, leading to a tension with the expectation from a generic weakly coupled loop-induced Higgs potential. This tension is the origin of the fine-tuning in these models: a fully natural loop-induced Higgs potential would require $f \sim v$, while EWPTs and Higgs couplings require $f > v$. In practice the tuning required to get around this tension is to have several contributions to a and b (along with their associated $g_{\rm SM}^2$ and Λ^2), which will then partially cancel to give an effective $a/b < 1$.

[1] In most cases this is not even necessary, given that the leading contributions to the potential can be arranged into only two definite functions of h/f.

Note that lowering the coupling g_* is actually not a possibility for finding non-tuned Higgs potentials with larger f: while formally the relation

$$\mu^2 = 2a\frac{g_{\rm SM}^2 g_*^2}{16\pi^2} f^2 \tag{2.5}$$

can be satisfied for $f > v$ if g_* is lowered, we actually know that $g_* f$ is a physical mass scale where new particles appear, and can thus not be too low experimentally. Also, in most models $g_{\rm SM}$ is a derived quantity (from couplings of several BSM states related to g_*) usually implying relations of the form $g_{\rm SM} < g_*$, which also sets a lower bound on how small g_* can be. Finally, taking $g_* < g_{\rm SM}$ would run counter to the philosophy of composite Higgs models, where a strongly interacting sector is expected to be responsible for generating the Higgs potential: in that case $g_* < g_{\rm SM}$ would likely require a separate tuning anyways within the strong sector. Thus we will not consider the possibility of very small g_* any further. Instead we will have to be content to live with some amount of tuning (the specific implementation of the little hierarchy problem), which we quantify below.

Clearly, the tuning here will be proportional to v^2/f^2. One simple way of quantifying it is to consider the magnitudes of the individual terms[2] that would contribute to a shift of the VEV of the Higgs

$$\Delta_{v^2} = \frac{\delta v^2}{v^2_{\rm exp}} \sim \frac{1}{(246\,{\rm GeV})^2}\frac{a_i}{b_i} f^2, \tag{2.6}$$

where a_i and b_i are the generic magnitudes of the terms appearing in the potential (which are then assumed to partially cancel against each other). Since this tuning involves the ratios of two terms generated in the potential (and since the magnitudes of the individual terms in the potential are known) it is better to instead separately consider the tuning in the mass term and the quartic term in the potential. The tuning for the mass parameter μ^2 is

$$\Delta_{\mu^2} = \frac{\delta\mu^2}{\mu^2_{\rm exp}} \sim \frac{1}{(800\,{\rm GeV})^2} a_i\, g^2_{{\rm SM},i}\Lambda_i^2, \tag{2.7}$$

while the tuning for the Higgs quartic is

$$\Delta_\lambda = \frac{\delta\lambda}{\lambda_{\rm exp}} \sim \frac{1}{3^2} b_i\, g^2_{{\rm SM},i} g^2_{*,i}, \tag{2.8}$$

where again a_i and b_i are the individual contributions to these terms before any cancelation. Notice that even in the most favorable situation for Δ_λ, that is, $g_* \simeq g_{\rm SM}$, an irreducible tuning remains from the mass parameter, given that $\Delta_{\mu^2} \sim (f/270\,{\rm GeV})^2$, where we have taken $g^2_{\rm SM} \sim N_c y_t^2$, and experimentally $f > v$ is required.

[2] We write the Higgs potential as $V(h) = \sum_i \Delta V_i(h)$, $\Delta V_i(h) = \frac{g^2_{{\rm SM},i}\Lambda_i^2}{16\pi^2}(-a_i|h|^2 + b_i\frac{|h|^4}{2f^2})$.

An important consequence of this discussion is that since the Higgs mass determines the value of the Higgs quartic, it is no longer reasonable to assume an order one Higgs quartic (since we know if is fixed to $\lambda \approx 0.13$). One popular way of reducing the fine-tuning in composite Higgs models was to assume that while the mass parameter is generated at loop level, the quartic is generated at tree level (corresponding to $a \sim 1, b \sim (4\pi)^2$). This would eliminate the tuning in v (due to the relation $v \sim f/(4\pi)$); however, now the quartic would come out too large, requiring in turn a tuning in λ to reduce the Higgs mass to the observed value.

We can summarize the discussion of the tuning in the Higgs potential in the following way: the experimental data suggests that both μ^2 and λ must be loop suppressed, and to minimize the tuning one would like f to be as close to v, and g_* as close to $g_{\rm SM}$, as possible.

3 Classification of the composite Higgs models based on Higgs potential

Based on the discussion of the previous section we can now classify the various types of composite Higgs models based on the generic magnitudes of the Higgs mass and quartic parameters they would be predicting.

3.1 Tree-level mass and quartic: $a = \mathcal{O}(1), b = \mathcal{O}(1)$, $g_* \sim 4\pi$. Bona fide composite Higgs

These models can be regarded as technicolor models with an enlarged global symmetry, the breaking of which yields an extra 'pion' with the quantum numbers of the Higgs [43]. However, they typically predict a too large Higgs mass term and quartic coupling, with generically $v \sim f$. Even if a is tuned by an amount $\sim \xi = v^2/f^2$, the Higgs is still too heavy, since $\lambda \sim g^2_{\rm SM} \sim N_c y_t^2$. Thus a second independent tuning must be made on b. Overall, we can roughly estimate the tuning required in this class of models as[3]

$$\Delta = \Delta_{\mu^2} \times \Delta_\lambda \sim (0.003\,\%)^{-1}\left(\frac{f}{1\,{\rm TeV}}\right)^2. \tag{3.1}$$

3.2 Loop-level mass, tree-level quartic: $a = \mathcal{O}(1)$, $b = \mathcal{O}(\frac{16\pi^2}{g_*^2})$, $g_* \ll 4\pi$. Little Higgs models

The 'little' Higgs models [26,27,44–49] were invented to provide a fully natural Higgs potential: one automatically obtains a hierarchy between the Higgs VEV and f: $v^2/f^2 \simeq g_*^2/16\pi^2 \ll 1$, without tuning. This, however, comes at the price of increasing Higgs mass: since $\lambda \sim g^2_{\rm SM}$, one would

[3] We will be assuming for simplicity that two uncorrelated cancelations, one in μ^2 and another in λ, take place.

expect $m_h \sim 2v g_{\rm SM} \sim 500$ GeV for $g_{\rm SM} \sim 1$. While a fully natural Higgs potential was very appealing before the value of the Higgs mass was known, once the Higgs mass is pinned down to 125 GeV one needs to perform additional tunings in a and b to obtain this mass. Thus the Higgs potential in little Higgs theories cannot be considered fully natural anymore. A naive estimate of the tuning involved is given by

$$\Delta = \Delta_{\mu^2} \times \Delta_\lambda \sim (1\,\%)^{-1} \left(\frac{f}{1\,\text{TeV}}\right)^2 \left(\frac{g_*}{\sqrt{N_c} y_t}\right)^2, \quad (3.2)$$

where we have taken $g_{\rm SM} \sim 1$.[4]

The crucial ingredient that allows the Higgs mass parameter to become loop suppressed in little Higgs models is called collective symmetry breaking: the Higgs doublet transforms under some extended global symmetry, which is not completely broken by any single interaction term. Since one needs a chain of these terms to feel the symmetry breaking, one-loop diagrams will not be quadratically divergent and hence will not be cut off by the naive scale of compositeness $\Lambda_{\rm C} = 4\pi f$, but rather at some earlier scale. This lower scale is set by the masses of the light composite resonances, $m_* = g_* f$, which are called top partners for the top loop, or vector partners for the gauge loop. It is technically natural for the top/vector partners to be lighter than the strong coupling scale $\Lambda_{\rm C} \sim 4\pi f$; in addition, the mechanism of partial compositeness, which we will discuss in detail in Sect. 4, naturally realizes light top partners for a sizable degree of compositeness of the top. Collective breaking then requires that g_* must not be much larger than $g_{\rm SM}$. In particular, this fact implies that the top/vector partners must be weakly coupled.

Little Higgs models are chosen such that the collective breaking protects the Higgs mass parameter hence $a = \mathcal{O}(1)$, while a tree-level quartic is generated by means of extra scalars leading to $b = \mathcal{O}(16\pi^2/g_*^2)$.[5] The collective breaking mechanism also ensures that the large tree-level effective quartic does not lead to enhanced corrections to the Higgs mass term, the so-called collective quartic [50,51].

3.3 Loop-level mass and quartic: $a = \mathcal{O}(1)$, $b = \mathcal{O}(1)$, $g_* \ll 4\pi$. Holographic composite Higgs

This is the scenario where the entire Higgs potential is loop generated. These models need one tuning in the Higgs potential of order $\xi = v^2/f^2$ in order to achieve the right Higgs VEV $v < f$. However, once this tuning is achieved, the Higgs mass will automatically be light. Again the divergences in the Higgs potential are cut off at the scale of the top and vector partners. Thus, the generic tuning required in this case scales as

$$\Delta = \Delta_{\mu^2} \times \Delta_\lambda \sim (7\,\%)^{-1} \left(\frac{f}{1\,\text{TeV}}\right)^2 \left(\frac{g_*}{\sqrt{N_c} y_t}\right)^4, \quad (3.3)$$

where $g_{\rm SM}^2 \sim N_c y_t^2$ has been taken.

These models were inspired by the AdS/CFT correspondence: some strongly interacting theories can be described by weakly coupled AdS duals. The existence of such a dual is intrinsically tied to the presence of 'weakly' coupled resonances in the large N regime, with coupling $g_* \sim 4\pi/\sqrt{N}$. One can include in this class of models their deconstructed [52] versions as well, with several sites and links [53–55].

The holographic composite Higgs models also feature a version of collective breaking mechanism both in the gauge and fermion sectors, which is a consequence of extra-dimensional locality (or theory-space locality, its discrete version for the deconstructed case) [56]. This protection is generically absent in the scalar sector for the holographic Higgs. However, since the quartic is already loop suppressed, the loop contribution to the Higgs mass from the Higgs self-interaction will be effectively two-loop suppressed, and hence it is not dominating even if it is cut off at a scale higher than the top/vector partners. The same will hold for contributions to the Higgs potential obtained from integrating out additional GBs. Thus we can summarize the two main differences between little Higgs models and holographic composite Higgs models: little Higgs models feature a tree-level collective quartic $b = O(16\pi^2/g_*^2)$, generated from integrating out a particular class of 'heavy' GBs [50,51], while holographic Higgs models have a loop-suppressed quartic. Collective breaking in little Higgs models will ensure that the Higgs mass contribution from scalar and self-interactions is suppressed despite the appearance of a large effective quartic, while no such mechanism is at work in holographic models. In those models the quartic is simply small, thus also ensuring the appropriate suppression of the Higgs mass term.

Then, the collective breaking in holographic Higgs models affects the Higgs mass term as well as the other pGBs, such that the Higgs is only lighter than these extra scalars at the expense of tuning the Higgs VEV, that is, $m_h^2 \sim L v^2$ while $m_H^2 \sim L f^2$. This is in contrast with little Higgs models, where generically only the Higgs mass term is protected, but not the other pGBs, in particular those involved in the generation of the quartic Higgs coupling. The result in this case is $m_h^2 \sim g_{\rm SM}^2 v^2$ while $m_H^2 \sim g_{\rm SM}^2 f^2$, which is the same

[4] In most little Higgs models the leading quartic Higgs coupling is not generated from the same SM coupling than the mass term, the latter typically arising from top loops.

[5] These scalars get $\sim f/v$ larger mass terms than the Higgs, and they can thus be consistently integrated out for what the Higgs potential concerns.

ratio as in holographic Higgs models but without the loop suppression.

3.4 Twin Higgs: $a = \mathcal{O}(1)$, $b = \mathcal{O}(1) - \mathcal{O}(\frac{16\pi^2}{g_*^2})$, $g_* = g_{\rm SM}$

The 'twin' Higgs models [57,58] yield the same prediction for a as little Higgs or holographic Higgs models, but the mechanism to eliminate the quadratic divergences in the Higgs mass term is based on a discrete Z_2 symmetry instead of collective breaking. Regarding b, the generic prediction is a loop-level Higgs quartic coupling; thus, as in holographic Higgs models $b = \mathcal{O}(1)$, although when these models were originally proposed, it was convenient to introduce by hand a tree-level quartic, such that $b = \mathcal{O}(16\pi^2/g_*^2)$ and a hierarchy $v < f$ was naturally generated, as in little Higgs models. However, since the overall scale of the Higgs potential is now known, the latter option is no longer preferred, as discussed in Sect. 2.

The most important difference with respect to the previous models is that the partners cutting off the potential do not necessarily carry SM charges, in particular color. Given the lack of positive signals of top partners at the LHC, this is a relatively unexplored scenario in which opportunities for model building are still open, with the potential to produce interesting developments.

3.5 Dilatonic Higgs

This scenario is quite different from the previous ones, and it is not very useful to compare them based on the form of the Higgs potential. In this case the dilaton (the pGB of spontaneously broken scale invariance) is playing the role of the 125 GeV Higgs-like particle [59–65]. The analog state in the warped extra dimensional models is the radion [66–69], the studies of which have inspired much of the work in the general 4D framework. However, for these 'dilatonic' Higgs models it is very important to point out that the dilaton VEV is not directly related to the electroweak VEV, or in other words $m_W^2 \neq g^2\langle h\rangle^2/4$, unlike for a genuine Higgs. Instead, the VEV of the dilaton actually fixes the overall scale of the potential, $\langle h\rangle \equiv f$, relative to a given UV scale μ_0. This explains why in the limit of exact scale invariance the dilaton potential only contains a quartic term (which itself is consistent with scale invariance). A non-trivial minimum is then achieved due to explicit scale invariance breaking induced by the running couplings, which introduces an implicit dependence of $g_{\rm SM}$ on h/μ_0, of the form $g_{\rm SM} \sim (h/\mu_0)^{\gamma_{\rm SM}}$, where $\gamma_{\rm SM}$ is the anomalous dimension associated to $g_{\rm SM}$. Furthermore, a minimum with $f \ll \mu_0$ only arises naturally for $g_{\rm SM} \sim 4\pi$ at the condensation scale, which is commonly taken as an indication that the potential of the dilaton is driven by a non-SM coupling.[6]

In order for the dilaton to resemble the SM Higgs, f must accidentally be close to v, for instance if only operators with the quantum numbers of the SM Higgs condense. Therefore the experimental constraints in this case go in the opposite direction that in the previous models, pushing towards $v \sim f$. Moreover, let us note that the dilaton could actually arise from a variety of scale invariant 'strong sectors', including those that are 'weakly' coupled, that is, $g_* \ll 4\pi$. However, explicit calculations using AdS/CFT imply that the large N limit associated with this scenario is not preferred, since it tends to push $f \gg v$.

As a final remark in this section, we would like to emphasize that twisted versions of the models reviewed above also exist. For instance, due to constraints from electroweak precision constraints, which affect more significantly the boson sector of little Higgs models, it is known that it is favored not to extend the SM gauge group, at the expense of a collective symmetry breaking in the gauge sector that resembles that of holographic models. This set-up was first proposed in [70], and later the littlest Higgs coset SU(5)/SO(5) was realized à la holographic Higgs, first as a warped extra-dimensional model in [71] and then using the 4D effective description [72].

As we have already done in this section, in the following we use the term 'partners' to denote the new light and weakly coupled states that cut off the Higgs potential.

4 Classification of the composite Higgs models based on flavor structure

Another important distinguishing feature of the various composite Higgs models is based on the mechanism for generating Yukawa couplings. The two main alternatives are condensation of 4-Fermi operators and partial compositeness. Further classification of the partially composite case can be done based on how the appropriate flavor hierarchies are actually achieved.

4.1 Condensation of 4-Fermi operators

This is the traditional way of obtaining Yukawa couplings in strongly coupled (technicolor) theories [73,74]: a SM bilinear interacts with the strong sector,

$$\lambda \bar{\psi}_{\rm L} \psi_{\rm R} \mathcal{O}, \tag{4.1}$$

where $\mathcal{O}$ is a scalar operator with the quantum numbers of the Higgs, for instance $\mathcal{O} = \bar{\psi}_{\rm TC}\psi_{\rm TC}$ in extended techni-

[6] Although one possibility is that the coupling of the top to the strong sector, which is related to its Yukawa, drives the spontaneous breaking of scale invariance.

color models. At low energies the operator $\mathcal{O}$ interpolates to a function of the Higgs, therefore giving rise to an ordinary Yukawa coupling of size

$$y_\psi \sim \lambda(\Lambda_F)\left(\frac{\Lambda_C}{\Lambda_F}\right)^{d-1}, \tag{4.2}$$

where $\lambda(\Lambda_F)$ is the value of the bilinear coupling at the flavor scale Λ_F, $\Lambda_C \sim 4\pi f$ is the strong sector scale, and d is the dimensionality of the operator $\mathcal{O}$. This is the mechanism relied on in the bona-fide composite Higgs models. The most refined version of it goes under the name of conformal technicolor [75], which tries to explain why the Higgs has properties similar to an elementary scalar in the Yukawa interactions where it is linearly coupled, but it is very different from an elementary scalar in the Higgs mass term where it appears quadratically. Conformal technicolor would assume that, while the dimensionality of the linear Higgs operator is close to one, in order to allow a large enough Λ_F as to satisfy flavor constraints while reproducing the sizable Yukawa of the top, that of the quadratic one is bigger than four, rendering it irrelevant. It also departs from the proposal of walking technicolor [76,77] in that the large-N limit of the strong gauge group is not taken, to avoid large contributions to the S-parameter. However, the basic assumption is under stress from recent general bounds on scaling dimensions in 4D CFTs using conformal bootstrap [78–81].

4.2 Partial compositeness

All the other composite Higgs models use the alternative mechanism for generating Yukawa couplings known as partial compositeness. Although this mechanism was originally proposed to address the flavor problem in technicolor models [82], its power was not appreciated until its realization, via the AdS/CFT correspondence, as the localization of bulk fermions along a warped extra dimension in Randall–Sundrum models [31,83–87]. Here each SM fermion chirality couples to a different composite fermionic operator $\mathcal{O}_{L,R}$ of the strong sector,

$$\lambda_L \bar{\psi}_L \mathcal{O}_R + \lambda_R \bar{\psi}_R \mathcal{O}_L. \tag{4.3}$$

At low energies the state to be identified with the SM fermion is a mixture of $\psi_{L,R}$ and the lowest excitation of $\mathcal{O}_{L,R}$, which we call $\Psi_{L,R}$, to be identified with the vectorlike fermionic partners of the SM fermions. The fraction of compositeness of the SM fields is characterized by the parameters $f_{L,R}$, which depend on the mixing matrices $\lambda_{L,R}$, as well as the fermionic composite spectrum, $m_{\Psi_{L,R}}$, as $f_{L,R} \simeq \lambda_{L,R} f/m_{\Psi_{L,R}}$. Assuming the Higgs is fully composite and has unsuppressed Yukawa couplings $Y_{u,d}$ with the composites $\Psi_{L,R}$, the effective SM Yukawa couplings $y_{u,d}$ for the SM fermions will be given by

$$y_u^{ij} = f_q^i Y_u^{ij} f_u^j, \quad y_d^{ij} = f_q^i Y_d^{ij} f_d^j. \tag{4.4}$$

There are two main approaches to obtaining the correct flavor hierarchy without introducing large flavor violating interactions involving the SM fermions. If the composite sector has no flavor symmetry, then $Y_{u,d}$ are matrices with random $\mathcal{O}(1)$ elements. In this case a hierarchical structure in the mixing matrices $f_{L,R}$ can yield the right flavor hierarchies together with a strong flavor protection mechanism called RS-GIM. The other option is that the composite sector has a flavor symmetry, which would then be the source of the flavor protection. In this case some of the mixing matrices $f_{L,R}$ should be directly proportional to the SM Yukawas $y_{u,d}$.

4.2.1 Anarchic Yukawa couplings

The most popular version of partial compositeness is called the anarchic approach to flavor, where the underlying Yukawa couplings of the composites $Y_{u,d}$ are generic $\mathcal{O}(1)$ numbers without any structure. The flavor hierarchy in this case arises due to the hierarchical nature of the mixings between the elementary and the composite states $f_{L,R}$, due to large anomalous dimensions of the composite operators $\mathcal{O}_{L,R}$. In this case the mixing is expected to be given by

$$f_{L,R}(\Lambda_C) \sim f_{L,R}(\Lambda_F)\left(\frac{\Lambda_C}{\Lambda_F}\right)^{d_{L,R}-5/2}, \tag{4.5}$$

where $d_{L,R}$ are the scaling dimensions of the composite operators, and $f_{L,R}(\Lambda_F)$ are the values of the mixing parameters at the flavor scale Λ_F. A hierarchical flavor structure arises naturally for $\mathcal{O}(1)$ anomalous dimensions. The CKM mixing matrix arises from the diagonalization of the anarchic Yukawa matrices (4.4) resulting in hierarchic left and right rotation matrices for the up and down sectors $L_u^{ij} \sim L_d^{ij} \sim \min(f_q^i/f_q^j, f_q^j/f_q^i)$, $R_{u,d}^{ij} \sim \min(f_{u,d}^i/f_{u,d}^j, f_{u,d}^j/f_{u,d}^i)$. This results in a hierarchical CKM matrix completely determined by the mixing of the LH states, and with the relations $f_q^1/f_q^2 \sim \lambda$, $f_q^2/f_q^3 \sim \lambda^2$, $f_q^1/f_q^3 \sim \lambda^3$ (where λ is the Cabibbo angle), while the diagonal quark masses are given by $m_{u,d}^i = f_q^i f_{u,d}^i v$.

One of the consequences of this mechanism is that for states where the mixing is close to maximal, the mass of the heavy state must be well below the compositeness scale Λ_C. We can understand this by considering the interplay between a single composite fermion multiplet with mass $m_\Psi = g_\Psi f$ and its couplings $\lambda_{L,R}$ with the elementary fermions $\psi_{L,R}$. The mixing parameter is given by

$$f_{L,R} = \frac{\lambda_{L,R}}{\sqrt{\lambda_{L,R}^2 + g_\Psi^2}}. \tag{4.6}$$

For this to approach unity we need $g_\Psi \ll 4\pi$, in agreement with our original expectation that the state responsible for

cutting off the quadratic dependence of the Higgs potential should appear well below the cutoff scale.

Flavor violations in this anarchic scenario are protected by the RS-GIM mechanism [87], which is simply the fact that every flavor violation must go through the composite sector; thus, all flavor violating operators will be suppressed by the appropriate mixing factors. For example, a typical $\Delta F = 2$ 4-Fermi operator mediated by a composite resonance of mass m_ρ and coupling g_ρ, will have the structure

$$f_q^i f_q^{\dagger j} f_q^k f_q^{l\dagger} \frac{g_\rho^2}{m_\rho^2} \bar{q}^i q^j \bar{q}^k q^l, \tag{4.7}$$

leading to a quark-mass dependent suppression of these operators. As we will review in Sect. 6.2, the RS-GIM mechanism with completely anarchic Yukawa couplings is not sufficient to avoid the stringent flavor constraints from the kaon system or from several dipole operators, pushing the compositeness scale f to the multi-TeV regime.

4.2.2 Flavor symmetries in the composite sector

Another possible way of protecting the flavor sector from large corrections is by imposing a flavor symmetry on the composite sector. In this case we will lose the explanation of the origin of the flavor hierarchy; however, we might be able to obtain a setup that is minimally flavor violating (MFV), or next-to-minimally flavor violating (NMFV). This was first carried out in the extra dimensional context in [88–90], and later it was implemented in the four dimensional language in [91,92]. The flavor symmetry structure is determined by the flavor structure of the mixing matrices $\lambda_{\mathrm{L,R}}$ as well as the composite Yukawa matrices $Y_{u,d}$. A flavor invariance of the composite sector will imply that the composite Yukawas are proportional to the unit matrix $Y_{u,d} \propto \mathrm{Id}_3$ for the case with maximal $\mathrm{U}(3)^3$ flavor symmetry in the composite sector. In order to have MFV, we need to make sure that the only sources of flavor violation are proportional to the SM Yukawa couplings. The simplest possibility is to make the LH mixing matrix proportional to the unit matrix, and the RH mixing matrices proportional to the up- and down-type SM Yukawa couplings:

$$\lambda_{\mathrm{L}} \propto \mathrm{Id}_3, \quad \lambda_{Ru} \propto y_u, \quad \lambda_{Rd} \propto y_d. \tag{4.8}$$

This scenario corresponds to the case with composite left-handed quarks and elementary right-handed quarks, and an explicit implementation of MFV. However, the fact that the left-handed quarks are composite will imply potentially large corrections to electroweak precision observables. The other possibility is to introduce the flavor structure in the left-handed mixing matrix. In order to be able to reproduce the full CKM structure, one needs to double the partners of the LH quarks to include Q_u and Q_d: the composite Yukawa of Q_u will give rise to up-type SM Yukawa couplings, while those of Q_d to down-type Yukawas, while their mixings $\lambda_{Lu}, \lambda_{Ld}$ are proportional to the SM Yukawas. Hence the ansatz for right-handed compositeness is

$$\lambda_{Lu} \propto y_u, \quad \lambda_{Ld} \propto y_d, \quad \lambda_{Ru} \propto \mathrm{Id}_3, \quad \lambda_{Rd} \propto \mathrm{Id}_3, \tag{4.9}$$

which is also an implementation of MFV.

In the MFV scenarios discussed above the composite sector has a $\mathrm{U}(3)^3$ flavor symmetry, and either the LH or RH quarks are substantially composite, the degree fixed such as to reproduce the Yukawa coupling of the top. However, the light quarks appear to be very SM-like, more so after LHC dijet production measurements $pp \to jj$ in agreement with the SM, and it might be advantageous to reduce the flavor symmetry, allowing only the third generation quarks to be composites. Furthermore, the models with large flavor symmetries can significantly influence the predictions for the Higgs potential. If parts of the first and second generation are largely composite, along with that of the third, their contributions to the Higgs potential will be enhanced beyond the usual expectations. Accordingly, the phenomenology of the fully MFV models can be significantly modified, as we comment in Sect. 6. A lot of effort has been put recently into exploring the models where the third generation is split from the first two. This next-to-minimal flavor violation corresponds to imposing a $\mathrm{U}(2)^3 \times \mathrm{U}(1)^3$ or $\mathrm{U}(3)^2 \times \mathrm{U}(2) \times \mathrm{U}(1)$ flavor symmetry on the composite sector: it is phenomenologically viable or even favored [92–94], keeping the natural expectations that the Higgs potential is saturated by the top and its partners. We will discuss the main phenomenological signatures of these scenarios in Sect. 6.2.

Finally, there are other possibilities to reproduce the flavor structure of the SM while avoiding the constraints from flavor observables. These rely as well on flavor symmetries. One scenario, originally proposed in [88], is to assume that all the mixing matrices $\lambda_{\mathrm{L,R}}$ are proportional to the identity, while all the flavor structure is provided by the composite sector, that is, $Y_{u,d} \propto y_{u,d}$. This setup satisfies the rules of MFV, and all the SM quarks must have a large degree of compositeness.

One last logical possibility to comply with experiments is that the composite sector respects CP, given that most of the bounds come from CP-violating observables. In this case the Yukawa couplings of the composite sector can be chosen to be real matrices, while the mixings introduce non-negligible CP phases if the SM fermions are coupled to more than one composite operator. It has been shown in [91] that this idea might give rise to a realistic theory of flavor.

5 Cosets of symmetry breaking

In this section we have compiled the most important symmetry breaking cosets $\mathcal{G}/\mathcal{H}$ from which a pseudo-Goldstone–

Table 1 Symmetry breaking patterns $\mathcal{G} \to \mathcal{H}$ for Lie groups. The third column denotes whether the breaking pattern incorporates custodial symmetry. The fourth column gives the dimension N_G of the coset, while the fifth contains the representations of the GBs under $\mathcal{H}$ and SO(4) $\cong$ $SU(2)_L \times SU(2)_R$ (or simply $SU(2)_L \times U(1)_Y$ if there is no custodial symmetry). In case of more than two SU(2)s in $\mathcal{H}$ and several different possible decompositions we quote the one with largest number of bi-doublets

$\mathcal{G}$	$\mathcal{H}$	C	N_G	$\mathbf{r}_\mathcal{H} = \mathbf{r}_{SU(2)\times SU(2)}$ ($\mathbf{r}_{SU(2)\times U(1)}$)	Ref.
SO(5)	SO(4)	✓	4	$\mathbf{4} = (\mathbf{2},\mathbf{2})$	[31]
SU(3) × U(1)	SU(2) × U(1)		5	$\mathbf{2_{\pm 1/2}} + \mathbf{1_0}$	[30,48]
SU(4)	Sp(4)	✓	5	$\mathbf{5} = (\mathbf{1},\mathbf{1}) + (\mathbf{2},\mathbf{2})$	[43,70,95]
SU(4)	$[SU(2)]^2 \times U(1)$	✓*	8	$(\mathbf{2},\mathbf{2})_{\pm 2} = 2 \cdot (\mathbf{2},\mathbf{2})$	[96]
SO(7)	SO(6)	✓	6	$\mathbf{6} = 2 \cdot (\mathbf{1},\mathbf{1}) + (\mathbf{2},\mathbf{2})$	–
SO(7)	G_2	✓*	7	$\mathbf{7} = (\mathbf{1},\mathbf{3}) + (\mathbf{2},\mathbf{2})$	[97]
SO(7)	SO(5) × U(1)	✓*	10	$\mathbf{10_0} = (\mathbf{3},\mathbf{1}) + (\mathbf{1},\mathbf{3}) + (\mathbf{2},\mathbf{2})$	–
SO(7)	$[SU(2)]^3$	✓*	12	$(\mathbf{2},\mathbf{2},\mathbf{3}) = 3 \cdot (\mathbf{2},\mathbf{2})$	–
Sp(6)	Sp(4) × SU(2)	✓	8	$(\mathbf{4},\mathbf{2}) = 2 \cdot (\mathbf{2},\mathbf{2})$	[96]
SU(5)	SU(4) × U(1)	✓*	8	$\mathbf{4_{-5}} + \bar{\mathbf{4}}_{\mathbf{+5}} = 2 \cdot (\mathbf{2},\mathbf{2})$	[98]
SU(5)	SO(5)	✓*	14	$\mathbf{14} = (\mathbf{3},\mathbf{3}) + (\mathbf{2},\mathbf{2}) + (\mathbf{1},\mathbf{1})$	[27,70,72]
SO(8)	SO(7)	✓	7	$\mathbf{7} = 3 \cdot (\mathbf{1},\mathbf{1}) + (\mathbf{2},\mathbf{2})$	–
SO(9)	SO(8)	✓	8	$\mathbf{8} = 2 \cdot (\mathbf{2},\mathbf{2})$	[98]
SO(9)	SO(5) × SO(4)	✓*	20	$(\mathbf{5},\mathbf{4}) = (\mathbf{2},\mathbf{2}) + (\mathbf{1}+\mathbf{3},\mathbf{1}+\mathbf{3})$	[99]
$[SU(3)]^2$	SU(3)		8	$\mathbf{8} = \mathbf{1_0} + \mathbf{2_{\pm 1/2}} + \mathbf{3_0}$	[26]
$[SO(5)]^2$	SO(5)	✓*	10	$\mathbf{10} = (\mathbf{1},\mathbf{3}) + (\mathbf{3},\mathbf{1}) + (\mathbf{2},\mathbf{2})$	[46]
SU(4) × U(1)	SU(3) × U(1)		7	$\mathbf{3_{-1/3}} + \bar{\mathbf{3}}_{\mathbf{+1/3}} + \mathbf{1_0} = 3 \cdot \mathbf{1_0} + \mathbf{2_{\pm 1/2}}$	[48,57,58]
SU(6)	Sp(6)	✓*	14	$\mathbf{14} = 2 \cdot (\mathbf{2},\mathbf{2}) + (\mathbf{1},\mathbf{3}) + 3 \cdot (\mathbf{1},\mathbf{1})$	[44,70]
$[SO(6)]^2$	SO(6)	✓*	15	$\mathbf{15} = (\mathbf{1},\mathbf{1}) + 2 \cdot (\mathbf{2},\mathbf{2}) + (\mathbf{3},\mathbf{1}) + (\mathbf{1},\mathbf{3})$	[49]

Higgs could arise. The result is given in Table 1. Most of the global symmetry breaking patterns $\mathcal{G} \to \mathcal{H}$ have been described in the literature, mainly in the context of the little and holographic Higgs models.

The minimal requirement on the global symmetries of the strong sector is that the unbroken $\mathcal{H}$ must contain an SU(2) × U(1) subgroup, while the coset $\mathcal{G}/\mathcal{H}$ must contain a $\mathbf{2_{\pm 1/2}}$ representation corresponding to the quantum numbers of the Higgs doublet under $SU(2)_L \times U(1)_Y$. However, in order to protect the T-parameter from large corrections, one may instead require the unbroken $\mathcal{H}$ to contain a larger 'custodial' symmetry SO(4) $\cong$ SU(2) × SU(2) (which in turn contains the previous SU(2) × U(1)). This ensures that the actual custodial $SU(2)_C$ is left unbroken after the Higgs gets its VEV, avoiding excessively large contributions to the T-parameter of order $\sim v^2/f^2$. In this case the coset must contain a 4-plet representation of SO(4) (that is a $\mathbf{4} = (\mathbf{2},\mathbf{2})$ of SU(2) × SU(2)). In Table 1 we have introduced the column C to mark the cases with custodial symmetry $\mathcal{H} \supset$ SU(2) × SU(2), with ✓, while for the cases with only $\mathcal{H} \supset$ SU(2) × U(1) this column is left blank. Notice, however, that if there are GBs in addition to the single Higgs which are charged under SU(2) × SU(2), such as extra doublets or triplets (under either of the two SU(2)s), the $SU(2)_C$ does not generically remain unbroken when all the scalars get a VEV. In such a case SO(4) is not large enough, and extra SU(2)s or extra discrete symmetries are required to ensure an unbroken custodial symmetry. When there are additional SU(2)s, misaligned VEVs can be allowed if a large enough 'custodial' symmetry is present for $SU(2)_C$ to remain unbroken in the vacuum, while for the case with discrete symmetries, the extra parities must enforce vanishing VEVs for the additional scalars. We denote the cases without extra custodial protection with ✓*. Aside from symmetries, the effects of these additional GBs could instead be tamed by the introduction of additional gauge bosons that eat them. This would allow the suppression of the dangerous violations of custodial symmetry if the corresponding gauge coupling can be taken large, effectively reducing the coset to a smaller one without the dangerous GBs (we also denote these cases with ✓*).

Several additional comments are in order regarding Table 1:

(1) Beyond rank 3 this is an incomplete list for $\mathcal{G}$s. We do not intend to be exhaustive here.
(2) Further cosets can be obtained stepwise from Table 1 via $\mathcal{G} \to \mathcal{H} \to \mathcal{H}' \to \cdots$.
(3) 'Moose'-type models are obtained by combining several copies of the cosets in Table 1. This is the case

for instance of the minimal moose of [26], given by $[SU(3)^2/SU(3)]^4$, and likewise for other mooses [46,48].

(4) In little Higgs models it is customary to gauge a subgroup of $\mathcal{G}$ beyond the SM $SU(2)_L \times U(1)_Y$, in order to implement the collective breaking in the gauge sector. Therefore, not all the GBs in Table 1 appear as physical states in the spectrum. In this regard, the gauge collective breaking in holographic models becomes apparent by extending the symmetry structure, for instance from $SO(5)/SO(4)$ to $[SO(5)]^2/SO(5)$, and gauging a SO(4) subgroup on one of the factors (or sites), while the SM $SU(2)_L \times U(1)_Y$ is gauged on the other. We do not include these possibilities as separate entries in Table 1.

(5) Finally, little Higgs models with T-parity [100,101] typically require extra global symmetries (and its breaking) beyond the model without T-parity they are built from. For instance, the 'littlest' Higgs model $SU(5)/SO(5)$ is extended with a $[SU(2)\times U(1)]^2/SU(2)\times U(1)$ in [291] (see [102,290] for other attempts). We do not include any of these extensions either in Table 1.

It is understood that the global symmetries of the strong sector contain an unbroken $SU(3)_C$ factor that is gauged by the SM strong interactions, that is, $\mathcal{G}\times SU(3)_C$. However, several models have been proposed that include the color group in a non-trivial way [103–106]. One of the main motivations of these models is to provide a rationale for the apparent unification of forces in the SM. By embedding $SU(3)_C$ in a simple group along with $SU(2)_L \times U(1)_Y$ (for instance in SO(10), $SU(4)_1 \times SU(4)_2 \times P_{12}$, or SO(11)), the central charges of the strong sector are the same for all the SM gauge interactions, thus ensuring that the differential running of the SM couplings remains the same than in the SM.[7] One of the main implications of these constructions is that some of the GBs carry color (also known as leptoquarks or diquarks).

At this point, it is worth to note which of these symmetry breaking patterns could arise from fermion bilinear condensation $\langle\psi\psi'\rangle$ [107]. The possible cosets are $[SU(N)]^2/SU(N)$, $SU(N)/SO(N)$, or $SU(2N)/Sp(2N)$, depending on the representation of ψ, ψ' under the strong gauge group, complex, real, or pseudo-real, respectively. This fact might be relevant when considering possible UV completions of the composite Higgs.

Let us end this section by noting that more exotic possibilities have also been considered for $\mathcal{G}/\mathcal{H}$, in particular non-compact Lie groups. Besides the case of the dilaton, corresponding to $SO(4,2)/ISO(3,1)$, other possibilities such as $SO(4,1)/SO(4)$ have also been considered [108,109], although much less investigation has been devoted to these cases, mainly due to the expectation that their UV completion is non-unitary.

5.1 The minimal model with custodial symmetry: $SO(5)/SO(4)$

The $SO(5)/SO(4)$ is the minimal coset containing custodial $SO(4) \cong SU(2)_L \times SU(2)_R$ symmetry that gives rise to a Higgs bi-doublet $(\mathbf{2},\mathbf{2})$. The $SU(2)_L$ factor and the $U(1)_Y$ inside $SU(2)_R$ are gauged by the SM electroweak interactions. Other models with larger cosets that also implement custodial symmetry reduce to this one when the symmetry breaking interactions make the other GBs heavy (or they are gauged away).

This model, whose origin can be traced back to [46] as a little Higgs moose model, and which was realized as a warped extra-dimensional construction in [31] (MCHM), has been thoroughly examined in light of the Higgs discovery. Besides the well-known fact that a certain degree of tuning is required to bring down μ^2 to the observed value [110,111] (see [112] for a recent assessment), several approaches have been recently used to render the potential finite and therefore calculable, nailing down the features that the SM partners (top and electroweak) must have in order to reproduce the observations. Among these it is worth mentioning the 'moose' extensions, either $SO(5)\times SO(5)/SO(5)$ with extra SO(4) gauged [113], or $SO(5) \times SO(5)/SO(5) \times SO(4)$ with extra SO(5) gauged [114], and the use of the Weinberg sum rules (an old idea used to compute the pion masses in the QCD chiral Lagrangian) [115,116].[8] The conclusions of these works are similar to those previously obtained in realizations in a warped extra dimension [118], and which we have explained in Sect. 2: light and weakly coupled top partners are needed, and some tuning, ∼5 %, is needed to push f somewhat larger than v and comply with the experimental constraints. We show in Fig. 1 the plot from [116] showing that at least one of the top partners (in a **1** and **4** representations of SO(4), with masses m_{Q_1} and m_{Q_4}, respectively) must be light in order to reproduce the observed Higgs mass.[9]

[7] Of course this feature could also be an accidental property of the strong sector in those cases where $SU(3)_C$ is factored out.

[8] It has also been shown in this set-up that extra colored vector resonances, or gluon partners, can mildly reduce the Higgs mass prediction via renormalization effects [117].

[9] Exceptions exist to this generic expectation [115,116]. These have been found in the context of a fully composite t_R, thus arising as a massless chiral composite. In this case t_R does not contribute to the Higgs potential, and the top Yukawa coupling is simply given by $y_t \simeq \lambda_L$, hence the degree of compositeness of t_L is fixed. Further, in these special cases the Higgs quartic is accidentally generated only at y_t^4 order, instead of $y_t^2 g_*^2$, thus losing the connection small λ − small g_*. Hence the observed Higgs mass can be reproduced with heavier top partners. However, this is at the expense of increasing the tuning in μ^2 (for fixed f), which scales as $y_t^2 g_*^2$, as expected.

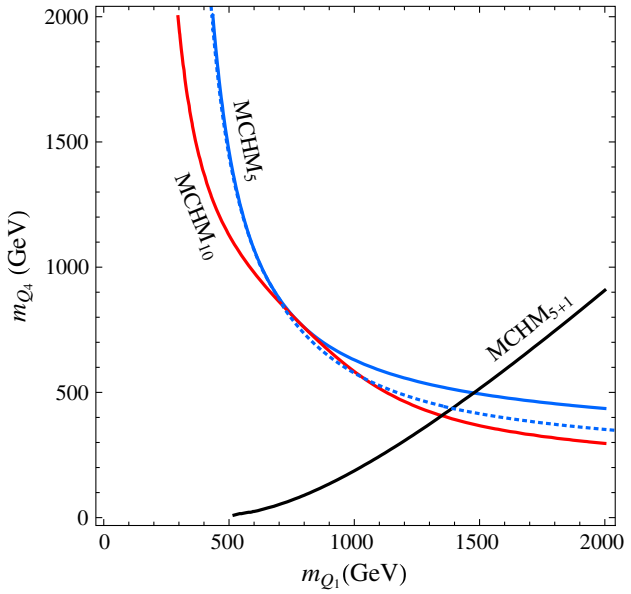

Fig. 1 Masses of the top partners Q_1 and Q_4 that reproduce the Higgs mass $m_h = 125\,\text{GeV}$ for $v^2/f^2 = 0.2$, from [116]. The different *lines* correspond to different SO(5) embeddings for the top quark. In *blue* $q_L, t_R \in \mathbf{5}$, in *red* $q_L, t_R \in \mathbf{10}$ (with $Q_1 \to Q_6$) and in *black* $q_L \in \mathbf{5}$ and $t_R \in \mathbf{1}$

Let us conclude this section with another comment on the ∼5 % tuning in μ^2. This tuning can be accomplished either by canceling two different top contributions, generically of $\mathcal{O}(\lambda_L^2)$ and $\mathcal{O}(\lambda_R^2)$, or by canceling the top versus the gauge contributions, of $\mathcal{O}(g^2)$. In this latter case the expectation is, as confirmed in explicit constructions, that the top and gauge contributions appear with different signs, creating some degree of cancelation. Assuming that this is the case, the current upper bound on the gauge partner masses, $m_\rho \simeq 2.5\,\text{TeV}$ (see Sect. 6.1), gives us a direct clue on where the top partners should be: the approximate cancelation $N_c y_t^2 m_T^2 \simeq (9/8) g^2 m_\rho^2$ yields $m_T \simeq 1\,\text{TeV}$. This mass range will be thoroughly explored in the next phase of the LHC.

6 Signals

The SM partners (new particles light compared to the cutoff $\Lambda_C \sim 4\pi f$) play an important role in the generation of the Higgs potential in the little, holographic and twin Higgs scenarios, which can be considered the weakly coupled versions of the bona fide composite Higgs case. The potential in these cases could be affected by large logs, $\log(\Lambda_C^2/m_*^2)$, where again Λ_C is the compositeness scale while m_* is a generic mass for the partners, unless another layer of partners is light. The partners, if present as suggested by the discussion in the previous section, generically give the leading contribution to electroweak precision tests (EWPT), in particular S, T, and $Zb\bar{b}$. They can also give rise to important flavor transitions beyond the SM. Also, they modify the couplings of the Higgs boson, to be taken into consideration along with the intrinsic deviations due to the composite nature of the Higgs.[10] Finally, such resonances should be produced at colliders, if they are sufficiently light and coupled to the SM matter. All of these issues will be discussed in this section.

6.1 Electroweak precision tests

The electroweak precision observables characterize the properties of the SM gauge bosons and their couplings to the SM fermions. Since we have not observed any particles beyond the standard model thus far, it is reasonable to assume that all new physics states are heavier than the electroweak scale. This allows us, as a leading approximation, to parametrize their effects at the electroweak scale and below via higher dimensional operators with SM fields only.

6.1.1 Universal

Most of the new physics effects are of the 'universal type' and can be encoded in the modifications of the SM gauge bosons' two-point functions [119–121]. The most relevant effects in each class can be parametrized by the parameters[11] $\hat{S}$, $\hat{T}$, W, and Y, where the first two generically yield the most stringent constraints, since the other two are typically suppressed by extra powers of g^2/g_*^2.

There are two generic contributions to the $\hat{S}$ parameter which arise in all composite Higgs models: the UV contribution from heavy spin-1 resonances that can be estimated as

$$\hat{S}_{\text{UV}} \sim \frac{m_W^2}{m_\rho^2}\,, \tag{6.1}$$

and an IR contribution associated with the reduced Higgs coupling c_V to the EW gauge bosons [42]. This second one can be understood as follows. For $m_h \gg m_Z$, the S-parameter in the SM scales logarithmically with the Higgs mass as result of a cancelation of the log-divergent one-loop contributions of virtual Goldstone and Higgs bosons, $\log m_h/m_Z = \log \Lambda/m_Z - \log \Lambda/m_h$. In composite Higgs models, while the Goldstone boson loop stays the same as in the SM, the Higgs boson loop is reduced and hence the cancelation is spoiled, leaving over $\log \Lambda/m_Z - c_V^2 \log \Lambda/m_h$. Thus the S-parameter becomes logarithmically sensitive to the new physics scale $\Lambda \sim m_\rho$ to be identified with the masses of the heavy resonances (of spin 0, 1, or 2) that couple to the W and the Z [42]

[10] Notice that the partners, being composite as is the Higgs, will generically be affected by higher-dimensional operators, suppressed by suitable powers of m_*/Λ_C.

[11] $\hat{S}$ and $\hat{T}$ are proportional to the Peskin–Takeuchi parameters $\hat{S} = g^2/(16\pi)S$ and $\hat{T} = \alpha_{\text{EM}} T$.

$$\hat{S}_{\rm IR} \simeq \hat{S}_{\rm SM}(m_h^{\rm eff}) = \frac{g^2}{96\pi^2}\log\left(\frac{m_h^{\rm eff}}{m_Z}\right),$$
$$m_h^{\rm eff} = m_h\left(\frac{\Lambda}{m_h}\right)^{1-c_V^2}. \quad (6.2)$$

Using a dispersion relation approach [122] one can refine these estimates and achieve a $\mathcal{O}(m_h/m_\rho)$ accuracy in $\hat{S}$ at leading order in g^2 if the spectral density of the strong sector is known. For example, using vector meson dominance as in [115,122], one finds

$$\hat{S} = \frac{g^2}{96\pi^2}\frac{v^2}{f^2}\left(\log\frac{m_\rho}{125\text{GeV}} - 0.29\right) + \frac{m_W^2}{f^2}\left(\frac{f_\rho^2}{m_\rho^2} - \frac{f_a^2}{m_a^2}\right), \quad (6.3)$$

where $f_{\rho,a}$ and $m_{\rho,a}$ denote the decay constants and the masses of vector and axial resonances. The new physics contribution to $\hat{S}$ can be kept under control if m_ρ^2 is sufficiently large, although this generically introduces some tuning in the Higgs potential, since m_ρ^2 fixes the scale where gauge-loop contributions are cut off. Another option is to invoke some degree of cancelation between different contributions directly in $\hat{S}$, for instance coming from extra scalars or fermions [123], although these are loop suppressed and generically model dependent.[12] Moreover, in [113] it was pointed out that fermion loops in composite Higgs models may provide additional sources of logarithmically enhanced contributions that can be understood in terms of the running of the two dimension-6 operators $\mathcal{O}_{W,B}$ related to $\hat{S}$ [41].

It was recognized long ago [126] that the $\hat{T}$-parameter can be protected against new physics contributions by a custodial symmetry $\mathrm{SU}(2)_C \subset \mathrm{SO}(4) \cong \mathrm{SU}(2)_L \times \mathrm{SU}(2)_R$. This requires that the new sector respects custodial symmetry to a very high degree, most often forbidding new sources of breaking beyond those already present in the SM, that is, the Yukawa coupling of the top and the hypercharge gauge coupling. In particular, it is required that the new states cutting off the Higgs potential, in particular the vector partners, come in complete representations of SO(4). This has been explicitly verified in many little Higgs models, see for instance [127–129]. In holographic Higgs models this requirement is satisfied by construction, since the partners always come in complete representations of the unbroken global symmetry subgroup, which contains SO(4) [130,131]. In addition, while the custodial SO(4) is sufficient to protect the $\hat{T}$-parameter when a single Higgs field breaks the electroweak symmetry spontaneously, as we discussed in Sect. 5 this is not the case when extra scalar fields charged under SO(4) are present, additional Higgs doublets, triplets, etc. In these cases, an 'enlarged' custodial symmetry is required (see [96] for a detailed explanation of the THDM case).

[12] See e.g. [124,125] for a discussion in the minimal SO(5)/SO(4) model (MCHM).

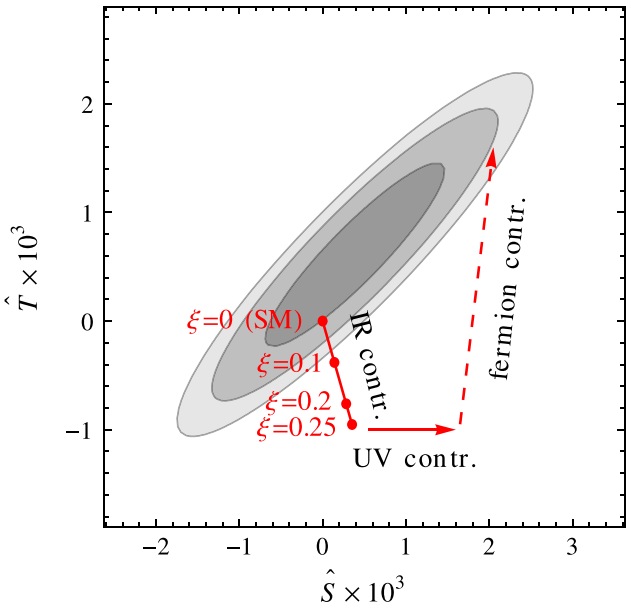

Fig. 2 Confidence-level contours (at 65, 95 and 99 %) for $\hat{S}$ and $\hat{T}$ from [132]. The IR contributions alone would imply $\xi = v^2/f^2 \lesssim 0.1$

With custodial protection, the leading corrections to $\hat{T}$ arise thus at one loop. Analogously to the case for $\hat{S}$, there is a universal IR contribution from the reduced coupling of the Higgs boson which can again be estimated in the heavy Higgs limit as

$$\hat{T}_{\rm IR} \simeq -\frac{3g'^2}{32\pi^2}\log\left[\frac{m_h}{m_Z}\left(\frac{\Lambda}{m_h}\right)^{1-c_V^2}\right]. \quad (6.4)$$

These IR contributions due to the modified Higgs couplings, Eqs. (6.2) and (6.4), form a line in the $\hat{S}-\hat{T}$ plane. If these were the only corrections, then they would imply $\xi = v^2/f^2 \lesssim 0.1$, see Fig. 2 reproduced from [132].

The one-loop contribution from fermions can be even more important: within the framework of partial compositeness it is generated by insertions of the mixings $\lambda_{L,R}$ and estimated as [41]

$$\hat{T}_{\rm fermions} \sim \frac{N_c}{16\pi^2}\frac{\lambda_L^4 f^2}{m_\Psi^2}\frac{v^2}{f^2}, \quad (6.5)$$

which can be the leading contribution. See e.g. [113,124,125] on concrete realizations and for examples. The above expression corresponds to the leading term in an expansion in λ_L/g_Ψ. However, if the degree of compositeness of the LH or RH top quark is large, the contributions to $\hat{T}$ are actually controlled by m_Ψ [41]. In that case $\hat{T}$ scales as m_Ψ^2/m_ρ^2, and it has been shown that such contributions can be positive for moderate values of $m_\Psi \sim 1$ TeV [133].

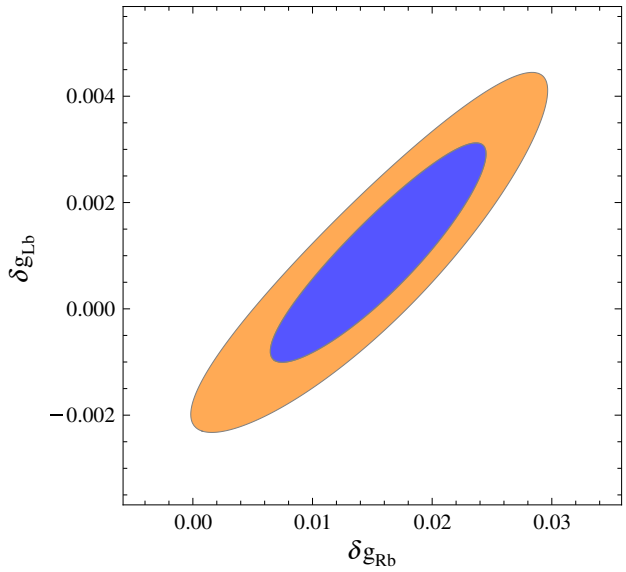

Fig. 3 Best fit region for the $Z\bar{b}b$ couplings from [137] favoring small positive δg_{Rb}. The SM is represented by the *green* point

As shown in Fig. 2, these contributions to $\hat{T}$ can be very important in order to bring the model into the $\hat{S}-\hat{T}$ ellipse and thus reduce the bound on f.

6.1.2 Non-universal

Besides the oblique parameters, strongly interacting models usually induce non-universal modifications to the couplings of the top, and due to $\mathrm{SU}(2)_{\mathrm{L}}$ invariance, also to those of the left-handed bottom [134,135]. This is due to the necessarily large coupling of the top quark to the strong sector, in order to reproduce its large Yukawa coupling. The strongest constraints come from measurements of the $Zb_{\mathrm{L}}\bar{b}_{\mathrm{L}}$ coupling, sensitive to the masses of the new-physics states. However, it was shown in [136] that the $Zb_{\mathrm{L}}\bar{b}_{\mathrm{L}}$ vertex can be protected from large corrections by a P_{LR} parity symmetry, as long as the b_{L} embedding does not break it, that is, if b_{L} has $-1/2$ charge under both $\mathrm{SU}(2)_{\mathrm{L}}$ and $\mathrm{SU}(2)_{\mathrm{R}}$.[13] As for the custodial symmetry, when this custodial parity is preserved by the strong sector, corrections to $Zb_{\mathrm{L}}\bar{b}_{\mathrm{L}}$ can be kept under control. Both symmetries yield important consequences for the quantum numbers and spectrum of the top partner resonances (for instance extended representations such as the $\mathbf{4}=(\mathbf{2},\mathbf{2})$).

Figure 3 reproduced from [137] shows the best fit region with a small positive δg_{Rb} where the following parametrization is used:[14]

$$\mathcal{L}=\frac{g}{c_W}Z_\mu\bar{b}\gamma^\mu\left[\left(g_{Lb}^{\mathrm{SM}}+\delta g_{LB}\right)P_{\mathrm{L}}+\left(g_{Rb}^{\mathrm{SM}}+\delta g_{RB}\right)P_{\mathrm{R}}\right]b. \tag{6.6}$$

The contribution from fermion loops to δg_{Lb} is generically logarithmically divergent as a result of insertions of the mixings that break the P_{LR} parity

$$\frac{\delta g_{Lb}}{g_{Lb}^{\mathrm{SM}}}\sim\frac{y_t^2}{16\pi^2}\frac{v^2}{f^2}\log\frac{\Lambda^2}{m_\Psi^2}\,. \tag{6.7}$$

Another sensitive test concerns the anomalous coupling of the right-handed top and bottom to the Z. This coupling is tightly constrained by $b\to s\gamma$ measurements. However, the size of the anomalous coupling is generically suppressed by y_b/y_t, yielding mild bounds on the new physics scale, see for instance [138]. Other top related measurements still lack of precision [133,139].

In the previous sections we have argued that due to its contribution to the Higgs potential, fermionic top partners should be the lightest new physics states. The effects of top-partners on precision tests, which we have reviewed in this section, have been thoroughly discussed in the literature, either in the context of little Higgs models [140], holographic Higgs models [42,92,125,133,141,142], or in more generality [132,143].

Finally, let us again note that modified Higgs couplings to electroweak gauge bosons can be indirectly probed through electroweak precision measurements, Eqs. (6.2) and (6.4). Such modified couplings arise whenever the operator $(\partial_\mu(H^\dagger H))^2$ is generated, to which new physics contributes even if the states responsible for taming the Higgs potential only couple to the Higgs (even if they do not carry electroweak charges in particular). Besides, this operator generically encodes the non-linear self-interactions of the Higgs, intrinsic of its GB nature. As such, it will be suppressed by α/f^2, with α a numerical factor that depends on the coset structure.

Also note that the case of a dilatonic Higgs needs to be considered separately for the EWPTs. Since a composite Higgs-like dilaton is not embedded into a SU(2) doublet, the argument before does not directly apply. Actually, the couplings of the dilaton to the gauge fields agree with those of the SM Higgs, except for a v/f suppression. Thus the corrections to $\hat{S}_{\mathrm{IR}}$ and $\hat{T}_{\mathrm{IR}}$ are minimized in the limit $v/f\to 1$, the opposite limit than in ordinary composite Higgs scenarios.

For a recent model independent analysis of the constraints from EWPT, see [144].

Another important direction for taming electroweak precision constraints has been the introduction of T-parity [100,101]: a Z_2 discrete symmetry under which all BSM states are odd. Such a symmetry ensures that all corrections to electroweak precision observables from the new states are at least one-loop suppressed, thus reducing the bounds on the

[13] Notice that in symmetry breaking cosets with unbroken SO(4), P_{LR} actually arises as an accidental symmetry of the leading order derivative Lagrangian [96].

[14] There exists another best fit region with a larger negative δg_{Rb}.

masses of the new states. In this case one can obtain a theory consistent with the electroweak precision observables, even with new states as light as $\sim$1 TeV. T-parity has been one of the leading themes for little Higgs models, and it can of course also be implemented in the general 4D versions.[15] An illustration of the electroweak precision observables in a little Higgs model with T-parity can be found in [146].

6.2 Flavor and CP violation

The interplay between electroweak symmetry breaking and the generation of the SM flavor structures has always been one of the major concerns in composite Higgs models. The degree of the problem, and thus the importance of the constraints, can be understood by the number and expected size of the flavor structures present in the SM low-energy effective theory. This crucially depends on the mechanism employed to generate the SM Yukawas (see Sect. 4).

6.2.1 4-Fermi operators

It has been long known that a simple mechanism to generate the interactions in Eq. (4.1) gives rise also to unsuppressed SM flavor violating 4-Fermi interactions

$$\frac{c^{ijkl}}{\Lambda_{\rm F}^2} q_i q_j \bar{q}_k \bar{q}_l, \tag{6.8}$$

which generically violate the stringent flavor constraints: for instance from the kaon system, $\Lambda_{\rm F} > 10^{3-5}$ TeV, while allowing for a sufficiently large top mass one would need $\Lambda_{\rm F} = \mathcal{O}(10)$ TeV. As explained in Sect. 4.1, this tension can be relaxed if the dimension of the operator $\mathcal{O}$ in Eq. (4.1) is sufficiently close to one, as long as the dimension of $\mathcal{O}^2$ does not decrease below four hence reintroducing the hierarchy problem.

It is worth mentioning that other alternatives might be viable, which rely on the flavor dynamics inducing additional suppression of the operators in Eq. (6.8), either via the Yukawa couplings, $c^{ijkl} \sim y_{u,d}^{ij}\, y_{u,d}^{kl}$, in which case the bounds on $\Lambda_{\rm F}$ can be relaxed close to the scale required to reproduce the top mass, or effectively imposing MFV, which could be realized if the couplings of the standard model fermions to the strong dynamics arise from the exchange of (supersymmetric) heavy scalars, such as in bosonic technicolor [147–149]. In the former case new physics is to be expected in flavor transitions, while in the latter supersymmetric states remnant of the flavor generation should be observable.

[15] In warped extra-dimensional models one can find constructions with KK parity [145], which also aim at reducing the tension with electroweak precision measurements.

6.2.2 Anarchic partial compositeness

As discussed in Sect. 4.2, the RS-GIM mechanism of partial compositeness significantly reduces the contributions to dangerous flavor transitions. However, it has been shown that the suppression is not quite enough as to provide a fully realistic theory of flavor. Even though $\Delta F = 2$ 4-Fermi operators

$$f_q^i f_q^{\dagger j} f_q^k f_q^{l\dagger} \frac{g_\rho^2}{m_\rho^2} \bar{q}^i q^j \bar{q}^k q^l \tag{6.9}$$

are effectively suppressed by four powers of the fermion masses m/v or CKM entries $V_{\rm CKM}$, measurements of CP violation in the kaon system, $\epsilon_{\rm K}$, put stringent bounds on the LR operators in Eq. (6.9), of the form $m_\rho \gtrsim 10 \frac{g_\rho}{Y_d}$ TeV [87,91,111,150–152], as well on LL operators. Although less significant, qualitatively similar bounds on LL operators arise from CP violation in the B system, $m_\rho \gtrsim 1 \frac{g_\rho}{Y_u}$ TeV. Given the expectation $m_\rho \sim g_\rho f$, these type of constraints bound the combination $Y_{d,u} f$. In explicit constructions of the pGB Higgs, the composite Yukawas $Y_{u,d}$ are correlated with the masses of the composite fermions cutting off the Higgs potential. These kind of bounds therefore have a significant impact on the fine-tuning. In addition, these bounds have to be contrasted with other potentially problematic flavor observables such as dipole operators

$$f_q^i f_q^{\dagger j} \frac{1}{16\pi^2} \frac{Y_{u,d}^3}{m_\Psi^2} \bar{q}_i \sigma_{\mu\nu} F^{\mu\nu} q_j, \tag{6.10}$$

generated by loops of composite fermions of mass m_Ψ and the Higgs. These induce large contributions to $b \to s\gamma$, direct CP violation in $\epsilon'/\epsilon_{\rm K}$, and contributions to the flavor conserving electric dipole moment of the neutron, all of them scaling with positive powers of Y_d; thus, the constraints $m_\Psi > \alpha Y_d$ TeV, with $\alpha \sim 0.5-2$ [91,92,152–154]. All these flavor bounds taken together force the scale of compositeness to be above 2 TeV along with composite couplings $g_{*=\rho,\Psi} \gg g_{\rm SM}$.[16]

Moreover, let us notice that the operators in Eq. (6.9) could also be mediated by the Higgs or other pGBs (of mass m_H), with the associated enhancement of their coefficients by $(m_\rho^2/m_h^2)(v/f)^4$ or (m_ρ^2/m_H^2), respectively.[17] However, it was pointed out in [96,156] that these unwanted effects can be avoided thanks to the Goldstone nature of these scalars, as long as the embedding of the SM fermions into the global symmetries of the strong sector only allows for a single Yukawa-type operator $\bar{q}_{\rm L} q_{\rm R} F(h, H)$, thus enforcing the MFV structure in the scalar interactions.[18]

[16] Other relevant effects which could also give rise to important constraints on m_Ψ arise from flavor transitions mediated by the Z [155].

[17] Higgs mediated FCNCs will arise from the operators $\bar{q}_i H q_j H^\dagger H$.

[18] Flavor transitions mediated by extra pGBs can also be suppressed by forbidding their couplings to fermions via symmetries [157,158].

This is, however, not the case for a dilatonic Higgs, since the lack of a direct connection with the electroweak VEV generically implies that the fermion mass matrices and the dilaton couplings are misaligned. In that case the best alternative is to assume that the composite sector is endowed with flavor symmetries.

Let us briefly comment on the lepton sector. First of all, given that neutrinos are much lighter than charged leptons, and that their mixings are not hierarchical, it is certainly plausible that neutrino masses come from a different source, or enjoy a different generation mechanism. Factoring out the discussion of neutrino mass generation, the constraints on partial compositeness for leptons with anarchic Yukawas come from [152,159,160] the electron EDM, and $\mu \to e\gamma$ transitions from penguin mediated dipole operators. The bounds from experimental data are even more stringent than in the quark sector, which makes the minimal implementation of leptonic partial compositeness not viable.

The most appealing option thus seems to rely on lepton flavor global symmetries, enforcing LMFV [161]. Another option to remove tree-level constraints on lepton partial compositeness is by imposing an A4 symmetry on the composite sector [162], alleviating the tension with the loop-induced processes. In that case the degree of compositeness of the leptons must increase in order to yield the proper Yukawa couplings, with the consequence of light tau partners [163].

6.2.3 $U(3)^3$ *symmetric partial compositeness*

As review in Sect. 4.2, the scenarios falling into this category can be classified as LH or RH quark compositeness. The degree of compositeness in each case is fixed by the requirement $f_{\mathrm{L,R}} \gtrsim y_t/Y_u$, in order to reproduce the top mass. Therefore, in every case the inevitable signal will come from flavor diagonal 4-quark operators,

$$\frac{g_\rho^2}{m_\rho^2} f_{\mathrm{L,R}}^4 (\bar{q}\gamma_\mu q)(\bar{q}'\gamma^\mu q'), \tag{6.11}$$

generated from the exchange of heavy resonances of mass m_ρ and coupling g_ρ. These have been recently probed at the LHC in $pp \to jj$ angular distributions. The individual bounds for the complete set of independent 4-quark operators, their coefficient normalized to Λ^{-2}, range between $\Lambda \gtrsim 1 - 5\,\mathrm{TeV}$ [164]. These place strong constraints on the degree of compositeness of the quarks, given the identification $\Lambda \sim f/f_{\mathrm{L,R}}^2$, for $m_\rho \sim g_\rho f$. Taking the most favorable situation, that is, $f_{\mathrm{L,R}} \sim y_t/Y_u$, the dijets constraints bound the combination $Y_u^2 f$, again implying large partners masses as in the anarchic case.

There is another class of constraints that apply only to LH or RH compositeness. If the LH quarks are composite, their (flavor diagonal) couplings to W and Z receive significant corrections, which affect precision observables such as quark–lepton universality in kaon and β decays or the hadronic width of the Z [91].[19] The corresponding bounds take the form $m_\Psi \gtrsim 35 f_{\mathrm{L}} Y_u v$, which again, taking $f_{\mathrm{L,R}} \sim y_t/Y_u$, implies a strong bound on the partners masses $m_\Psi \gtrsim 35 m_t$. For the case of RH composite quarks, given that their coupling to W and Z are still poorly measured (and can be easily protected by their proper embedding into the global symmetries of the strong sector), the previous measurements do not yield important constraints. However, flavor violating LL 4-Fermi operators Eq. (6.9) are still generated with a significant coefficient $(y_u y_u^\dagger)^2/(f^2 Y_u^4 f_{\mathrm{R}}^4)$ [92], which even though MFV suppressed, still yields $Y_u^2 f_{\mathrm{R}}^2 f \gtrsim 6\,\mathrm{TeV}$. Notice in particular that while this constraint prefers f_{R} large, the dijet bounds push towards f_{R} small.

In summary, flavor models with $\mathrm{U}(3)^3$ symmetry are under a significant stress from recent measurements of dijet production at the LHC. With the increase of energy at the next run of the LHC, such measurements will provide conclusive results about this possibility.

6.2.4 $U(2)^3$ *symmetric partial compositeness and variants*

In models where the flavor symmetry is reduced in order to uncouple the fraction of compositeness of the light generations and that of the top quark, the compositeness constraints from measurements of W and Z couplings or dijet production (discussed above), are irrelevant. Therefore in these scenarios the only phenomenologically relevant flavor constraints are the consequences of the third generation (LH chirality, RH, or both) being distinct from the first two. In this case it is important to point out that the R rotation matrices are very close to the identity in all the scenarios, with the corresponding suppression of the most dangerous LR 4-Fermi operators in Eq. (6.9) [92,94]. Still the most sensitive flavor observables come from the kaon and B systems (and the D system in the case of RH compositeness), as in the anarchic case, but with correlations among them, depending on the particular symmetry implementation. Most importantly, the associated bounds can now be satisfied for relatively low values of f or the partner masses. This makes the U(2) scenarios the most favored ones for a natural electroweak scale, while still offering good prospects of new physics effects in flavor physics.

Let us conclude this section by commenting on the particulars of little Higgs models. Although their UV completion is not a priori determined, thus making an assessment of flavor and CP violation more model dependent, solely from the interactions of the low energy degrees of freedom valuable

[19] If the compositeness fraction of the LH leptons is equal to that of the LH quarks, there will be universal shifts in couplings to gauge bosons, which can be interpreted as a (too large) contribution to the S-parameter.

lessons can be inferred, which are of course similar to those discussed in this section. Gauge and top partners contribute to neutral meson mixing and CP violation, with bounds at the same level or in some cases milder than those coming from EWPT [165–171] (and see [140] for a recent review on the top partners effects).

6.3 Higgs production and decay

Higgs physics is a direct probe of the electroweak symmetry breaking sector, making the measurement and study of its couplings one of the major goals in particle physics today. This is particularly relevant in the composite Higgs scenario, given that its GB nature unavoidably implies non-linearities in its couplings to SM fields, i.e. corrections of order v^2/f^2 with respect to the SM predictions. Importantly, this is regardless of any new states that might be present in the spectrum, given that such GB effects cannot be decoupled.

6.3.1 Single-Higgs production

After the Higgs discovery, one of the major enterprises in particle physics has been the extraction of the linear couplings of the Higgs to the other SM fields. These are obtained by fitting the experimental data on $\sigma \times BR$, see [172–174] and references therein. The best tested Higgs couplings to date are those to electroweak gauge bosons hZZ and hWW (with less precision), and to massless gauge bosons hgg and $h\gamma\gamma$, induced at one loop in the SM. Indirectly, through its contribution to hgg and $h\gamma\gamma$, the coupling to top quarks, $ht\bar{t}$ is also being tested. The first results on the coupling to tau leptons $h\tau\bar{\tau}$ and bottom quarks $hb\bar{b}$ have also been obtained.

In order to make connection with the experimental data and compare with different models, we parametrize the linear interactions of the Higgs by the following Lagrangian:

$$\begin{aligned}\mathcal{L}^{(h)}_{eff} = &\left(c_V\left(2m_W^2 W_\mu^+ W^{-\mu} + m_Z^2 Z_\mu^2\right)\right.\\ &\left.-c_t m_t \bar{t}t - c_b m_b \bar{b}b - c_\tau m_\tau \bar{\tau}\tau\right)\frac{h}{v}\\ &+\left(\frac{c_{\gamma\gamma}}{2}A_{\mu\nu}A^{\mu\nu} + c_{Z\gamma}Z_{\mu\nu}\gamma^{\mu\nu} + \frac{c_{gg}}{2}G^a_{\mu\nu}G^{a,\mu\nu}\right)\frac{h}{v},\end{aligned} \tag{6.12}$$

and present in Table 2 the predictions for two distinct composite Higgs models, the SO(5)/SO(4) model of [31], known as the Minimal Composite Higgs Model (MCHM), and the dilatonic Higgs following [63]. For the MCHM, we only include the predictions associated to the GB non-linear nature of the Higgs, dictated by the symmetry structure of the model, and we comment on the effects of the light SM partners below, which in any case give subleading corrections. For the case of the dilaton the couplings are entirely determined by scale invariance and its breaking.

Table 2 Coefficients of the linear Higgs couplings in Eq. (6.12), for the SM, the SO(5)/SO(4) composite Higgs (MCHM), and the dilaton Higgs

Coupling	SM	MCHM	Dilaton
c_V	1	$\sqrt{1-\xi}$	$\sqrt{\xi}$
c_ψ	1	$\frac{1-(1+n_\psi)\xi}{\sqrt{1-\xi}}$	$(1+\gamma_\psi)\sqrt{\xi}$
$c_{\gamma\gamma}$	0	0	$\frac{\alpha}{4\pi}(b^{(\mathrm{EM})}_{\mathrm{IR}} - b^{(\mathrm{EM})}_{\mathrm{UV}})\sqrt{\xi}$
$c_{Z\gamma}$	0	0	$\frac{\alpha}{4\pi t_W}(b^{(2)}_{\mathrm{IR}} - b^{(2)}_{\mathrm{UV}})\sqrt{\xi}$
c_{gg}	0	0	$\frac{\alpha_s}{4\pi}(b^{(3)}_{\mathrm{IR}} - b^{(3)}_{\mathrm{UV}})\sqrt{\xi}$

In Table 2 we have defined $\xi = v^2/f^2$, and we notice first the important fact that in the MCHM the deviations from the SM scale with ξ; thus, the SM limit is reproduced for $\xi \to 0$. This is a common feature of all the composite Higgs models except for the dilatonic Higgs, where instead the SM limit is recovered when $\xi \to 1$. For the dilaton, however, this is not the only requirement to reproduce the SM. The anomalous dimensions of the SM operators, which encode the explicit breaking of scale invariance from the SM fields, must also vanish. These are associated to the Yukawa coupling of the fermion, $\psi = t, b, \tau, \gamma_\psi$, and to the gauge field strength tensors, $\gamma_{g_i} = (b^{(i)}_{\mathrm{UV}} - b^{(i)}_{\mathrm{IR}})g_i^2/(4\pi)^2$. Importantly, the interaction of the dilaton with massless gauge fields receives its leading corrections from the trace anomaly, in contrast with the MCHM where these corrections arise only after integrating out light composite states, generically small and not included in Table 2. Let us also note that for the MCHM, the numerical factor multiplying ξ in the coupling to electroweak gauge bosons, 1/2 when expanded in powers of ξ, is fixed by the SO(5)/SO(4) symmetry. In larger cosets such factor might be different, for instance in SU(5)/SO(5) it is 1/8. However, one should bear in mind that if the additional GBs in these extended cosets are decoupled via large explicit breakings, the prediction for hVV should approach those of the MCHM (as long as custodial symmetry is preserved).[20] Let us also point out that the Higgs interactions with fermions depend on the specific form of the fermion couplings to the composite sector, in particular on the embeddings into the global symmetries. Using the general structure presented in [116] for the mass of the fermion, $m_\psi(h) \propto \sin(h/f)\cos^{n_\psi}(h/f)$, with $m_W(h) = gf\sin(h/f)/2$, one can derive the c_ψ presented in Table 2.

To parametrize this model dependence, the deviations in the Higgs couplings can be analyzed in general by encoding the effects of new physics in higher-dimensional opera-

[20] In the littlest Higgs model of [27], based on the SU(5)/SO(5) coset, once the extra vector resonances are integrated out and the custodial breaking triplet VEV is fine-tuned to vanish, one obtains a factor 5/32 [41]. This is far from the MCHM, but only because the corrections g_{SM}/g_* are important in that particular realization.

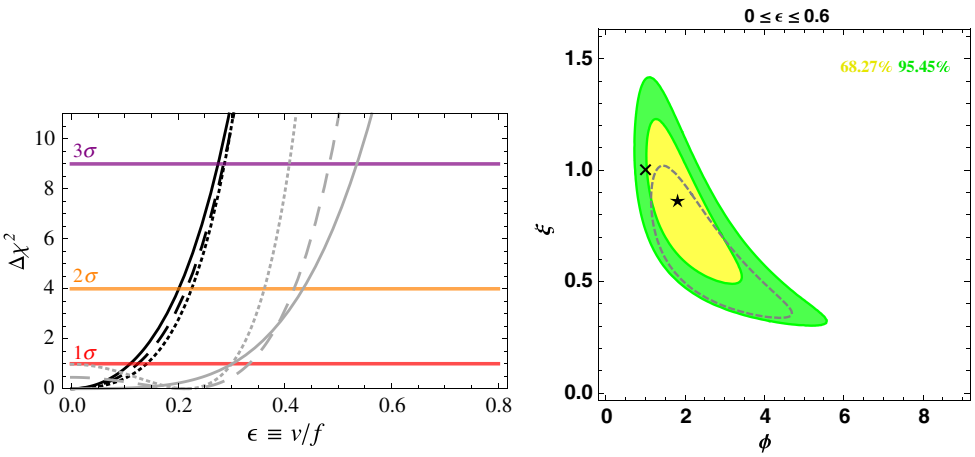

Fig. 4 Higgs fits from [173] (*left panel*) and [182] (*right panel*). *Left panel* Fit to v/f for the MCHM with (*black*) or without (*gray*) including electroweak precision data, with $n_\psi = 0$ (*solid*), $n_\psi = 1$ (*dashed*), and $n_\psi = 2$ (*dot-dashed*). *Right panel* Fit to $\xi = v^2/f^2$ and $c_{\gamma\gamma}/\xi$ from Higgs data, with $\epsilon \equiv \gamma_\psi$ marginalized in the range $0 \leqslant \epsilon \leqslant 0.6$. The star is the best-fit point, while the cross corresponds to a Higgs-like dilaton limit

tors involving the Higgs complex doublet field [41,175]. The most relevant ones are: (1) Universal corrections to all Higgs couplings, arising as a modification of the Higgs kinetic term from the operator $(\partial_\mu (H^\dagger H))^2$. This is generically generated by the non-linear structure of the coset interactions, extra scalars mixing with the Higgs, tree-level exchange of vector partners, and at one loop by top partners and extra GBs. Notice that this term gives rise to modified Higgs coupling to electroweak gauge bosons correlated with the modification in the couplings to fermions; (2) This correlation is broken by the operator $H^\dagger H \bar{\psi}_{\rm L} H \psi_{\rm R}$, which affects only the fermionic couplings of the Higgs; (3) Given its importance for Higgs production and decay, the operators $H^\dagger H F^2_{\mu\nu}$ parametrize the corrections of the Higgs couplings to massless gauge bosons. The contributions of these operators to the parameters of Eq. (6.12) can be found in Table 1 of [176].[21] Several other works have also recently reassessed such effective Lagrangians in the context of the newly discovered Higgs boson [177–180]. Given a proper complete basis of operators for physics beyond the SM, corrections and correlations on observables can be consistently derived, allowing one for instance to identify which new physics Higgs signals are still poorly constrained [179,180]. One particularly interesting unconstrained channel is the $h \to Z\gamma$ decay rate [179,181].

The odd case is again that of the dilatonic Higgs [63,182], where the proper effective Lagrangian disengages the longitudinal components of the W and Z from the Higgs particle, see for instance [177].

Given all these considerations, we come back to the particular models discussed above, to show in Fig. 4 left panel the fit for the MCHM in terms of v/f (ϵ in the plot) for $n_\psi = 0, 1, 2$, taken from [173], and in the right panel for the dilaton in terms of $\xi = v^2/f^2$ and $c_{\gamma\gamma}/\xi$ (ϕ in the plot) for γ_ψ (ϵ in the plot) between 0 and 0.6 and $c_{gg} = 0$, taken from [182]. For the MCHM, given the absence of significant deviations from the SM predictions, a lower bound on the compositeness scale $f \gtrsim 700\,\text{GeV}$ at 1σ level can be obtained from Higgs couplings measurements only (gray lines), while $f \gtrsim 1.5\,\text{TeV}$ if the electroweak precision data, mostly affecting c_V, is included in the fit (black lines). As explained above, these bounds apply to most of the composite Higgs models, although they can be somewhat relaxed if there is an extended GB sector [72,183,184] (see also [185]), or extra contributions to $\hat{T}$ as explained in Sect. 6.1. For the Higgs-like dilaton, if the electroweak precision data is not included there is still a significant allowed range for ξ around 0.8, correlated with the values of $c_{\gamma\gamma}$ and c_{gg}, which in this case can display $\mathcal{O}(1)$ deviations from the SM. However, if the bound on c_V from EWPT is taken into account, it forces $f \lesssim 300\,\text{GeV}$ and small anomalous dimensions $\gamma_\psi, \gamma_{g_i} \ll 1$.

At this point it is worth pointing out that deviations in the $ht\bar{t}$ coupling and direct contributions to the hgg coupling both affect the Higgs production channel via gluon fusion. Given that in models such as the MCHM, the leading new physics effects modify c_t, while for the dilaton it is c_{gg} that receives the largest corrections, one important subject is to disentangle them. Several approaches have been proposed to achieve this: th production [186,187], $t\bar{t}h$ production [188,189], and hj production [190,191].

It is thus clear that it is very important to identify which new physics contributions to the Higgs one-loop couplings to gluons and photons are predicted in scenarios such as the MCHM due to the presence of light states (the top and vector partners). Since the Higgs is assumed to be a pGB, these contributions are expected to scale with $g^2_{\rm SM}/m^2_*$, in addition to the loop factor $g^2/16\pi^2$. Several analyses have considered such deviations due to the light top partners [192–194], and the same behavior is expected for the vector partners. In these corrections collective symmetry breaking plays an important role: it basically eliminates the dependence on masses of the partners, leading to a shift in the hgg coupling which

[21] In that table the contributions of several other operators to a more complete set of effective interactions of the Higgs are also shown, which are relevant for 3-body $V\psi\psi$ Higgs decays, $V = W, Z$.

scales as v^2/f^2, and independent of $g_* = m_*/f$ to leading order in m_h^2/m_*^2. This shift is the same as in the $ht\bar{t}$ coupling to leading order in $\lambda_{\mathrm{L,R}}^2/g_*^2$. This was first pointed out in [195] in the holographic Higgs framework, followed by recent works [196,197]. This pattern of deviations no longer holds if the partners for the light SM fields, such as the bottom quark, are light. This is due to the fact that light SM fields do not contribute to loop-mediated Higgs couplings, while their partners do [196,198]. In this case the hgg and $h\gamma\gamma$ couplings are sensitive to the spectrum of partners, their corrections scaling with the expected $\lambda_{\mathrm{L,R}}^2/m_*^2$ ratio. Also, if the low-energy theory contains more than one LR Yukawa-type operator, non-trivial dependence on m_* can arise.[22] It is important to point out at this point that the GB suppression does not hold for $hZ\gamma$, since this coupling involves both a massless and a massive SM gauge boson; thus, it does not need to be suppressed by the GB symmetry [181].

Finally, notice that in twin Higgs models, where the SM partners are not charged under the SM gauge symmetries, no effects are present except through Higgs operators [200].

6.3.2 Double-Higgs production

We begin this section by noticing an important but obvious point. Since the recently discovered Higgs boson has SM-like couplings, in particular to the massive gauge bosons $V = W, Z$, the unitarization of their scattering amplitudes $VV \to VV$ is accomplished to a high degree by the Higgs itself, without the need of any new resonances up to at least $\sim$3 TeV [201–203]. For the case that the Higgs arises as a 4-plet of GBs, the above statement, in effective field theory language, is equivalent to the confirmation that the operator $(\partial_\mu (H^\dagger H))^2$ is suppressed by a scale f hierarchically larger than the electroweak scale. Furthermore, in this case the properties of the W and Z are intrinsically tied to those of the Higgs boson, and as such their behavior at high energies is completely correlated by the SO(4) symmetry. Because of this, the high energy behavior of double Higgs production does not offer a new (compared to WW scattering) avenue where beyond the SM behavior might be expected. However, two important comments are in order. First, there is a composite Higgs candidate which does not exhibit the above features by construction: the dilatonic Higgs. Second, the production of Higgs boson pairs can be affected by several other new-physics effects, as we now show.

As in the previous section, we parametrize the double interactions of the Higgs by a phenomenological Lagrangian [204]

[22] Besides, Higgs plus jet production has been shown to display a higher sensitivity to the top partners masses and couplings [199].

Table 3 Higgs couplings in Eq. (6.13) for the SM, the MCHM, and the dilaton

Coupling	SM	MCHM	Dilaton
d_V	1	$1-2\xi$	ξ
d_ψ	0	$\frac{-\xi(1+3n_\psi-(1+n_\psi)^2\xi)}{2(1-\xi)}$	$\frac{1}{2}\gamma_\psi\xi$
d_{gg}	0	0	$-\frac{\alpha_s}{8\pi}(b_{\mathrm{IR}}^{(3)}-b_{\mathrm{UV}}^{(3)})\xi$
c_3	1	$\frac{1-(1+\tilde{n}_\psi)\xi}{\sqrt{1-\xi}}$	$\frac{1}{3}(5+\mathrm{d}\beta/\mathrm{d}\lambda)\sqrt{\xi}$

$$\mathcal{L}_{\mathrm{eff}}^{(h^2)} = \left(\frac{d_V}{2}\left(m_W^2 W_\mu^+ W^{-\mu} + m_Z^2 Z_\mu^2\right) - d_t m_t \bar{t}t - d_b m_b \bar{b}b - d_\tau m_\tau \bar{\tau}\tau\right)\frac{h^2}{v^2} + \left(\frac{d_{gg}}{2} G_{\mu\nu}^a G^{a,\mu\nu}\right)\frac{h^2}{v^2} - \frac{c_3}{2}\frac{m_h^2}{v}h^3\,, \tag{6.13}$$

and present in Table 3 the predictions for the MCHM of [31] and the dilatonic Higgs [63]. For the MCHM we omit again the effects of the light SM partners, but we comment on those below. As for the linear Higgs couplings, the deviations from the SM vanish in the limit $\xi \to 0$ for the MCHM, as well as in other models where the Higgs boson belongs to the same multiplet as the scalars eaten by the W and the Z. Once again, the dilaton mimics the SM prediction in the opposite limit $\xi \to 1$, along with vanishing anomalous dimensions, except for one notable exception, the trilinear Higgs self-interaction c_3. This can be understood by noticing that the SM result $c_3 = 1$ is reproduced if the perturbation explicitly breaking scale invariance is a pure mass term, as in the SM, since then $d\beta/\mathrm{d}\lambda = -2$ (where in the SM case $\lambda = \mu$). However, the natural realization of the Higgs-like dilaton scenario (with a sufficiently light dilaton) implies $\mathrm{d}\beta/\mathrm{d}\lambda \propto m_d^2/\Lambda_C^2$, which makes this a subleading contribution. This fact then establishes double-Higgs production as the key test to distinguish the dilatonic Higgs scenario from an ordinary Higgs. Let us also note that for the MCHM the numerical factor multiplying ξ in d_V is again fixed by the SO(5)/SO(4) symmetry, and for larger cosets these coefficients could be different. This also applies to double Higgs couplings to fermions, which are embedding dependent, and which we have derived again from $m_\psi(h) \propto \sin(h/f)\cos^{n_\psi}(h/f)$. The prediction for c_3 in the MCHM is more model dependent, since it depends on what the leading contribution to the Higgs potential is. We have assumed here that it is of the form $V(h) = \cos^{1+\tilde{n}_\psi}(h/f)(\alpha - \beta\cos^{1+\tilde{n}_\psi}(h/f))$. All this model dependence can again be encoded in the coefficients of higher-dimensional operators beyond the SM, in particular $(\partial_\mu(H^\dagger H))^2$, $H^\dagger H \bar{\psi}_{\mathrm{L}} H \psi_{\mathrm{R}}$, $H^\dagger H G_{\mu\nu}^2$, and $(H^\dagger H)^6$, for d_V, d_ψ, d_{gg}, and c_3, respectively [201]. In any case it is important to stress that double-Higgs production via gluon fusion is not only sensitive to the trilinear Higgs coupling, but

also to the $hht\bar{t}$ and $hhgg$ couplings. The actual sensitivity is more promising for the latter rather than the former [204]. The effects of the top partners on these couplings have also been studied [193], with the important result that the process $gg \to hh$ gets sizable contributions, contrary to the expectations for single-Higgs production in $gg \to h$.

Let us conclude this section with more comments on the high energy behavior of W, Z and h scattering. We stress the fact that in most composite Higgs models at the high energies the relation $\mathcal{A}(W^+W^- \to hh) \simeq \mathcal{A}(W^+W^- \to ZZ)$ is expected to hold due to the Higgs being part of an SO(4) vector, unlike for the dilaton. The relation between the linear and double dilaton couplings to the massive gauge bosons $V = W, Z$ ensures that the growth with energy in $VV \to hh$ is absent at leading order $\mathcal{A}(W^+W^- \to hh) \simeq (d_V - c_V^2)(s/v^2) = 0$. However, this relation is affected by higher derivative terms, such as $\partial_\mu h \partial_\nu h \partial^\mu \partial^\nu h$ or $2m_V^2 V_\mu V_\nu \partial^\mu h \partial^\nu h$. The first of these operators breaks the $h \to -h$ parity symmetry present in the chiral Lagrangian of the MCHM (a property that is shared by all the composite Higgses except for the dilaton). The feasibility of probing these interactions at the LHC is quite limited, with better perspectives at a linear collider [205].

6.3.3 Invisible decays

Composite Higgs models providing a dark matter candidate may predict invisible Higgs decays which in turn affect the various branching ratios into visible final states. Because of the small Higgs width in the SM, $\Gamma_{\rm SM} \sim 10^{-5} m_h$, even relatively small couplings of the Higgs boson to dark matter (or to other undetectable final states) may result into relatively large modifications of the branching ratios. CMS has placed a direct upper bound of 69 % (at 95 % CL) on the invisible branching ratio in the VBF channel [206]. The upper bounds on the Higgs invisible branching ratio in the Zh associated production channel are 75 % from CMS [207], and 65 % from ATLAS [208]. The invisible Higgs branching ratio is also constrained indirectly by $BR_{\rm inv} \lesssim 0.6$ [209,210] obtained from fitting the Higgs couplings. Milder bounds in the 35–50 % range can be obtained by allowing variations of the Higgs couplings to gluons and photons in the fit [173,174].

6.4 Direct searches

The SM partners are constrained indirectly from electroweak, flavor, and Higgs physics, as we have reviewed in the previous sections. Already from LEP the bounds on generic vector partners is quite strong, $m_\rho \gtrsim 2.5\,\text{TeV}$. On the other hand pre-LHC bounds on fermion partners were less constraining, and LHC Higgs couplings measurements are not contributing much to the bounds on the partner masses. Nevertheless, these indirect measurement can be sensitive to the UV properties of the models around the strong coupling scale $\Lambda_{\rm C}$, while direct searches do not have that problem. The latter thus constitute a direct probe of the fine-tuning in any given model.

There are many studies on the phenomenology of the SM partners, either in little Higgs [211–214] or in holographic Higgs models [215,216]. We will classify them based on the spin.

Spin-1 gauge partners: These vector resonances are the $W_{\rm H}, Z_{\rm H}$ gauge boson partners in little Higgs models [217,218], in warped extra dimensions they are the KK gauge bosons [219–221], or generically they are simply ρ mesons. These states could have played an important role [203] in the unitarization of the WW scattering amplitudes; however, since the Higgs couplings are SM-like there is not much need for that. Therefore their main role is to tame the radiative contributions to the Higgs potential from the $\mathrm{SU}(2)_{\rm L} \times \mathrm{U}(1)_Y$ gauge bosons. For studies of the 4D general effective Lagrangians describing these fields see [202,203,222].

Due to the strong indirect bounds, we focus on the limit of strong coupling $g_\rho \gg g$ (which increases the mass of the ρ to several TeV). These resonances have coupling g_ρ to the composite states (including the Higgs and longitudinal gauge bosons), while the coupling to quarks, leptons and transverse gauge boson are expected to be significantly smaller, g^2/g_ρ (unless one has a U(3) flavor symmetry [223] and light quark compositeness or simply $g_\rho \sim g$, though the latter is disfavored by EWPTs). Note that these latter couplings are not necessary to cut off the Higgs potential. In this case the branching ratios of the ρ are dominated by the decays $\rho \to WW, WZ, Wh, Zh$. Also decays to $t\bar{t}$ are plausible given the assumption of the compositeness of the top. Moreover, given the necessary hierarchy implied by the constraints and the fine-tuning arguments, decays to top partners could actually dominate. The production of the ρ is expected to be dominated by single Drell–Yan production, through their mixing with the W and Z. Another important channel might be associated production with jets if they are coupled more strongly to light quarks. At a linear collider, effects on $e^+e^- \to f\bar{f}$ due to the ρ have been studied for instance in [218].

While 4D models do not necessarily include them, excitations of the gluon are an integral part of most extra dimensional models, and they have been thoroughly investigated [224–226]. In fact this is one of the most prominent signals of the extra dimensional versions, due to the enhanced production rate of the KK gluons at hadron colliders. In fact, it is possible that such color-octet excited states show up in generic models as well, since some of the fields in the composite sector must be charged under color in order to be able to generate the top partners (even though the mass of the gluon partners has no direct connection with naturalness).

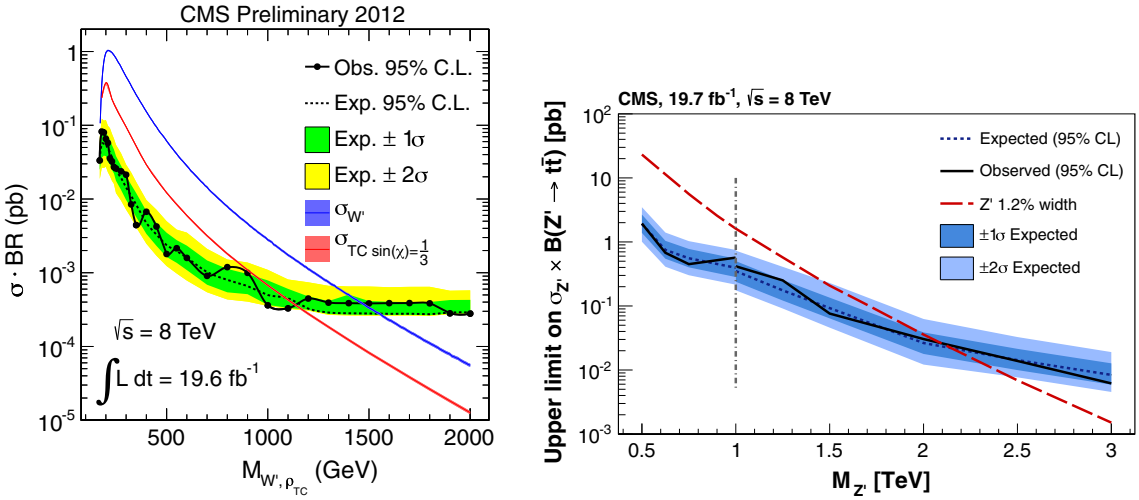

Fig. 5 Preliminary CMS bounds from run 1 of the LHC on the production of spin 1 resonances. *Left panel* bound on $\rho^{\pm}$ using decays to WZ, from [227]. *Right panel* bound on the KK gluon decaying to $t\bar{t}$, from [229]. Note that the dashed curve is for a Z', the KK gluon bound from the same plot is around 2.5 TeV

The direct searches at ATLAS and CMS are most sensitive to $\rho^{\pm}$ production with decays to WZ. The final CMS run 1 bound is $m_{\rho} \gtrsim 1.1\,\text{TeV}$ at 95 % CL ($\sim 20\,\text{fb}^{-1}$ at 8 TeV) [227], see Fig. 5 left panel. One obtains similar bounds in ATLAS [228] although the integrated luminosity in the most recent analysis is somewhat lower $\sim 14\,\text{fb}^{-1}$, leading to a slightly reduced bound. Important constraints can arise also from resonance searches in $t\bar{t}$ production. The resulting bounds depend on the degree of compositeness of the top, generically for the ρ they are milder than those from WZ searches. On the other hand for the KK gluon this is the leading channel, since the branching ratio is usually strongly dominated by $t\bar{t}$. The resulting run 1 CMS bound is $m_G \gtrsim 2.5\,\text{TeV}$ at 95 % CL ($\sim 20\,\text{fb}^{-1}$ at 8 TeV) [229] (and again slightly weaker for ATLAS due to less luminosity [230]). Notice that if the decays to $t\bar{t}$ and $t\bar{b}$ are non-negligible then the BR to VV and Vh will be reduced; thus, the above bounds can be weakened (to date no analysis for a combined bound in both channels has been performed).

Spin-1/2 top partners: The investigation of the phenomenology and collider physics of the top partners has been initiated in the framework of the Little Higgs models [231], for recent analyses in this context see [140,232]. As discussed throughout this review, these states are also predicted in the warped extra-dimensional models or pure 4D descriptions [233–238] as they are responsible for taming the radiative contributions to the Higgs potential from the top quark. Recent analyses of 4D effective Lagrangian descriptions parametrizing the most general possible interactions of the top partners can be found in [239–242].

The properties of the top partners depend on their quantum numbers under the global symmetries of the composite sector. If custodial SO(4) is assumed, it is common to find a **4** (required to couple to q_{L}) and **1** (required to couple to t_{R}). In almost all composite models they are triplets of color (the exception being twin Higgs models). Searches are typically classified by their electric charges: $T_{5/3}$, $T_{2/3}$, and $T_{-1/3} \equiv B$, although even more exotic charges have been proposed e.g. $T_{8/3}$ [243], arising from a **9** of SO(4).

The phenomenology of the top partners depends on their production and decay. The leading gluon fusion initiated production is more model independent. However, single production via W, Z exchange is also very important for relatively heavy states. Their decays are usually fixed by symmetry. The Goldstone boson equivalence theorem mostly fixes the couplings and therefore the decay rates: (1) $BR(T \to Zt) \simeq BR(T \to ht) \simeq BR(T \to W^+b)/2$ for the $T_{2/3}$ singlet under SO(4) (or $\text{SU}(2)_{\text{L}}$). (2) $BR(B \to W^-t) \simeq 1$ for the B doublet (under $\text{SU}(2)_{\text{L}}$). (3) $BR(T \to Zt) \simeq BR(T \to ht)$ for the $T_{2/3}$ doublet (under $\text{SU}(2)_{\text{L}}$). (4) $BR(T \to W^+t) \simeq 1$ for the $T_{5/3}$ doublet (under $\text{SU}(2)_{\text{L}}$). It is important to recall that this is somewhat dependent on the spectrum. There could be cascade decays or extra light GBs that can reduce the branching ratios [244,245]. The phenomenology of composite light generations with various flavor symmetries can be found in [246].

The 95 % CL final run 1 bounds from CMS using $\sim 20\,\text{fb}^{-1}$ luminosity at 8 TeV are shown in Fig. 6: $m_{T_{5/3}} \gtrsim 800\,\text{GeV}$ left panel [247], $m_{T_{2/3}} \gtrsim 700\,\text{GeV}$ for the singlet, middle panel [248], $m_{\tilde{B}} \gtrsim 700\,\text{GeV}$ right panel [249], where $\tilde{B}$ is asinglet under $\text{SU}(2)_{\text{L}}$; thus, $BR(\tilde{B} \to Zb) \simeq BR(\tilde{B} \to hb) \simeq BR(\tilde{B} \to W^-t)/2$. The references also contain limits for 'non-standard' BR. Reference [250] recast experimental searches for single and doubly produced top partners and showed that the single-lepton search could be more sensitive than the same-sign lepton search.

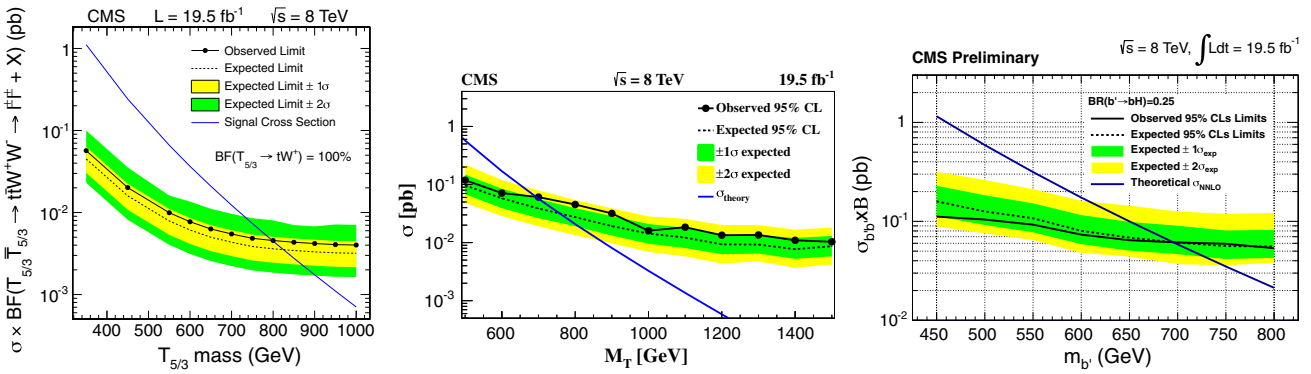

Fig. 6 CMS bounds on spin 1/2 top partners after run 1. *Left* the bound on the charge 5/3 top partner from [247], middle: the bound on the charge 2/3 singlet from [248], *right* the bound on the charge $-1/3$ singlet bottom partner from [249]

The most recent ATLAS bounds are for slightly lower luminosity $\sim 14\,\text{fb}^{-1}$ at 8 TeV, yielding somewhat milder bounds. The ATLAS analyses are organized by collider signatures and thus they apply to several top partners: lepton plus jets corresponding to mainly $T_{2/3} \to ht$ is found in [251], $T_{2/3} \to W^+b$ is in [252], same-sign dileptons corresponding to all possible kinds of $T_{2/3}$ and B decays (singlets and doublets under $\text{SU}(2)_\text{L}$) [253], and Z plus jets corresponding mainly to $T_{2/3} \to Zt$ and $B \to Zb$ decays (singlets as well as doublets) can be found in [254]. These analyses also provide limits as a function of branching ratios.

6.5 Dark matter

Dark matter (DM) candidates in composite models are of several nature. We can find partners of the SM states that enjoy a protecting global or discrete symmetry that renders them stable. Alternatively, the coset space $\mathcal{G}/\mathcal{H}$ may have non-trivial homotopy groups and give rise to topologically conserved charges.

Non-trivial homotopy groups $\pi_n(\mathcal{G}/\mathcal{H})$ lead to $(2-n)$-dimensional defects such as domain walls ($n = 0$), strings ($n = 1$), and magnetic monopoles ($n = 2$) whose cosmological abundances were studied e.g. in [255]. The case of Skyrmions, $\pi_3(\mathcal{G}/\mathcal{H}) \neq 0$, has been explored recently within Little Higgs models in [256,257] where it was shown that the geometric annihilation cross-section $\sigma = \pi\langle r^2\rangle$ may account for the observed DM relic density provided a quite large Skyrme parameter is chosen. One generic problem of the models based on skyrmions is the stability of their masses and sizes which is achieved by balancing two operators with different dimensions, going beyond the regime of validity of the EFT. Nevertheless, there exist 5D realizations [258] where the size of the skyrmion is in fact larger than the inverse cutoff of the theory and the predictions can thus be trusted.

Models with extra conserved U(1)s were proposed originally within technicolor models [259,260] where the lighest 'technibaryon' (which may or may not be a PNGB) is stable and can have the observed DM relic density [261–263], which is typically linked to the ordinary baryon asymmetry, similarly to the case of asymmetric DM models [264].

Other models with conserved U(1) baryon and lepton numbers have been considered within holographic versions of composite grand unified theories [103,106,265] where the $U(1)$s are gauged and then spontaneously broken at the UV brane. Similarly to R parity in SUSY, the resulting accidental Z_n symmetry is enough to ensure DM stability over cosmological time scales [266].

Models with large cosets may give stable PNGBs by invoking suitable discrete symmetries acting on $\mathcal{G}/\mathcal{H}$. For example, the next-to-minimal composite Higgs model O(6)/O(5) studied in [267] features an extra PNGB η, which is a SM singlet stabilized by one of the O(6) parities, $\eta \to -\eta$. Interestingly, the model is particularly predictive in the region of parameter space that is consistent with the latest bounds from the LUX [268] and XENON100 [269] experiments. In particular, the η can provide all the relic DM abundance, while naturally accommodating all the constraints, by choosing $m_\eta \gtrsim 100$ GeV and $f \sim 1$ TeV. In this case, the annihilation cross-section mediated by the Higgs boson is controlled only by f, which fixes all the PNGB derivative coupling terms of the states parametrizing the coset as

$$\mathcal{L} = \frac{1}{2}(\partial_\mu \eta)^2 + \frac{1}{2f^2}\left(\partial_\mu |H|^2 + \frac{1}{2}\partial_\mu \eta^2\right)^2 . \tag{6.14}$$

Notice also that in the regime $m_\eta < m_h/2$ bounds from the invisible BR of the Higgs boson are among the strongest in this scenario [267].

Models with T-parity [100,101] naturally contain a dark matter candidate, the lightest T-odd particle. Within little Higgs models this often turns out to be the partner of the neutral gauge boson B. A lot of work has been devoted to analyzing the viability of this scenario [270–273].

7 UV completions

The models presented here are all effective theories with a cutoff scale $\Lambda_C \simeq 4\pi f \sim 5$–$10$ TeV. An important question is what these theories would look at a scale beyond the cutoff, which is not too far above the LHC energies. This motivates the search for UV completions. Assuming that one wants to avoid reintroducing the hierarchy problem, UV completions generically fall into two categories. The first are non-supersymmetric strongly coupled theories similar to QCD/technicolor, but with modified dynamics. In this case one needs to guess the right symmetry breaking pattern and low-energy degrees of freedom, which should then be verified by lattice simulations. The second are supersymmetric UV completions, which may also involve some strong dynamics (but is usually under control due to the added constraint of supersymmetry).

One should emphasize that there are several different ways of trying to combine the pGB Higgs ideas with supersymmetry. In many cases, the low-energy theory (at a few 100 GeV) is actually a SUSY theory, which due to the pGB nature of the Higgs has interesting properties different from the ordinary MSSM. These include so-called super-little Higgs [274–280] and buried Higgs [281,282] models. A particularly interesting SUSY model is where only the idea of partial compositeness is implemented [283,284]—due to SUSY there is no need to further protect the Higgs potential. Partial compositeness could rather raise the physical Higgs mass, and also it could provide a reason for hierarchical soft breaking terms [285]. Purely composite SUSY Higgs models usually go under the name of 'fat Higgs' [286,287]. While all of these models contain some of the ingredients used in the non-SUSY pGB composite Higgs models, they are not true UV completions, since there is no regime where the theory is truly non-supersymmetric composite Higgs model, with only a composite Higgs, the top partners and the vector partners in the spectrum. An attempt at such a SUSY UV completion for the MCHM was recently proposed in [288,289]: the effective theory below 10 TeV is the SO(5)/SO(4) MCHM with top and vector partners (and perhaps a few scalar superpartners of the top partners). Other superpartners show up at 10 TeV. The model is based on the $SO(4)_m$ magnetic dual of a strongly coupled electric SO(N) theory, where the flavor symmetries contain an additional SO(5) factor. A different type of SUSY UV completion is based on a weakly coupled SUSY theory, a concrete example has been worked out for the case of little Higgs models in [290,291].

The non-supersymmetric UV completions include a strongly coupled (non-QCD-like) SO(7) theory for the littlest Higgs model [292], as well as condensing 4-Fermi oparators à la NJL [293].

Of course many of the composite Higgs models originate from extra dimensional constructions. These have their own cutoff scales, which depends on the parameters of the theory. The theory below the cutoff generically describes the first few weakly coupled KK Modes of the theory, the lightest of which can be identified with the top and gauge partners. However, to find a true UV completion one either needs to find a string theory construction, or use a deconstructed version without elementary scalars.

Acknowledgments We thank Ignatios Antoniadis and Dumitru Ghilencea for tasking us with this review, and for their patience with us. We also thank Maxim Perelstein for useful conversations. B.B. thanks Filippo Sala for reading and commenting on the paper. B.B. is supported in part by the MIUR-FIRB grant RBFR12H1MW, and by the Agence Nationale de la Recherche under contract ANR 2010 BLANC 0413 01. C.C. and J.S. are supported in part by the NSF grant PHY-0757868.

References

1. S. Chatrchyan et al., CMS Collaboration, Phys. Lett. B **716**, 30 (2012). [arXiv:1207.7235 [hep-ex]]
2. G. Aad et al., ATLAS Collaboration, Phys. Lett. B **716**, 1 (2012). [arXiv:1207.7214 [hep-ex]]
3. S. Weinberg, Phys. Rev. D **13**, 974 (1976)
4. L. Susskind, Phys. Rev. D **20**, 2619 (1979)
5. C. Csaki, C. Grojean, H. Murayama, L. Pilo, J. Terning, Phys. Rev. D **69**, 055006 (2004). [hep-ph/0305237]
6. C. Csaki, C. Grojean, L. Pilo, J. Terning, Phys. Rev. Lett. **92**, 101802 (2004). [hep-ph/0308038]
7. P. Ramond, SUSY: the early years (1966–1976). Eur. Phys. J. C **74**, 2698 (2014). doi:10.1140/epjc/s10052-013-2698-x. arXiv:1401.5977
8. P. Fayet, The supersymmetric standard model. Eur. Phys. J. C **74**, 2837 (2014). doi:10.1140/epjc/s10052-014-2837-z. arXiv:1403.5951
9. I. Melzer-Pellmann, P. Pralavorio, Lessons for SUSY from the LHC after the first run. Eur. Phys. J. C **74**, 2801 (2014). doi:10.1140/epjc/s10052-014-2801-y. arXiv:1404.7191
10. J. Ellis, Supersymmetric fits after the Higgs discovery and implications for model building. Eur. Phys. J. C **74**, 2732 (2014). doi:10.1140/epjc/s10052-014-2732-7. arXiv:1312.5426
11. A. Djouadi, Implications of the Higgs discovery for the MSSM. doi:10.1140/epjc/s10052-013-2704-3. arXiv:1311.0720
12. G. G. Ross, SUSY: Quo Vadis? Eur. Phys. J. C **74**, 2699 (2014). doi:10.1140/epjc/s10052-013-2699-9
13. R. Catena, L. Covi, SUSY dark matter(s). doi:10.1140/epjc/s10052-013-2703-4. arXiv:1310.4776
14. H. P. Nilles, The strings connection: MSSM-like models from strings. Eur. Phys. J. C **74**, 2712 (2014). doi:10.1140/epjc/s10052-013-2712-3
15. D.B. Kaplan, H. Georgi, Phys. Lett. B **136**, 183 (1984)
16. D.B. Kaplan, H. Georgi, S. Dimopoulos, Phys. Lett. B **136**, 187 (1984)
17. H. Georgi, D.B. Kaplan, P. Galison, Phys. Lett. B **143**, 152 (1984)
18. T. Banks, Nucl. Phys. B **243**, 125 (1984)
19. H. Georgi, D.B. Kaplan, Phys. Lett. B **145**, 216 (1984)
20. M.J. Dugan, H. Georgi, D.B. Kaplan, Nucl. Phys. B **254**, 299 (1985)

21. H. Georgi, Nucl. Phys. B **266**, 274 (1986)
22. L. Randall, R. Sundrum, Phys. Rev. Lett. **83**, 3370 (1999). [hep-ph/9905221]
23. K. Agashe, A. Delgado, M.J. May, R. Sundrum, JHEP **0308**, 050 (2003). [hep-ph/0308036]
24. H. Davoudiasl, J.L. Hewett, T.G. Rizzo, Phys. Lett. B **473**, 43 (2000). [hep-ph/9911262]
25. A. Pomarol, Phys. Lett. B **486**, 153 (2000). [hep-ph/9911294]
26. N. Arkani-Hamed, A.G. Cohen, E. Katz, A.E. Nelson, T. Gregoire, J.G. Wacker, JHEP **0208**, 021 (2002). [arXiv:hep-ph/0206020]
27. N. Arkani-Hamed, A.G. Cohen, E. Katz, A.E. Nelson, JHEP **0207**, 034 (2002). [arXiv:hep-ph/0206021]
28. N. Arkani-Hamed, A.G. Cohen, H. Georgi, Phys. Rev. Lett. **86**, 4757 (2001). [hep-th/0104005]
29. C.T. Hill, S. Pokorski, J. Wang, Phys. Rev. D **64**, 105005 (2001). [hep-th/0104035]
30. R. Contino, Y. Nomura, A. Pomarol, Nucl. Phys. B **671**, 148 (2003). [arXiv:hep-ph/0306259]
31. K. Agashe, R. Contino, A. Pomarol, Nucl. Phys. B **719**, 165 (2005). [hep-ph/0412089]
32. Y. Hosotani, Phys. Lett. B **126**, 309 (1983)
33. I. Antoniadis, K. Benakli, M. Quiros, New J. Phys. **3**, 20 (2001). [hep-th/0108005]
34. N.S. Manton, Nucl. Phys. B **158**, 141 (1979)
35. H. Hatanaka, T. Inami, C.S. Lim, Mod. Phys. Lett. A **13**, 2601 (1998). [hep-th/9805067]
36. G. von Gersdorff, N. Irges, M. Quiros, Nucl. Phys. B **635**, 127 (2002). [hep-th/0204223]
37. L.J. Hall, Y. Nomura, D. Tucker-Smith, Nucl. Phys. B **639**, 307 (2002). [hep-ph/0107331]
38. C. Csaki, C. Grojean, H. Murayama, Phys. Rev. D **67**, 085012 (2003). [hep-ph/0210133]
39. C.A. Scrucca, M. Serone, L. Silvestrini, Nucl. Phys. B **669**, 128 (2003). [hep-ph/0304220]
40. C.A. Scrucca, M. Serone, L. Silvestrini, A. Wulzer, JHEP **0402**, 049 (2004). [hep-th/0312267]
41. G.F. Giudice, C. Grojean, A. Pomarol, R. Rattazzi, JHEP **0706**, 045 (2007). [arXiv:hep-ph/0703164]
42. R. Barbieri, B. Bellazzini, V.S. Rychkov, A. Varagnolo, Phys. Rev. D **76**, 115008 (2007). [arXiv:0706.0432 [hep-ph]]
43. J. Galloway, J.A. Evans, M.A. Luty, R.A. Tacchi, JHEP **1010**, 086 (2010). [arXiv:1001.1361 [hep-ph]]
44. I. Low, W. Skiba, D. Tucker-Smith, Phys. Rev. D **66**, 072001 (2002). [hep-ph/0207243]
45. D.E. Kaplan, M. Schmaltz, JHEP **0310**, 039 (2003). [arXiv:hep-ph/0302049]
46. S. Chang, J.G. Wacker, Phys. Rev. D **69**, 035002 (2004). [arXiv:hep-ph/0303001]
47. W. Skiba, J. Terning, Phys. Rev. D **68**, 075001 (2003). [hep-ph/0305302]
48. M. Schmaltz, JHEP **0408**, 056 (2004). [hep-ph/0407143]
49. M. Schmaltz, D. Stolarski, J. Thaler, JHEP **1009**, 018 (2010). [arXiv:1006.1356 [hep-ph]]
50. M. Schmaltz, J. Thaler, JHEP **0903**, 137 (2009). [arXiv:0812.2477 [hep-ph]]
51. A. Hook, J.G. Wacker, JHEP **1006**, 041 (2010). [arXiv:0912.0937 [hep-ph]]
52. N. Arkani-Hamed, A.G. Cohen, H. Georgi, Phys. Lett. B **513**, 232 (2001). [arXiv:hep-ph/0105239]
53. R. Contino, T. Kramer, M. Son, R. Sundrum, JHEP **0705**, 074 (2007). [arXiv:hep-ph/0612180]
54. G. Panico, A. Wulzer, [arXiv:1106.2719 [hep-ph]]
55. S. De Curtis, M. Redi, A. Tesi, [arXiv:1110.1613 [hep-ph]]
56. J. Thaler, JHEP **0507**, 024 (2005). [arXiv:hep-ph/0502175]
57. Z. Chacko, H.S. Goh, R. Harnik, Phys. Rev. Lett. **96**, 231802 (2006). [arXiv:hep-ph/0506256]
58. Z. Chacko, Y. Nomura, M. Papucci, G. Perez, JHEP **0601**, 126 (2006). [arXiv:hep-ph/0510273]
59. W.D. Goldberger, B. Grinstein, W. Skiba, Phys. Rev. Lett. **100**, 111802 (2008). [arXiv:0708.1463 [hep-ph]]
60. J. Fan, W.D. Goldberger, A. Ross, W. Skiba, Phys. Rev. D **79**, 035017 (2009). [arXiv:0803.2040 [hep-ph]]
61. L. Vecchi, Phys. Rev. D **82**, 076009 (2010). [arXiv:1002.1721 [hep-ph]]
62. Z. Chacko, R.K. Mishra, [arXiv:1209.3022 [hep-ph]]
63. B. Bellazzini, C. Csaki, J. Hubisz, J. Serra, J. Terning, Eur. Phys. J. C **73**, 2333 (2013). [arXiv:1209.3299 [hep-ph]]
64. B. Bellazzini, C. Csaki, J. Hubisz, J. Serra, J. Terning, [arXiv:1305.3919 [hep-th]]
65. F. Coradeschi, P. Lodone, D. Pappadopulo, R. Rattazzi, L. Vitale, JHEP **1311**, 057 (2013). [arXiv:1306.4601 [hep-th]]
66. C. Csaki, M. Graesser, L. Randall, J. Terning, Phys. Rev. D **62**, 045015 (2000). [hep-ph/9911406]
67. W.D. Goldberger, M.B. Wise, Phys. Lett. B **475**, 275 (2000). [hep-ph/9911457]
68. C. Csaki, M.L. Graesser, G.D. Kribs, Phys. Rev. D **63**, 065002 (2001). [hep-th/0008151]
69. C. Csaki, J. Hubisz, S.J. Lee, Phys. Rev. D **76**, 125015 (2007). [arXiv:0705.3844 [hep-ph]]
70. E. Katz, A.E. Nelson, D.G.E. Walker, JHEP **0508**, 074 (2005). [arXiv:hep-ph/0504252]
71. J. Thaler, I. Yavin, JHEP **0508**, 022 (2005). [hep-ph/0501036]
72. L. Vecchi, [arXiv:1304.4579 [hep-ph]]
73. S. Dimopoulos, L. Susskind, Nucl. Phys. B **155**, 237 (1979)
74. E. Eichten, K.D. Lane, Phys. Lett. B **90**, 125 (1980)
75. M.A. Luty, T. Okui, JHEP **0609**, 070 (2006). [arXiv:hep-ph/0409274]
76. B. Holdom, Phys. Lett. B **150**, 301 (1985)
77. D.B. Kaplan, J.-W. Lee, D.T. Son, M.A. Stephanov, Phys. Rev. D **80**, 125005 (2009). [arXiv:0905.4752 [hep-th]]
78. R. Rattazzi, V.S. Rychkov, E. Tonni, A. Vichi, JHEP **0812**, 031 (2008). [arXiv:0807.0004 [hep-th]]
79. R. Rattazzi, S. Rychkov, A. Vichi, J. Phys. A **44**, 035402 (2011). [arXiv:1009.5985 [hep-th]]
80. A. Vichi, JHEP **1201**, 162 (2012). [arXiv:1106.4037 [hep-th]]
81. D. Poland, D. Simmons-Duffin, A. Vichi, JHEP **1205**, 110 (2012). [arXiv:1109.5176 [hep-th]]
82. D.B. Kaplan, Nucl. Phys. B **365**, 259 (1991)
83. Y. Grossman, M. Neubert, Phys. Lett. B **474**, 361 (2000). [hep-ph/9912408]
84. S.J. Huber, Q. Shafi, Phys. Lett. B **498**, 256 (2001). [arXiv:hep-ph/0010195]
85. T. Gherghetta, A. Pomarol, Nucl. Phys. B **586**, 141 (2000). [arXiv:hep-ph/0003129]
86. S.J. Huber, Nucl. Phys. B **666**, 269 (2003). [arXiv:hep-ph/0303183]
87. K. Agashe, G. Perez, A. Soni, Phys. Rev. D **71**, 016002 (2005). [arXiv:hep-ph/0408134]
88. R. Rattazzi, A. Zaffaroni, JHEP **0104**, 021 (2001). [arXiv:hep-th/0012248]
89. G. Cacciapaglia, C. Csaki, J. Galloway, G. Marandella, J. Terning, A. Weiler, JHEP **0804**, 006 (2008). [arXiv:0709.1714 [hep-ph]]
90. J. Santiago, JHEP **0812**, 046 (2008). [arXiv:0806.1230 [hep-ph]]
91. M. Redi, A. Weiler, JHEP **1111**, 108 (2011). [arXiv:1106.6357 [hep-ph]]
92. R. Barbieri, D. Buttazzo, F. Sala, D.M. Straub, A. Tesi, JHEP **1305**, 069 (2013). [arXiv:1211.5085 [hep-ph]]
93. R. Barbieri, D. Buttazzo, F. Sala, D.M. Straub, JHEP **1207**, 181 (2012). [arXiv:1203.4218 [hep-ph]]
94. M. Redi, Eur. Phys. J. C **72**, 2030 (2012). [arXiv:1203.4220 [hep-ph]]

95. B. Gripaios, A. Pomarol, F. Riva, J. Serra, JHEP **0904**, 070 (2009). [arXiv:0902.1483 [hep-ph]]
96. J. Mrazek, A. Pomarol, R. Rattazzi, M. Redi, J. Serra, A. Wulzer, Nucl. Phys. B **853**, 1–48 (2011). [arXiv:1105.5403 [hep-ph]]
97. M. Chala, JHEP **1301**, 122 (2013). [arXiv:1210.6208 [hep-ph]]
98. E. Bertuzzo, T.S. Ray, H. de Sandes, C.A. Savoy, JHEP **1305**, 153 (2013). [arXiv:1206.2623 [hep-ph]]
99. S. Chang, JHEP **0312**, 057 (2003). [hep-ph/0306034]
100. H.C. Cheng, I. Low, JHEP **0309**, 051 (2003). [arXiv:hep-ph/0308199]
101. H.C. Cheng, I. Low, JHEP **0408**, 061 (2004). [arXiv:hep-ph/0405243]
102. I. Low, JHEP **0410**, 067 (2004). [hep-ph/0409025]
103. K. Agashe, G. Servant, Phys. Rev. Lett. **93**, 231805 (2004). [arXiv:hep-ph/0403143]
104. K. Agashe, R. Contino, R. Sundrum, Phys. Rev. Lett. **95**, 171804 (2005). [arXiv:hep-ph/0502222]
105. B. Gripaios, JHEP **1002**, 045 (2010). [arXiv:0910.1789 [hep-ph]]
106. M. Frigerio, J. Serra, A. Varagnolo, JHEP **1106**, 029 (2011). [arXiv:1103.2997 [hep-ph]]
107. E. Witten, Nucl. Phys. B **223**, 433 (1983)
108. R. Rattazzi talk at "The Zurich phenomenology workshop: Higgs search confronts theory" (2012)
109. A. Urbano, [arXiv:1310.5733 [hep-ph]]
110. M.S. Carena, E. Ponton, J. Santiago, C.E.M. Wagner, Phys. Rev. D **76**, 035006 (2007). [hep-ph/0701055]
111. C. Csaki, A. Falkowski, A. Weiler, JHEP **0809**, 008 (2008). [arXiv:0804.1954 [hep-ph]]
112. G. Panico, M. Redi, A. Tesi, A. Wulzer, JHEP **1303**, 051 (2013). [arXiv:1210.7114 [hep-ph]]
113. O. Matsedonskyi, G. Panico, A. Wulzer, JHEP **1301**, 164 (2013). [arXiv:1204.6333 [hep-ph]]
114. M. Redi, A. Tesi, JHEP **1210**, 166 (2012). [arXiv:1205.0232 [hep-ph]]
115. D. Marzocca, M. Serone, J. Shu, JHEP **1208**, 013 (2012). [arXiv:1205.0770 [hep-ph]]
116. A. Pomarol, F. Riva, JHEP **1208**, 135 (2012). [arXiv:1205.6434 [hep-ph]]
117. J. Barnard, T. Gherghetta, A. Medina, T.S. Ray, [arXiv:1307.4778 [hep-ph]]
118. R. Contino, L. Da Rold, A. Pomarol, Phys. Rev. D **75**, 055014 (2007). [arXiv:hep-ph/0612048]
119. M.E. Peskin, T. Takeuchi, Phys. Rev. Lett. **65**, 964 (1990)
120. M.E. Peskin, T. Takeuchi, Phys. Rev. D **46**, 381 (1992)
121. R. Barbieri, A. Pomarol, R. Rattazzi, A. Strumia, Nucl. Phys. B **703**, 127 (2004). [arXiv:hep-ph/0405040]
122. A. Orgogozo, S. Rychkov, [arXiv:1211.5543 [hep-ph]]
123. M.J. Dugan, L. Randall, Phys. Lett. B **264**, 154 (1991)
124. R. Barbieri, G. Isidori, D. Pappadopulo, JHEP **0902**, 029 (2009). [arXiv:0811.2888 [hep-ph]]
125. P. Lodone, JHEP **0812**, 029 (2008). [arXiv:0806.1472 [hep-ph]]
126. P. Sikivie, L. Susskind, M.B. Voloshin, V.I. Zakharov, Nucl. Phys. B **173**, 189 (1980)
127. C. Csaki, J. Hubisz, G.D. Kribs, P. Meade, J. Terning, Phys. Rev. D **67**, 115002 (2003). [arXiv:hep-ph/0211124]
128. C. Csaki, J. Hubisz, G.D. Kribs, P. Meade, J. Terning, Phys. Rev. D **68**, 035009 (2003). [hep-ph/0303236]
129. G. Marandella, C. Schappacher, A. Strumia, Phys. Rev. D **72**, 035014 (2005). [hep-ph/0502096]
130. K. Agashe, R. Contino, Nucl. Phys. B **742**, 59 (2006). [arXiv:hep-ph/0510164]
131. M.S. Carena, E. Ponton, J. Santiago, C.E.M. Wagner, Phys. Rev. D **76**, 035006 (2007). [arXiv:hep-ph/0701055]
132. C. Grojean, O. Matsedonskyi, G. Panico, [arXiv:1306.4655 [hep-ph]]
133. A. Pomarol, J. Serra, Phys. Rev. D **78**, 074026 (2008). [arXiv:0806.3247 [hep-ph]]
134. R.S. Chivukula, S.B. Selipsky, E.H. Simmons, Phys. Rev. Lett. **69**, 575 (1992). [arXiv:hep-ph/9204214]
135. G. Cacciapaglia, C. Csaki, G. Marandella, A. Strumia, Phys. Rev. D **74**, 033011 (2006). [hep-ph/0604111]
136. K. Agashe, R. Contino, L. Da Rold, A. Pomarol, Phys. Lett. B **641**, 62 (2006). [arXiv:hep-ph/0605341]
137. B. Batell, S. Gori, L.-T. Wang, JHEP **1301**, 139 (2013). [arXiv:1209.6382 [hep-ph]]
138. N. Vignaroli, [arXiv:1204.0478 [hep-ph]]
139. J.A. Aguilar-Saavedra, N.F. Castro, A. Onofre, Phys. Rev. D **83**, 117301 (2011). [arXiv:1105.0117 [hep-ph]]
140. J. Berger, J. Hubisz, M. Perelstein, JHEP **1207**, 016 (2012). [arXiv:1205.0013 [hep-ph]]
141. M. Gillioz, Phys. Rev. D **80**, 055003 (2009). [arXiv:0806.3450 [hep-ph]]
142. C. Anastasiou, E. Furlan, J. Santiago, Phys. Rev. D **79**, 075003 (2009). [arXiv:0901.2117 [hep-ph]]
143. G. Cacciapaglia, A. Deandrea, D. Harada, Y. Okada, JHEP **1011**, 159 (2010). [arXiv:1007.2933 [hep-ph]]
144. M. Ciuchini, E. Franco, S. Mishima, L. Silvestrini, [arXiv:1306.4644 [hep-ph]]
145. K. Agashe, A. Falkowski, I. Low, G. Servant, JHEP **0804**, 027 (2008). [arXiv:0712.2455 [hep-ph]]
146. J. Hubisz, P. Meade, A. Noble, M. Perelstein, JHEP **0601**, 135 (2006). [hep-ph/0506042]
147. S. Samuel, Nucl. Phys. B **347**, 625 (1990)
148. M. Dine, A. Kagan, S. Samuel, Phys. Lett. B **243**, 250 (1990)
149. J.A. Evans, J. Galloway, M.A. Luty, R.A. Tacchi, JHEP **1104**, 003 (2011). [arXiv:1012.4808 [hep-ph]]
150. M. Blanke, A.J. Buras, B. Duling, S. Gori, A. Weiler, JHEP **0903**, 001 (2009). [arXiv:0809.1073 [hep-ph]]
151. M. Bauer, S. Casagrande, U. Haisch, M. Neubert, JHEP **1009**, 017 (2010). [arXiv:0912.1625 [hep-ph]]
152. B. Keren-Zur, P. Lodone, M. Nardecchia, D. Pappadopulo, R. Rattazzi, L. Vecchi, Nucl. Phys. B **867**, 429 (2013). [arXiv:1205.5803 [hep-ph]]
153. O. Gedalia, G. Isidori, G. Perez, Phys. Lett. B **682**, 200 (2009). [arXiv:0905.3264 [hep-ph]]
154. W. Altmannshofer, P. Paradisi, D.M. Straub, JHEP **1204**, 008 (2012). [arXiv:1111.1257 [hep-ph]]
155. A.J. Buras, C. Grojean, S. Pokorski, R. Ziegler, JHEP **1108**, 028 (2011). [arXiv:1105.3725 [hep-ph]]
156. K. Agashe, R. Contino, Phys. Rev. D **80**, 075016 (2009). [arXiv:0906.1542 [hep-ph]]
157. S.L. Glashow, S. Weinberg, Phys. Rev. D **15**, 1958 (1977)
158. A.J. Buras, M.V. Carlucci, S. Gori, G. Isidori, JHEP **1010**, 009 (2010). [arXiv:1005.5310 [hep-ph]]
159. K. Agashe, A.E. Blechman, F. Petriello, Phys. Rev. D **74**, 053011 (2006). [hep-ph/0606021]
160. C. Csaki, Y. Grossman, P. Tanedo, Y. Tsai, Phys. Rev. D **83**, 073002 (2011). [arXiv:1004.2037 [hep-ph]]
161. M. Redi, JHEP **1309**, 060 (2013). [arXiv:1306.1525 [hep-ph]]
162. C. Csaki, C. Delaunay, C. Grojean, Y. Grossman, JHEP **0810**, 055 (2008). [arXiv:0806.0356 [hep-ph]]
163. F. del Aguila, A. Carmona, J. Santiago, JHEP **1008**, 127 (2010). [arXiv:1001.5151 [hep-ph]]
164. O. Domenech, A. Pomarol, J. Serra, Phys. Rev. D **85**, 074030 (2012). [arXiv:1201.6510 [hep-ph]]
165. W.-J. Huo, S.-H. Zhu, Phys. Rev. D **68**, 097301 (2003). [hep-ph/0306029]
166. S.R. Choudhury, N. Gaur, A. Goyal, N. Mahajan, Phys. Lett. B **601**, 164 (2004). [hep-ph/0407050]
167. J.Y. Lee, JHEP **0412**, 065 (2004). [hep-ph/0408362]

168. A.J. Buras, A. Poschenrieder, S. Uhlig, Nucl. Phys. B **716**, 173 (2005). [hep-ph/0410309]
169. A. J. Buras, A. Poschenrieder, S. Uhlig, [hep-ph/0501230]
170. J. Hubisz, S.J. Lee, G. Paz, JHEP **0606**, 041 (2006). [hep-ph/0512169]
171. M. Blanke, A.J. Buras, B. Duling, S. Recksiegel, C. Tarantino, Acta Phys. Polon. B **41**, 657 (2010). [arXiv:0906.5454 [hep-ph]]
172. A. Azatov, J. Galloway, Int. J. Mod. Phys. A **28**, 1330004 (2013). [arXiv:1212.1380]
173. A. Falkowski, F. Riva, A. Urbano, [arXiv:1303.1812 [hep-ph]]
174. P.P. Giardino, K. Kannike, I. Masina, M. Raidal, A. Strumia, [arXiv:1303.3570 [hep-ph]]
175. I. Low, R. Rattazzi, A. Vichi, JHEP **1004**, 126 (2010). [arXiv:0907.5413 [hep-ph]]
176. R. Contino, M. Ghezzi, C. Grojean, M. Muhlleitner, M. Spira, JHEP **1307**, 035 (2013). [arXiv:1303.3876 [hep-ph]]
177. R. Alonso, M.B. Gavela, L. Merlo, S. Rigolin, J. Yepes, Phys. Lett. B **722**, 330 (2013). [arXiv:1212.3305 [hep-ph]]
178. I. Brivio, T. Corbett, O.J.P. Éboli, M.B. Gavela, J. Gonzalez-Fraile, M.C. Gonzalez-Garcia, L. Merlo, S. Rigolin, [arXiv:1311.1823 [hep-ph]]
179. J. Elias-Miro, J.R. Espinosa, E. Masso, A. Pomarol, [arXiv:1308.1879 [hep-ph]]
180. A. Pomarol, F. Riva, [arXiv:1308.2803 [hep-ph]]
181. A. Azatov, R. Contino, A. Di Iura, J. Galloway, Phys. Rev. D **88**, 075019 (2013). [arXiv:1308.2676 [hep-ph]]
182. Z. Chacko, R. Franceschini, R.K. Mishra, [arXiv:1209.3259 [hep-ph]]
183. M. Montull, F. Riva, JHEP **1211**, 018 (2012). [arXiv:1207.1716 [hep-ph]]
184. J. Reuter, M. Tonini, JHEP **1302**, 077 (2013). [arXiv:1212.5930 [hep-ph]]
185. G. Belanger, B. Dumont, U. Ellwanger, J.F. Gunion, S. Kraml, [arXiv:1306.2941 [hep-ph]]
186. M. Farina, C. Grojean, F. Maltoni, E. Salvioni, A. Thamm, JHEP **1305**, 022 (2013). [arXiv:1211.3736 [hep-ph]]
187. S. Biswas, E. Gabrielli, F. Margaroli, B. Mele, JHEP **07**, 073 (2013). [arXiv:1304.1822 [hep-ph]]
188. C. Degrande, J.M. Gerard, C. Grojean, F. Maltoni, G. Servant, JHEP **1207**, 036 (2012) [Erratum-ibid. 1303 (2013) 032] [arXiv:1205.1065 [hep-ph]]
189. D. Curtin, J. Galloway, J.G. Wacker, [arXiv:1306.5695 [hep-ph]]
190. C. Grojean, E. Salvioni, M. Schlaffer, A. Weiler, [arXiv:1312.3317 [hep-ph]]
191. A. Azatov, A. Paul, JHEP **1401** 014(2014) [arXiv:1309.5273 [hep-ph]]
192. I. Low, A. Vichi, Phys. Rev. D **84**, 045019 (2011). [arXiv:1010.2753 [hep-ph]]
193. M. Gillioz, R. Grober, C. Grojean, M. Muhlleitner, E. Salvioni, JHEP **1210**, 004 (2012). [arXiv:1206.7120 [hep-ph]]
194. M. Farina, M. Perelstein, N.R. -L. Lorier, [arXiv:1305.6068 [hep-ph]]
195. A. Falkowski, Phys. Rev. D **77**, 055018 (2008). [arXiv:0711.0828 [hep-ph]]
196. A. Azatov, J. Galloway, Phys. Rev. D **85**, 055013 (2012). [arXiv:1110.5646 [hep-ph]]
197. M. Montull, F. Riva, E. Salvioni, R. Torre, [arXiv:1308.0559 [hep-ph]]
198. C. Delaunay, C. Grojean, G. Perez, [arXiv:1303.5701 [hep-ph]]
199. A. Banfi, A. Martin, V. Sanz, [arXiv:1308.4771 [hep-ph]]
200. N. Craig, C. Englert, M. McCullough, [arXiv:1305.5251 [hep-ph]]
201. R. Contino, C. Grojean, M. Moretti, F. Piccinini, R. Rattazzi, JHEP **1005**, 089 (2010). [arXiv:1002.1011 [hep-ph]]
202. R. Contino, D. Marzocca, D. Pappadopulo, R. Rattazzi, JHEP **1110**, 081 (2011). [arXiv:1109.1570 [hep-ph]]
203. B. Bellazzini, C. Csaki, J. Hubisz, J. Serra, J. Terning, JHEP **1211**, 003 (2012). [arXiv:1205.4032 [hep-ph]]
204. R. Contino, M. Ghezzi, M. Moretti, G. Panico, F. Piccinini, A. Wulzer, JHEP **1208**, 154 (2012). [arXiv:1205.5444 [hep-ph]]
205. R. Contino, C. Grojean, D. Pappadopulo, R. Rattazzi, A. Thamm, [arXiv:1309.7038 [hep-ph]]
206. CMS Collaboration [CMS Collaboration], CMS-PAS-HIG-13-013
207. CMS Collaboration [CMS Collaboration], CMS-PAS-HIG-13-018
208. [ATLAS Collaboration], ATLAS-CONF-2013-011
209. [ATLAS Collaboration], ATLAS-CONF-2013-034
210. J.R. Espinosa, M. Muhlleitner, C. Grojean, M. Trott, JHEP **1209**, 126 (2012). [arXiv:1205.6790 [hep-ph]]
211. N. Arkani-Hamed, A.G. Cohen, T. Gregoire, J.G. Wacker, JHEP **0208**, 020 (2002). [hep-ph/0202089]
212. J.L. Hewett, F.J. Petriello, T.G. Rizzo, JHEP **0310**, 062 (2003). [hep-ph/0211218]
213. T. Han, H.E. Logan, B. McElrath, L.-T. Wang, Phys. Rev. D **67**, 095004 (2003). [hep-ph/0301040]
214. T. Han, H.E. Logan, L.-T. Wang, JHEP **0601**, 099 (2006). [hep-ph/0506313]
215. M.S. Carena, E. Ponton, J. Santiago, C.E.M. Wagner, Nucl. Phys. B **759**, 202 (2006). [hep-ph/0607106]
216. M. Carena, A.D. Medina, B. Panes, N.R. Shah, C.E.M. Wagner, Phys. Rev. D **77**, 076003 (2008). [arXiv:0712.0095 [hep-ph]]
217. G. Burdman, M. Perelstein and A. Pierce, Phys. Rev. Lett. **90**, 241802 (2003). [Erratum-ibid. 92 (2004) 049903] [hep-ph/0212228]
218. J.A. Conley, J.L. Hewett, M.P. Le, Phys. Rev. D **72**, 115014 (2005). [hep-ph/0507198]
219. K. Agashe, H. Davoudiasl, S. Gopalakrishna, T. Han, G.-Y. Huang, G. Perez, Z.-G. Si, A. Soni, Phys. Rev. D **76**, 115015 (2007). [arXiv:0709.0007 [hep-ph]]
220. K. Agashe, S. Gopalakrishna, T. Han, G.-Y. Huang, A. Soni, Phys. Rev. D **80**, 075007 (2009). [arXiv:0810.1497 [hep-ph]]
221. K. Agashe, A. Azatov, T. Han, Y. Li, Z.-G. Si, L. Zhu, Phys. Rev. D **81**, 096002 (2010). [arXiv:0911.0059 [hep-ph]]
222. F. del Aguila, J. de Blas, M. Perez-Victoria, JHEP **1009**, 033 (2010). [arXiv:1005.3998 [hep-ph]]
223. M. Redi, V. Sanz, M. de Vries, A. Weiler, JHEP **1308**, 008 (2013). [arXiv:1305.3818 [hep-ph]]
224. K. Agashe, A. Belyaev, T. Krupovnickas, G. Perez, J. Virzi, Phys. Rev. D **77**, 015003 (2008). [hep-ph/0612015]
225. B. Lillie, L. Randall, L.-T. Wang, JHEP **0709**, 074 (2007). [hep-ph/0701166]
226. B. Lillie, J. Shu, T.M.P. Tait, Phys. Rev. D **76**, 115016 (2007). [arXiv:0706.3960 [hep-ph]]
227. CMS Collaboration [CMS Collaboration], CMS-PAS-EXO-12-025
228. [ATLAS Collaboration], ATLAS-CONF-2013-015
229. S. Chatrchyan et al., CMS Collaboration, Phys. Rev. Lett. **111**, 211804 (2013). [arXiv:1309.2030 [hep-ex]]
230. The ATLAS collaboration, ATLAS-CONF-2013-052
231. M. Perelstein, M.E. Peskin, A. Pierce, Phys. Rev. D **69**, 075002 (2004). [hep-ph/0310039]
232. S. Godfrey, T. Gregoire, P. Kalyniak, T.A.W. Martin, K. Moats, JHEP **1204**, 032 (2012). [arXiv:1201.1951 [hep-ph]]
233. R. Contino, G. Servant, JHEP **0806**, 026 (2008). [arXiv:0801.1679 [hep-ph]]
234. J. Mrazek, A. Wulzer, Phys. Rev. D **81**, 075006 (2010). [arXiv:0909.3977 [hep-ph]]
235. G. Dissertori, E. Furlan, F. Moortgat, P. Nef, JHEP **1009**, 019 (2010). [arXiv:1005.4414 [hep-ph]]
236. N. Vignaroli, Phys. Rev. D **86**, 075017 (2012). [arXiv:1207.0830 [hep-ph]]

237. G. Cacciapaglia, A. Deandrea, L. Panizzi, S. Perries, V. Sordini, JHEP **1303**, 004 (2013). [arXiv:1211.4034 [hep-ph]]
238. J. Li, D. Liu, J. Shu, JHEP **1311**, 047 (2013). [arXiv:1306.5841 [hep-ph]]
239. J.A. Aguilar-Saavedra, JHEP **0911**, 030 (2009). [arXiv:0907.3155 [hep-ph]]
240. A. De Simone, O. Matsedonskyi, R. Rattazzi, A. Wulzer, JHEP **1304**, 004 (2013). [arXiv:1211.5663 [hep-ph]]
241. M. Buchkremer, G. Cacciapaglia, A. Deandrea, L. Panizzi, Nucl. Phys. B **876**, 376 (2013). [arXiv:1305.4172 [hep-ph]]
242. J.A. Aguilar-Saavedra, R. Benbrik, S. Heinemeyer, M. Perez-Victoria, Phys. Rev. D **88**, 094010 (2013). [arXiv:1306.0572 [hep-ph]]
243. D. Pappadopulo, A. Thamm, R. Torre, JHEP **1307**, 058 (2013). [arXiv:1303.3062 [hep-ph]]
244. J. Kearney, A. Pierce, J. Thaler, JHEP **1308**, 130 (2013). [arXiv:1304.4233 [hep-ph]]
245. J. Kearney, A. Pierce, J. Thaler, JHEP **1310**, 230 (2013). [arXiv:1306.4314 [hep-ph]]
246. C. Delaunay, T. Flacke, J. Gonzalez-Fraile, S.J. Lee, G. Panico, G. Perez, [arXiv:1311.2072 [hep-ph]]
247. S. Chatrchyan et al., CMS Collaboration, arXiv:1312.2391 [hep-ex]
248. S. Chatrchyan et al., CMS Collaboration, [arXiv:1311.7667 [hep-ex]]
249. CMS Collaboration, CMS Collaboration, CMS-PAS-B2G-13-003
250. A. Azatov, M. Salvarezza, M. Son and M. Spannowsky, arXiv:1308.6601 [hep-ph]
251. [ATLAS Collaboration], ATLAS-CONF-2013-018
252. [The ATLAS collaboration], ATLAS-CONF-2013-060
253. [The ATLAS collaboration], ATLAS-CONF-2013-051
254. [The ATLAS collaboration], ATLAS-CONF-2013-056
255. H. Murayama, J. Shu, Phys. Lett. B **686**, 162 (2010). [arXiv:0905.1720 [hep-ph]]
256. A. Joseph, S.G. Rajeev, Phys. Rev. D **80**, 074009 (2009). [arXiv:0905.2772 [hep-ph]]
257. M. Gillioz, A. von Manteuffel, P. Schwaller, D. Wyler, JHEP **1103**, 048 (2011). [arXiv:1012.5288 [hep-ph]]
258. A. Pomarol, A. Wulzer, JHEP **0803**, 051 (2008). [arXiv:0712.3276 [hep-th]]
259. S. Nussinov, Phys. Lett. B **165**, 55 (1985)
260. S.M. Barr, R.S. Chivukula, E. Farhi, Phys. Lett. B **241**, 387 (1990)
261. S.B. Gudnason, C. Kouvaris, F. Sannino, Phys. Rev. D **73**, 115003 (2006). [hep-ph/0603014]
262. S.B. Gudnason, C. Kouvaris, F. Sannino, Phys. Rev. D **74**, 095008 (2006). [hep-ph/0608055]
263. R. Foadi, M.T. Frandsen, F. Sannino, Phys. Rev. D **80**, 037702 (2009). [arXiv:0812.3406 [hep-ph]]
264. D.E. Kaplan, M.A. Luty, K.M. Zurek, Phys. Rev. D **79**, 115016 (2009). [arXiv:0901.4117 [hep-ph]]
265. K. Agashe, A. Delgado, R. Sundrum, Ann. Phys. **304**, 145 (2003). [hep-ph/0212028]
266. L. Vecchi, [arXiv:1310.7862 [hep-ph]]
267. M. Frigerio, A. Pomarol, F. Riva, A. Urbano, JHEP **1207**, 015 (2012). [arXiv:1204.2808 [hep-ph]]
268. D.S. Akerib et al., LUX Collaboration, [arXiv:1310.8214 [astro-ph.CO]]
269. E. Aprile et al., XENON100 Collaboration, Phys. Rev. Lett. **109**, 181301 (2012). [arXiv:1207.5988 [astro-ph.CO]]
270. J. Hubisz, P. Meade, Phys. Rev. D **71**, 035016 (2005). [hep-ph/0411264]
271. A. Birkedal, A. Noble, M. Perelstein, A. Spray, Phys. Rev. D **74**, 035002 (2006). [hep-ph/0603077]
272. M. Perelstein, A. Spray, Phys. Rev. D **75**, 083519 (2007). [hep-ph/0610357]
273. D. Hooper, G. Zaharijas, Phys. Rev. D **75**, 035010 (2007). [hep-ph/0612137]
274. A. Birkedal, Z. Chacko, M.K. Gaillard, JHEP **0410**, 036 (2004). [hep-ph/0404197]
275. Z. Berezhiani, P.H. Chankowski, A. Falkowski, S. Pokorski, Phys. Rev. Lett. **96**, 031801 (2006). [hep-ph/0509311]
276. T.S. Roy, M. Schmaltz, JHEP **0601**, 149 (2006). [hep-ph/0509357]
277. C. Csaki, G. Marandella, Y. Shirman, A. Strumia, Phys. Rev. D **73**, 035006 (2006). [hep-ph/0510294]
278. B. Bellazzini, S. Pokorski, V.S. Rychkov, A. Varagnolo, JHEP **0811**, 027 (2008). [arXiv:0805.2107 [hep-ph]]
279. B. Bellazzini, C. Csaki, A. Delgado, A. Weiler, Phys. Rev. D **79**, 095003 (2009). [arXiv:0902.0015 [hep-ph]]
280. N. Craig, K. Howe, [arXiv:1312.1341 [hep-ph]]
281. B. Bellazzini, C. Csaki, A. Falkowski, A. Weiler, Phys. Rev. D **80**, 075008 (2009). [arXiv:0906.3026 [hep-ph]]
282. B. Bellazzini, C. Csaki, A. Falkowski, A. Weiler, Phys. Rev. D **81**, 075017 (2010). [arXiv:0910.3210 [hep-ph]]
283. C. Csaki, Y. Shirman, J. Terning, Phys. Rev. D **84**, 095011 (2011). [arXiv:1106.3074 [hep-ph]]
284. N. Craig, D. Stolarski, J. Thaler, JHEP **1111**, 145 (2011). [arXiv:1106.2164 [hep-ph]]
285. C. Csaki, L. Randall, J. Terning, Phys. Rev. D **86**, 075009 (2012). [arXiv:1201.1293 [hep-ph]]
286. M.A. Luty, J. Terning, A.K. Grant, Phys. Rev. D **63**, 075001 (2001). [hep-ph/0006224]
287. R. Harnik, G.D. Kribs, D.T. Larson, H. Murayama, Phys. Rev. D **70**, 015002 (2004). [hep-ph/0311349]
288. F. Caracciolo, A. Parolini, M. Serone, JHEP **1302**, 066 (2013). [arXiv:1211.7290 [hep-ph]]
289. D. Marzocca, A. Parolini, M. Serone, [arXiv:1312.5664 [hep-ph]]
290. C. Csaki, J. Heinonen, M. Perelstein, C. Spethmann, Phys. Rev. D **79**, 035014 (2009). [arXiv:0804.0622 [hep-ph]]
291. D. Pappadopulo, A. Vichi, JHEP **1103**, 072 (2011). [arXiv:1007.4807 [hep-ph]]
292. E. Katz, J.-y. Lee, A.E. Nelson, D.G.E. Walker, JHEP **0510**, 088 (2005). [hep-ph/0312287]
293. J. Barnard, T. Gherghetta, T.S. Ray, [arXiv:1311.6562 [hep-ph]]